Supramolecular Devices and Materials

A thesis submitted for the degree of

Doctor of Philosophy

of The Australian National University by

Charlotte Kirsty Rouse

Australian National University

Research School of Chemistry

The Australian National University, Canberra, Australia

August 2016

Author's Statement

This is to declare that the work in this thesis represents original work that I have undertaken during my Ph.D. degree at the Research School of Chemistry, The Australian National University from 2012 to 2016, with the following exceptions; the crystal structure of compound **83** reported in Chapter 4 was obtained, solved and refined by Dr Paul Carr at The Australian National University, and the rheological, AFM and FT-IR analysis of compound **112** in Chapter 7 was performed by Dr Adam Martin at The University of New South Wales.

To the best of my knowledge, the thesis does not contain material that has been published or written by another person or accepted for the award of any other degree or diploma in any other university or tertiary institution, unless due reference has been made in the text. All figures that do not cite permission to publish are my own work.

I give consent to this copy of my thesis, when deposited in the University library, being available for loan or photocopying.

Charlotte Rouse

August 2016

Acknowledgements

First and foremost I would like to thank Professor Chris Easton for his excellent supervision during my Ph.D. studies. Not only has he provided guidance and support, he has also allowed me the independence to explore my own ideas and has always pushed me to achieve more.

I am also indebted to Dr Hideki Onagi who has been a constant source of advice throughout this project and whose dedication to research is an inspiration. Thank you also to all the past and present members of the Easton group, particularly Dr Lee Alissandratos, Dr Hye Kyung Kim and Dr Tim Altimore for their insightful discussions and whose input has been invaluable.

Thank you to the RSC staff, particularly Anithahini Jeyasingham, Chris Blake and Dr Paul Carr for your fantasic support.

Thank you to Professor Pall Thordarson and Dr Adam Martin at The University of New South Wales for your contribution and collaboration.

Thank you to Dr David Fulton at the University of Newcastle upon Tyne, whose mentorship and encouragement during my undergraduate studies initiated my interest in supramolecular chemistry and without whom I would not have even considered studying for a Ph.D.

Thank you to my family; mum, dad and Jordan, and Daniel Bartkus for your unerring support and belief.

Finally, thank you to the ANU SCUBA club for providing a much needed distraction from my studies!

Conference Presentations

Charlotte K. Rouse, Hideki Onagi, Stephen F. Lincoln, Christopher J. Easton, 'Self-Assembly of a Metal Receptor *via* Peptide Structure Modification' poster presentation, *Self-Assembly and Supramolecular Chemistry Gordon Research Conference,* 2015, Lucca, Italy

Charlotte K. Rouse, Hideki Onagi, Stephen F. Lincoln, Christopher J. Easton, 'Self-Assembly of a Metal Receptor *via* Peptide Structure Modification' invited oral presentation, *Self-Assembly and Supramolecular Chemistry Gordon Research Seminar,* 2015, Lucca, Italy

Charlotte K. Rouse, Hideki Onagi, Stephen F. Lincoln, Christopher J. Easton, 'Modification of Peptide Structure by Cyclodextrin-based Molecular Machines' oral presentation, *RACI National Congress,* 2014, Adelaide, Australia

Charlotte K. Rouse, Hideki Onagi, Stephen F. Lincoln, Christopher J. Easton, 'Modification of Peptide Structure and Function' oral presentation, *RACI NSW Branch Organic One-Day Symposium*, 2014, Canberra, Australia

Charlotte K. Rouse, Hideki Onagi, Stephen F. Lincoln, Christopher J. Easton, 'Peptidic Molecular Machines' oral presentation, *7th Asian Cyclodextrin Conference,* 2013, Bangkok, Thailand

Abstract

This thesis describes work towards the development of a range of supramolecular devices and materials based on cyclodextrin host-guest interactions, and/or short peptide structures.

The first such device targeted was a photoswitchable molecular lariat composed of a [*c*2] (cyclic, two-component) asymmetric daisy chain. Upon combining the two hetero monomer units it was found that a [*c*2]-dimer was not formed.

The next phase of research involved the design of a second type of supramolecular device, also based on cyclodextrin host-guest inclusion complexes, this time serving to produce a change in peptide secondary structure. A range of devices were synthesised giving several modifications; increasing the stability of hexavaline β-sheets, reducing the PPII (polyproline type II) helicity in pentaalanine and introducing β-sheet character to pentaalanine. Furthermore, an azobenzene moiety was introduced as a photo-switchable cyclodextrin guest, enabling PPII helicity to be switched between states of increased and decreased structure *via* photoirraditation.

This principle was then developed to give a device which not only produced a change in peptide structure but also brought about a change in function, in this case metal-binding ability. Upon cyclodextrin host-guest [*c*2]-dimer formation, β-sheet structure was induced in a short peptide strand which facilitated the arrangement of histidine residues in order to bind to a metal ion in a pseudo-chelating arrangement. The unmodified peptide, with no cyclodextrin or guest attached did not bind to Zn^{2+}, whereas the cyclodextrin dimer was found to bind to Zn^{2+} with a K_a of 2,223 M^{-1}. The system was then investigated in the solid-phase and a crystal was grown wherein [*c*1]-complexes were bound to Zn^{2+} in tetrameric assemblies. In addition, the same crystal structure was observed in the absence of Zn^{2+} showing that the system pre-assembles to form a crystal lattice with vacant metal binding sites.

A number of smaller studies were also performed to explore the possibility of the application of peptide chemistry techniques and principles to supramolecular concepts. The solid-phase synthesis technique used to make peptide sequences was investigated as a method for the preparation of rotaxanes. Despite several attempts no interlocked structures were synthesised, however a method was established for the mobilisation of a cyclodextrin onto a stationary phase. β-Sheet peptide-peptide interactions, in conjunction with cyclodextrin host-guest interactions were then explored as a method for the generation of self-assembling polymers. A range of polymeric structures were considered, however within all the systems examined it was found that none formed.

Finally, it was observed that a peptide amphiphile (PA), synthesized during the preparation of a metal-binding cyclodextrin dimer, formed a gel in acetonitrile/water mixtures, DMF and acetone at just 0.06 wt.%. The compound did not form a gel in water, despite its structural similarity to previously reported PAs, but did obey the structure-property relationships determined for these hydrogels. This suggests that despite the difference in solvents, assembly of these organo and hydrogels is the same and indicates a new strategy for the modification of PAs in order to gel target solvents.

Glossary

δ	chemical shift (ppm)
°C	degrees Celsius
2D	two-dimensional
3D	three-dimensional
ADP	adenosine diphosphate
AFM	atomic force microscopy
Ala	alanine
ATP	adenosine triphosphate
AU	arbitrary unit
Boc	di-*tert*-butyl dicarbonate
BOM	benzyloxymethyl acetal
BOP	benzotiazol-1-yloxy-tris(dimethylamino)phosphonium hexafluorophosphate (Castro's reagent)
br	broad
$C_2D_2Cl_4$	deuterated tetrachloroethane
ca.	circa
calcd	calculated
CD	cyclodextrin
CD CX	cyclodextrin carbons, X = 1-6
CD HX	cyclodextrin protons, X = 1-6
CD OHX	cyclodextrin hydroxyl protons, X = 1-6
CD_3OD	deuterated methanol
$CDCl_3$	deuterated chloroform
cGMP	cyclic guanosine monophosphate
cr	crude
D_2O	deuterium oxide
DCL	dynamic combinatorial library
DCM	dichloromethane
dec.	decomposition
DIC	N,N-diisopropylcarbodiimide

DIPEA	diisopropylethylamine
DMAP	4-dimethylaminopyridine
DMF	N,N'-dimethylformamide
DMSO	dimethylsulfoxide
DMSO-d_6	deuterated dimethylsulfoxide
DMTMM	4-(4,6-dimethoxy-1,3,5-triazin-2-yl)-4-methylmorpholinium chloride
DNA	deoxyribonucleic acid
eq	equivalents
ESI	electrospray ionisation
et al.	et alia
Et_2O	diethyl ether
EtOAc	ethyl acetate
Fmoc	fluoroenylmethyloxycarbonyl
G	Gibb's free energy
g	gram
GDP	guanosine diphosphate
Gly	glycine
GTP	guanosine triphosphate
H	enthalpy
HBTU	N,N,N',N'-tetramethyl-*O*-(1*H*-benzotriazol-1-yl)uranium hexaflurophosphate
His	histidine
HOBt	hydroxybenzotriazole
HOD	mono-deuterated water
HOMO	highest occupied molecular orbital
HPLC	high performance liquid chromatography
h	hour
HRMS	high-resolution mass spectrometry
Hz	hertz
ITC	isothermal titration calorimetry
J	coupling constant
K	Kelvin

K_a	association constant
K_d	dissociation constant
LC-MS	liquid chromatography mass spectrometry
lit.	literature
LR	low resolution
LUMO	lowest unoccupied molecular orbital
M	moles per litre
m.p.	melting point
m/*z*	mass-to-charge ratio
M^+	molecular ion
MeCN	acetonitrile
MeOH	methanol
mg	milligram
mgc	minimum gel concentration
min	minutes
mL	millilitres
mol	moles
n	number of molecules
nm	nanometre
NMP	N-methyl-2-pyrrolidone
NMR	nuclear magnetic resonance
nOe	nuclear Overhauser effect
PA	peptide amphiphile
p*K*a	logarithmic acid dissociation constant
PPII	polyproline type II helix
R	gas constant
R_f	retention factor
ROESY	rotating-frame Overhauser effect spectroscopy
RT	room temperature
S	entropy
TFA	trifluoroacetic acid
TIPS	triisopropylsilane

TLC	thin layer chromatography
T_m	mid-point transition
TNBS	2,4,6-trinitrobenzenesulfonic acid
Tos	tosylate
t_R	retention time
TSPA-d_4	deuterated (trimethylsilyl)-3,3,2,2-tetradeuteropropionic acid
UV-vis	ultraviolet-visible
v	volume
Val	valine
w	weight

Contents

Chapter 1: Introduction

1.1 Supramolecular Chemistry

'If atoms are letters, molecules are the words, supramolecular entities are the sentences and the chapters' so Jean-Marie Lehn[1] analogised the field of supramolecular chemistry or 'chemistry beyond the molecule'. Just as words can be arranged to create meaning, supramolecular chemists can arrange molecules to create devices and materials that go beyond the scope of size, complexity and capabilities that can typically be achieved with conventional single molecule chemistry.

Following Lehn's likeness of chemistry to language, the grammatical rules that govern the organization of words can be compared to the connections that control the way in which molecules interact. Supramolecular chemistry therefore focuses on the study and control of what is *between* molecules, that is intermolecular interactions. Although typically much weaker than covalent, intramolecular bonds, non-covalent intermolecular interactions can be combined in a cooperative fashion to produce strong attractive forces,[2] similar to the way in which Velcro® works (Figure **1.1**).

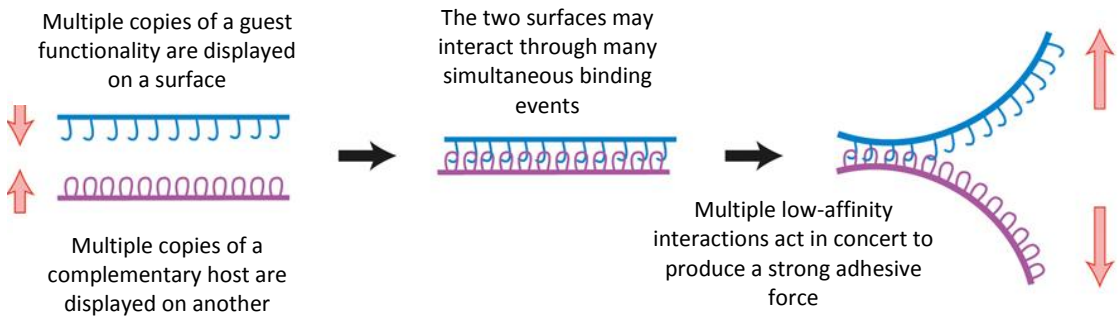

Figure 1.1 Weak, non-covalent bonds can be combined cooperatively to create strong interactions similar to the way in which Velcro® works.[2] Reproduced with permission from Nature Publishing Group.

This strategy allows for the formation of complex, stable molecular architectures which still remain thermodynamically responsive.[3, 4] Life itself relies upon such construction, as in the DNA double helix (Figure **1.2**) which is held together by hydrogen bonds but

can be readily unzipped to enable essential processes such as transcription and replication to occur. This disruption of the hydrogen bonds between DNA strands can also be achieved thermally in a process termed as 'DNA melting', as used in the polymerase chain reaction (PCR) DNA amplification technique.[5]

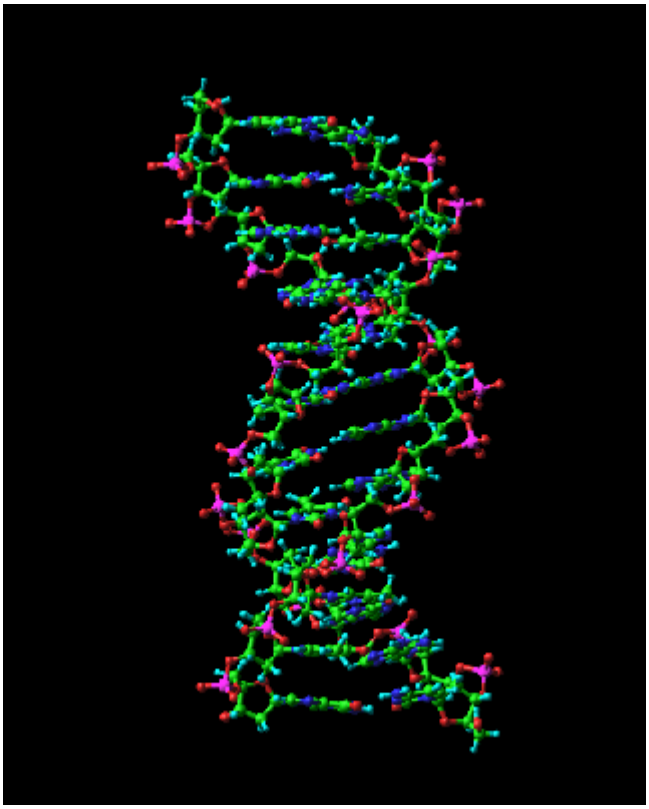

Figure 1.2 The DNA double helix is held together by many weak hydrogen bonds.[6] Reproduced with permission from Elsevier.

During replication, a helicase enzyme unzips the DNA helix to expose the bases on two strands. A second enzyme, DNA polymerase, then binds free nucelotides to the phosphate backbone according to complementary hydrogen bonding with the existing sequence; guanidine binds to cytosine and adenine binds to thymine (Figure **1.3**).[7] As a consequence of the dynamic nature of this pairing, an inherent error-checking system is also present. If the 'wrong' base-pairs become linked, they are quickly displaced by the 'right' base-pairs which form a more thermodynamically favourable interaction, giving highly accurate molecular recognition. This results in the production of an anti-parallel copy of DNA with mistakes only once in every 10^4-10^6 base pairs[8] (although *in vivo*, replication is even more precise on account of proof-reading enzymes). This process, of components in equilibrium adopting the most energetically favourable, defined

arrangement is termed 'self-assembly' and is an integral aspect of supramolecular chemistry.[9]

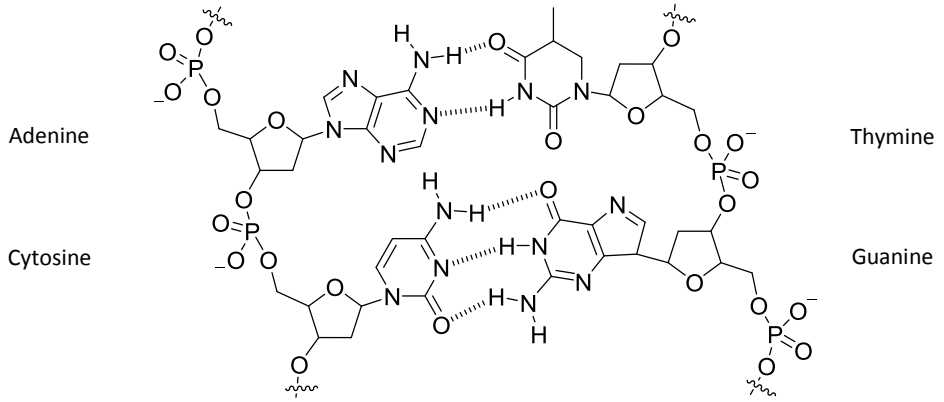

Figure 1.3 DNA assembles *via* hydrogen bonding between complementary base pairs. Adenine binds to thymine (*above*) and cytosine binds to guanine (*below*).

Self-assembly is a 'bottom-up' approach to synthesis, beginning from the smallest construction materials possible and using them as building blocks. As this is usually a one-pot procedure, it is much quicker than traditional step-wise methods to reach nano-sized structures with high complexity (Figure **1.4**).

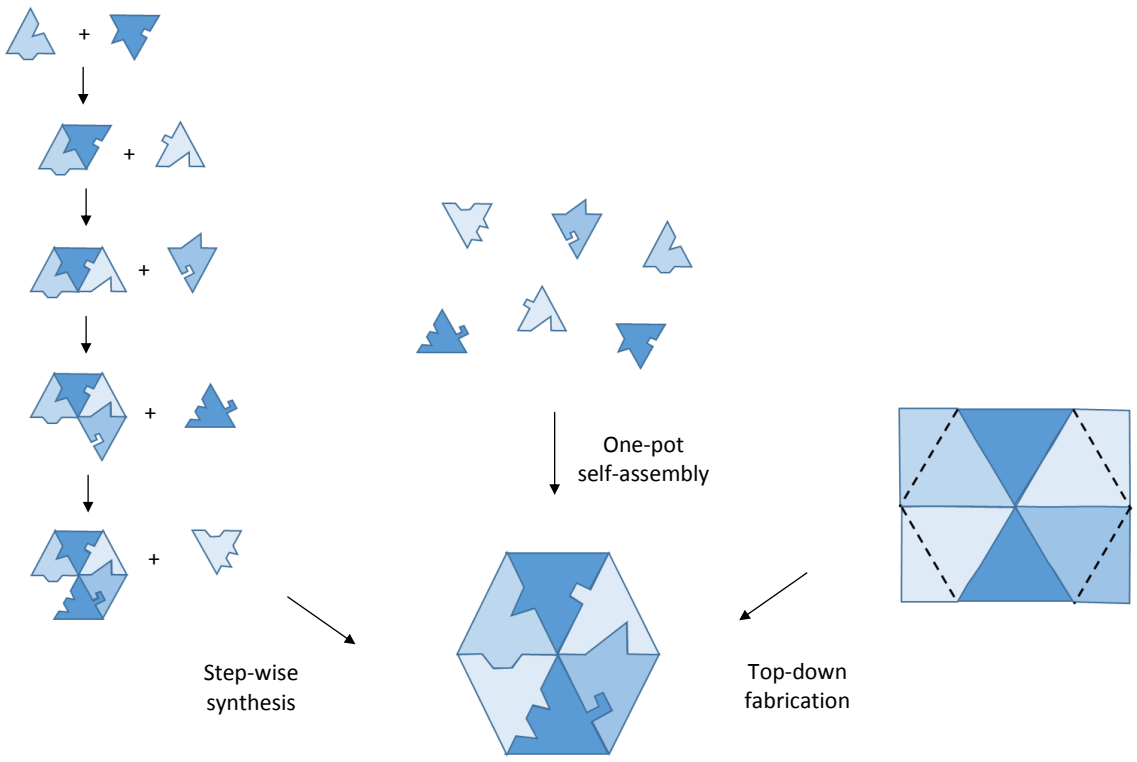

Figure 1.4 Different strategies towards the synthesis of nano-sized structures.

'Top-down' fabrication methods, namely lithography, have also been traditionally used for nano-scale synthesis. In 1985 Tom Newman collected one of Richard Feynman's US$1,000 prizes by writing the first page of Charles Dickens' '*A Tale of Two Cities*' on a 1/25,000 scale using electron beam lithography (Figure **1.5**).[10] The letters were about 75 nm in height, the scale required in order to write the entire Encyclopedia Brittanica on the head of a pin. Current techniques can now etch 1.5 nm letters,[11] however the self-assembly in supramolecular chemistry offers construction down to the same magnitude but with molecular-level resolution, as well as the potential for three-dimensional structures around the full 360° (as they do not require a solid surface), and the formation of mechanically interlocked species.

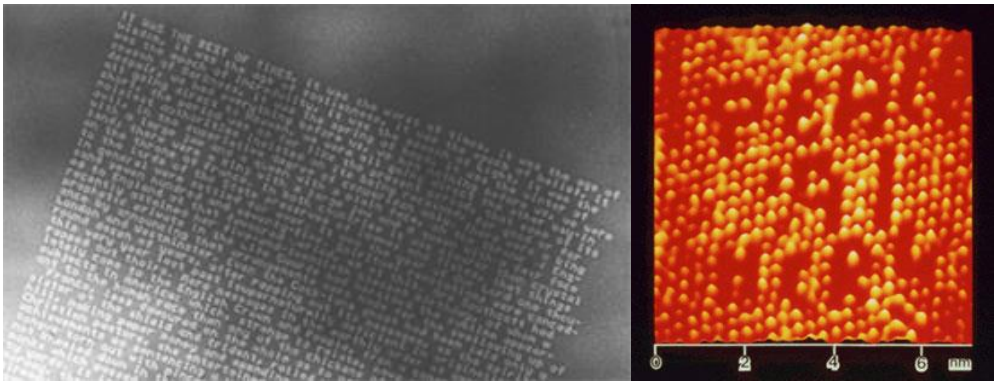

Figure 1.5 Lithographic techniques to etch the smallest letters possible in 1985 (*left*)[10] and 1992 (*right*).[11] Reproduced with permission from AIP Publishing LLC and Elsevier.

The combinatorial approach in supramolecular chemistry not only allows access to large molecules, but also high complexity systems. If we have n molecules in a system, there are $\frac{n(n+1)}{2}$ possible interactions between them all (including interactions with themselves), and if sequence is applied for example in a polymer chain, there are $n!$ possible combinations of these molecules. This allows for an immense amount of information storage using comparatively simple components and is seen in biological systems; entire genetic codes are written using just four DNA bases, and proteins with diverse functions are constructed using combinations of just twenty amino acids.

As opposed to conventional covalently bound molecules, supramolecular systems are not static. This gives rise to the field of dynamic combinatorial chemistry, which uses the lability of components in supramolecular systems in order to generate responsive

systems, termed dynamic combinatorial libraries (DCLs).[12] As DCLs can then adapt to the addition of a material, e.g. a bioactive substance, specifically optimised combinations are generated which can then be isolated *via* an irreversible reaction (Figure **1.6**).[13] The formation of these optimum arrangements are not as a statistical distribution, rather they are selected for by way of specific intermolecular interactions, spontaneously forming the most thermodynamically stable product.

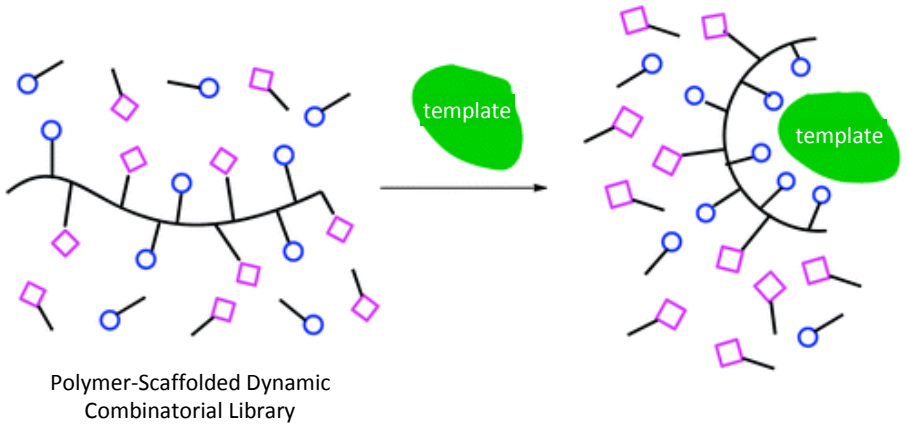

Figure 1.6 Templation of a dynamic combinatorial library.[14] Reproduced with permission from the Royal Society of Chemistry.

Nano-scale structures feature unique supramolecular functionalities that are not apparent at either the atomic scale or micrometre scale, and are also the size range at which biological compounds operate (Figure **1.7**). They are large enough to attain sophisticated, emergent functionalities that are simply not possible with small molecules, but are small enough that effects such as equilibrium, Brownian motion and viscosity are still applicable. Forces such as friction and gravity are limited, yet it is possible for nano-sized compounds to have an effect at the macroscopic level, for example the unidirectional movement of myosins along actin filaments producing the contraction of muscles.[15]

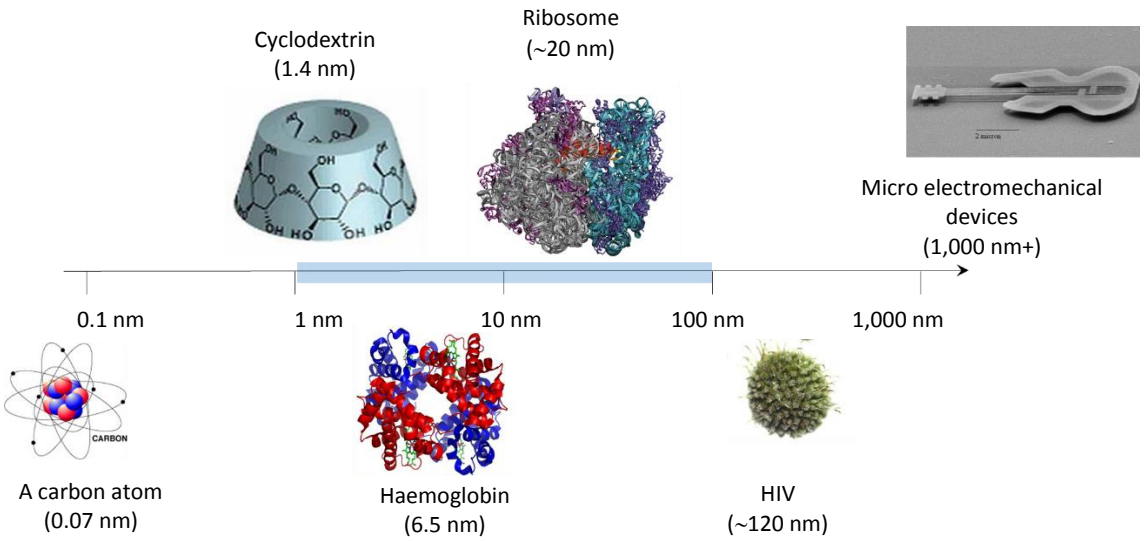

Figure 1.7 The scope of supramolecular chemistry.[16-18]

If we hope to synthesise compounds that approach the level of functionality observed in natural systems or interact with them, we must also construct at the nanometre size. The potential significance of construction at the nano-scale has long been realised by forward-thinking scientists and even science fiction writers. Whilst the perils of robots that reproduce themselves, i.e. the 'grey goo'[19] may not be a realistic fear for now, certainly the application of molecular-sized wires[20] that could power molecular sized computers, or the construction of molecular machines[21, 22] that could eventually be turned into molecular surgeons[23] are in the beginnings of being realised. Such molecular robots could be sent into places no human hand could ever operate - from the inside of a human heart valve, to the inside of a nuclear reactor, or even act as preventative devices, patrolling the bloodstream looking for clots and tumours (Figure **1.8**).

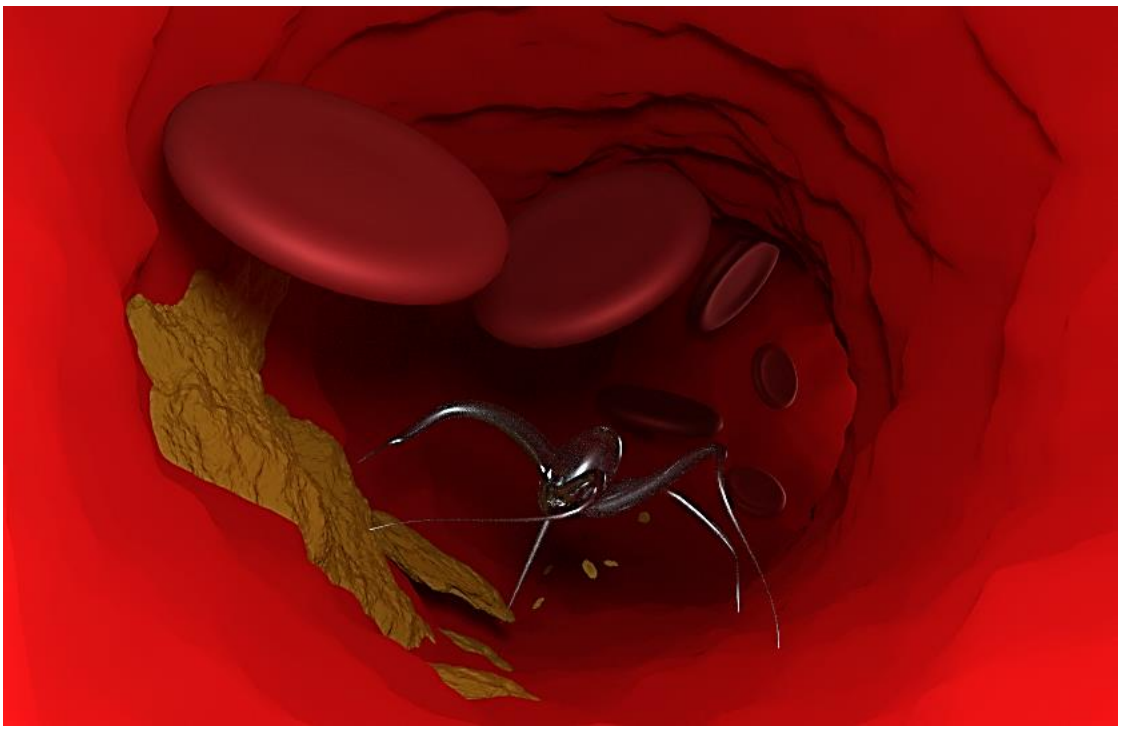

Figure 1.8 Conceptual artwork of a 'molecular surgeon' removing plaque from a blood vessel.

1.2 Non-Covalent Interactions

Supramolecular chemistry is characterised by the use of non-covalent interactions. They allow for features such as bottom-up synthesis *via* self-assembly, thermodynamic responsiveness, error-checking, multi-valency and combinatorial complexity. Non-covalent bonds are broadly categorised into electrostatic, π-interactions and hydrophobic effects. Each has their own properties which are exploited to build and control structures and devices, and often form the basis of supramolecular functionality.

Non-covalent interactions also allow for the formation of the mechanical bond. This takes the form of interlocked rings (catenanes), or rings threaded onto axles (rotaxanes) with nomenclature giving the number of components in the structure as [n]. Rotaxanes can be fixed in place by 'stoppers' or 'capping groups' which prevent de-threading, otherwise they are termed 'pseudo-rotaxanes', and polyrotaxanes can also be formed wherein multiple rings are threaded onto the same axle. Catenanes can be made by either single or double cyclisation, and rotaxanes by clipping, stoppering, slippage, snapping or swelling (Figure **1.9**).[24]

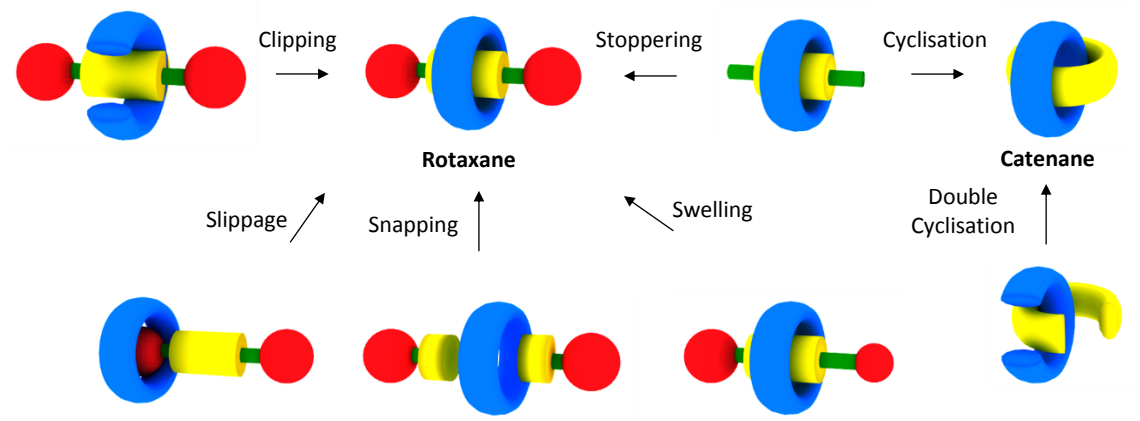

Figure 1.9 Approaches to rotaxane and catenane synthesis adapted from Caballero and coworkers.[24]

Almost all types of non-covalent interactions have been used in supramolecular chemistry and many examples use combinations, such as in the synthesis of the molecular pentafoil knot **1** (Figure **1.10**).[25] In this architecture, relatively weak interactions are multiplied five-fold giving a large effect on the thermodynamic stability of the structure. Metal-ion interactions promote helicate formation of bi-pyridine ligands, hydrogen bonds with the central chloride ion template the cyclic arrangement and stereoelectronic effects favour the looped conformations of aldehyde ligands. The aldehyde and amine ligands then react to give imine bond formation which, although covalent, is reversible until quenched thereby giving an 'error-checking' mechanism under which the most thermodynamically stable product is formed, hence its wide use in supramolecular chemistry.[26]

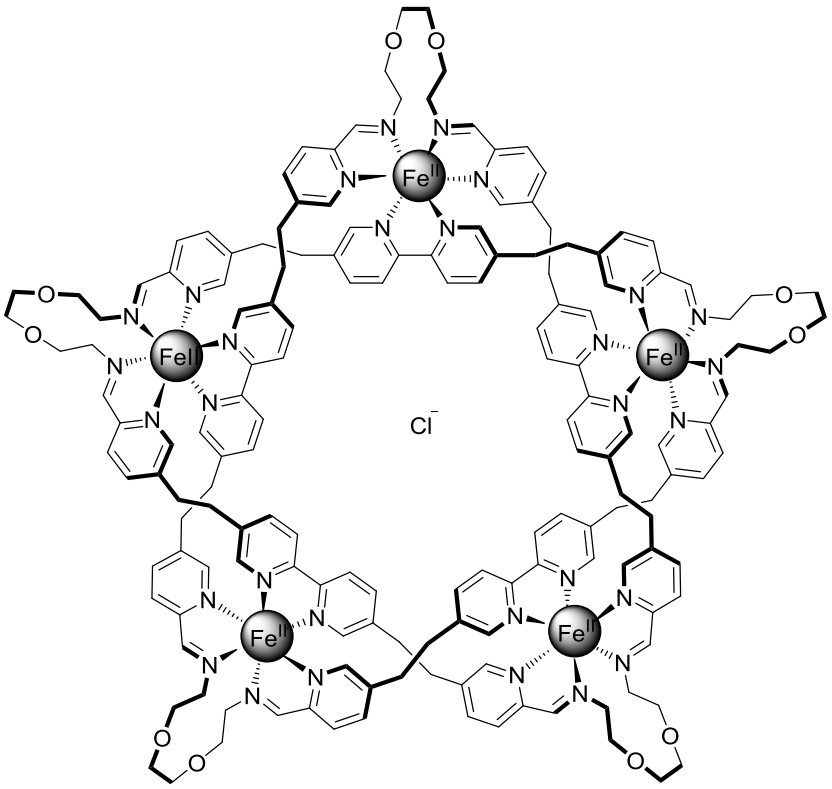

1

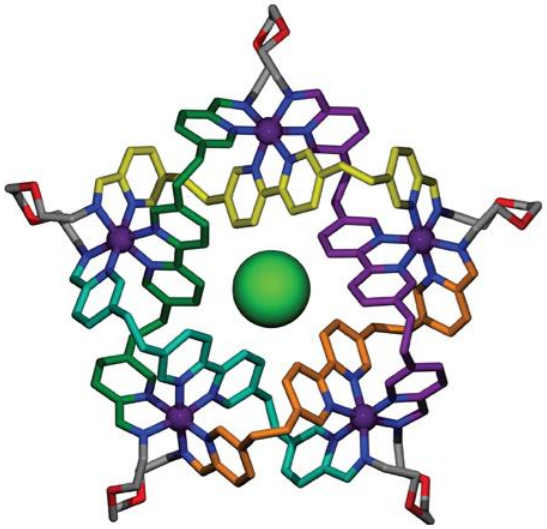

Figure 1.10 Molecular structure (*above*) and crystal structure (*below*) of a molecular pentafoil knot synthesised by self-assembly of aldehyde and amine ligands.[25] Reproduced with permission from Nature Publishing Group.

The first synthetic examples of supramolecular host-guest chemistry (natural systems of course were operating much earlier!) used ion-dipole interactions to selectively encapsulate cation guests, for example the crown ether host **2** which binds K^+ ions (Figure **1.11**).[27] Although ion-dipole interactions are usually non-selective, the fixed cavity of the crown ether results in high size-dependent selectivity of the cation. Since the first example in 1967, this molecular recognition principle has been extended to

azacrowns, thiacrowns, lariat ethers,[28] azacycloalkanes, azacyclophanes,[29] cryptands, and spherands,[30] and used to form rotaxanes.[31]

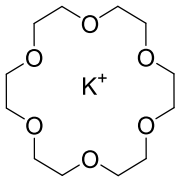

2

Figure 1.11 18-Crown-6, one of the crown ether hosts reported by Pederson[27] that selectively encapsulates a cation.

The most prevalent non-covalent interaction in biological systems is the hydrogen bond, and not surprisingly it is found throughout synthetic supramolecular chemistry. Hydrogen bonds between the NH donors on the wheel of rotaxane **3** and the carbonyl groups on its axle have been used to form a 'station' on which the wheel sits, preventing free rotational and directional movement (Figure **1.12**). These interactions can then be switched off with the introduction of DMSO solvent which outcompete the axle as a hydrogen bond acceptor.[32]

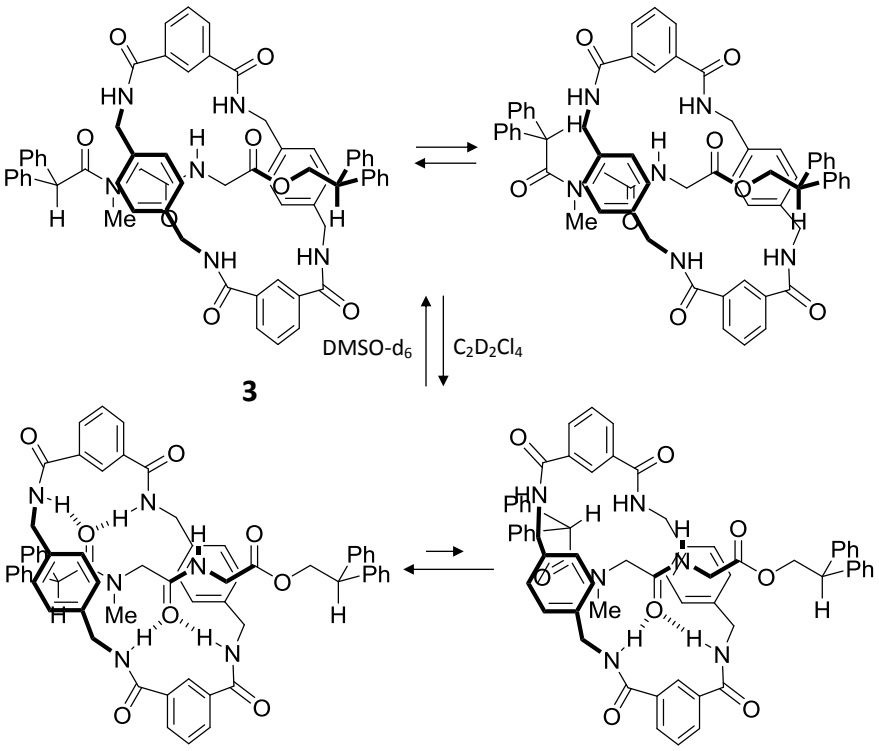

3

Figure 1.12 An amide rotaxane wheel is threaded onto the axle *via* hydrogen bonding, which is disrupted when the solvent is changed to DMSO.[32]

Other electrostatic interactions have been less widely used in supramolecular chemistry, nevertheless ionic interactions have been employed to drive the copolymerisation of dendritic cationic and anionic monomers **4** and **5** into nanotubes (Figure **1.13**).[33] These high-order aggregates remain stable at pH 7, but can be disassembled when the pH is brought away from physiological conditions.

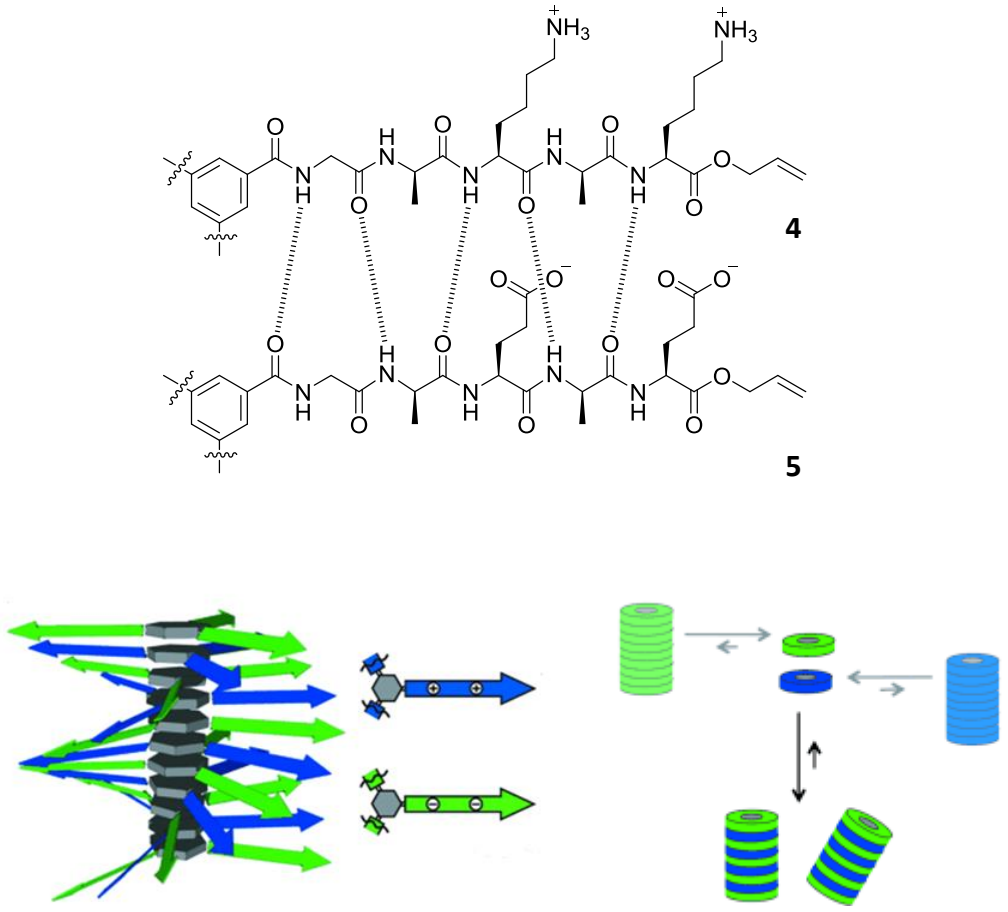

Figure 1.13 Peptide monomers **4** and **5** (*above*) assemble *via* ionic interactions into nanotubes (*below*).[33] Reproduced with permission from John Wiley and Sons.

Different forms of π-interactions have also been used throughout supramolecular chemistry. Conjugated π-π systems have conducting properties, making this an ideal interaction from which to make self-assembling molecular wires.[34] If the conjugated π-π systems are made to form the axle of a rotaxane, the use of a suitable wheel gives a strategy for the formation of insulated molecular wires. This has been demonstrated with the use of conjugated stilbene axles, threaded through a cyclodextrin wheel to give rotaxane **6** which forms extended molecular wires in both solution and the crystal structure (Figure **1.14**).[35]

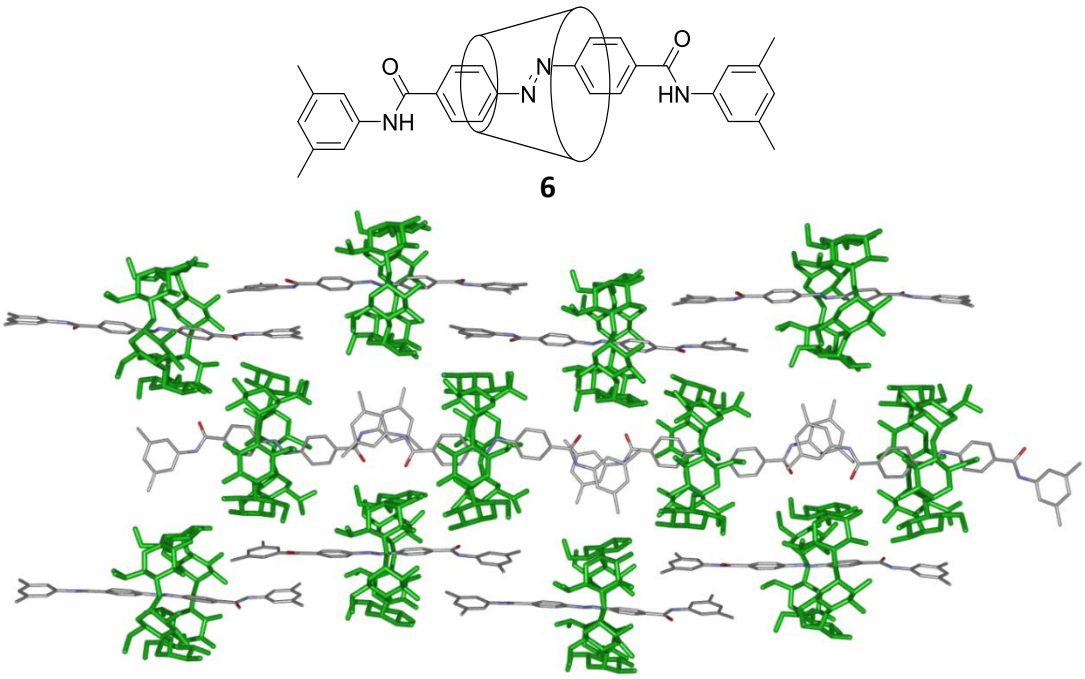

6

Figure 1.14 π-π Stacking of the rotaxane **6** (*above*) gives conjugated molecular wires in the crystal structure (*below*).[35] Reproduced with permission from the American Chemical Society.

π-Interactions not only exist between two conjugated systems however, they can also be formed between an ion and a π system, as in the case of ferrocene. Ferrocene formation has been widely used throughout supramolecular chemistry, for example in the formation of the [3]rotaxane **7** (Figure **1.15**).[36] Here, ferrocene is not only part of the axle of the rotaxane, it also acts as a redox-active sensor, giving a voltammetric response in the presence of bound chloride or sulfate anions.

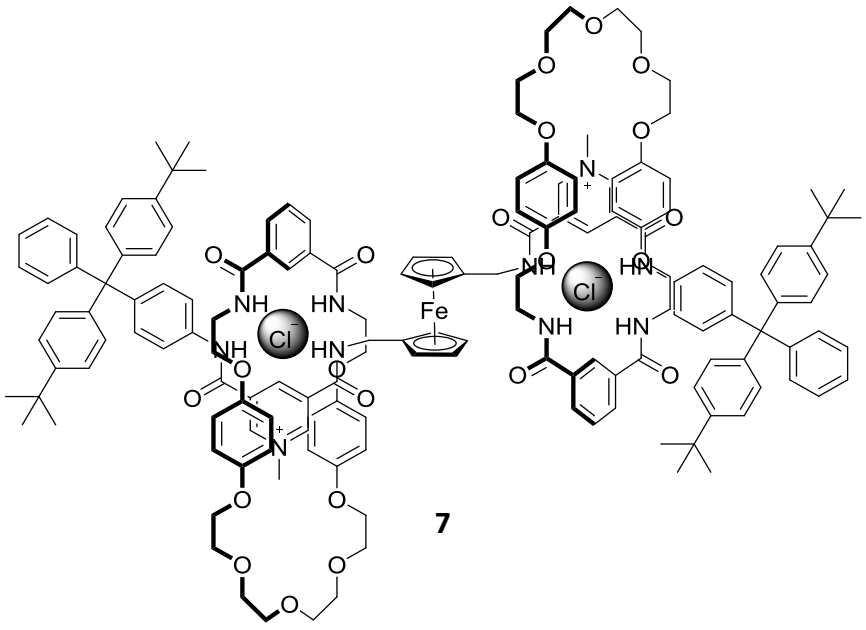

7

Figure 1.15 A ferrocene π-cation interaction forms part of the axle of the [3]rotaxane **7**.[36]

Donor-acceptor π-π stacking systems have also been used to create interlocked molecules, for example the [3]catenane **8** assembles *via* the interaction of π-electron rich tetrathiafulvalene units with π-electron poor cyclobis(paraquat-4,4'-biphenylene) units (Figure **1.16**).[37] This structure was then used as a 'molecular flask' as it gives ideal geometric arrangements and high effective concentrations that stabilise mixed-valence and radical-cation species upon oxidation.

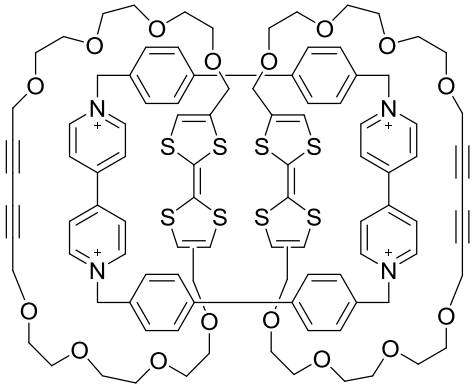

8

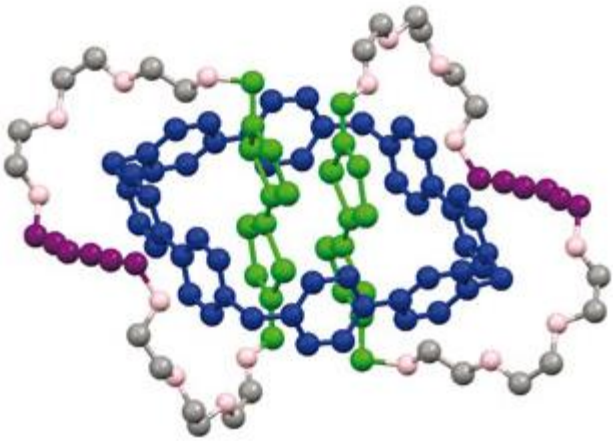

Figure 1.16 A 'molecular flask' constructed from the [3]catenane **8** which is assembled by interactions between π-electron poor and π-electron rich units.[37] Reproduced with permission from Nature Publishing Group.

Another category of non-covalent interaction is hydrophobic effects, which drive the formation of cyclodextrin host-guest complexes. In aqueous solutions, hydrophobic guest groups form inclusion complexes with the hydrophobic cavities of the cyclodextrins. This interaction has been widely used in supramolecular chemistry, and has even been used to direct the assembly of macroscopic objects. Polyacrylamide gels **9** and **10** functionalised with either cyclodextrin or adamantane guest moieties are able

to self-assemble and their interaction may be visualised on the macro-scale (Figure **1.17**).[38]

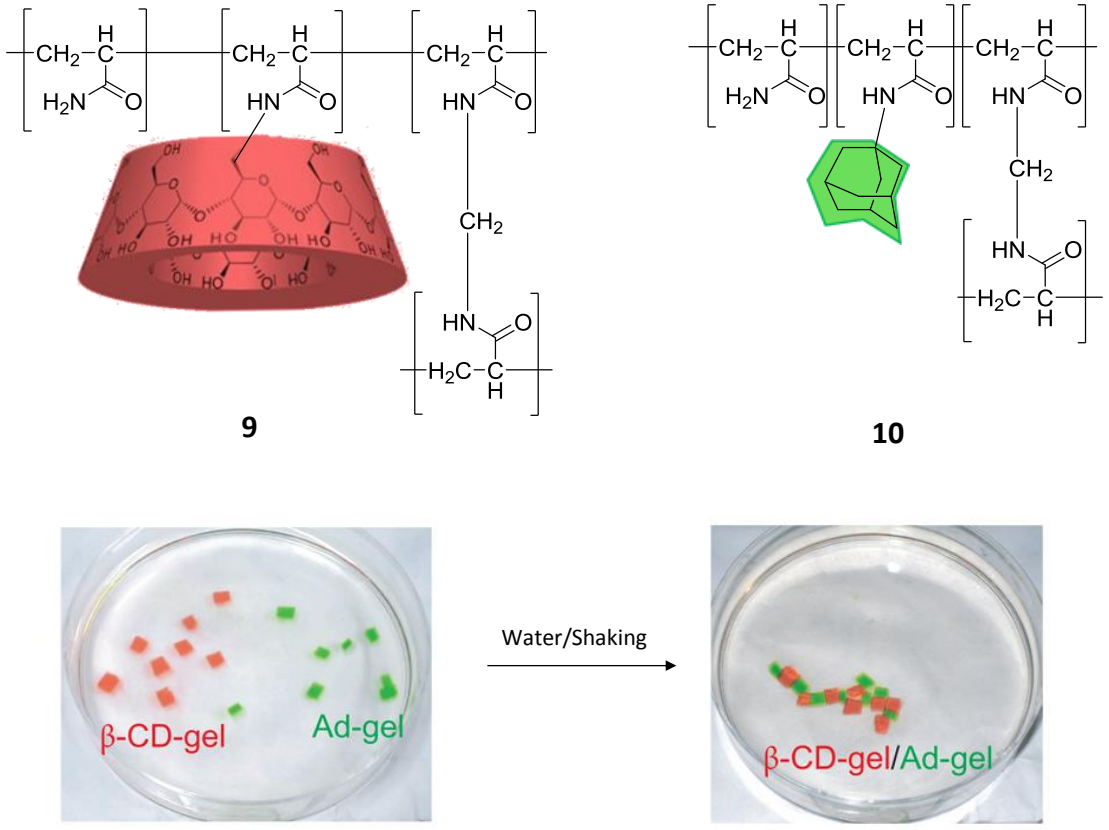

Figure 1.17 Functionalised polyacrylamide gels **9** and **10** (*above*) exhibit host-guest interactions which can be visualised on the macro-scale (*below*).[38] Reproduced with permission from Nature Publishing Group.

The use of cyclodextrin host-guest interactions as a molecular recognition process has been used in this thesis to develop a range of supramolecular devices and materials.

1.3 Cyclodextrins

Cyclodextrins were first observed by Antoine Villiers[39] in 1891 as a product in the bacterial fermentation of potato starch with *Bacillus macerans*. Although it was noted that these new compounds were quite different to the known saccharides of the time, it wasn't until 1948 that their structures were elucidated by Freudenberg and Cramer[40] as cyclic, chiral oligomers of 1,4-α-linked glucopyranose units. The most common cyclodextrins consist of 6, 7 and 8 of these sugar units termed as α, β and γ, respectively. The 1,4-linkages position all the primary hydroxyl groups on one face (the primary face), and all the secondary hydroxyl groups on the opposite face (the secondary face).

Cyclodextrins exist as a slightly truncated cone and are often represented as the simplified 3D shape with carbons and hydrogens numbered 1-6 in a clockwise direction around each glucopyranose ring (Figure **1.18**).

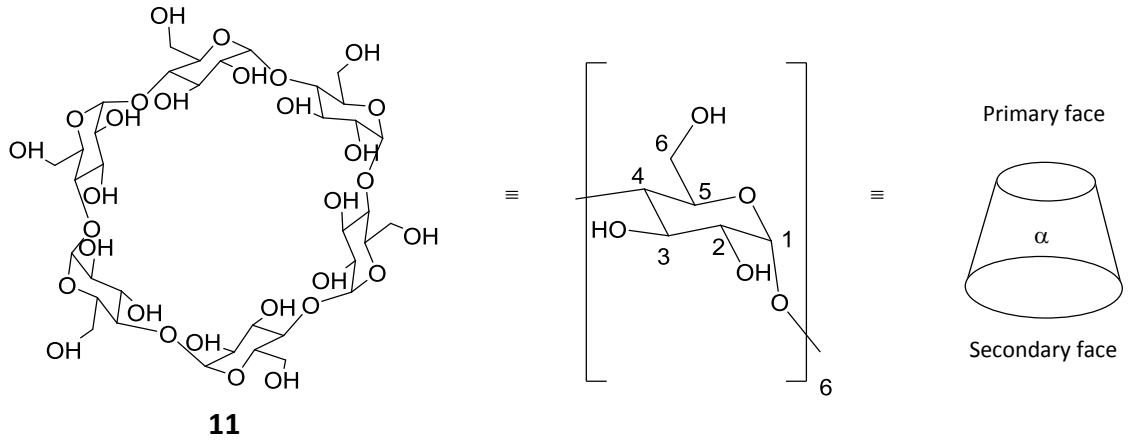

11

Figure 1.18 Chemical structure of α-cyclodextrin **11** (*left*), numbering of atom positions on the pyranose rings (*centre*) and the simplified representation of the cyclodextrin (*right*).

The α-link denotes that the O at the C1 position is in the axial, rather than the equatorial position, even though this conformation is more sterically hindered. This arrangement is an anomeric or Edward Lemieux effect, attributable to hyperconjugation between the HOMO of the adjacent oxygen and the LUMO of the C-O bond (Figure **1.19**).[41]

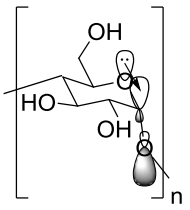

Figure 1.19 Proposed hyperconjugation that results in the axial positioning of the C1 oxygen in cyclodextrins.

The arrangement of the glucopyranose units also allows for the formation of hydrogen bonds between the C2-hydroxyl groups and the C3-hydroxyl groups of the next units. In β-cyclodextrin this bonding extends all the way around the sugar ring forming a secondary hydrogen 'belt' giving it a more rigid structure and making it much less soluble in water than α- and γ-cyclodextrins.[42]

The arrangement of the hydroxyl groups on the exterior of the cyclodextrins gives their most interesting property; a hydrophilic exterior and a hydrophobic interior, which imparts the ability of the cyclodextrins to form inclusion complexes with hydrophobic guests in aqueous solution. Complexation is a thermodynamic process, enthalpically driven by the displacement of water molecules from within the hydrophobic cyclodextrin cavity and around the hydrophobic guest (Figure **1.20**).

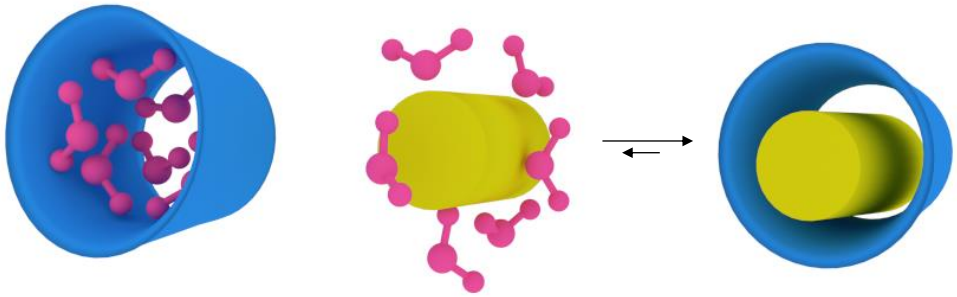

Figure 1.20 Cartoon representation of a hydrophobic guest (*yellow*) complexing with the hydrophobic cavity of a cyclodextrin (*blue*) resulting in the displacement of water molecules (*pink*).

As different cyclodextrins comprise different numbers of glucopyranose units, they also differ in the size of their cavities (Table **1.1**) resulting in selectivity in complexing different sized guests.

	α	β	γ
Glucopyranose units	6	7	8
Diameter between C5 H	4.7 Å	6.0 Å	7.5 Å
Diameter between C3 H	5.2 Å	6.4 Å	8.3 Å
Volume	174 Å	262 Å	472 Å
Solubility in H_2O at 298 K[43]	0.1211 mol L^{-1}	0.0163 mol L^{-1}	0.168 mol L^{-1}

Table 1.1 Properties of α-, β- and γ-cyclodextrins.

As cyclodextrins become larger than 8 glucopyranose units, the annulus begins to distort under steric strain and some units adopt a *trans* configuration with β- rather than α-1,4 links.[44] This collapsed structure persists up until υ-cyclodextrin which consists of 26 units and forms a 'figure of eight' annulus.[45] The largest cyclodextrin that has been isolated and characterised has 39 units[46] however the existence of cyclodextrins composed of

hundreds of units has been detected.[47] Despite reports of inclusion complexes of large-ring cyclodextrins with Buckminster fullerene,[48] carbon nanotubes[49] and even proteins,[50] their use is restricted as a consequence of the difficulty in their separation.

Since the first report of iodine complexation in 1911,[51] the application of cyclodextrin host-guest formation has become wide-spread thanks to the low-cost production of α-, β- and γ-cyclodextrins by the enzyme cyclodextrin glucosyl transferase [CGT-ase], and their low inherent toxicity. As early as 1953, Freudenberg, Cramer and Plieninger[52] obtained a patent covering the use of cyclodextrins in a range medical applications, and today they are part of a number of pharmaceutical preparations (Figure **1.21**). They form complexes with nicotine in Nicorette®, diclofenac in Voltaren® and estradiol in Aerodiol® enhancing the water solubility of lipophilic drugs, protecting easily oxidisable substances and reducing the volatility and hence the loss of pharmaceutically active compounds. 2-Hydroxypropyl-β-cyclodextrin is currently being trialled in the treatment of Niemann-Pick disease as it is thought to complex with accumulated cholesterol and glycolipids in lysosomes, helping to transport them out.[53]

Figure 1.21 Examples of commercial products which contain cyclodextrin.

Cyclodextrin host-guest complexes are also used in many industrial processes and everyday applications. Complexation decreases the volatility of guests and so is used to retain flavour in foods such as coffee, green tea, wasabi and chewing gum. Cyclodextrin guests are also protected against degradation, for example fatty acids in fish oil and

colourants in confectionery. Cyclodextrins are used as 'slow release' agents of fragrant molecules, as well as the moisture-maintaining compound ceramide, and antibacterial oils in perfumes and cosmetics, and agricultural chemicals. Compounds with useful properties have also been combined with cyclodextrins, and coated onto fabric and wrapping materials, after which they are released over time. Cyclodextrins are also used to capture unwanted compounds such as the bitter flavoured naringin in grapefruit juice and catechins in tea, and the fabric freshener Febreze includes cyclodextrin to capture hydrophobic compounds that cause bad odours.[54]

Cyclodextrins play a major role in supramolecular research including in enantioseparation, nanoparticles, catalysis,[55] and the construction of supramolecular structures and devices. Inclusion can be analysed directly by the use of techniques such as isothermal titration calorimetry (ITC), X-ray crystallography and 2D rotating frame nuclear Overhauser effect spectroscopy (ROESY), or indirectly by measuring a change in the properties of the guest (for example increased solubility, nuclear magnetic resonance (NMR) spectroscopy shifts, Cotton effects in circular dichroism spectroscopy, UV-Vis spectra, fluorescence spectra, reactivity and diffusion). Differences between the free and included guest may not only serve as a tool for topology characterisation but may also afford functionality such as in molecular sensors.[56]

Synthetic modification of cyclodextrins further increases their versatility. The 6-hydroxy groups are the most basic and the most nucleophilic, whereas the 2-hydroxy groups are the most acidic. This difference in reactivity allows for the selective modification of cyclodextrins at either the primary or secondary face. For example reacting α-cyclodextrin **11** with tosyl chloride and pyridine leads to tosylation of the primary face,[57] whereas reaction with tosyl chloride and NaOH leads to tosylation of the secondary face (Figure **1.22**).[58] Pyridine also sits inside the α-cyclodextrin cavity, further directing reaction at the C6-OH positions.[59]

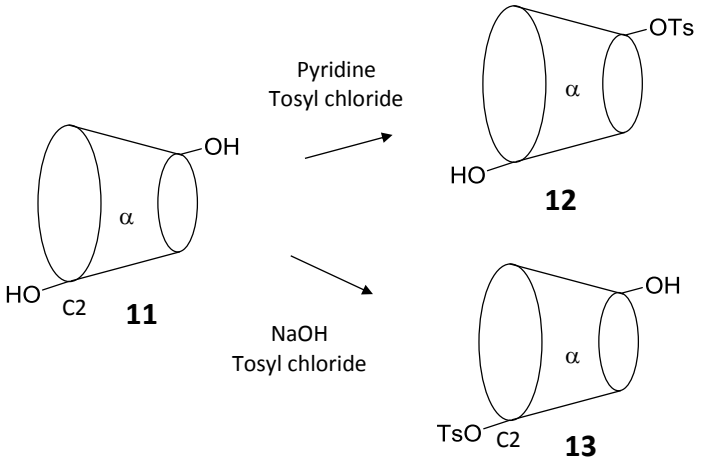

Figure 1.22 Different bases are used to selectively tosylate α-cyclodextrin **11** at either the C6-OH position or the C2-OH position.

Synthesis with cyclodextrins is made all the more easier with the use of an acidic naphthalene-1,3-diol thin-layer chromatography (TLC) dip which produces pink-coloured spots in the presence of cyclodextrin-containing compounds (Figure **1.23**). As each naphthalene molecule reacts with a glucopyranose unit, the dip is fairly sensitive. The mechanism, although not proven, is thought to involve electrophilic aromatic substitution.

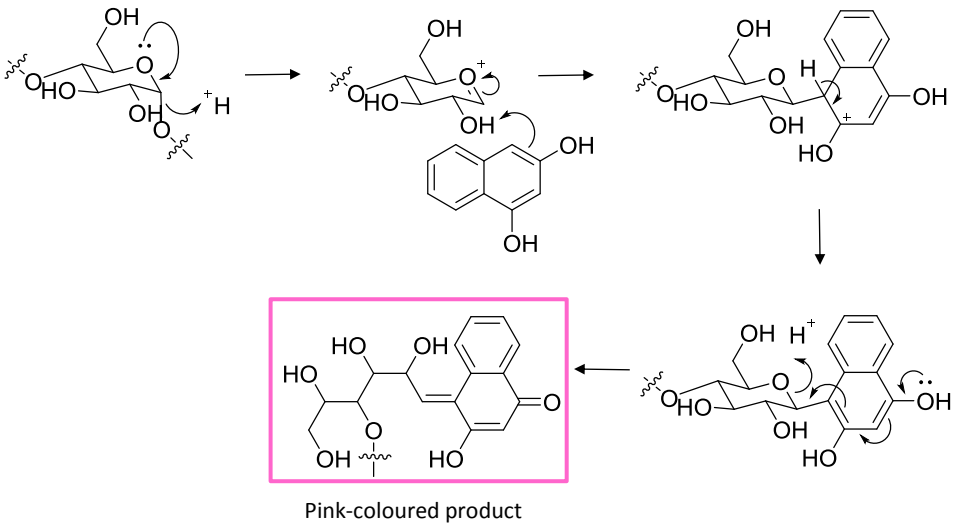

Figure 1.23 Proposed mechanism for the TLC dip which produces pink spots on the plate where cyclodextrin-containing products elute.

Many cyclodextrin-based interlocked molecules have been fabricated using host-guest complexation to thread axles, with the first stoppered cyclodextrin rotaxane **14** reported in 1981,[60] and the first cyclodextrin catenane **15** in 1993 (Figure **1.24**).[61]

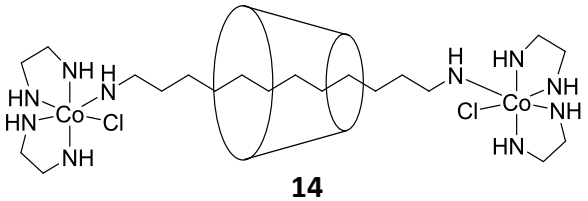

14

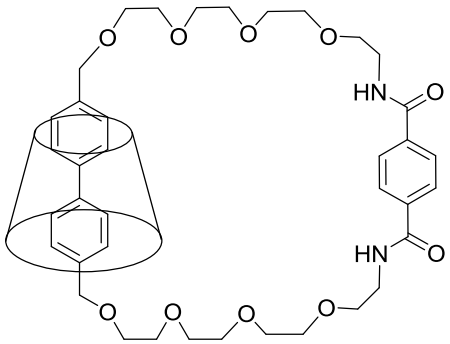

15

Figure 1.24 The first cyclodextrin based rotaxane **14** (*above*)[60] and catenane **15** (*below*).[61]

The molecular recognition process can also be switched on and off forming the basis of cyclodextrin molecular switches, an important component of molecular devices.

1.4 Cyclodextrin-Based Molecular Switches

Molecular switches can be defined as systems which reversibly shift between two or more stable states in response to an external stimulus.[62] Their effect is described as influence as a function of state, rather than influence as a function of trajectory, which applies to molecular machines.[63] True molecular machines perform cumulative work with each switching step moving farther and farther from the initial state in a single direction, for example Feringa's molecular rotor[64] and Leigh's walking molecule[65] and artificial ribosome.[22]

Cyclodextrins form the basis of synthetic molecular switches where an external stimulus influences the equilibrium process that governs the initial host-guest complex formation. This is expressed by a change in the association constant K_a which, for a 1:1 cyclodextrin:guest complex is determined by Equation **1.1**.

$$K_a = \frac{[\text{Complex}]}{[\text{Cyclodextrin}]\,[\text{Guest}]}$$

Equation 1.1 Expression for the association constant for the formation of a 1:1 cyclodextrin:guest complex.

Cyclodextrin-based switching can involve removal and inclusion of a single guest (simple 'in and out' switching), displacement of a guest by another competing guest in 'displacement' switching, or 'back and forth' switching where the cyclodextrin shuttles between two linked guest sites or stations.[66]

The stimulus for this switching varies. Solvent can be used to switch between structures, for example the contracted or extended state of the [*c*2] dimer **16** which depends on the polarity of the solvent (Figure **1.25**).[67] In DMSO the cyclodextrin units sit over the amide bonds of the cinnamide unit, however upon the addition of H_2O (to a 1:1 ratio) the cyclodextrin shuttles to include the hexyl chain. This is because the presence of more polar solvent inside the apolar cyclodextrin cavity results in a thermodynamically unfavourable system which is alleviated by switching to the apolar alkyl chain.

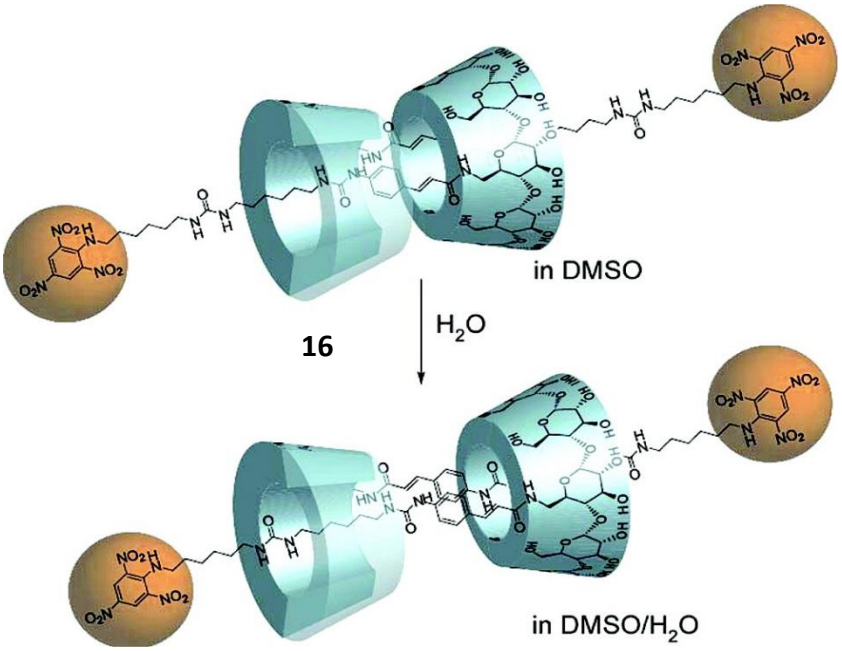

Figure 1.25 Solvent is used to switch between an extended and contracted [*c*2]-cyclodextrin dimer **16**.[67] Reproduced with permission from the American Chemical Society.

Switching solvent has also been used to exert a macroscopic effect, by incorporating cyclodextrins and a pyrene host into polyacrylamide gels. Here the oligomerisation of the pyrene guest and hence interaction with different sized cyclodextrin cavities is

dependent on DMSO/H_2O solvent mixtures (Figure **1.26**).[68] When the volume fraction of DMSO (X_{DMSO}) is 0, i.e. only water, pyrene exists mainly as a dimer which interacts with γ-cyclodextrin but not β-cyclodextrin. As the polarity of the solvent is decreased, to X_{DMSO} = 0.2, a mixture of pyrene monomers and dimers exist, allowing the pyrene gels to interact with both γ- and β-cyclodextrin gels. Finally, at X_{DMSO} = 0.5 pyrene exists mainly as a monomer, interacting with only β-cyclodextrin.

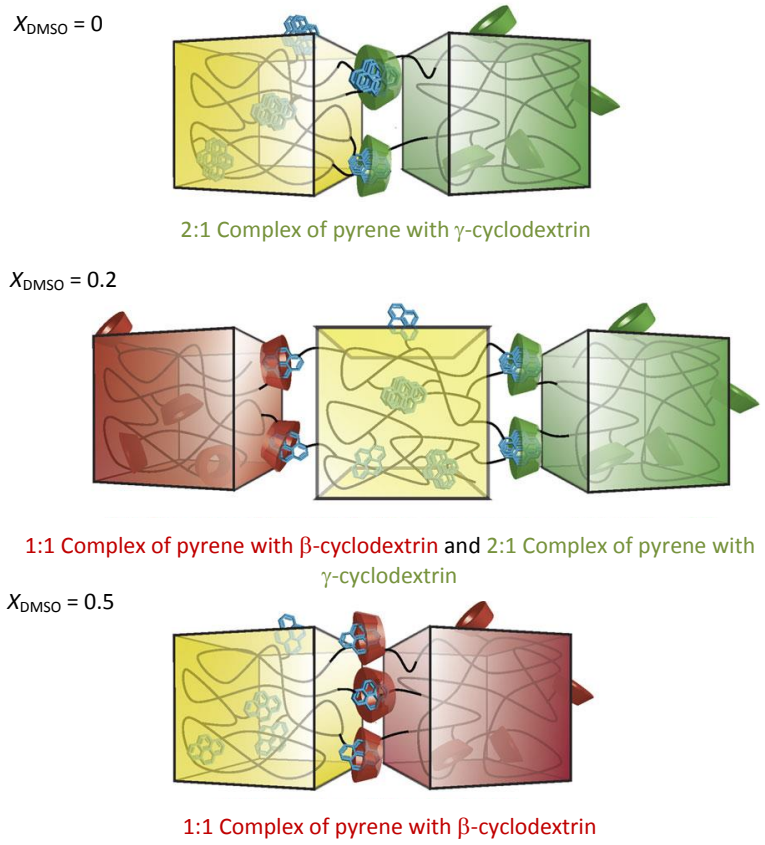

Figure 1.26 Changing solvent alters pyrene oligomerisation, which then dictates the cyclodextrin that binds the guest.[68] Reproduced with permission from Nature Publishing Group.

Switching can also be executed with the addition of a competing guest as observed in the mechanism of the molecular piston **17**. The decompression stroke is performed when 1-adamantol is incorporated in place of the cinnamide guest, and the compression stroke when the alkyl guest is extracted with a non-polar solvent (Figure **1.27**).[69] Work performed by the system, as calculated by the difference in *E/Z* amide ratios, was measured as 2.1 kcal mol^{-1} during compression. Photoisomerisation of the cinnamide alkene switches the machine on and off.

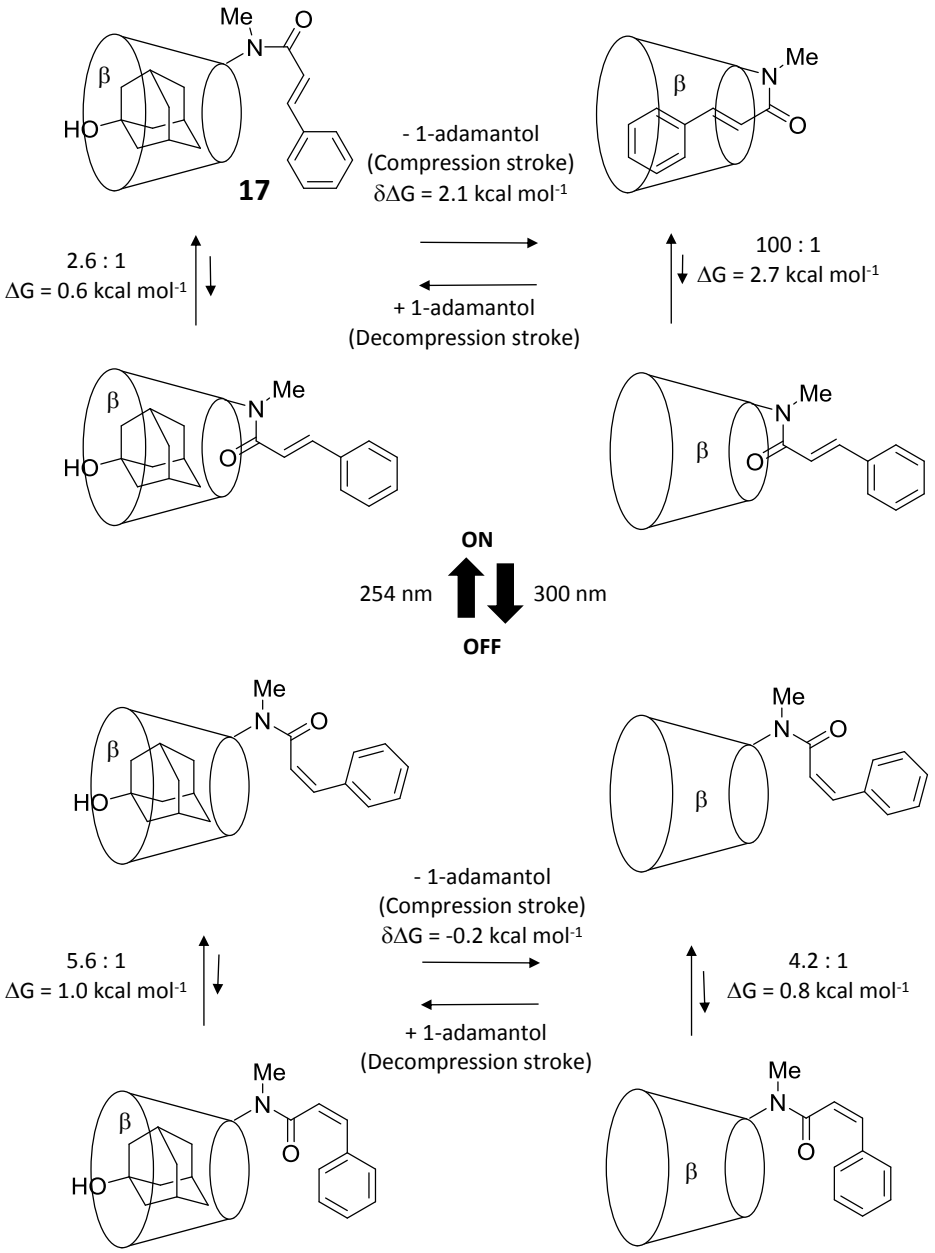

Figure 1.27 A molecular piston wherein the compression stroke is performed by a competing adamantol guest displacing the tethered cinnamide guest.[69]

The external stimulus used for cyclodextrin switching can also be a change in pH. Liu et al.[70] demonstrated that in a pyridine-dicarboxamide-bridged bis-β-cyclodextrin compound, the pyridine group sits outside the cyclodextrin cavities at neutral pH, whereas at acidic pH it is shallowly included into one of the hosts (Figure **1.28**). Inclusion is observed by the appearance of an induced circular dichroism peak when the chromophoric linker sits inside the chiral cyclodextrin cavity. It was also noted that the linking guest was able to partially displace a number of short oligopeptides from cyclodextrin, giving a pH-switchable binding mode.

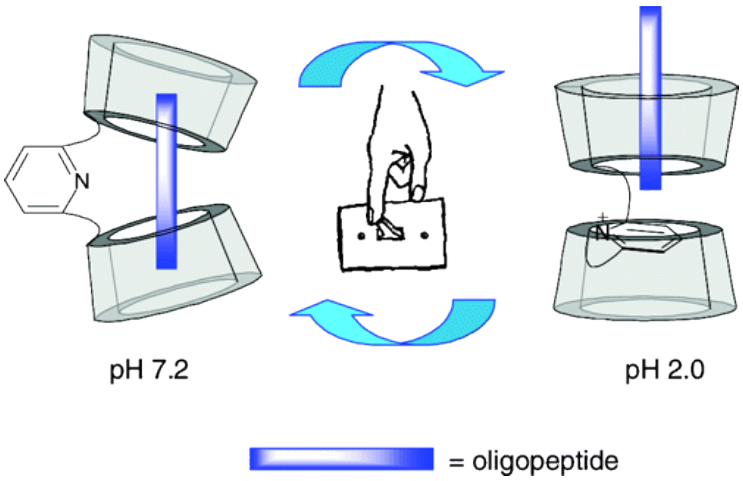

Figure 1.28 Change in binding of the cyclodextrin bridge upon pH change induces a change in the binding mode of oligopeptides.[70] Reproduced with permission from the American Chemical Society.

Switching can be redox-responsive, as shown in the shuttling rotaxane **18** reported by Stoddart et al.[71] The cyclodextrin initially includes the tetrathiafulvalene unit, whereas upon oxidation this becomes positively charged and the triazole unit becomes the most energetically favoured guest, inducing shuttling of the cyclodextrin ring (Figure **1.29**).

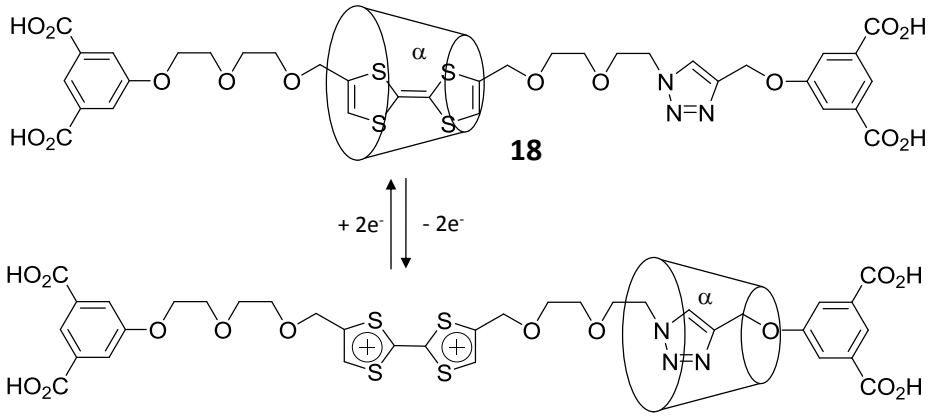

Figure 1.29 Oxidation of the tetrathiafulvane unit shuttles the cyclodextrin from this station to the triazole station.[71]

Finally, probably the most useful stimulus for synthetic molecular switches is light as it is non-invasive, chemo-selective and highly controllable.[72] The ability of a number of cyclodextrin guests to form inclusion complexes can be switched on and off *via* photoisomersation between *trans* and *cis* isomers. In the molecular muscle **19**, stilbene is incorporated into a [*c*2]-cyclodextrin dimer (Figure **1.30**).[73] In the *trans* configuration the α-cyclodextrin ring sits on the stilbene guest station. Upon photoisomerisation to

the *cis* configuration, the stilbene becomes too sterically bulky to sit inside the α-cyclodextrin cavity and the host shuttles to the secondary, propyl guest station resulting in overall contraction.

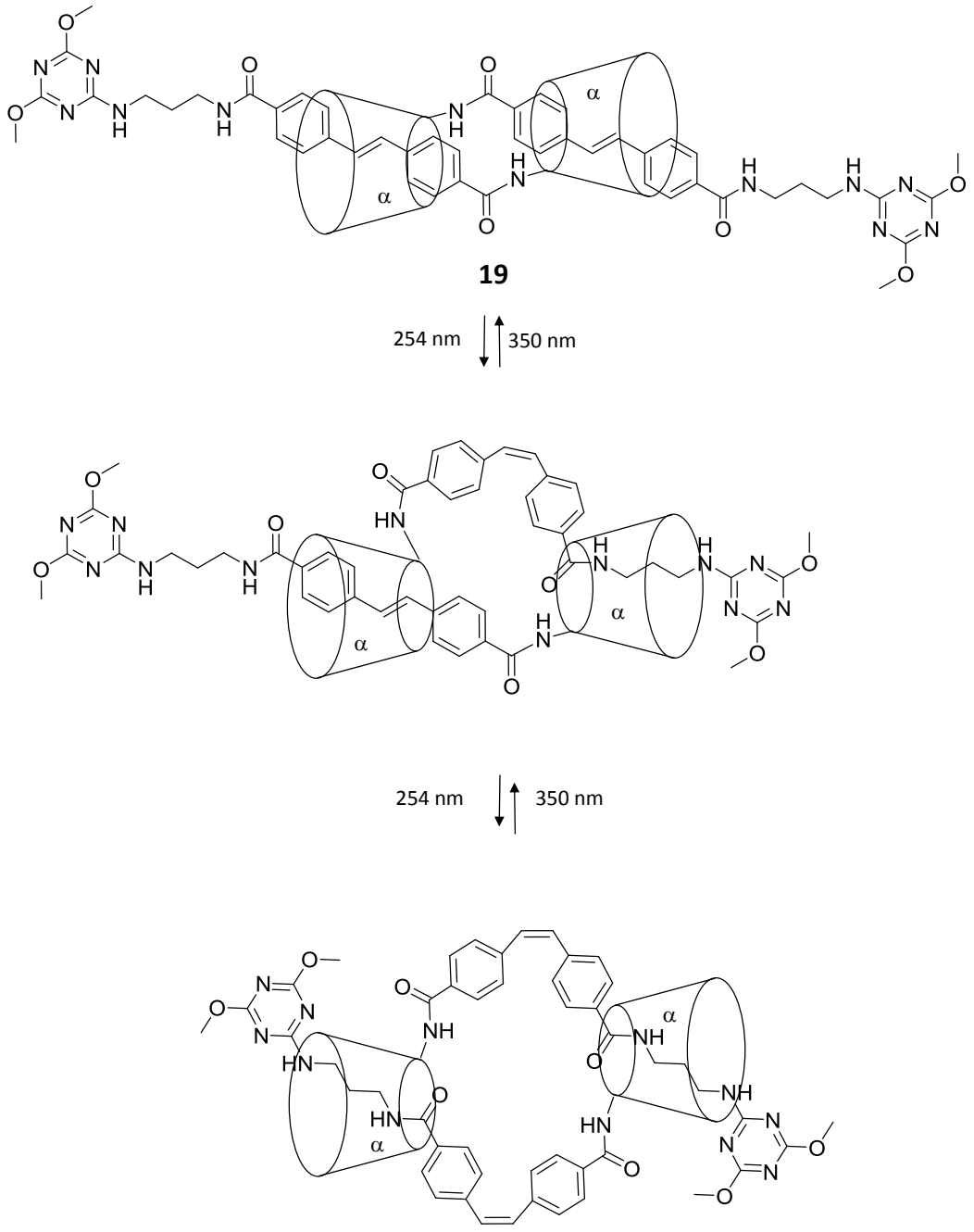

Figure 1.30 Photoisomerisation of stilbene guests shuttle the α-cyclodextrins to secondary propyl guests, resulting in overall contraction of the [*c*2]-dimer **19**.[73]

1.5 Molecular Switches in Nature

Many natural systems feature molecular switches, where an external stimulus produces a change in state or conformation of a protein or peptide. An initial change can then act as the stimulus for a succeeding switching step producing a cascade of switches. If one of the steps involves the activation of an enzyme, the initial stimulus is amplified throughout the signalling cascade.

For example the vision process begins with the photoisomerisation of retinal, the chromophore bound to the opsin protein, from the *cis* to the *trans* state (Figure **1.31**). This is followed by a conformation change of opsin to metarhodopsin II, causing it to split and activate the regulatory protein transducin. A release of GTP occurs, activating phosphodiesterase and amplifying the signal, leading to an increase in cGMP concentration and the closure of sodium channels. This causes hyperpolarisation of the cell and closure of calcium channels which gives nerve signal.[74]

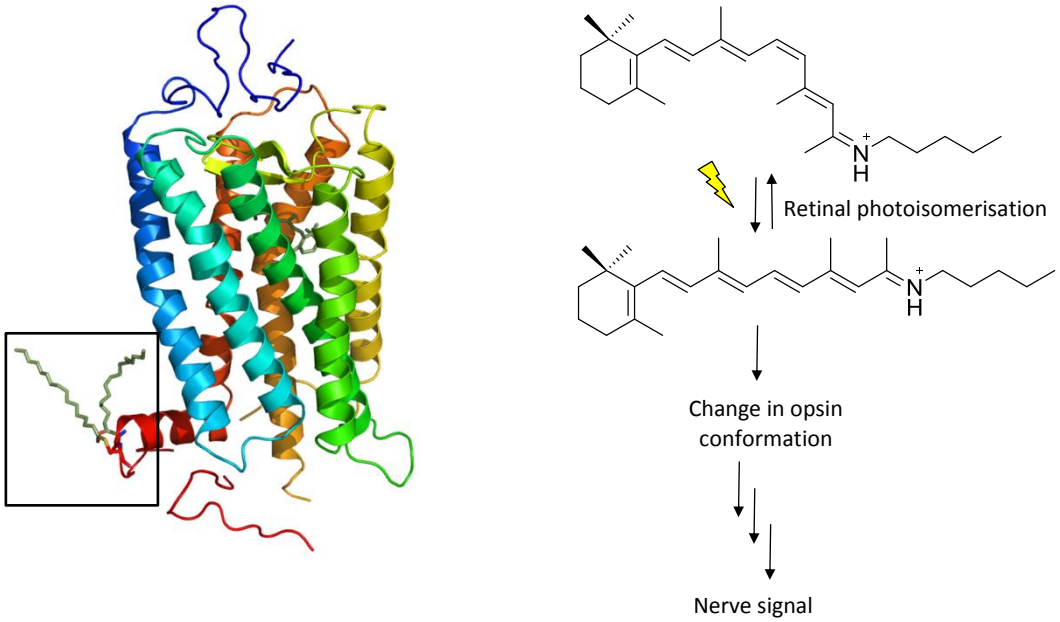

Figure 1.31 The protein opsin with retinal highlighted (*left*)[75] and a simplified mechanism of the vision process (*right*). Reproduced with permission from Elsevier.

A molecular switching process is also a key component of calcium signalling, wherein Ca^{2+} ions bind to the regulatory protein calmodulin. This induces a large change in conformation, exposing hydrophobic domains which then bind to and control other

proteins, such as cadmodulin-dependent protein kinases which are involved in the regulation of fuel metabolism, ionic permeability, and neurotransmitter synthesis and release.

Molecular switches are also a part of molecular devices that drive biochemical systems, such as kinesins and dyneins,[76] myosins[77] and the rotational motor protein ATP synthase, which is made up of a F_0 rotational unit and the F_1 catalytic unit (Figure **1.32**).[78] Rotational movement is driven by a pH gradient between the high $[H^+]$ in the cell cytoplasm and the lower $[H^+]$ in the cell matrix. The α-subunit of the c-ring contains two half-channels that allow contact with two of the c-subunits; in the subunit next to the acidic channel an aspartic acid residue is protonated which results in rotation of the c-ring to position the protonated subunit next to the proton-poor environment of the matrix channel, where the proton is released. Rotational movement of the c-ring is directly transferred to the $\gamma\varepsilon$-stalk of the F_1 unit. As the stalk turns, it induces different conformations in the β-subunits of the catalytic unit leading to different binding capabilities in a so-called binding change mechanism. The 'loose' conformation binds ADP and orthophosphate (HPO_4^{2-}), they then form ATP in the 'tight' conformation and are finally released in the 'open' conformation. Thus, the proton gradient drives rotation which in turn drives switching between these three conformations and hence ATP synthesis and release.

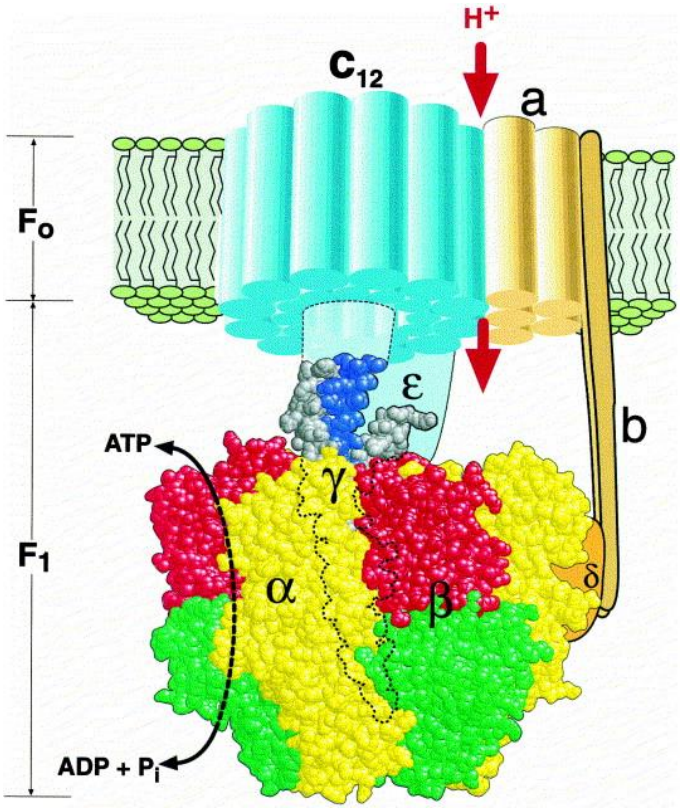

Figure 1.32 The structure of ATP synthase showing the rotatational unit (F_o) and the catalytic unit (F_1).[78] Reproduced with permission from Elsevier.

If we hope to mimic Nature and produce our own synthetic molecular switches that replicate the high-level functions that biological systems demonstrate, or even develop synthetic systems that can interact with natural ones for example to correct disease states, one strategy is to combine non-peptidic, supramolecular systems such as cyclodextrin host-guest inclusions complexes, with peptides.

1.6 Combining Peptidic and Non-Peptidic Supramolecular Entities

Supramolecular chemists have often sought inspiration from Nature for the assembly and operation of nano-sized constructions and devices,[65, 79, 80] as both are governed by the same fundamental principles of equilibrium, Brownian motion, viscosity, and the use of non-covalent, cooperative bonds. It is logical therefore, that natural structures are also borrowed and incorporated into semi-synthetic devices and materials, combining the features of both biological and synthetic supramolecular moieties to generate new functionalities and achieve new applications.

Of the available natural substances, peptides present a particularly attractive building material being supramolecular structures in their own right.[81, 82] The peptide bond provides a stable backbone, secondary structures are well-studied and occur in a variety of different architectures which are easily analysed,[83] and amino acid residues are capable of a wide range of non-covalent interactions such as π-π stacking, hydrogen bonding and metal binding. Solid-phase synthesis methods are highly efficient meaning that chemists are not restricted to natural sequences, rather de novo sequence design is possible and there is no restriction to the palette of naturally encoded amino acids. Peptides exhibit their inherent properties under physiological conditions and many examples are themselves biologically active, therefore they are advantageous for use in systems with biological applications.

New, acquired properties arise through the combination of peptides with other, non-peptidic supramolecular components presenting two strategies to achieve such emergent functionalities. In one approach functionality is conferred by the inherent structure of the peptide (Figure **1.33**), in the other supramolecular function affords control over peptide structure (Figure **1.34**).

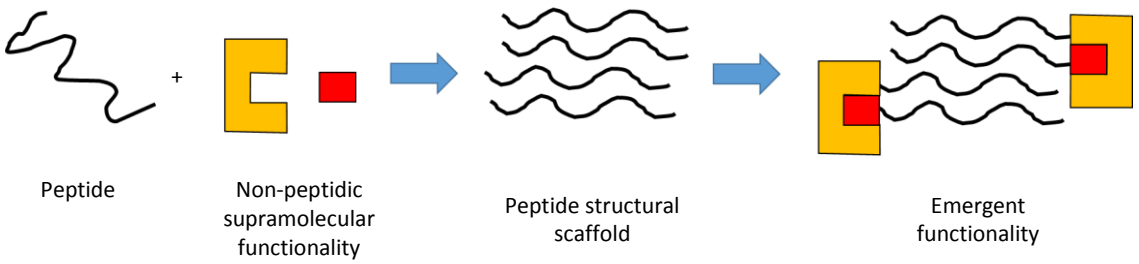

Figure 1.33 Conceptual scheme illustrating an approach to combining peptides with non-peptidic supramolecular components, wherein the inherent structure of a peptide determines function.

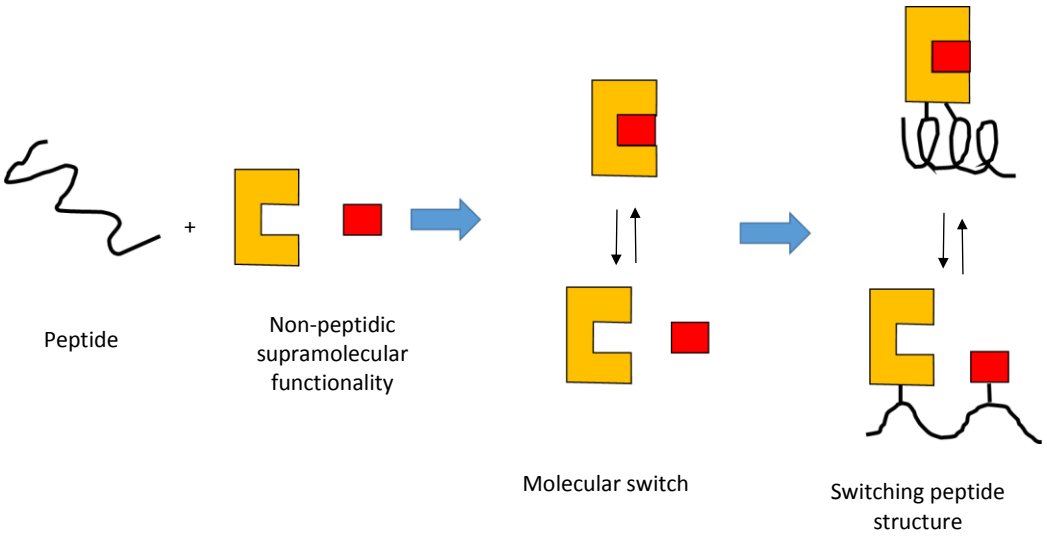

Figure 1.34 Conceptual scheme illustrating an approach to combining peptides with non-peptidic supramolecular components, wherein the property of a non-peptidic supramolecular moiety affects peptide structure.

Peptides are supramolecular moieties in their own right as they fold into three-dimensional structures by way of non-covalent interactions, and some have been designed (or evolved in the case of collagens, for example) to form a variety of nanostructures such as nanotubes,[84] gels,[85] fibres[86] and vesicles[87]. When non-peptidic components are applied to these scaffolds, new supramolecular functionalities emerge. Peptide structure is therefore considered as a tool or building block in synthetic supramolecular systems.

In the simplest type of scaffold, a single peptide strand is used as a structural backbone for supramolecular assembly. Primary amines, such as those present on lysine side-chains form complexes with crown ethers, and accordingly an oligolysine peptide chain was used as a 'molecular track' along which crown ether moieties were shown to undergo direct binding-site hopping (Figure **1.35**).[88]

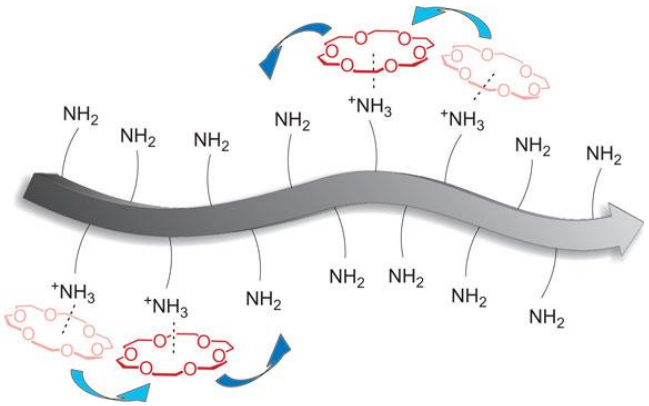

Figure 1.35 A single peptide strand acts as a scaffold for crown ethers to undergo binding site hopping.[88] Reproduced with permission from Nature Publishing Group.

Peptides have also been employed as the axle in a rotaxane, where the capability of the amide backbone to form hydrogen bonds has been used to create stations for amide-based wheels (Figure **1.12**).[32, 89, 90]

A peptide strand has also been used as a template for inorganic materials, as demonstrated by the Stevens group[91] when they used a helical peptide strand on which to grow a gold nanocluster (Figure **1.36**). Cysteine residues provide sites for concentrated nucleation, but it is the cavity of the helix which controls growth and determines the size of the final nanocluster.

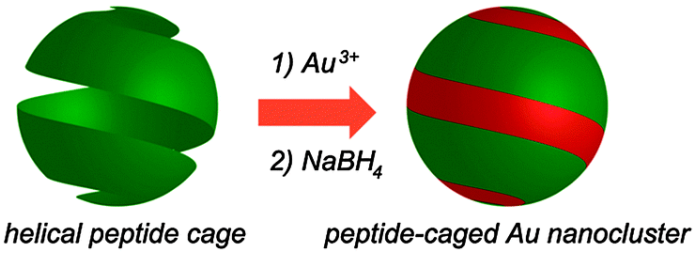

Figure 1.36 A single peptide strand acts as a scaffold for the control of growth of a gold nanocluster.[91] Reproduced with permission from the Royal Society of Chemistry.

Some peptides self-assemble into higher order, nano-scale structures such as fibrils, of which many exhibit interesting mechanical properties, for example gelation. These arrangements are highly ordered at the molecular scale and, if the peptides are functionalised with other moieties, they also adopt the same level of organisation. Placing electronically active residues at pre-determined, regular spacings promotes π-π stacking interactions, leading to electron transfer capabilities. The use of self-assembling

peptides as a scaffold for these types of functionalities has therefore led to the development of peptide-based molecular wires. This was demonstrated by Ghadiri et al.[92] who used a cyclic peptide, decorated with naphthalene diimide functionalities, to form nanotubes with delocalised electron states (Figure **1.37**). The peptides have the added advantage of being electronically insulating. The same principle was later employed by Ashkenasy and Ashkenasy et al.[93] with a similar naphthalene diimide electronically-active functionality, this time incorporated onto a β-sheet fibril-forming peptide. The use of a fibril forming peptide as a scaffold for molecular electronics has also been shown with porphyrin functionalities.[94]

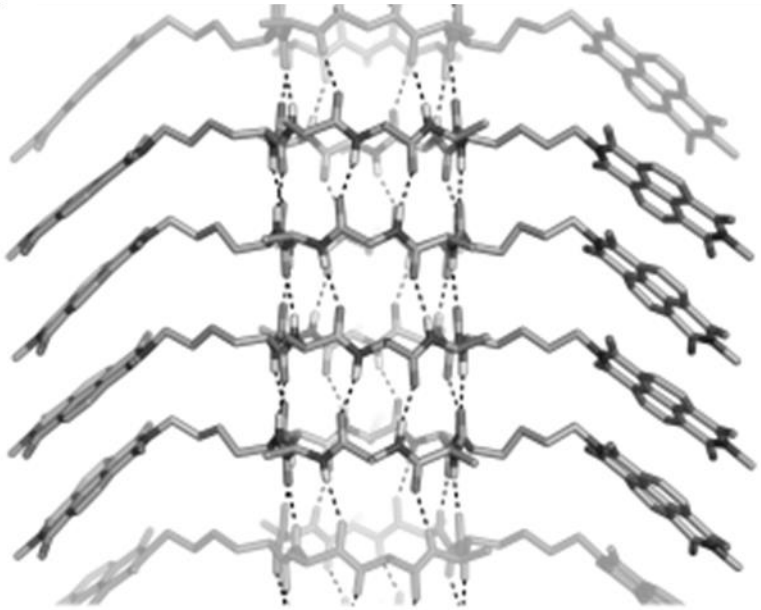

Figure 1.37 A fibril forming peptide is decorated with naphthalene diimide functionalities giving molecular wires.[92] Reproduced with permission from John Wiley and Sons.

Closely related to molecular wires is the field of molecular optics which also requires functionalities to be regularly spaced, a condition fulfilled by decorating peptide nanostructures with chromophores. This strategy also allows distances between chromophores to be adjusted by altering their positioning along the peptide scaffold, enabling optical properties to be modified and optimised in a logical, pre-determinable fashion. Park et al.[95] demonstrated the formation of photoluminescent peptide nanotubes, simply by in situ incorporation of various sensitisers and lanthanide ions with the fibril-forming dipeptide phenylalanyl-phenylalanine, with different combinations producing different luminescent colours. To gain control over the assembly and

therefore properties of such systems, the optically active residues have been covalently bound to the peptide scaffold. MacPhee et al.[96] have shown that fibril forming peptides, modified with fluorophores, demonstrate exciton migration in the resulting structures. As assembly is fully controlled by the peptide, the optically active residue could then be independently altered, introducing both donor and acceptor moieties to give light-harvesting properties, whilst retaining the core self-assembled structure (Figure **1.38**).[97] Energy transfer has also been facilitated by the arrangement of donor/acceptor chromophores within a peptide hydrogel, resulting in an optically active material that also has potentially useful mechanical properties.[98]

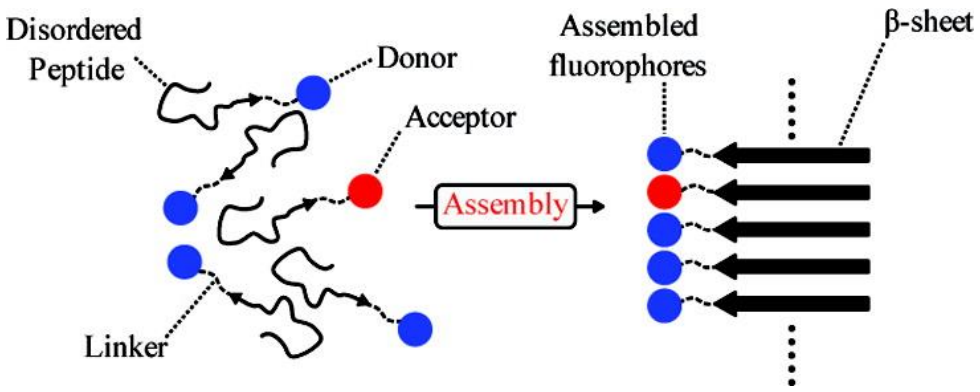

Figure 1.38 A fibril forming peptide is decorated with donor and acceptor fluorophores resulting in a light harvesting system.[96] Reproduced with permission from the American Chemical Society.

Regulation of the aggregation of nanomaterials, and hence control over their properties, has been achieved with the use of switchable peptide-peptide interactions. Amphiphilic, helical peptides have been used to coat carbon nanotubes to not only aid solubilisation but also to control their assembly *via* ionic interactions, enabling oligomerisation of the carbon nanotubes to be modified as a function of solution ionic strength (Figure **1.39**).[99]

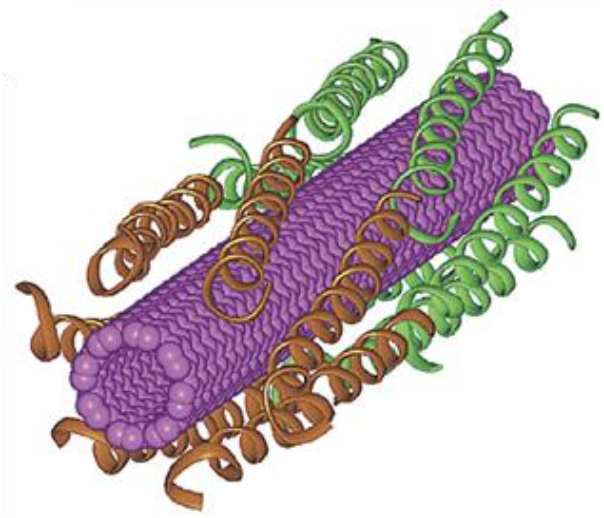

Figure 1.39 Carbon nanotubes are coated with peptides that assemble *via* ionic interactions.[99] Reproduced with permission from the American Chemical Society.

Other nano-technological materials which require control of aggregation are inorganic nanoparticles, and the attachment of a peptide which has pH dependent secondary structure has led to control over the aggregation of gold nanoparticles[100] and gold nanorods (Figure **1.40**).[101] At acidic pH, the polyglutamic acid peptide exists as an α-helix, interacts with other attached peptides and causes aggregation or assembly of the nanoparticles. Upon raising the pH, the peptide switches to a random coil structure, disrupting interactions and dispersing the nanoparticles back into solution.

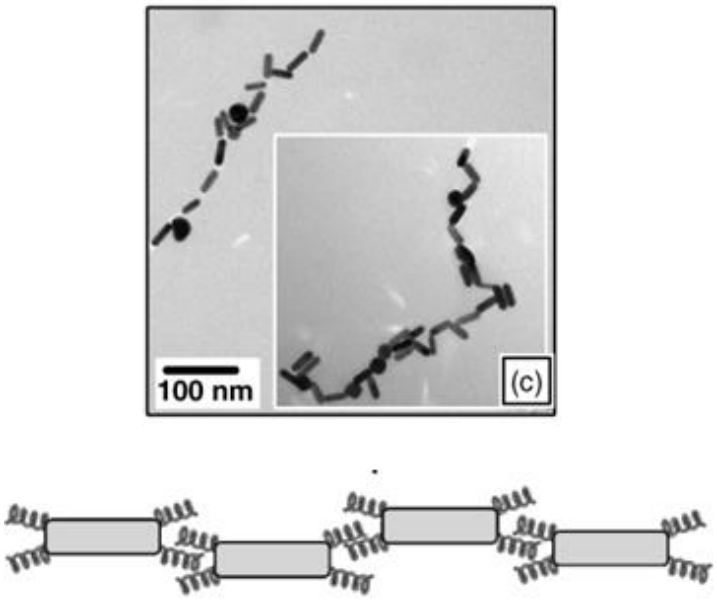

Figure 1.40 Peptide-peptide interactions which are pH-switchable are used to control the aggregation of gold nanorods.[101] Reproduced with permission from IOP Publishing Ltd.

Gold nanoparticles exhibit a colour change when switching between aggregated and dispersed states, a feature that makes them good candidates for use in detectors. Nanoparticles have been functionalised at the cysteine residue of protease cleavable peptide sequences, which leads to aggregation *via* π-π stacking at the Fmoc-protected *N*-termini and gives the nanoparticles a blue colour. The system then acts as a biological sensor in the presence of thermolysin, which cleaves the peptides. The segments containing the aggregating Fmoc functionality are removed and the remaining peptide segments are left with positively charged unprotected $-NH_3^+$ *N*-termini. These charged peptides then repel each other resulting in dispersion of the nanoparticles and a visible colour change (Figure **1.41**).[102] As the control of aggregation and dispersion is wholly dependent on the change in the peptides' *N*-termini from protected Fmoc to charged amines, this concept can be applied to detect any peptidase by simply changing the peptide sequence to a corresponding recognised cleavage site.

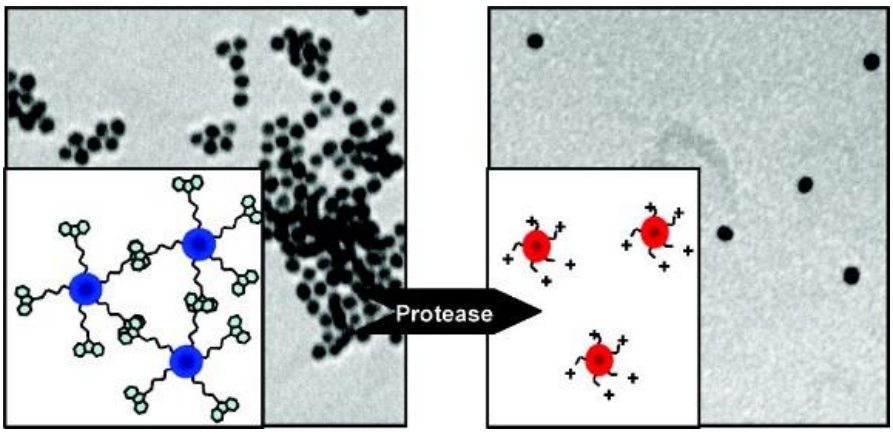

Figure 1.41 *N*-Fmoc protected peptides cause aggregation of nanoparticles, which are dispersed when a protease cleaves the peptide and exposes charged *N*-termini.[102] Reproduced with permission from the American Chemical Society.

Controlling change in peptide structure is an essential part of natural systems such as signaling cascades,[75, 103] or as part of protein assemblies in the performance of overall work.[15] Although these mechanisms consist of many components, they can be broken down into a series of discrete steps that are broadly described as a change in peptide structure in response to a specific stimulus. In order to emulate these biological switches, non-peptidic switching functionalities have been introduced to short peptides that elicit changes in structure thereby producing a 'pared down' synthetic peptide

switch without the need to replicate an entire globular protein structure. In another technique de novo peptides have been designed with careful sequencing that gives inherent structural duality,[104] however this method imposes tight restrictions on the sequence making modifications for functionality difficult. The use of a non-peptidic switch enables structure change that is independent of peptide sequence, allowing for the introduction of functional peptides whose activity can be switched on and off by way of change in their structure. Many examples are also universally applicable, in that the non-peptidic switch functionality can be applied to any peptide sequence.

Molecular switches can modify secondary, tertiary, or quaternary structure, including extended macromolecular structures such as fibrils, some of which have interesting mechanical properties like gelation. If responsive functionalities are introduced, 'smart' materials that in one state disrupt fibril formation and hence material state are produced. As previously mentioned, perhaps most useful are light-responsive switches such as azobenzene, as photo-irradiation is chemo-selective, non-invasive and highly controllable.[72] The incorporation of an azobenzene functionality into a hydrogelating peptide was demonstrated by Lee et al.,[105] giving a substance that is able to be switched between solution and gel-phase *via* photoirradiation (Figure **1.42**). Hydrogels are used as biomaterials to affect cell morphology,[106] therefore enabling switchable hydrogelation allows for the facile external control of cell environment and hence type of cell growth.

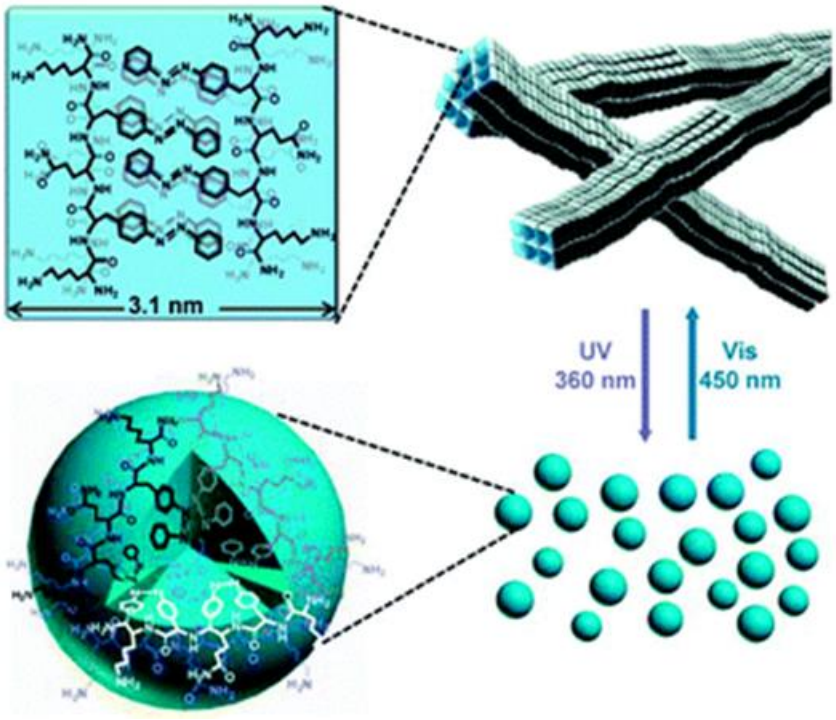

Figure 1.42 Photocontrol of peptide aggregation resulting in switching between gel and solution phases.[107] Reproduced with permission from the Royal Society of Chemistry.

The work of Zhang and co-workers[108] also features azobenzene, this time to link two interacting α-helical peptides which form a variety of nano-structures depending on both *cis*-*trans* configuration and pH (Figure **1.43**). In the *trans* configuration the peptides have a linear arrangement which at acidic pH forms fibres, but at basic pH, with weaker hydrogen bonding and stacking, forms spheres. Upon photo-irradiation to the *cis* azobenzene the peptides are arranged in a horseshoe shape and form spheres at acidic pH and vesicles at basic pH.

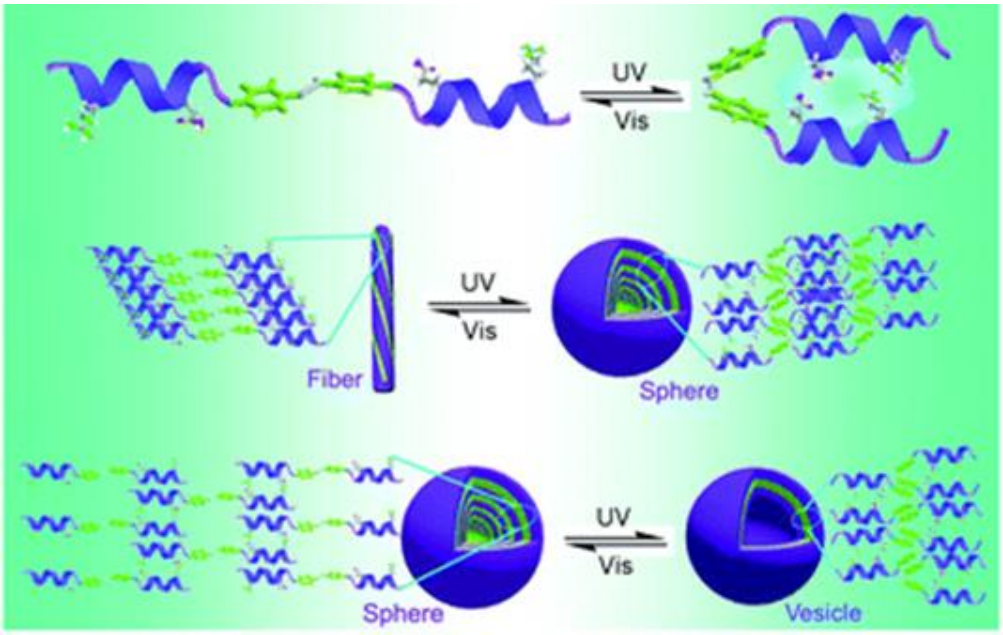

Figure 1.43 Photocontrol of peptide aggregation, resulting in switching between fibres and spheres at basic pH, and spheres and vesicles at acidic pH.[108] Reproduced with permission from the Royal Society of Chemistry.

Molecular switches demonstrate control over quaternary organisation, for example transcriptional activator proteins which only bind to DNA in the dimeric form. In the wild-type peptide dimerization is effected with a leucine-zipper, however Morii et al.[109] demonstrated that this interaction could be replaced with cyclodextrin-adamantane host-guest inclusion (Figure **1.44**). This strategy potentially allows for transcriptional DNA binding to be switched on and off by the disruption of cyclodextrin molecular recognition, for example with the introduction of a competitive guest.

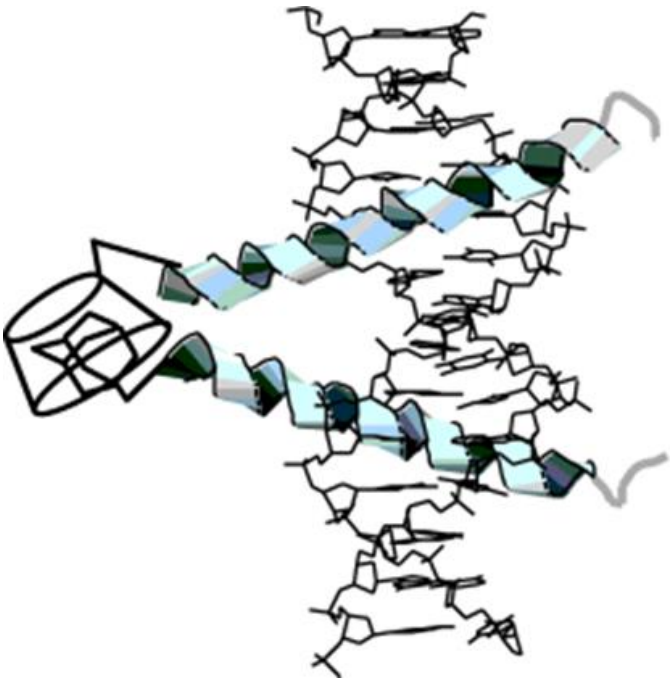

Figure 1.44 Cyclodextrin-adamantane complex formation arranges a transcriptional factor protein into a dimeric form, enabling it to bind to DNA.[110] Reproduced with permission from the American Chemical Society.

Since this first example, similar replacement of the wild-type leucine-zipper for dimer formation has been achieved with other non-peptidic switching functionalities. Peacock et al.[111] attached the two arms of the same transcriptional peptide dimer to a terpyridine moiety (Figure **1.45**). Upon the addition of Cu^{2+} or Zn^{2+}, the metal ions bind to the terpyridine, resulting in a shift from the *trans* conformation to the *cis*. This in turn brings the peptide arms to the same distance as in the dimeric form, enabling binding to DNA.

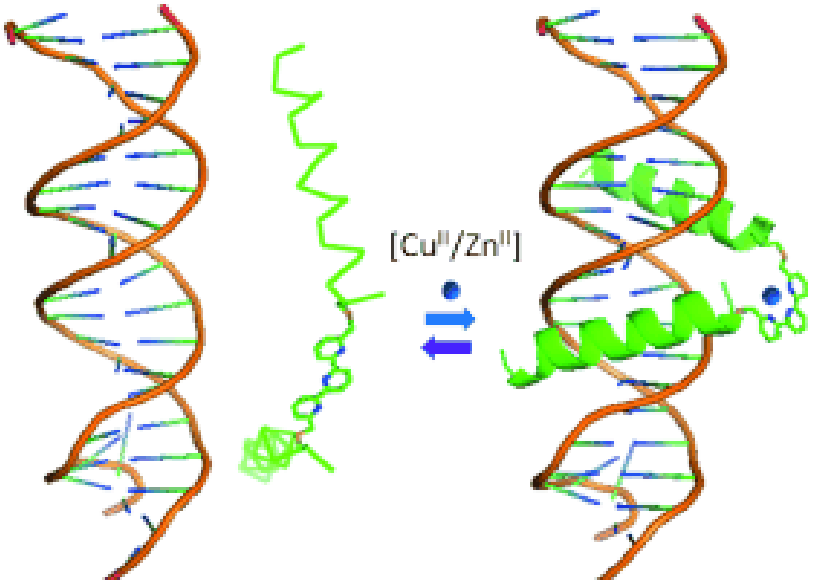

Figure 1.45 Two arms of a transcriptional peptide dimer are arranged into a DNA binding configuration with the use of metal coordination.[111] Reproduced with permission from John Wiley and Sons.

Vazquez, Mascarenas and co-workers[112] also used the formation of a metal complex to assemble the arms of a transcription peptide into an arrangement that resembles dimer formation and hence allows for DNA binding (Figure **1.46**). This ruthenium complex was also photolysed, which resulted in the detachment of one of the peptides from the complex and therefore switched off DNA binding.

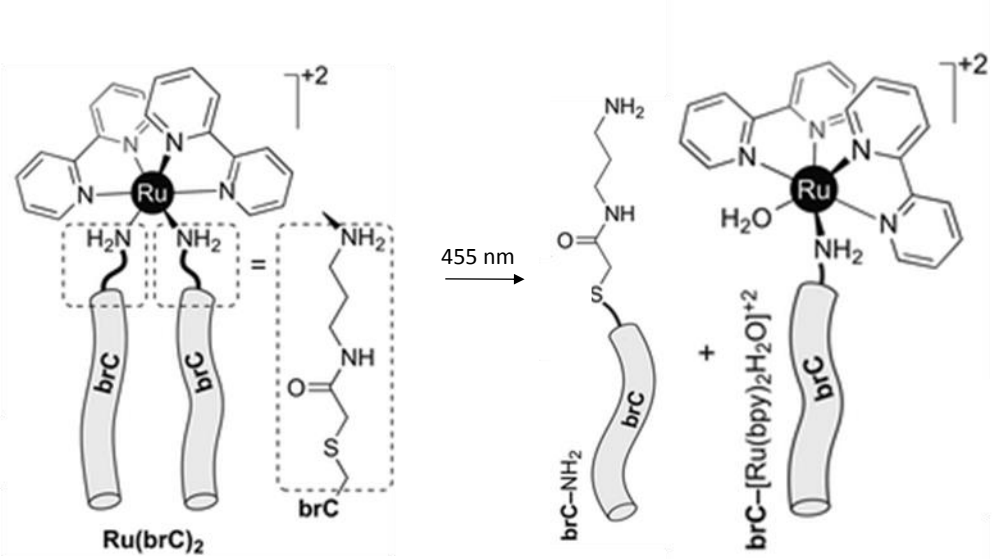

Figure 1.46 Control over the quaternary structure of peptides is afforded with the formation of a metal complex.[112] Reproduced with permission from the Royal Society of Chemistry.

In addition to DNA binding activity quaternary structure switches have also been used to control the activity of capase, cleavage proteins that are active in the dimeric form and non-active in the monomeric form. Brusnveld et al.[113] labelled the *N*-terminus of the capase-9 monomer with phenylalanyl-glycyl-glycine sites which are selectively included in the cavity of cucurbit[8]uril in a 2:1 binding ratio (Figure **1.47**). This host-guest recognition could therefore be used to bring together the two inactive capase monomers to form an active dimer.

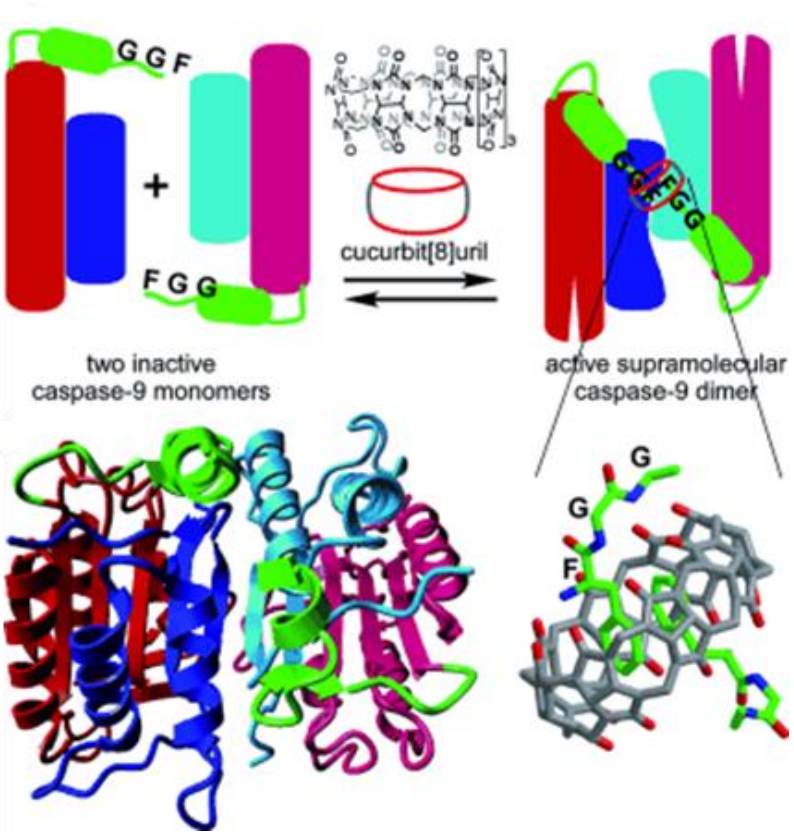

Figure 1.47 Cucurbit[8]uril host-guest interactions are used to control dimerisation of a capase protein.[113] Reproduced with permission from John Wiley and Sons.

The use of host-guest interactions to mediate oligomerisation has also been applied to protein p53, a transcription factor which exists as a homotetramer. In some cancers however, p53 is mutated causing a destabilisation of quaternary folding and favouring the monomeric form. Mendoza et al.[114] used modified calix[4]arene which sits inside hydrophobic clefts in the mutated peptide, to hold together monomers *via* ion-pair interactions between positively charged guanidiniomethyl groups on the calixarene ring and negatively charged peptide arginines, restoring wild-type tetramer structure (Figure **1.48**).

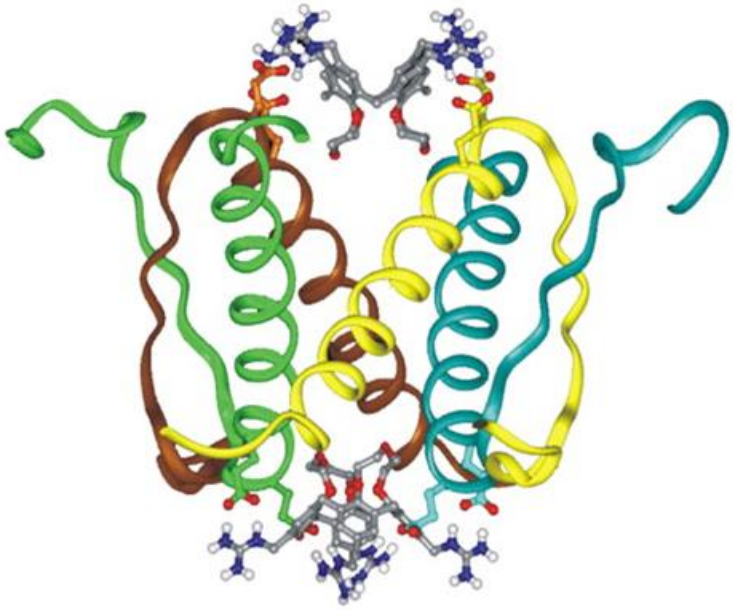

Figure 1.48 Calix[4]arene host-guest interactions stabilize the quaternary structure of a mutated p53 protein.[114] Reproduced with permission from the National Academy of Sciences.

The tertiary folding of peptides is controllable using host-guest chemistry. Urbach et al.[115] made use of the specific recognition of cucurbit[8]uril for methyl viologen and tryptophan pairs in order to create a tryptophan sequence recognition receptor (Figure **1.49**). Peptides modified with methyl viologen residues could be matched to their tryptophan counterparts with the same spacing between amino-acids when cucurbit[8]uril included both moieties, linking the strands. Although the work has focussed on the binding properties of the system, it is easy to see how this could also be applied to selectively unfold the tertiary structure of tryptophan containing peptides, by the use of corresponding methyl viologen modified peptides. Another example of host-guest-mediated tertiary peptide unfolding, is the use of cucurbit[8]uril to reversibly denature ubiquitin as the host binds to a lysine residue guest.[116] The refolded protein could then be recovered with the addition of a competing guest for the cucurbit[8]uril cavity.

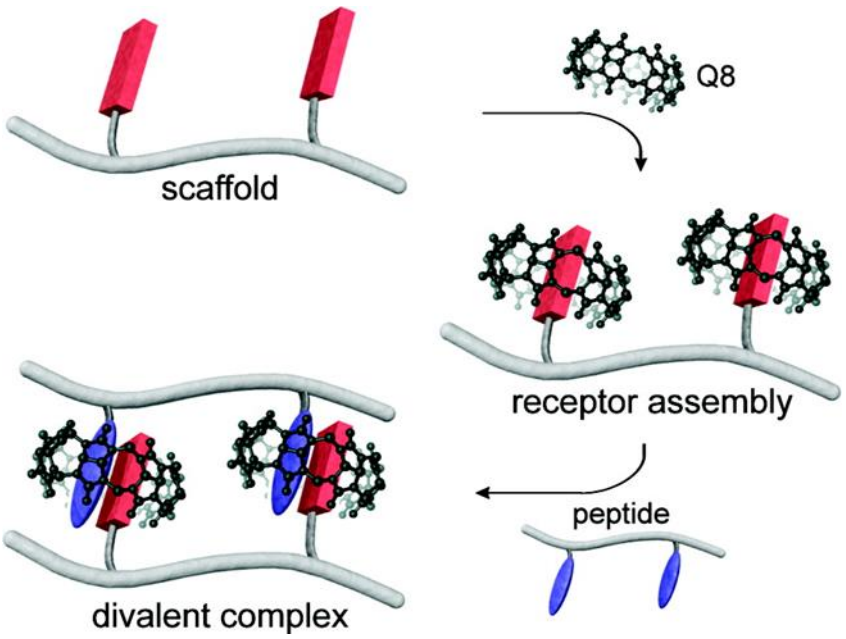

Figure 1.49 Control over the tertiary structure of peptides is demonstrated with systems that use cucurbit[8]uril and methyl viologen-tryptophan interactions.[115] Reproduced with permission from the American Chemical Society.

In another strategy, the activity of green fluorescent protein is controlled by the introduction of a cyclodextrin-coumarin host-guest pair to either terminus of a short peptide section that has been detached from the complete structure (Figure **1.50**).[117] The formation of an inclusion complex forces the tertiary structure of this peptide into a misfolded conformation preventing it from associating with the bulk protein. Upon addition of a competing guest molecule the cyclodextrin-coumarin host-guest interaction is disrupted allowing the peptide to refold back within the protein, restoring fluorescent activity.

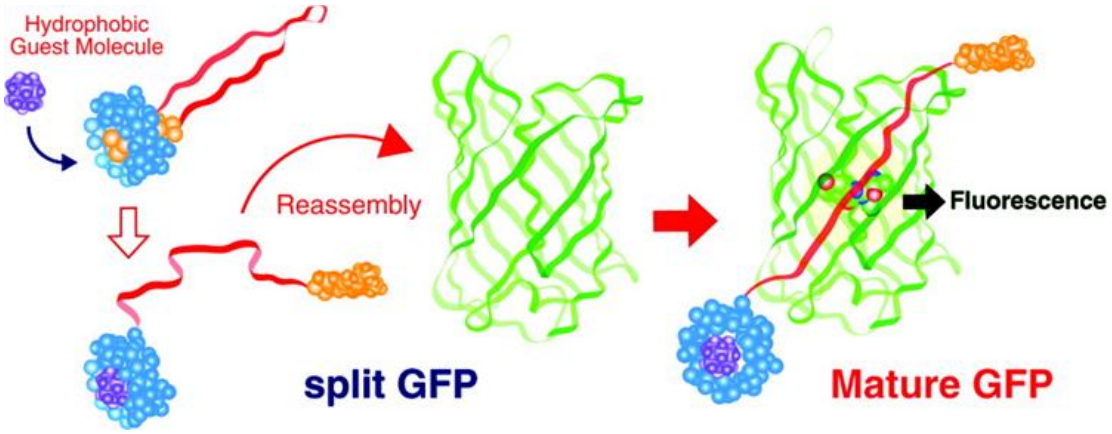

Figure 1.50 The short peptide section of split GFP is modified with cyclodextrin-coumarin groups, enabling control of this host-guest interaction to influence refolding within the mature protein.[117] Reproduced with permission from the American Chemical Society.

The most precise control of peptide structure involves the ordering and disordering of specific secondary structure, such as α-helices, β-sheets and 3_{10} polyproline type II (PPII) helices. Switching between secondary structure states has been demonstrated with the incorporation of photo-isomerisable units into peptide structures as part of the backbone, or as single or bridging amino-acid side-chains (Figure **1.51**).[118] The conformation change of the photoresponsive moiety from *trans* to *cis* initiates a change in peptide secondary structure which translates to enhancement of an existing structure, the disruption of an existing structure or the switch from one distinct type of structure to another.

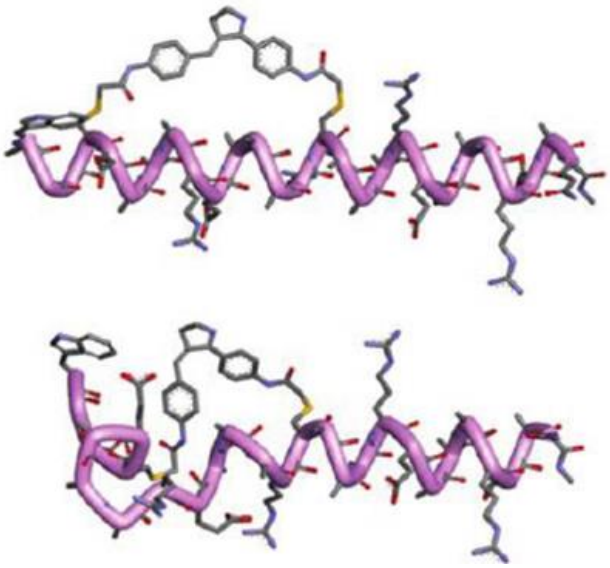

Figure 1.51 A photoresponsive bridging moiety disrupts the secondary structure of a peptide backbone upon photoisomerisation.[119] Reproduced with permission from the American Chemical Society.

As with stilbene compounds previously mentioned, photo-isomerisation of azobenzene switches its ability to form a host-guest interaction with cyclodextrin, with the *trans* conformation forming an inclusion complex and the *cis* conformation unable to. Ueno et al.[120] incorporated this molecular switching process into an α-helical peptide by modification of a glutamic acid residue with a cyclodextrin, and a lysine residue with azobenzene (Figure **1.52**). They found that when the inclusion complex formed the α-helix was stabilised, but upon photo-irradiation to the non-complexing *cis* azobenzene conformation the peptide secondary structure returned to that observed in the wild-type.

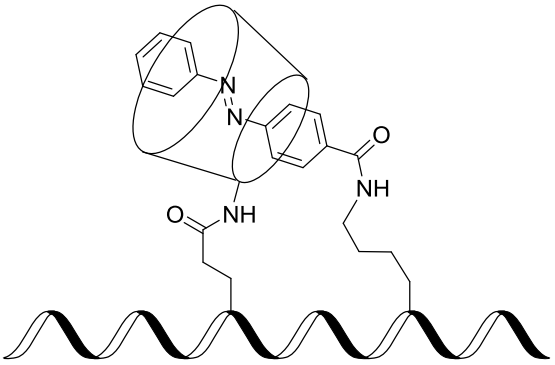

Figure 1.52 The extent of α-helicity in a peptide backbone is increased with azobenzene-cyclodextrin host-guest inclusion.[120]

Other methods that use host-guest interactions to induce a change in peptide secondary structure include the work of Fujita and co-workers[121] who used a palladium-porphyrin host to entirely encapsulate a trialanine peptide, resulting into its folding into a β-turn structure (Figure **1.53**).

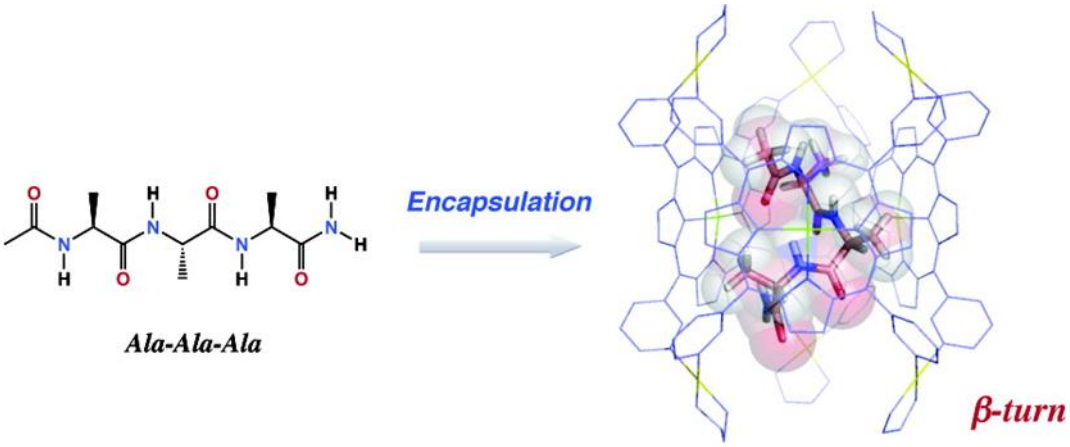

Figure 1.53 Trialanine forms a β-turn when encapsulated in a palladium-porphyrin host.[121] Reproduced with permission from the American Chemical Society.

Coutrot et al.[122] also used switchable inclusion complex formation this time with the preparation of a self-included 'lasso' type crown ether monomer, featuring two pH dependent guest stations and a triglycine peptide linker (Figure **1.54**). In acidic conditions the crown ether sits on the furthest guest station from the host giving a looser lasso and a more flexible triglycine structure, whereas in basic conditions the crown ether sits on the closer guest station giving a tightened lasso and a more constrained, bent peptide structure.

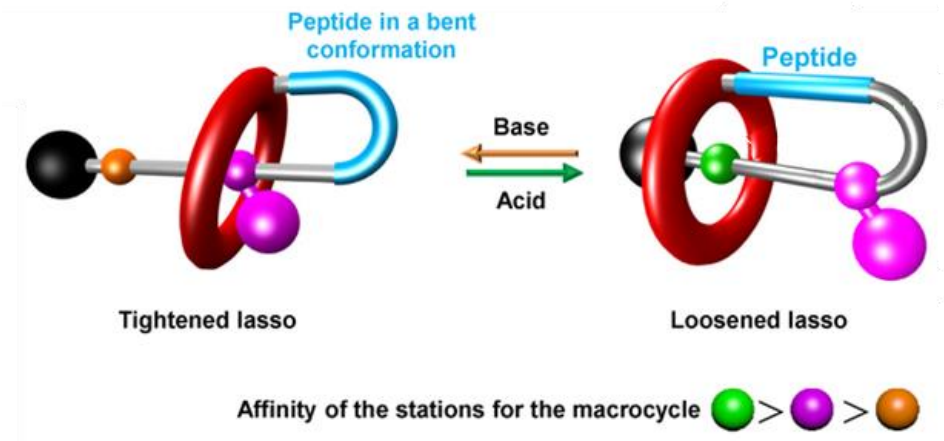

Figure 1.54 Control over peptide secondary structure is provided by pH switching of a crown ether host-guest interaction.[122] Reproduced with permission from the Multidisciplinary Digital Publishing Institute.

Cyclodextrins are an attractive input for switches that affect peptide structure as they operate under aqueous conditions and are bio-orthognal. This enables the non-peptidic supramolecular system to be developed separately to the peptide, allowing widespread application of a device to influence multiple peptidic sequences.

1.7 Self-Assembling Polymers and Daisy Chains

Among the wide variety of possible structures, the self-assembly process has been used to make polymers which consist of many small molecules (termed 'low molecular weight building blocks') held together by non-covalent intermolecular bonds. As with smaller oligomer supramolecular structures, many different types of non-covalent bonds can be used to self-assemble polymers such as metal-ligand bonds,[123] hydrogen bonding,[124] π-π stacking[125] and protein-protein interactions.[126] The polymers themselves have been shown to exhibit properties such as switchability and conductance, and physical features such as gelation.[127] Polymerisation can also be controlled by doping in a competing molecule that terminates the polymer chain.[128] If the bond controlling polymerisation is switchable, changes on the molecular scale have the potential to be translated into an effect on the macro scale by the cumulative effect of many interactions.[129]

Self-assembled polymers can also be constructed from the formation of inclusion complexes, giving special types of polymers including polyrotaxanes,[130] polycatenanes[131] and daisy chains. For example, a di-alkyl bromide functionalised

pillar[5]arene has been used to form an interlocked [*c*2]-dimer with one of these functionalities acting as a guest leaving the other as as an unbound recognition site (Figure **1.55**).[132] The [*c*2]-daisy chains are then linked using a bis-pillar[5]arene compound to give a self-assembled polymer chain **20**.

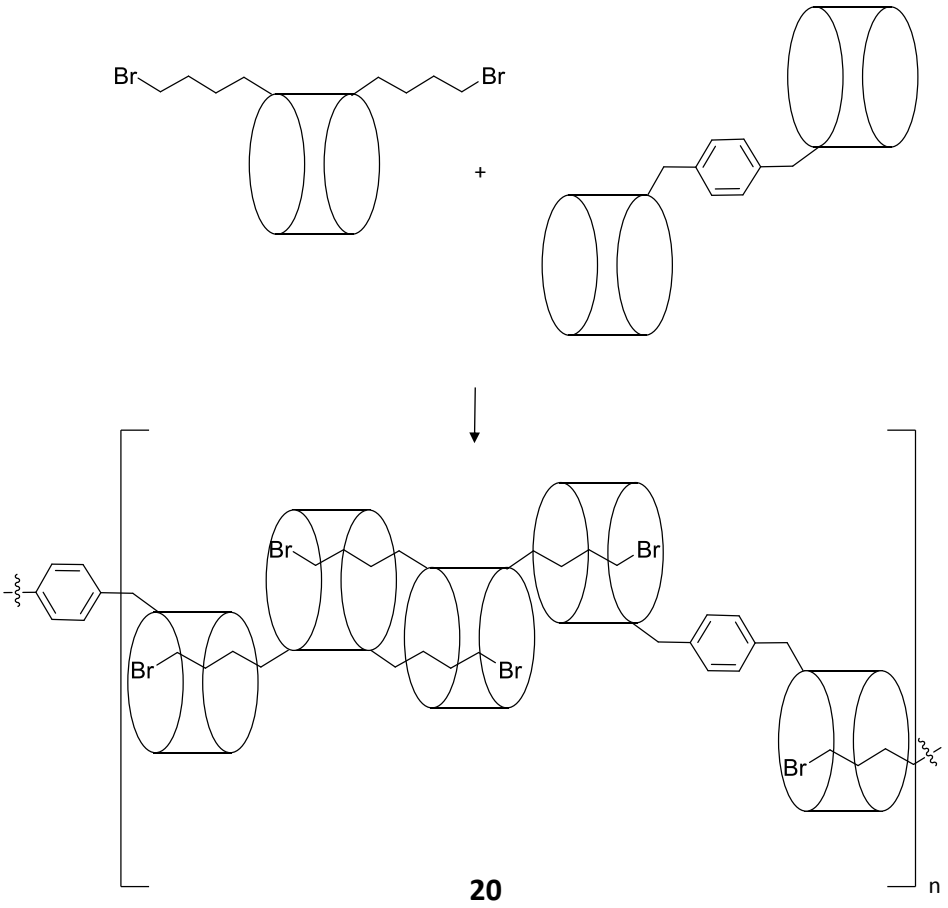

20

Figure 1.55 A pillar[5]arene based polymer composed of a di-guest and di-host unit.[132]

Once the low molecular weight building blocks have assembled into polymeric structures, they can then be mechanically locked with the use of a stoppering moiety which prevents disassembly, usually by steric bulk (Figure **1.56**). This enables the polymeric mixtures to be separated and characterised.

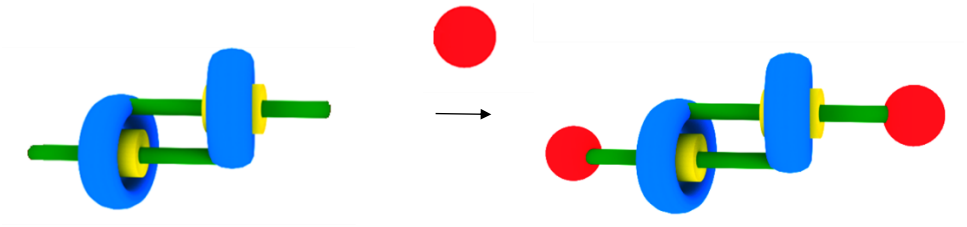

Figure 1.56 Conceptual image of a [*c*2]-daisy chain mechanically locked by a stopper (*red*) which prevents dissociation of the interlocked product by steric hinderance.

Daisy chain polymers are so-called because the construction emulates that of the traditional flower craft; the stem is the axle, the hole in the stem is the ring and the stopper is the flower (Figure **1.57**). Nomenclature gives *a* or *c* for acyclic or cyclic systems, and *n* as the number of bound monomers (Figure **1.58**).

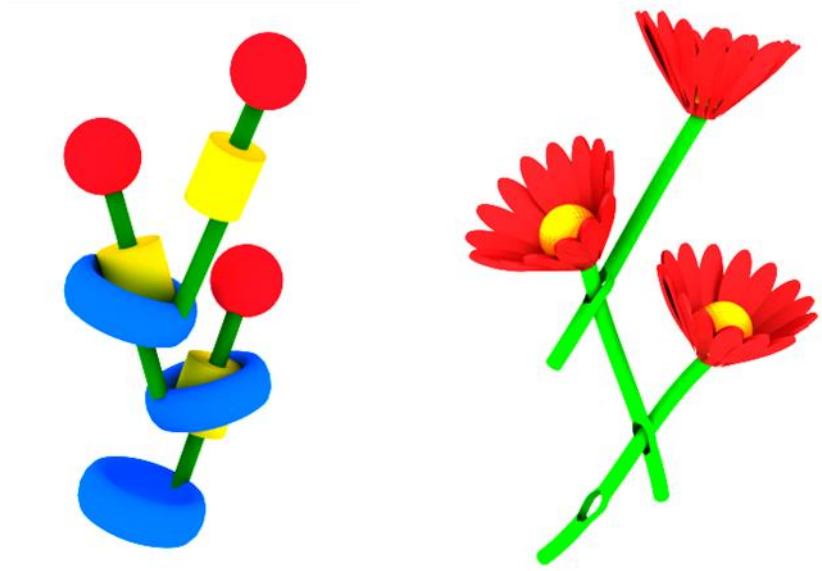

Figure 1.57 Structure of a molecular daisy chain (*left*) constructed from host rings (*blue*), linkers (*green*), guests (*yellow*) and stoppers (*red*), and its comparison with the structure of a traditional daisy chain (*right*).

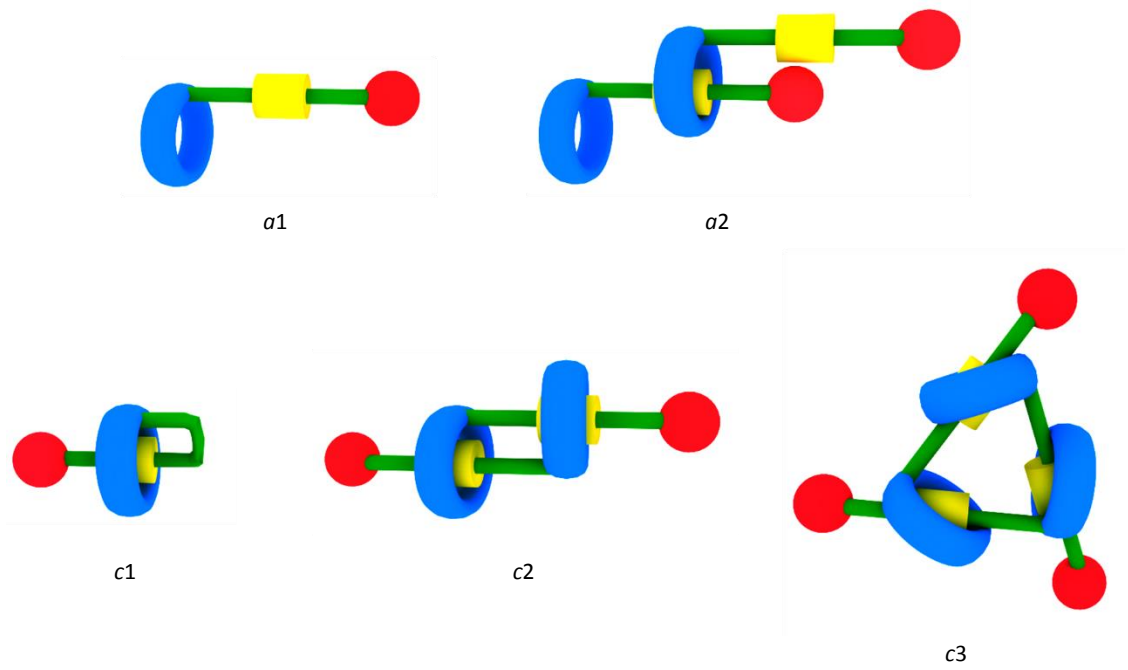

Figure 1.58 Configurations of various stoppered daisy chains.

Daisy chains with more than two components are difficult to synthesize in one-pot reactions however, because the loss of entropy as the polymer increases outweighs the enthalpy gain that comes from forming the ring/axle inclusion complex. Moreover, even if the daisy chain is created, it can be very difficult to analyse and may exist as a mixture of different sized polymers. The ratio of daisy chain polymer to monomeric and dimeric species within the mixture may also be very small.

Only a handful of cyclodextrin based daisy chain polymers have been reported including the formation of a [*c*5]-daisy chain from the azobenzene-napthalene methylated α-cyclodextrin monomer **21**,[133] a polymer assembled from nitrophenyl-β-cyclodextrin **22**[134] and a range of oligomers and cyclic trimers formed from the cinnamoyl-based cyclodextrin compounds **23**-**26** (Figure **1.59**).[135-137]

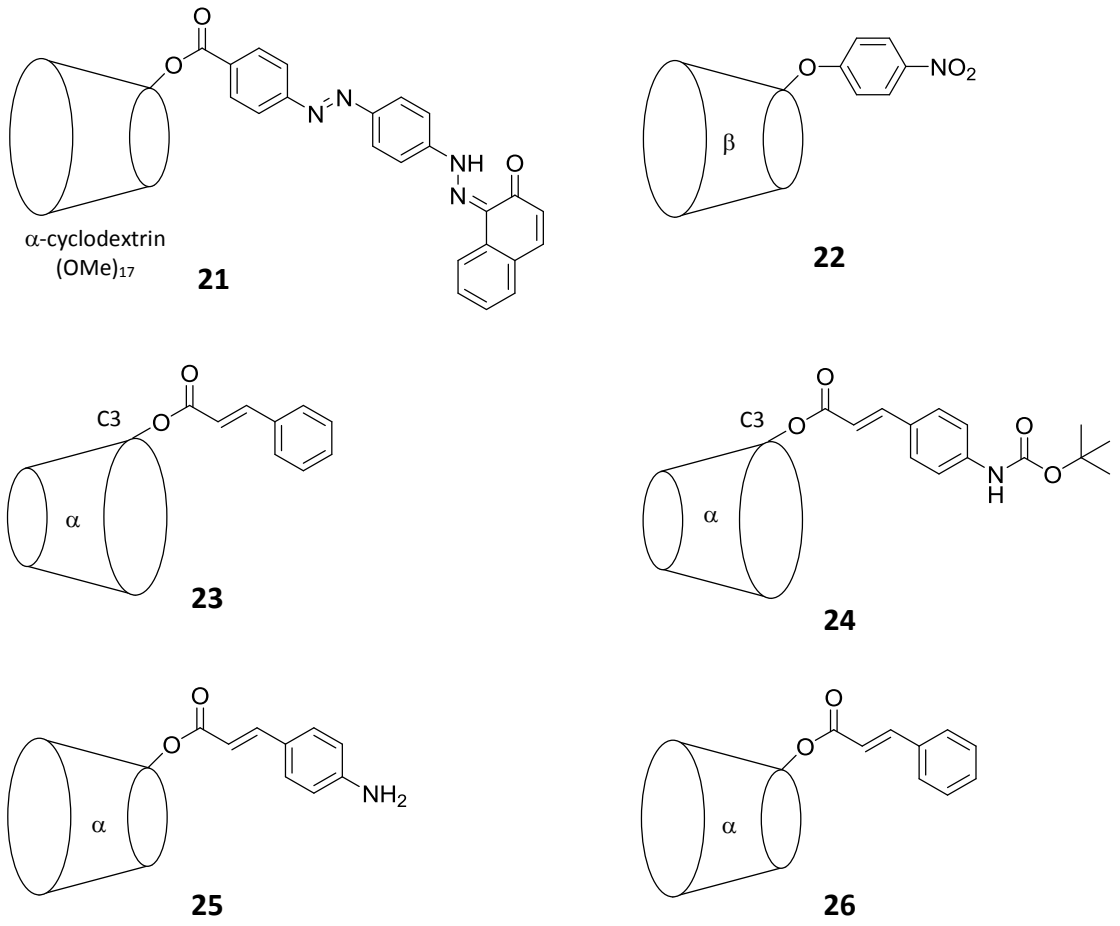

Figure 1.59 Cyclodextrin compounds from which daisy chain polymers have been reported.[133-137]

Work by the Harada group highlights the difficulty in obtaining cyclodextrin daisy chains larger than the [*c*2]-dimer, and the fact that small differences in structure yield very different oligomerisation behaviour. For example, functionalisation of α-cyclodextrin with a cinnamoyl moiety at the C6 position **26** gives a cyclic trimer,[137] whereas modification with the same group at the C3 position **23** yields a polymer,[136] and at the C2 position a dimer.[135] Changing the guest group to a hydrocinnamoyl group, with an alkyl chain in place of the alkene led to only weakly complexing, intramolecular [*c*1]-monomers.

Liu et al.[138] also found that the spatial arrangement of the guest in relation to the cyclodextrin is vital to daisy chain formation, with their triazine-azobenzene β-cyclodextrin compounds. A hydrothermal reaction to link the guest to the cyclodextrin results in a 1,5-orientated guest **28** giving a [*c*2]-daisy chain. Using a copper catalyst

however, gives a 1,4-orientated guest **27** which results in a polymer structure (Figure **1.60**).

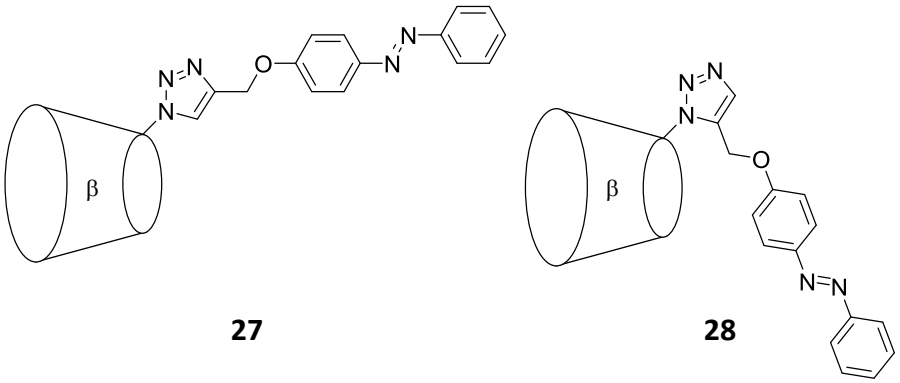

Figure 1.60 The 1,4-substitued triazine guest gives a polymeric structure whereas the 1,5-substituted triazine guest gives a dimer.[138]

Self-assembling polymers have also be made with the combination of two types of non-covalent bond, for example when a daisy chain structure formed by host-guest interactions then itself self-assembles into a polymeric structure. Giuseppone et al.[139] demonstrated this with the formation of a crown ether based [*c*2]-dimer which was then functionalised using click chemistry to attach terpyridine stopper groups. With the addition of Zn^{2+} or Fe^{2+}, the [*c*2]-daisy chains were then linked *via* the formation of octahedral metal complexes to give the polymer **29** assembled by both crown ether host-guest interactions and metal binding (Figure **1.61**). Furthermore, pH-controlled expansions and contractions of the individual daisy chains could be observed as mesoscale changes in the length of the polymer. A similar approach was used by Huang et al.[140] when they formed a [*c*2]-daisy chain with a pillar[5]arene modified with an alkyl chain. This interlocked [*c*2]-architecture was then itself assembled into a polymeric structure **30** with the addition of a terpyridine capping group which formed a complex with added Fe^{2+}.

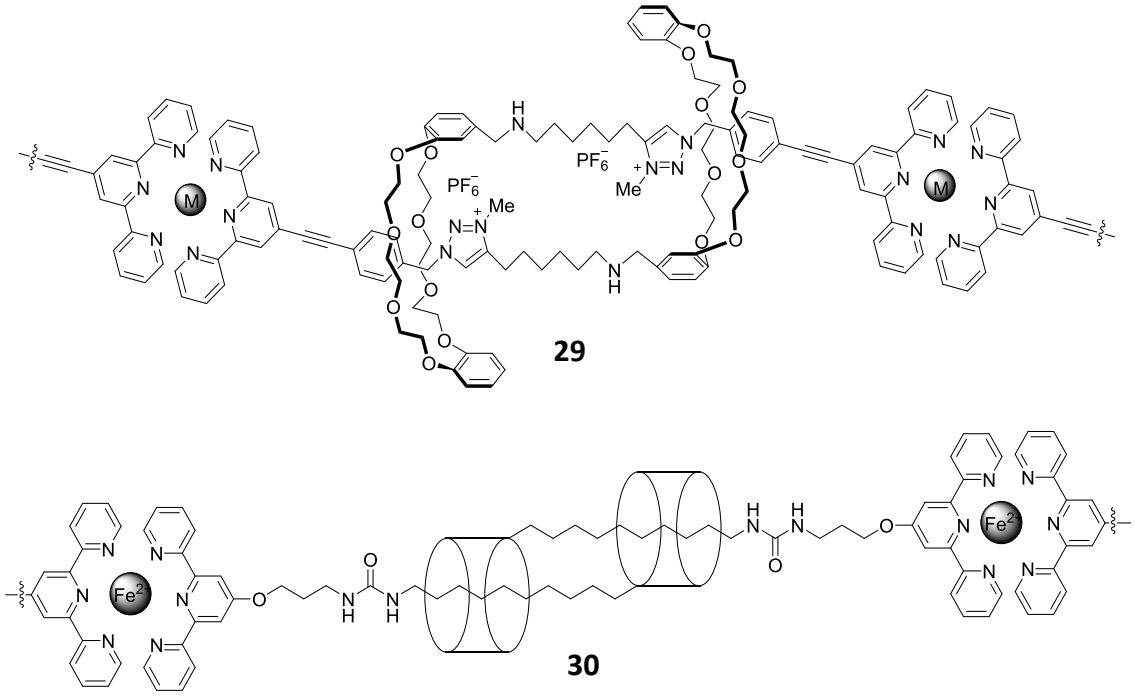

Figure 1.61 [*c*2]-Dimer daisy chains polymerised *via* metal-chelating ligands.[139, 140]

1.8 Aims of the Project

The aim of this project was to design and synthesise molecular devices and assemblies based on cyclodextrin host-guest chemistry and/or short peptide structures.

The first type of device investigated in the work described in Chapter 2 was a molecular lariat, constructed from a cyclodextrin host-guest cyclic, two-membered [*c*2]-daisy chain. [*c*2]-Daisy chains are common motifs in molecular devices[141-143] as they enable the harnessing of linear movement. The [*c*2]-architecture has been employed in the construction of molecular muscles in order to produce contraction and expansion[144] in response to a variety of external stimuli such as the incorporation of a transition metal,[145] pH change[146] and photo-irradiation.[73]

As mentioned in previous examples, light is an attractive external control for molecular machines as it is non-invasive, reliable, easily reversible and reacts selectively.[119] Previous work in the group[147] describes the preparation of a symmetrical [*c*2]-azobenzene molecular muscle **31** in which contraction and expansion is achieved *via* photo-irradiation (Figure **1.62**). In the extended state, α-cyclodextrin preferentially

includes the *trans*-azobenzene moiety. Upon photo-irradiation, the azobenzene isomerises to the *cis* configuration which can no longer form a complex and α-cyclodextrin shuttles to the secondary complexation site, the propyl moiety, affording the contracted state.

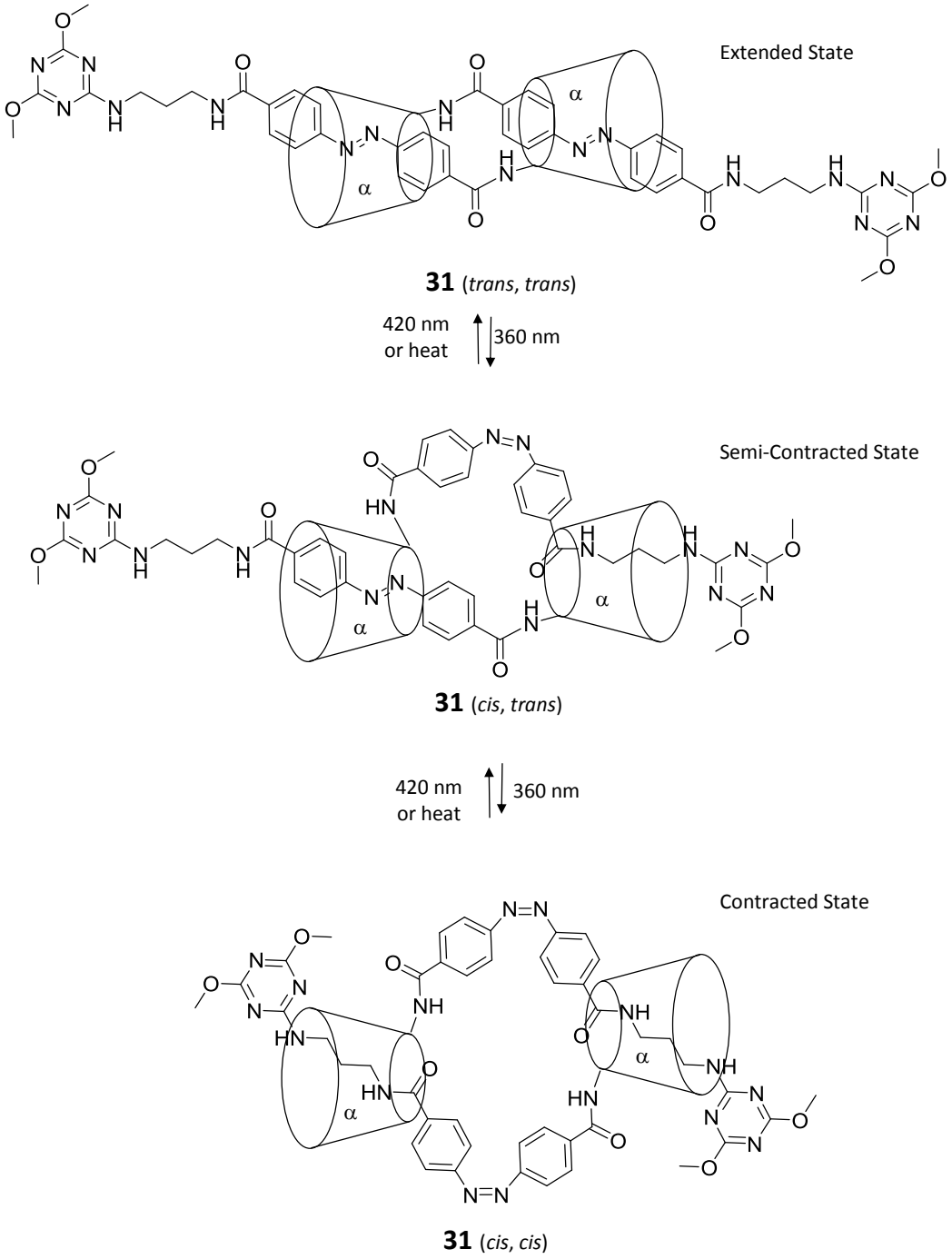

Figure 1.62 Contraction and expansion of the symmetrical azobenzene molecular muscle **31** by Easton *et al.*[73]

The presence of two photo-switchable 'arms' gives rise to three switchable stages; fully extended, semi-contracted and fully contracted. In order to achieve the transition

between the extended and contracted states, two photo-chemical events must occur thereby limiting the efficiency of the molecular machine. An asymmetric molecular muscle **32** with only one photo-switchable arm was therefore prepared by the group (Figure **1.63**),[147] giving a more efficient device as it only requires one event to interconvert between contracted and expanded forms.

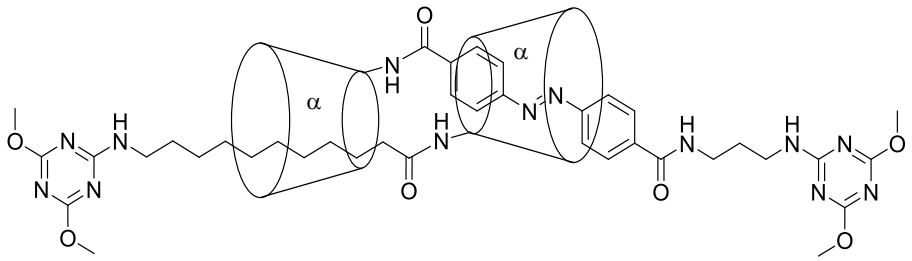

32 (*trans*)

Figure 1.63 Asymmetric molecular muscle **32** synthesised by Easton *et al*.[147]

The asymmetric device **32** is more photo-chemically efficient than molecular muscles comprising two photo-switchable moieties, and establishes a method for the preparation of asymmetric daisy chains. In Chapter 2 it was investigated as to whether a shorter alkyl chain could be used in a similar asymmetric [*c*2]-daisy chain construction, and if it could act as a hinge to give a device that worked as a molecular lariat.

In the investigations described in Chapter 3, daisy chain motifs were also studied, incorporating short peptide sequences to explore the effect of cyclodextrin host-guest complexation on their secondary structures. The devices were left mechanically unlocked, allowing for a variety of assemblies, such as [*a*1]- [*c*1]- and [*c*2]-daisy chains to form under equilbrium. Incorporation of a switchable guest was also investigated, which would switch inclusion on and off by an external stimulus (Figure **1.64**).

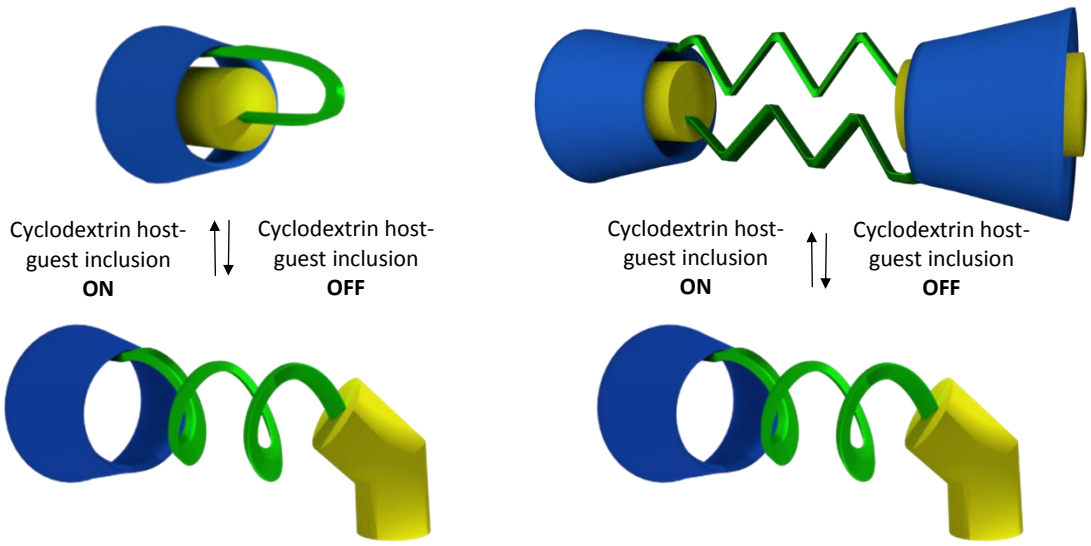

Figure 1.64 Conceptual image of the molecular devices investigated in Chapter 3 featuring cyclodextrin (*blue*), a guest (*yellow*) and a peptide (*green*).

The concept of using cyclodextrin host-guest complex formation to influence peptide structure was further developed in the study described in Chapter 4. Here, a peptide sequence was incorporated into a device that could also give a change in function upon formation of a host-guest inclusion complex.

Peptides are commonly prepared by solid-phase synthesis, a technique wherein amino acids are coupled onto a resin with reagents and unreacted material is washed off at each step. The work described in Chapter 5 investigated this method as a route to cyclodextrin daisy chains whereby desired interlocked species could be mechanically trapped on the solid resin and non-included species could be washed off.

In addition to daisy chain polymers, a number of other self-assembling polymers were attempted in the work presented in Chapter 6. These were designed to assemble *via* two types of non-covalent interactions; cyclodextrin host-guest recognition and peptide-peptide β-sheet formation.

Finally, a peptide amphiphile synthesized during the work described in Chapter 4 was noted to have gelation properties in various solvents. In the investigation described in Chapter 7 the nature of self-assembly and characteristics of the gel were investigated.

Chapter 2: Results and Discussion

Attempted Synthesis of a Photo-Responsive Molecular Lariat

2.1 Introduction

As described in Chapter 1, the design for a photo-responsive lariat was based on the asymmetric molecular muscle **32** previously synthesized in the group which features a photo-switchable azobenzene arm and a non-photo-responsive undecane arm (Figure **2.1**).

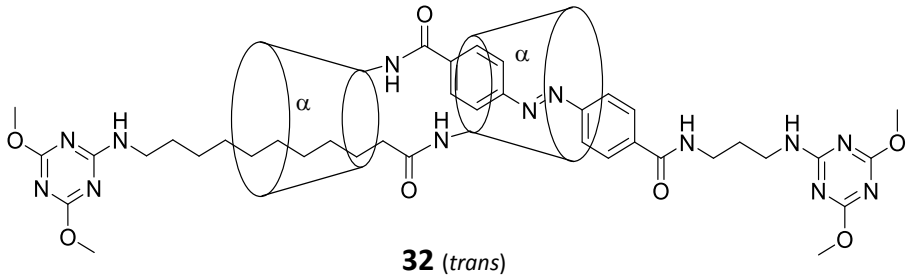

32 (*trans*)

Figure 2.1 Asymmetric molecular muscle **32** synthesised by Easton *et al.*[147]

In order to minimise movement along the non-photo-responsive arm and create the hinge required for a lariat device an octyl chain length was chosen as this is the shortest, and therefore most restrictive, alkyl chain which still forms a rotaxane with α-cyclodextrin in a reasonable yield.[148] The designed molecular lariat **33** therefore comprises a photo-responsive azobenzene arm and an octyl chain hinging arm. Molecular movement would then be manifest as the expansion and contraction of the lariat 'loop' (Figure **2.2**).

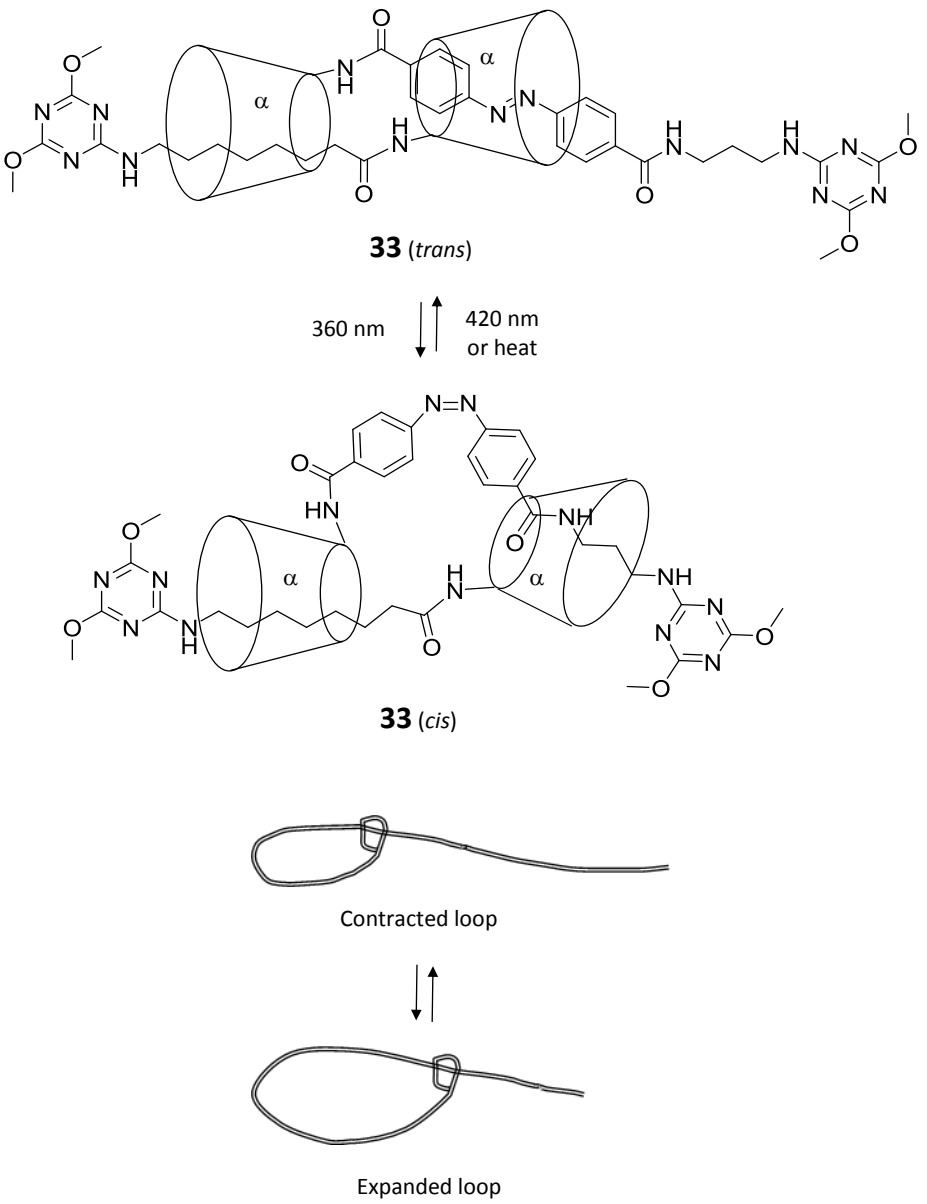

Figure 2.2 Opening and closing of the proposed asymmetric molecular lariat **33**.

2.2 Synthesis of the Molecular Lariat Components

The molecular lariat was based on an asymmetric [*c*2]-dimer construct with one arm intended to act as a photo-responsive moiety and the other a hinge. The photo-responsive arm featured two cyclodextrin guest stations; the primary station, azobenzene, upon which cyclodextrin was expected to preferentially sit in the initial unirradiated state, and the secondary station, a propyl group, to which cyclodextrin was anticipated to move when the azobenzene station was photoisomerised to the *cis* conformation.

The cyclodextrin **39** was synthesised according to previous experimental methods developed in the group (Scheme **2.1**).[147]

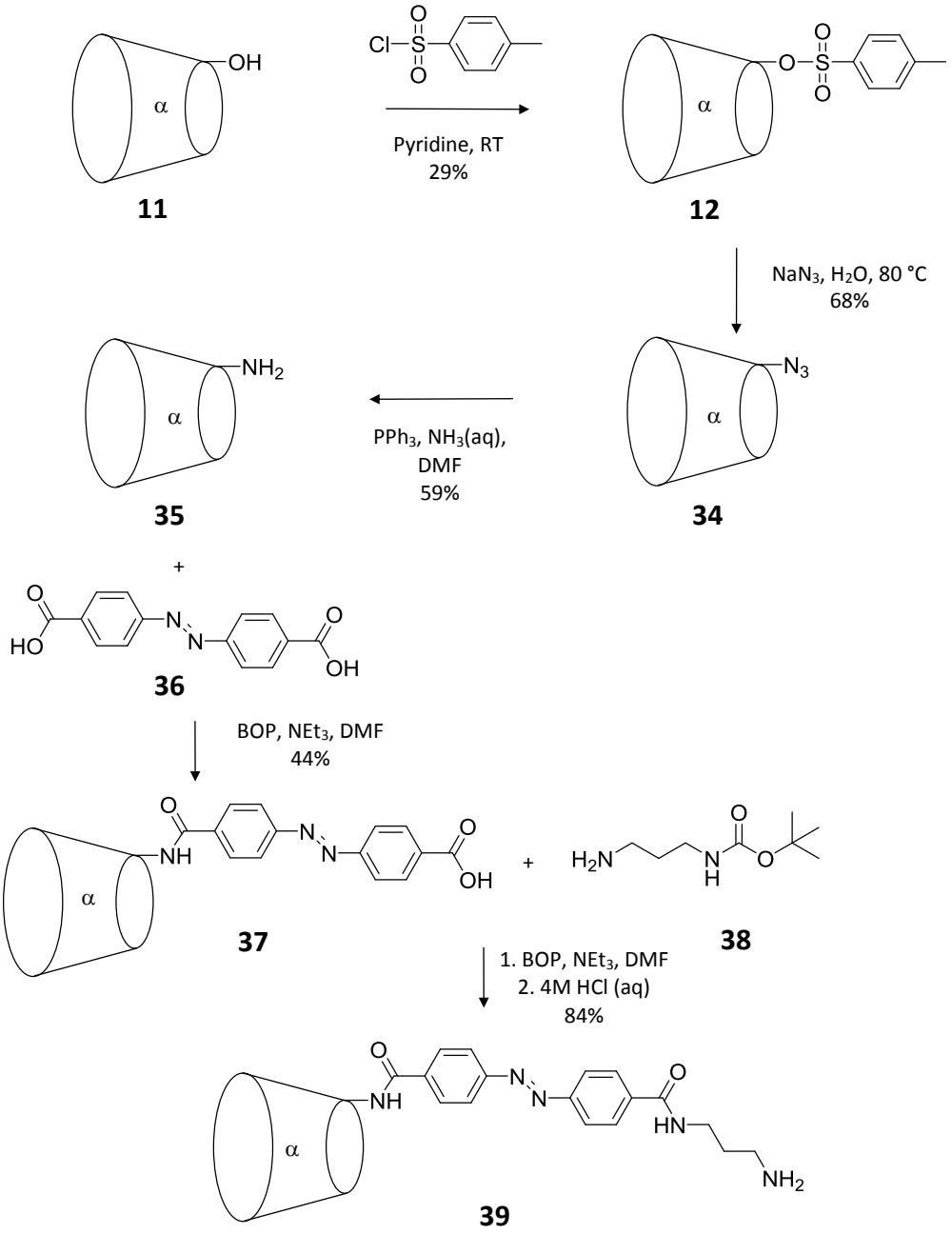

Scheme 2.1 Synthesis of the photo-responsive component **39** of the molecular lariat.

Natural α-cyclodextrin **11** was first tosylated at the C6-OH position using tosyl chloride and pyridine. As discussed in Chapter 1, the use of a weak base such as pyridine enables selective reaction at C6-OH over the C2-OH and C3-OH postions. In these conditions the hydroxyl functionalities remain protonated meaning that the primary groups are more nucleophilic and hence more reactive than the secondary groups.[149] As discussed in

Chapter 1, pyridine also sits inside the α-cyclodextrin cavity, further directing reaction at the C6-OH positions.[59] The reaction mixture was carefully monitored by TLC and after 4 h, when TLC of the reaction indicated that α-cyclodextrin **11** starting material, mono-tosylated α-cyclodextrin product **12** and combined multiply-tosylated products were present in roughly equal proportions, the reaction was quenched with water which hydrolyses remaining tosyl chloride and prevents further reaction. Work-up involved pipetting the crude reaction mixture into ice-cold, stirring acetone which resulted in the precipitation of cyclodextrin species whilst other reagents remained in solution. This method was used throughout the experimental procedures in this thesis as an effective way of isolating cyclodextrin-containing compounds from a reaction mixture. The mono-tosylated α-cyclodextrin product **12** was then separated from unreacted α-cyclodextrin **11** and multiply-tosylated α-cyclodextrins by column chromatography in a yield of 29%. This is an excellent recovery considering that at the point of quenching, TLC of the reaction indicated roughly a 33% formation of the mono-tosylated α-cyclodextrin product **12**.

NaN_3 was then added to tosylated-α-cyclodextrin **12** to form azido-α-cyclodextrin **34**. This reaction occurred cleanly with displacement of the tosyl group with an azido group and no side-products formed, enabling the crude product to be used with no purification. Azido-α-cyclodextrin **34** was reduced in a Staudinger reaction to give amino-α-cyclodextrin **35**, which was isolated by elution from a SP-650M cation exchange column. The solid phase in this column is a polystyrene functionalised with sulfonate groups which have a p*K*a of ~2. At neutral pH, the sulfonate groups are negatively charged and interact with the positively charged amino-α-cyclodextrin **35** retaining it on the column, whilst neutral species such as azido-α-cyclodextrin **34** or tosylated-α-cyclodextrin **12** are eluted. The amino-α-cyclodextrin **35** can then be eluted separately, by increasing the basicity of the liquid phase to above the p*K*a of the amino group which causes it to deprotonate and prevents interaction with the solid-phase. This purification method was used to isolate amino-α-cyclodextrin **35** in a 59% yield.

Cyclodextrin **37** was then synthesised from amino-α-cyclodextrin **35** with the use of BOP coupling chemistry with azobenzene-4,4'-dicarboxylic acid **36**. Although the

carnicogenic by-product hexamethylphosphoramide (HMPA) is produced in this reaction, use of the precipitation work-up retains HMPA in an acetone solution allowing for appropriate disposal before purification thus minimizing contact. Azobenzene-4,4'-dicarboxylic acid **36** may react with one equivalent of amino-α-cyclodextrin **35** to form the desired cyclodextrin **37**, or with two equivalents to give a di-cyclodextrin substituted compound. In order to bias the reaction to favour the mono-substituted product an excess of azobenzene-4,4'-dicarboxylic acid **36** was used (3.7 equivalents compared to 1 equivalent of amino-α-cyclodextrin **35**), and a solution of amino-α-cyclodextrin **35** added dropwise to a more concentrated solution of azobenzene-4,4'-dicarboxylic acid **36**. This experimental design was reasoned to expose a relatively smaller concentration of amino-α-cyclodextrin **35** to each azobenzene-4,4'-dicarboxylic acid **36** molecule, thus making di-substitution less likely. Column chromatography was used to isolate the cyclodextrin **37** in a 44% yield.

The azobenzene monomer **39**, which was to act as the photo-responsive arm in the molecular lariat was obtained by firstly coupling the cyclodextrin **37** with Boc-protected 1,3-diaminopropane **38** which was previously synthesised by the group.[150] The Boc protecting group was then removed by treatment with 4M HCl and the resulting cyclodextrin **39** isolated by elution from a SP-650M cation exchange column in a 84% yield with the ^{1}H NMR spectrum shown in Figure **2.3**. Care had to be taken with the deprotection step as harsh acidic conditions can lead to breakdown of the cyclodextrin ring, such that occurs in the naphthalene-1,3-diol TLC dip described in Chapter 1. As with the purification of amino-α-cyclodextrin **35**, the p*K*a of the amino group in the cyclodextrin **39** was exploited to facilitate retention on the column at neutral pH, allowing by-products and unreacted starting material to be washed off, and separate elution of the product at basic pH. The isolated azobenzene monomer **39** was stored under vacuum in order to prevent carbamate formation which results upon extended exposure to carbon dioxide.

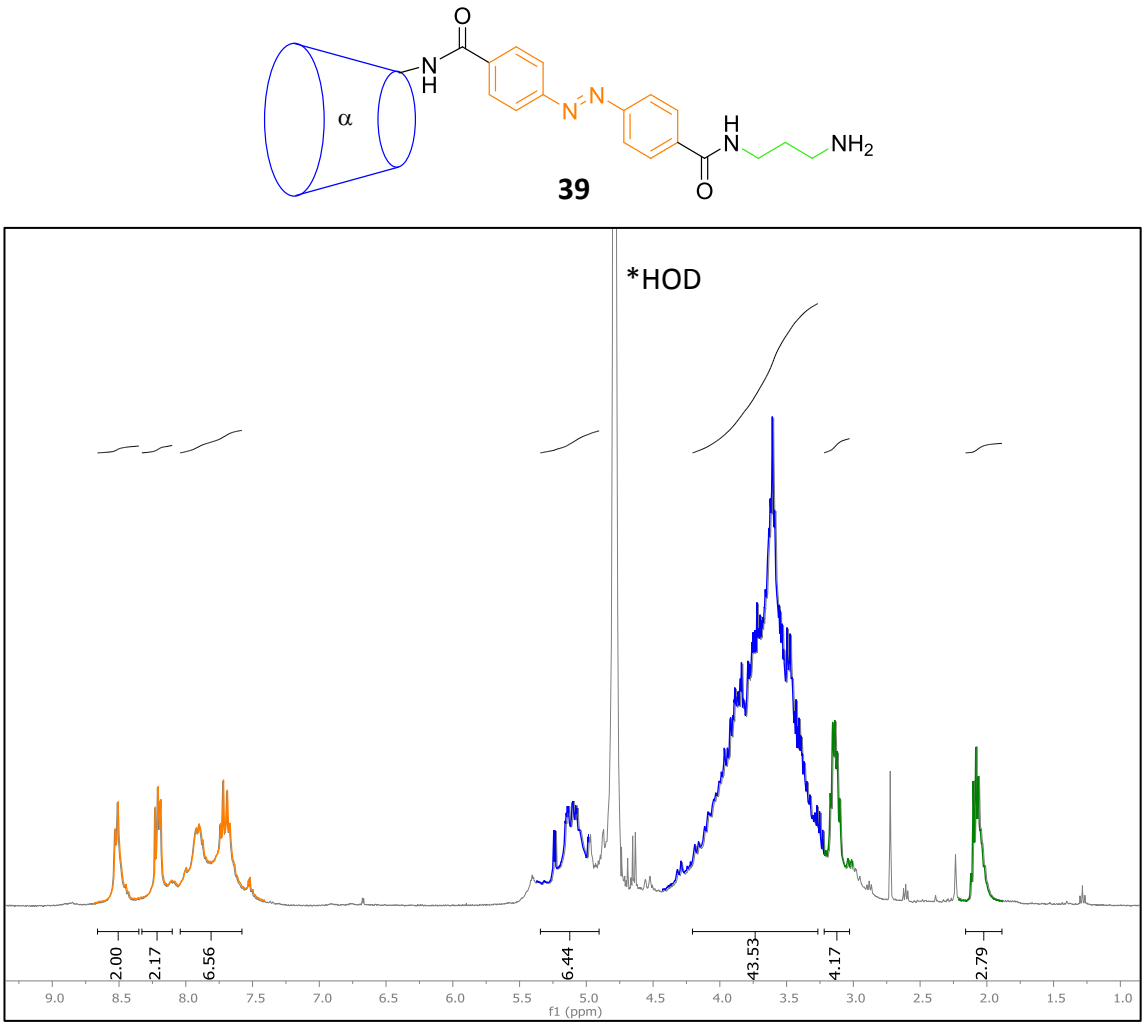

Figure 2.3 400 MHz ^{1}H NMR spectrum of the cyclodextrin **39** in D_2O at 25 °C. Cyclodextrin proton signals are shown in blue, azobenzene proton signals in orange and alkyl proton signals in green. *Denotes residual HOD solvent signal.

The octyl monomer **42**, designed to act as the hinge in the molecular lariat, was then separately synthesised (Scheme **2.2**).

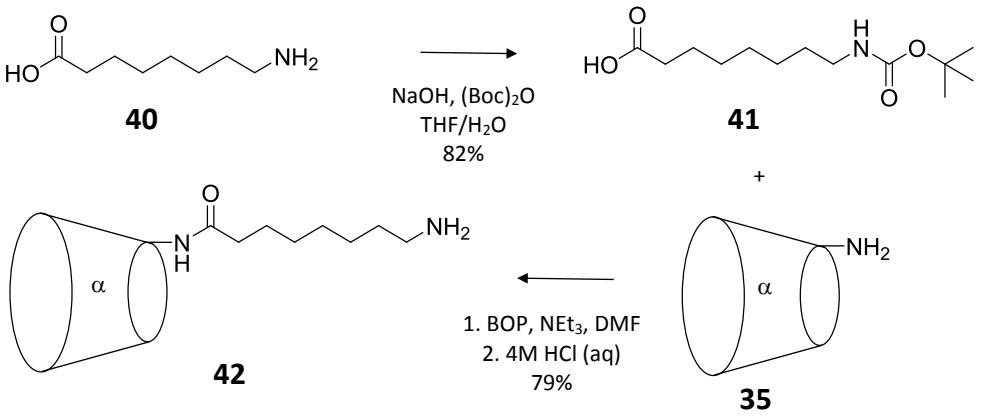

Scheme 2.2 Synthesis of the hinging component **42** of the asymmetric molecular lariat.

8-Amino-octanoic acid **40** was protected with a Boc-group to give 8-*tert*-butoxycarbonylamino-octanoic acid **41** which was isolated in 82% yield by recrystallization. 8-*tert*-Butoxycarbonylamino-octanoic acid **41** was then coupled with amino-α-cyclodextrin **35**, and the Boc protecting group removed by treatment with 4M HCl. Cation exchange was used to isolate the cyclodextrin **42** in a 79% yield with the ^{1}H NMR spectrum shown in Figure **2.4**. As previously described, the p*K*a of the amino group in the cyclodextrin **42** was exploited in order to give retention on the cation exchange column at neutral pH. Unreacted starting material **41** and other reagents were eluted, with separate elution of the product **42** at basic pH.

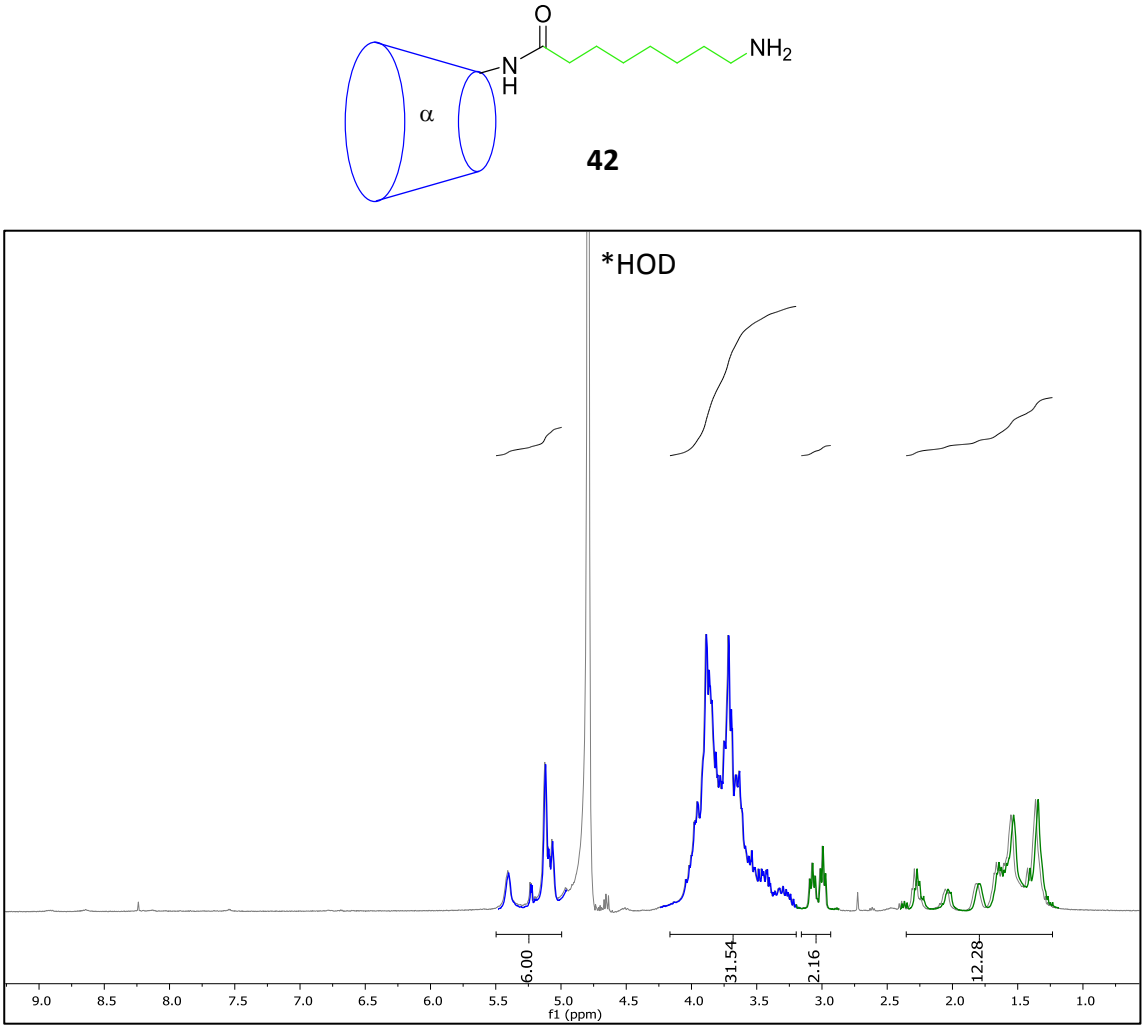

Figure 2.4 400 MHz ^{1}H NMR spectrum of the cyclodextrin **42** in D_2O at 25 °C. Cyclodextrin proton signals are shown in blue and alkyl proton signals in green. *Denotes residual HOD solvent signal.

2.3 Attempted Synthesis of the Molecular Lariat

Having synthesised the two components required for the molecular lariat, the photo-responsive arm **39** and the hinging arm **42**, synthesis of the asymmetric [*c*2]-dimer **33** was attempted. The experimental design involved equilibration of the two modified cyclodextrins **39** and **42** in water allowing supramolecular assemblies to form, followed by a capping reaction with 2-chloro-4,6-dimethoxy-1,3,5-triazine **43** to mechanically trap interlocked products (Scheme **2.3**). This prevents dissociation of any cyclodextrin host-guest inclusion complexes, enabling their isolation by chromatographic techniques.

As a consequence of the use of two different cyclodextrin monomers, three different capped [*c*2]-daisy chains could be potentially formed; the azobenzene homo-[*c*2]-dimer **31**, the octane homo-[*c*2]-dimer **44** and the desired hetero-[*c*2]-dimer **33**. The association constant (K_a) of cyclodextrin-azobenzene inclusion[151] is much higher than that of cyclodextrin-octane inclusion.[152] In equilibrium the azobenzene homo-dimer is therefore the most thermodynamically stable [*c*2]-dimer structure, followed by the azobenzene octane hetero-dimer, with the octane homo-dimer being the least stable. To bias the equilibrium towards the asymmetric product an excess of the octane monomer **42** was used. Previous work in the group[147] showed that a 5:1 ratio of alkane:azobenzene monomer led to an increased product ratio of the asymmetric molecular muscle **32**, therefore the same ratio was evaluated for formation of the asymmetric molecular lariat **33**.

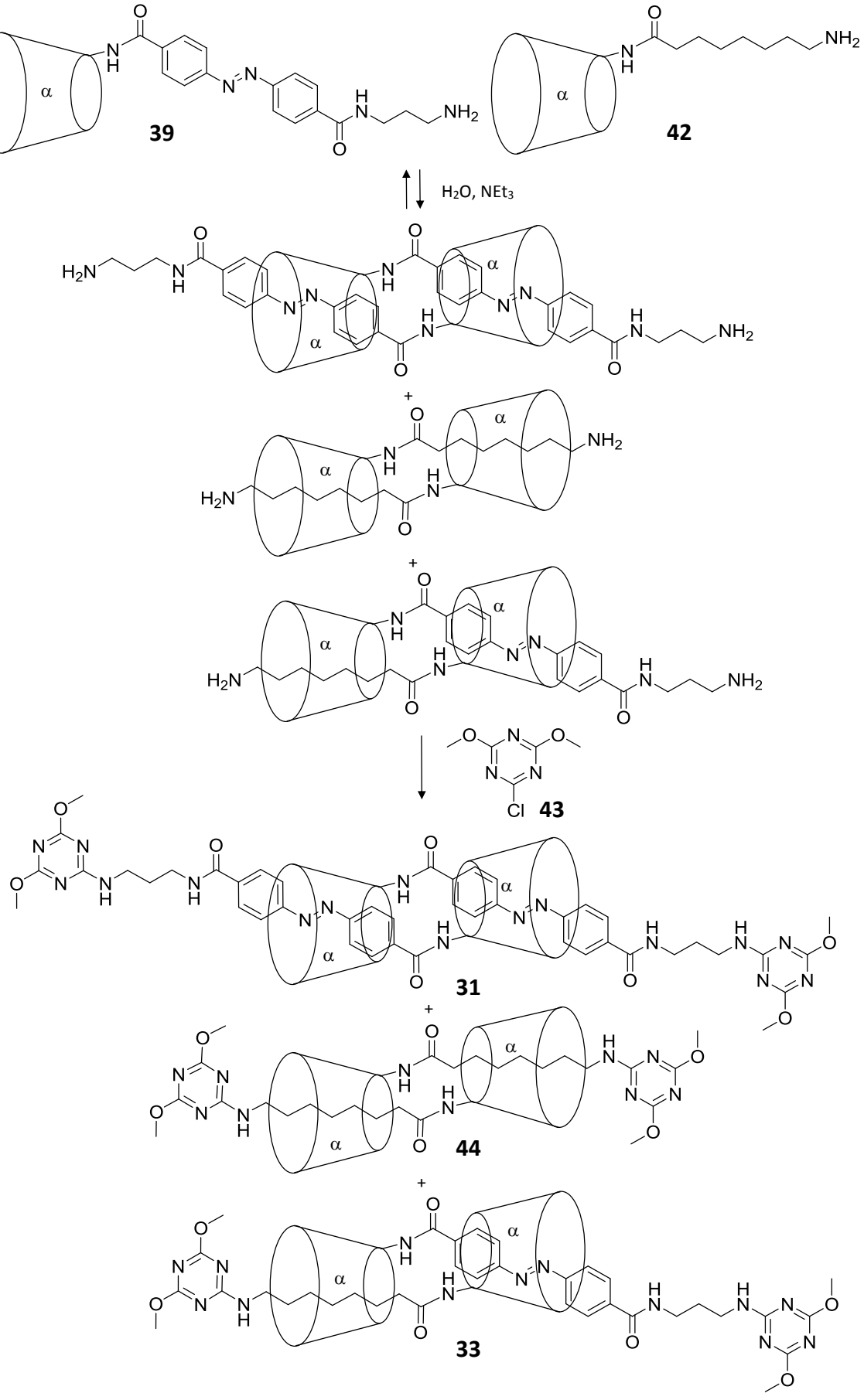

Scheme 2.3 Possible [*c*2]-dimeric products **33**, **31** and **44** that could be formed after the addition of the stoppering reagent **43** to an equilibrated mixture of the cyclodextrin monomers **39** and **42**.

A solution of the cyclodextrin monomer **39** was added dropwise to a solution of the cyclodextrin **42**, both in aqueous solution at pH 9.5. The stoppering reagent **43** (1 eq of the combined cyclodextrin monomers) was then added and after 24 h the crude reaction mixture was analysed by HPLC at 340 nm (Figure **2.5**). Compounds that do not contain azobenzene, such as the octane monomer **42** and related derivatives are not observable at this wavelength, greatly simplifying the task of identification of any asymmetric [*c*2]-dimer **33** peak.

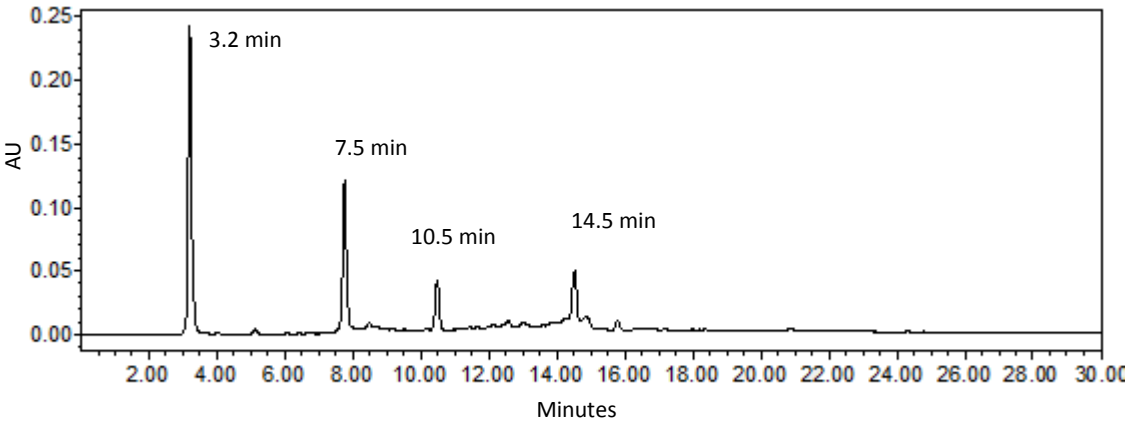

Figure 2.5 Chromatogram acquired by reverse phase HPLC of the crude reaction mixture of cyclodextrin monomers **39** and **42** (1eq of combined monomers) with 1 eq of the stoppering reagent **43**, monitored at 340 nm.

Although only four main peaks were detected in the HPLC trace at 360 nm, they could be attributed to a range of possible compounds. In addition to both the fully-stoppered homo-[*c*2]-dimer **31** and the hetero-[*c*2]-dimer **33**, singly-stoppered versions of these [*c*2]-dimers could be present, as well as unreacted azobenzene monomer **39**, and capped azobenzene monomer **45**.

In order to identify peaks arising from products that do not feature the octane monomer **42**, and therefore eliminate them as candidates for the desired hetero-[*c*2]-dimer **33** product peak, it was hypothesised that a reaction using only the azobenzene monomer **39** to form the homo-[*c*2]-dimer **31** and related by-products could be analysed under the same HPLC conditions as in Figure **2.5**. The azobenzene monomer **39** was allowed to equilibrate in aqueous solution at pH 9.5, followed by addition of the stoppering reagent **43** (1 eq based on cyclodextrin monomer) (Scheme **2.4**). After 24 h the crude reaction mixture was analysed by HPLC (Figure **2.6**).

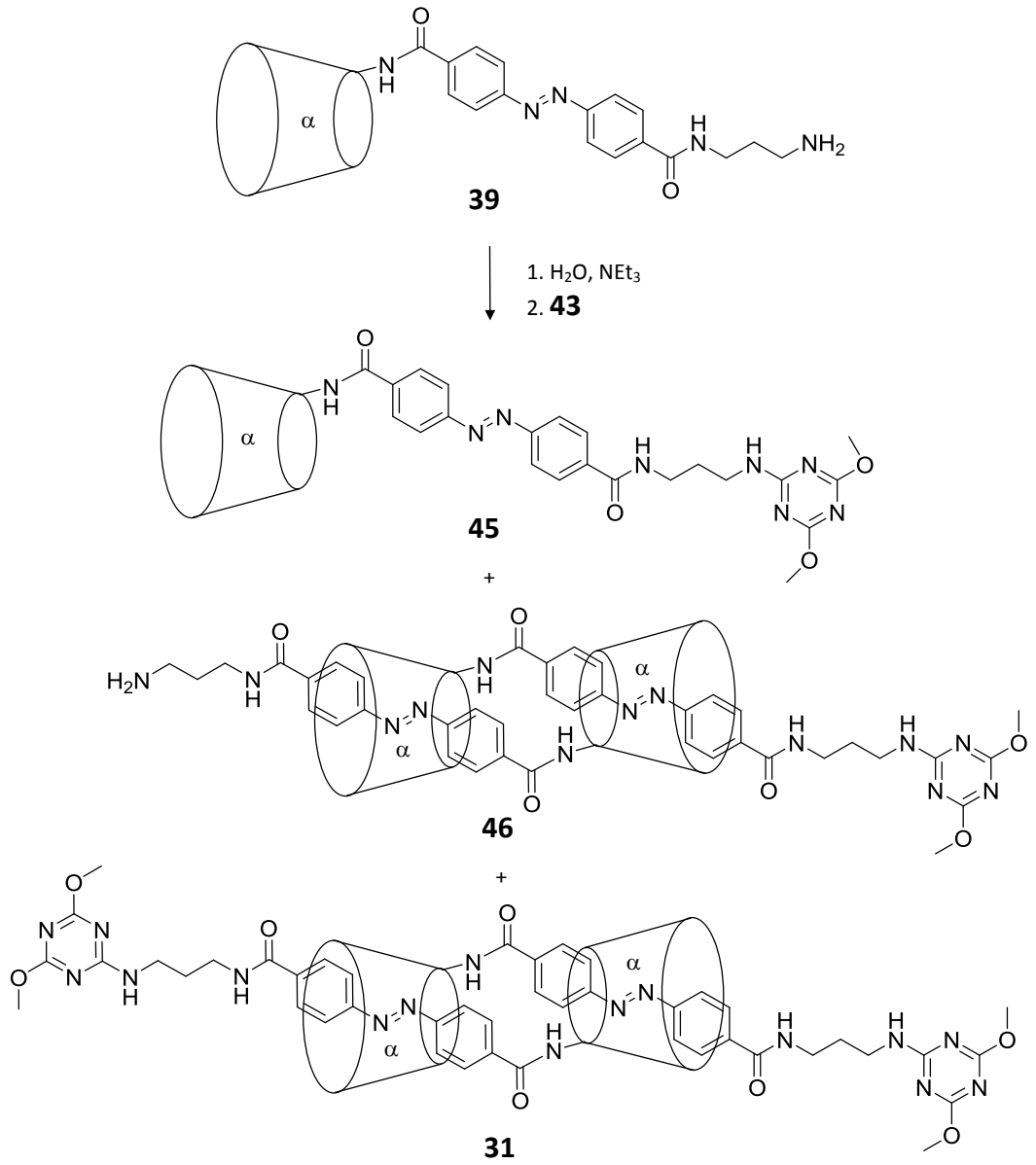

Scheme 2.4 Possible products **31**, **45** and **46** that could be formed after the addition of the stoppering reagent **43** to an equilibrated mixture of the cyclodextrin monomer **39**.

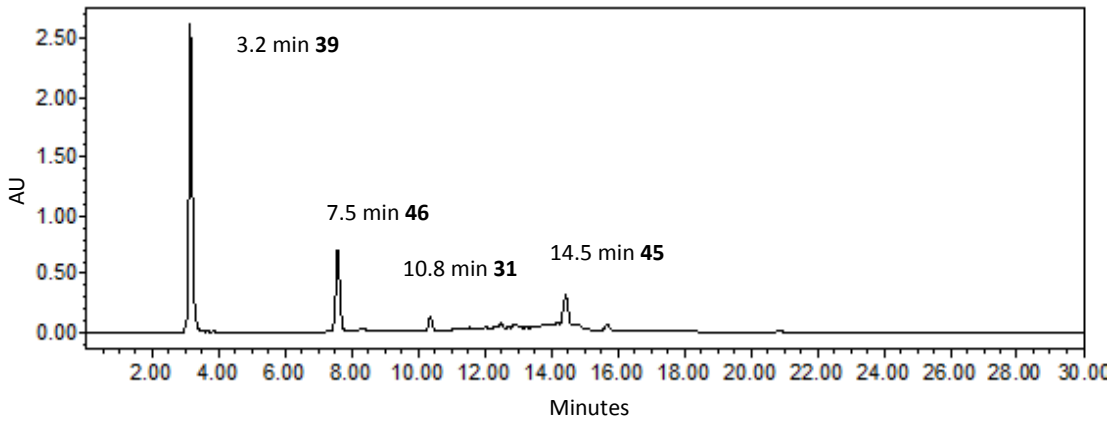

Figure 2.6 Chromatogram acquired by reverse phase HPLC of the crude mixture of the cyclodextrin monomer **39** (1 eq) with 1 eq of the stoppering reagent **43**, monitored at 340 nm.

The HPLC trace shows four main peaks which were collected and analysed by mass spectrometry. On this basis, the peak appearing at 3.2 min was assigned as unreacted azobenzene monomer **39**, the peak at 7.5 min as the singly-capped azobenzene [*c*2]-dimer **46**, the peak at 10.8 min as the fully-capped azobenzene [*c*2]-dimer **31**, and the peak at 14.5 mins as the capped azobenzene monomer **45**.

Comparing this trace to that obtained from the equilibration of cyclodextrins **39** and **42** (Figure **2.5**), no different peaks could be observed, indicating that an asymmetric product had not formed in that case.

Another attempt of the synthesis of the homo-[*c*2]-dimer **31** was made, wherein the equivalents of the stoppering reagent **43** were increased from 1 eq to 7 eq (based on cyclodextrin monomer). When the crude reaction mixture with this experimental change was analysed by HPLC, it was found that the reaction had been driven to completion and that the fully-capped azobenzene [*c*2]-dimer **31** had formed almost exclusively (Figure **2.7**) and none of the capped azobenzene monomer **45** had formed.

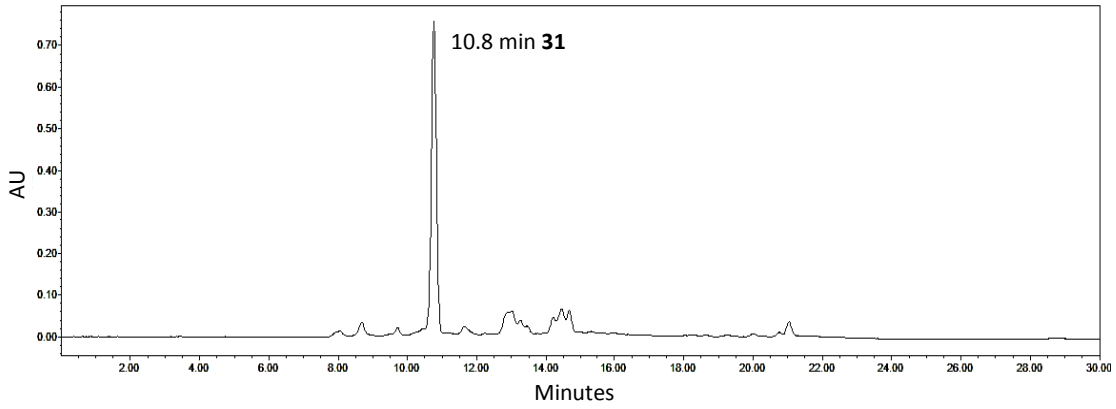

Figure 2.7 Chromatogram acquired by reverse phase HPLC of the crude reaction mixture of the cyclodextrin monomer **39** with 7 eq of the stoppering reagent **43**, monitored at 340 nm.

The increased concentration of the stoppering reagent **43** clearly facilitates the complete capping of all available sites, as no uncapped monomer **39** or singly capped dimer **46** is present. The reason for the enhanced formation of the fully capped dimer **31** over the capped monomer **45** is unclear but may reflect an increased rate of capping, which limits the re-establishment of equilibrium between the precursor complexes.

As the addition of an increased amount of stoppering reagent **43** had resulted in almost exclusive formation of the azobenzene homo-[*c*2]-dimer **31**, it was considered that this methodology could also be used to promote the production of the azobenzene octane hetero-[*c*2]-dimer **33**. A reaction was therefore set up wherein 7 eq of the stoppering reagent **43** (based on combined cyclodextrin monomers) were added to a solution of monomers **39** and **42**. After 24 h the crude reaction mixture was analysed by HPLC (Figure **2.8**).

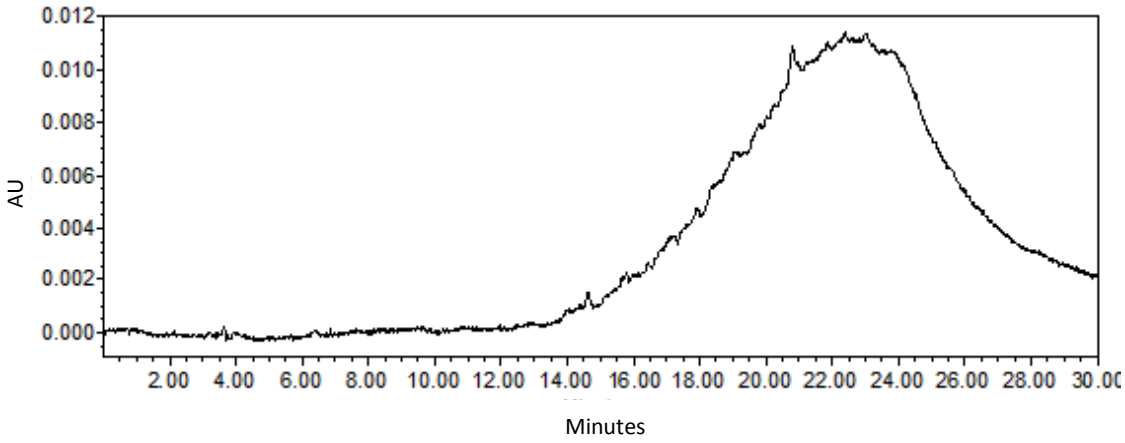

Figure 2.8 Chromatogram acquired by reverse phase HPLC of the crude reaction mixture of cyclodextrin monomers **39** and **42** (1 eq of combined monomers) with 7 eq of the stoppering reagent **43**, monitored at 340 nm.

The analytical HPLC trace of the crude reaction mixture of cyclodextrin monomers **39** and **42** (1 eq of combined monomers) with 7 eq of stoppering reagent (Figure **2.8**) is clearly very different to that with only 1 eq of the stoppering reagent **43** (Figure **2.5**). The peaks at 3.2 min, 7.5 min and 10.8 min corresponding to unreacted azobenzene monomer **39**, singly-capped azobenzene [*c*2]-dimer **46** and the fully-capped azobenzene [*c*2]-dimer **31** do not appear. It is unclear whether or not the peak at 14.5 min which corresponds to the capped, unincluded azobenzene monomer **45** is present as it is partially obscured by a large, broad peak.

The analytical HPLC method used for the trace shown in Figure **2.8** was altered to increase the hydrophobicity of the mobile phase, resulting in a much sharper peak (Figure **2.9**).

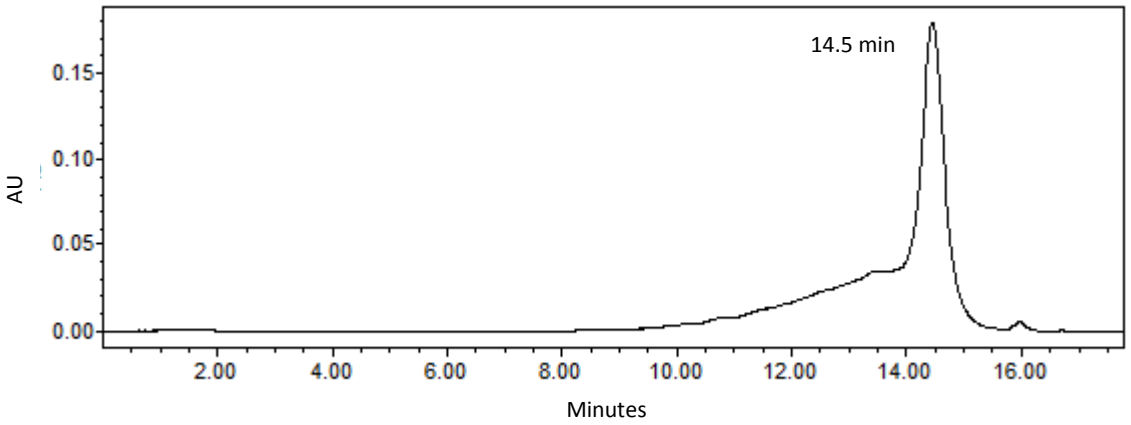

Figure 2.9 Chromatogram acquired by reverse phase HPLC of the crude reaction mixture of cyclodextrin monomers **39** and **42** (1 eq of combined monomers) with 7 eq of the stoppering reagent **43**, monitored at 340 nm, with a more hydrophobic mobile phase.

The peak shown in the HPLC trace was then isolated by size-exclusion chromatography and analysed by mass spectrometry (Figure **2.10** and Figure **2.11**).

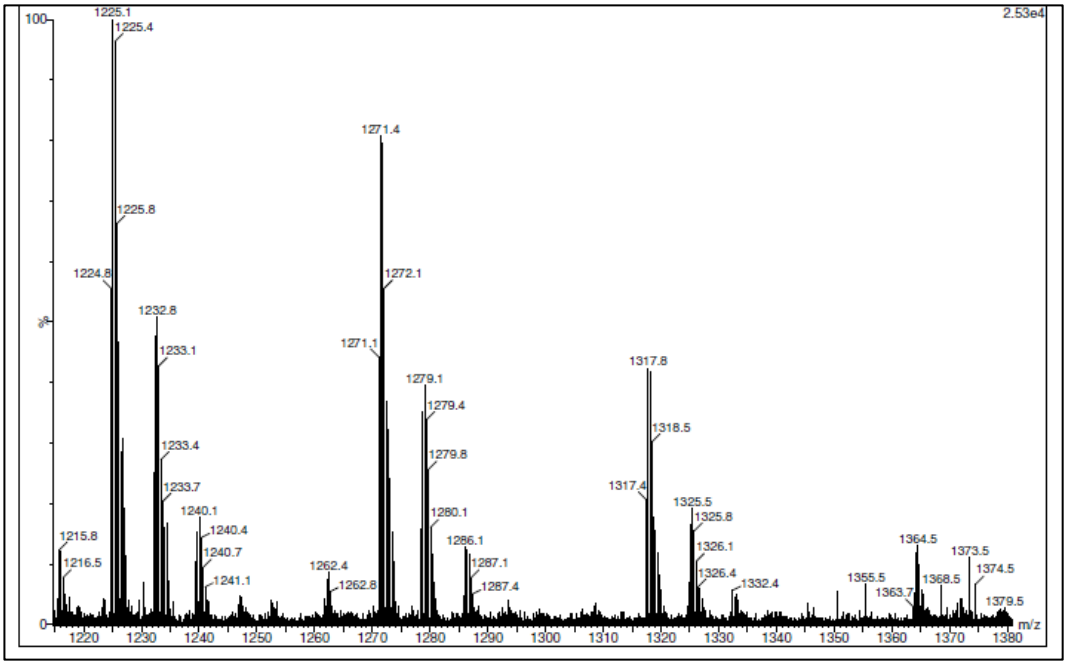

Figure 2.10 LCT-ESI mass spectrum from *m/z* 1215-1380 of the material isolated from the the crude reaction mixture of cyclodextrin monomers **39** and **42** (1 eq of combined monomers) with 7 eq of the stoppering reagent **43** by size-exclusion chromatography.

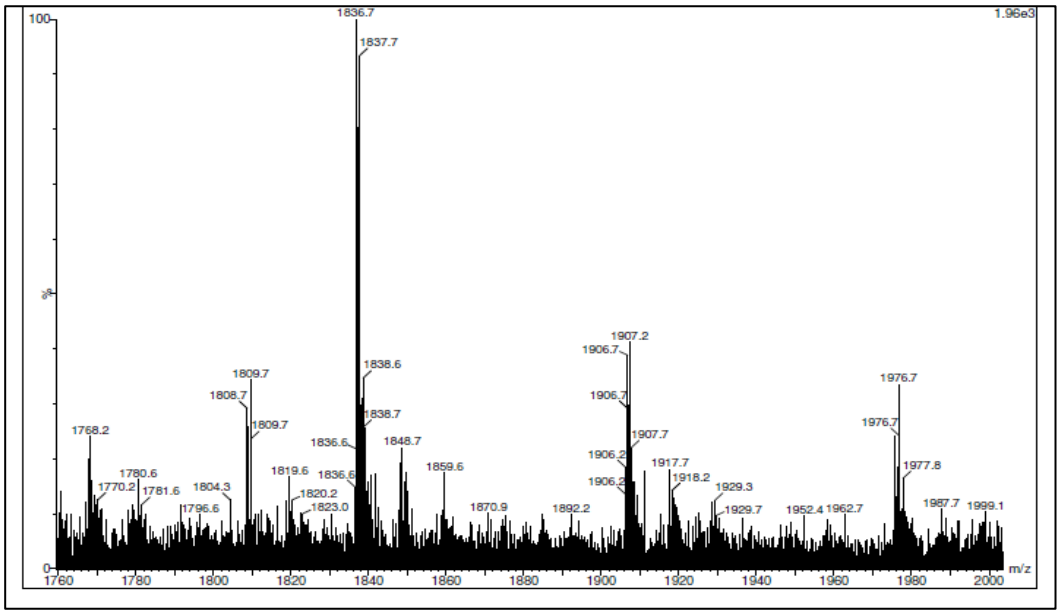

Figure 2.11 LCT-ESI mass spectrum from *m/z* 1760-2000 of the material isolated from the the crude reaction mixture of cyclodextrin monomers **39** and **42** (1 eq of combined monomers) with 7 eq of the stoppering reagent **43** by size-exclusion chromatography.

Observed *m/z* peaks show that the isolated material is one or more trimeric species, each consisting of two azobenzene monomer units and one octane unit and three stopper groups (Table **2.1**). Molecular ion peaks corresponding to triply charged trimers (M) appear at *m/z* 1364.5 and 1373.5, with other fragment peaks corresponding to the loss of varying numbers of capping groups.

The ^{1}H NMR spectrum of the material isolated by size-exclusion chromatography (Figure **2.12**) also supports the formation of trimeric species, with the integration of cyclodextrin, azobenzene and alkyl proton peaks approximately corresponding to two azobenzene monomer units and one octyl monomer unit. If the H6-α-cyclodextrin proton peak integral at 5.02 ppm, shown in blue, is defined as 18H as for three α-cyclodextrin moieties, the azobenzene proton peaks at 8.46 ppm, 8.14 ppm and 7.64 ppm, shown in orange, integrate to a total of 15H representing roughly a 2:1 ratio of α-cyclodextrin:azobenzene moieties. The alkyl proton peaks at 2.02 ppm, 1.95 ppm and 1.55-1.44 ppm, shown in green, then integrate to a total of 17H giving a roughly 3:1 ratio of α-cyclodextrin:octane moieties. The methyl ester protons on the stopper groups have an expected shift of around 3.9 ppm and therefore overlap with the H2-6-α-cyclodextrin proton peaks. The protons in this region integrate to 129H, accounting for the presence of three α-cyclodextrin moieties and three 4,6-dimethoxy-1,3,5-triazine stoppers. This

provides further evidence that the isolated trimeric species are fully capped, and that *m/z* peaks in the mass spectrum corresponding to species with less than three stoppers are fragments as opposed to discrete compounds.

Species	Observed *m/z*
$[M - 3x\ stoppers + 3H]^{3+}$	1225.1
$[M - 3x\ stoppers + 2H + Na]^{3+}$	1232.8
$[M - 3x\ stoppers + H + 2Na]^{3+}$	1240.1
$[M - 2x\ stoppers + 3H]^{3+}$	1271.4
$[M - 2x\ stoppers + 2H + Na]^{3+}$	1279.1
$[M - 2x\ stoppers + H + 2Na]^{3+}$	1286.1
$[M - 1x\ stopper + 3H]^{3+}$	1317.8
$[M - 1x\ stopper + 2H + Na]^{3+}$	1325.5
$[M - 1x\ stopper + H + 2Na]^{3+}$	1332.4
$[M + 3H]^{3+}$	1364.5
$[M + 2H + Na]^{3+}$	1373.5
$[M - 3x\ stoppers + 2H]^{2+}$	1836.7
$[M - 3x\ stoppers + H + Na]^{2+}$	1848.7
$[M - 3x\ stoppers + 2Na]^{2+}$	1859.6
$[M - 2x\ stoppers + 2H]^{2+}$	1907.2
$[M - 2x\ stoppers + H + Na]^{2+}$	1917.7
$[M - 2x\ stoppers + 2Na]^{2+}$	1929.3
$[M - 1x\ stopper + 2H]^{2+}$	1976.7
$[M - 1x\ stopper + H + Na]^{2+}$	1987.7

Table 2.1 Observed m/z peaks in the LCT-ESI spectrum of the material isolated from the the crude reaction mixture of cyclodextrin monomers **39** and **42** (1 eq of combined monomers) with 7 eq of the stoppering reagent **43** by size-exclusion chromatography. M = trimeric species comprising two azobenzene and one octane cyclodextrin monomer, and three stoppers.

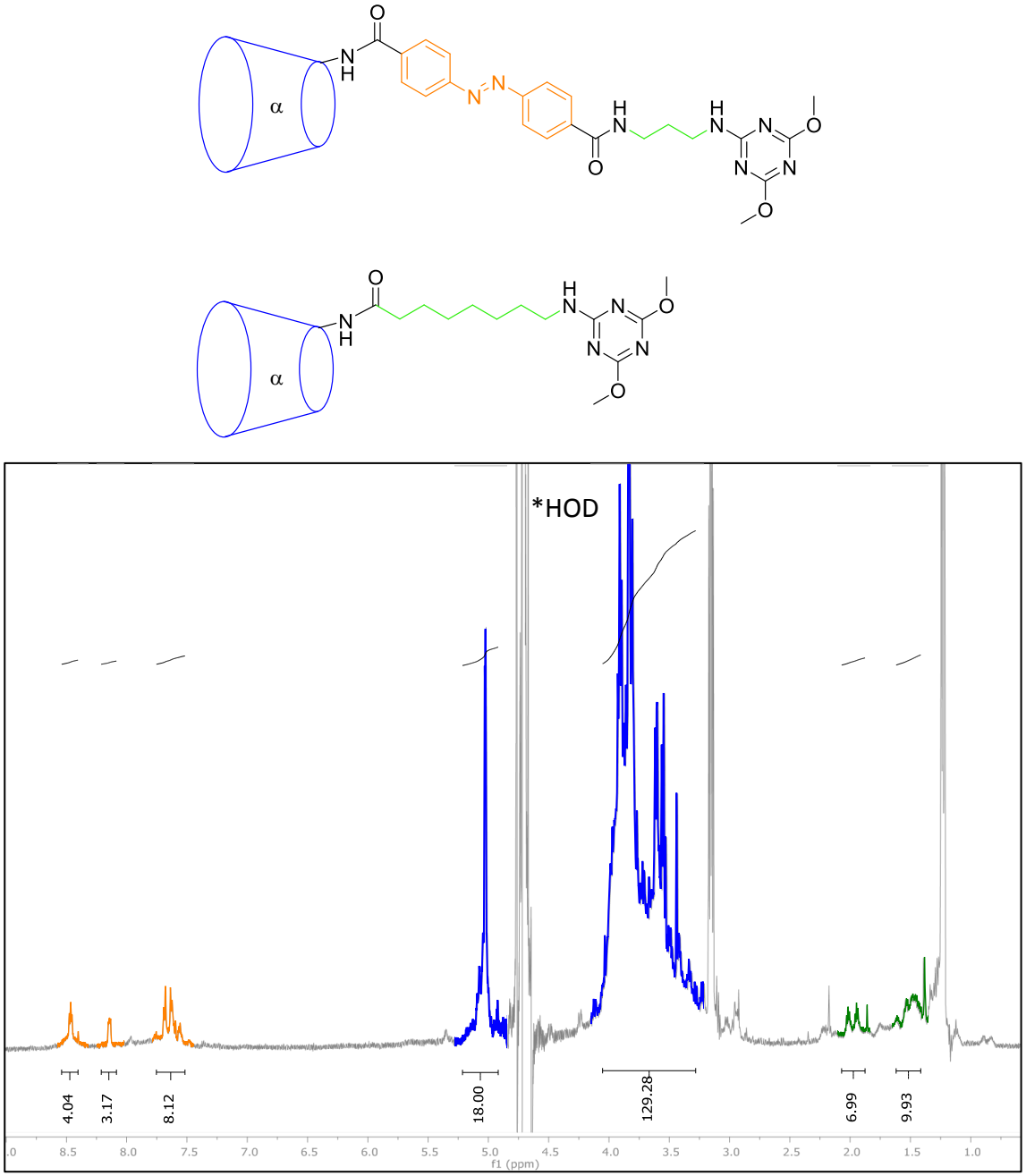

Figure 2.12 600 MHz ^{1}H NMR spectrum of the material isolated by size-exclusion chromatography in D_2O at 25 °C. Cyclodextrin proton signals are shown in blue, azobenzene proton signals in orange and alkyl proton signals in green. *Denotes residual HOD solvent signal.

The lack of formation of the azobenzene octane hetero-[*c*2]-dimer **33** is possibly a result of the length of the octyl chain, that it is too short to form a capped inclusion complex. In this case the mono-capped complex **47** would therefore not be formed, however the mono-capped complex **48** could form but would not be fully capped to give the dimer **33** (Scheme **2.5**). Instead the complex **48** could be the precursor to trimers through the octane guest being displaced by an azobenzene monomer **39** which is then capped to

give compound **49** as two possible regioisomeric trimers, depending on the orientation of the second included azobenzene monomer **39** (Scheme **2.6**).

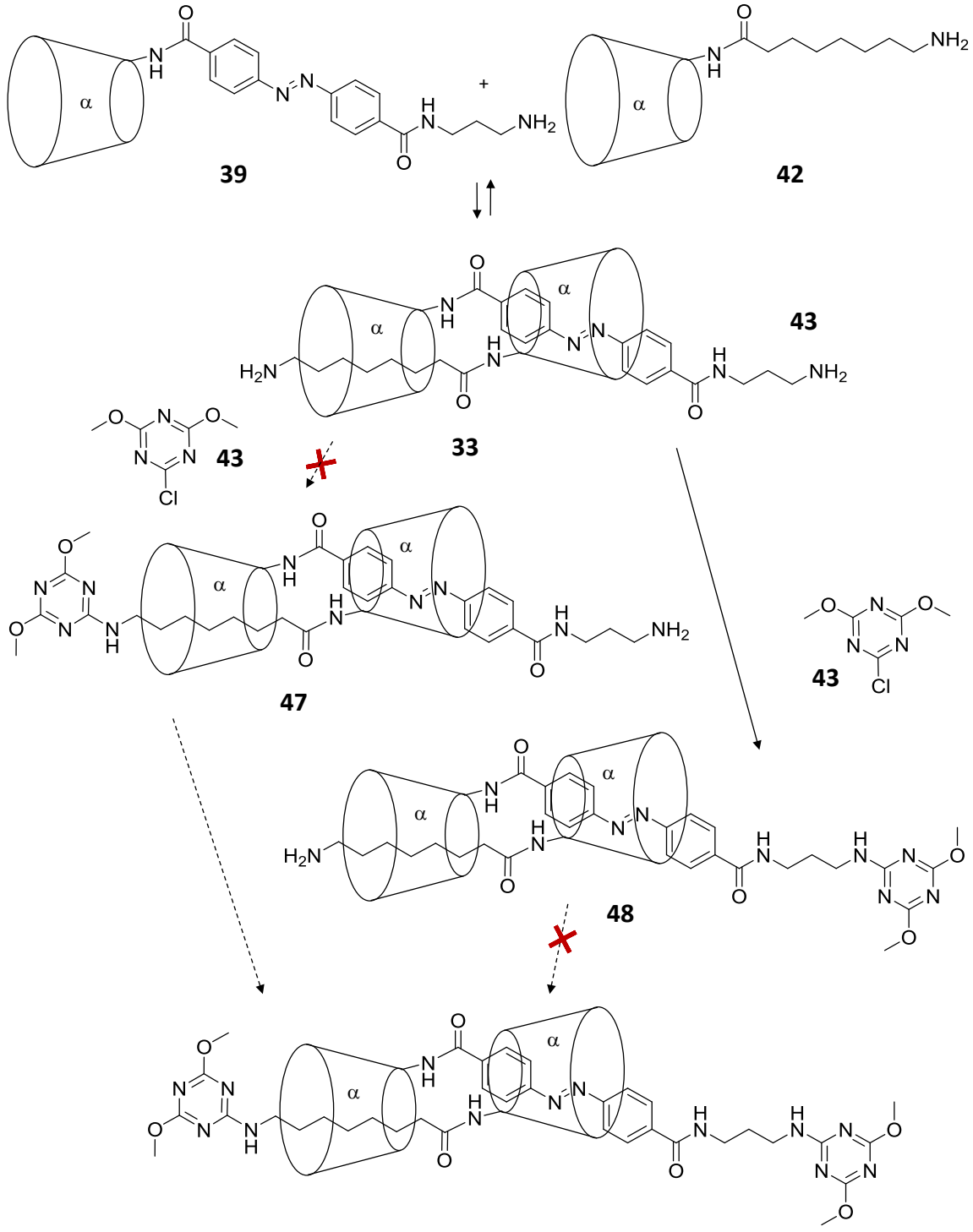

Scheme 2.5 Possible route to the formation of complex **48**.

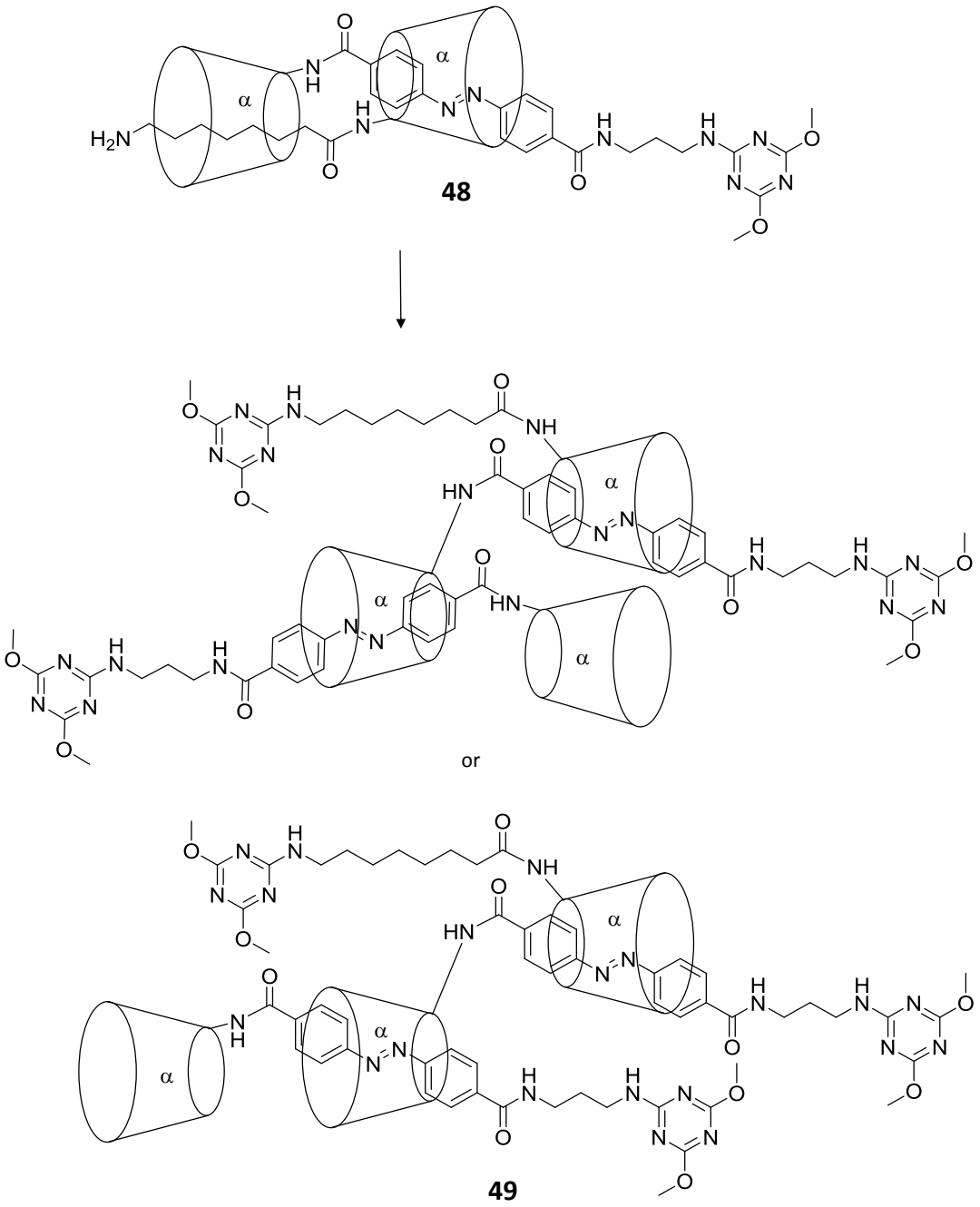

Scheme 2.6 Possible route to the formation of the trimeric rotaxanes.

2.4 Conclusions

Synthesis of the octane azobenzene hetero-[*c*2]-dimer **33**, attempted in an endeavour to develop a photo-responsive molecular lariat, was unsuccessful. As previous studies[147] have shown that the use of an undecane cyclodextrin monomer was successful in the synthesis of the azobenzene undecane [*c*2]-hetero-dimer **32**, it is concluded that the octyl chain is too short to form a capped inclusion complex with cyclodextrin.

Under reaction conditions using a 5:1 ratio of octane:azobenzene cyclodextrin monomers **42** and **39** and an excess of stoppering reagent **43**, material with a much longer HPLC elution time than expected for the hetero-[*c*2]-dimer **33** was isolated by size-exclusion chromatography. Mass spectrometry and ^{1}H NMR spectroscopy showed that this was one or more trimeric species, each comprising two azobenzene and one octane cyclodextrin monomer and three stoppering groups.

It is possible that the trimer is the rotaxane **49**, but since the desired hetero-[*c*2]-dimer **33** was not obtained, this line of research was abandoned, to pursue more fruitful avenues of investigation.

Chapter 3: Results and Discussion

Molecular Devices that Elicit Change in Peptide Secondary Structure

3.1 Introduction

As the strategy for the development of the photo-responsive molecular lariat described in Chapter 2 proved to be unsuccessful, efforts were focussed on the investigation of a different type of molecular device.

As discussed in Chapter 1, supramolecular assemblies with more than two components are not common and [*a*1]-, [*c*1]- and [*c*2]-assemblies are usually the most thermodynamically favourable. In solution, before stoppering mechanically traps these species, they exist in equilbirum with each other. It was decided to investigate whether this molecular recognition process, of shifting between non-included [*a*1]-species and included [*c*1]- and [*c*2]-species, could be used as an input to influence the state of an additional moiety in these self-assembled cyclodextrin-guest structures.

The formation of host-guest inclusion complexes has been used successfully to modify peptide secondary structure, earlier highlighted in Chapter 1. It was therefore hypothesised that in a cyclodextrin-peptide-guest monomer (Figure **1.64**) the formation of [*c*1]- and [*c*2]-cyclodextrin complexes might be used to produce an effect on peptide secondary structure. This change was predicted to be observable by circular dichroism spectroscopy. If a responsive guest was to be used, this structural modification could in principle be switched on and off by switching cyclodextrin host-guest inclusion on and off.

Circular dichroism spectroscopy is a measurement of the difference in absorbance of left and right circularly polarised light by a compound. As peptides consist of chiral

amino acids they can be analysed this way, specifically by the absorbance of the n $\rightarrow \pi^*$ and $\pi \rightarrow \pi^*$ transitions which occur in the near-UV region (190 nm – 225 nm). Secondary structures have characteristic circular dichroism spectra; α-helices exhibit a typical double minima at 208 nm and 222 nm, β-sheets give a minimum at 218 nm and polyproline type II (PPII) helices give a minimum at 198 nm (Figure **3.1**).[83]

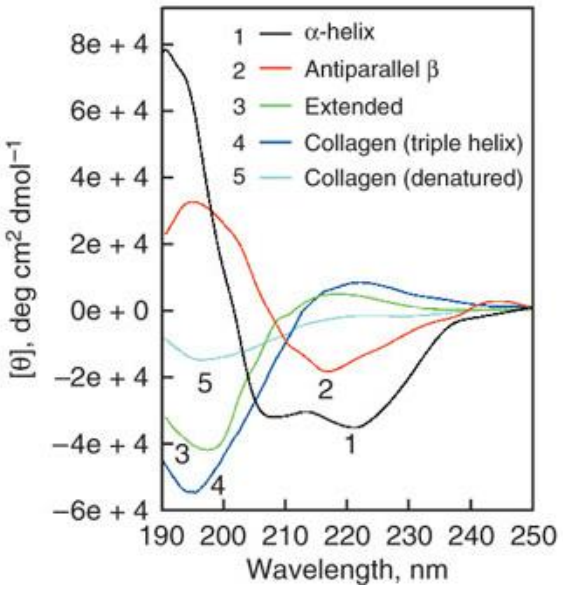

Figure 3.1 Circular dichroism spectra showing typical traces for defined peptide secondary structures.[83]

Apart from absolute structure, circular dichroism spectroscopy can also be used to determine the physical characteristics of a peptide by analysing temperature profiles of secondary structures. The mid-point transitions (T_m) of thermal folding or unfolding can be derived, as well as the ΔG, ΔS and ΔH of these process.[153]

3.2 Synthesis of a Peptide Structure Photo-Switch

The initial design for a cyclodextrin-peptide-guest monomer included an α-cyclodextrin and an azobenzene guest. As previously discussed in Chapter 1, photo-irradiation has many benefits as an external switching mechanism and azobenzene is a well-known photo-responsive guest for α-cyclodextrin.[154-158] The *trans* configuration has the capability to form a host-guest complex, which is lost upon photoisomerization to the *cis* configuration.

The peptide that was used to study potential changes in secondary structure was pentaalanine. Pentaalanine was chosen as it demonstrates some inherent structural duality with an approximately 90:10 distribution of PPII helix to β-sheet conformation.[159-162] This made it a good candidate as it is not 'locked' in a single thermodynamically favourable folded structure, making the relatively weak interaction of the cyclodextrin with the guest more likely to have an observable effect.

The molecular device **54** was synthesised according to Scheme **3.1**. Amino-α-cyclodextrin **35** was prepared by the method discussed in Chapter 2, and coupled to commercially obtained *N*-Cbz-pentaalanine **50**. The crude reaction mixture was pipetted into ice-cold, stirring acetone to precipitate cyclodextrin and peptidic compounds, leaving the other species in solution. This work-up procedure was used during synthesis in Chapter 2 to isolate cyclodextrin-containing products and although the peptides used in this Chapter also precipitate in acetone, it has been used throughout the experimental procedures. The desired product **51** proved too polar to be purified by silica-based chromatography and too apolar to be purified by HP-20 chromatography. Solubility in HPLC solvents was poor, therefore in order to avoid lengthy HPLC purification, isolation was achieved by application to a cation exchange cartridge followed by an anion exchange cartridge. In aqueous solvent at neutral pH the cation and anion exchange cartridges retain the positively charged unreacted amino-α-cyclodextrin **35**, and the negatively charged *N*-Cbz-pentaalanine **50** respectively allowing the desired compound to elute through both solid phases. The Cbz-protected peptide **51** was thus prepared in a yield of 50% and this purification method used throughout the synthesis described in this Chapter.

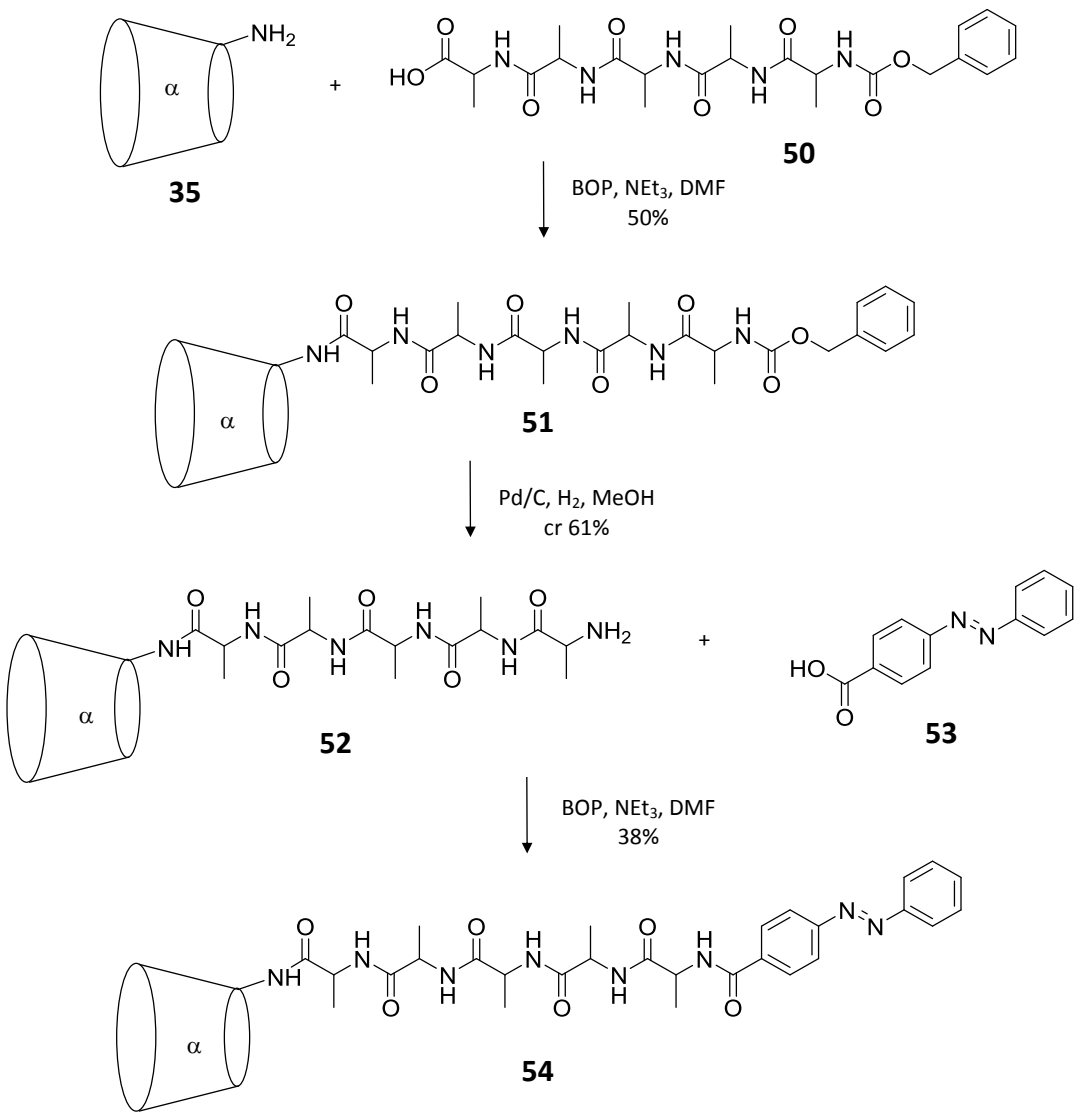

Scheme 3.1 Synthesis of the azobenzenyl peptide **54**.

The Cbz-protected peptide **51** was then deprotected using hydrogen and palladium on carbon reduction conditions. According to the ^{1}H NMR spectrum, this reaction proceeded to completion, therefore the deprotected peptide **52** was used with no further purification and a crude yield of 61% was recorded.

The peptide **52** was then coupled with 4-(phenylazo)benzoic acid **53**, and the desired azobenzenyl peptide **54** obtained by the previously described method of precipitation into acetone, followed by application to a cation and anion exchange column. This was then further purified by HPLC to give a yield of 38% with the ^{1}H NMR spectrum shown in Figure **3.2**.

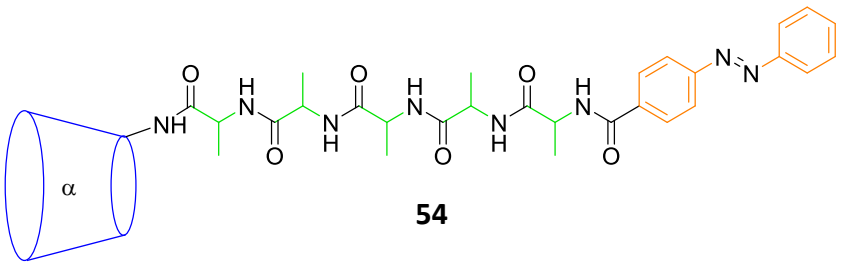

54

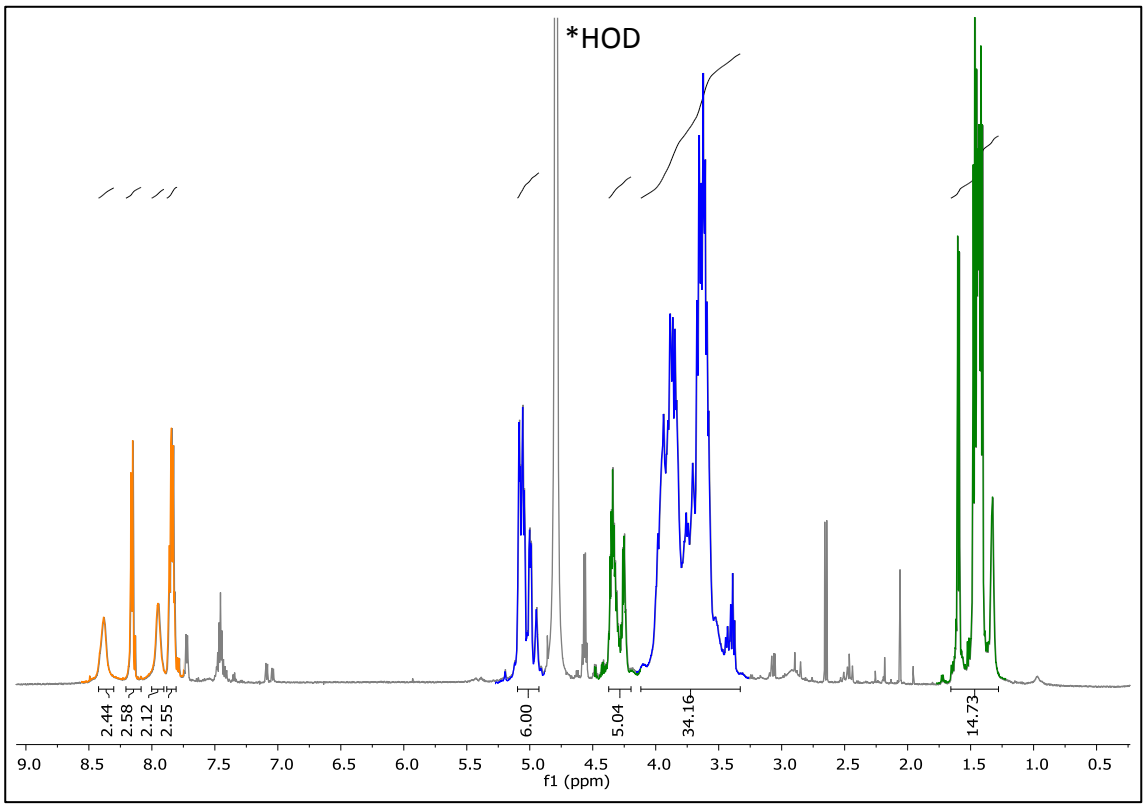

Figure 3.2 400 MHz ^{1}H NMR spectrum of the azobenzenyl peptide **54** (5 mM) in D_2O at 25 °C. Cyclodextrin proton signals are shown in blue, azobenzene proton signals in orange and alanine proton signals in green. *Denotes residual HOD solvent signal.

In aqueous solution at equilbrium the azobenzenyl peptide **54** may exist as the non-included [*a*1]-species, the self-included [*c*1]-complex and the [*c*2]-complex (Figure **3.3**) with higher oligomers possible but thermodynamically unlikely. In order to determine the nature of this equilibrium a dimer dissociation experiment was conducted using isothermal titration calorimetry (ITC).

The extent of any [*c*2]-dimer formation in equilibrium is concentration dependent, with a greater amount present at higher concentrations. In an ITC dimer dissociation experiment a solution with a high concentration of compound, where any [*c*2]-structure is most likely to prevail, is titrated from a syringe into a cell containing a blank solution. As the compound moves from a very high concentration to a very low concentration,

[*c*2]-dimer dissociates to monomeric species and the associated energy change is measured. As the titration progresses, the concentration of the compound in the cell increases thereby decreasing dimer dissociation and therefore energy change. The titration reaches an end point where the concentration in the cell is such that [*c*2]-complex no longer dissociates enough to be detectable. The data of energy change per mole of monomer vs equivalent monomer concentration can then be fitted to a dimer dissocation model curve and the dissociation constant (K_d) derived. From this, the association constant (K_a) can also be calculated ($K_a = 1/K_d$). A compound that does not form a concentration dependent species gives linear ITC data.

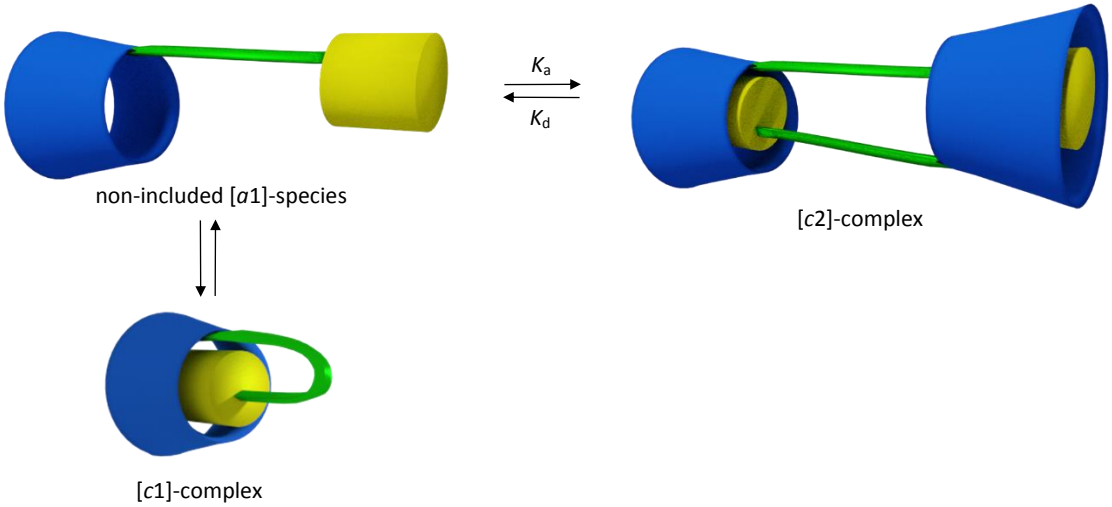

Figure 3.3 Conceptual image of the equilbirum between a non-included [*a*1]-species, a [*c*1]-complex and a [*c*2]-complex. Higher oligomer species are not shown.

An ITC dimer dissociation experiment was performed with the azobenzenyl peptide **54** using a syringe concentration of 5 mM. At lower concentrations a linear response of energy change with concentration was observed and the ITC data could not be fitted to a dimer dissociation model curve because a plateau was not reached. At higher concentrations the azobenzenyl peptide **54** precipitates such that heat of dissolution is measured during titrations, invalidating the measurements of heat of dimer dissociation.

Analysis of the ITC data shows a titration curve (Figure **3.4**) which fits a dimer dissociation model (Figure **3.5**) from which a K_d of 5.30 mM was derived, corresponding to a K_a of 188 M^{-1} ($K_a = 1/K_d$). The close fit to the dimeric model establishes that [*c*2]-dimer was present in the 5 mM azobenzenyl peptide **54** syringe solution. The measured K_d value can also be used to calculate the concentrations where either the [*c*2]-complex

or the monomer is predominant; above 240 mM the azobenzenyl peptide **54** exists as >90% dimer whereas at 0.33 mM it exists at >90% monomer (see Appendix A for calculations).

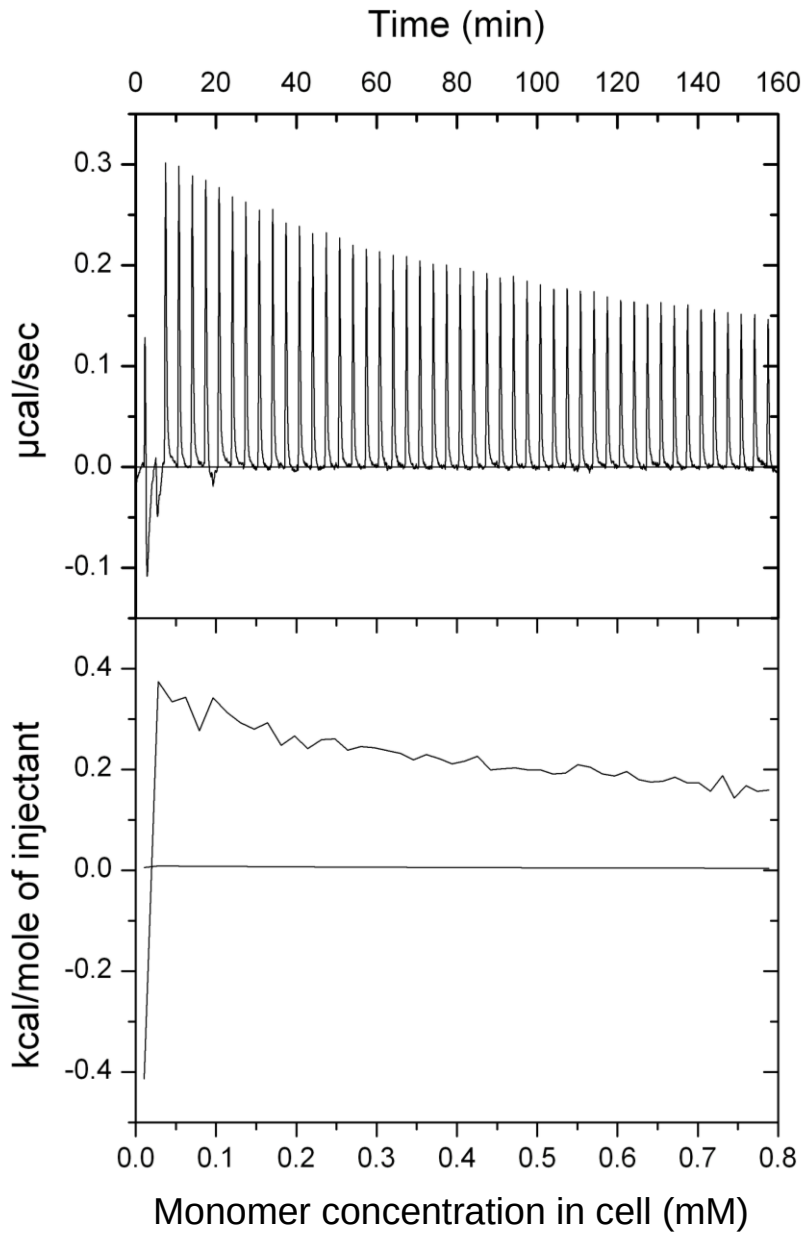

Figure 3.4 ITC data of the azobenzenyl peptide **54** (5 mM) with 5 µL injections into phosphate buffer (1.4365 mL, 5 mM, pH 7).

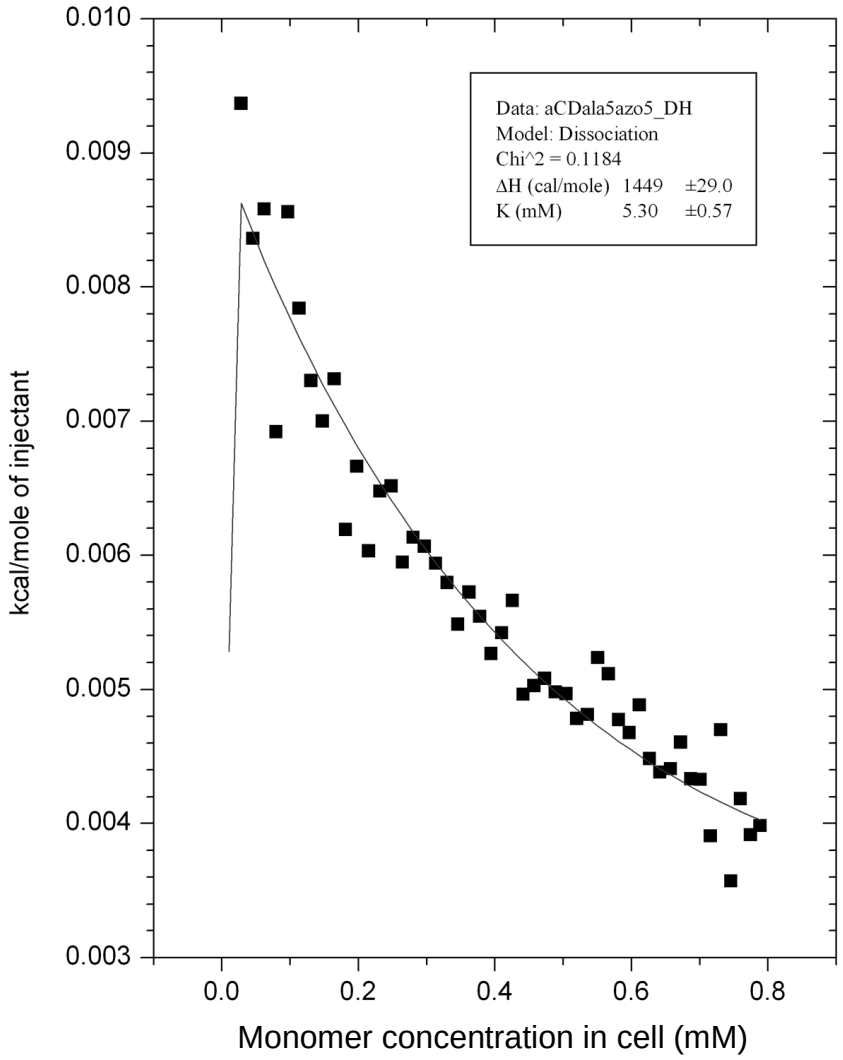

Figure 3.5 Fitted dimer dissociation curve to the azobenzenyl peptide **54** ITC data.

In order to assess whether the azobenzenyl peptide **54** forms species that assemble *via* cyclodextrin host-guest interactions, a 2D ^{1}H-^{1}H ROESY experiment (Figure **3.6**) was performed. Solubility limits of the azobenzenyl peptide **54** in aqueous conditions imposed a maximum concentration for this study of 5 mM. From the K_d value measured by ITC, this corresponds to 49% of the compound **54** existing as a dimer and 51% as a monomer. NOe cross-peaks are observed between cyclodextrin protons and azobenzene protons showing that the guest sits inside the host cavity, consistent with cyclodextrin host-guest interactions. It is unknown however, if the host-guest interactions result from the dimer complex, the monomeric complex or a contribution of both.

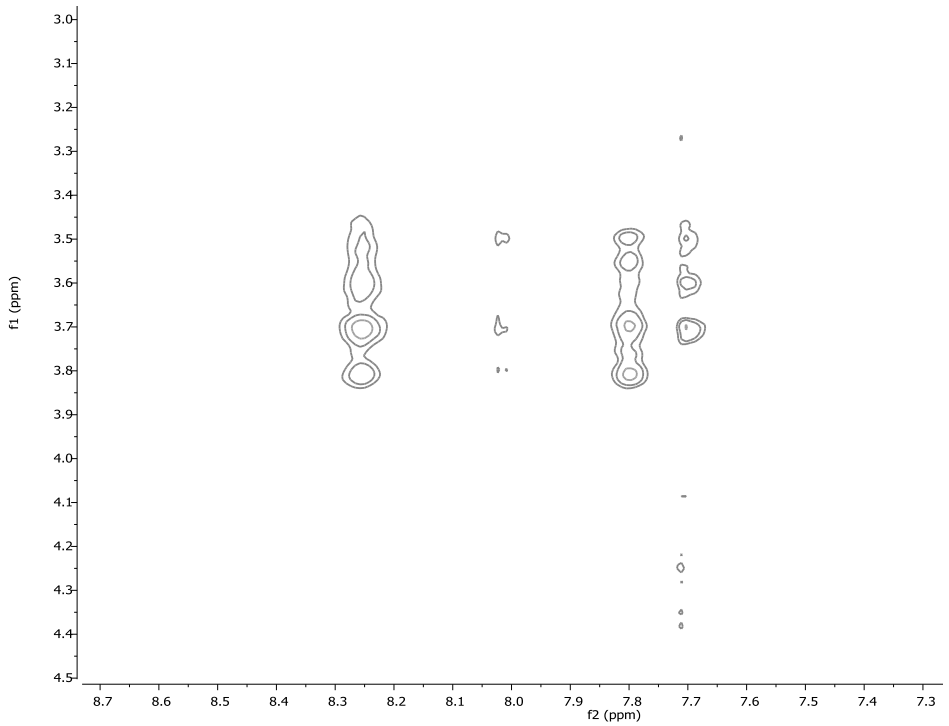

Figure 3.6 2D ^{1}H-^{1}H ROESY spectrum of the azobenzenyl peptide **54** (5 mM) in *d*-phosphate buffer (5 mM, pH 7) at 500 MHz.

Solubility limits preclude the measurement of a 2D ^{1}H-^{1}H ROESY spectrum at a high enough concentration that the azobenzenyl peptide **54** is mainly the dimer, and the sensitivity of the method also prevents measurement at a low enough concentration that a majority of monomer exists. Instead, circular dichroism spectroscopy was used as it involves analysis of solutions at low concentrations where monomer is present almost exclusively. The monomeric azobenzenyl peptide **54** was therefore evaluated to determine whether it exists as a non-included [*a*1]-species or a self-included [*c*1]-complex using circular dichroism spectroscopy.

When an achiral guest sits inside or very close to the cavity of a chiral host such as a cyclodextrin, induced Cotton effects arise at the wavelength that the guest absorbs. These are typically very weak signals compared to non-induced signals from chiral compounds. Positive induced signals arise when the polarised electronic transition of the guest (the $\pi \rightarrow \pi^*$ transition in azobenzene) is orbitally aligned parallel to the long axis of the host's cavity, and negative signals when the polarised electronic transition of the guest is perpendicular to the long axis of the host's cavity (Figure **3.7**).[163]

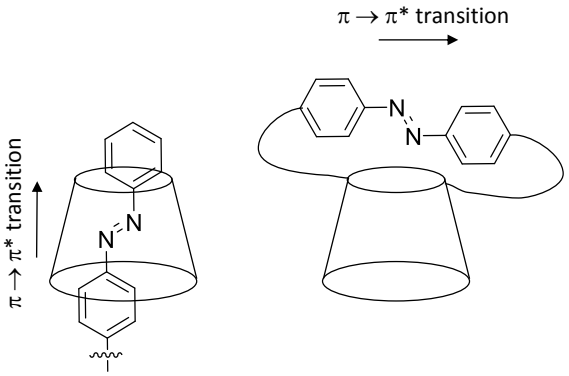

Figure 3.7 An azobenzene guest which lies with the $\pi \rightarrow \pi^*$ transition orbitally parallel with the long axis of the cavity of a cyclodextrin, such that occurs in an inclusion complex (*left*), exhibits positive induced Cotton effects in its circular dichroism spectra. An azobenzene guest which lies with the $\pi \rightarrow \pi^*$ transition perpendicular to the long axis of the cavity of a cyclodextrin (*right*) exhibits negative induced Cotton effects.[163]

A 50 μM solution of the azobenzenyl peptide **54** was analysed by circular dichroism spectroscopy (Figure **3.8**), a concentration at which according to the K_a value measured by ITC, 98% monomer is present. The spectrum shows a positive Cotton effect at 335 nm and a weaker positive signal at 240 nm, wavelengths very close to the λ_{max} in the UV-absorption spectrum of the azobenzenyl peptide **54**. The positive sign of the signals shows that azobenzene lies with its $\pi \rightarrow \pi^*$ transition orbitally parallel to the long axis of the cyclodextrin cavity, such as would occur in the formation of an inclusion complex. This demonstrates that the azobenzenyl peptide **54** monomer is present as a [*c*1]-complex, in a sufficient ratio compared to the [*a*1]-species to observe induced circular dichroism signals. Although the ratio of [*a*1]- to [*c*1]-species could not be determined, this study indicated that the [*c*1]-complex forms in a sufficient proportion to be likely to affect peptide structure, as induced Cotton effects are typically very weak and would be unlikely to be observable if an inclusion complex had formed in only a small amount. The effect on the secondary structure of the pentaalanine moiety was therefore investigated.

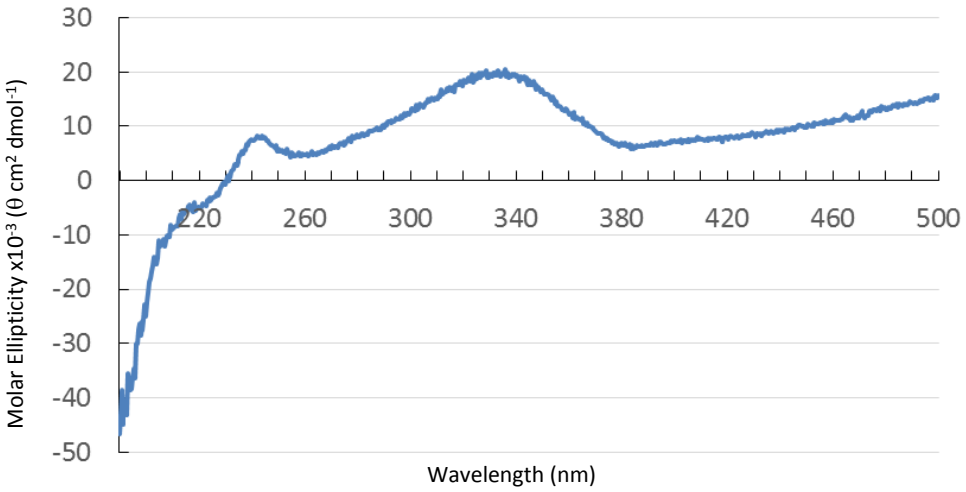

Figure 3.8 Circular dichroism spectrum of the azobenzenyl peptide **54** (50 μM) showing induced Cotton effects at 335 and 240 nm attributable to the inclusion of azobenzene in the chiral cyclodextrin cavity.

For comparison, the secondary structure of a pentaalanine without the influence of cyclodextrin host-guest complex formation was also ascertained, by measuring the circular dichroism spectra of commercially available *N*-Cbz-pentaalanine **50** (Figure **3.9**). Concentrations were used at which the azobenzenyl peptide **54** predominantly exists as the monomer. Spectra at a range of concentrations were measured in order to rule out any concentration-dependent effects, with the highest concentration being the maximum possible before saturation of the detector, and the lowest being the minimum where the signal to noise ratio was acceptable. Spectra of *N*-Cbz-pentaalanine **50** exhibited a strong minimum at 196 nm, a signal characteristic of PPII helices. Although this minimum is very close to the minimum observed in random coil structures, previous studies have established by NMR spectroscopy that pentaalanine exists as a PPII helix.[159-162]

The circular dichroism spectra of the azobenzenyl peptide **54** were then measured (Figure **3.10**) and show a negative signal with maximum molar ellipticity at 190-193 nm, consistent with random coil peptide structure. The absence of a minimum at 196 nm indicates substantial disruption of the PPII helix structure observed in *N*-Cbz-pentaalanine **50**, however complete loss of PPII helix is difficult to affirm as the 190-193 nm signal could be masking a shoulder.

This modification of peptide structure is likely to be a consequence of significant [*c*1]-complex formation as such effects are unlikely to arise from the presence of a non-included [*a*1]-structure, which only differs from *N*-Cbz-pentaalanine **50** in that the termini of the peptide are modified.

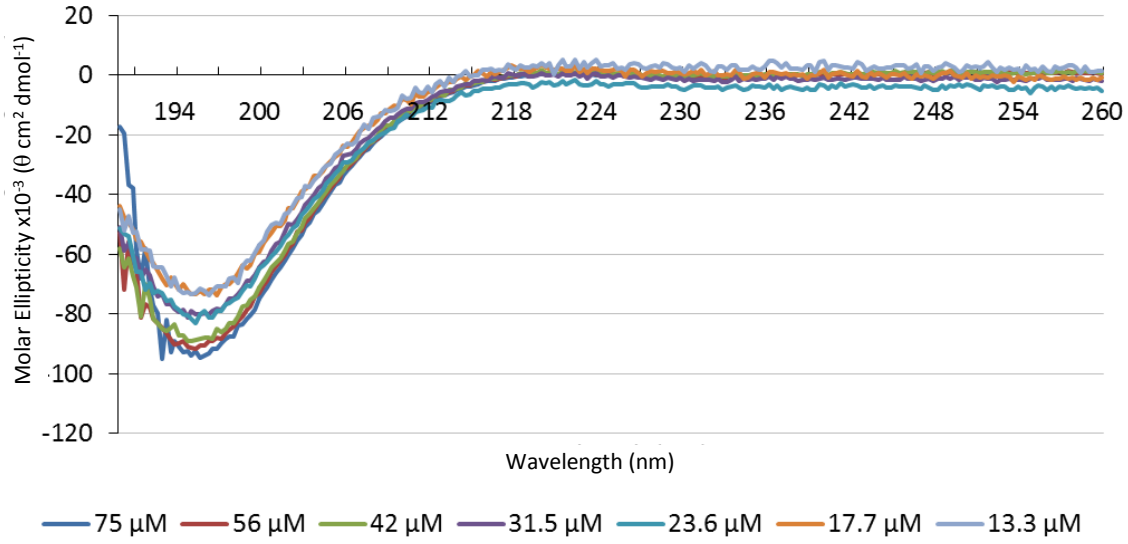

Figure 3.9 Circular dichroism spectra of *N*-Cbz-pentaalanine **50** (13.3-75 µM).

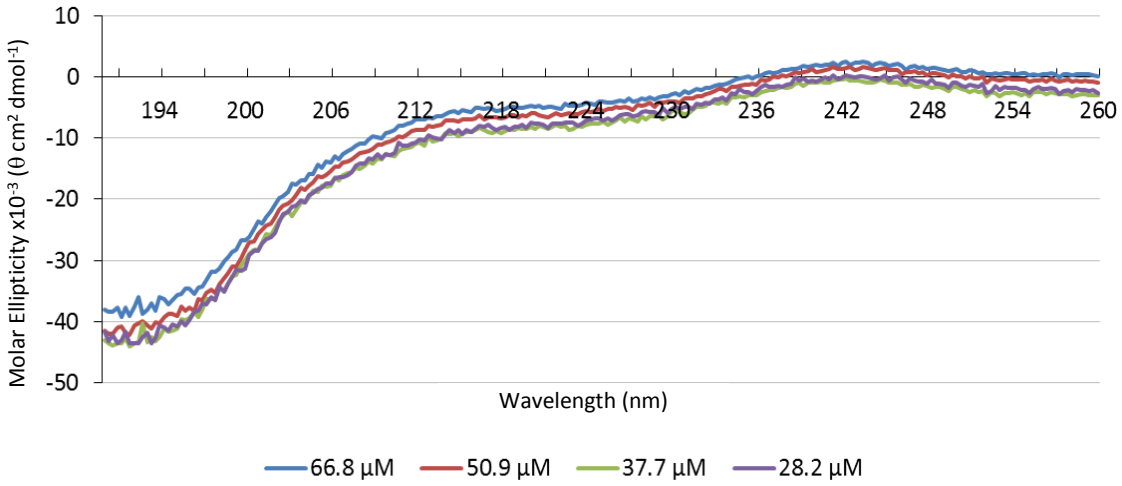

Figure 3.10 Circular dichroism spectra of the azobenzenyl peptide **54** (28.2-66.8 µM).

An azobenzene is known to reversibly isomerise between *trans* and *cis* conformations with the use of photo-irradiation and optimal wavelengths of 360 nm to convert to the *cis* and 420 nm to convert to the *trans* isomer have been established.[154-158] It is also known that this photoisomerisation process switches the propensity for azobenzene-

cyclodextrin host-guest complexation between being favoured to highly unfavoured, as the *trans* isomer has a much higher affinity for the α-cyclodextrin cavity than the *cis* isomer. Cyclodextrin host-guest interactions in the azobenzenyl peptide **54** appeared to affect pentaalanine structure, therefore photoisomerisation of the azobenzene was investigated to examine the effect on complexation propensity and peptide structure.

In order to examine the photoswitchable behaviour, analytical HPLC was used to observe the ratio of the *trans* azobenzenyl peptide **54** and its *cis* isomer during irradiation cycles. The isosbestic point of the *trans* azobenzenyl peptide **54** and its *cis* isomer in their UV-vis sepctra (the wavelength at which both compounds absorb equally) was determined. HPLC analysis at this wavelength then allowed direct comparison of the integrations of the isomer peaks to determine relative ratios, without the requirement of calibration curves.

The UV-vis spectrum of the *trans* azobenzenyl peptide **54** was measured before irradiation (Figure **3.11**) to determine the absorbance profile of this isomer. The *trans* azobenzenyl peptide **54** was then irradiated at 360 nm, the optimum wavelength for isomerisation of *trans* azobenzene to the *cis* isomer, in 30 second bursts with the UV-vis spectrum measured after each irradiation. Short exposures were used in order to track the change in the UV-profile as the *trans* azobenzenyl peptide **54** was converted to its *cis* isomer, until a new photostationary state was reached where the UV-profile showed no further change with irradiation at 360 nm. The isosbestic points of the *trans* azobenzenyl peptide **54** and its *cis* isomer, where absorbance is the same in both, could then be identified. Several such points were observed, however 293 nm was chosen for HPLC analysis as both isomers absorb significantly here, improving signal to noise and enabling more accurate peak integration.

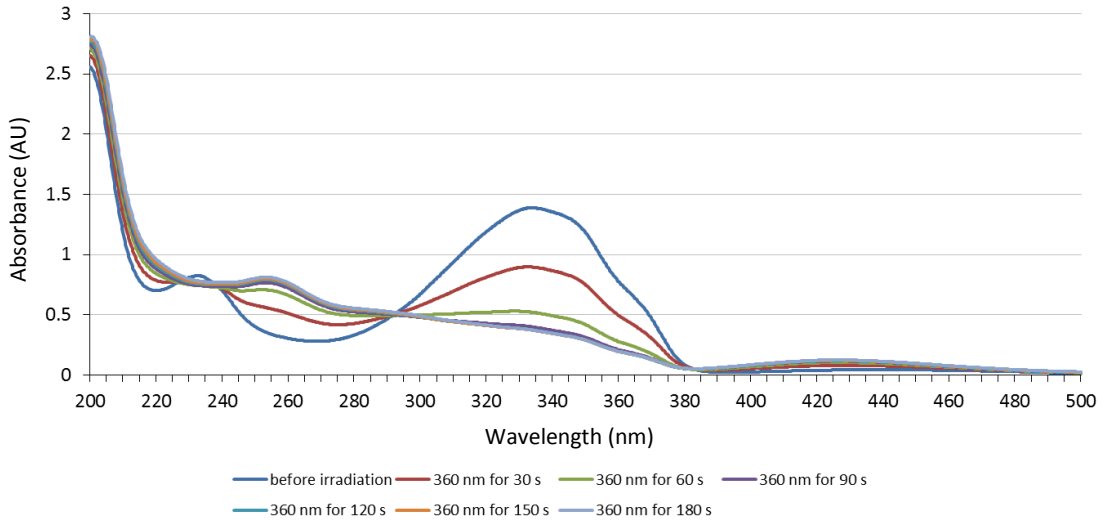

Figure 3.11 UV-vis absorbance spectra of the azobenzenyl peptide **54** during irradiation at 360 nm.

A solution of the azobenzenyl peptide **54** (50 μM) was therefore analysed by HPLC at 293 nm at a concentration where the monomer is the dominant species, separation of peaks is good and absorbance is strong enough to give a good signal to noise ratio. Two peaks were observed in the HPLC trace and assigned as the *trans* azobenzenyl peptide **54** and its *cis* isomer as they absorb at the expected wavelength and exhibit the expected behaviour during photoirradiation. After irradiation of the azobenzenyl peptide **54** at 360 nm, the smallest peak was assigned as the *trans* isomer and the largest as the *cis* isomer. After irradiation at 420 nm, the known optimum wavelength for the conversion of a *cis* azobenzene to the *trans* isomer, the HPLC peak assigned to the *trans* isomer greatly increased in intensity and the peak assigned to the *cis* isomer greatly decreased. The adherence of the peaks changes upon irradiation to expected photochemical behaviour provides strong evidence for their assignment as the *trans* azobenzenyl peptide **54** and its *cis* isomer.

HPLC analysis of the azobenzenyl peptide **54** was performed over four photochemical cycles, wherein the solution was irradiated at 360 nm for 10 min (half-cycles) then at 420 nm for 10 min (full cycles). Each irradiation was conducted for a long enough period to achieve maximum extent of isomerisation, as determined by UV-absorbance spectra over the course of irradiation (Figure **3.11**). Integration of the isomer HPLC peaks during each cycle (Figure **3.12**) shows that the azobenzenyl peptide **54** undergoes expected photoisomerisation,[164] with the level of *trans* isomer switched between 95% and 28%

during irradiation cycles. The proportions of each isomer are constant in each progressive switching cycle and no additional HPLC peaks were observed, showing that no photochemical degradation occurs.

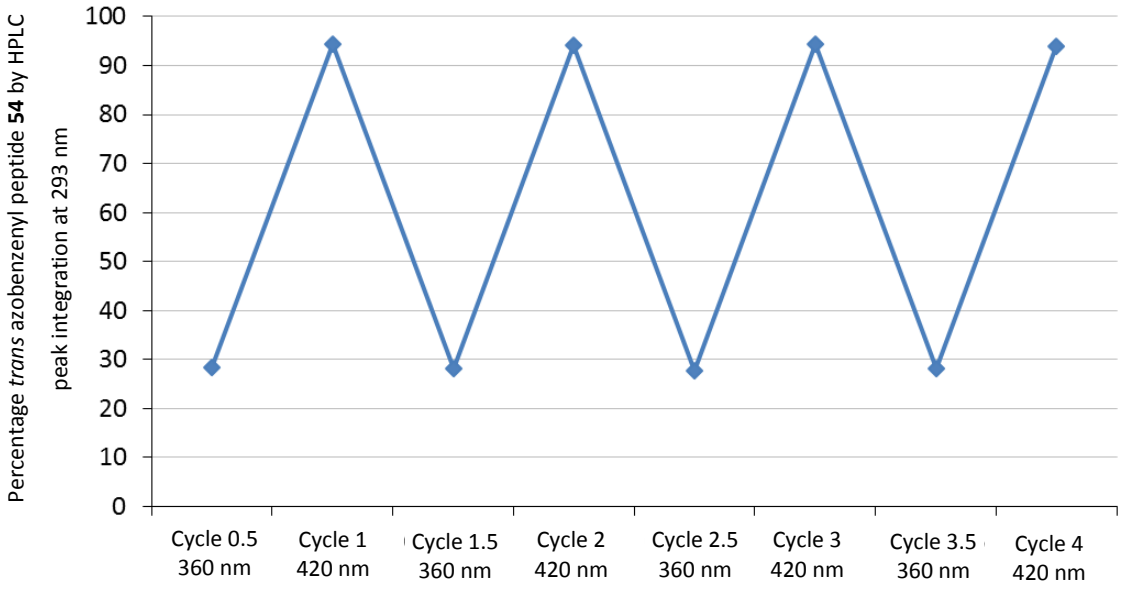

Figure 3.12 Percentage *trans* azobenzenyl peptide **54** during irradiation cycles of a 50 μM solution.

Having determined that the azobenzenyl peptide **54** undergoes *trans-cis* photoisomerisation, the effect of this on pentaalanine secondary structure was assessed by circular dichroism spectroscopy. A solution of the azobenzenyl peptide **54** (16.5 μM) was analysed before irradiation, after irradiation at 360 nm and again after irradiation at 420 nm (Figure **3.13**). The spectrum before irradiation, when the azobenzenyl peptide **54** exists as the *trans* isomer, shows a minimum at 190-193 nm, indicative of a random coil peptide structure. When the compound is irradiated at 360 nm switching the azobenzene to the *cis* isomer, the spectrum shows a large increase in the maximum negative molar ellipticity and a strong minimum is observed at 196 nm, characteristic of PPII helix and matching the signal observed with *N*-Cbz-pentaalanine **50** (Figure **3.9**). Irradiation at 420 nm to give the *trans* azobenzenyl peptide **54** restores the circular dichroism spectroscopy signal to that observed before irradiation.

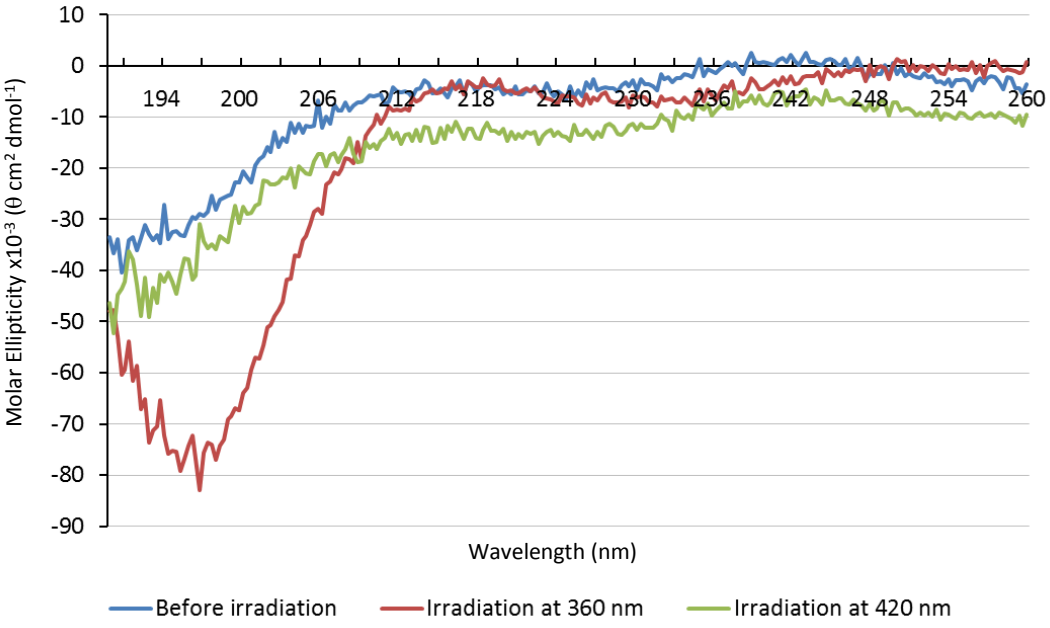

Figure 3.13 Circular dichroism spectra of the azobenzenyl peptide **54** (16.5 μM) at different stages of photoirradiation.

The secondary structure of the pentaalanine moiety in the azobenzenyl peptide **54** was observed over four photochemical cycles by circular dichroism spectroscopy (Figure **3.14**). Photoswitching between *trans* and *cis* isomers results in the reversible and repeatable switching of pentaalanine structure between states of extensive PPII helicity and random coil/greatly reduced PPII helicity.

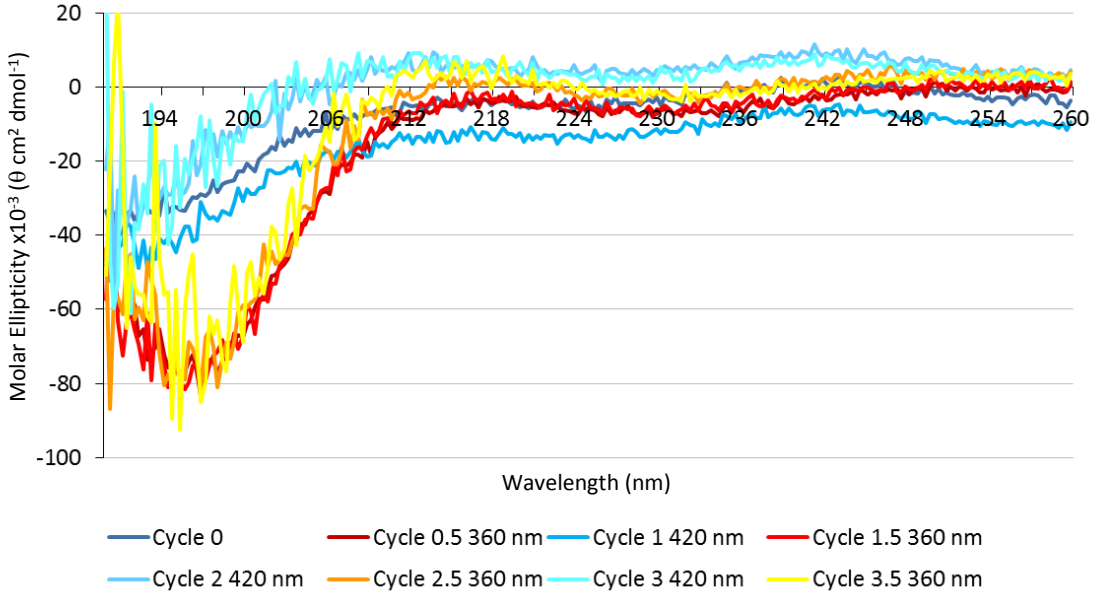

Figure 3.14 Circular dichroism spectra of the azobenzenyl-peptide **54** (16.5 μM) over multiple cycles of photoirradiation.

Monomeric species are predominant at the concentration where the circular dichroism spectra were measured, therefore the photoswitching between azobenzene isomers that produces switching of peptide structure is attributable to conversion between a non-included [*a*1]-species and a [*c*1]-complex. That the circular dichroism spectrum of the *cis* isomer is the same as that observed with *N*-Cbz-pentaalanine **50** confirms that the *cis* isomer favours an [*a*1]-structure. The azobenzenyl peptide **54** can therefore act as a molecular switch, where photoisomeriation is the input to switch between the favouring of complexed and uncomplexed structures, resulting in switching of the extent of PPII helicity in peptide structure.

3.3 Effect of the Strength of the Cyclodextrin Host-Guest Interaction

The azobenzenyl peptide **54** described in Section 3.2 was found to exhibit a change in peptide secondary structure upon cyclodextrin host-guest complexation, and it is logical that the strength of this interaction would affect the extent of structure change. In order to test this hypothesis, the Cbz-protected peptide **51**, prepared during the synthesis of the azobenzenyl peptide **54**, was also investigated for effect on peptide structure as a result of cyclodextrin host-guest inclusion formation. A free phenyl guest has a lower K_a with α-cyclodextrin than a free azobenzene guest,[165] therefore it seemed likely that a smaller effect on peptide structure would be observed with the Cbz-protected peptide **51** compared to the azobenzenyl peptide **54**.

An ITC dimer dissociation experiment was performed with the Cbz-protected peptide **51** in an attempt to determine the K_a of dimer association and derive the proportion of dimer present at different concentrations. Using a syringe solution at 3 mM however, the noise to signal ratio of the resulting titration was too high for a dimer dissociation curve to be fitted to the data. The Cbz-protected peptide **51** was insoluble at higher concentrations, adding energy of dissolution to the titrations which invalidates the measurement of energy of dimer dissociation. Nevertheless, the ITC data indicates a weaker dimer interaction than was observed with the azobenzenyl peptide **54** as less dissociation energy was detected at a similar concentration, suggesting less dimer present in the syringe solution.

Although ITC dimer dissociation data could not be obtained, the presence of cyclodextrin host-guest complexes in the Cbz-protected peptide **51** could be explored by 2D ^{1}H-^{1}H ROESY NMR spectroscopy. A spectrum was obtained with a peptide **51** solution at 3 mM (Figure **3.16**) with the 1D ^{1}H NMR spectrum shown in Figure **3.15**.

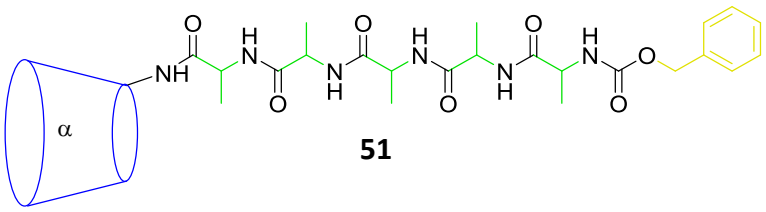

51

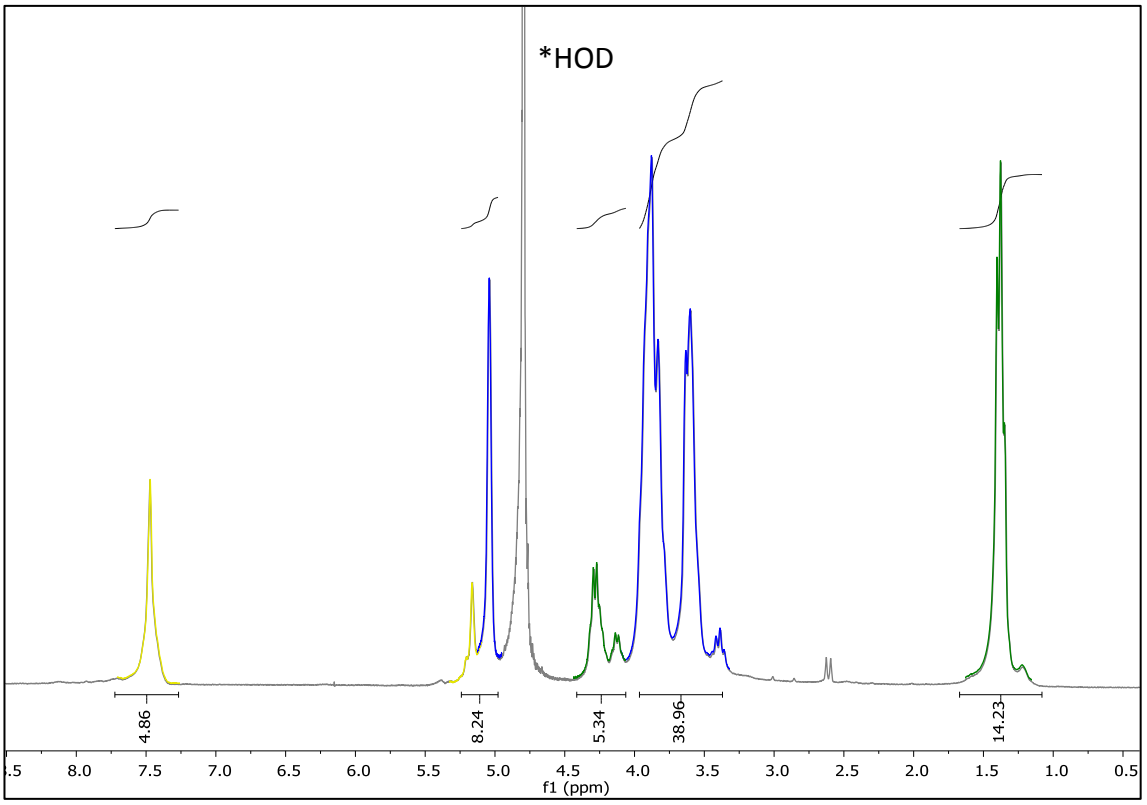

Figure 3.15 400 MHz ^{1}H NMR spectrum of the Cbz-protected peptide **51** (3 mM) in D_2O at 25 °C. Cyclodextrin proton signals are shown in blue, Cbz guest proton signals in yellow and alanine proton signals in green. *Denotes residual HOD solvent signal.

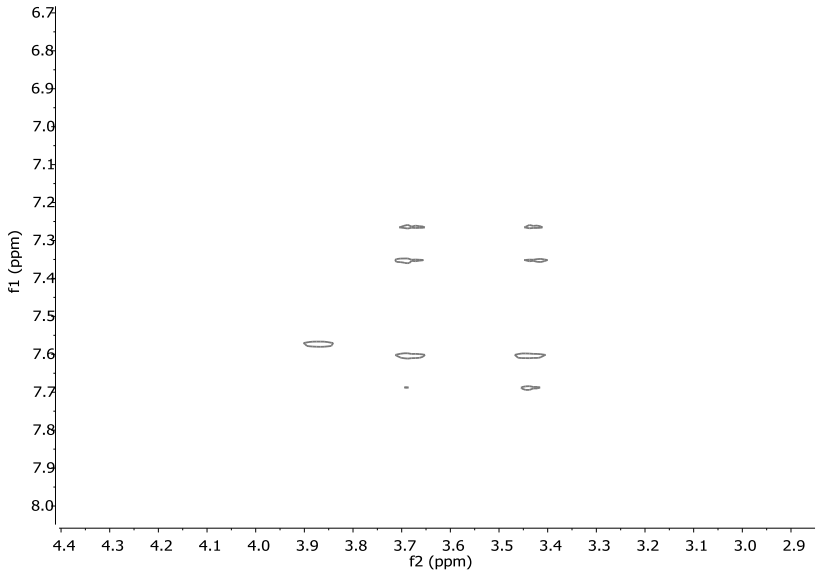

Figure 3.16 2D ^{1}H-^{1}H ROESY spectrum of the Cbz-protected peptide **51** (3 mM) in *d*-phosphate buffer (5 mM, pH 7) at 500 MHz.

The 2D ^{1}H-^{1}H ROESY spectrum shows nOe cross-peaks between cyclodextrin protons and the Cbz protons indicating that host-guest inclusion complexes are formed, however they are very weak in comparison to those observed with the azobenzenyl peptide **54**. Although this is strictly a qualitative observation it provides additional evidence that the interaction between the host and guest with the Cbz-protected peptide **51** is weaker than that with the azobenzenyl peptide **54**.

As ITC data indicated that dimer formation by the Cbz-protected peptide **51** is weaker than for the azobenzenyl peptide **54**, investigation of the peptide structure with the Cbz-protected peptide **51** was focussed on the monomeric species. ITC suggests that the azobenzenyl peptide **54** forms a higher proportion of dimer than the Cbz-protected peptide **51** at a similar concentration, so concentrations of less than 50 μM were used to study the monomeric Cbz-protected peptide **51**, as at this concentration the azobenzenyl peptide **54** exists as 98% monomer, meaning that the Cbz-protected peptide **51** must exist as >98% monomer.

The circular dichroism spectrum of the Cbz-protected peptide **51** was examined for induced Cotton effects arising from Cbz inclusion, however no such signals could be detected. This is consistent with the proportion of [*a*1]-species being higher for the Cbz-protected peptide **51** than for the azobenzenyl peptide **54**.

Having established that less [*c*1]-complex is formed, circular dichroism spectroscopy was used to investigate the effect on pentaalanine structure. The circular dichroism spectra of the Cbz-protected peptide **51** at 37.2-11.8 μM were measured (Figure **3.17**), and show a strong minimum at 195 nm. Comparing these spectra to those obtained for *N*-Cbz-pentaalanine **50** (Figure **3.9**), only a small decrease in the extent of molar ellipticity and only a very small shift in wavelength occurs with the Cbz-protected peptide **51**, indicative of little reduction in pentaalanine PPII helicity.

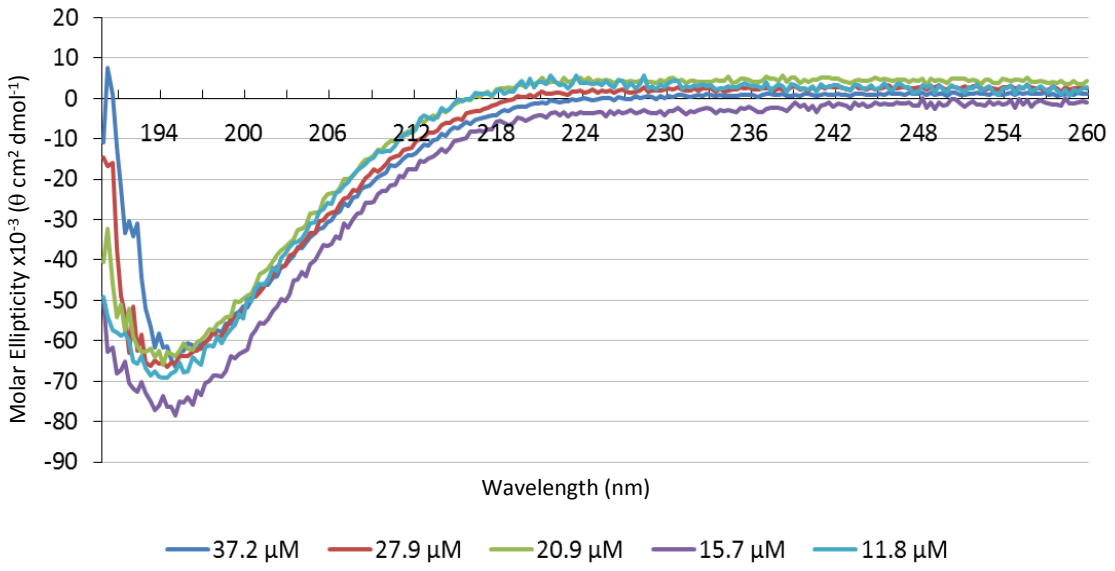

Figure 3.17 Circular dichroism spectra of the Cbz-protected peptide **51** (11.8-37.2 μM) in phosphate buffer (5 mM, pH 7).

Compared to the changes in peptide structure observed with the azobenzenyl peptide **54** (Figure **3.10**), the modification of pentaalanine structure in the Cbz-protected peptide **51** from that observed with *N*-Cbz-pentaalanine **50** is small, reflective of the weaker host-guest interaction and the presence of less [*c*1]-complex. This indicated that in a construct with a host-guest interaction stronger than that with the azobenzenyl peptide **54**, a stronger effect on peptide structure might be observed. A system was therefore designed to maximise the cyclodextrin host-guest recognition, and a β-cyclodextrin and adamantane, known to have a very high binding affinity,[166] were incorporated into the construction of the proposed molecular device **60** (Scheme **3.2**).

In a method analogous to that used for the synthesis of amino-α-cyclodextrin **35** described in Chapter 2, amino-β-cyclodextrin **56** was prepared by reduction of azido-β-

cyclodextrin (synthesised previously in the group[167]) and the product was isolated by cation exchange column chromatography in a 33% yield.

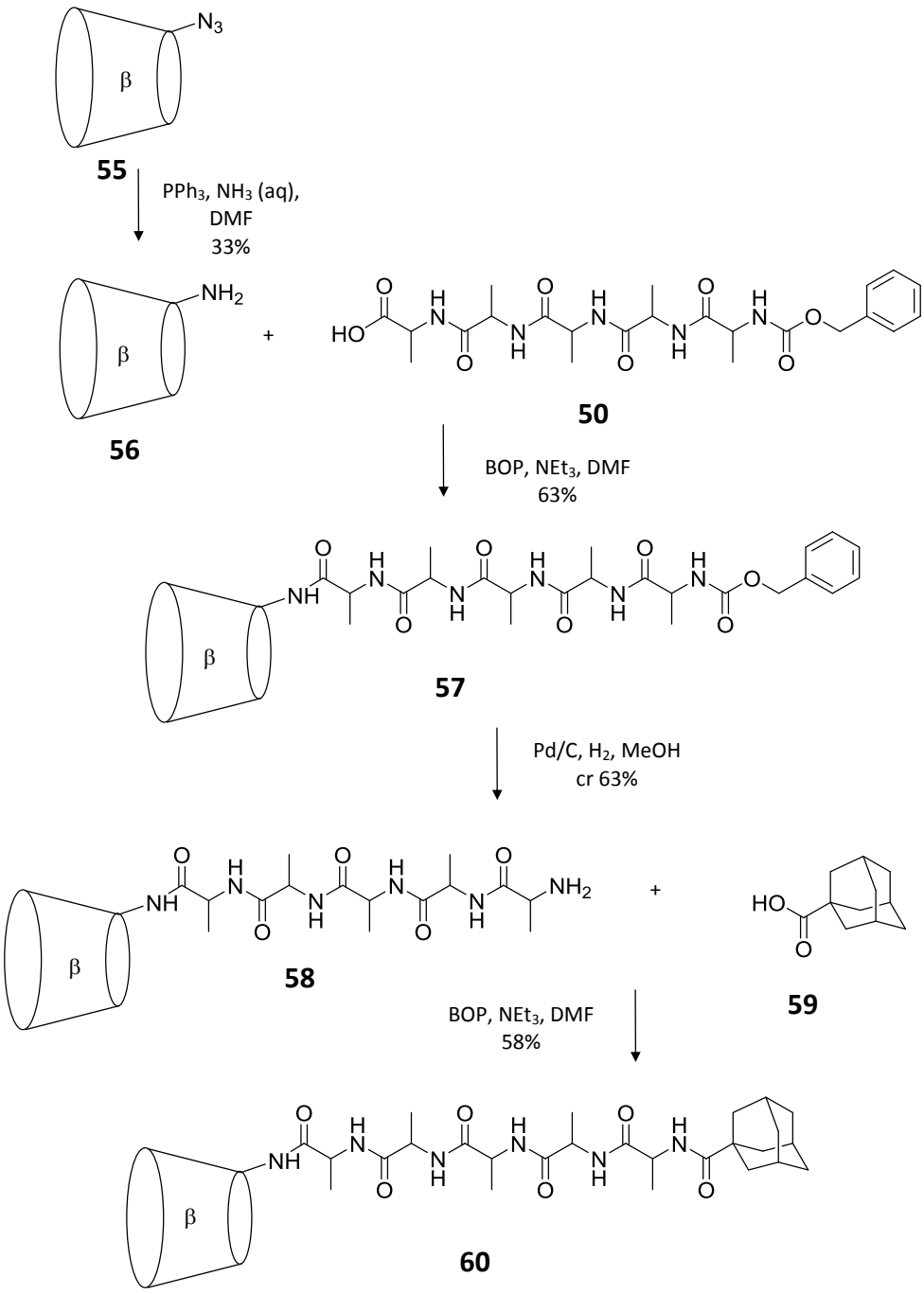

Scheme 3.2 Synthesis of the adamantyl peptide **60**.

Experimental conditions similar to those used for the synthesis of the azobenzenyl peptide **54** were then followed. Amino-β-cyclodextrin **56** was coupled to *N*-Cbz-pentaalanine **50** and the Cbz-protected peptide **57** isolated by application to a cation- then anion-exchange column to give a yield of 63%. The Cbz protecting group was removed by reduction to give the peptide **58** in a crude yield of 63%. As the ^{1}H NMR

spectrum indicated complete deprotection, the compound was used with no further purification. The peptide **58** was coupled to 1-carboxyadamantane **59** and the desired adamantyl peptide **60** isolated in a 58% yield by application to a cation- then anion-exchange column. The ^{1}H NMR spectrum of the adamantyl peptide **60** is shown in Figure **3.18**.

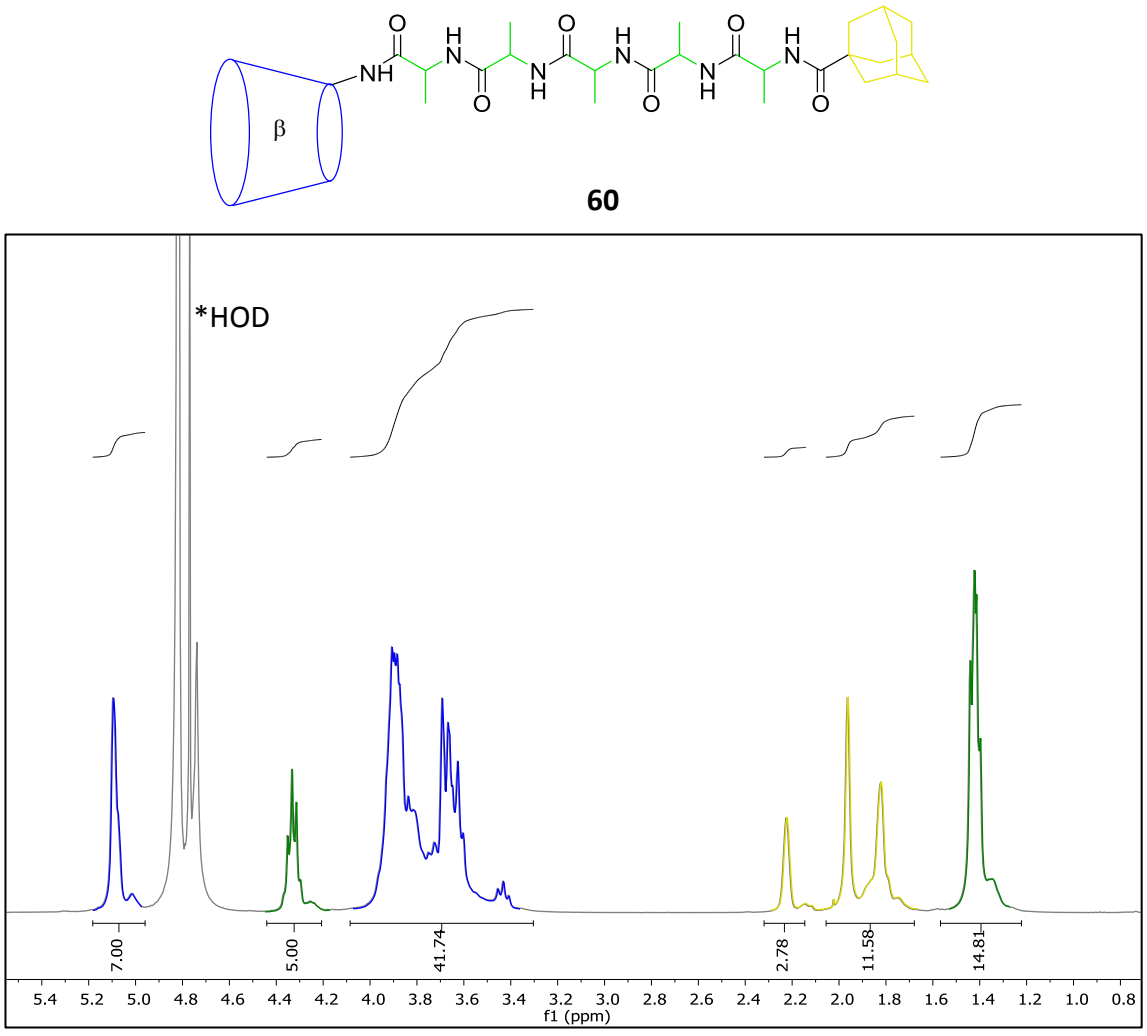

60

Figure 3.18 400 MHz ^{1}H NMR spectrum of the adamantyl peptide **60** (3 mM) in D_2O at 25 °C. Cyclodextrin proton signals are shown in blue, adamantane guest proton signals in yellow and alanine proton signals in green. *Denotes residual HOD solvent signal.

An ITC dimer dissociation experiment was conducted with the adamantyl peptide **60** in order to determine the K_a of dimer association and derive the proportion of dimer present at different concentrations. A 3 mM syringe solution of the adamantyl peptide **60** in phosphate buffer was titrated into a blank phosphate buffer solution (Figure **3.19**). The data were fitted to a dimer dissociation curve (Figure **3.20**) from which a K_d of 0.359 mM was derived, corresponding to a K_a of 2786 M^{-1} ($K_a = 1/K_d$). As with the ITC data

obtained from the azobenzenyl peptide **54** dimer dissociation, the close fit to the dimeric model establishes that a [*c*2]-dimer was present in the 3 mM adamantyl peptide **60** syringe solution. The measured K_d value can also be used to calculate the concentrations where either the [*c*2]-complex or the monomer is predominant; at 16 mM the adamantyl peptide **60** exists as over 90% dimer and at 0.02 mM exists as over 90% monomer (see Appendix A for calculations).

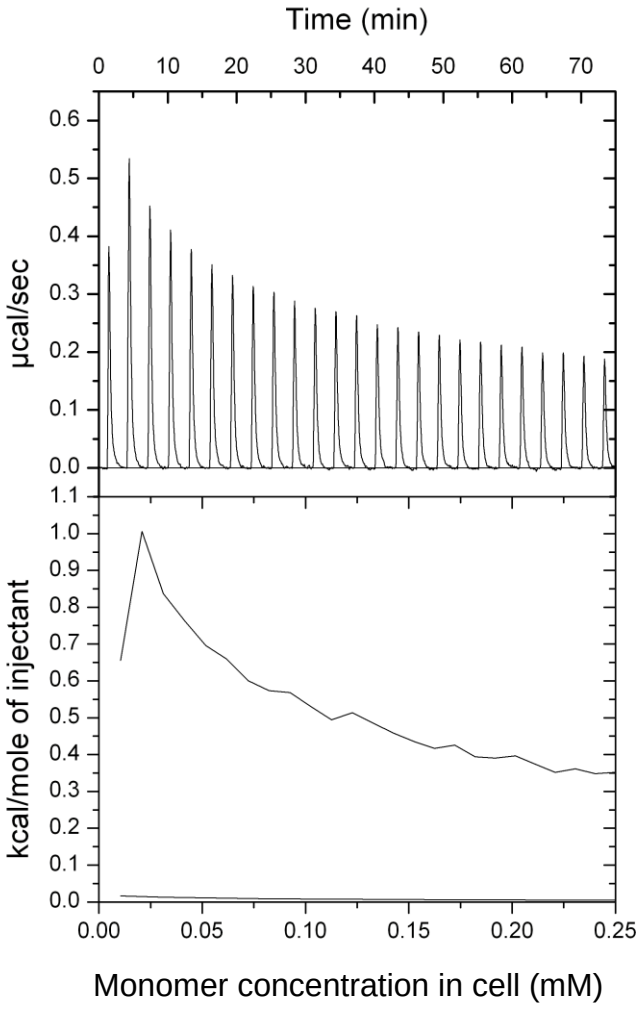

Figure 3.19 ITC data of the adamantyl peptide **60** (3 mM) with 5 µL injections in phosphate buffer (1.4365 mL, 5 mM, pH 7).

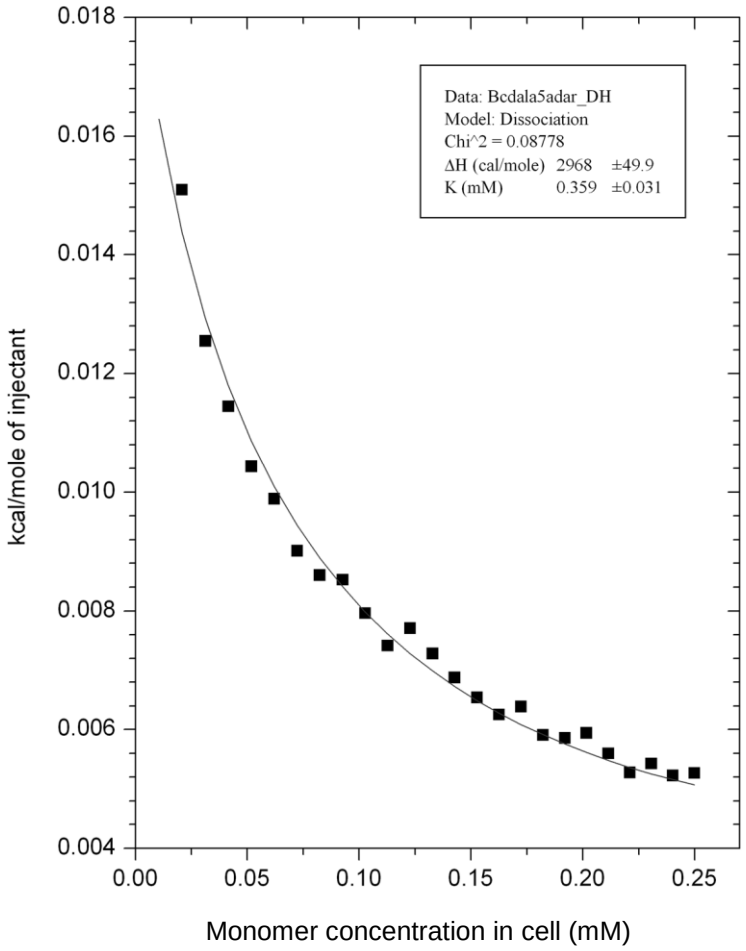

Figure 3.20 Fitted dimer dissociation curve to the adamantyl peptide **60** ITC data.

The higher K_a of adamantyl peptide **60** dimer association compared to azobenzenyl peptide **54** dimer association indicates stronger dimer-forming interactions. To examine cyclodextrin host-guest interactions in adamantyl peptide **60** solutions, 2D ^{1}H-^{1}H ROESY NMR spectroscopy was performed at 3 mM (Figure **3.21**). From the K_d value measured by ITC this corresponds to 78% of the peptide **60** existing as a dimer and 22% as a monomer. The spectrum shows nOe peaks between the cyclodextrin host and the adamantane guest demonstrating that at this concentration the guest sits inside the host cavity, strongly suggesting that the dimer observed by ITC is assembled *via* cyclodextrin host-guest interactions. As the extent of monomer at this concentration is fairly low, it is unlikely that the nOe signals observed in the 2D ^{1}H-^{1}H ROESY spectrum arise solely from a monomeric complex, however it is unkown if they result exclusively from the dimeric complex, or both species.

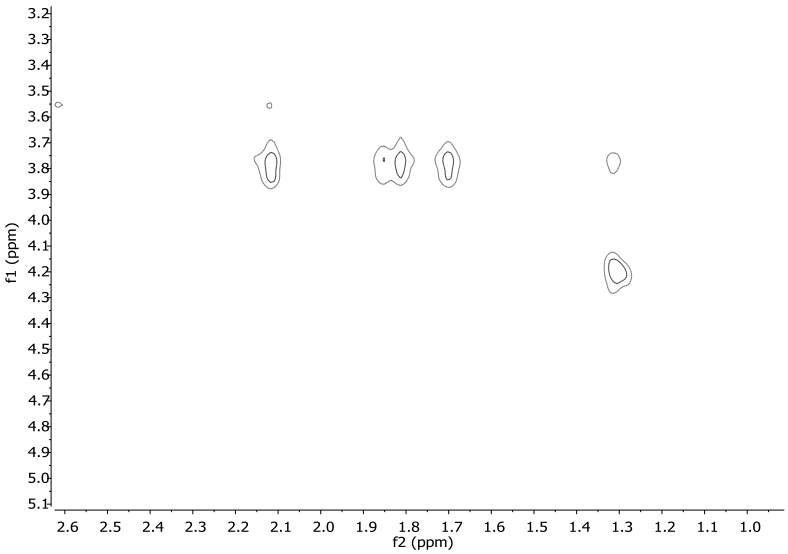

Figure 3.21 2D ^{1}H-^{1}H ROESY spectrum of the adamantyl peptide **60** (3 mM) in *d*-phosphate buffer (5 mM, pH 7) at 500 MHz.

As sensitivity constraints of the method preclude measurement of a 2D ^{1}H-^{1}H ROESY NMR spectrum of adamantyl peptide **60** at a low concentration where the monomeric species is predominant, the presence of a [*c*1]-complex formed by cyclodextrin host-guest interactions could not be investigated using this technique. Induced circular dichroism was also unsuitable as a method for detection of induced Cotton effects associated with any [*c*1]-complex, as the adamantane guest does not absorb at a wavelength separate to the peptide.

Instead, the effect of adamantyl peptide **60** [*c*2]-complex formation on pentaalanine structure was examined. The circular dichroism spectrum of the adamantyl peptide **60** at 2.7 mM (with the use of a 0.1 mm pathlength cuvette) corresponding to 77% dimer was recorded, showing a signal with a maximum at 196 nm and a minimum at 203 nm (Figure **3.22**). Although a specific type of secondary structure cannot be assigned, it can be concluded that formation of the [*c*2]-complex brings about a complete disordering of pentaalanine PPII helix, as no minimum at ~196 nm is observed.

Circular dichroism spectra of adamantyl peptide **60** were also recorded at concentrations where the monomer is the major species. The circular dichroism spectra of the adamantyl peptide **60** (Figure **3.22**) at 15.8-100 μM, corresponding to 92-72% monomer, show signals with a strong minimum at 199 nm. Molar ellipticity at 196 nm, the wavelength at which the PPII helix in *N*-Cbz-pentaalanine **50** absorbs (Figure **3.9**), is

roughly halved showing that the peptide is at least half unfolded in the adamantyl system **60**. It is unclear however, if the minimum at 199 nm is a result of remaining PPII helix, random coil structure or a different type of structure. The circular dichroism spectra of the adamantyl peptide **60** also show a shoulder at 214-222 nm. This suggests two possible explanations. One is where a mixture of [*c*1]-complex and [*a*1]-species exists, with the complexed structure contributing to a β-sheet signal at 214-222 nm and loss of PPII helicity, and the uncomplexed structure resulting in residual PPII helical signal. Another possibility is that the adamantyl peptide **60** exists mainly as a [*c*1]-complex which folds the pentaalanine into a β-turn, a structure which exhibits a circular dichroism signal similar to that observed, with minima at both ~199 nm and ~218 nm.[168]

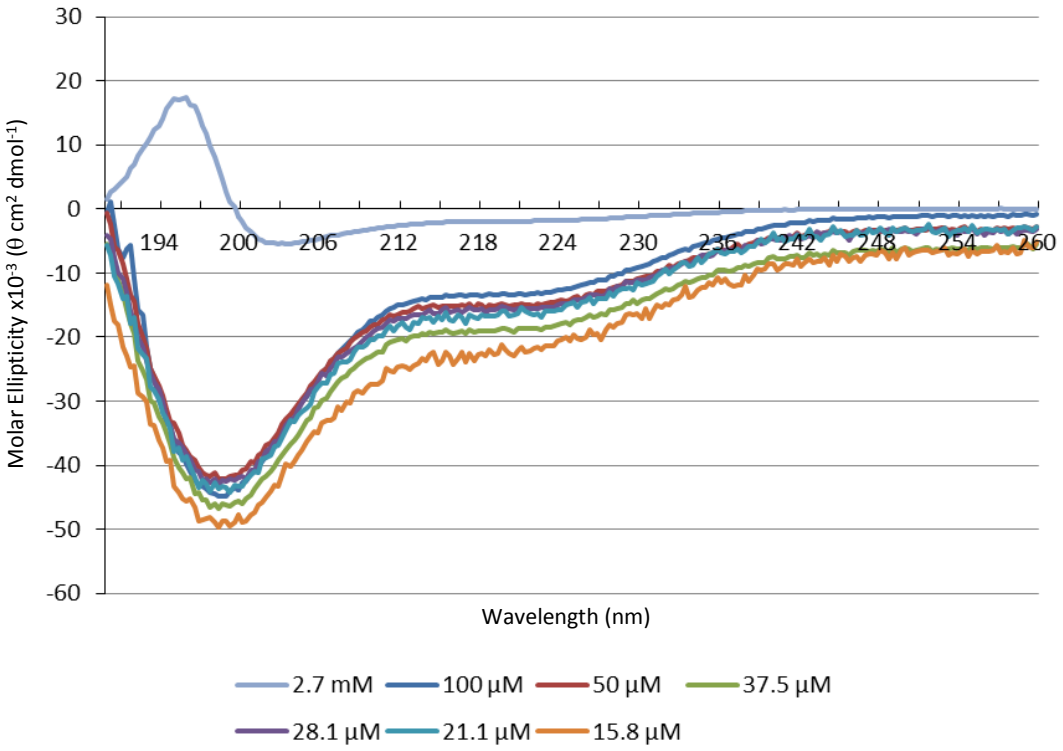

Figure 3.22 Circular dichroism spectra of the adamantyl peptide **60** (15.8 µM-2.7 mM) in phosphate buffer (5 mM, pH 7).

3.4 Thermodynamics of Peptide Structure Transition in Molecular Devices

Having studied the Cbz-protected peptide **51**, the azobenzenyl peptide **54** and the adamantyl peptide **60** at 20 °C, the thermal profiles of the circular dichroism spectra of these compounds were investigated. For comparison, pentaalanine **61** was also studied, prepared by deprotection of *N*-Cbz-pentaalanine **50** in a 68% yield.

Circular dichroism spectra of pentaalanine **61** were recorded from 5 to 90 °C at 5 °C increments (Figure **3.23**). After each spectrum measurement, the temperature was returned to 20 °C and the spectrum re-measured in order to ensure that changes in peptide structure were reversible. As the peptide is heated, the signal at 194 nm undergoes a loss of molar ellipticity and the minimum wavelength is red-shifted, consistent with unfolding of a PPII helix.

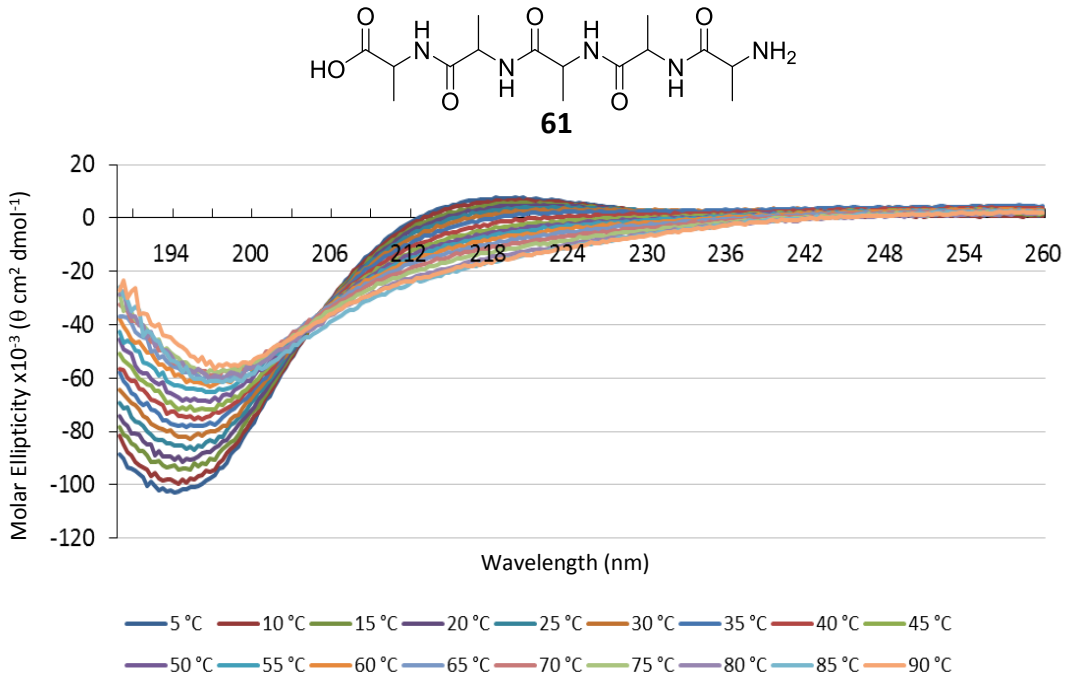

Figure 3.23 Circular dichroism spectra of pentaalanine **61** (60 μM) in phosphate buffer (5 mM, pH 7) over a 5-90 °C temperature range

The circular dichroism spectra of the Cbz-protected peptide **51** were then recorded over 5-90 °C at 5 °C increments. Returned measurements at 20 °C showed that above 70 °C the Cbz-protected peptide **51** underwent an irreversible structure change, therefore spectra recorded at 70-90 °C were omitted from the analysis (Figure **3.24**). The spectra show that as the Cbz-protected peptide **51** is heated, there is a loss of molar ellipticity in the signal at 194 nm, and the minimum wavelength in this region is red-shifted. This observation is consistent with unfolding of PPII helix with heating, similar to the structure transition in pentaalanine **61**. Although the two sets of spectra are very similar, molar ellipticity corresponding to PPII helix in the Cbz-protected peptide **51** is slightly reduced compared to that in pentaalanine **61**. This was observed in comparison of the spectra in Section 3.3 at 20 °C, and is shown here to hold true over a temperature range.

The small decrease is consistent with a small amount of [*c*1]-complex formation with the Cbz-protected peptide **51** which disrupts PPII helix formation. Even so, the similarity of the circular dichroism spectra of pentaalanine **61** and the Cbz-protected peptide **51** over a temperature range indicates similar peptide structures are dominant in both compounds.

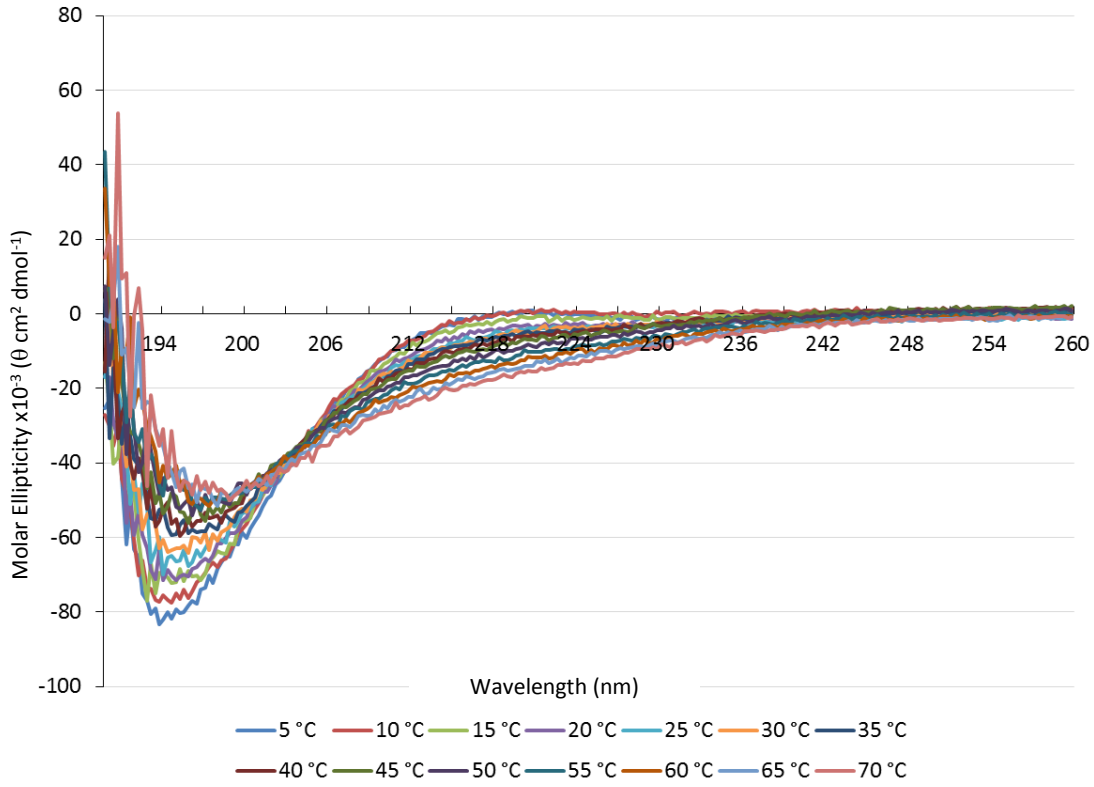

Figure 3.24 Circular dichroism spectra of the Cbz-protected peptide **51** (40 μM) in phosphate buffer (5 mM, pH 7) over a 5-70 °C temperature range

The circular dichroism spectra of the azobenzenyl peptide **54** were also measured over 5-90 °C at 5 °C increments. Spectra at returned temperatures of 20 °C showed that over 70 °C an irreversible structure change occurs, therefore data at 70-90 °C were also omitted from this analysis (Figure **3.25**). Signals in the 190-198 nm region show no temperature dependency, with spectra exhibiting a high degree of disorder consistent with a random coil/disordered peptide structure.

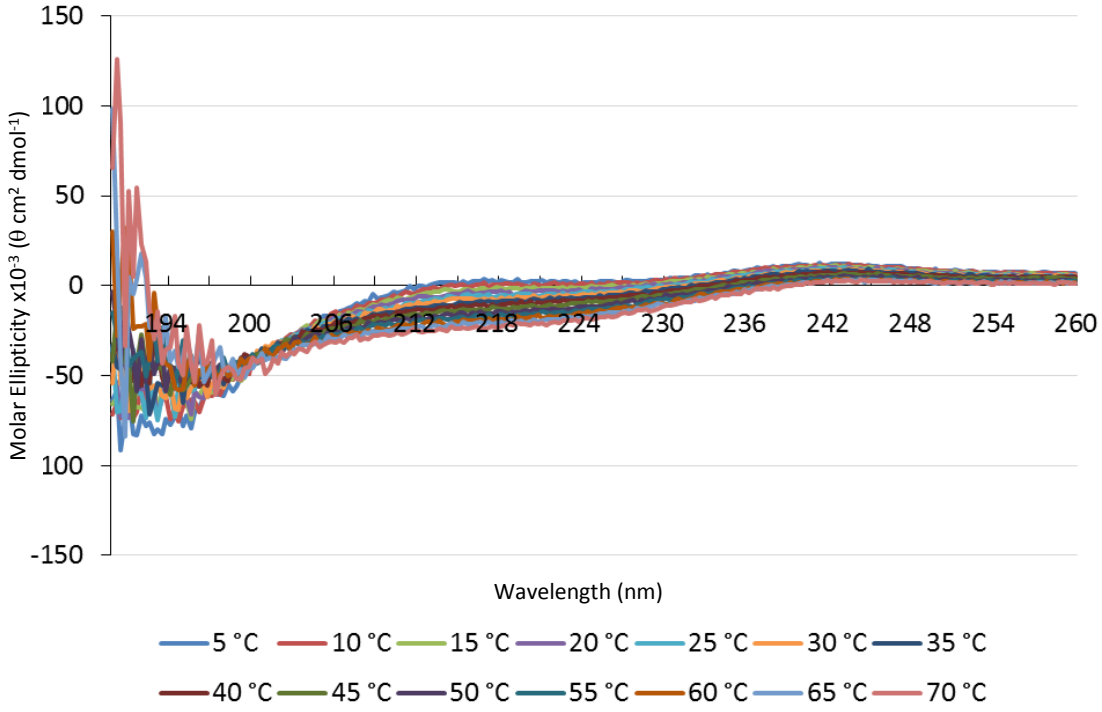

Figure 3.25 Circular dichroism spectra of the azobenzenyl peptide **54** (50 μM) in phosphate buffer (5 mM, pH 7) over a 5-70 °C temperature range.

The circular dichroism spectra of the adamantyl peptide **60** were also measured at 5-90 °C at 5 °C increments. Returned measurements at 20 °C showed that the peptide underwent an irreversible structure change in this case above 75 °C, therefore data above this temperature were not included in the analysis (Figure **3.26**).

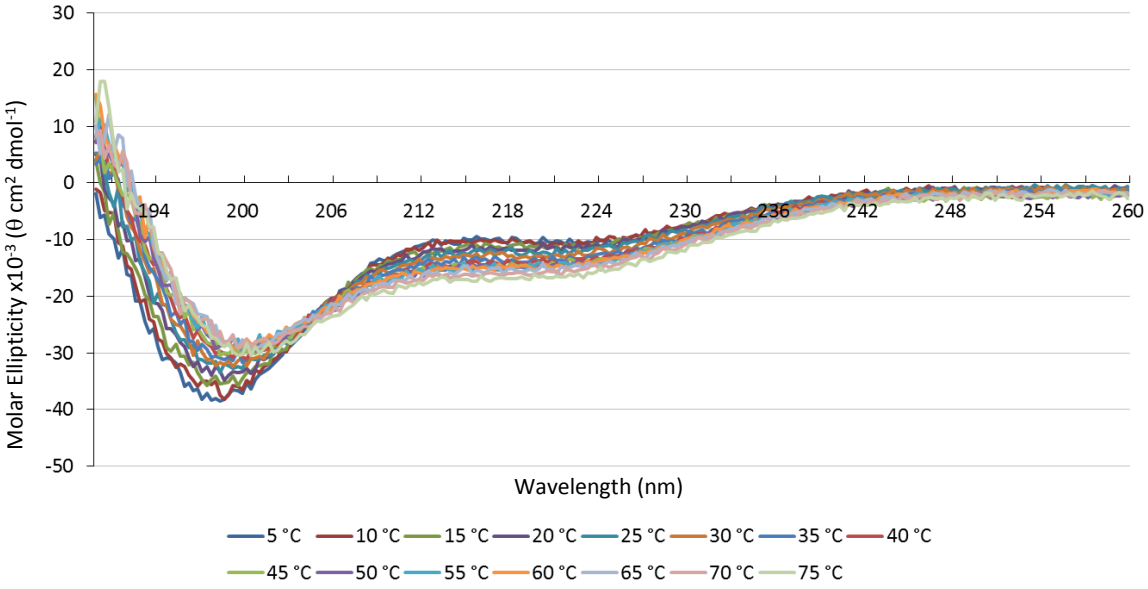

Figure 3.26 Circular dichroism spectra of the adamantyl peptide **60** (50 μM) in phosphate buffer (5 mM, pH 7) over a 5-75 °C temperature range.

The spectra show a decrease in the molar ellipticty in the 198-199 nm region and a small red-shift in the minimum wavelength with increasing temperature up to 50 °C. At higher temperatures, molar ellipticity begins to increase and the minimum wavelength stays roughly the same (Figure **3.27**). The biphasic nature of signal change at this wavelength suggests that at least two different types of structure are present.

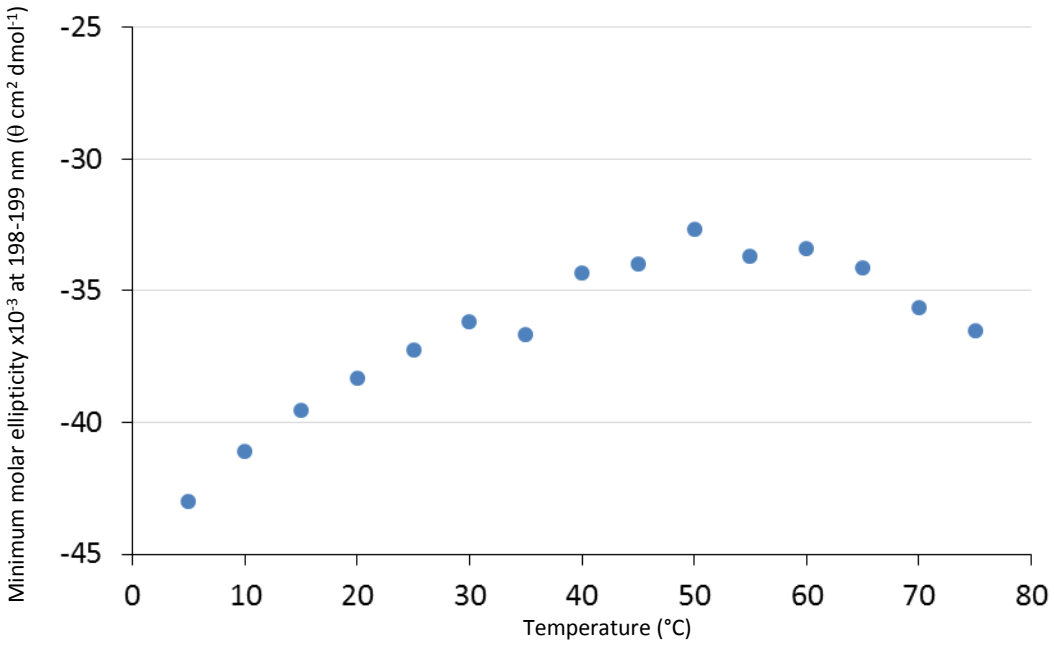

Figure 3.27 Minimum molar ellipticity of the adamantyl peptide **60** at 198-199 nm vs temperature.

The circular dichroism spectra of the adamantyl peptide **60** also show temperature dependency in the molar ellipticity at 218 nm (Figure **3.28**). The biphasic change in molar ellipticity observed at 198-199 nm is also seen at 218 nm suggesting that the structure transitions are related. This indicates that the adamantyl peptide **60** does not exist exclusively as a [*c*1]-complex, but is more likely to form a mixture of [*a*1]- and [*c*1]-species. Although absolute structures cannot be assigned, the spectra could be interpreted as the pentaalanine in the [*a*1]-species existing as a PPII helical structure and in the [*c*1]-complex as a β-turn.

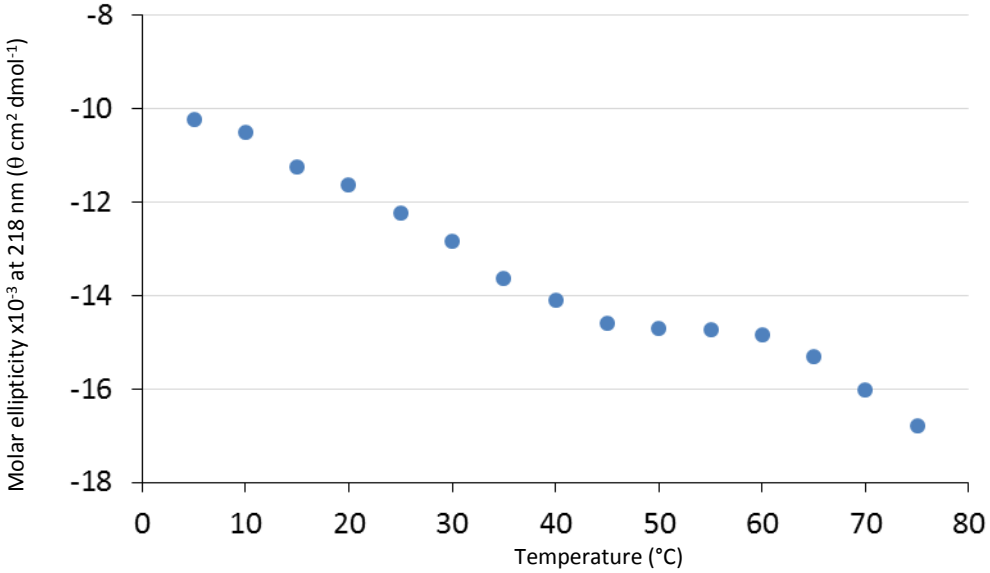

Figure 3.28 Molar ellipticity of the adamantyl peptide **60** at 218 nm vs temperature.

In all the cyclodextrin host-guest modified peptides studied, a reduction of PPII helix is observed, although to different extents. The energy required to unfold the PPII helix found in pentaalanine **61**, corresponding to 'work performed' by these systems was calculated.

The circular dichroism spectra of pentaalanine **61** from 5-90 °C (Figure **3.23**) were used to find the fraction of unfolded PPII helix across this temperature range. The signal minimum at 5 °C is considered as fully folded and the minimum at 90 °C as fully unfolded. By plotting Ln*K* vs 1/*T* (where *K* = fraction unfolded / (1- fraction unfolded)) (Figure **3.29**), a ΔG of 3.2 kcal mol^{-1} was derived from the resulting graph where ΔG = gradient/R (gas constant = 1.987 cal K^{-1} mol^{-1}).

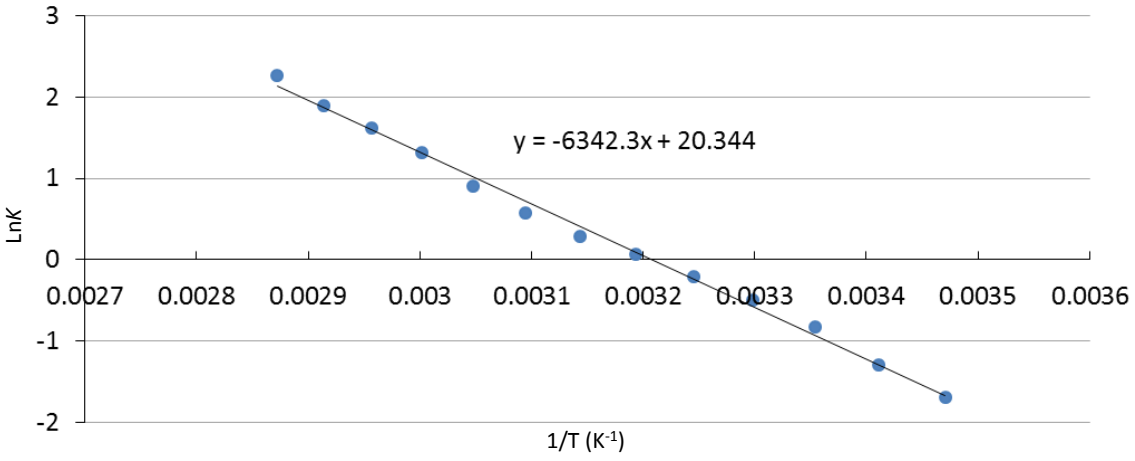

Figure 3.29 Relationship between fraction of unfolded PPII helix in pentaalanine **61** and temperature change.

From the calculated ΔG, ΔH and ΔS of PPII helix unfolding could also be derived as 12.6 kcal mol^{-1} and 0.04 kcal K^{-1} mol^{-1} respectively at 25 °C, using Equation **3.1** and Equation **3.2**.

$$\Delta G = \Delta H(1-T/T_m)-\Delta Cp((T_m-T) + T\ln(T/T_m))$$

Equation 3.1 The modified Gibbs-Helmholtz equation which describes unfolding of a monomeric peptide. Change in heat capacity (ΔC_p) is set at 0.[153]

$$\Delta G = \Delta H\text{-}T\Delta S$$

Equation 3.2 Equation for Gibbs free energy in a thermodynamic system.

These results show that at 25 °C the unfolding of the PPII helix in pentaalanine is a process contributed to roughly equally by enthalpy and entropy.

3.5 Synthesis of a System wherein Cyclodextrin Complexation Enhances Peptide Structure

The azobenzenyl peptide **54**, Cbz-protected peptide **51** and adamantyl peptide **60** described in this Chapter produce various effects on the secondary structure of pentaalanine upon cyclodextrin host-guest complexation. These changes however, largely involve the disruption of structure. A better alternative would be a construct where structure was enhanced, and with this aim a new design was explored using a peptide sequence that preferentially forms β-sheet structure. This secondary structure is more difficult to disorder and it was thought it might be retained and even enhanced in a [*c*2]-complex. A new cyclodextrin and guest modified peptide construct was therefore designed employing hexavaline, which is reported to mainly form β-sheet structure,[169] α-cyclodextrin and azobenzene (Scheme **3.3**).

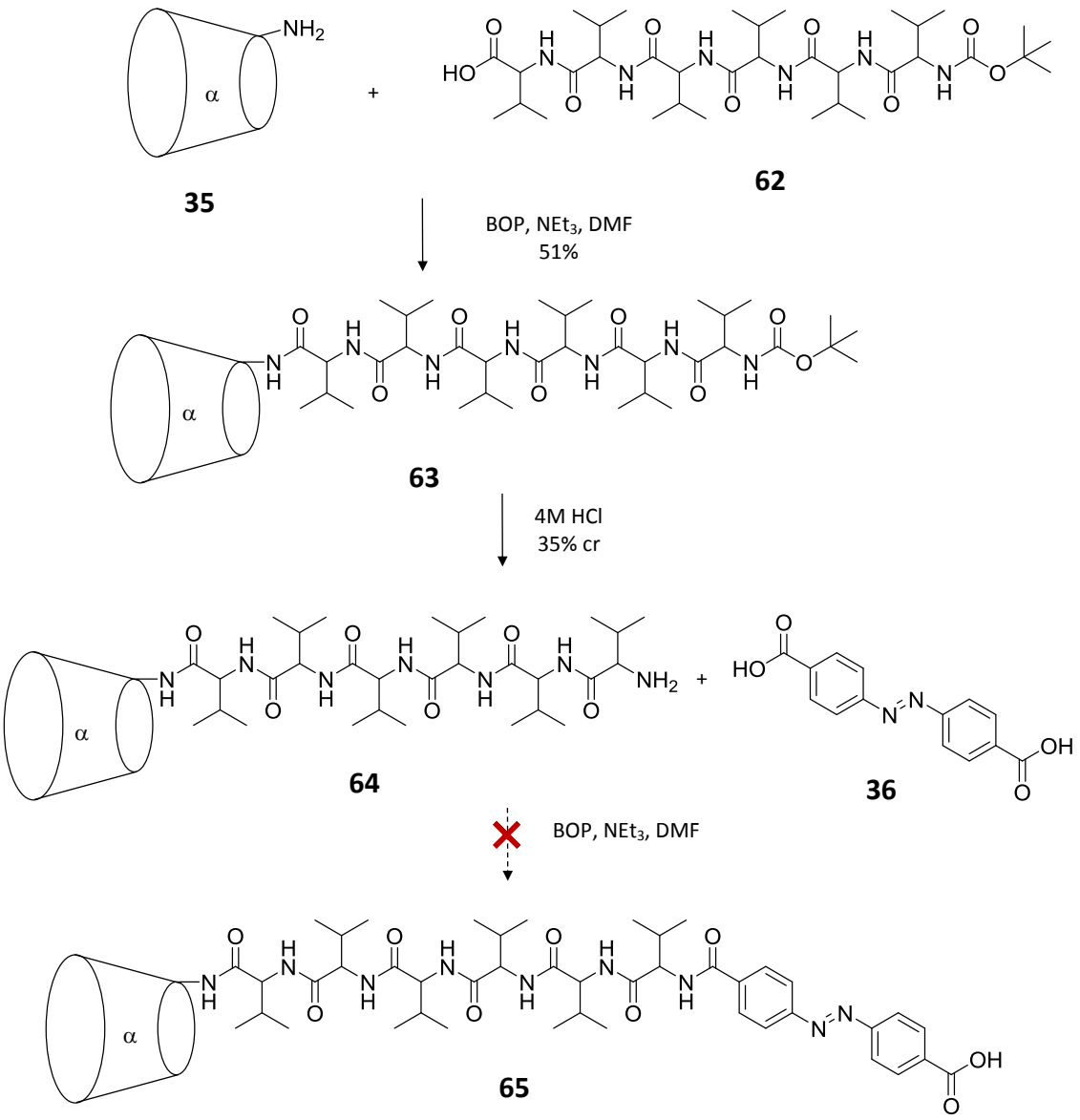

Scheme 3.3 Attempted synthesis of the photoswitchable hexavaline molecular switch **65**.

Amino-α-cyclodextrin **35** was coupled with commercially available *N*-Boc-hexavaline **62** and the Boc-protected peptide **63** isolated by application to a cation-exchange column then an anion-exchange cartridge in a 51% yield. Both the *N*-Boc-hexavaline **62** starting material and the Boc-protected peptide **63** have relatively low solubility in aqueous solution, therefore a very dilute solution of the crude product mixture with a high volume was used. This method of purification is particularly suitable in this case as the use of a dilute mobile phase does not result in slow diffusion across the solid phase which would cause coelution in techniques such as column chromatography.

The Boc protecting group was then removed from peptide **63** in acidic conditions to give the deprotected peptide **64** in a crude yield of 35%. As the ^{1}H NMR spectrum showed complete deprotection, the compound was used with no further purification.

An attempt was then made to introduce the azobenzene photoisomerisable guest by coupling the deprotected peptide **64** with azobenzene-4,4'-dicarboxylic acid **36**. The dicarboxyazobenzene was used over the monocarboxyazobenzene as it was predicted that the free carboxylic acid in the product would aid solubility in aqueous conditions. Although the desired azobenzenyl peptide **65** was detected in the crude reaction mixture by mass spectrometry, and appeared by TLC to have been synthesised in a reasonable yield, purification and further characterisation proved impractical as a consequence of the compound's insolubility.

Although isolation of the azobenzenyl peptide **65** was unsuccessful, the Boc-protected peptide **63** was identified as a candidate for the investigation of the effect of cyclodextrin host-guest complex formation on hexavaline secondary structure, as the tertiary butyl group can act as a guest for α-cyclodextrin.[170] For comparison, hexavaline **66** was prepared from *N*-Boc-hexavaline **62** by removal of the protecting group under acidic conditions (Scheme **3.4**)

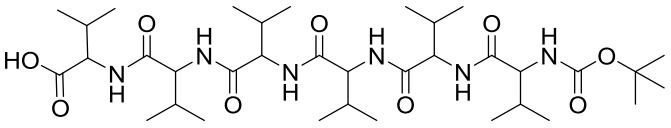

62

4M HCl
73%

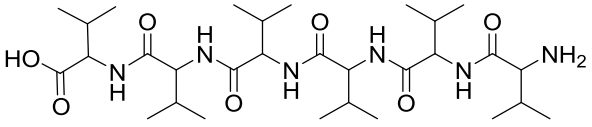

66

Scheme 3.4 Synthesis of hexavaline **66**.

The Boc-protected peptide **63** was analysed by 2D ^{1}H-^{1}H ROESY NMR spectroscopy to determine whether host-guest interactions are present (Figure **3.30**). The spectrum shows nOe crosspeaks between proton signals of α-cyclodextrin and the Boc group, and also between α-cyclodextrin protons and valine γ-protons, showing that an inclusion complex is formed.

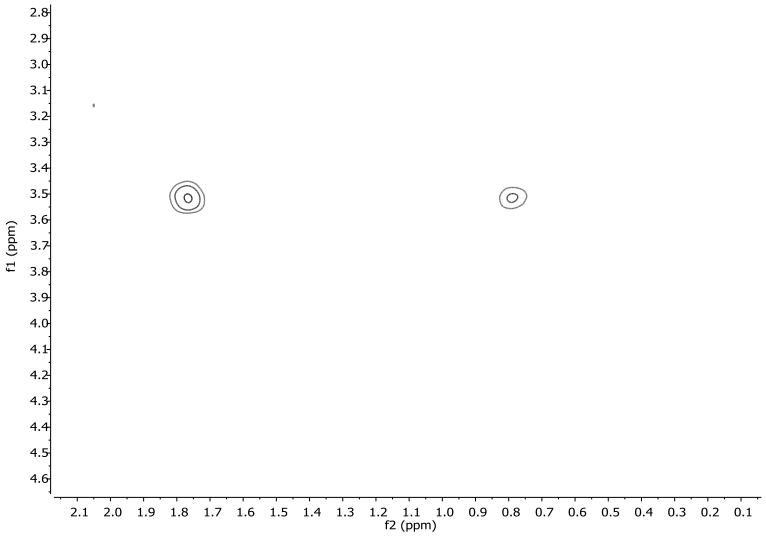

Figure 3.30 2D ^{1}H-^{1}H ROESY spectrum of the Boc-protected peptide **63** (1 mM) in *d*-phosphate buffer (5 mM, pH 7) at 500 MHz.

An ITC dimer dissociation experiment was then performed in an attempt to determine if complex formation is in the form of a [*c*1]- or [*c*2]-complex. An initial syringe solution of 1 mM Boc-protected peptide **63** in buffer was used, the maximum concentration possible before precipitation occurred, and titrated into blank buffer solution (Figure **3.31**). The absence of an endothermic titration curve, such as those observed in the ITC experiments performed with the azobenzenyl peptide **54**, the Cbz-protected peptide **51** and the adamantyl peptide **60**, indicates that no cyclodextrin host-guest dimer dissociation is occurring. This could be because either the initial syringe solution of the Boc-protected peptide **63** did not contain dimeric structures and dimer formation is very weak, or because after titration into the blank solution any dimer did not dissociate and dimer formation is very strong. A weak exothermic titration curve is observed, possibly as a result of a β-sheet dissociation.[171]

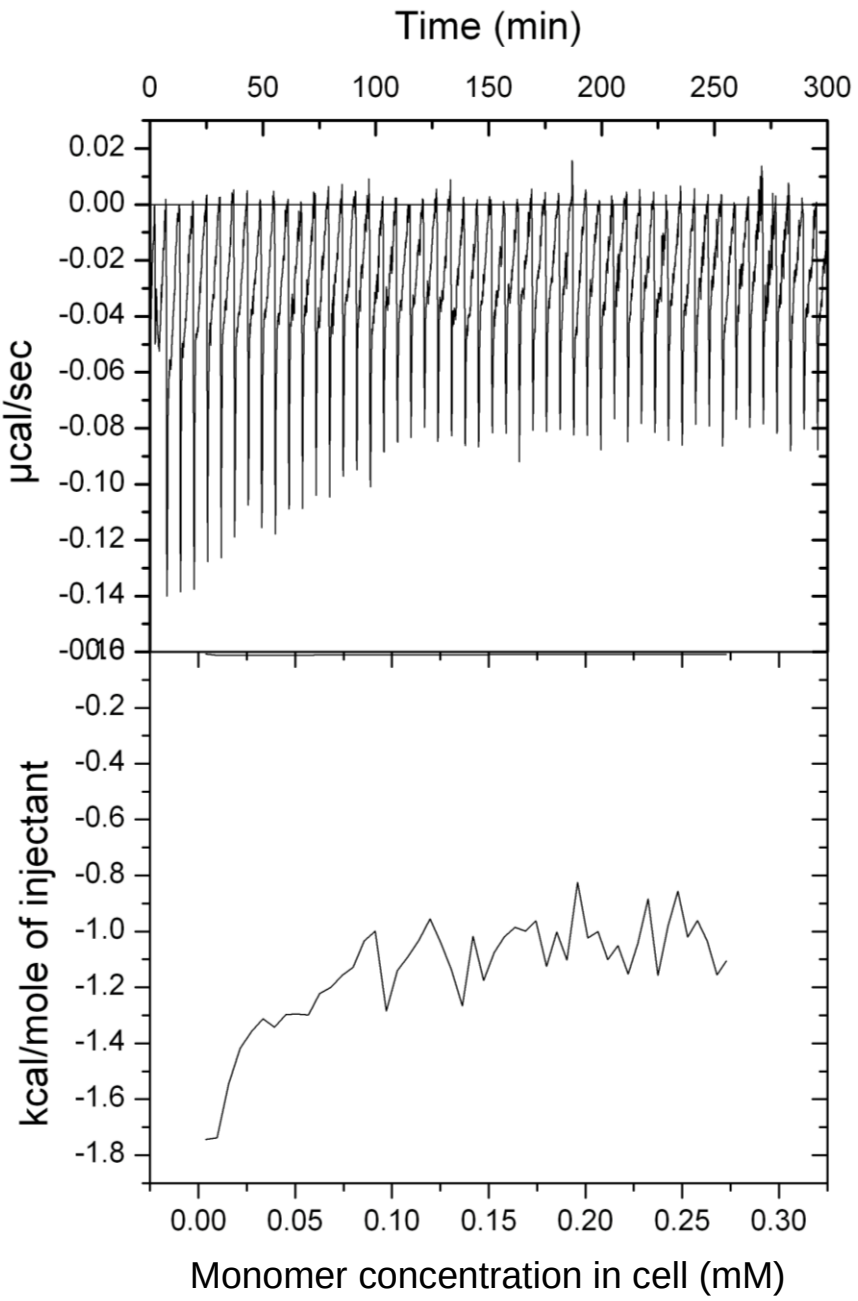

Figure 3.31 ITC of the Boc-protected peptide **63** (1 mM) with 5 µL injections into phosphate buffer (1.4365 mL, 5 mM, pH 7).

Although it could not be determined whether the Boc-peptide **63** forms a [*c*1]- or [*c*2]-complex, 2D ^{1}H-^{1}H ROESY NMR spectroscopy showed that the compound does form host-guest interactions. The effect of inclusion complex formation on the secondary structure of hexavaline was therefore investigated. The circular dichroism spectrum of the Boc-protected peptide **63** was measured (Figure **3.32**) and compared to that of the unmodified peptide, hexavaline **66** (Figure **3.33**). Both compounds demonstrate a signal with a negative trough at ~217 nm which is characteristic of β-sheet formation. Molar

ellipticity in both compounds is also about the same (taking into account the baseline shift in the spectra of the Boc-protected peptide **63**), indicating a similar extent of β-sheet structure. The lack of concentration dependency in the spectra of the Boc-protected peptide **63** again suggests that either a [*c*2]-complex is not formed, or that dimer complexation is so strong that no difference in the extent of dimer formation is observed over this concentration range.

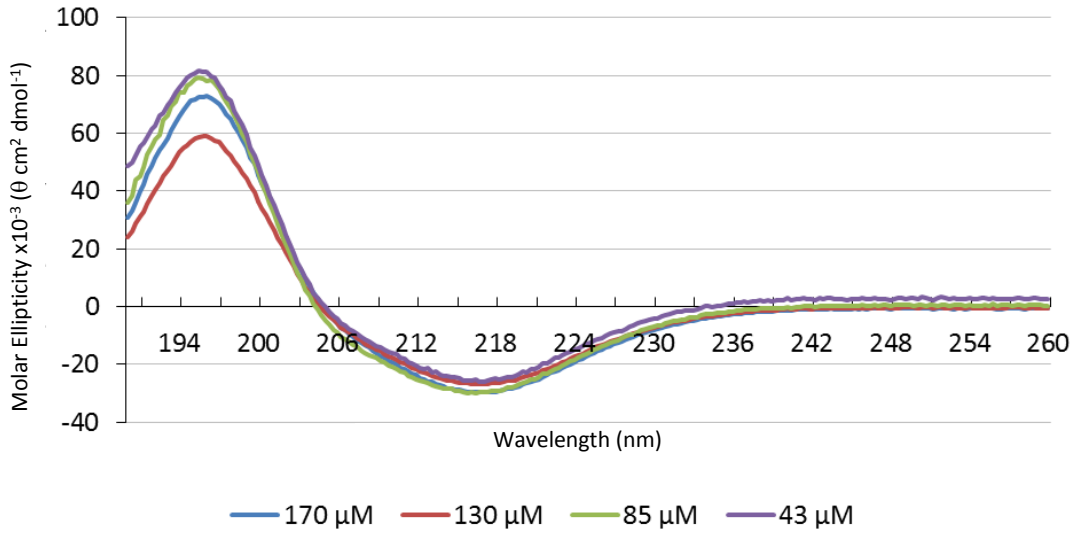

Figure 3.32 Circular dichroism spectra of hexavaline **66** (43-170 µM) in phosphate buffer (5 mM, pH 7).

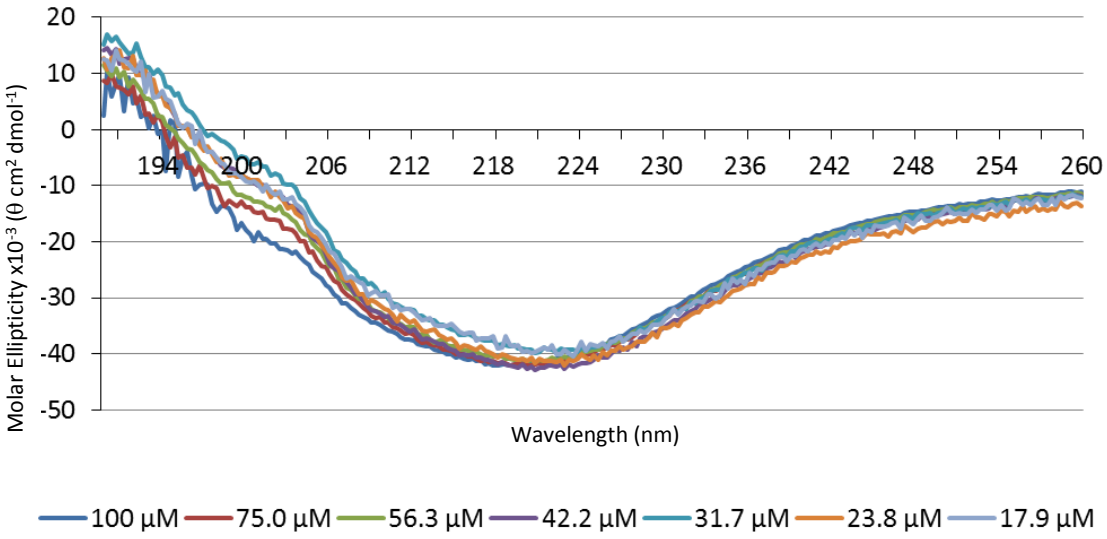

Figure 3.33 Circular dichroism spectra of the Boc-protected peptide **63** (17.9-100 µM) in phosphate buffer (5 mM, pH 7).

As no effect of cyclodextrin host-guest complex formation on the structure of hexavaline with the Boc-protected peptide **63** was observed at room temperature, the effect on

the thermal stability of hexavaline β-sheets was explored. Circular dichroism spectroscopy from 5 °C to 90 °C was measured to give temperature profiles of β-sheet structure in hexavaline **66** (Figure **3.34**) and the Boc-protected peptide **63** (Figure **3.35**). With both compounds, molar ellipticity at 217 nm decreased with increasing temperature.

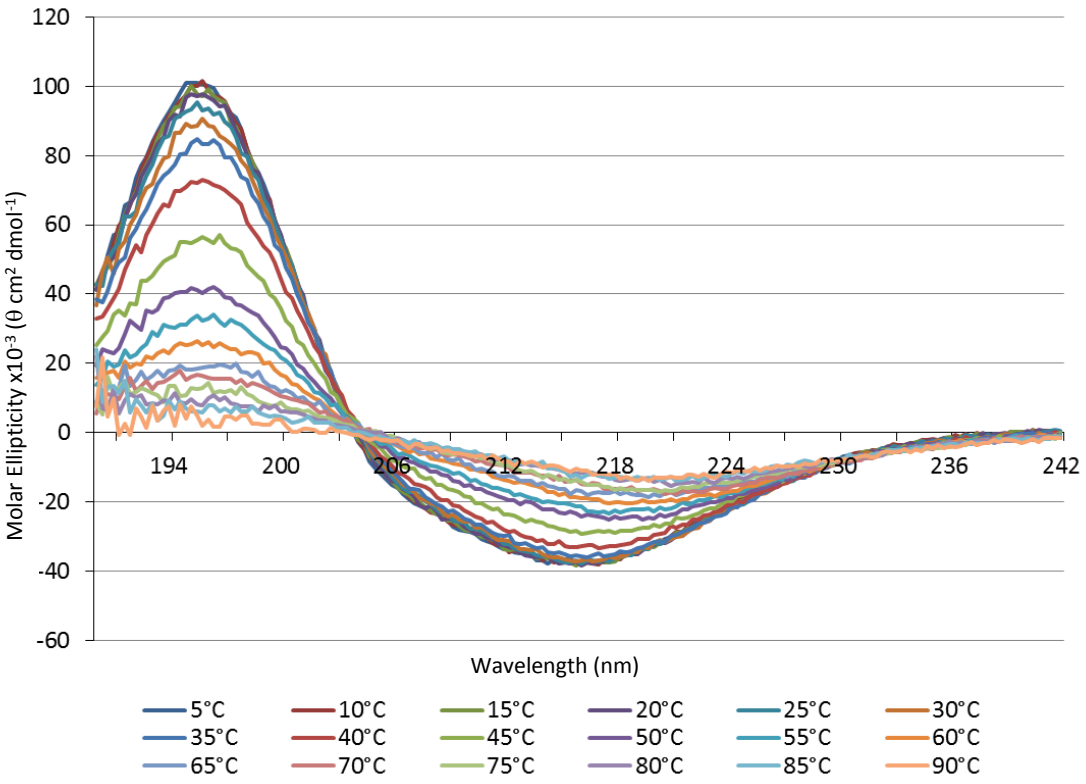

Figure 3.34 Circular dichroism spectra of hexavaline **66** (100 μM) in phosphate buffer (5 mM, pH 7) over a temperature range of 5-90 °C.

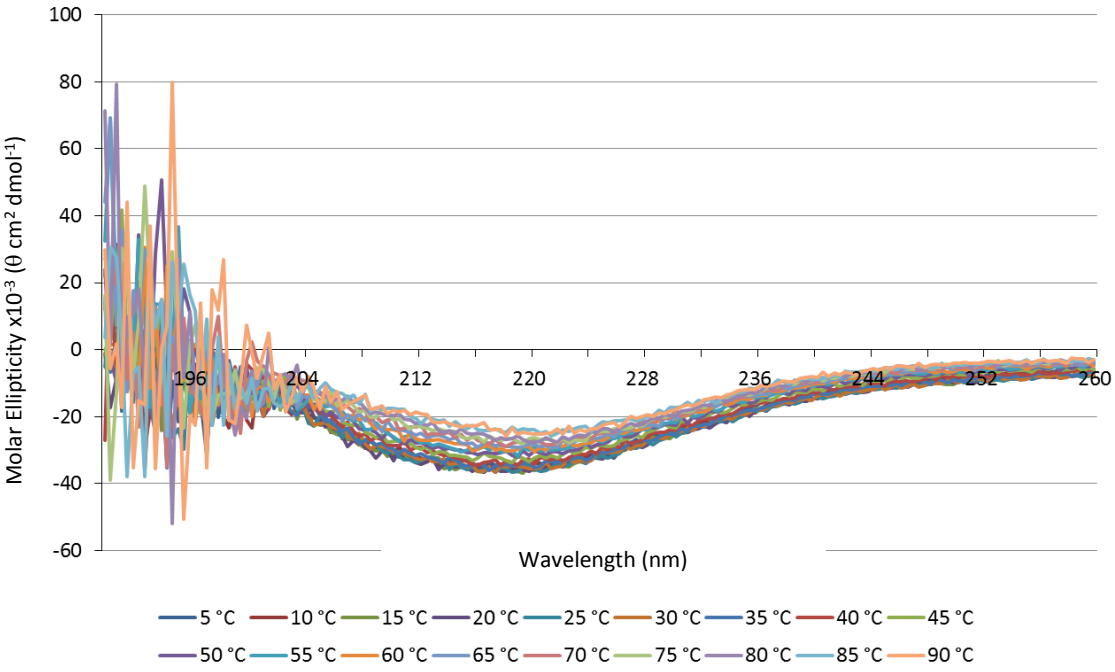

Figure 3.35 Circular dichroism spectra of the Boc-protected peptide **63** (100 μM) in phosphate buffer (5 mM, pH 7) over a temperature range of 5-90 °C.

Molar ellipticity at 217 nm was then plotted against temperature for the Boc-protected peptide **63** and hexavaline **66** to give melting curves of β-sheet unfolding (Figure **3.36**). The mid-point temperature for this transition (T_m) from a folded to an unfolded state in hexavaline **66** was 51 °C. The temperature profile of β-sheet structure in the Boc-protected peptide **63** reaches no minimum ellipticity plateau, and even at 90 °C molar ellipticity is around twice that observed in hexavaline **66**. This indicates that even at such high temperatures the β-sheets in the dimer complex are not fully unfolded, therefore a true T_m value cannot be calculated and only the mid-point for the incomplete unfolding process can be given as 65 °C. This corresponds to an increase in the thermal stability of hexavaline β-sheets in the cyclodextrin complex of at least 14 °C.

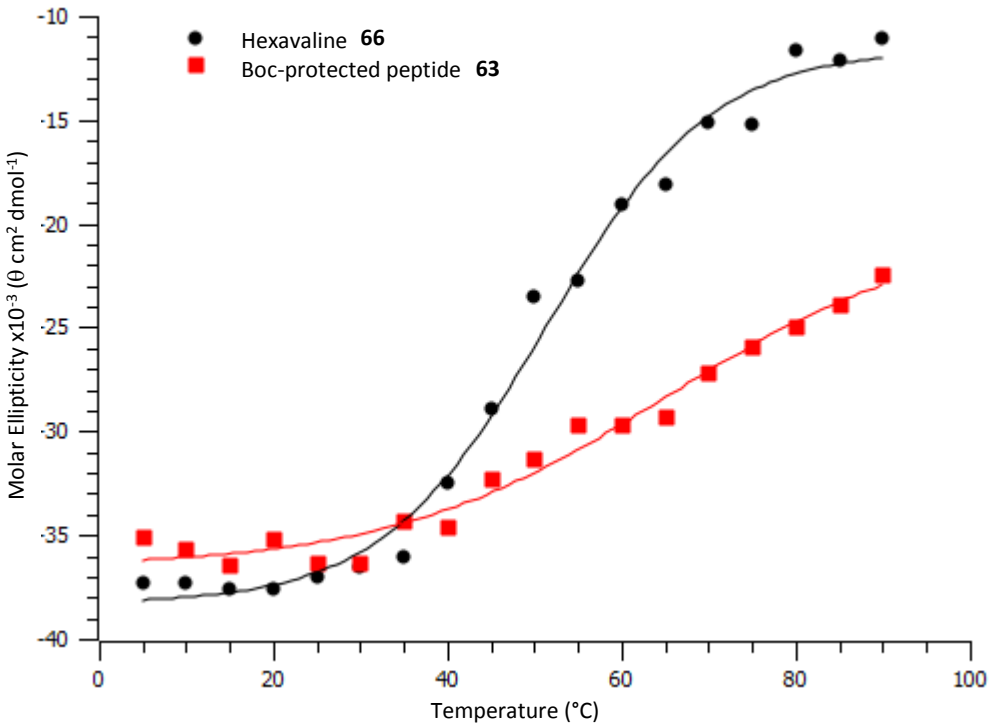

Figure 3.36 Temperature profiles of β-sheet structure in hexavaline **66** and the Boc-protected peptide **63**.

The observations with the Boc-protected peptide **63** suggest that formation of a [*c*2]-complex is more likely than formation of a [*c*1]-complex. As the amount of β-sheet character remains the same in both the Boc-protected peptide **63** and hexavaline **66** at room temperature, a [*c*1]-complex is unlikely as this would be expected to incur a loss in β-sheet character. Even if a β-turn structure was formed within a [*c*1]-assembly, at least two amino acids would not be involved in β-sheet formation where the turn is made, which would also result in a loss of β-sheet character. It is logical that β-sheets formed between hexavaline moieties therefore strengthen [*c*2]-complexation to such an extent that no dissociation could be observed in the ITC experiment, and no concentration dependency on β-sheet structure was observed in the circular dichroism spectra of the Boc-protected peptide **63**.

3.6 Conclusions

In this Chapter, a range of molecular devices constructed from short peptides and cyclodextrin host-guest pairs were investigated for their effect on the secondary structure of the peptide moiety. Varying the host-guest pair resulted in the unfolding of

PPII helices in pentaalanine sequences to differing extents, as a consequence of changes in host-guest complexation strength. A photo-reponsive guest was also incorporated into a device, facilitating its activity as a peptide structure photoswitch.

The use of a hexavaline sequence, which preferentially forms β-sheet structures, resulted in a cyclodextrin host-guest device which positively influenced secondary structure. β-Sheets in the host-peptide-guest construct had an enhanced thermal stability compared to the unmodified hexavaline peptide, with a significant proportion of folded structure present even at 90 °C.

The results in this Chapter demonstrate that these type of cyclodextrin-peptide-guest structures are suitable as devices to produce changes in peptide structure upon cyclodextrin host-guest complexation. As this system does not rely on the inherent properties of the peptide itself, it provides a universal scaffold wherein any short peptide sequence can be used. It was envisaged that this work could be further developed with the use of a peptide sequence which also exhibits a change in function upon secondary structure modification. This concept is explored in Chapter 4.

Chapter 4: Results and Discussion

Self-Assembly of a Peptidic Zinc-Binding Site

4.1 Introduction

Having established in the work discussed in Chapter 3 a series of cyclodextrin-based molecular devices that produce a modification in the secondary structure of short peptides, it was anticipated that the same type of construct could be used in the preparation of an artificial metal binding site. Artificial binding sites are useful in furthering the understanding of natural mechanisms, and the development of new functionalities. One strategy to achieve this is the modification of existing natural proteins through residue mutation[172-174] or the addition of prosthetic groups.[175, 176] Another strategy for the preparation of artificial binding sites is the use of non-peptidic, supramolecular scaffolds.[177, 178]

Previous studies have used peptide-peptide interactions to assemble artificial binding sites,[179-182] for example with helical bundles that fold to give a zinc binding site,[183] bundling of β-peptides to give cadmium-binding sites[184] and β-sheet amyloids that bind zinc metal ions.[185] Despite successes using this strategy, the use of peptide-peptide interactions for assembly still requires good knowledge of structure-sequence relationships,[186] a grand challenge in itself, and the components for assembly are themselves potentially bioactive. As outlined in Chapter 1, an alternative approach to the development of devices such as artificial binding sites, is the combination of non-peptidic supramolecular moieties with peptidic elements. Non-peptidic functionalities have the potential to self-assemble a peptide binding site, thereby giving a simplified version of the protein construct which is easier to synthesise than a whole protein, whilst retaining a biologically relevant, naturally encoded amino acid-based binding site. The use of cyclodextrin host-guest interactions is therefore a suitable non-peptidic assembly mechanism as the components are bio-orthogonal and assembly operates

under aqueous conditions. Furthermore, the separation of components that impart assembly and binding functionality is advantageous as they can be separately modified in order to produce variations in properties.

Based on the constructs explored in Chapter 3, a system was envisaged wherein cyclodextrin host-guest complexation could give an assembled structure which could then induce secondary structure in a peptide, in turn assembling a binding site (Figure **4.1**). A suitable peptide sequence, modified with a cyclodextrin at one terminus and a complementary guest moiety at the other terminus, was therefore designed, prepared and investigated.

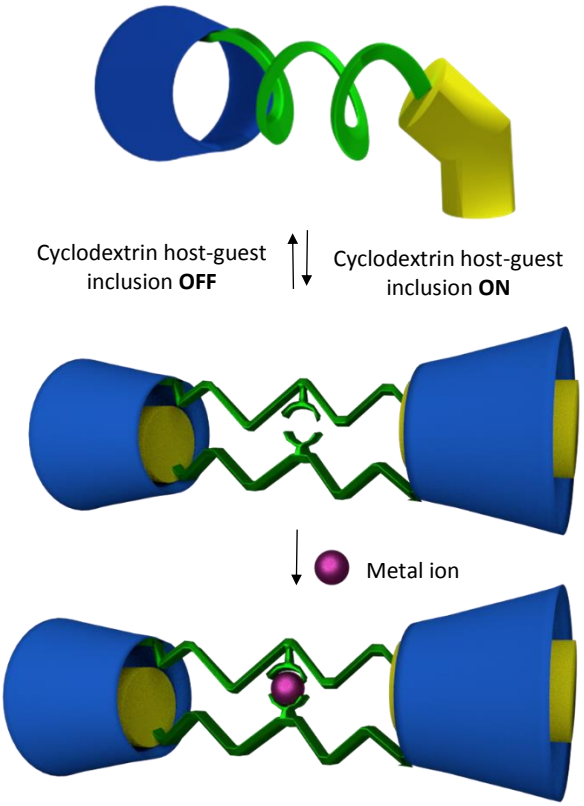

Figure 4.1 Conceptual image of the metal binding molecular device investigated in Chapter 4 with the cyclodextrin moiety in blue, the guest in yellow, the peptide in green and the metal ion in pink.

4.2 Design of the Peptide Sequence

The overall design for a self-assembling metal binding site consequently used the peptide sequence Val-Val-Val-His-Gly-Val-Val-Val, functionalised with a cyclodextrin and a complementary guest at the termini (Figure **4.2**). As the amino-cyclodextrin **35** had

previously been synthesised, the peptide was designed with a cyclodextrin modification at the *C*-terminus and a guest at the *N*-terminus.

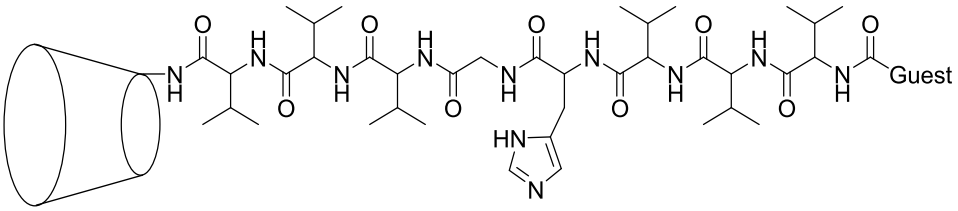

Figure 4.2 Design for the monomer unit of the self-assembling metal-binder.

In order for the device to act as designed, the metal-binding interaction needed to be strong enough to be detectable, yet not so strong that a metal would bind to the peptide sequence in the absence of cyclodextrin host-guest interactions. This balance reduces the likelihood of the metal interaction directing assembly, and also gives the potential for binding to be switched on and off by switching cyclodextrin host-guest inclusion on and off. Based on these criteria it was decided to use a combination of two histidine residues (with one on each monomer of a [*c*2]-assembly) and zinc as the metal ion. Previous studies have shown that zinc binding to two histidine residues on the same short peptide occurs with a K_a of around 4,571 M^{-1} but that no binding is observed with a single histidine residue.[187]

Results in Chapter 3 showed that a [*c*2]-complex was favoured with the use of a β-sheet forming peptide, hexavaline.[169] The design of the peptide sequence therefore used hexavaline, with the insertion of a histidine metal binding residue in the middle of the oligomer. It was envisaged that the pre-assembled [*c*2]-complex would afford a bidentate ligand for the metal ion in a pseudo-chelating manner, with the binding site further arranged for metal-coordination with the formation of adjacent β-sheets.

The trivaline sequences were expected to form anti-parallel β-sheets with residue side-chains orientated perpendicular to the amide backbone in alternate ‘up’ and ‘down’ orientations. An even number of residues in the peptide sequence would give a structure where the metal-binding histidine would be ‘up’ in one strand and ‘down’ in the other, giving a three-dimensionally more enclosed metal-binding site. An extra

residue, glycine, which does not participate in binding was therefore included in the sequence to facilitate this arrangement (Figure **4.3**).

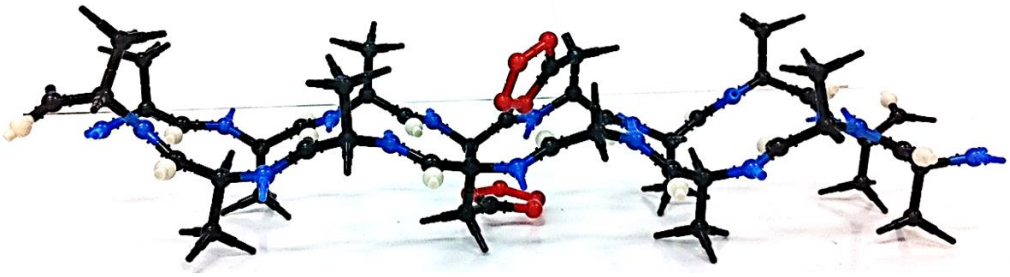

Figure 4.3 3D Molecular model of the designed peptide sequence in an antiparallel β-sheet arrangement. Carbon atoms are shown in black, oxygen atoms in white and nitrogen atoms in blue, with the two histidine side-chains in red.

4.3 Attempted Synthesis of Host-Peptide-Guest Constructs by Coupling of Peptide Segments

The initial scheme for the synthesis of a host-peptide-guest construct as the basis for an artificial metal binding site involved the preparation of separate, short peptide segments consisting of a cyclodextrin modified section, a glycine-histidine section and a guest modified section. These would then have been coupled to give the complete monomer of which two were designed and their synthesis begun in parallel; the azobenzenyl-peptide **72** (Scheme **4.1**) and the adamantyl-peptide **76** (Scheme **4.2**). α-Cyclodextrin and azobenzene were examined as this pair forms a photo-responsive complex giving the potential for the development of a photoswitch. β-Cyclodextrin and adamantane were incorporated into the other design as it was demonstrated in Chapter 3 that the strong interactions between this host-guest pair produce a large effect on peptide structure, which was expected to translate into a stronger metal-binding capability. The synthesis was designed to be highly convergent with the idea that if a particular aspect of the device required alteration, only a short peptide segment would need to be re-synthesised.

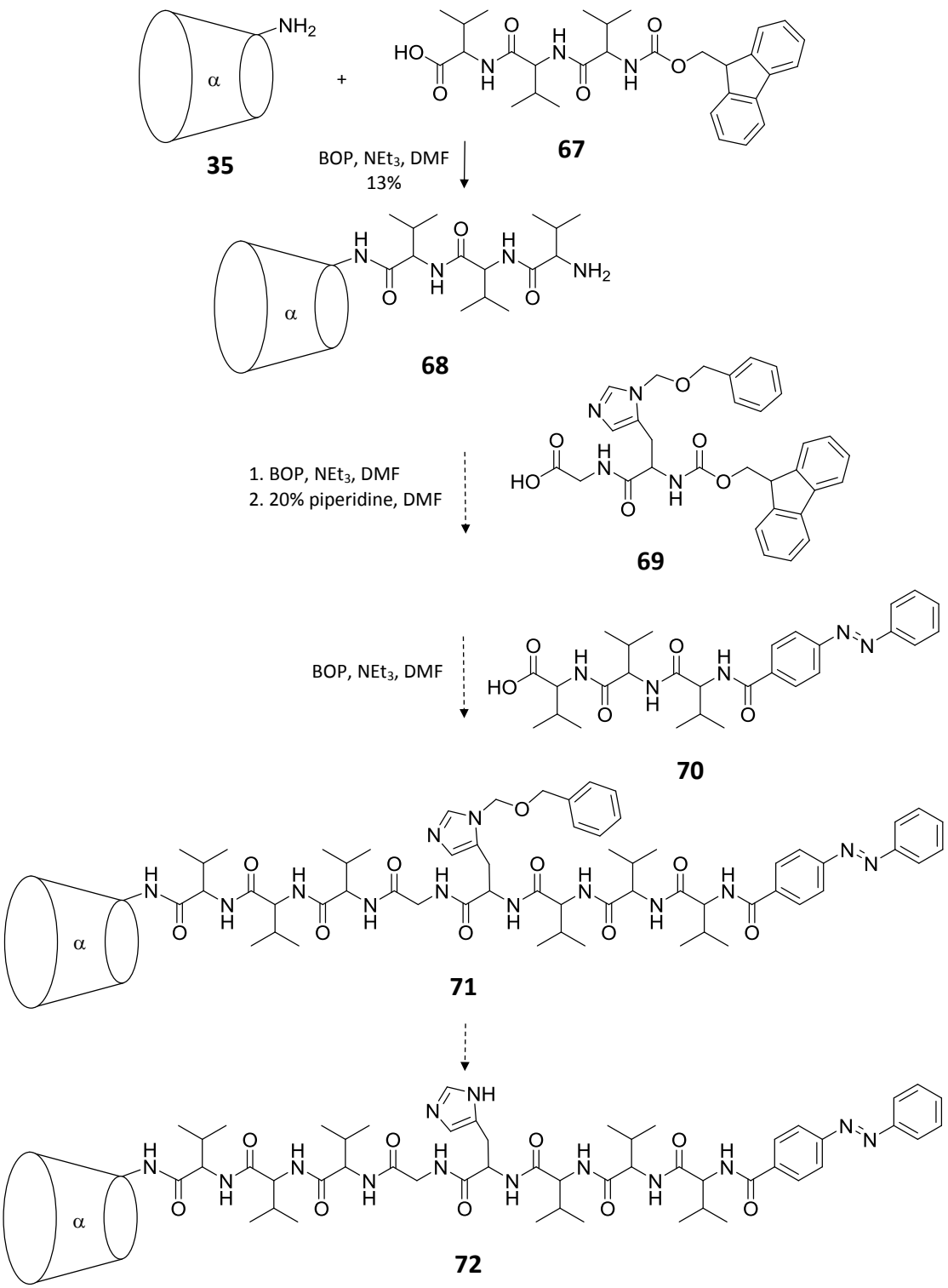

Scheme 4.1 Planned synthesis of the azobenzenyl-peptide **72** from peptide fragments.

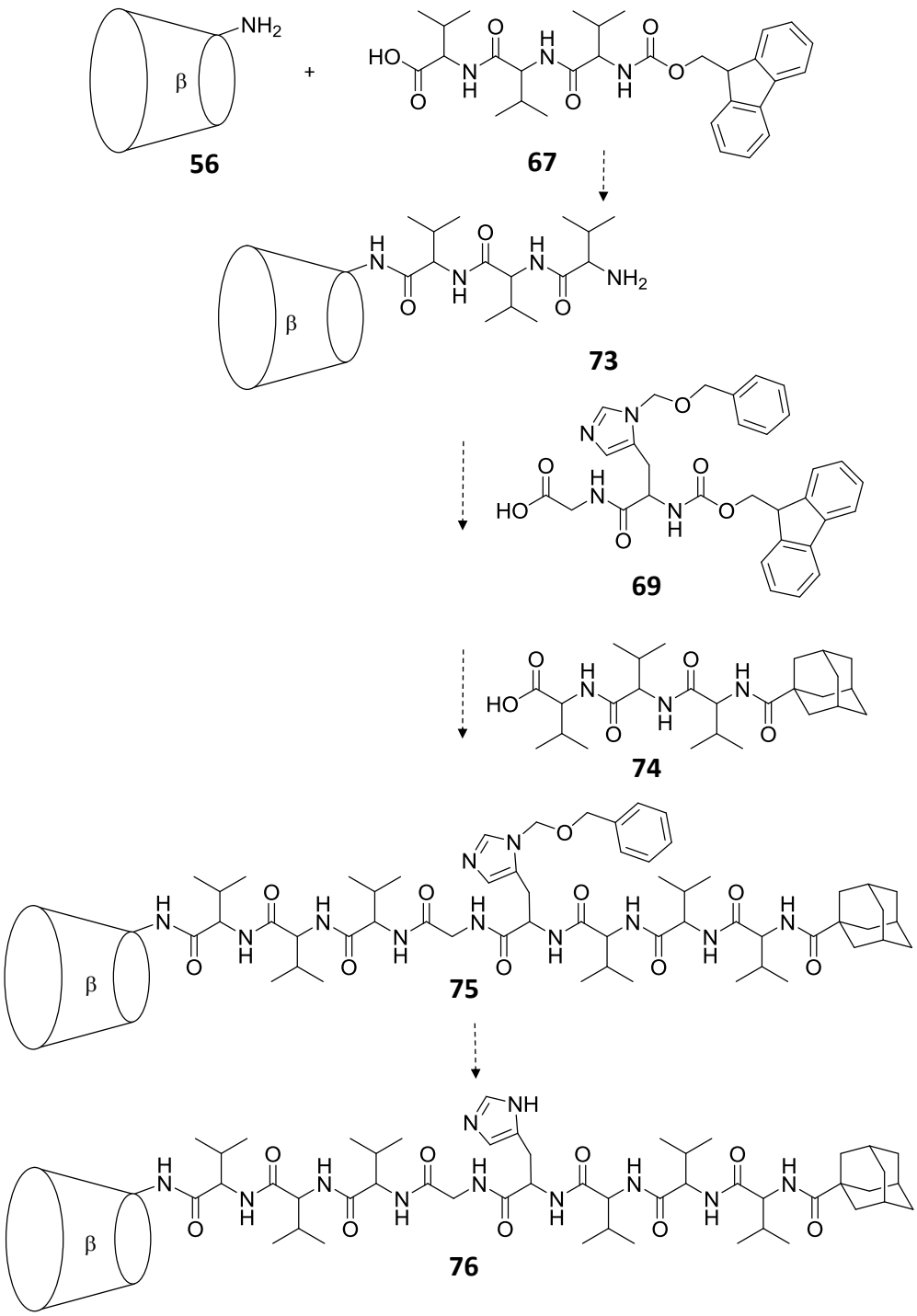

Scheme 4.2 Planned synthesis of the adamantyl-peptide **76** from peptide fragments.

N-Fmoc-trivaline **67** was prepared by standard Fmoc-coupling solid-phase synthesis and cleaved from the resin to give a yield of 37%. As the ^{1}H NMR spectrum indicated a pure product, no purification was required. *N*-Fmoc-trivaline **67** was then coupled to amino-α-cyclodextrin **35**, under conditions which also cleaved the Fmoc group to give the cyclodextrin **68**. The product was isolated by precipitation into acetone, followed by

application to a cation exchange cartridge in neutral aqueous solution and elution in a basic solution to give a 13% yield.

N-Fmoc-His(π-BOM)-Gly **69** was prepared by standard Fmoc-coupling solid-phase synthesis and cleaved from the resin. As the ^{1}H NMR spectrum showed that a pure product had formed, no purification was required and a yield of 22% recorded. The BOM-protected histidine was used throughout the synthesis described in this Chapter, as this protecting group is not removed under Fmoc solid-phase peptide synthesis cleavage conditions and prevents unwanted coupling to the histidine π-nitrogen in subsequent steps.

Two guest-modified peptides were then synthesised; the azobenzenyltrivaline **70** and the adamantyltrivaline **74** both prepared by solid-phase synthesis with either 4-phenylazobenzoic acid **53** or 1-carboxyadamantane **59** in the final coupling stage of on-resin synthesis. The azobenzenyltrivaline **70** was cleaved from the resin and purified by HPLC to give the product in a 21% yield. The adamantyltrivaline **74** was also purified by HPLC after cleavage from the resin to give a yield of 11%.

An attempt was then made to synthesise the azobenzenyl-peptide **71** by coupling the cyclodextrin **68** with *N*-Fmoc-His(π-BOM)-Gly **69** followed by removal of the Fmoc protecting group and subsequent coupling of the azobenzenyltrivaline **70**. This compound was focussed on over the adamantane-β-cyclodextrin system as it incorporates a potential photo-responsive switching mechanism. The desired azobenzenyl-peptide product **71** was detected by mass spectrometry, however when purification was attempted by HPLC it was evident that the desired product had formed in a very low yield. Isolation of the azobenzenyl-peptide **71** was therefore not pursued and subsequent reduction to the peptide **72** was not performed.

The convergent synthesis of the azobenzenyl-peptide **72** (Scheme **4.1**) entailed the solid-phase synthesis of three separate fragments, peptides **67**, **69** and **70** which were prepared in moderate yields. The peptide **67** was then coupled to amino-cyclodextrin **35** in a low-yielding reaction to give the cyclodextrin **68**, which was then coupled to peptides **69** and **70** in a synthetic step which resulted in a negligible quantity of the

peptide **71**. In order to be investigated as a biomimetic metal-binding system, the peptide **71** would also be required to undergo an additional step in order to remove the BOM protecting group. The high number of synthetic steps in this scheme, many of which are very low-yielding made it unsuitable for the preparation of the azobenzenyl-peptide **72**, as enough material for investigation into assembly and metal-binding behaviour of the compound would be difficult to obtain by this method. An alternative approach, wherein the entire peptide sequence was synthesised on solid-phase resin in one preparation was proving to be more successful, therefore the coupling of smaller fragments was abandoned and the synthesis of the adamantyl-peptide **75** was not attempted.

4.4 Attempted Synthesis of an α-Cyclodextrin-Peptide-Azobenzene Construct

As the synthetic steps in the convergent approach described in Section 4.3 proved to be too low yielding to be practically useful, a scheme where the entire guest-modified peptide was to be synthesised in one preparation was implemented in the attempted synthesis of the azobenzenyl-peptide **72** (Scheme **4.3**).

The azobenzenyl-peptide **77** was prepared using standard Fmoc coupling solid-phase synthesis with 4-phenylazobenzoic acid **53** used the final on-resin coupling step. The product was cleaved from the resin and purified by HPLC to give a yield of 8%. This yield is fairly low possibly as a consequence of the large ratio of hydrophobic valine residues in the sequence which can lower coupling efficiency.[188, 189]

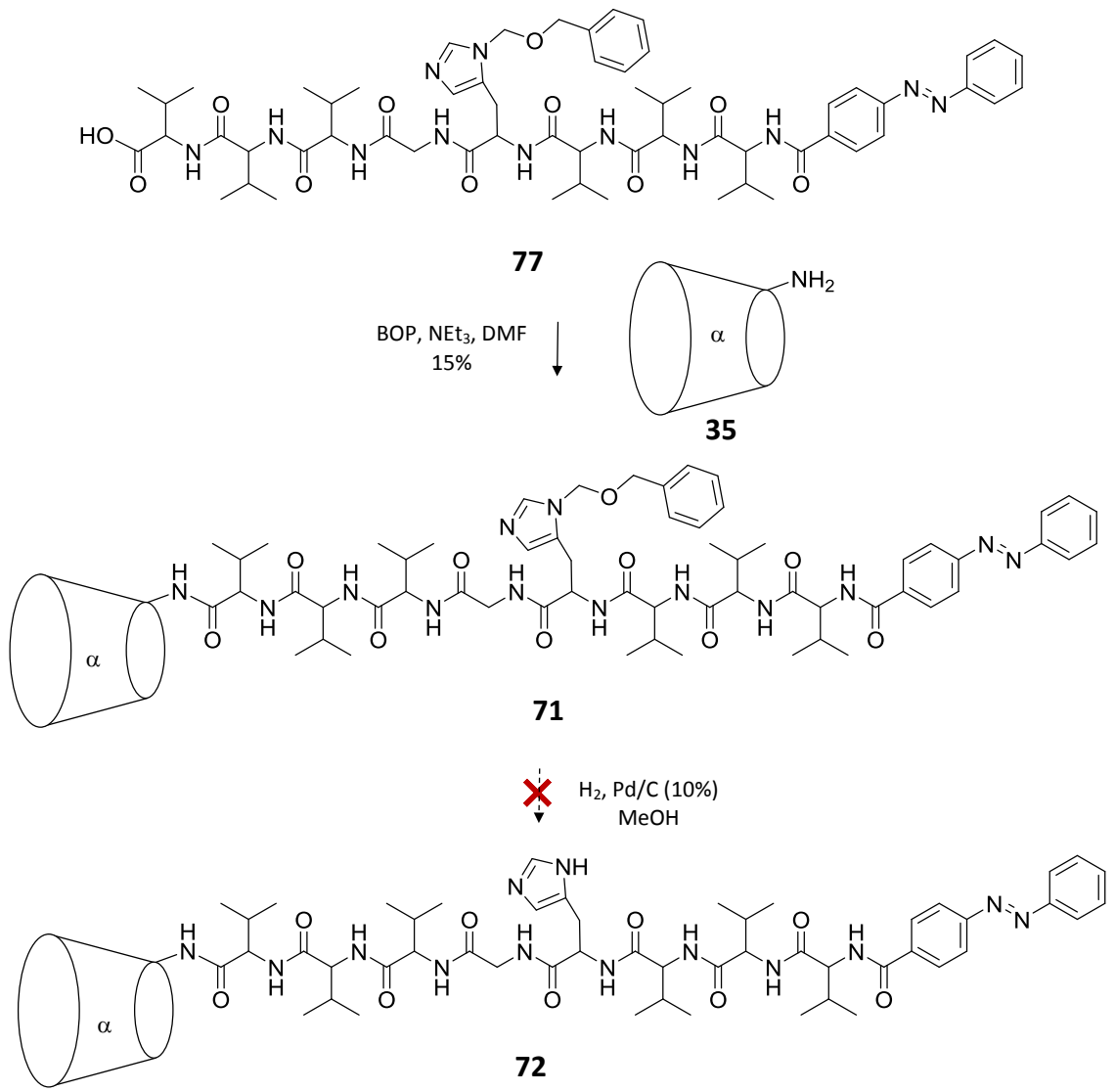

Scheme 4.3 Attempted synthesis of the azobenzenyl-peptide **72**.

The peptide **77** was then coupled to amino-α-cyclodextrin **35** and the azobenzenyl-peptide **71** isolated by HPLC in a 15% yield. The BOM protecting group was then removed by reduction with hydrogen and palladium on carbon. Although the BOM-protected histidine would likely be capable of metal-binding, the deprotected version was sought as this features biologically relevant residues. The desired azobenzenyl peptide product **72** was detected by mass spectrometry, however analytical HPLC of the crude reaction mixture revealed a large number of products had formed. ^{1}H NMR spectroscopy showed many small peaks in the aromatic proton region, indicating that the azobenzene moiety had suffered decomposition. The formation of a large amount of byproducts in the reduction step meant that the yield of the azobenzenyl-peptide **72** would be too low to be practically useful for further investigations.

4.5 Attempted Synthesis of a β-Cyclodextrin-Peptide-Adamantane Construct

As it was demonstrated that an azobenzene guest group is incompatable with the reduction conditions required to remove the histidine BOM protecting group, the focus of study was switched back to the β-cyclodextrin-adamantane host-guest pair. Synthesis of the adamantyl-peptide **75** was attempted according to Scheme **4.4**, with preparation of the entire peptide sequence performed in one solid-phase synthetic procedure.

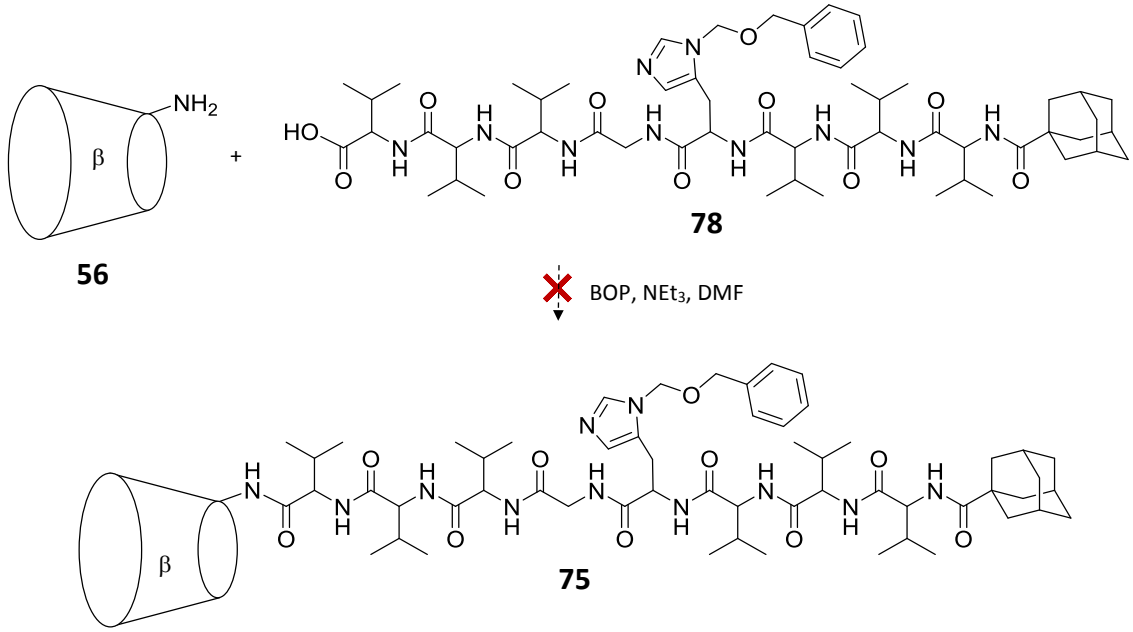

Scheme 4.4 Attempted synthesis of the adamantyl-peptide **75**.

The peptide **78** was prepared using standard Fmoc coupling solid-phase synthesis with the final on-resin coupling step performed with 1-carboxyadamantane **59**. The product was cleaved from the resin and purified by HPLC in 23% yield. An attempt was then made to couple peptide **78** with amino-β-cyclodextrin **56**, however no evidence of the desired product **75** was obtained by TLC or mass spectrometry.

It was considered that the presence of the adamantane guest could be interfering with the coupling of amino-β-cyclodextrin **56** to the peptide **78**, therefore an alternative synthesis (Scheme **4.5**) was attempted wherein the cyclodextrin moiety was introduced before the adamantane guest. The peptide **79** was prepared by solid-phase synthesis and the product cleaved from the resin and purified by HPLC to give a yield of 9%. This

was then coupled with amino-β-cyclodextrin **56** to give the cyclodextrin **80**, which was purified by HPLC in a 13% yield. An attempt was then made to couple the cyclodextrin **80** with 1-carboxyadamantane **59**, however no evidence of the desired product **75** could be obtained by TLC or mass spectrometry. The failure of the synthesis of the adamantyl peptide **75** is possibly as a consequence of the strong host-guest interaction between the β-cyclodextrin and adamantane moieties. The host-peptide-guest construct was therefore redesigned to incorporate a weaker complexing host-guest pair.

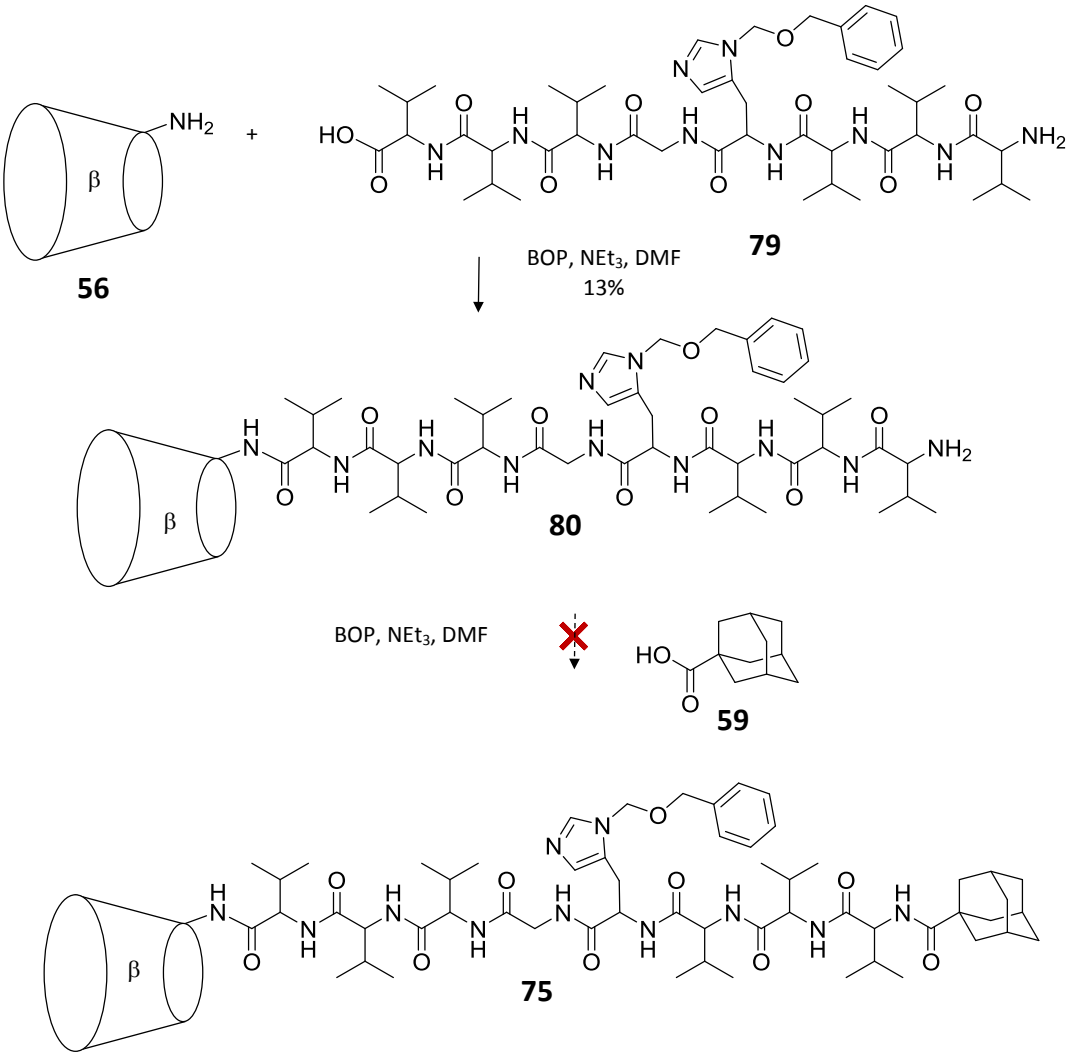

Scheme 4.5 Attempted synthesis of the adamantyl-peptide **75**.

4.6 Synthesis of an α-Cyclodextrin-Peptide-Octane Construct

In an effort to reduce possible interference of host-guest complexation in the synthesis of a host-peptide-guest construct, an α-cyclodextrin host and alkyl chain guest were

incorporated into the design of the octyl-peptide **83** which was synthesised according to Scheme **4.6**. The peptide **81** was prepared using Fmoc coupling solid-phase synthesis, with octanoic acid used in the final on-resin coupling step. In standard peptide synthesis methods, the peptide is cleaved from the resin then precipitated into diethyl ether to remove reagents used in the cleavage, however the peptide **81** was soluble in this solvent. The method was therefore modified, using a 10% acetonitrile in water solution for the precipitation step. Although 100% water also produced precipitation, the product tended to float on top of the supernatant making recovery by centrifugation difficult. The addition of a small amount of acetonitrile prevented this.

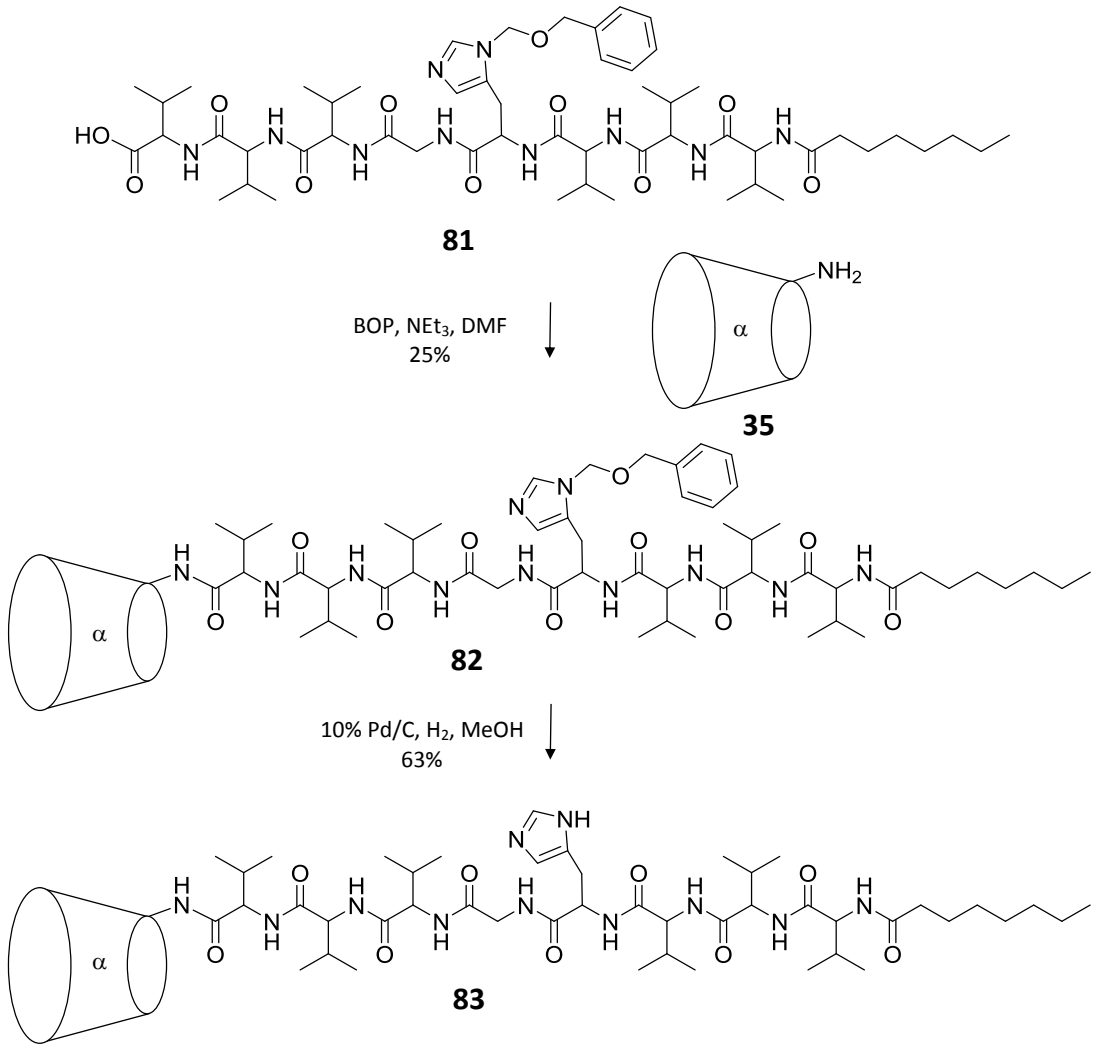

Scheme 4.6 Synthesis of the octyl-peptide **83**.

The crude octyl-peptide **81** was subjected to HPLC, which proved challenging as the compound was difficult to solubilise on account of its amphiphilic nature, and tended to gelate in the HPLC solvent (50% MeCN and H_2O). The purified octyl-peptide **81** was analysed by HPLC (Figure **4.4**) and integration of the product peak at 28.07 min showed

96% purity. The peak at 25.84 min is likely to be truncated peptide as a consequence of incomplete coupling on the solid-phase, considering its similarity in elution time to the product **81** and absorbance profile. Given this similarity and the yield of only 16%, further purification by HPLC or recrystallisation was not practical and the octyl-peptide **81** was used with this purity.

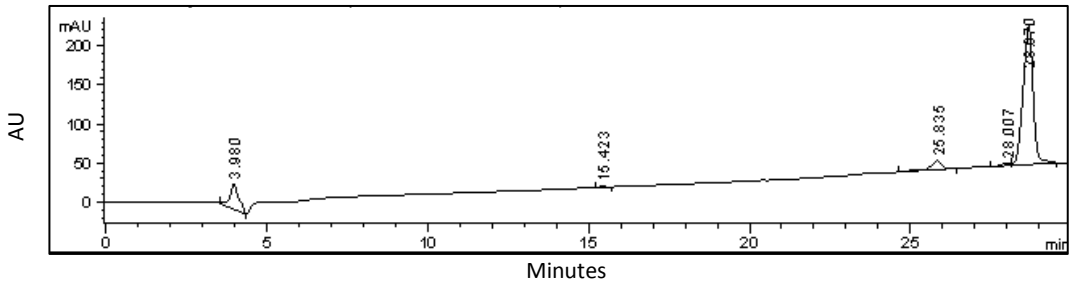

Figure 4.4 Chromatogram acquired by reverse phase analytical HPLC of the octyl-peptide **81**, monitored at 220 nm.

The ^{1}H NMR spectrum of the octyl-peptide **81** (Figure **4.5**) shows the proton signals arising from this compound. The valine protons are assigned to the signals that occur at 4.30-4.08 (α-protons), 2.18-1.87 (β-protons, with contribution to the integration from two of the octyl protons) and 0.87-0.75 ppm (γ-protons, with contribution to the integration from the octyl chain methyl protons). The glycine residue protons are assigned to signals that occur at 3.82-3.70 ppm. The histidine residue protons are assigned to signals at 8.35 (ε-proton), 7.38-7.28 (δ-proton, with contribution to the integration from the aromatic BOM protons), 4.64 (α-proton) and 3.04-2.98 ppm (a β-proton, with the other β-proton partially obscured by the HOD solvent signal), and the BOM-protecting group also giving signals assigned at 7.38-7.28 (aromatic, with contribution to the integration from the histidine δ-proton), 5.70 (O-CH_2-N), 5.64 (O-CH_2-N) and 4.54 ppm (Ar-CH_2-O). Finally, octyl chain protons are assigned to signals at 2.18-1.87 (contributing two protons to the integration here), 1.50-1.43 (integrating to two protons), 1.22 (integrating to eight protons) and the methyl protons occurring in the signal at 0.94-0.72 ppm.

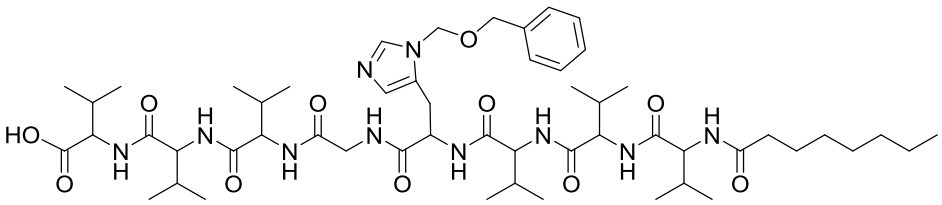

81

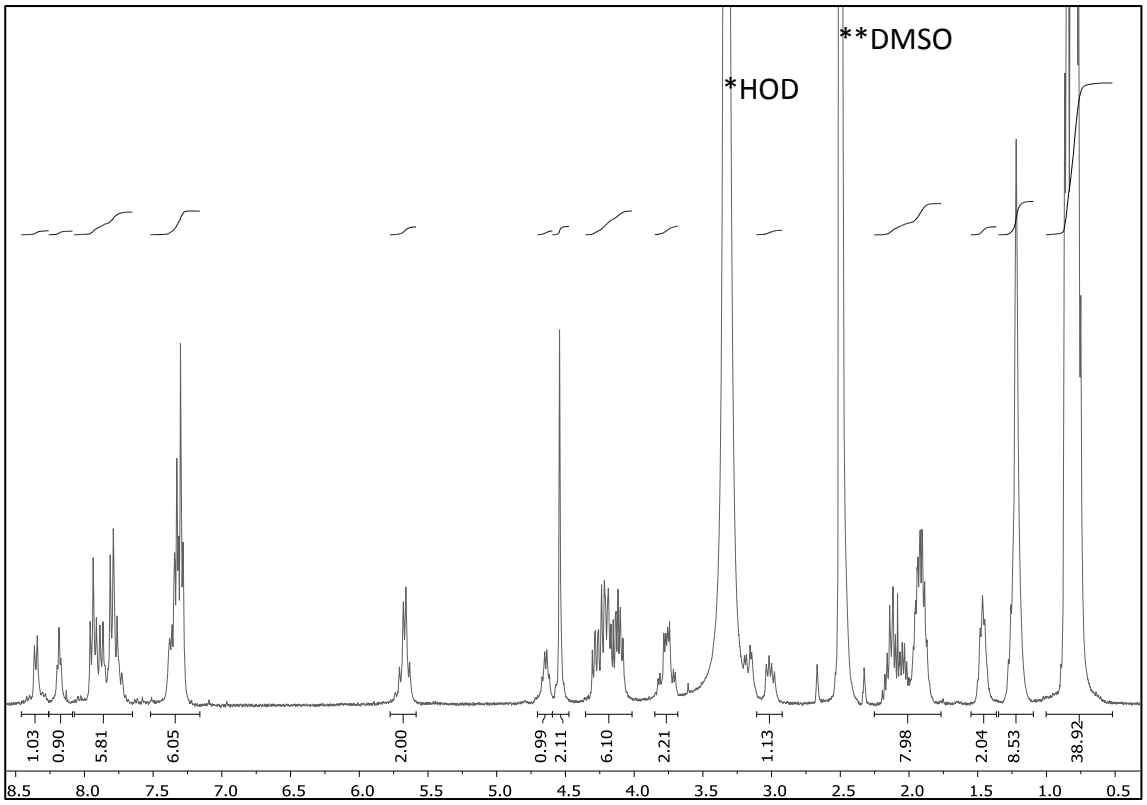

Figure 4.5 400 MHz ^{1}H NMR spectrum of the octyl-peptide **81** (2 mM) in DMSO-d_6 at 25 °C. *Denotes residual HOD solvent signal, **denotes residual DMSO solvent signal.

The peptide **81** was then coupled with amino-α-cyclodextrin **35** and the crude octyl-peptide **82** was subjected to HPLC. Analysis after HPLC (Figure **4.6**) showed the presence of impurities, but the close elution of these impurities to the product peak made further purification impractical. The crude yield of this material was 25%.

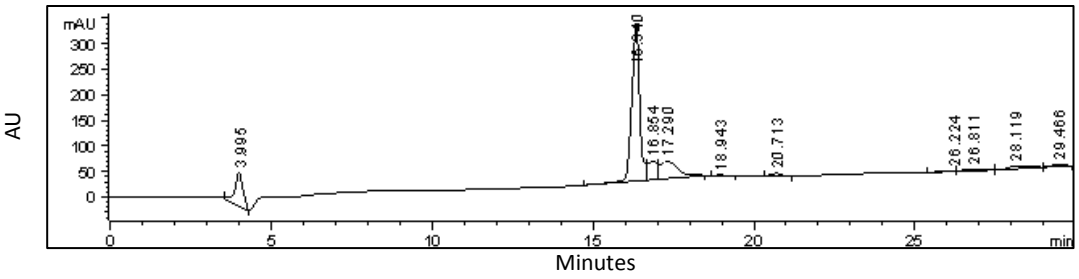

Figure 4.6 Chromatogram acquired by reverse phase analytical HPLC of the octyl-peptide **82**, monitored at 220 nm.

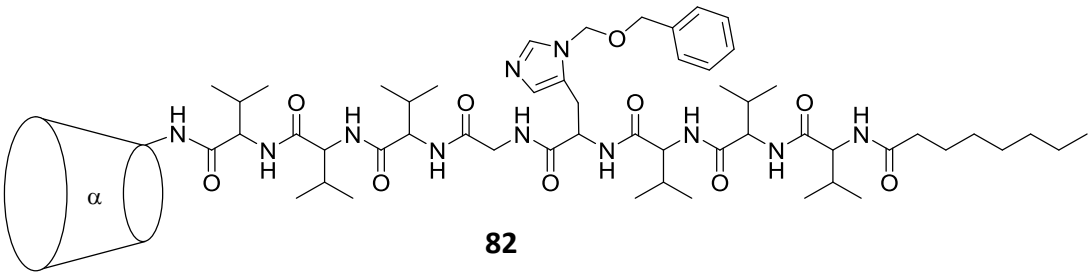

82

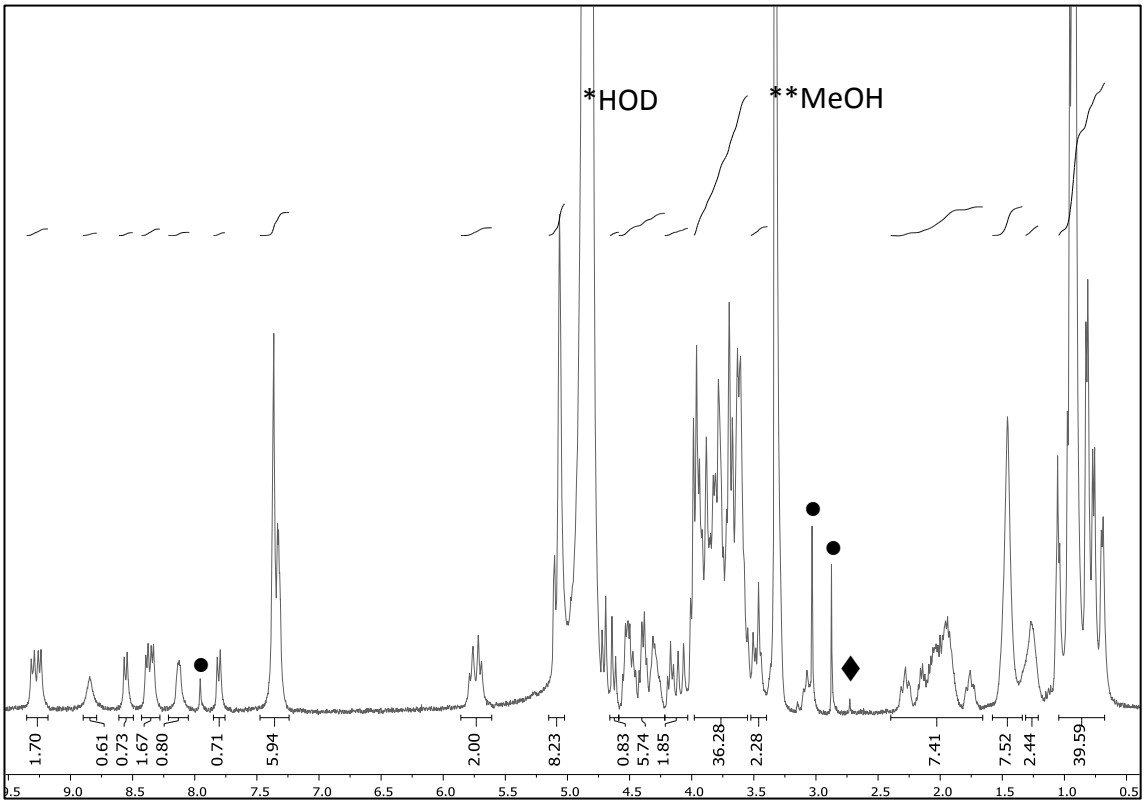

Figure 4.7 400 MHz ^{1}H NMR spectrum of the octyl-peptide **82** (2 mM) in CD_3OD at 25 °C. *Denotes residual HOD solvent signal, **denotes residual MeOH solvent signal, ● denotes DMF solvent impurity, ♦ denotes HMPA impurity.

The ^{1}H NMR spectrum of the product (Figure **4.7**) shows proton signals that are closely similar to those observed in the spectrum of the octyl-peptide **81** with the addition of signals assigned to the α-cyclodextrin moiety at 5.11 (H1, integration is affected by the HOD solvent peak) and 4.02-3.45 ppm (H2-6). A small amount of residual DMF solvent, and HMPA coupling by-product is also observed in the ^{1}H NMR spectrum.

The histidine BOM protecting group in the octyl-peptide **82** was then removed by reduction with hydrogen over palladium on charcoal. Analysis by HPLC (Figure **4.8**) showed the desired product **83** in a 95% purity. Although the octyl-peptide **83** contains an impurity, eluting at 20.17 min, purification was not practical as the low overall yield

of the synthesis resulted in only 12 mg of material for subsequent study. Any attempt at purification by HPLC would reduce this yield even further and purification by recrystallisation would be unlikely with such an amphiphilic compound. As such, further purification was not performed and a yield of 63% recorded.

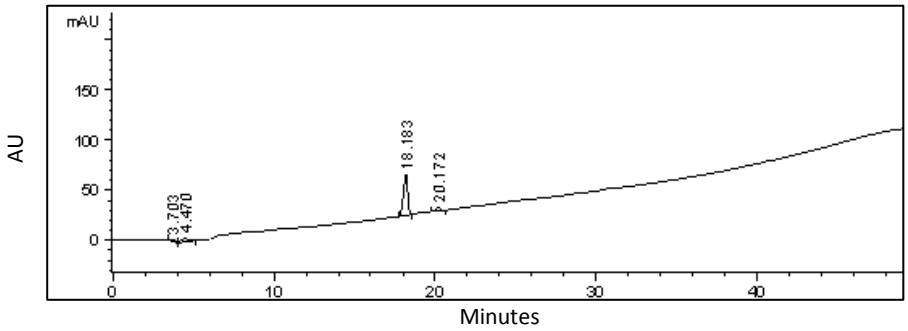

Figure 4.8 Chromatogram acquired by reverse phase analytical HPLC of the octyl-peptide **83**, monitored at 220 nm.

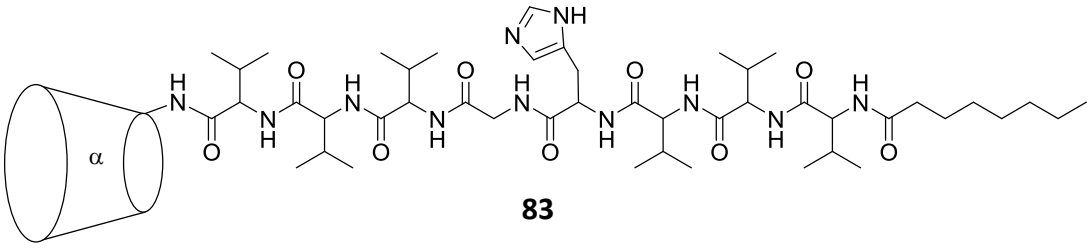

83

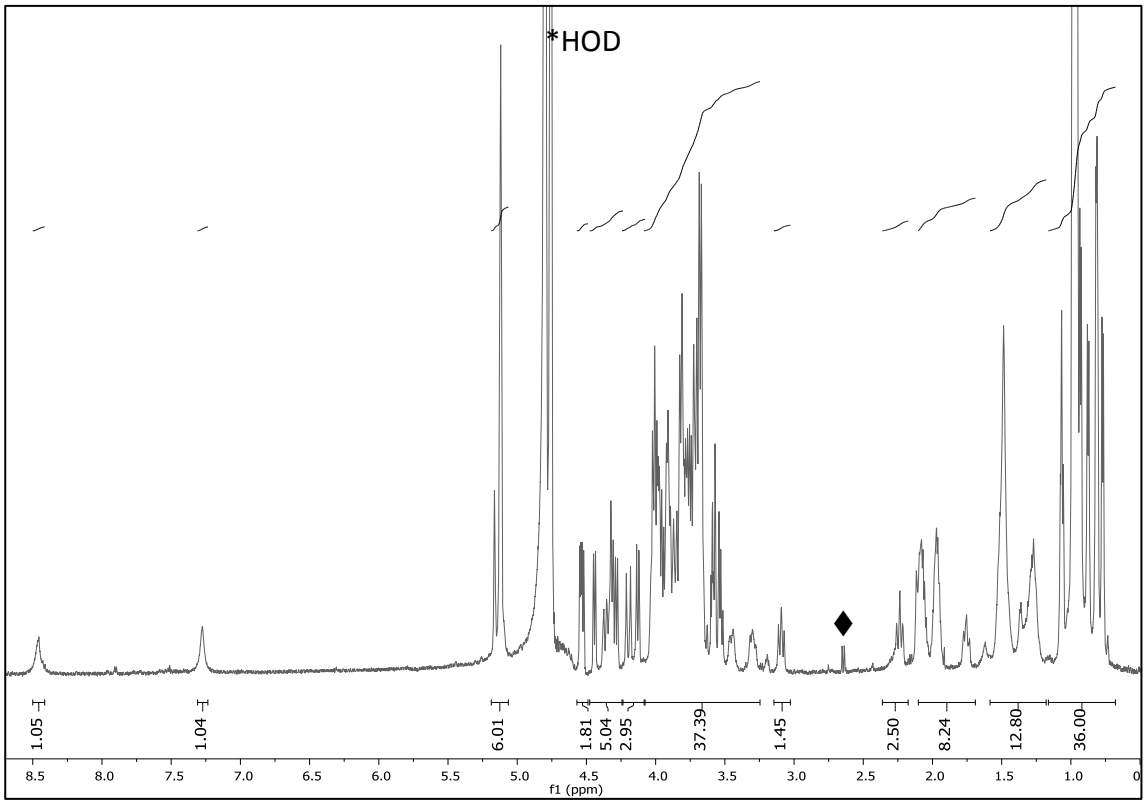

Figure 4.9 600 MHz ^{1}H NMR spectrum of the octyl-peptide **83** (2 mM) in D_2O at 25 °C. *Denotes residual HOD solvent signal and ♦ denotes HMPA impurity.

The ^{1}H NMR spectrum indicated that the removal of the BOM protecting group had proceeded to completion (Figure **4.9**), with the absence of BOM-proton signals at ~7.3 and ~5.7 ppm.

4.7 Synthesis of a Control Peptide

In order to differentiate between binding effects of the peptide sequence itself and those arising from any self-assembled structures, a peptide sequence with no cyclodextrin or guest moiety was synthesised to act as a control. To discount effects from the presence of free *C*- and *N*-termini, the acylated, amidated peptide **85** was prepared by solid-phase peptide synthesis. This was achieved by reacting the synthesised on-resin peptide with 10% acetic anhydride in pyridine to give *N*-terminus acetylation, and using Rink amide resin as the solid-phase which gives an amide at the *C*-terminus upon cleavage of the peptide. The peptide **85** was then purified by HPLC in a yield of 7% (Figure **4.10**) however the compound was insoluble under the aqueous conditions in which cyclodextrin host-guest self-assembly and therefore metal binding by the peptide **83** would be examined, and therefore was not useful. Instead, the unmodified peptide **84**, which was soluble under aqueous conditions, was prepared by solid-phase synthesis and purified by HPLC in a 19% yield. The free termini in the peptide **84** do not affect its validity as a control against the octyl-peptide **83**, as it has been previously reported that the carboxyl and amine groups can act as metal binding sites.[187] Any increase in metal-binding ability in the functionalised peptide **83**, where these sites are no longer available, will therefore be attributable to effects of cyclodextrin host-guest binding.

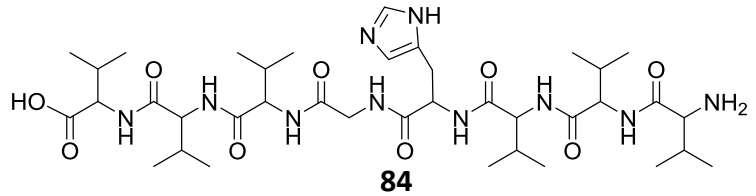

84

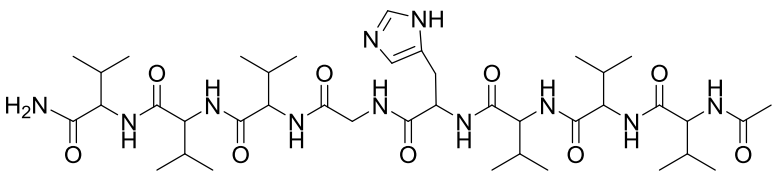

85

Figure 4.10 The unmodified control peptide **84** and the *C*- and *N*-terminally protected peptide **85**.

The ^{1}H NMR spectrum of the peptide **84** (Figure **4.11**) shows proton signals assigned to the histidine residue at 8.68 (ε-proton), 7.38 (δ-proton) 4.74-4.71 (α-protons) and 3.37-3.32 ppm (β-protons). The glycine residue protons are assigned to contribute to the integration of the peaks at 4.29-3.88 ppm, which are also assigned to the valine α-protons. The valine β-protons are assigned to the signal at 2.26-1.99 ppm, and the γ-protons to the signal at 1.04-0.84 ppm.

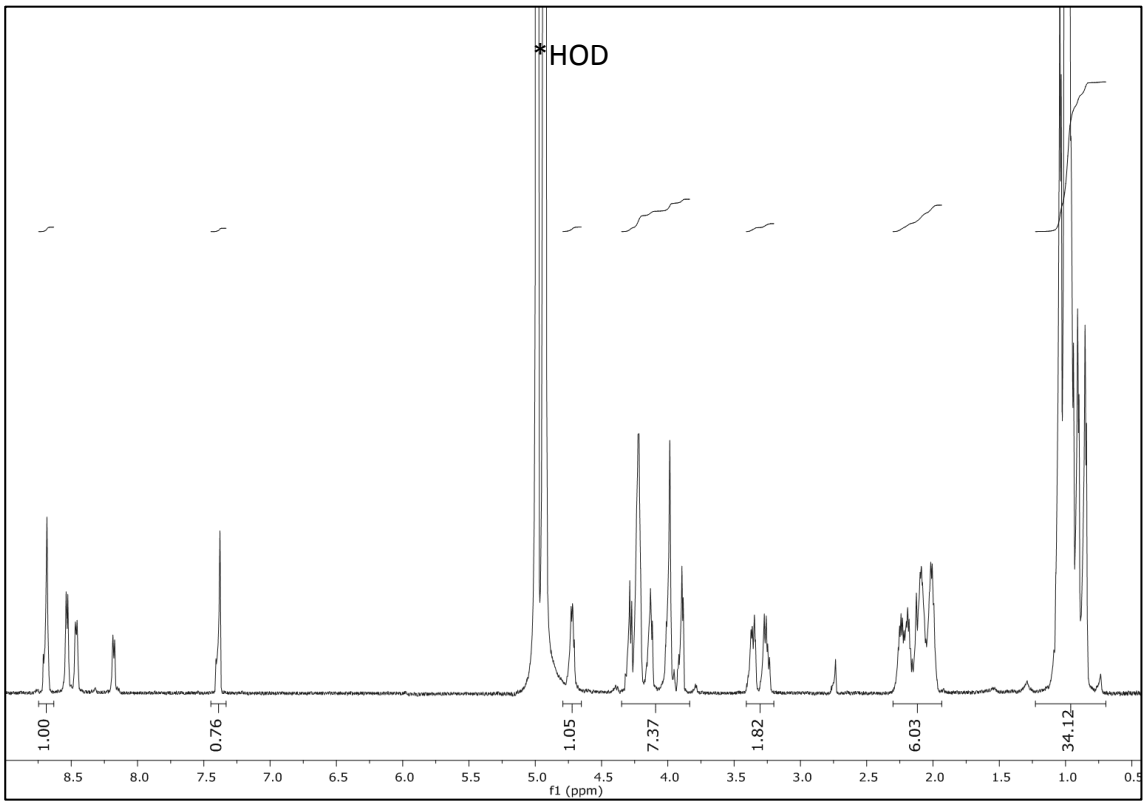

Figure 4.11 400 MHz ^{1}H NMR spectrum of the octyl-peptide **84** (2 mM) in D_2O at 25 °C. *Denotes residual HOD solvent signal.

4.8 Self-Assembly Behaviour of the α-Cyclodextrin-Peptide-Octane Construct

Having successfully synthesised the monomer **83**, its self-assembly behaviour was investigated. An ITC dimer dissociation experiment was performed with a 1.4 mM syringe solution of the octyl peptide **83** in buffer, titrating into a blank buffer solution (Figure **4.12**). A pH of 7.5 was used as this is the pH at which metal-binding experiments were to be conducted, where the histidine imidazole is neutral.[190] A data curve was

obtained (Figure **4.13**) however it appears to be biphasic and does not strictly follow a simple dimer dissociation model. The data peaks also change sign from endothermic to exothermic as the titration progresses. As the data was unexpected, the experiment was repeated with similar conditions (octyl-peptide **83** syringe solution of 1.5 mM) but gave an almost identical data curve, showing that these results are reproducible.

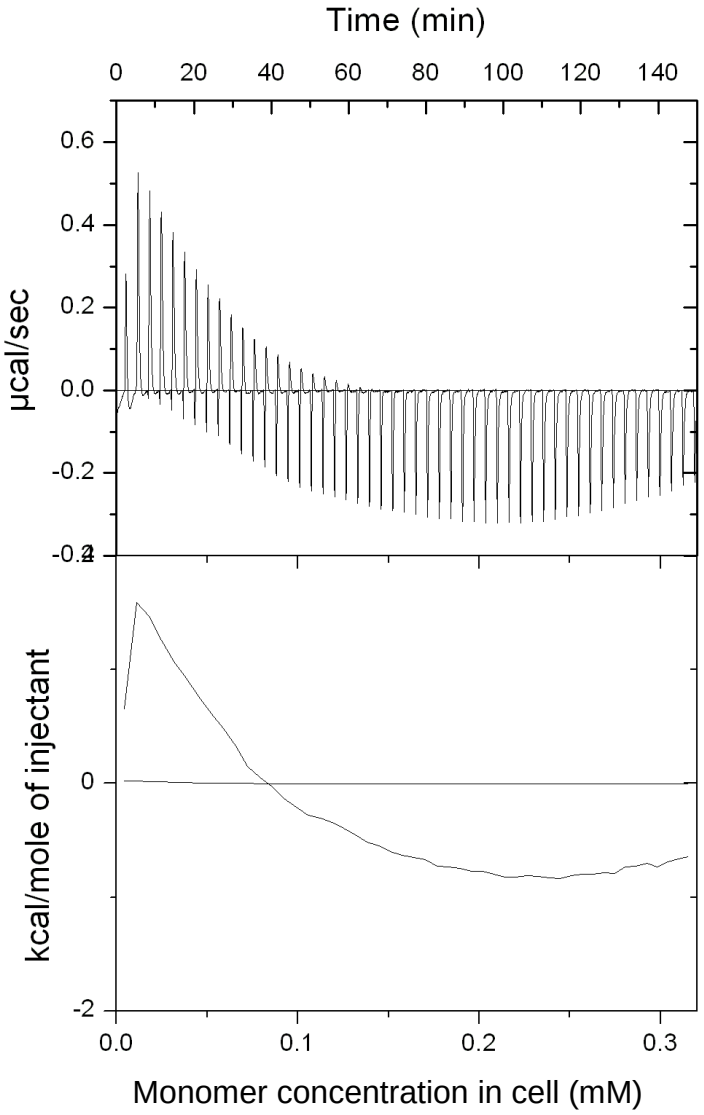

Figure 4.12 ITC data of the octyl peptide **83** (1.4 mM) with 5 µL injections into phosphate buffer (1.4365 mL, 5 mM, pH 7.5).

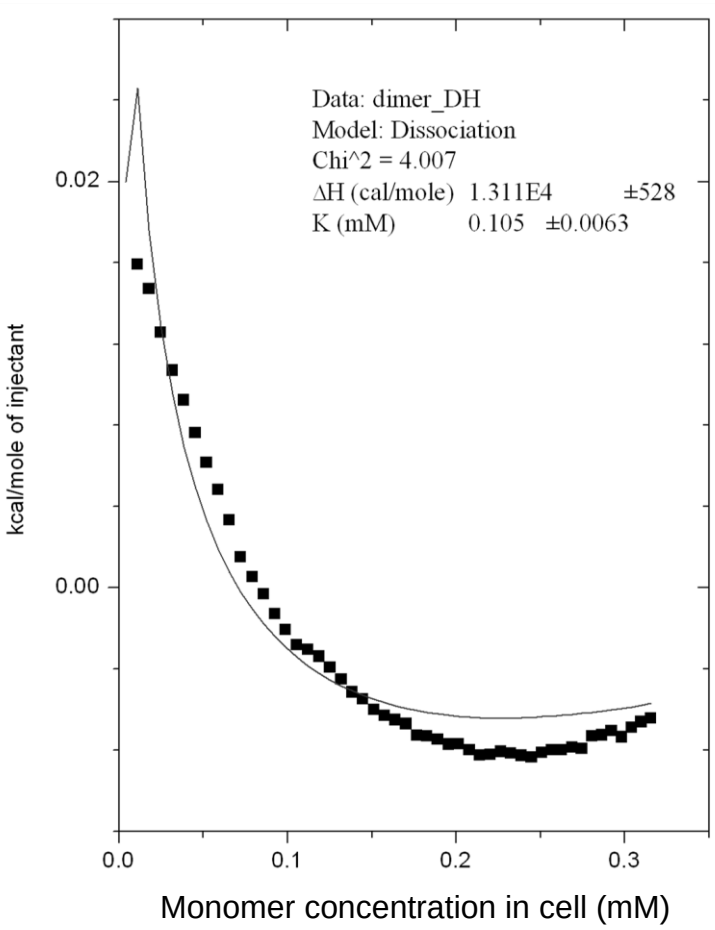

Figure 4.13 Fitted dimer dissociation curve to the octyl-peptide **83** ITC data.

It seemed likely that the data curve may be reflective of two concurrent thermodynamic processes with the lower monomer cell concentration data dominated by dimer dissociation energy and data at the higher concentration revealing a weaker, secondary interaction. This type of system would also account for the change in sign of the data peaks from endothermic to exothermic,[191, 192] as over the course of the titration endothermic dimer dissociation energy becomes less apparent and an exothermic curve is revealed.

The ITC curve was replotted using only data up to a 0.165 mM monomer cell concentration (Figure **4.14**). The derived K_d value for dimer dissociation is slightly higher than that obtained with the extended concentration range in Figure **4.13**. This again indicates that the secondary interaction observed in the titration of the octyl-peptide **83** is weaker than the primary one and more significant over the higher concentration range.

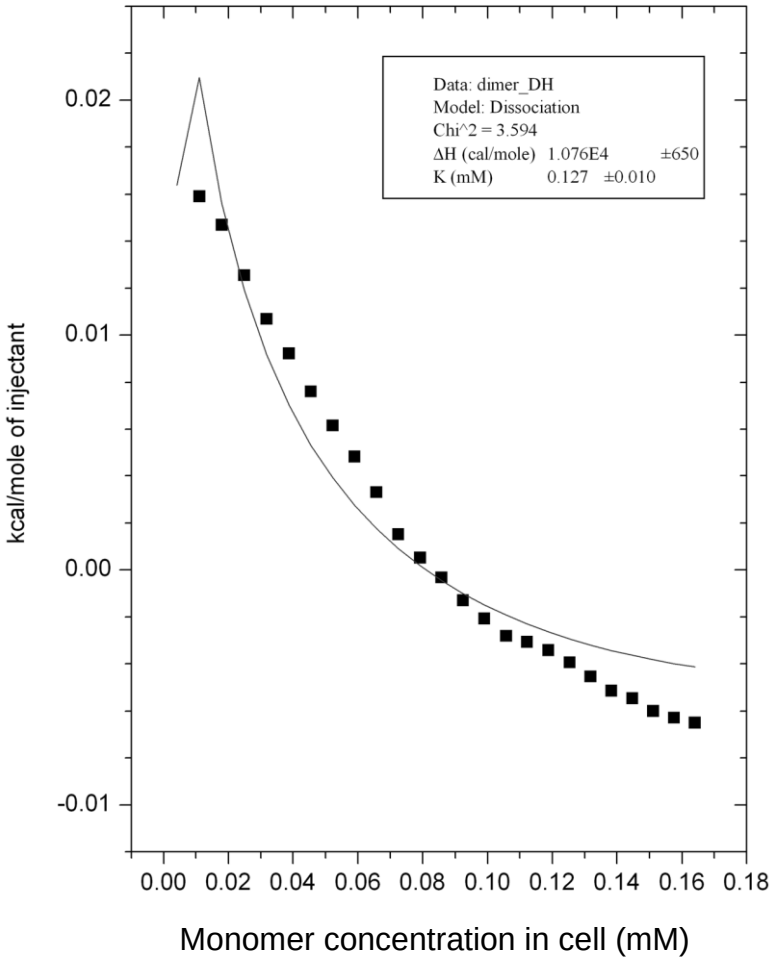

Figure 4.14 Fitted dimer dissociation curve to the octyl-peptide **83** ITC data up to 0.165 mM monomer cell concentration.

In order to further investigate the nature of the second interaction, another ITC dissociation experiment was performed with a higher octyl-peptide **83** syringe concentration of 4.1 mM and the data fitted to a dimer dissociation curve (Figure **4.15**). The K_d derived from this data however, is very different to that derived from the data in Figure **4.14** and is unusually small. Again, this suggests that a weaker secondary interaction becomes more significant at higher concentrations.

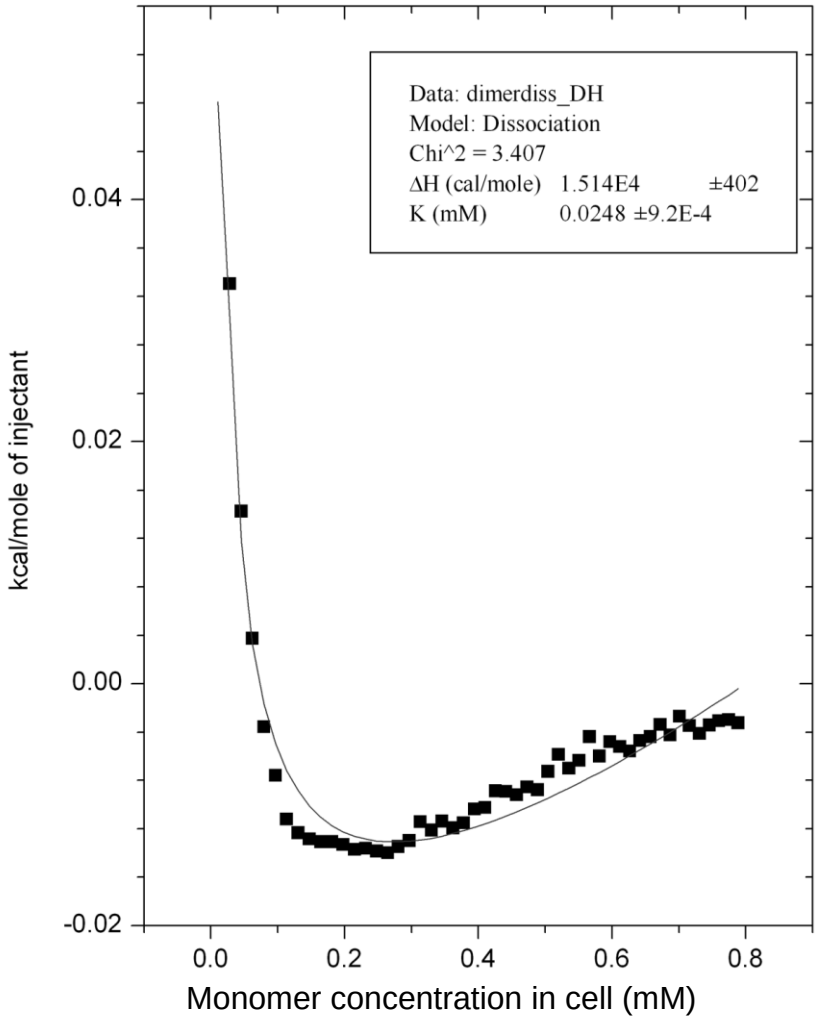

Figure 4.15 Fitted dimer dissociation curve to the octyl-peptide **83** ITC data with a 4.1 mM initial syringe concentration.

It follows that the data at low concentrations provides the best measurement of the dimer dissociation constant K_d and the value of 0.127 mM obtained as shown in Figure **4.14** was therefore taken as being the most accurate. The K_d of dimer dissociation derived from the data shown in Figure **4.14** corresponds to a K_a of 7,874 M^{-1}. The determined dimer association constant for the compound **83** is higher than that for the free cyclodextrin and guest group (the K_a of α-cyclodextrin with octanoic acid is 1,820 M^{-1})[193] indicating that another thermodynamically favourable interaction, such as β-sheet formation, also contributes to dimer formation. The measured K_d value can be used to calculate the concentrations where either the dimer or the monomer is predominant; above 5.7 mM the octyl-peptide **83** exists as >90% dimer and at 8 μM it exists at >90% monomer (see Appendix A for calculations).

An ITC dissociation experiment was then performed with the control peptide **84** in order to compare the effect of the presence of the cyclodextrin-octane host-guest pair on self-assembly behaviour. Titration of a 2 mM syringe solution of the control peptide **84** in buffer into blank buffer solution gave linear ITC data showing that over the concentration range observed no concentration dependent species such as dimers are formed (Figure **4.16**). As the unmodified peptide **84** does not assemble but the cyclodextrin and guest-modified peptide **83** does, this indicates that host-guest interactions are responsible for this behaviour as opposed to an inherent property of the peptide sequence.

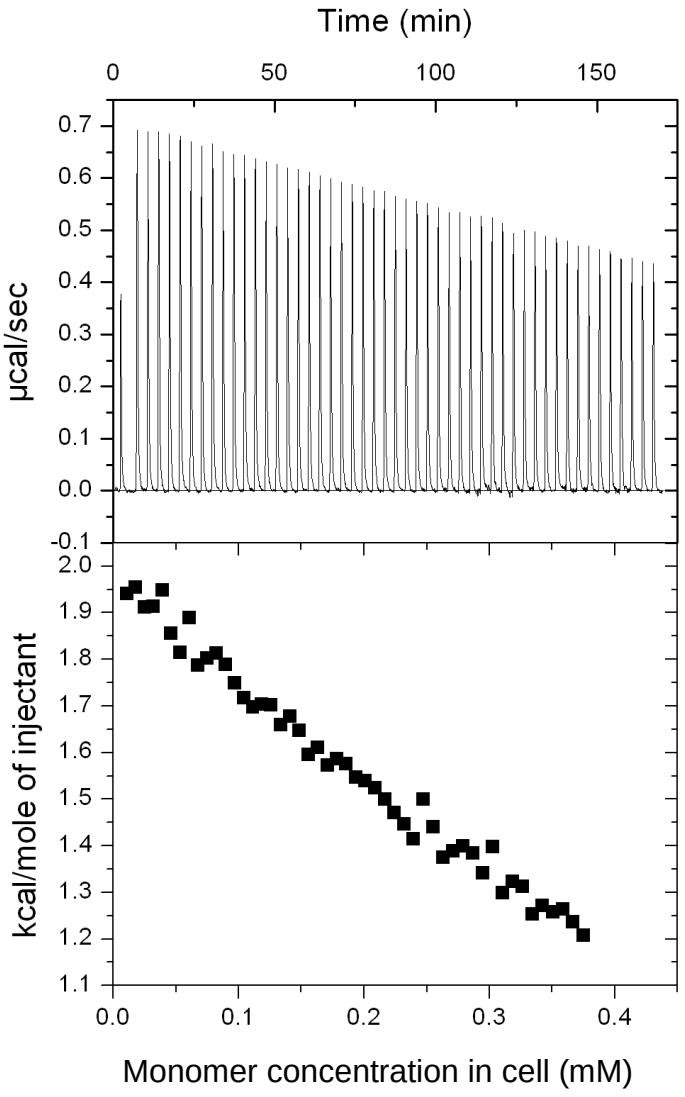

Figure 4.16 ITC data of the control peptide **84** (2 mM) with 5 µL injections into phosphate buffer (1.4365 mL, 5 mM, pH 7.5).

In order to further assess the assembling behaviour observed in the ITC experiments with the peptide **83** is a result of cyclodextrin host-guest complexation, the compound

was analysed by 2D ^{1}H-^{1}H ROESY NMR spectroscopy. The spectrum shows nOe signals between cyclodextrin protons at 4.02, 3.84 and 3.72 ppm and octane protons at 1.44 and 1.23 ppm (Figure **4.17**), indicating the octyl moiety is inside the cyclodextrin cavity. The spectrum was observed in a 5 mM solution of the octyl-peptide **83** which according to the measured K_d corresponds to 89% dimer formation. As the octyl-peptide **83** exists mainly as a dimer under these conditions, this suggests that the observed nOe interactions arise from the formation of a [*c*2]-complex assembled *via* cyclodextrin host-guest inclusion.

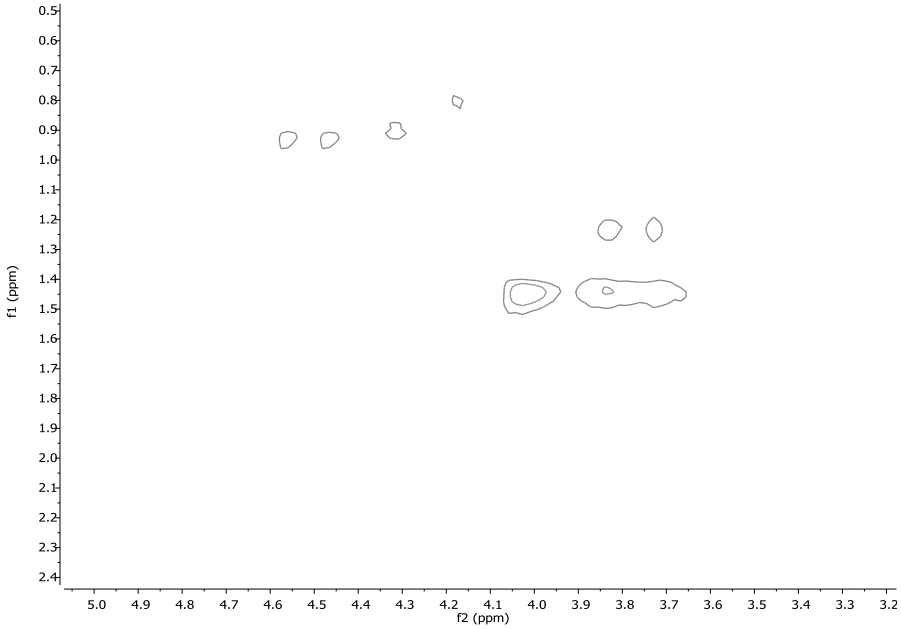

Figure 4.17 2D ^{1}H-^{1}H ROESY spectrum of the octyl-peptide **83** (5 mM) in *d*-phosphate buffer (5 mM, pH 7.5) at 500 MHz.

It is not possible to determine from the 2D ^{1}H-^{1}H ROESY NMR spectrum of the octyl-peptide **83** whether the monomeric proportion is a [*c*1]- or [*a*1]-species as any nOe signals would be masked by those of the dimer. As it was not practical to investigate solutions of the octyl-peptide **83** where mainly monomer is present, the compound was instead examined over a range of concentrations to see if structural changes in the peptide moiety correlated with extent of dimer formation.

4.9 Effect of Complex Formation on Peptide Structure in the α-Cyclodextrin-Peptide-Octane Construct

Circular dichroism spectroscopy was used to investigate the effect of [*c*2]-complex formation on peptide structure by measuring spectra over a series of concentrations which give a range in the extent of dimer formation. For comparison, the secondary structure of the peptide sequence without the influence of cyclodextrin host-guest complex formation was ascertained by measuring the circular dichroism spectra of the control peptide **84**.

The spectra of the peptide **84** show a strong minimum at ~197 nm, indicative of a random coil structure (Figure **4.18**). The spectra do not display any concentration dependency, supporting the conclusion drawn from the ITC dimer dissociation data of peptide **84** that at these concentrations no oligomeric species are formed.

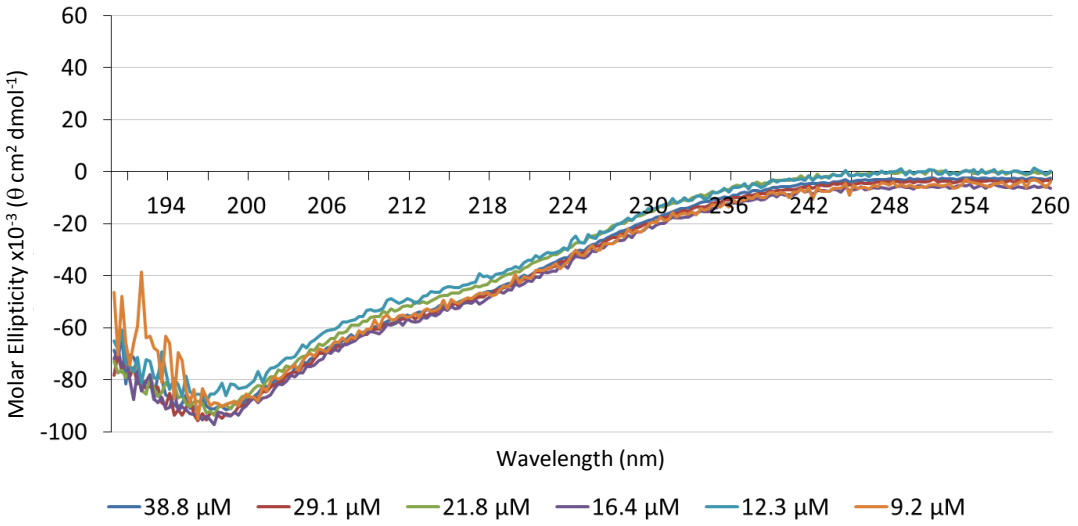

Figure 4.18 Circular dichroism spectra of the control peptide **84** (9.2-38.8 µM) in phosphate buffer (5 mM, pH 7.5).

The circular dichroism spectra of the octyl peptide **83** were then measured and show a strong minimum at ~214 nm, a signal characteristic of β-sheet structure (Figure **4.19**). The random coil signal at ~197 nm observed with the control peptide **84** (Figure **4.18**) is not observed. These differences in the circular dichroism spectra of the two peptides, which only differ in the presence or absence of a cyclodextrin and guest moiety, indicate that the formation of a cyclodextrin host-guest complex with the octyl-peptide **83** induces β-sheet formation in the peptide sequence which otherwise has very little

inherent secondary structure. The spectra of the octyl-peptide **83** also display concentration dependency in the signal at ~214 nm, with molar ellipticity increasing as concentration increases. This indicates that β-sheet structure in the peptide **83** is concentration dependent.

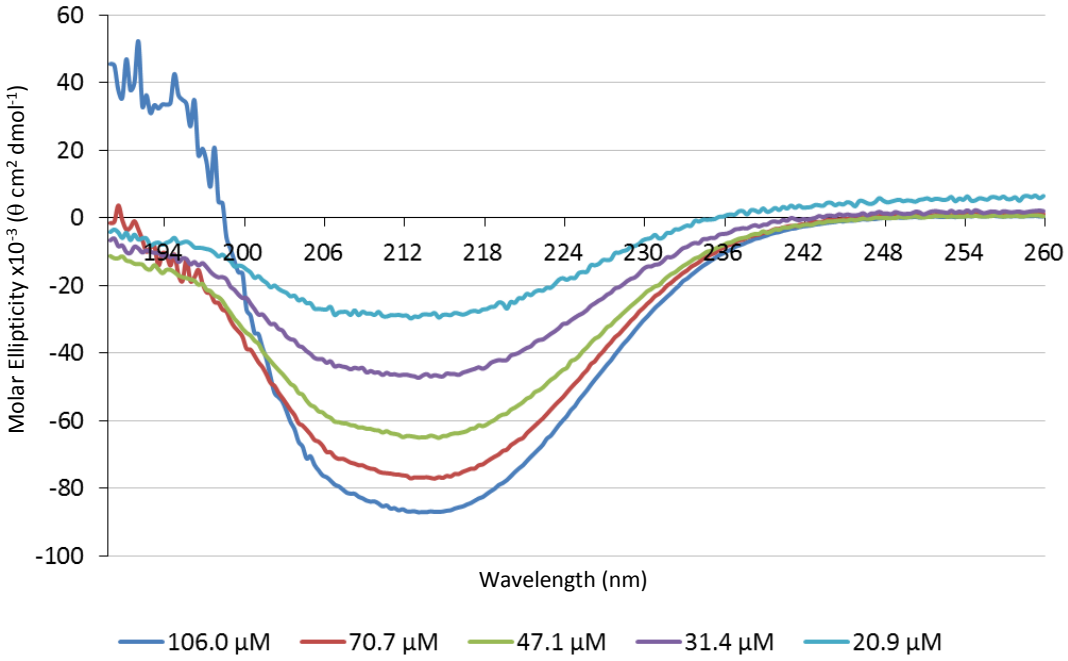

Figure 4.19 Circular dichroism spectra of the octyl peptide **83** (20.9-106.0 µM) in phosphate buffer (5 mM, pH 7.5).

According to the K_d of dimer dissociation, the octyl peptide **83** exists as 21-47% dimer at the concentrations where circular dichroism spectra were measured. The extent of dimer formation plotted against molar ellipticity at 214 nm (Figure **4.20**) shows a strong linear relationship, indicating that β-sheet structure in the peptide sequence is a result of [*c*2]-complex formation. This trend also suggests that the K_d value obtained from Figure **4.14** is appropriate, and that the secondary assembly interaction does not affect the extent of β-sheet character in the peptide moiety of the octyl peptide **83** at these concentrations.

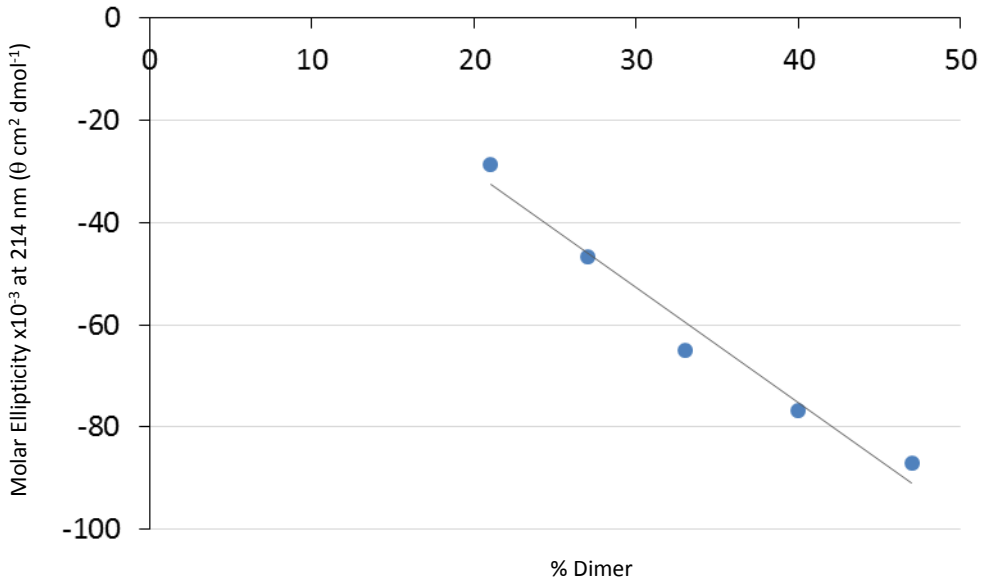

Figure 4.20 Relationship between the extent of β-sheet formation in the octyl peptide **83** and % dimer at varying concentrations.

4.10 Determination of Zinc Metal-Binding Capabilities of the α-Cyclodextrin-Peptide-Octane Construct

Having established that the octyl peptide **83** forms a [*c*2]-complex *via* cyclodextrin host-guest complexation, which then induces β-sheet formation in the peptide sequence, it was then investigated whether the self-assembled complex operates as a binding site. As the Zn^{2+} metal ion chosen in the design of this device is diamagnetic, binding could be investigated by NMR spectroscopy.

The control peptide **84** was first examined, to establish if the peptide sequence itself has any Zn^{2+} metal binding ability. $ZnCl_2$ was titrated into a 2 mM solution of the peptide **84**. It was not possible to perform this experiment in a suitable buffer as phosphate buffer interacts with Zn^{2+}, and non-interacting buffers such as HEPES were not available in a deuterated form. To minimise effects from pH and to ensure that the histidine imidazole remained neutral and therefore available for binding, the $ZnCl_2$ and peptide **84** solutions were made from the same stock solution which was adjusted to pH 7 with NaOD. ^1H NMR spectra after each titration of $ZnCl_2$ were obtained (Figure **4.21**), however there were no changes in the chemical shift of δ and ε histidine protons indicating that no binding was occurring at this residue. None of the other protons in the spectrum

changed in chemical shift upon $ZnCl_2$ titration, showing that binding was also not occurring at other sites.

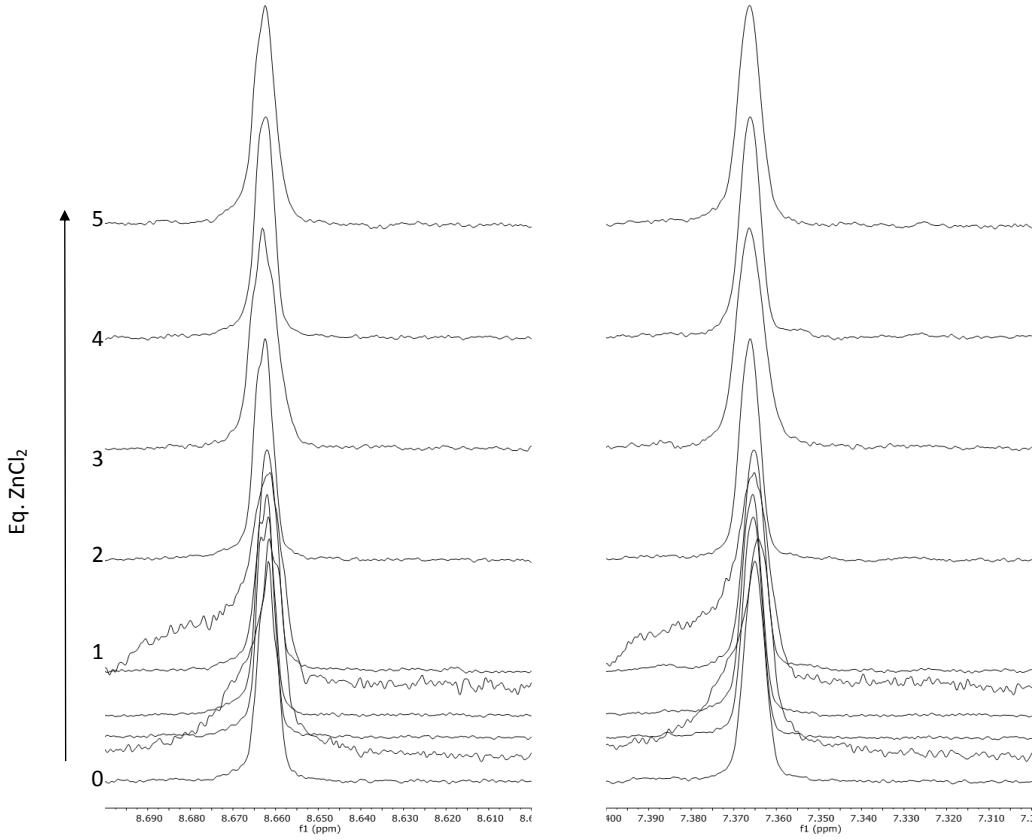

Figure 4.21 ^{1}H NMR spectra of the peptide **84** (2 mM) with addition of $ZnCl_2$, showing no change in the chemical shift of the histidine εH (*left*) or the histidine δH (*right*).

$ZnCl_2$ was then titrated into 2-3 mM solutions of the octyl peptide **83**, which corresponds to solutions where 84-86% dimer is formed. After each addition of $ZnCl_2$ solution a ^{1}H NMR spectrum was obtained (Figure **4.22**), showing that upon titration the chemical shifts of the δ and ε histidine protons moved downfield. No other protons were affected, indicating that binding occurs at the histidine residues only.

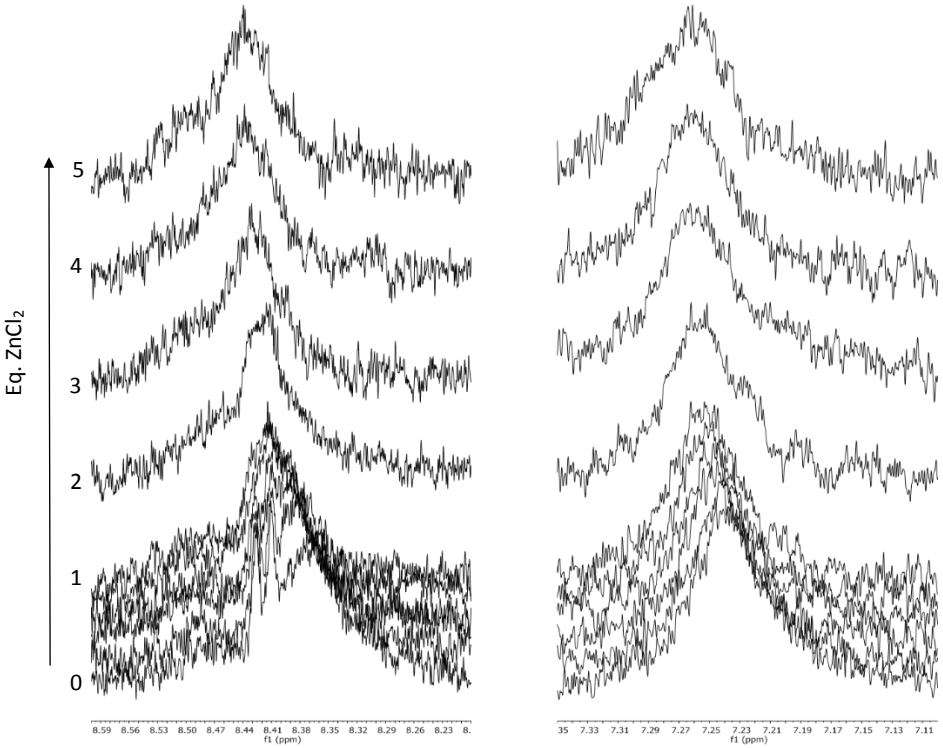

Figure 4.22 ^{1}H NMR spectra of the octyl peptide **83** (2 mM) with addition of $ZnCl_2$, showing a change in the chemical shift of the histidine εH (*left*) and the histidine δH (*right*).

The changes in chemical shift of the δ and ε histidine protons could then be plotted against $ZnCl_2$ equivalents to give a binding curve (Figure **4.23**) from which a K_a of Zn^{2+} association could be derived using a fitting program[194] written for Matlab. Titrations were performed in triplicate, giving K_a values of 2,319 M^{-1}, 2,325 M^{-1} and 2,441 M^{-1} and an average K_a of 2,362 M^{-1}. Calculations were made treating the octyl peptide **83** dimer as a single ligand, with host concentrations of the dimer rather than the monomer. The K_a of Zn^{2+} binding is close to the literature value measured for a short peptide containing two histidine residues, of 4,571 M^{-1}.[187] This is a good indication that the self-assembled octyl peptide **83** [*c*2]-complex is acting as a pseudo-chelated ligand with two histidine residues, one in each monomer, contributing to binding.

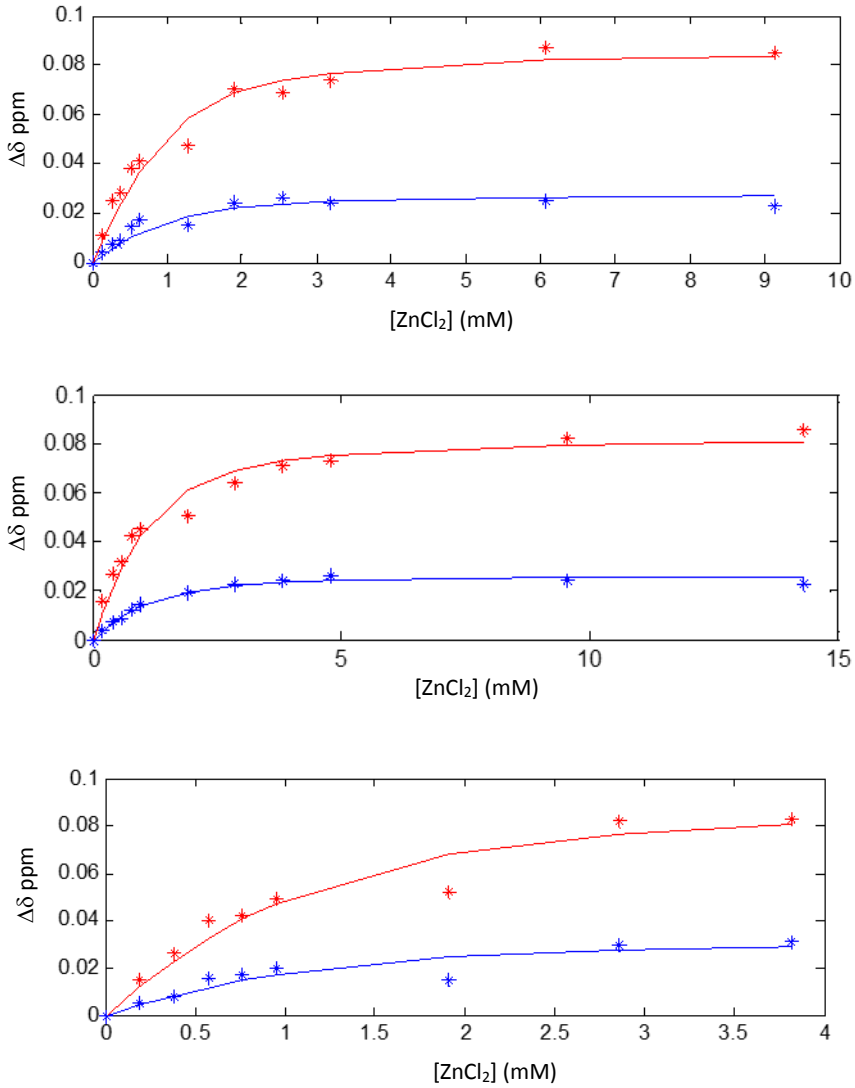

Figure 4.23 Binding curves fitted to the change in chemical shift of histidine εH (*red*) and δH (*blue*) in octyl cyclodextrin peptide **83** upon addition of $ZnCl_2$. Association constants were calculated as K_a 2319 M^{-1} (*top*), 2325 M^{-1} (*centre*) and 2441 M^{-1} (*bottom*) for each titration, giving an average of K_a 2362 M^{-1}. The sum of squares for the fit to the binding model for each titration are 0.00036129 (*top*), 0.00032090 (*centre*) and 0.00131922 (*bottom*).

A Job plot of the ^1H NMR spectroscopy titration data was also made (Figure **4.24**), plotting the change in chemical shift of the δ and ε histidine protons in each titration experiment multiplied by the mole fraction, against the mole fraction. Mole fraction was calculated using Equation **4.1**, where the concentration of the host was considered as the concentration of the octyl peptide **83** dimer.

$$\text{Mole fraction} = \frac{[\text{Host}]}{[\text{Host}] + [ZnCl_2]}$$

Equation 4.1 Expression for the calculation of mole fraction used to create Job plots.

The plots for δ and ε histidine protons in all titrations show a maximum in the curve at 0.5. This indicates that the binding ratio between the octyl peptide **83** dimer and Zn^{2+} is 1:1, providing further evidence that [*c*2]-dimer formation gives the device binding capability. This binding ratio also suggests that the other aggregates observed in the ITC dissociation experiments are not the foundation of the compound's metal-binding property.

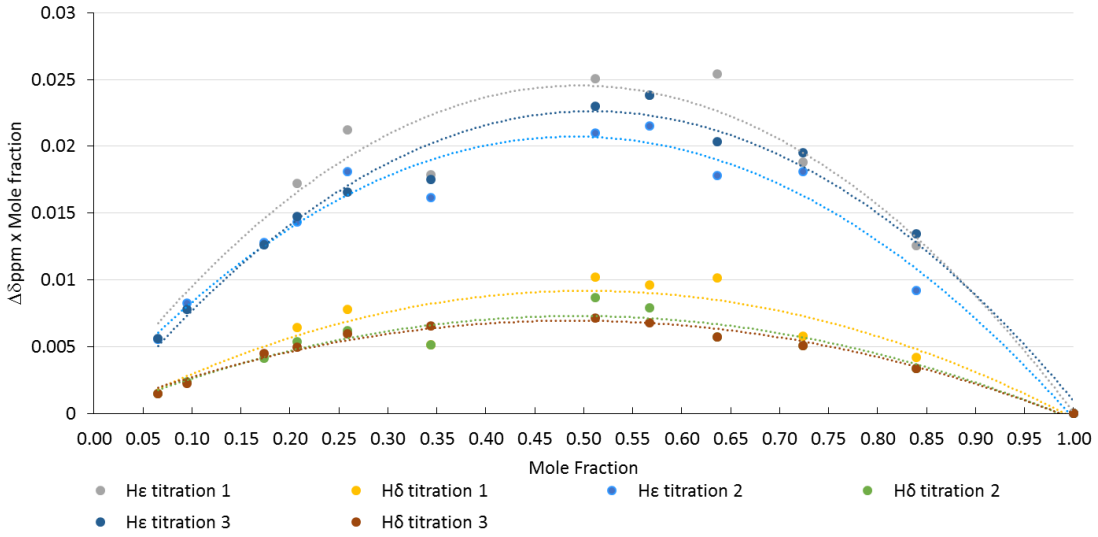

Figure 4.24 Job plot of ^{1}H NMR titration data where mole fraction = [dimer]/[dimer]+[$ZnCl_2$]

These titration experiments demonstrate that the octyl-peptide **83** operates as designed. Cyclodextrin host-guest complexation results in the assembly of a [*c*2]-complex, which induces a change in secondary structure in the peptide moiety as β-sheets are induced. This in turn affords the assembly zinc-binding capability with a K_a of 2,362 M^{-1}, a function which is not present at all in the unmodified peptide sequence.

4.11 Crystal Structure of the Zinc Metal-Binding α-Cyclodextrin-Peptide-Octane Construct

Having established that in solution the octyl-peptide **83** self-assembles into a [*c*2]-complex which then binds a Zn^{2+} metal ion, the solid-phase behaviour of the compound was explored. A crystal was successfully grown by vapour diffusion from a solution of the octyl-peptide **83** (5 mM) and $ZnCl_2$ (5 mM) in 1M ammonium sulphate and 0.1 M tris HCl buffer, macro-seeded with smaller crystals from a previous crystal growth experiment.

The crystal structure shows the octyl peptide **83** as a self-included [*c*1]-complex, bound to a Zn^{2+} ion *via* the histidine residue (Figure **4.25**) (see Appendix B for coordinates). Four molecules of the octyl peptide **83** [*c*1]-complex are bound to each Zn^{2+} ion in a square planar configuration (Figure **4.26** and Figure **4.27**). The packing of the crystal consists of these tetramers arranged in a 2D plane, with each at 180 ° to its adjacent neighbour (Figure **4.28**). These planes are then stacked along a third axis, with the cyclodextrin moieties of the tetramers and the Zn^{2+} ions facing each other (Figure **4.29**).

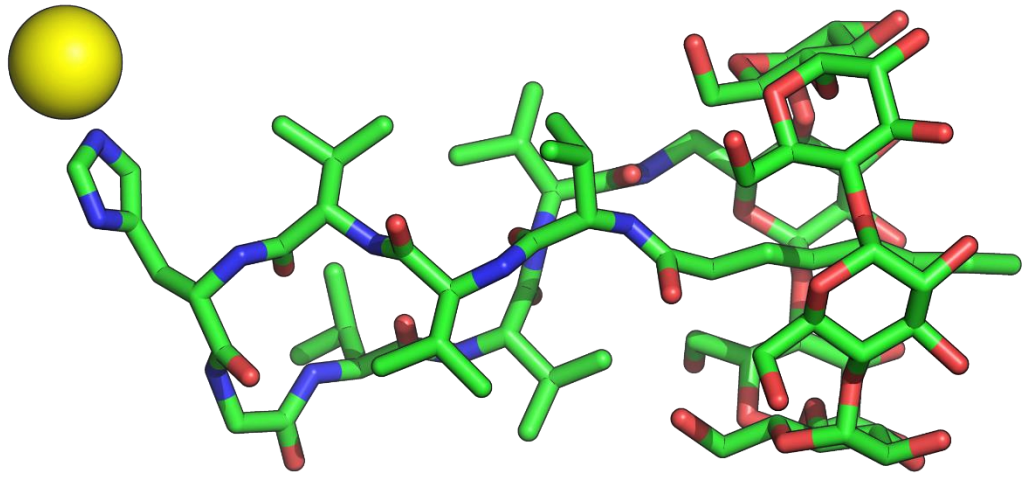

Figure 4.25 Crystal structure of the octyl-peptide **83** showing the self-included complex bound to Zn^{2+}. Carbon atoms are shown in green, oxygen in red, nitrogen in blue and Zn^{2+} in yellow.

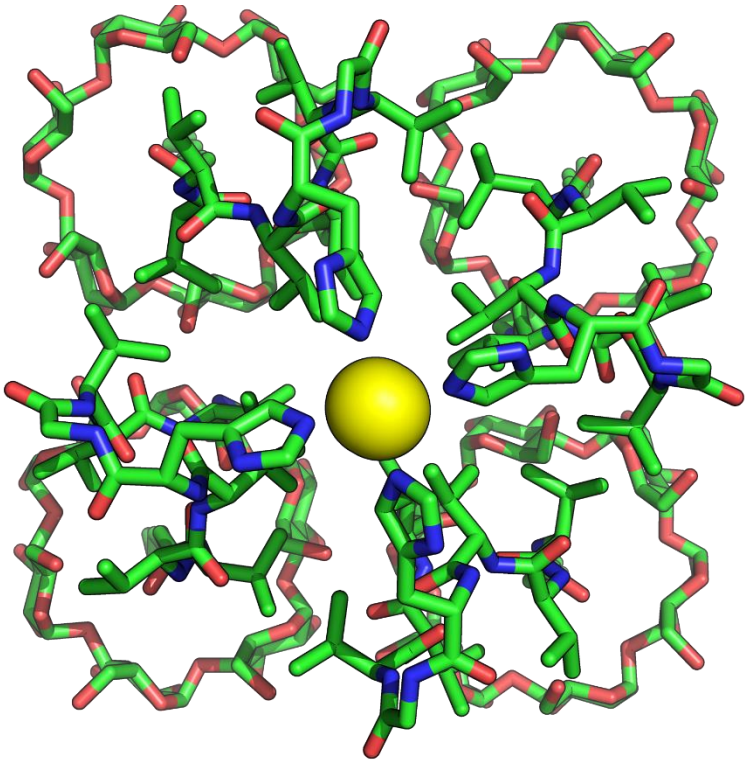

Figure 4.26 Crystal structure of the octyl-peptide **83** showing four modified peptides are bound to each Zn^{2+} in a square planar configuration.

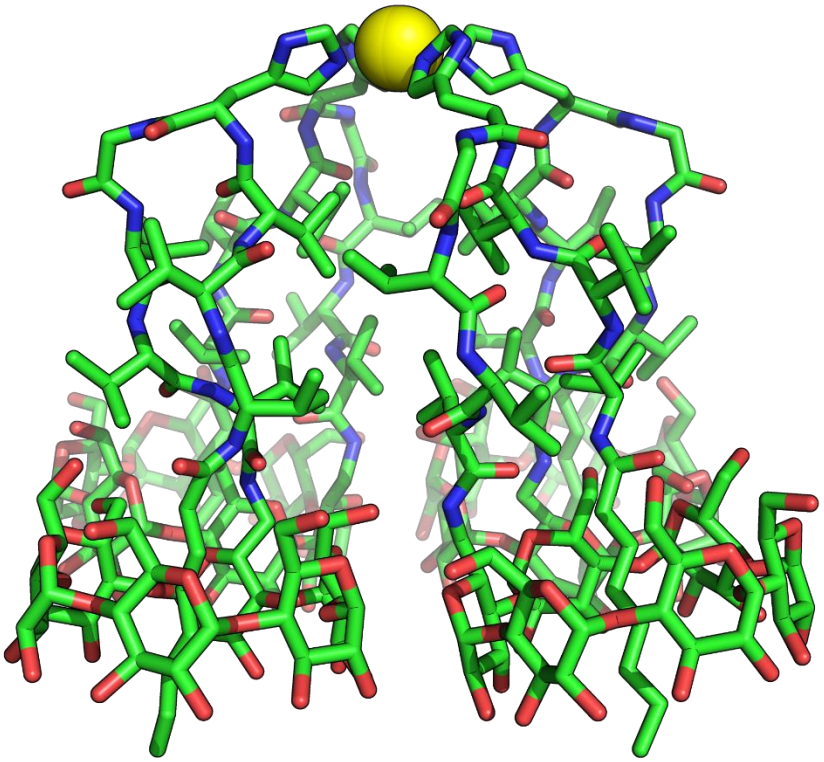

Figure 4.27 Side view of the crystal structure of the octyl-peptide **83**.

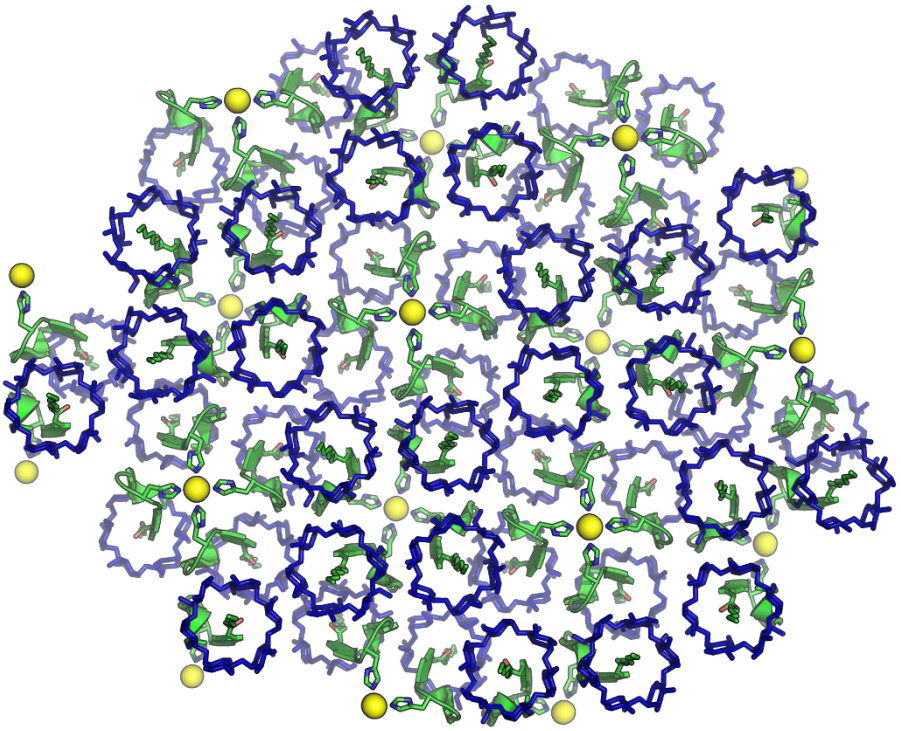

Figure 4.28 The packing of the crystal of the octyl-peptide **83** with cyclodextrin moieties shown in blue, peptides in green and Zn^{2+} in yellow. Each Zn-tetramer is orientated 180 ° to its adjacent neighbour.

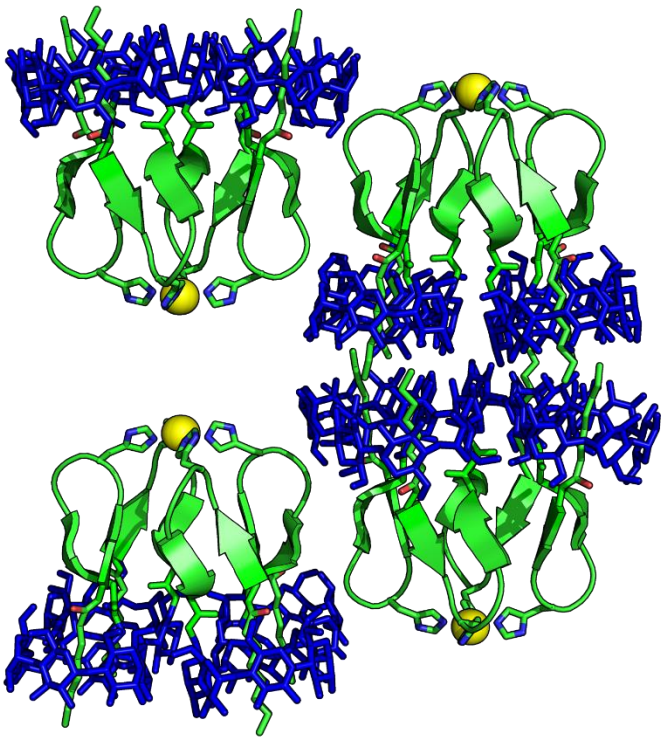

Figure 4.29 The packing of the crystal of the octyl-peptide **83** showing that along a third axis, tetramers are stacked so that cyclodextrin moieties and Zn^{2+} ions are facing.

Although the Zn^{2+}-octyl peptide **83** crystal was grown from a 5 mM solution, which according to the K_d of dimer dissociation represents 89% octyl-peptide **83** dimer assembly, the [*c*1]-complex preferentially crystalises. This is likely because of more favourable crystal packing interactions between the cyclodextrin and exposed peptide moieties, enabled by self-included arrangement. The low initial ratio of monomer does not affect crystalisation as any [*c*1]-monomer which crystalises out of solution leads to a re-establishment of the monomer-dimer equilbrium in solution.

A crystal of the octyl peptide **83** in the absence of Zn^{2+} was also grown, with the structure again showing a self-included [*c*1]-complex (Figure **4.30**) (see Appendix C for coordinates). The side-chain of the histidine residue could not be refined, probably because the absence of metal-binding results in more freedom of movement within the crystal at this position. As the octyl peptide **83** not only adopts the same structure with or without the metal, but also has the same packing behaviour (Figure **4.31** to Figure **4.34**), this suggests that metal binding does not template structure formation and assembly of the octyl-peptide **83**. Rather, the cyclodextrin host-guest inclusion complex forms first and it is this pre-assembled structure that facilitates metal binding, a

mechanism reminiscent of the folding of metalloproteins into binding sites for metal ions.

Attempts were then made to grow a crystal of the control peptide **84**, however these were not successful. Although an exhaustive study of crystal growth conditions was not conducted, this suggests that the control peptide **84** does not form an ordered structure in the solid state.

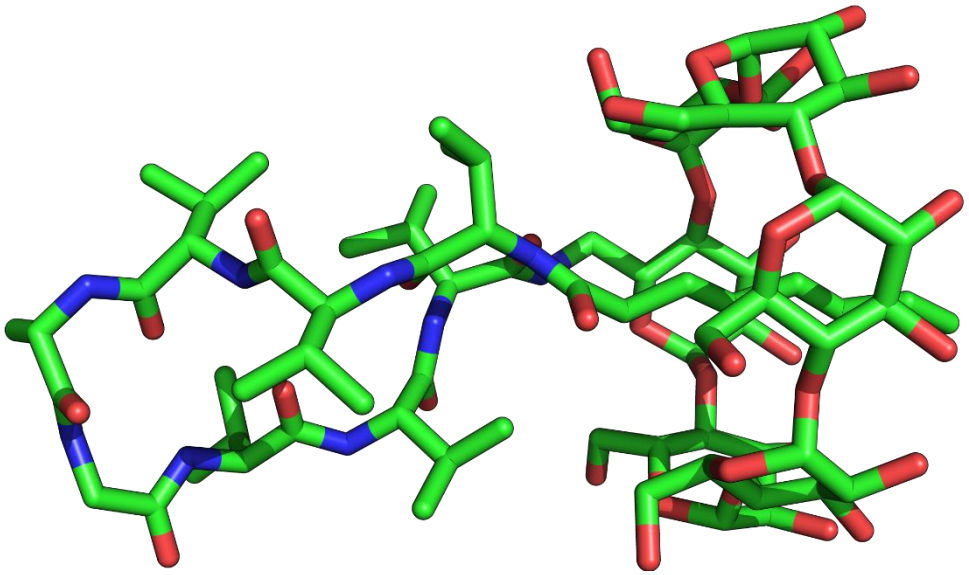

Figure 4.30 Crystal structure of the octyl peptide **83** in the absence of Zn^{2+} showing a self-included complex. The histidine residue could not be resolved, indicating it has a high degree of movement when not bound to Zn^{2+}.

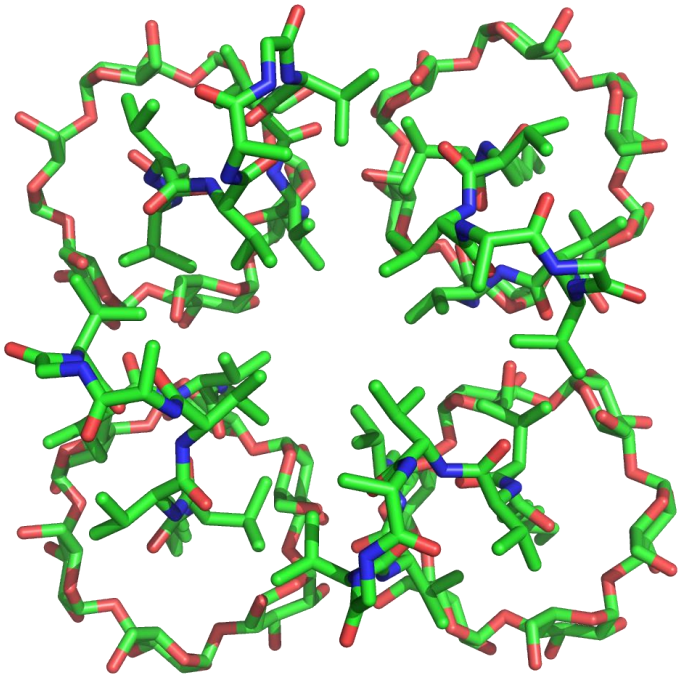

Figure 4.31 Crystal structure of the octyl-peptide **83** in the absence of Zn^{2+} showing four [*c*1]-complexes pack in a tetrameric arrangement even without metal-binding interactions.

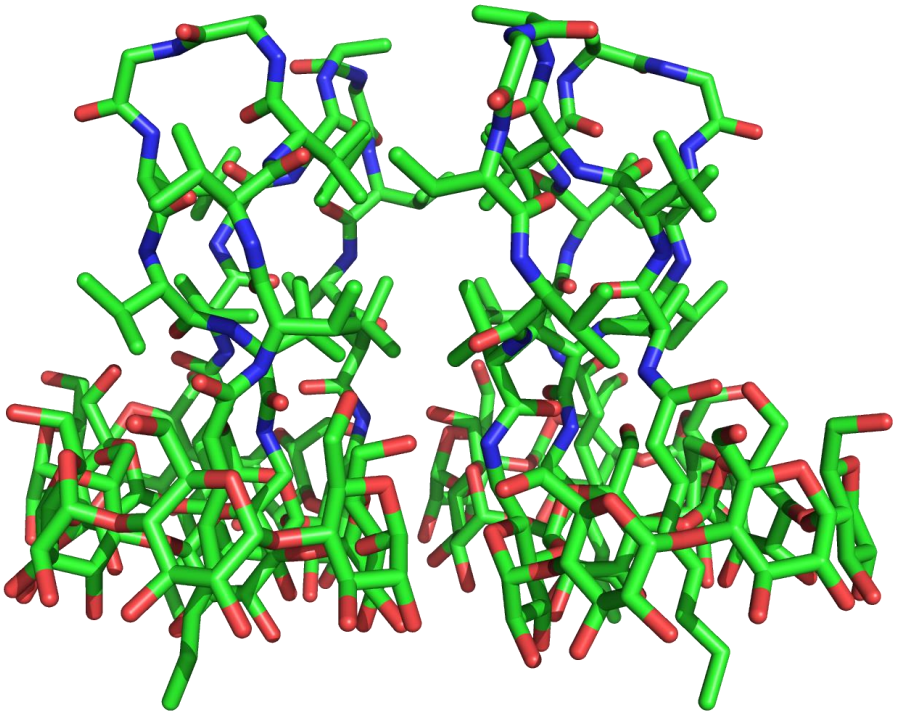

Figure 4.32 Side view of the crystal structure of the octyl-peptide **83** tetramer in the absence of Zn^{2+}.

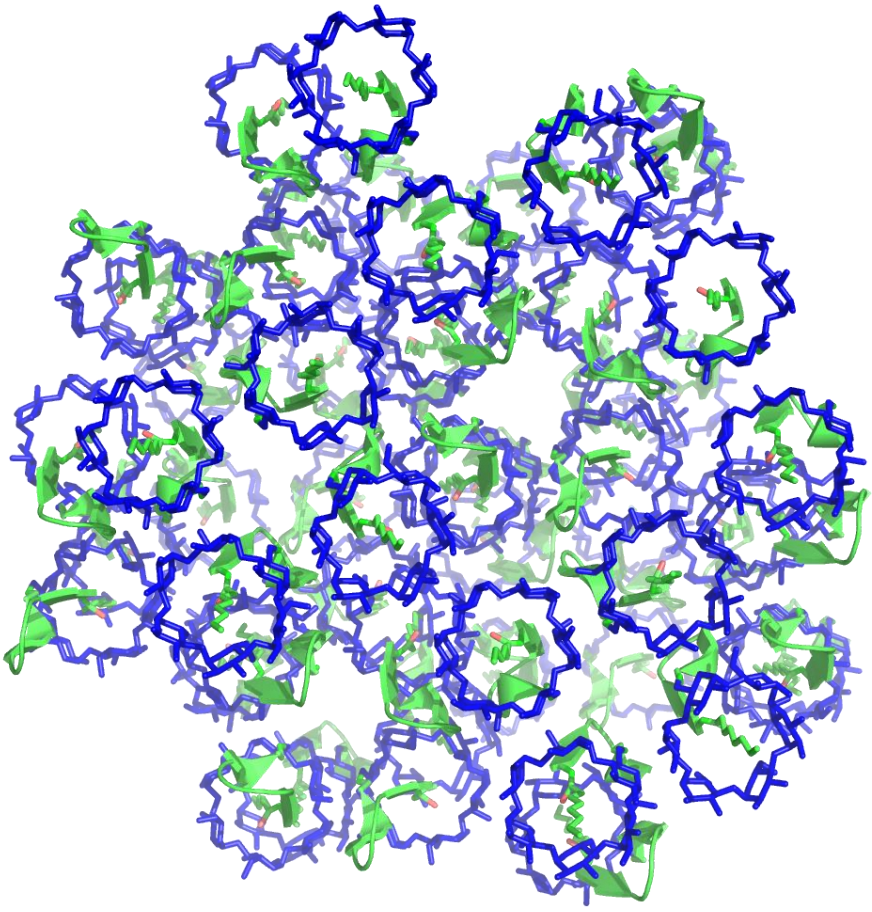

Figure 4.33 The packing of the crystal of the octyl-peptide **83** in the absence of Zn^{2+} with cyclodextrin moieties shown in blue and peptides in green. Each tetramer is orientated 180 ° to its adjacent neighbour.

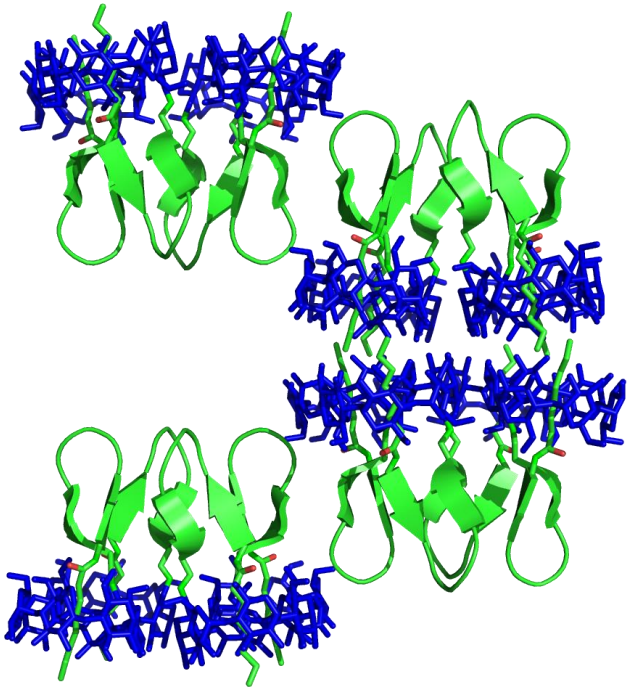

Figure 4.34 The packing of the crystal of the octyl-peptide **83** in the absence of Zn^{2+} showing that along a third axis, tetramers are stacked so that cyclodextrin moieties and peptides are facing.

4.12 Conclusions

A peptide sequence modified with an α-cyclodextrin and an octane guest was designed to act as an artificial, self-assembling metal-binding site. The host-peptide-guest construct **83** was envisaged to assemble into a [*c*2]-complex, giving a change in the secondary structure of the peptide which would in turn facilitate the arrangement of a metal binding site.

ITC experiments and 2D ^{1}H-^{1}H ROESY NMR spectroscopy demonstrated that the octyl-peptide **83** assembles *via* cyclodextrin host-guest complexation into a [*c*2]-dimer structure with a K_a of 7,874 M^{-1}. Circular dichroism spectroscopy then showed that the assembly of this dimeric complex induces β-sheet secondary structure in the peptide sequence and that the extent of β-sheet formation is directly related to extent of [*c*2]-dimerisation, which is concentration dependent. Comparison with a control peptide, **84** shows that the peptide sequence itself has no inherent ordered secondary structure and does not form dimers.

Titration of the octyl-peptide **83** with $ZnCl_2$ was then used to measure a K_a of Zn^{2+}, plotting a binding curve of changes in the chemical shifts of the δ and ε histidine protons. Metal binding was measured with a K_a 2,362 M^{-1}, compared to the control peptide **84** which demonstrated no binding at all. Job plots indicate that binding is 1:1 for the octyl peptide **83** dimer:Zn^{2+}.

The octyl-peptide **83** was then investigated for its behaviour in the solid-phase using crystallography. A crystal structure of the octyl-peptide **83** in the presence of Zn^{2+} shows that the compound crystallises as a [*c*1]-complex, four of which are bound to each Zn^{2+} ion in a tetrameric fashion. A crystal structure of octyl-peptide **83** in the absence of Zn^{2+} shows that the compound assembles and packs in the same way in the absence of metal-binding. This indicates that metal-binding does not template the assembly of the octyl-peptide **83**, rather the compound pre-assembles into an arrangement which acts as an artifical binding-site.

The design of the self-assembling zinc-binding site has the potential to be modified to afford various types of biomimetic sites by changing the peptide sequence, which is independent of the host-guest assembly process. Functionalities other than metal-binding, such as small molecule binding sites and catalysis could be developed using the same cyclodextrin host-guest complex formation to assemble different peptide sequences. This concept is further outlined in Chapter 8.

Chapter 5: Results and Discussion

Options for Solid-Phase Synthesis of Cyclodextrin Rotaxanes

5.1 Introduction

Although the studies described in Chapters 3 and 4 represent the main aims of this thesis project, observations made during these investigations raised some interesting ideas which are briefly explored in Chapters 5, 6 and 7. The short peptides described in Chapter 4 were prepared by solid-phase synthesis, a well-established technique for making peptides that was first developed in 1963 by Merrifield.[195] The general strategy involves coupling protected amino acids to a plastic, functionalised resin followed by deprotection, with final cleavage of the entire sequence. Two common approaches use either Boc-protected or Fmoc-protected amino acids, wherein coupling conditions are orthogonal to deprotection conditions.

The main advantage to solid-phase synthesis is that the cleaved product is usually very pure as reagents are used in excess and the excess is washed away from the resin at each stage.[196] It was hypothesised that this technique could be used for the synthesis of acyclic daisy chain compounds, where the acyclic species is built upon the insoluble resin and undesired species could be washed away.

The formation of daisy chains in solution is a thermodynamic self-assembly process where a mixture of products that can be cyclic or acyclic, and consist of multiple monomer members can assemble. The most thermodynamically stable structures are cyclic as in these cases host-guest interactions are maximised and hence favourable enthalpy is also maximised, and acyclic structures also feature an uncomplexed guest which leads to unfavourable solvent interactions. As the number of members in the system increases, so does unfavourable entropy until favourable host-guest interactions

are no longer enough to compensate and higher oligomers do not form. Consequently, very few examples of daisy chains with greater than two members exist in the literature[133-137] and none have been characterised as acyclic. The development of a solid-phase acyclic daisy chain synthesis method would therefore be highly advantageous as any species that is attached to the resin can only exist in the acyclic form, allowing cyclic daisy chains to be washed away. Although the technique would require more steps than a one-pot self-assembling synthesis, it potentially gives access to products that may form in only small amounts, or not at all under equilibrium in solution.

Solid-phase peptide synthesis is performed in organic solvents (usually DMF), and commercial resins such as Wang resin and Rink Amide resin have properties that allow them to swell in these conditions and hence undergo reaction efficiently. In order to thread a guest through a cyclodextrin host and consequently synthesise a daisy chain, at least some reactions would be required to be undertaken in aqueous solution. Tentagel® resin was therefore used for solid-phase daisy chain synthesis as this gives good swelling properties in both aqueous and organic solutions (Table **5.1**).[197]

Resin \ Solvent	Water	DMF
Wang	0	4.1
Tentagel®	3.6	4.7

Table 5.1 Swelling volumes of Wang and Tentagel® resin (mL g^{-1}).[197]

5.2 Attempted Daisy Chain Synthesis from a Guest-Modified Resin

Initially, a reaction scheme for the synthesis of a daisy chain was designed whereupon a guest would be coupled to the resin, upon which a cyclodextrin host could be threaded (Scheme **5.1**). Peptides are synthesised using amino acids with one protected functional group and one reactive functional group, ensuring that at each coupling step only one amino acid is added. Similarly, this design also required a guest with an Fmoc-protected amine functionality and a carboxylic acid functionality for coupling. Once the guest was coupled, a cyclodextrin moiety was to be threaded onto it which necessitated a third orthogonal functionality which would be unmasked to react with the carboxylic acid of the next guest, but not the stopper. An azido group was used, which could then be

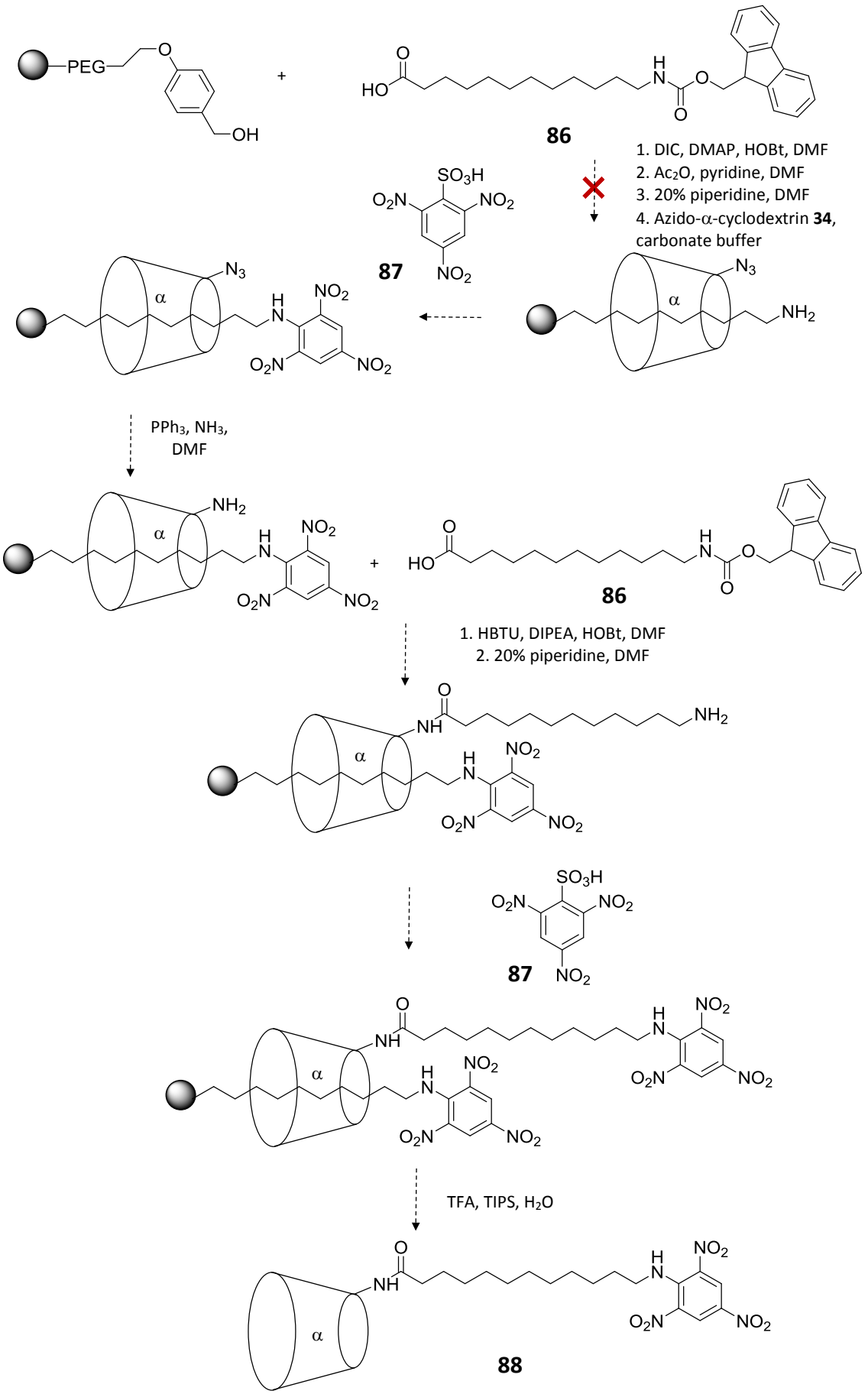

Scheme 5.1 Attempted synthesis of the [*a*1]-product **88**.

reduced to an amino group after stoppering in order to couple to the next guest. This scheme also avoids the possible formation of undesired complexes in solution as the free guest and free cyclodextrin moiety are never together in the same reaction step.

The guest was chosen as a simple alkane as the amino acid functionalised compound was commercially available, and a dodecyl length as this alkyl chain gives the highest yield of rotaxane formed with α-cyclodextrin.[148]

The Fmoc-protected dodecanoic acid guest **86** was synthesised using 9-fluorenylmethyl *N*-succinimidyl carbonate in dioxane, and purified by silica chromatography to give the product in a 34% yield. This guest was then coupled to the solid resin using standard amino acid DIC coupling conditions.[198] As the progress of each reaction could not be monitored without cleavage of each intermediate from the resin, the synthesis was continued to further stages before analysis.

After coupling of the guest **86**, the resin was washed with DMF to remove reagents. This washing step was performed after each reaction, and where the solvent was changed to water the resin was also washed with methanol as an intermediate solvent. The resin was then acylated using acetic anhydride and pyridine to ensure that any unreacted resin functionalities are unable to undergo coupling with reagents in subsequent steps, and the Fmoc-protecting group removed with a 20% piperidine solution in DMF. Azido-α-cyclodextrin **34** was then equilibrated with the resin-bound guest in aqueous carbonate buffer, before capping with the stoppering group[199] 2,4,6-trinitrobenzenesulfonic acid (TNBS) **87**. Azido-α-cyclodextrin **34**, then thought to be mechanically bound to the resin, was reduced to amino-α-cyclodextrin and coupled to the Fmoc-protected dodecanoic acid guest **86**. The guest was then deprotected and stoppered with TNBS **87** in an attempt to give a product which demonstrates the hypothetical continuation of an acyclic daisy chain structure.

The cleaved reaction mixture from the attempted synthesis of the [*a*1]-product **88** was analysed by HPLC (Figure **5.1**) and the peaks absorbing at 335 nm (the absorbance of the TNBS stoppering group) collected and analysed by mass spectrometry and ^{1}H NMR spectroscopy. None however, corresponded to the [*a*1]-product **88**, and furthermore no

peaks displayed cyclodextrin signals in their ^{1}H NMR spectra. The only HPLC peak that could be recognized was that at 13.9 min, which was identified as the capped dodecamino acid guest **89** (Figure **5.2**).

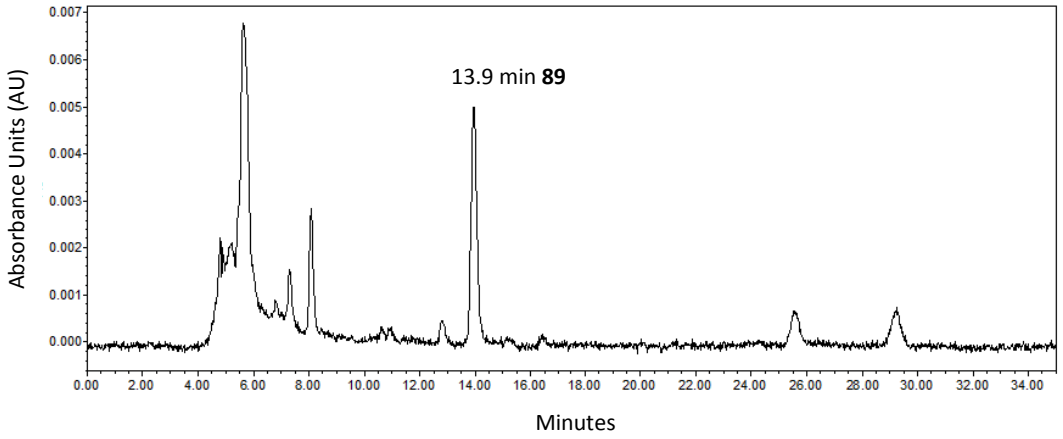

Figure 5.1 Chromatogram acquired by reverse phase HPLC of the cleaved product mixture from the attempted synthesis of the [*a*1]-material **88**, monitored at 335 nm.

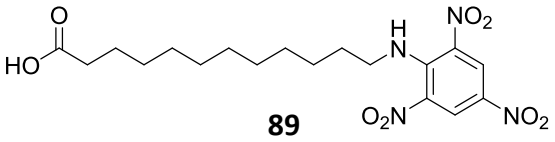

89

Figure 5.2 The TNBS-capped guest **89** identified as the 13.9 min HPLC peak.

The presence of compound **89** and the absence of any cyclodextrin products indicates that coupling of the guest to the resin, Fmoc deprotection and TNBS capping were successful, however the synthesis failed at the step where azido-α-cyclodextrin **34** was threaded onto the guest. It is possible that this is as a consequence of the low solubility of azido-α-cyclodextrin **34** in aqueous solution. Mass spectrometry of the crude cleaved reaction mixture also showed the presence of *m/z* peaks separated by 42 mass units, suggesting that compounds had been modified *via* acylation. A new synthetic scheme, which employs a more soluble cyclodextrin-based compound and omits the acylation step, was therefore designed and tested.

5.3 Attempted Daisy Chain Synthesis from a Cyclodextrin-Modified Resin

In order to avoid the synthetic step of threading the poorly soluble azido-α-cyclodextrin **34** onto the resin-bound guest, a new scheme was devised which uses the much more

water soluble amino-α-cyclodextrin **35** (Scheme **5.2**). Here, the cyclodextrin **90**, synthesised in a 94% yield using a previously decribed method,[200] was first coupled to the resin. The mono-protected dodecanoic acid axle **91** was then synthesised by coupling 3,5-dimethylaniline to dodecandoic acid, which was used in a five-fold excess to avoid overreaction. The desired product **91** was then isolated from the starting materials by acidification, enabling extraction into an organic layer. The coupling reagents were then washed away using acetone and a 23% product yield recorded. The mono-protected dodecanoic acid axle **91** was then equilibrated with the resin-bound cyclodextrin which was anticipated to give a resin-bound pseudo-rotaxane. This complex was then to be stoppered with amino-α-cyclodextrin **35** to give a resin-bound [*a*2]-daisy chain.

This scheme introduces the possibility of the formation of an unbound rotaxane by-product **92**, where the amino-α-cyclodextrin **35** used for stoppering could react with the uncomplexed axle **91**. In an attempt to favour formation of the resin-bound [*a*2]-daisy chain, the axle **91** was equilibrated with resin-bound cyclodextrin overnight before addition of the 4-(4,6-dimethoxy-1,3,5-triazin-2-yl)-4-methylmorpholinium chloride (DMTMM) activator and amino-α-cyclodextrin **35**. It was reasoned that the extended equilibrium time would maximise the amount of complexed axle **91** with the resin-bound cyclodextrin.

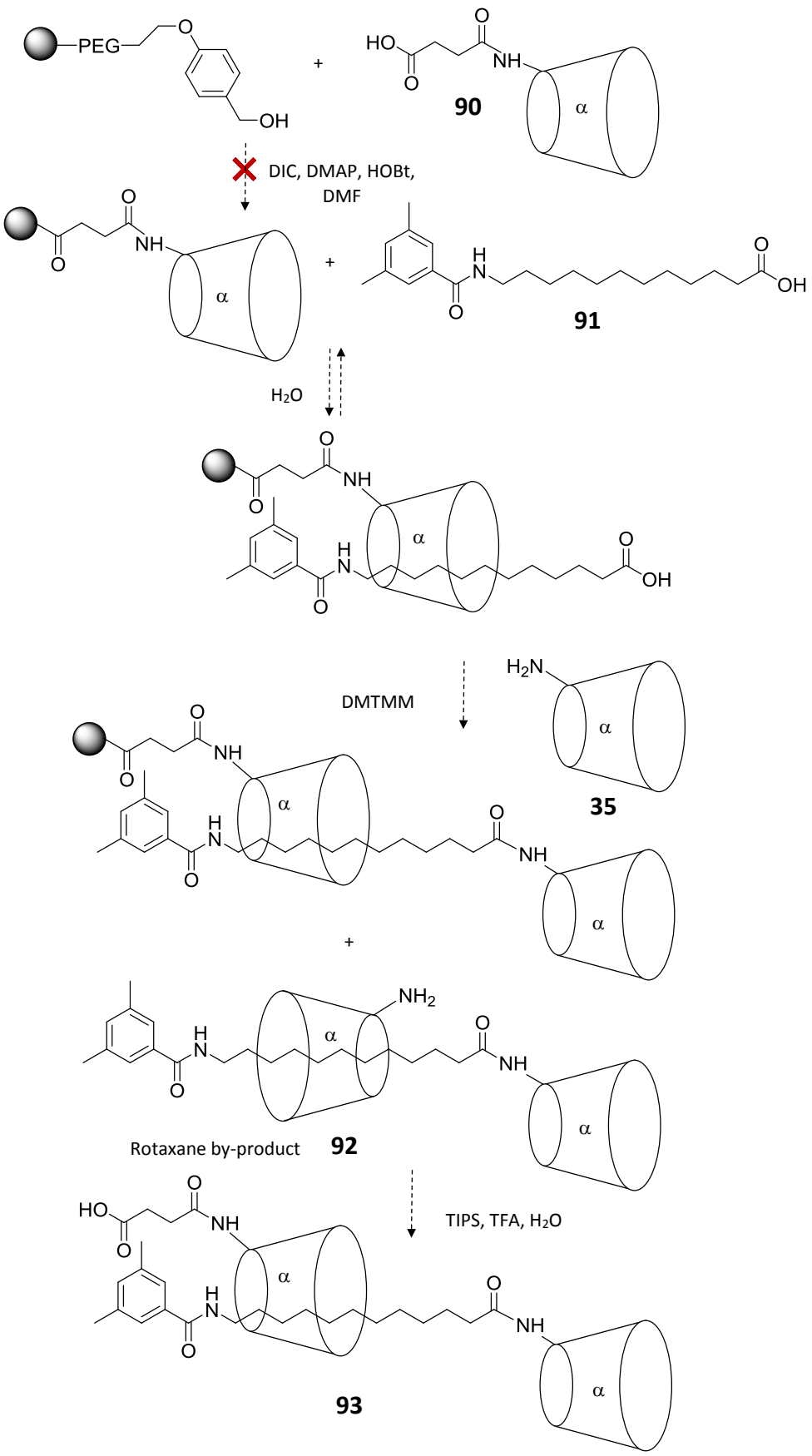

Scheme 5.2 Attempted synthesis of the [*a*2]-daisy chain **93**.

The cleaved reaction mixture from the attempted synthesis of the [*a*2]-daisy chain **93** was analysed by HPLC at 254 nm, the absorbance of the dimethylphenyl stopper group (Figure **5.3**), and the resulting peaks analysed by mass spectrometry. The desired [*a*2]-daisy chain **93** could not be detected however and only the peak at 28.0 min could be identified, as the 12-(3,5-dimethylphenylamido)-dodecanoic acid **91**.

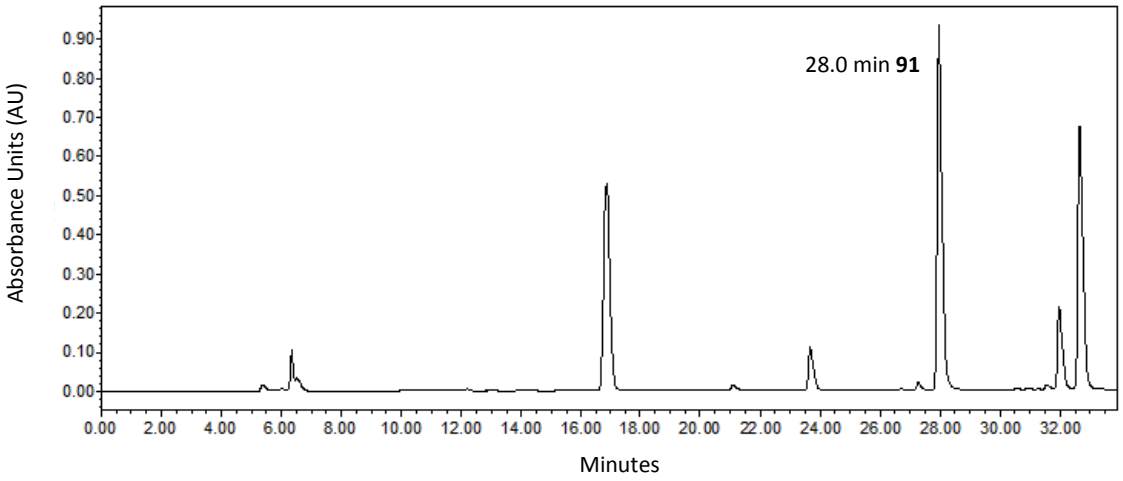

Figure 5.3 Chromatogram acquired by reverse phase HPLC of the cleaved mixture from the attempted synthesis of the [*a*2]-daisy chain **93**, monitored at 254 nm.

No cyclodextrin products were detected in the cleaved product mixture from Scheme **5.2**, including carboxypropionic acid-α-cyclodextrin **90**. This indicated that the initial step, coupling carboxypropionic acid-α-cyclodextrin **90** to the resin was unsuccessful. The failure of the synthesis is possibly because the propyl cyclodextrin linker was too short, therefore the synthesis was re-designed with a longer alkyl chain between the cyclodextrin and the resin.

5.4 Attempted Daisy Chain Synthesis with an Extended Cyclodextrin-Resin Linker

As it was speculated that carboxypropionic acid-α-cyclodextrin **90** may be too hindered to couple to the resin, this step was attempted with a longer linker than the propyl chain. A modified synthetic scheme was therefore devised, using a hexyl linker (Scheme **5.3**). Rather than synthesise a separate cyclodextrin, direct coupling of adipic acid **94** to the resin was attempted, followed by amino-α-cyclodextrin **35** coupling. The remainder of the synthetic scheme was unchanged to that shown in Scheme **5.2**.

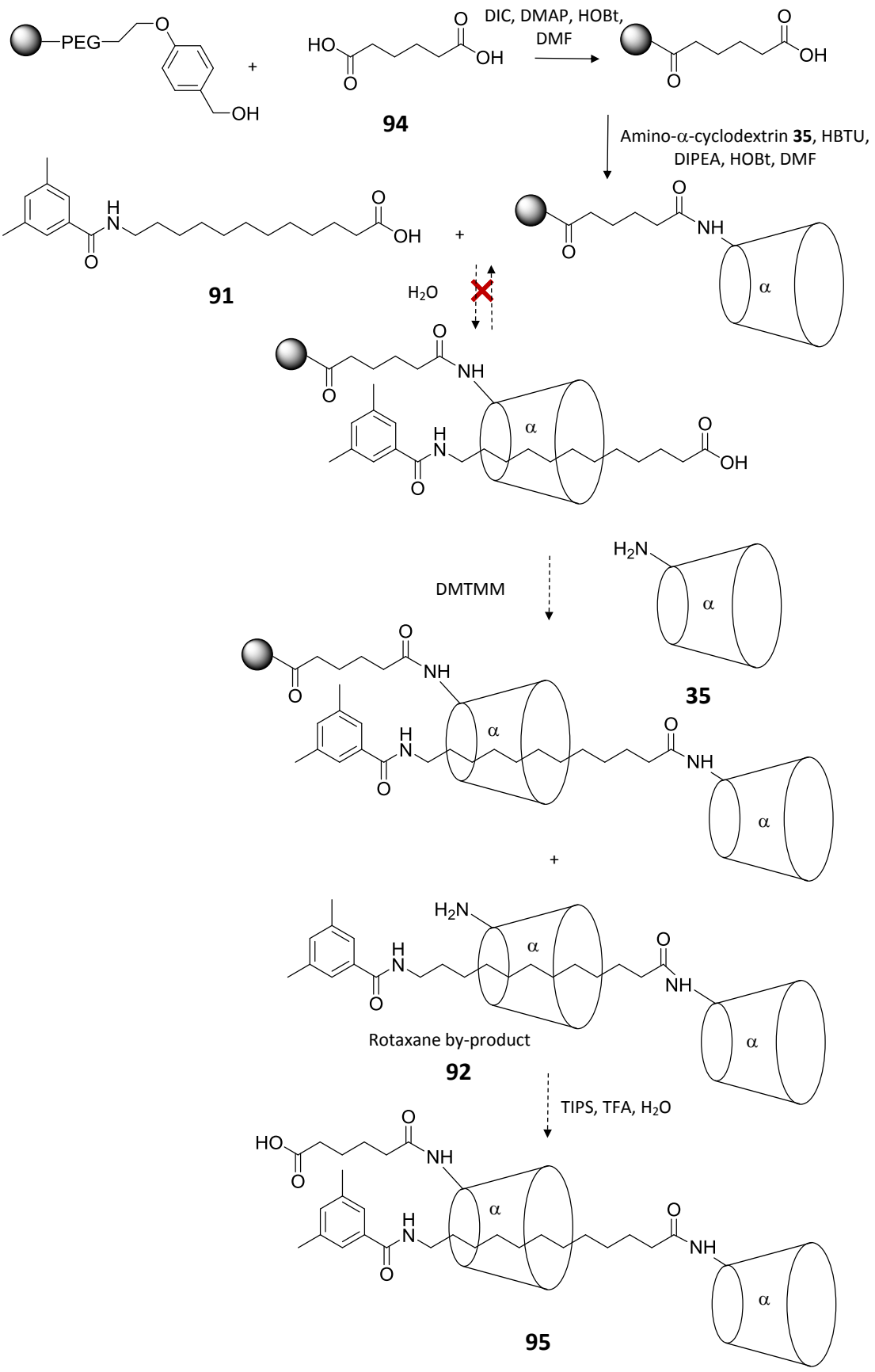

Scheme 5.3 Attempted synthesis of the [*a*2]-daisy chain **95**.

The cleaved reaction mixture was then analysed by LC-MS (Figure **5.4**). Although no [*a*2]-daisy chain product **95** could be detected, a *m/z* peak corresponding to the cyclodextrin **96** was identified. It could therefore be confirmed that the two initial steps in this synthesis were successful, and that a protocol for the attachment of a cyclodextrin to resin had been developed.

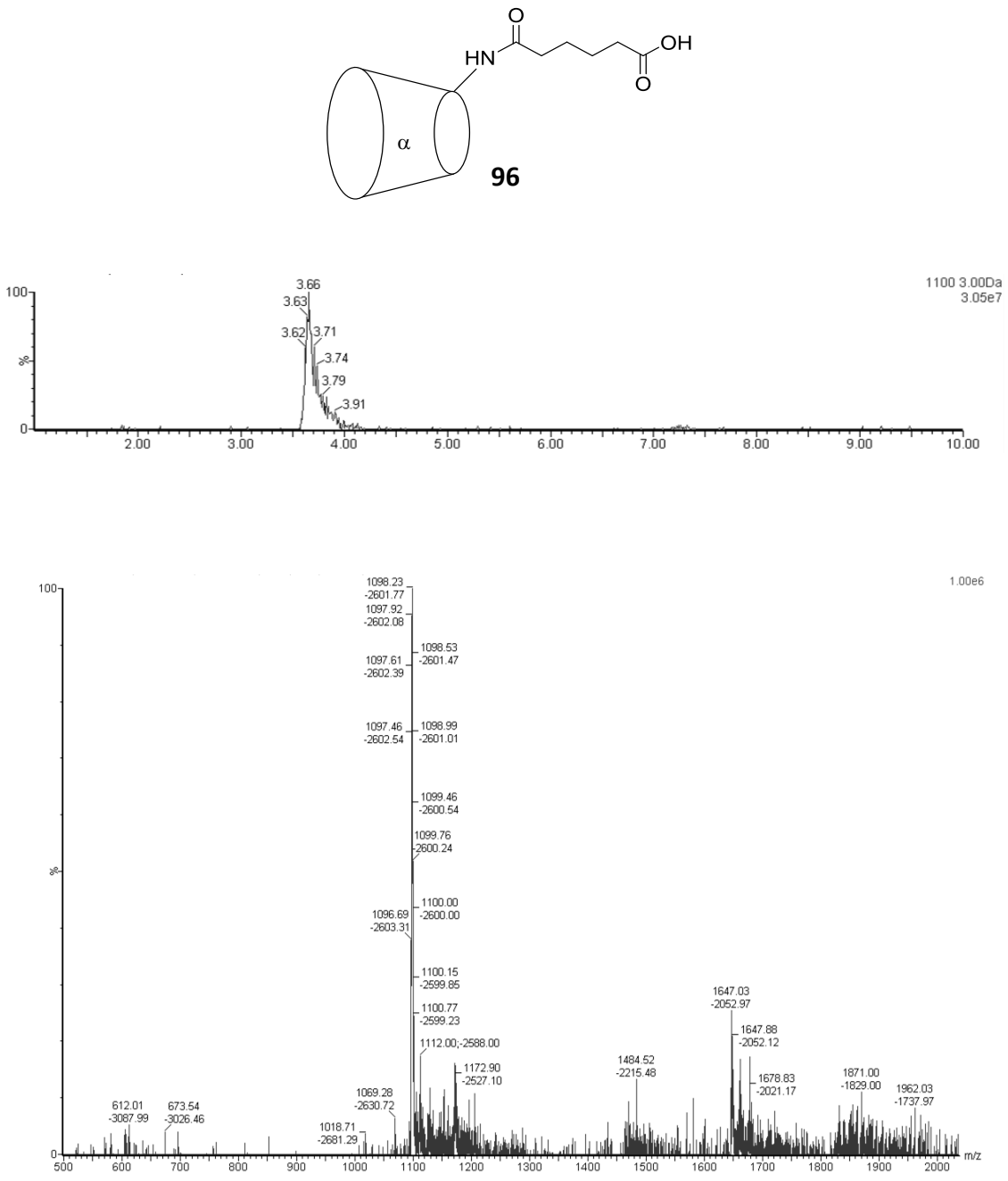

Figure 5.4 Chromatogram of the cleaved product mixture from the attempted synthesis of the [*a*2]-daisy chain **95** analysed for the *m/z* of compound **96** (*above*) and mass spectrum at 3.66 min (*below*).

Having established that the attachment of a cyclodextrin moiety to the resin was successful, it could be deduced that either complex formation with the axle **91** or stoppering with amino-α-cyclodextrin **35** was unsuccessful. It is possible that the low solubility of the axle **91** in aqueous solution is the reason that the [*a*2]-daisy chain **95** did not form. A modified synthetic scheme was therefore devised using a more soluble guest, and a stoppering group that has been previously reported in rotaxane synthesis.[35]

5.5 Attempted Rotaxane Synthesis with an Azobenzene Guest

As the axle **91** was poorly water soluble an alternative guest group, azobenzene-4,4'-dicarboxylic acid **36**, was used in a modified scheme in the development of the solid-phase synthesis of an interlocked product (Scheme **5.4**). It was also unknown if stoppering with amino-α-cyclodextrin **35** was successful therefore a previously reported dimethylaniline capping group **97**, that has been used to form rotaxanes in solution,[35] was employed.

Although this synthetic scheme would not yield a daisy chain product, only a rotaxane, it would act as a proof-of-principle and could be adapted to daisy chain synthesis if the capping group was switched to a cyclodextrin moiety. The experimental design also removes the possibility of the formation of unwanted, unbound inclusion complexes.

The cleaved product mixture was analysed by LC-MS, however no rotaxane product **98** could be detected and only the cyclodextrin **96** was identified. It could therefore be determined that either complexation of the axle or stoppering were still not successful, despite the experimental changes.

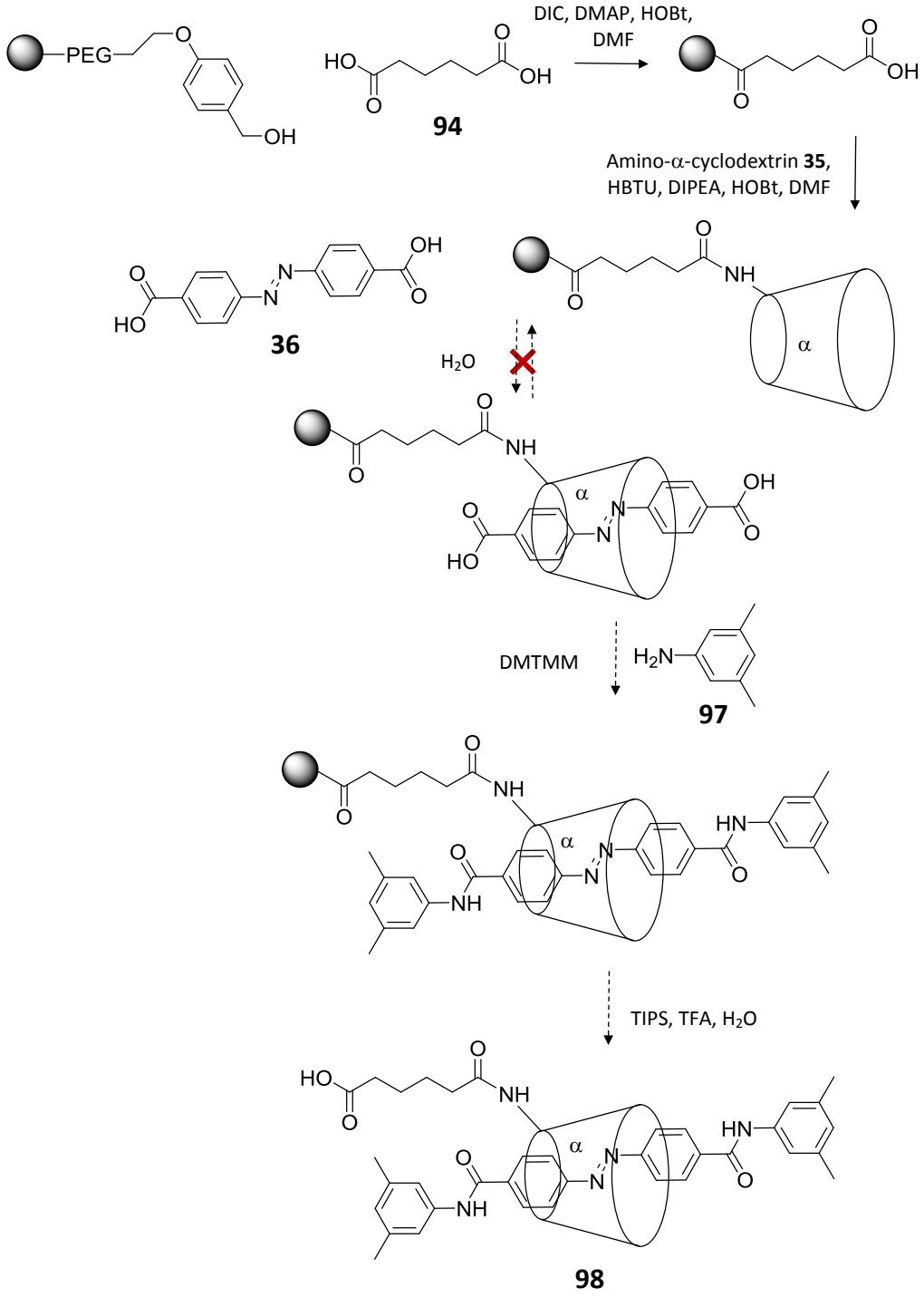

Scheme 5.4 Attempted synthesis of the rotaxane **98**.

5.6 Attempted Rotaxane Synthesis with a TNBS Stoppering Reagent

In another attempt at the solid-phase synthesis of a cyclodextrin rotaxane, a TNBS stoppering reagent **87** was used (Scheme **5.5**). The coupling of this capping group to a guest upon Tentagel resin had already been demonstrated in Scheme **5.1**, therefore if

this reaction was unsuccessful it would be more likely that it is the formation of the inclusion complex which prevents synthesis of the final product. The synthetic scheme was analogous to that shown in Scheme **5.4**, with the stoppering reagent replaced with TNBS **87** and the azobenzene-4,4'-dicarboxylic acid **36** guest replaced with diamino azobenzene **99** to give compatible functional groups for coupling.

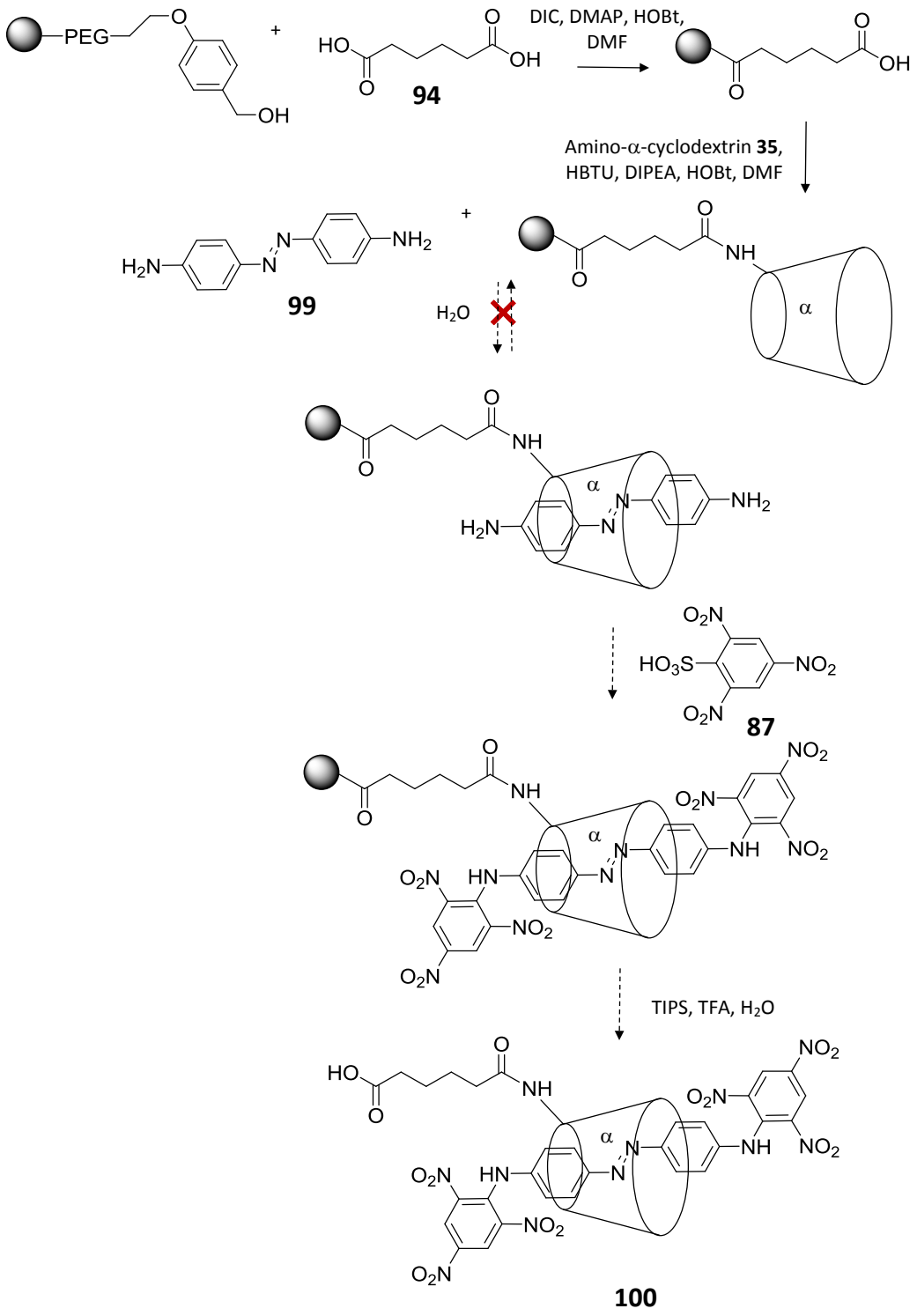

Scheme 5.5 Attempted synthesis of the rotaxane **100**.

The cleaved product mixture was analysed by LC-MS, however no rotaxane product **100** could be detected and the only identifiable product was the cyclodextrin **96**. The absence of other product formation under these conditions indicates that formation of the cyclodextrin host-guest inclusion complex is not occurring, and it is possible that the resin itself could be preventing this interaction.

5.7 Attempted Rotaxane Synthesis on Wang Resin

Despite the success of coupling a cyclodextrin to resin, synthesis of a resin-bound inclusion complex had so far failed. It was considered that the Tentagel resin could be interfering with cyclodextrin host-guest complexation, as PEG chains are known to be able to complex with cyclodextrin.[201] Although this has only been reported at very high, almost saturated concentrations of both host and guest, a high effective concentration at the resin could still be resulting in PEG groups outcompeting the guest in solution for the cyclodextrin cavity. The synthetic scheme described in Scheme **5.4** was therefore repeated, this time using Wang resin which has no PEG groups.

The cleaved product mixture from the Wang resin was analysed by LC-MS, however only adipic acid **94** was found to have successfully been coupled to the resin and no cyclodextrin-containing products were detected. It could not be confirmed whether the use of the Tentagel resin was preventing the formation of an inclusion complex, however it demonstrates that the Wang resin is not suitable for coupling the highly polar amino-α-cyclodextrin **35**.

5.8 Attempted Demonstration of Macromolecular Host-Guest Recognition

As it had been demonstrated that a cyclodextrin functionality could be attached to Tentagel resin, it was hypothesised that with the use of a complementary guest functionalised resin, host-guest recognition could be observed on the macro-scale (Scheme **5.6**). Similar systems have been demonstrated with complementary cyclodextrin host-guest functionliased acrylamide gels.[38] Tentagel resin has also been

used to observe molecular interactions on the macro-scale, in an on-bead peptide-peptide binding assay, which used a fluorescent tag to indicate interactions.[202]

Cyclodextrin-functionalised resin **101** and azobenzene-functionalised resin **102** were synthesised by coupling either adipic acid followed by amino-α-cyclodextrin **35**, or 4-phenylazobenzoic acid **53** to the resin. A small portion of each resin-bound product was cleaved and analysed by LC-MS to confirm that coupling had been successful.

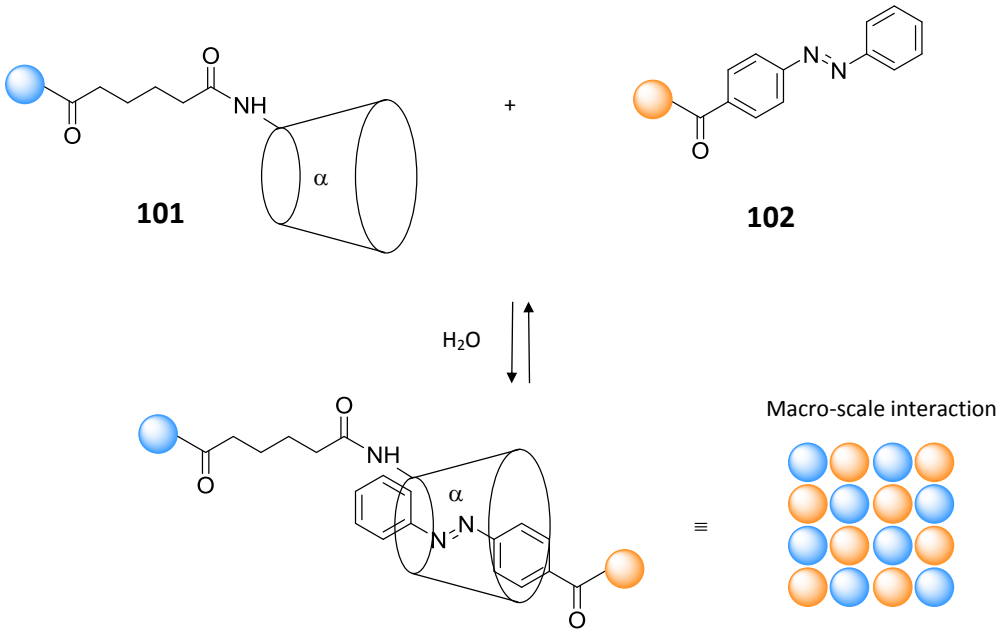

Scheme 5.6 Modified resins for the study of cyclodextrin host-guest complexation on the macro-scale.

A mixture of the two functionalised resins **101** and **102** was allowed to equilibrate in aqueous solvent before observing under a microscope (Figure **5.6**). As a control, unmodified Tentagel resin and the azobenzene functionalised resin **102** were also analysed under the same conditions (Figure **5.5**).

Visual inspection of the two systems shows that the use of the coloured, azobenzene guest is suitable for the recognition of macro-scale interactions as the orange azobenzene-functionalised resin **102** can be differentiated from the colourless cyclodextrin-functionalised resin **101**. No difference in the macro-assembly behaviour between the two however, could be observed. This indicates that no inclusion complex is forming between the cyclodextrin and azobenzene functionalised resins. This could possibly be because the effective concentration of the functionalities on the solid resins

are too low to facilitate inclusion, the curved nature of the resins prevents enough contact to demonstrate macro-scale molecular recognition, or that the PEG groups on the resin are outcompeting the azobenzene group for inclusion in the cyclodextrin cavity.

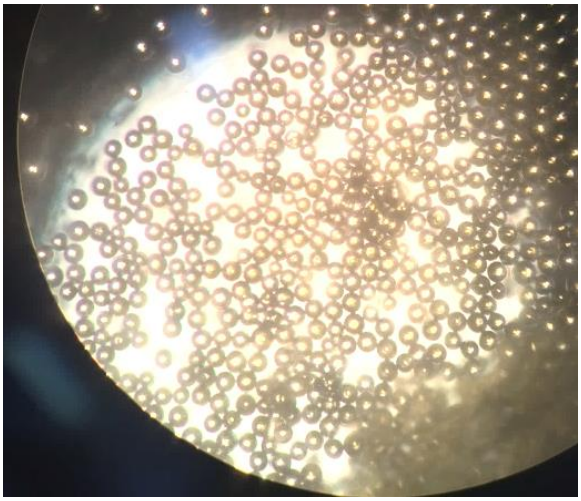

Figure 5.5 Microscopic image of a solution of the azobenzene-modified resin **102** and unmodified resin.

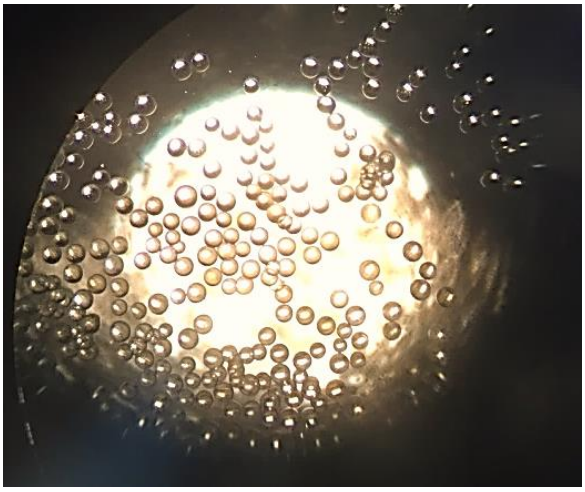

Figure 5.6 Microscopic image of a solution of the azobenzene-modified resin **102** and the cyclodextrin-modified resin **101**.

5.9 Conclusions

Two general strategies were attempted in the solid-phase synthesis of cyclodextrin rotaxanes; attaching an axle directly to the resin upon which cyclodextrin could be threaded, and attaching cyclodextrin directly to the resin through which an axle could

be threaded. Despite several attempts with varying guest and stopper groups the synthesis of a mechanically bound inclusion complex on resin could not be achieved, however a protocol was successfully developed for the attachment of either a guest group or a cyclodextrin moiety onto resin.

An attempt was made to translate molecular host-guest recognition to the macro-scale using the newfound procedure to functionalise resin with either α-cyclodextrin or an azobenzene guest. The two modified resins were then equilibrated in water and observed under a microscope, however no evidence of molecular interactions could be observed.

It is concluded that the absence of host-guest inclusion complexes produced in these experiments is likely a consequence of the PEG groups on the Tentagel resin interfering with complex formation, by competing with the added guest for inclusion in the cyclodextrin cavity. This hypothesis could be tested with the use of β-cyclodextrin functionalities replacing α-cyclodextrins in the schemes attempted in this Chapter. Although less soluble than their α-cyclodextrin counterparts, β-cyclodextrins do not form complexes with PEG polymers[201] therefore formation of resin-bound inclusion complexes may be more likely. Alternatively, a polypropylene glycol (PPG) functionalised resin could be used. This polymer should have similar swelling properties to PEG, but does not form a complex with α-cyclodextrin, however at the time of writing no commercially produced PPG functionalised resin was available.

Chapter 6: Results and Discussion

Self-Assembling Polymeric Systems

6.1 Introduction

Following investigations described in Chapters 3 and 4, where β-sheet interactions were combined with cyclodextrin host-guest complexes in the development of self-assembling molecular devices, it was anticipated that they could also be applied to the design of self-assembling polymers. Peptide-peptide interactions have been employed in the self-assembly of polymers with a range of physical features and applications.[203] Their assembly can be made to be responsive to stimuli such as change in pH,[204] addition of metal ions,[205] enzyme activity[206, 207] and photo-switching[208] to give 'smart' materials.

The responsive nature of cyclodextrin inclusion complexes would give potential for the material to be dependent on an external stimulus, enabling switching between monomeric and polymeric species. A range of systems was therefore designed and investigated, wherein cyclodextrin host-guest interlocked complexes could be linked by oligovaline β-sheet interactions.

6.2 Study of an α-Cyclodextrin-Azobenzene, β-sheet Self-Assembling Polymer

The initial design for a self-assembling polymer was with the use of the cyclodextrin monomer **103**. The aim was that this compound would form a [*c*2]-dimer in aqueous conditions with the azobenzene acting as the guest group. The trivaline peptides could then act as 'tabs', linking the interlocked structures *via* β-sheet formation to form a polymer (Scheme **6.1**). Photoisomerisation of the azobenzene guest would then dissociate the [*c*2]-complex, resulting in switching of the polymeric structure to monomers, conceivably resulting in a sol-gel switching system.

A trivaline peptide sequence was chosen, as according to previous studies,[169] they are the shortest valine structure that are able to form β-sheets. Longer valine sequences become increasingly insoluble in water and if the β-sheets were too strong, the peptide-peptide interactions might prevent switching from polymeric assemblies to monomers.

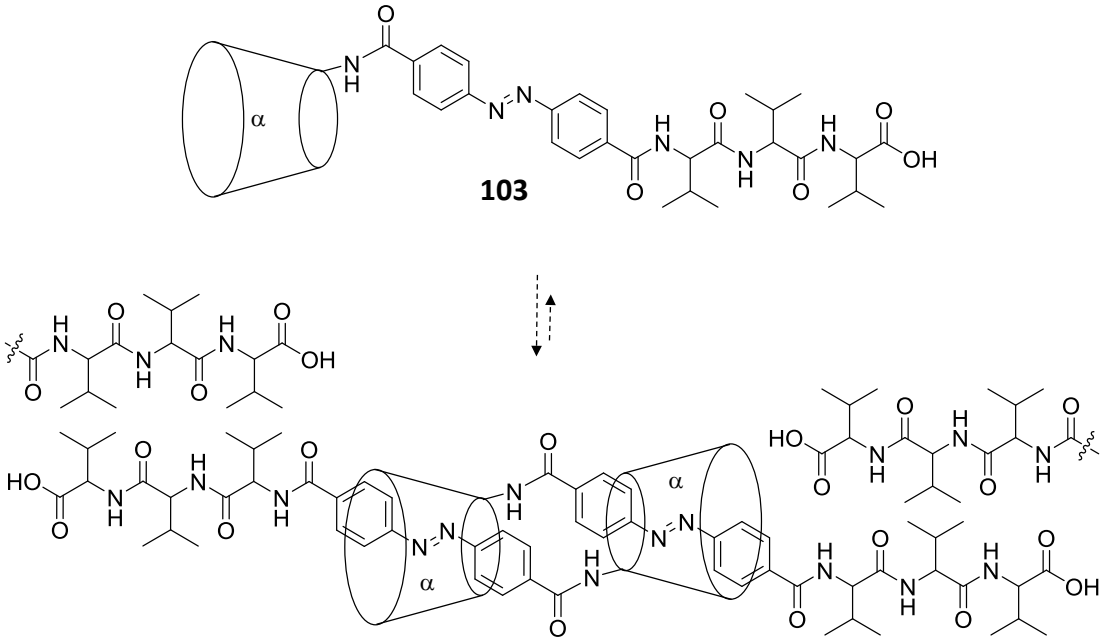

Scheme 6.1 Proposed self-assembly of a polymer, linked by the formation of [*c*2]-cyclodextrin host-guest dimers which would then polymerize *via* β-sheet formation between trivaline sections.

The cyclodextrin monomer **103** was prepared by solid-phase synthesis, with the cyclodextrin **37** used in the final on-resin coupling step. The crude product was cleaved from the resin and purified by HPLC to give the final product in a 12% yield. The cyclodextrin monomer **103** was then dissolved in water, however its solubility was very low and no evidence of polymerisation (i.e. gel formation) was observed. 2D ^{1}H-^{1}H ROESY NMR spectroscopy (Figure **6.1**) showed that no inclusion complex formed between the azobenzene and cyclodextrin.

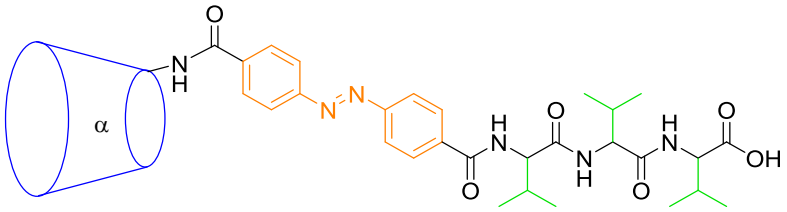

103

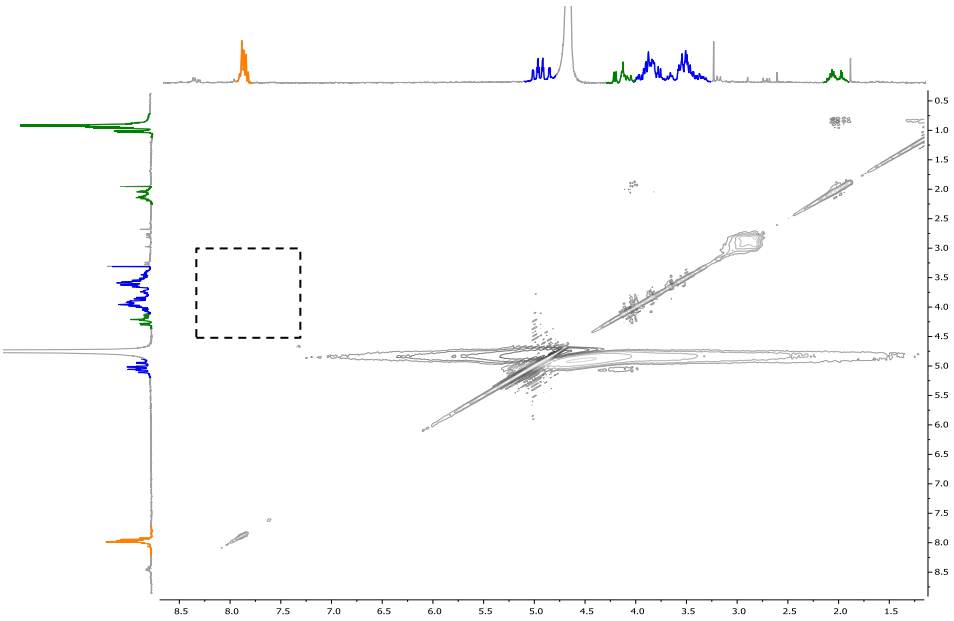

Figure 6.1 2D ^{1}H-^{1}H ROESY spectrum of the cyclodextrin **103** in D_2O, showing no nOe crosspeaks between azobenzene and cyclodextrin protons (dashed square denotes area where these would lie), indicating that no inclusion complex formed.

Although the cyclodextrin **103** did not form an inclusion complex as predicted, the suitability of the trivaline peptide sequence, in terms of extent of β-sheet formation could be examined. The circular dichroism spectra of the cyclodextrin **103** (Figure **6.3**) show two minima in the signal at around 198 nm and 215 nm, indicating a mixture of random coil and β-sheet structures.

The effect of the addition of cyclodextrin and azobenzene moieties was also examined by comparison with the circular dichroism spectra of unmodified trivaline **104** (Figure **6.3**), prepared by solid-phase synthesis in a 43% yield. The two compounds have almost identical circular dichroism signals, showing that coupling of the peptide to the cyclodextrin **37** has not affected its secondary structure. It was therefore concluded that the trivaline peptide sequence is suitable for use in a self-assembling polymer design.

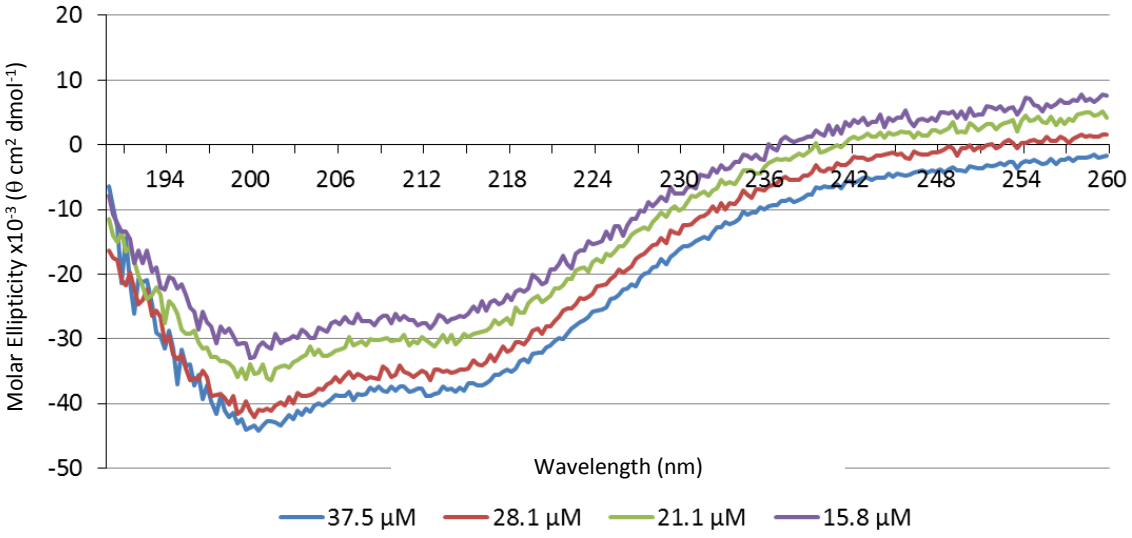

Figure 6.2 Circular dichroism spectra of the cyclodextrin **103**.

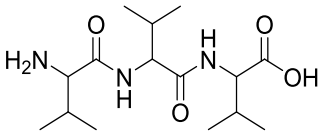

104

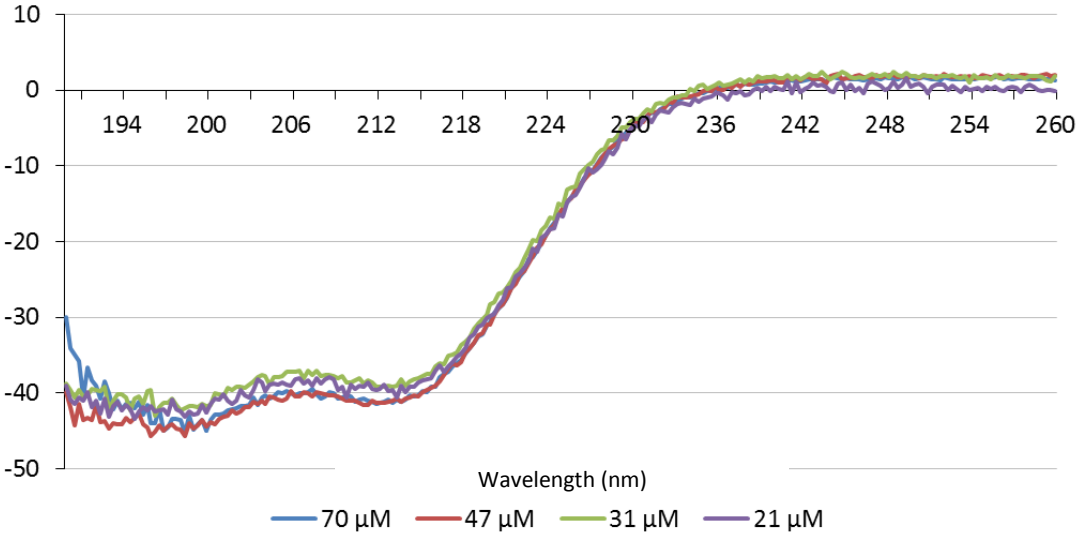

Figure 6.3 Circular dichroism spectra of trivaline **104**.

The lack of complex formation with the cyclodextrin **103** may be caused by the steric bulk of the valine side-chains, preventing the α-cyclodextrin ring slipping over them and including the azobenzene moiety. The compound was therefore redesigned to feature the larger annulus β-cyclodextrin.

6.3 Study of a β-Cyclodextrin-Azobenzene, β-sheet Self-Assembling Polymer

Having established that the cyclodextrin **103** does not form a host-guest inclusion complex, the synthesis of a similar compound with β-cyclodextrin in place of α-cyclodextrin was attempted (Scheme **6.2**). It was considered that if the steric bulk of the valine residue side-chains was preventing inclusion, the larger annulus cyclodextrin could overcome this restriction whilst still acting as a host for the azobenzene guest.[209]

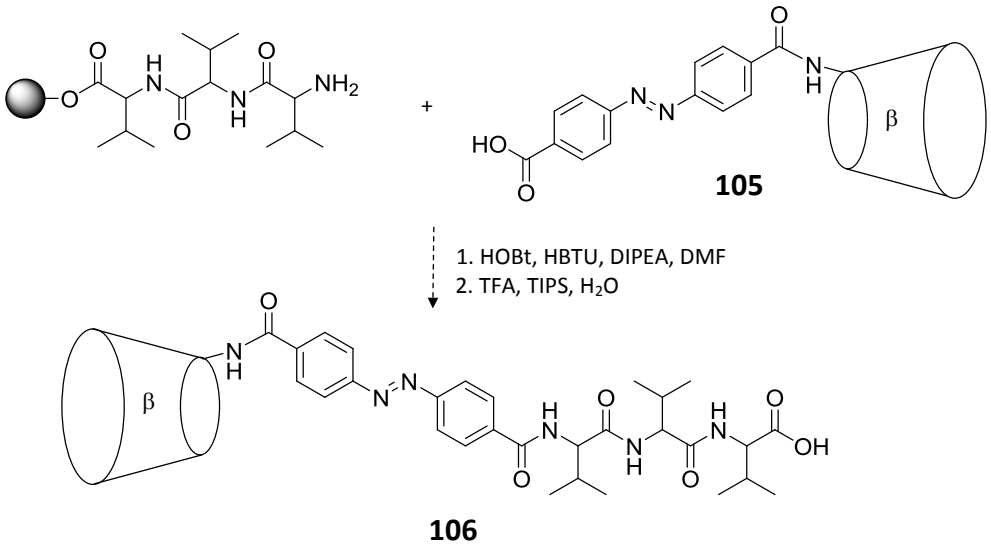

Scheme 6.2 Attempted synthesis of the cyclodextrin **106**.

The β-cyclodextrin **105** was synthesised by coupling amino-β-cyclodextrin **56** with azobenzene-4,4'-dicarboxylic acid **36**, and purified by column chromatography to give a 17% yield. An attempt was then made to prepare the β-cyclodextrin **106** by solid-phase synthesis, with the cyclodextrin **105** used in the final on-resin coupling step. Analysis of the reaction mixture after cleavage from the resin showed none of the desired product had formed, and this line of investigation was abandoned in favour of polymer studies with other compounds.

6.4 Second Study of an α-Cyclodextrin-Azobenzene, β-sheet Self-Assembling Polymer

As the α-cyclodextrin **103** does not form a [*c*2]-dimer and synthesis of the β-cyclodextrin **106** was unsuccessful, a new synthetic strategy for a self-assembling polymer was devised. Rather than synthesising the α-cyclodextrin monomer **103** first and then allowing it to self-assemble, it was proposed that an azobenzene-cyclodextrin [*c*2]-dimer could be assembled in aqueous solution and the trivaline peptide coupled to this pre-formed structure (Scheme **6.3**). It was hypothesised that if the valine residue side-chains were preventing formation of the [*c*2]-dimer of the α-cyclodextrin **103** as shown in Scheme **6.1**, in this approach they might act as stoppers, preventing dissociation. Work described in Chapter 2 showed that the α-cyclodextrin monomer **39** readily forms a [*c*2]-dimer, therefore this compound was used in this strategy to form a self-assembling polymer.

The cyclodextrin **39** was allowed to equilibrate in water, before the addition of trivaline **104** and DMTMM. The reaction mixture was then pipetted into acetone, and the resulting precipitate analysed by LC-MS. None of the dimer of **107** could be detected however, only the monomer of **107** and the monomer of the hexavalyl cyclodextrin **108** could be identified (Scheme **6.4**).

The LC-MS results indicate that although the coupling of trivaline **104** to the cyclodextrin **39** could be achieved, it either could not occur once the [*c*2]-dimer had formed, or the trivaline peptide does not prevent dimer dissociation. It is unlikely that the dimer of the cyclodextrin **39** does not form at all as previous work in the group,[147] and results in Chapter 2 show that this assembly forms readily and can be stoppered with alternative groups.

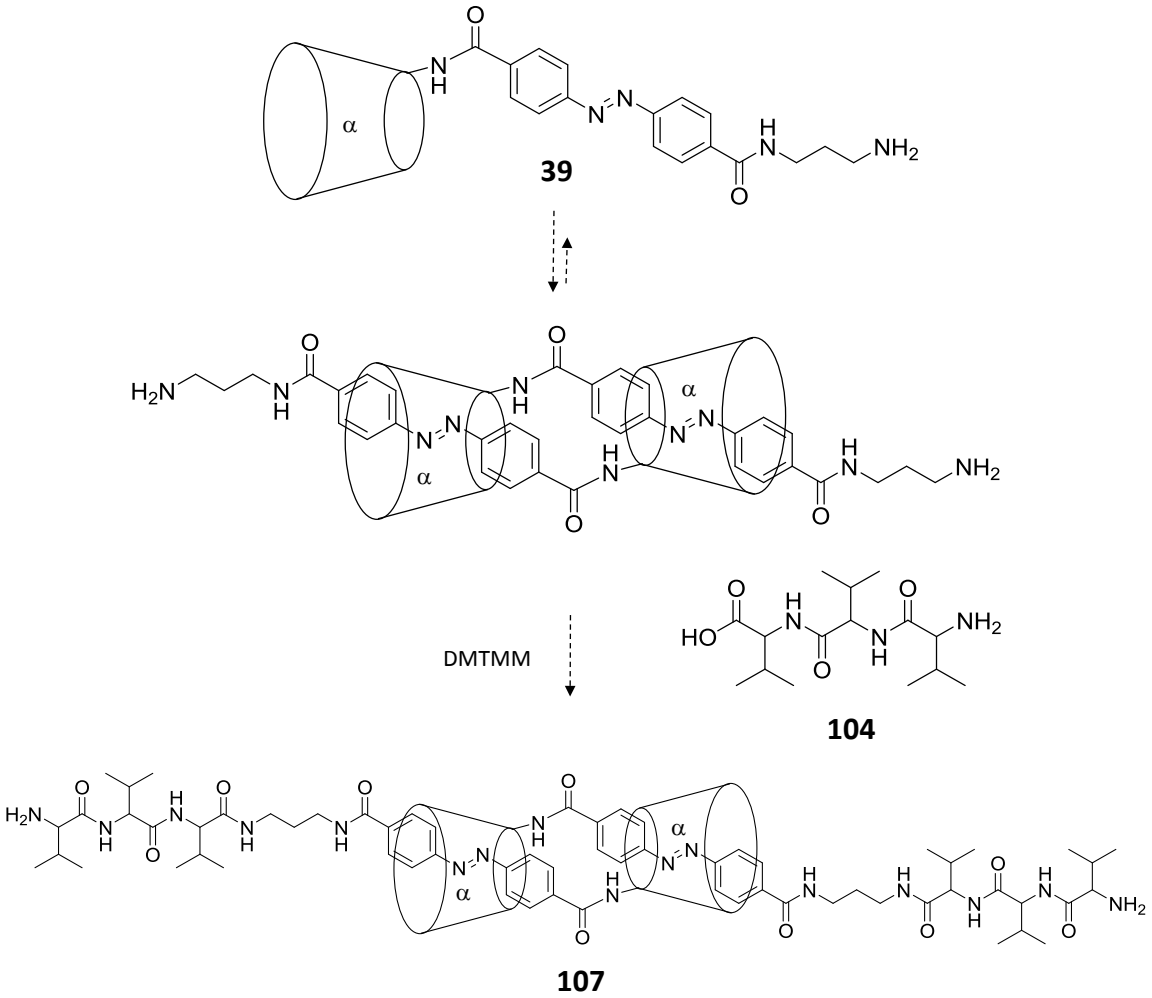

Scheme 6.3 Proposed formation of the dimer of **107**, anticipated to polymerise by β-sheet interactions.

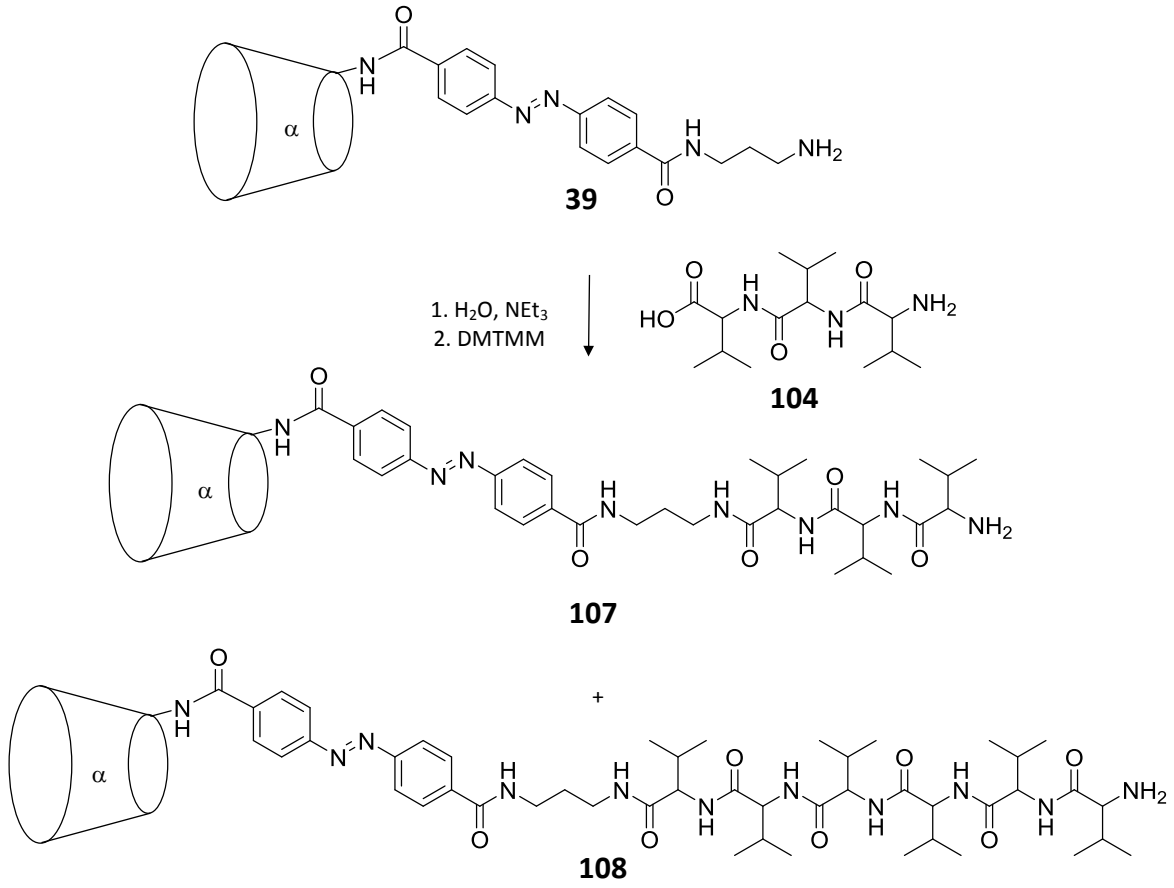

Scheme 6.4 Coupling of trivaline **104** to the cyclodextrin **39** produced the monomer of the cyclodextrin **107** and the monomer of the cyclodextrin **108**.

6.5 Study of a γ-Cyclodextrin-Azobenzene, β-sheet Self-Assembling Polymer

Attempts to generate a self-assembling polymer *via* [*c*2]-dimerisation were unsuccessful. A new system was designed that would utilise the formation of a 1:2 cyclodextrin host:guest complex in the form of a [3]-pseudo-rotaxane, which could then be polymerically linked by way of trivaline β-sheets (Scheme **6.5**). γ-Cyclodextrin **109** and an azobenzene guest were used in the design, as the structurally similar stilbene guest is known to form a 1:2 inclusion complex with this cyclodextrin.[210]

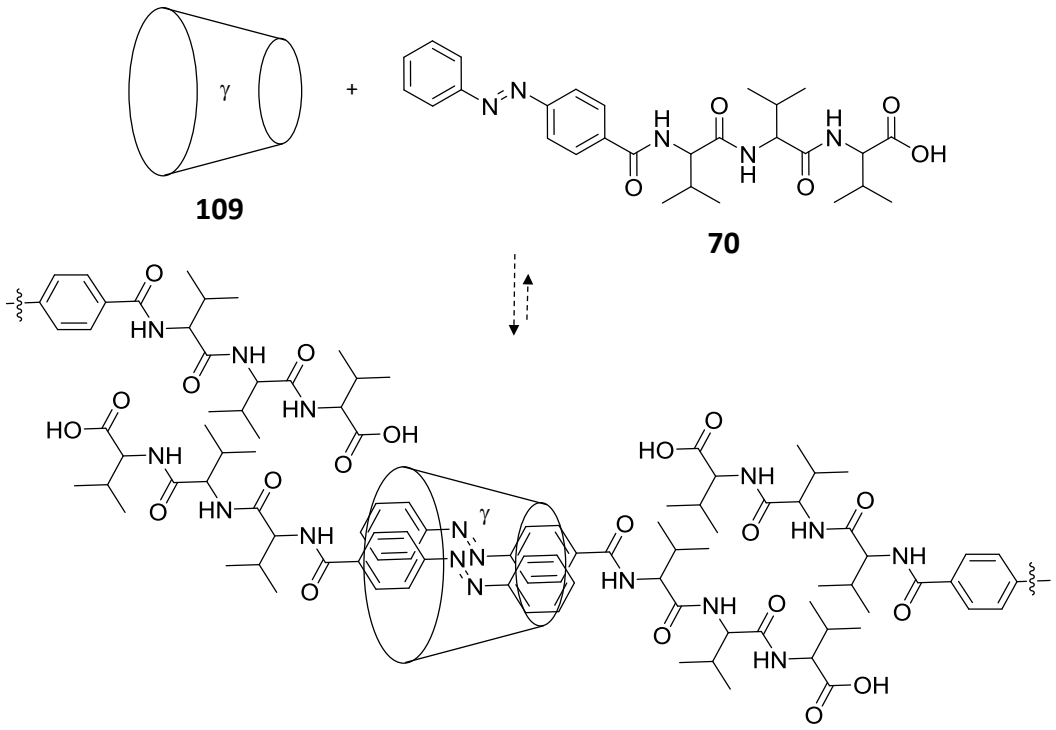

Scheme 6.5 Proposed formation of a [3]-pseudo-rotaxane, designed to polymerize by β-sheet formation between trivaline sequences.

The azobenzene **70**, prepared during the work described in Chapter 4, was allowed to equilibrate in D_2O with γ-cyclodextrin **109** and the solution analysed by 2D ^1H-^1H ROESY NMR spectroscopy (Figure **6.4**). The mixture however was poorly soluble, and the lack of nOe cross-peaks between the γ-cyclodextrin protons and the azobenzene guest protons showed that host-guest complexation was not present.

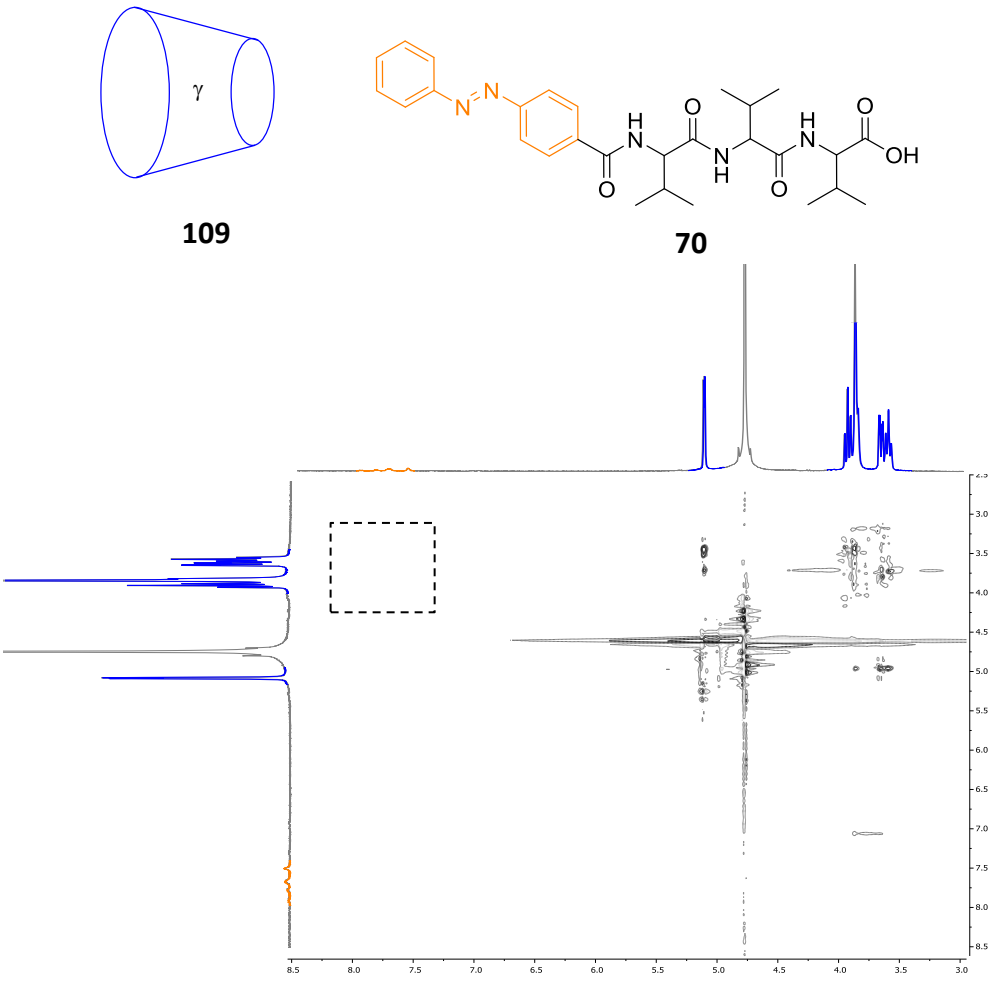

Figure 6.4 2D ^{1}H-^{1}H ROESY spectrum of the azobenzene **70** and γ-cyclodextrin **109** in D_2O, showing no nOe crosspeaks between azobenzene and cyclodextrin protons (dashed square denotes area where these would lie), indicating that no inclusion complex formed.

6.6 Study of a bis β-Cyclodextrin-Adamantane, β-sheet Self-Assembling Polymer

The 1:2 γ-cyclodextrin:azobenzene system suffered from poor aqueous solubility, therefore a new strategy was devised wherein the ratio of the more soluble cyclodextrin moiety compared to the hydrophobic guest moiety was increased to 1:1 in each complex. There was also a concern that a trivaline sequence does not have a high enough β-sheet propensity to polymerise assembled structures, and so a tetravaline sequence was employed.

In this design strategy a urea bridged bis-β-cyclodextrin **110** was used in an attempt to form an inclusion complex with two monomers of the adamantane **111**, which could in

turn be linked by β-sheet interactions (Scheme **6.6**). The bis-β-cyclodextrin **110** had been previously synthesised in the group,[211] and the adamantane **111** was prepared by solid-phase synthesis with 1-carboxy adamantane **59** used in the final on-resin coupling step, to give the product in a 22% yield.

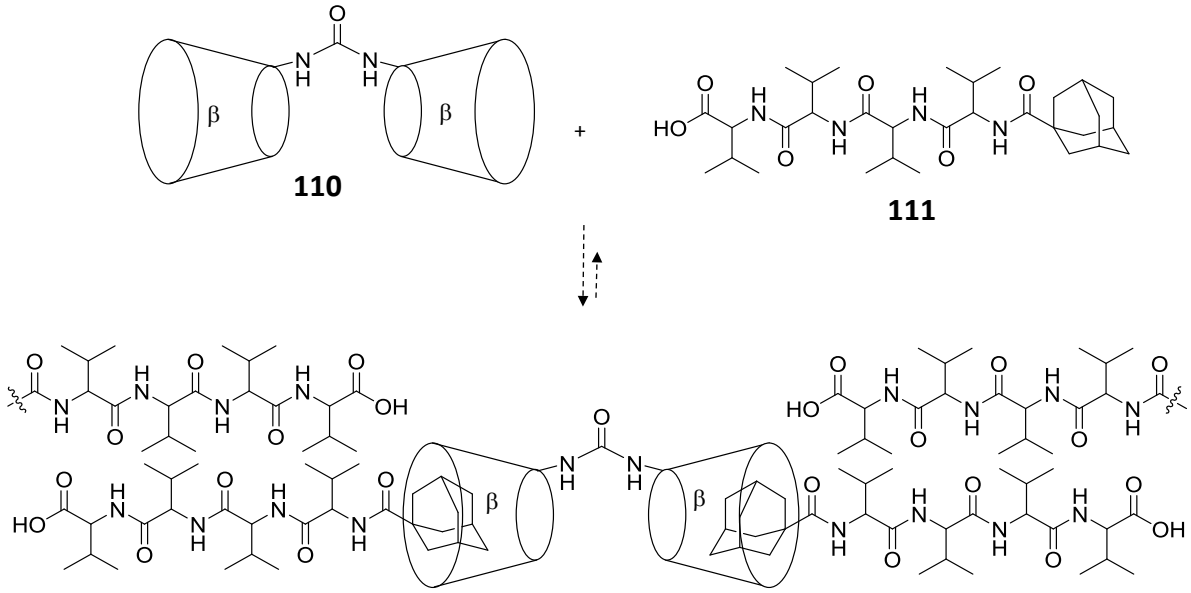

Scheme 6.6 Proposed formation of a [3]-pseudo-rotaxane, which was designed to polymerise through β-sheet formation between trivalines.

Bis-β-cyclodextrin **110** and the adamantane **111** were then allowed to equilibrate in D_2O and the solution analysed by 2D ^1H-^1H ROESY NMR spectroscopy (Figure **6.5**). The mixture however, exhibited no nOe interactions between the cyclodextrin and admantane guest protons showing that no cyclodextrin inclusion complex had formed.

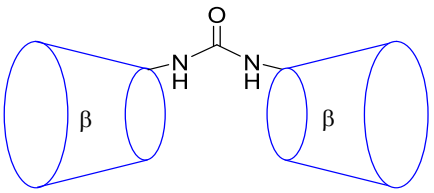

110

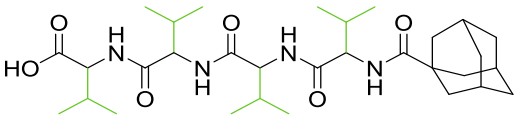

111

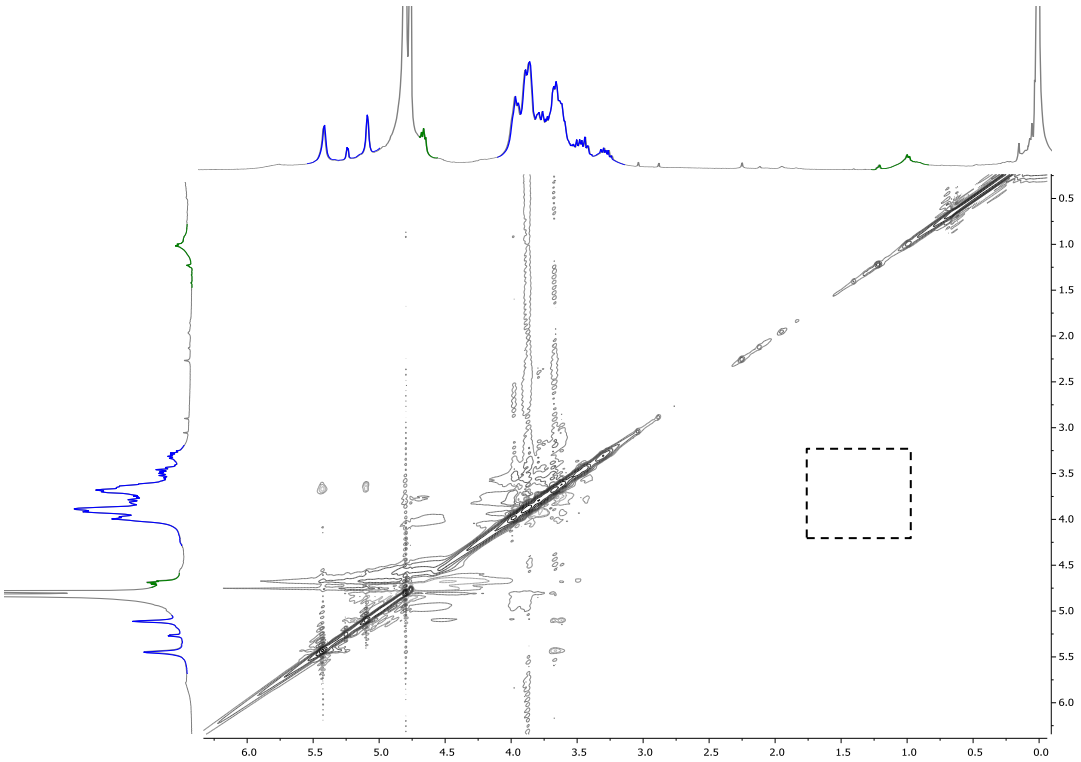

Figure 6.5 2D ^{1}H-^{1}H ROESY spectrum of adamantane **111** and bis β-cyclodextrin **110** in D_2O, showing no nOe crosspeaks between adamantane and cyclodextrin protons (dashed square denotes area where these would lie), indicating that no inclusion complex formed.

6.7 Conclusions

Five different strategies were employed in an effort to generate a self-assembling polymer, linked by both cyclodextrin host-guest inclusion complexes and β-sheet interactions. These involved various cyclodextrin host-guest complexed structures that were designed to polymerise *via* β-sheet formation between oligovaline peptide sequences.

None of the tested systems formed polymers in solution, evident from the lack of gel formation, and furthermore none formed inclusion complexes that could be detected by 2D ^{1}H-^{1}H ROESY NMR spectroscopy. It is probable that this lack of self-assembly is a

consequence of poor aqueous solubility of the guest compounds in the systems studied. The replacement of β-sheet interactions, which utilize hydrophobic peptide sequences, could be replaced by ionic peptide interactions which employ much more water-soluble, charged amino acids. This concept is further described in Chapter 8.

Chapter 7: Results and Discussion

A Peptide Amphiphile Organogelator

7.1 Introduction

Peptide amphiphiles (PAs) are a class of compounds which feature a lipophilic group (typically an alkyl chain) and a peptide which includes a charged, hydrophilic head group.[212] A number of these structures have been found to self-assemble *via* interactions such as π-π stacking,[213-215] hydrogen bonding[216-218] (including β-sheet formation) and hydrophobic interactions, into supramolecular structures that lead to gelation of a solution.[86, 219]

Peptide amphiphile gelation has previously focussed on studies in aqueous solutions, however it was noted during the synthesis of compounds presented in Chapter 4 that the octyl-peptide **81** formed a gel in a mixture of acetonitrile and water. As a consequence of the limited available material of the peptide **81** the deprotected version **112**, which is simpler and cheaper to synthesise as it uses the common trityl-protected histidine rather than the specialised BOM-protected amino acid, was explored as an organogel (Figure **7.1**). The deprotected peptide also retains biological relevance.

Organogelators have numerous potential applications including in the containment of oil spills,[220-222] drug delivery,[223] as additives in food[224] and cosmetics,[225] dye-sensitised solar cells,[226] materials for imaging,[227] removal of toxins from water[228] and light-harvesting materials.[229] Low-molecular weight gelators are particularly attractive as modifications at the molecular level can be used to tune the properties of the gel.[230-233] For comparison, the unalkylated peptide **84** was also studied.

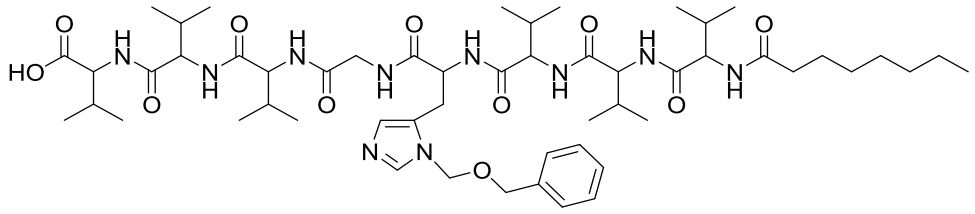

81

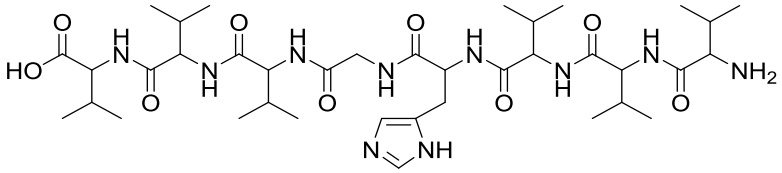

84

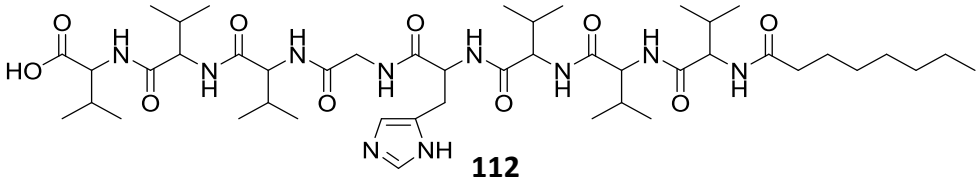

112

Figure 7.1 The organogelator **81** identified during work in Chapter 4, the unalkylated peptide **84** used for comparison, and the deprotected peptide amphiphile **112** investigated in this Chapter.

7.2 Gelation Behaviour

The peptide amphiphile **112** was prepared by solid-phase synthesis, with octanoic acid used in the final on-resin coupling step. The crude product was purified by HPLC in a yield of 22%.

The peptide amphiphile **112** displayed very limited solubility in water regardless of pH, temperature and sonication, and was therefore unable to form a hydrogel. The peptide amphiphile **112** was also insoluble in acetonitrile, however with sonication dissolved in mixtures of acetonitrile and water, forming a self-supporting gel upon standing. A range of acetonitrile/water ratios were examined with 10% solutions gelling after 10 days, and higher acetonitrile ratios resulting in faster gelation up to a 50% solution which gelled in less than 1 day (Figure **7.2**). Unsurprisingly, increasing the concentration of the peptide amphiphile **112** also sped up gelation with 0.8 wt.% (8.56 mM) solutions in 50:50 acetonitrile/water forming gels within minutes of initial sonication.

A 50:50 mixture of acetonitrile/water was used for subsequent gel characterisation, as these gels formed on useful timescales. The minimum gel concentration (mgc) of the peptide amphiphile **112** in a 50:50 acetonitrile/water mixture was determined to be 0.06 wt.% (0.64 mM). Peptide **84** was also soluble in the aforementioned acetonitrile/water mixtures, however did not form a gel at any of the ratios examined.

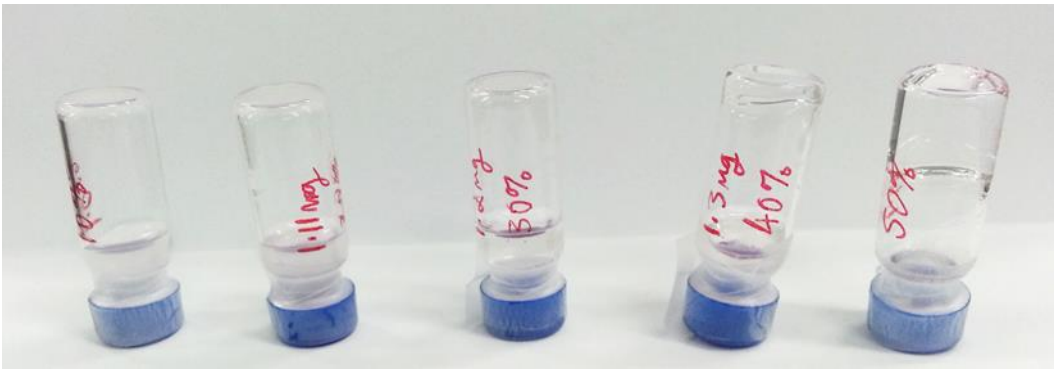

10% MeCN/H_2O | 20% MeCN/H_2O | 30% MeCN/H_2O | 40% MeCN/H_2O | 50% MeCN/H_2O

Figure 7.2 Peptide amphiphile **112** in varying proportions of acetonitrile after 1 day in an example of the inversion test for gelation.

Considering solvents other than acetonitrile/water, the peptide amphiphile **112** did not dissolve in ethyl acetate, diethyl ether or hexane. The compound dissolved in dimethyl sulfoxide, methanol, ethanol, isopropanol, chloroform, dichloromethane and toluene but did not form gels from those solutions. The peptide amphiphile **112** dissolved in DMF and acetone to give solutions that form gels with mgcs of 0.06 wt.% in each case.

In order to visualise ordered structures formed by the peptide that would be causing gelation, atomic force microscopy (AFM) was performed on the xerogels obtained from the gelation of each solvent. AFM of the xerogel from the gelation of 50% acetonitrile/water by peptide **112** (Figure **7.3**) shows short fibrils ranging in diameter from 8-12 nm. These structures exhibit a valley along the long axis of each fibril, most likely as a result of the collapse of a solvent-filled core during sample preparation.

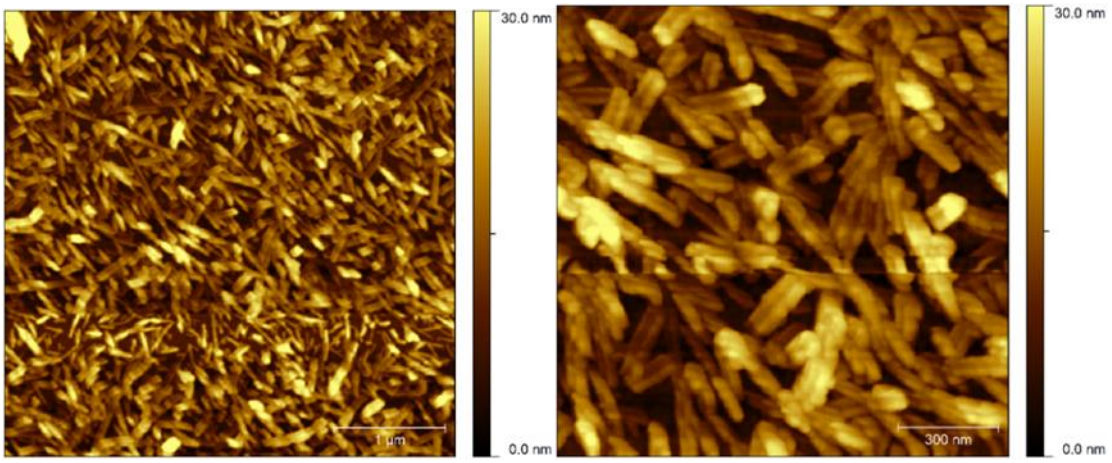

Figure 7.3 AFM images of the xerogel from gelation of 0.20 wt.% peptide amphiphile **112** in 50% acetonitrile/water at a 1 µm (*left*) and 300 nm (*right*) scale.

AFM images were also obtained from the DMF and acetone organogels of the peptide amphiphile **112** (Figure **7.4**). The DMF xerogel shows a similar morphology to the acetonitrile/water gels, although with larger fibre diameters (10-20 nm) and longer fibres (on the order of microns). Despite being a densely packed fibrous network, the acetone xerogel of the peptide amphiphile **112** also show short fibril morphology. The similarity in supramolecular structure assembly and comaparable mgcs suggests that the gelation mechanism of the peptide amphiphile **112** is the same in acetonitrile/water, DMF and acetone.

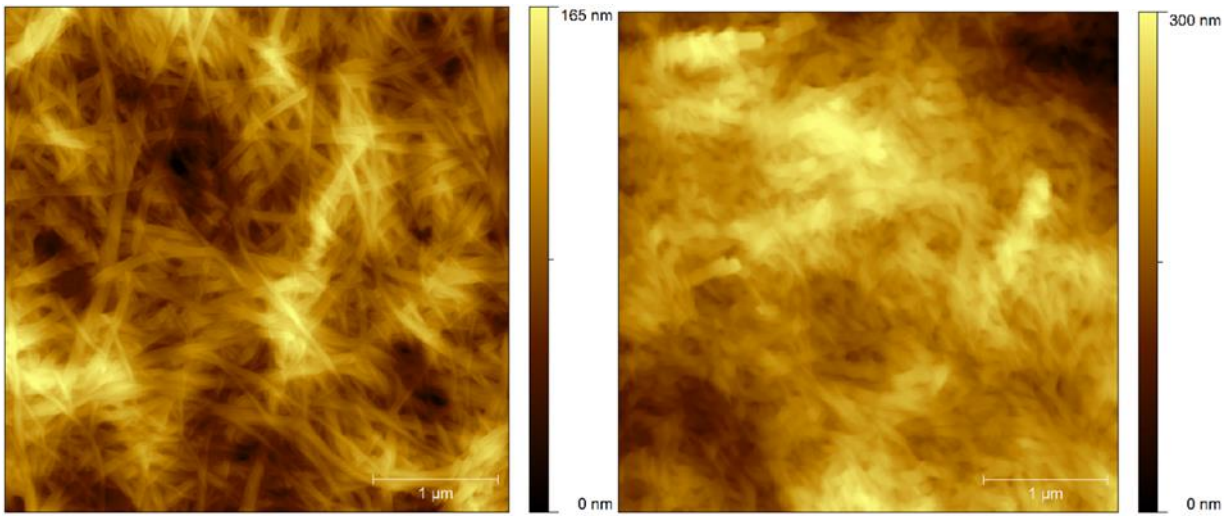

Figure 7.4 AFM images of the xerogel from gelation of 0.20 wt.% peptide amphiphile **112** in DMF (*left*) and acetone (*right*).

7.3 Rheological Properties of the Gel

In order to quantify mechanical strength, oscillatory rheology was performed on peptide amphiphile **112** gels from a 0.20 wt.% solution in 50% acetonitrile/water. Rheological experiments were not performed on the DMF and acetone gels as the slow and fast evaporation of these respective solvents makes measurements practically difficult. As the mechanism of gelation of the peptide amphiphile **112** gels across all solvents is likely to be the same, it is also likely that rheological behaviour will be the same.

A frequency sweep performed shows frequency-independent behaviour over the range studied, with a storage modulus (which is commonly used to approximate gel stiffness) of 1.5 $x10^5$ Pa (Figure **7.5**), which is high for a supramolecular gel. Strain sweeps show that these stiff gels are quite brittle however, with deviation from the linear viscoelastic region at only 1% strain (Figure **7.6**), followed a gel to liquid transition at 3% strain.

Thixotropy tests were also performed, where periods of large strain (100%) and low strain (0.2%) are alternated in order to observe gel recovery behaviour after disruption of the gel network. These tests show a rapid initial recovery of the gel network after application of a large strain, however a full recovery to the initial storage modulus of the gel is not achieved (Figure **7.7**). This lack of full recovery is most likely as a consequence of incomplete formation of the initial gel network. A full recovery is expected to occur over a longer time period than that measured here, however the ability of the peptide amphiphile **112** to reform a gel within 30 seconds of cessation of a large strain is notable, and relevant for the use of this gel as an injectable material. Although rheological measurements were not performed at higher concentrations, rapid gel recovery is observed in solutions above 0.8 wt.% (8.56 mM) with simple inversion tests.

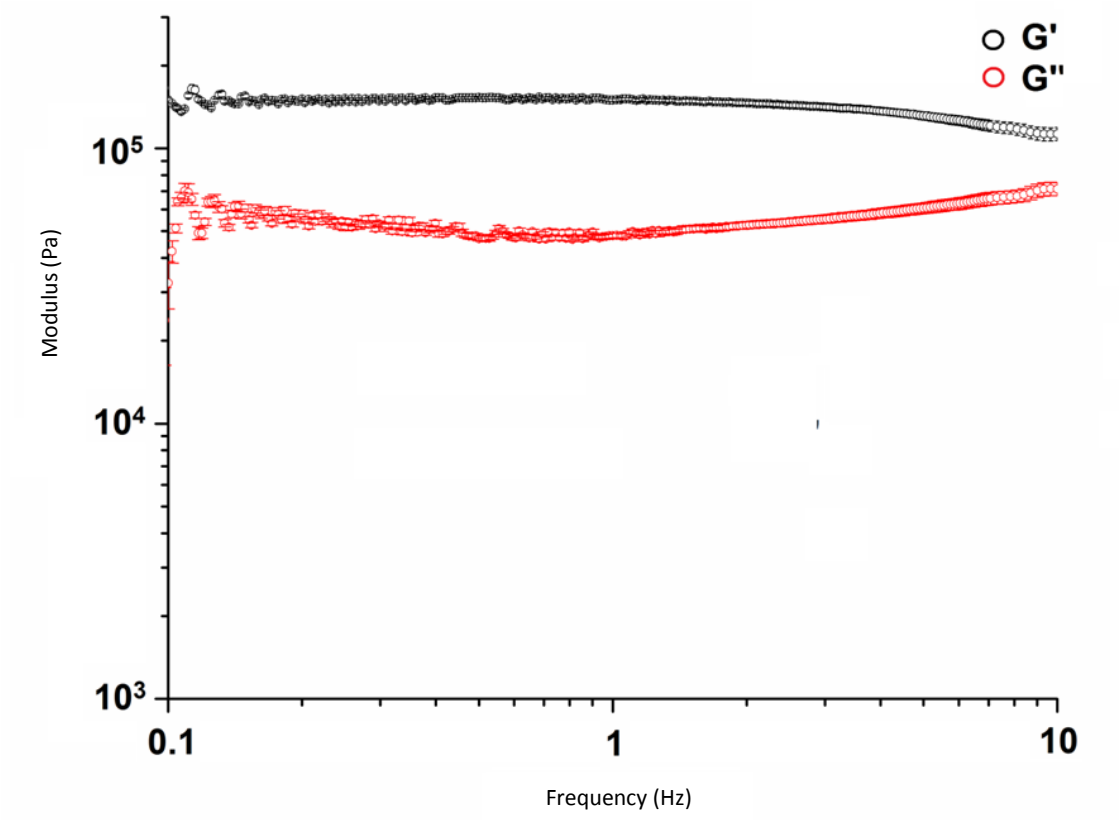

Figure 7.5 Storage and loss modulus of a 0.20 wt.% (2.14 mM) solution of the peptide amphiphile **112** in 50% acetonitrile/water as a function of frequency.

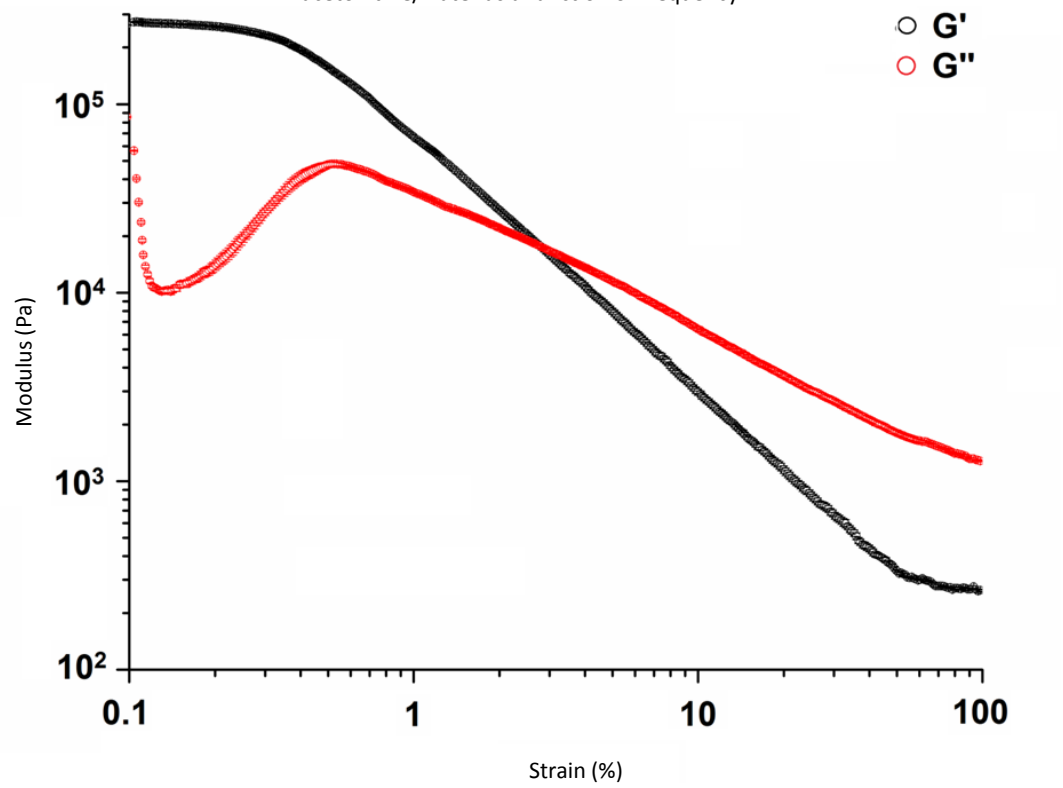

Figure 7.6 Storage and loss modulus of a 0.20 wt.% (2.14 mM) solution of the peptide amphiphile **112** in 50% acetonitrile/water as a function of strain.

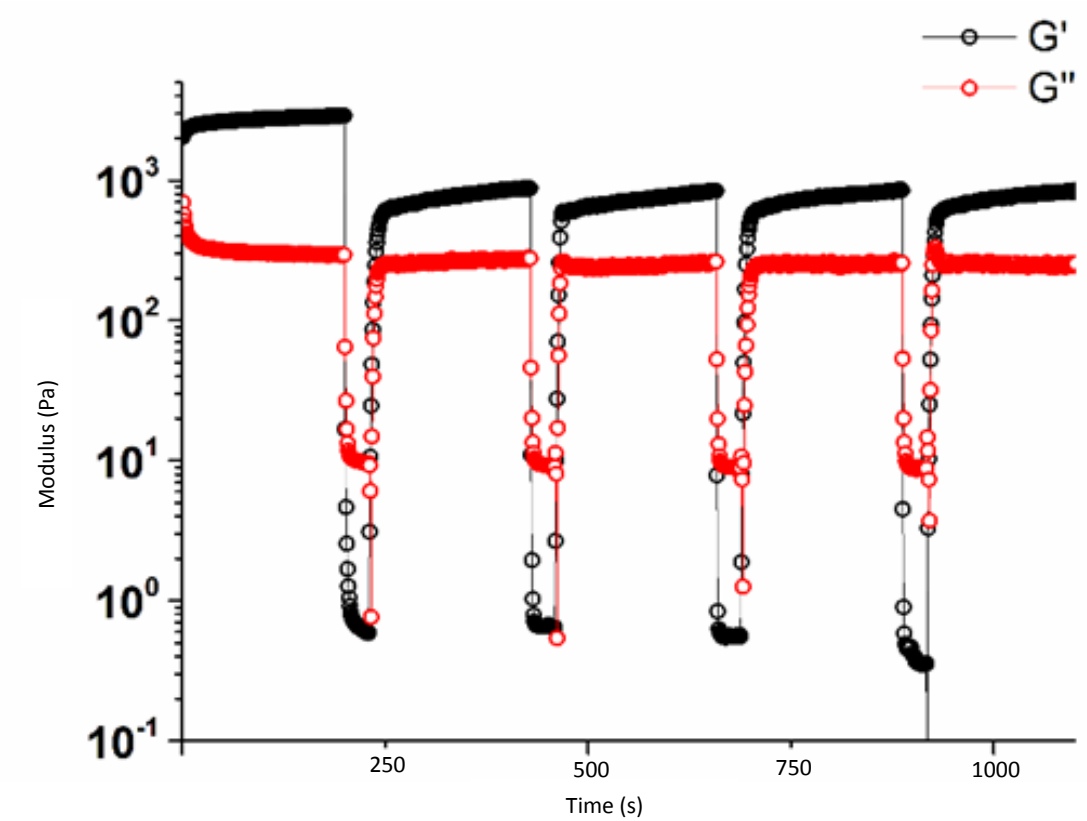

Figure 7.7 Thixotropic test of the 0.20 wt.% (2.14 mM) gel of the peptide amphiphile **112** in 50% acetonitrile/water.

7.4 Effect of Gelation on Peptide Structure

Having established the physical characteristics of the gel formed by the peptide amphiphile **112** in 50% acetonitrile/water, the role of peptide secondary structure in gelation was then investigated. The circular dichroism spectrum of the gel (Figure **7.8**) shows a minimum at 218 nm, characteristic of β-sheet secondary structure.[234] The spectrum of a corresponding solution of the peptide amphiphile **112** before it was let stand for gelation to occur shows a minimum at 201 nm with a shoulder at ~215 nm, indicating a mixture of random coil/disordered and β-sheet structures respectively. The differences between these spectra show that gelation involves ordering of the peptide into a sheet assembly. Even though the unalkylated peptide **84** does not form a gel, its circular dichroism spectrum also shows an intense minimum at 214 nm characteristic of β-sheet formation, demonstrating that gelation is not solely determined by interactions between peptide chains and the alkyl moiety of the peptide amphiphile **112** is key to gel formation.

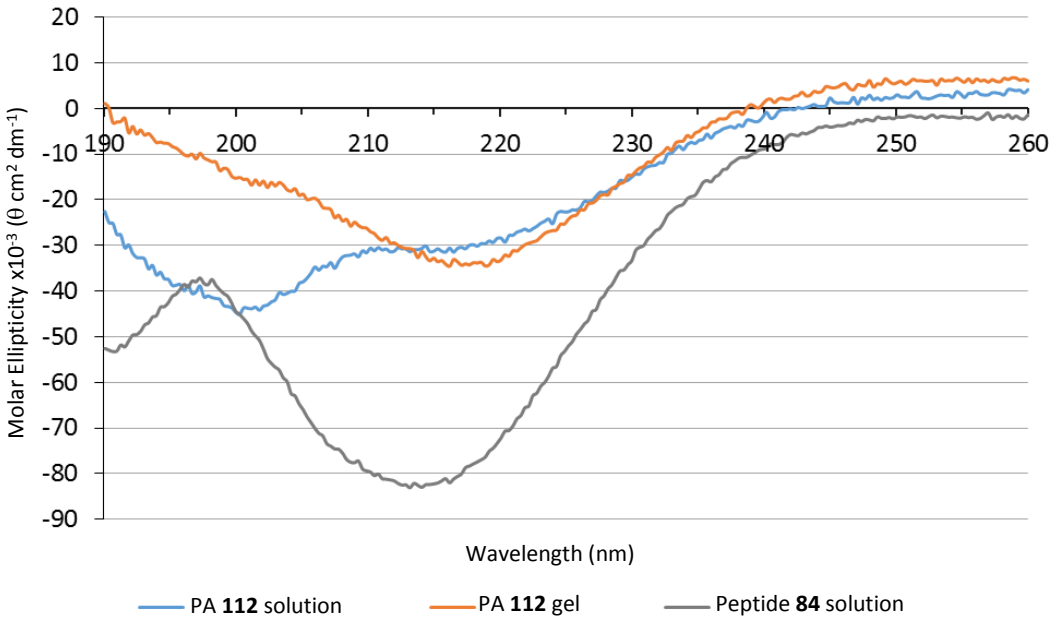

Figure 7.8 Circular dichroism spectra of the peptide amphiphile **112** in solution and after gelation (average of 27.5-11.6 μM), and peptide **84** in solution (average of 29.1-12.3 μM).

The structural information provided by circular dichroism spectroscopy is mirrored in results obtained using FT-IR spectroscopy. The gel of the peptide amphiphile **112**, prepared in 50% acetonitrile/D_2O instead of acetonitrile/water so as to eliminate interference from H_2O,[235] showed an amide I carbonyl signal at 1624 cm^{-1} corresponding to a β-sheet structure (Figure **7.9** and Figure **7.10**).[236] The signal at 1626 cm^{-1} in the corresponding spectrum of the unalkylated peptide **84** shows a similar structure (Figure **7.11** and Figure **7.12**), again demonstrating that gelation is not only dependent on peptide secondary structure and that the alkyl moiety of the peptide amphiphile **112** is required.

The carbonyl signals in the spectra of both the gel of the peptide amphiphile **112** and the solution of peptide **84** in 50% acetonitrile/D_2O are each red-shifted by approximately 5 cm^{-1}, relative to those of the corresponding powders, which appear at 1630 and 1631 cm^{-1}, respectively. Shifts in β-sheet carbonyl FT-IR spectroscopic signals are indicative of the characteristics of the hydrogen bonding that is present,[237] therefore this observation provides some tentative evidence that the interactions between the peptide chains in the gel of the peptide amphiphile **112** are similar to those in the solution of peptide **84**, and further supports the argument that peptide structure is not the only requirement for gelation.

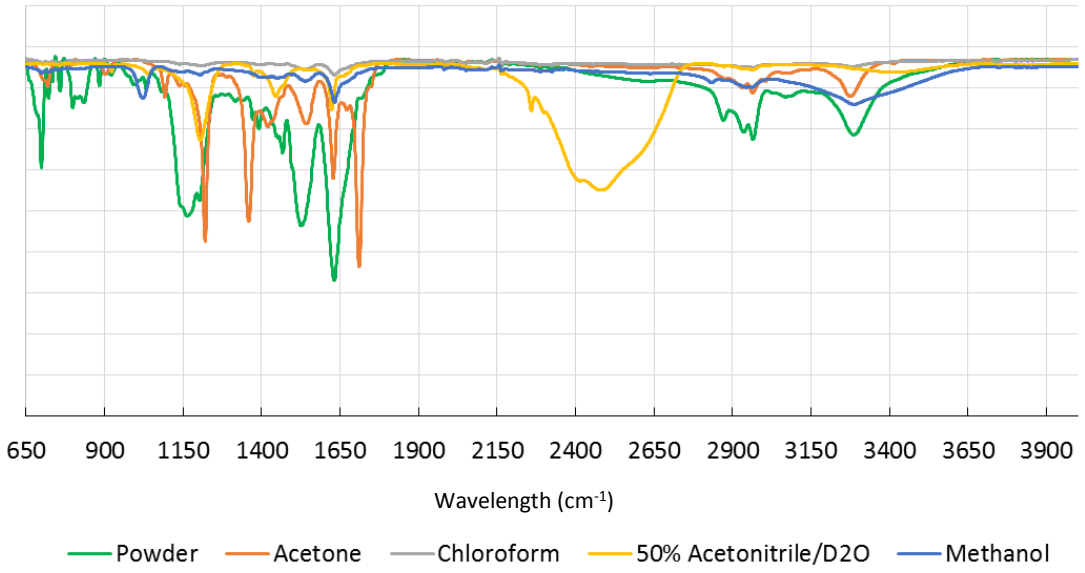

Figure 7.9 FT-IR spectra of the peptide amphiphile **112** 0.20 wt.% (2.14 mM) in acetone, chloroform, 50% acetonitrile/D_2O and methanol, and as a powder.

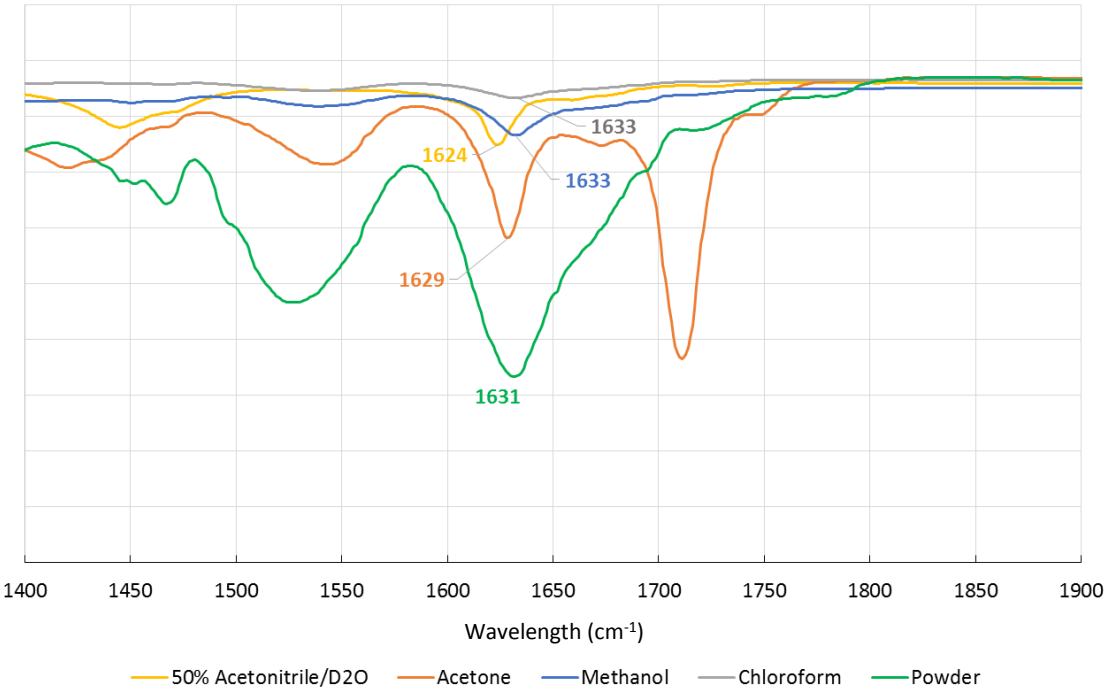

Figure 7.10 β-Sheet carbonyl region of the FT-IR spectra of the peptide amphiphile **112** 0.20 wt.% (2.14 mM) in acetone, chloroform, 50% acetonitrile/D_2O and methanol, and as a powder.

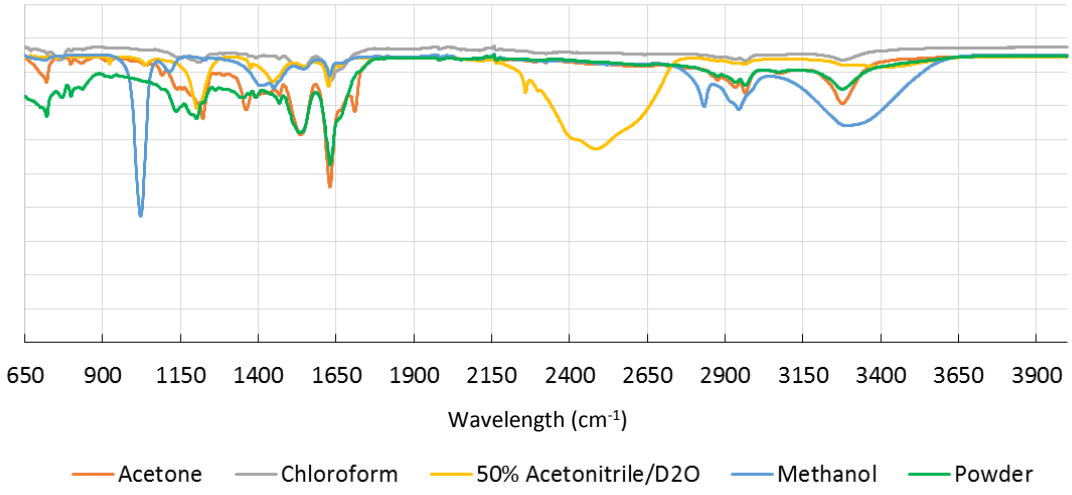

Figure 7.11 FT-IR spectra of peptide **84** 0.20 wt.% (2.14 mM) in acetone, chloroform, 50% acetonitrile/D_2O and methanol, and as a powder.

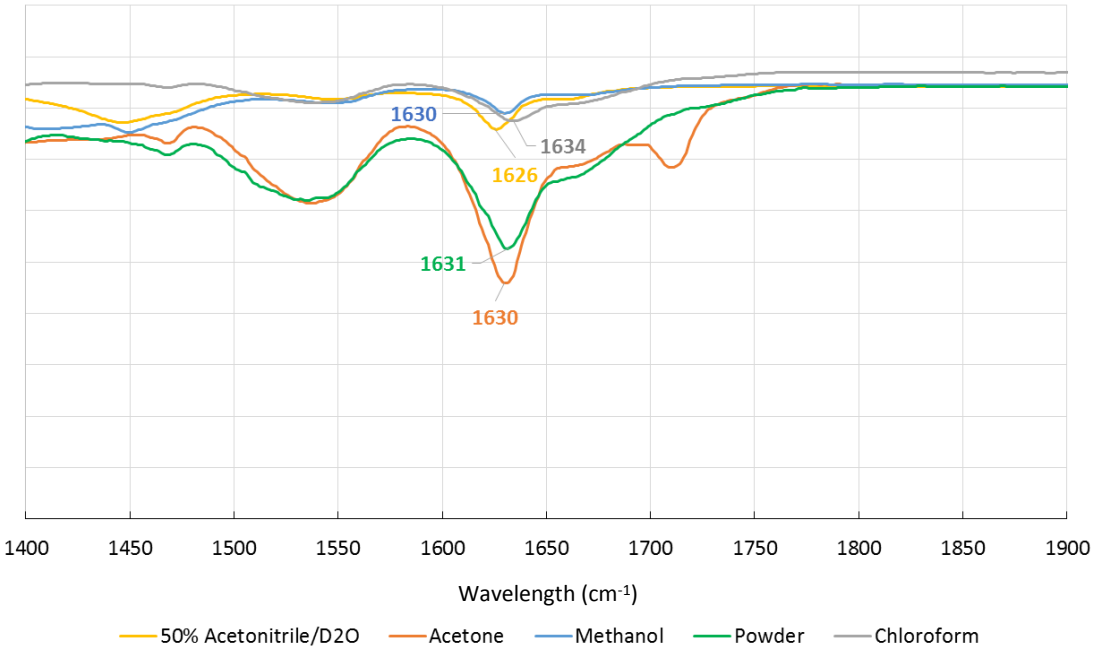

Figure 7.12 β-Sheet carbonyl region of the FT-IR spectra of peptide **84** 0.20 wt.% (2.14 mM) in acetone, chloroform, 50% acetonitrile/D_2O and methanol, and as a powder.

7.5 Structure-Property Relationships

The peptide amphiphile **112** is structurally similar to PAs that form hydrogels such as **113**, featuring a charged head group, a β-sheet forming peptide region and an alkyl chain. A series of these types of peptide amphiphiles have previously been investigated

to determine structure-property relationships between modification of the β-sheet forming peptide and gel stiffness.[238] The molecular structure and stiffness of the resulting organogel formed by the peptide **112** were analysed to determine if they fit the structure-property rules established for the peptide hydrogels.

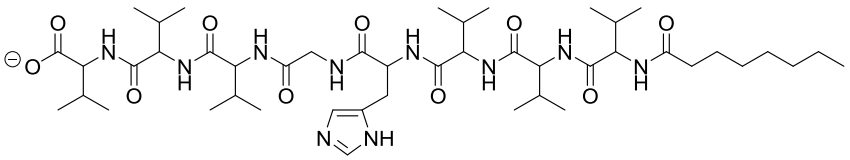

112

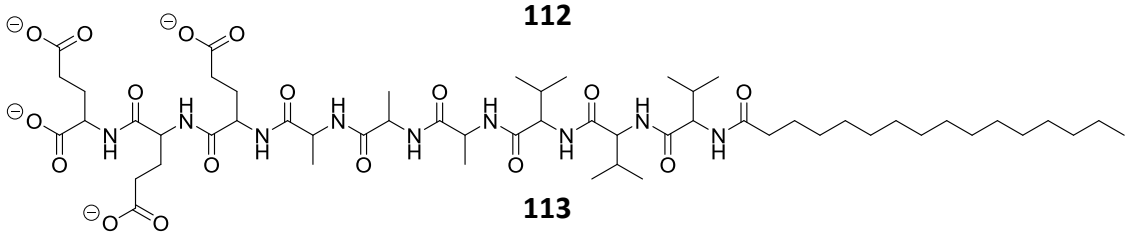

113

Figure 7.13 A comparison of the structures of the peptide amphiphile organogelator **112** and a previously reported peptide amphiphile hydrogelator **113**.[238]

Stupp et al.[238] found that increasing the proportion of valines in the β-sheet forming region of a peptide amphiphile results in an increase in gel stiffness. The peptide amphiphile **112** contains a higher proportion of valine residues to non-valine residues (75%) than any PAs analysed in this study (the highest contained 50% valines), and is also of a much higher stiffness of 1.5 x10^5 Pa compared to the stiffest hydrogelating PA which was measured as ~10^4 Pa. The minimum of the β-sheet signal in the circular dichroism spectra of the hydrogelating PAs in the same study, was noted to be red-shifted by a magnitude that inversely correlates with gel stiffness. This has been attributed to the extent of twisting of the sheets, i.e., stiffer gels involve stronger peptide interactions with the least twisting.[238] Again, the gel of the organogelator peptide amphiphile **112** fits this trend as the corresponding signal is red-shifted by only 2.3 nm, consistent with a very stiff gel. With hydrogelating PAs it has also been shown that an alkyl chain of more than six carbons is necessary for gelation to occur,[239] a condition which is fulfilled by the organogelating peptide amphiphile **112**.

The consistency of the peptide amphiphile organogelator **112** with the structure-property relationships observed in the hydrogelating PAs suggest that they gelate *via* a similar mechanism despite the difference in solvent. Hydrogelating PAs such as **113** are

understood to gelate by means micelle-type hydrophobic aggregation of alkyl chains which propagates down the fibre axis, then is reinforced by peptide β-sheet interactions extending along the length of the fibre.[240] Comparison of the non-gelating peptide **84** and the organogelator **112** show that alkyl chain interactions are required for gelation, supporting this assembly theory. AFM images of the xerogel of the peptide amphiphile **112** from acetonitrile/water solution (Figure **7.3**) also show a valley along the axis of the fibres as would occur in the collapsed core of a micelle.

The identification of the organogelating peptide amphiphile **112** as analogous to hydrogelating peptide amphiphiles provides the unique opportunity to examine the role of the hydrophilic head group. It is postulated that the reduced charge of this moiety in peptide **112** is responsible for its insolubility in aqueous solvents and therefore inability to form a hydrogel, and lends itself towards organogel formation. This hypothesis is in line with a previous study which showed that Boc-protection of a charged amine in a peptide amphiphile resulted in a switch from a hydrogelator to an organogelator.[241] Unlike other systems however, the design rules for β-sheet-forming peptide amphiphiles such as peptide **112** are established and can therefore be drawn upon to give a strategy for not only the development of gelators for targeted solvents for particular technological applications, but also materials with predictable properties.

7.6 Conclusions

The peptide amphiphile **112** has been shown to act as an organogelator in mixtures of acetonitrile and water, DMF and acetone at mgcs of 0.06 wt.% (0.64 mM), giving its classification as a supergelator. Circular dichroism spectroscopy and FT-IR spectroscopy show that self-assembly occurs by way of β-sheet interactions that become more ordered during the gelation process. Comparison with the non-gelating unalkylated peptide **84**, which also forms a similar extent of β-sheets, demonstrates that interactions between alkyl chains is critical for gelation.

The peptide amphiphile **112** bears a high structural similarity to a series of previously reported hydrogelating PAs, including **113**, enabling a direct comparison between the two types of gelators. Results indicate that despite the difference in solvent, these PA

hydrogelators and organogelators assemble *via* the same mechanism, and that the peptide amphiphile **112** adheres to the structure-property relationships previously established for the series of hydrogelating PAs. It is likely that the basis for the variation in solvent gelation capability between the PA **112** and **113**, is the change in charge of the head group component which influences solubility in aqueous and organic solvents. This suggests that a solvent could be targeted for gelation by a peptide amphiphile, by tuning the charge of the head group. Furthermore, the structure-property relationships that govern peptide amphiphile hydrogels could be applied to the design for peptide amphiphile gelators of other solvents.

Chapter 8: Conclusions and Future Work

In this thesis a range of supramolecular devices based on cyclodextrin-peptide-guest constructs were investigated. Studies demonstrated that the formation of host-guest inclusion complexes could effect modification in the secondary structures of the peptides, and that the use of a photoswitchable guest enables switching of the structural change. As the self-assembling component of the design is independent of the peptide moiety, in principle any sequence could be incorporated into the construct. This technique therefore allows for the facile study of biologically relevant short sequences which can adopt secondary and even tertiary structures without the complexity of the whole protein. The method could be used to delineate structural properties of protein fragments and for analysis in complex biological systems such as in the presence of enzymes, as the cyclodextrin host-guest interaction is bio-orthogonal.

The structural effects of both [*c*1]- and [*c*2]-complex formation on various peptides have been investigated. The assembly of [*c*1]-complexes can compared to artificial models of loops,[242-244] turns[245, 246] and hairpins,[247, 248] common structural features in proteins. An interesting research direction would be to use [*c*1]-structure formation to investigate the properties of folded peptide sequences without the influence and complication of the larger protein structure. These folds often have an effect on subsequent biological properties such as binding to other molecules.[249]

The formation of cyclodextrin-peptide-guest [*c*2]-dimers represents a maximisation in the effective concentration of the peptide sequence used and could therefore be used as a tool to recreate biological macromolecular crowding without requiring the use of crowding agents. The use of orthogonal cyclodextrin and guest pairs also gives the possibility for the formation of asymmetric peptide dimers. Macromolecular crowding is observed in a wide range of environments including the lens of the eye,[250] red blood cells[251] and the mitochondrial matrix.[252] It is associated with a number of positive effects such as protein stabilization, oligomer assembly and enhancement of protein-protein

interactions, and also negative effects such as protein destabilization, protein misfolding and aggregate and amyloid formation.[253] Macromolecular crowding is also implicated in disease states such as Parkinson's disease,[254, 255] Alzheimer's disease and type II diabetes,[256] and in the impairment of the effectiveness of antiviral peptide drugs such as those used to inhibit HIV and the foot-and-mouth disease virus.[257] Cyclodextrin-peptide-guest [*c*2]-dimer formation poses an attractive system for the in-depth study of macromolecular crowding effects on protein fragments.

In addition to peptide structural modifications, change in peptide function was also explored using the same type of cyclodextrin-peptide-guest construct to confer Zn^{2+} binding capability to a histidine-containing sequence which ordinarily has none. The same system could be used to study the binding of different metal ions such as Cu^{2+}, Ni^{2+}, Co^{2+} and Cd^{2+} which are known to bind to histidine residues.[258-260] The peptide sequence could also be modified with the introduction of additional histidine residues with the prediction that the strength of metal-binding in the complex can be increased.

In a further progression to this project, it is possible that a system that binds a metal ion such as has been developed, may also be capable of catalysis. This is observed in many natural metalloenzymes such as carboxypeptidase A and has also been demonstrated in artificial systems where short peptides that self-assemble into amyloids are reported to act as carbonic anhydrases as a result of their Zn^{2+} histidine binding capability, hydrolysing *p*-nitrophenylacetate with a k_{cat}/K_M of 360 M^{-1} s^{-1}.[185] Although this activity is much lower than the natural carbonic anhydrase enzyme, on a weight-for-weight basis the fibril has over twice the activity. The same assay could therefore be used to test the cyclodextrin host-guest peptide system developed in Chapter 4 for catalytic activity (Figure **8.1**).

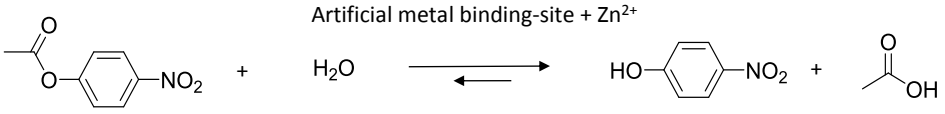

Figure 8.1 *p*-Nitrophenylacetate assay for ester hydrolysis activity, where production of the hydrolysed product can be monitored by absorption at 400 nm.

This assay represents a benchmark for hydrolytic enzymes, but other reactions might also be catalysed, for example the hydrolysis of bicarbonate to form CO_2. If the cyclodextrin host-guest peptide system could also catalyse the reverse reaction, it would have applications as a low-molecular weight carbon capture device.

In the work described in Chapters 5 and 6, concepts in peptide chemistry were applied to supramolecular systems. Attempts to prepare cyclodextrin rotaxanes by solid-phase synthesis were unsuccessful, however only a narrow range of conditions were examined. The concept remains interesting as it potentially gives access to supramolecular assemblies that are not usually formed under thermodynamic equilibrium in solution, therefore efforts to develop a better protocol with changes in resin, reaction conditions and host-guest pairs would be worthwhile. The development of a method to mobilise cyclodextrin onto the resin solid-phase was successful, and has potential in applications such as complexation-based separation and extraction.

Self-assembling systems were designed to form using both cyclodextrin host-guest interactions and peptide-peptide β-sheet interactions in order to generate non-covalent polymers. Evidence of supramolecular assembly i.e., gel formation was not observed, reasoned to be as a consequence of the low aqueous solubility of the oligovaline peptides used in the studies. A variation in this strategy for the formation of a self-assembling polymer would be to replace the β-sheet interactions that require a hydrophobic peptide sequence, with ionic interactions which exist between highly water-soluble, charged sequences. Furthermore a polymer comprising both ionic and cyclodextrin host-guest interactions would be dually responsive, sensitive to both inputs that switch complexation on and off such as azobenzene photoirradiation and pH.

The work described in Chapter 7 investigates the properties of the peptide amphiphile organogelator **112**, and draws a direct comparison to a set of previously reported hydrogelators including the peptide amphiphile **113**. This study has led to the proposal that these types of peptide amphiphiles can be tuned to gelate in specific solvents by adjustment of the size of the charged head group with relation to the size of the alkyl chain. A series of peptide amphiphiles with such structural modifications could therefore be investigated in a more extensive study in order to test this hypothesis.

In conclusion, the work presented in this thesis demonstrates that cyclodextrin and peptide moieties can be synthetically combined to give supramolecular devices and materials. The nature of most of these constructions enables the incorporation of almost any small peptide sequence, thereby giving potential for a wide range of associated sequence-dependent functionalities and properties to be integrated into cyclodextrin-based devices and materials. The virtually unlimited library of possible peptide combinations in turn gives conceivable applications that lie in a diverse scope of fields from structural biology to biomimetic chemistry to supramolecular materials.

Chapter 9: Experimental Methods

9.1 General Methods

Reagents and Solvents: Hexavaline, pentaalanine and Fmoc-His (π-BOM) were purchased from Auspep and all other chemicals from Sigma Aldrich or Tokyo Chemical Industry Co. and were used as received without further purification. α-Cyclodextrin was purchased from Nihon Shokuhin Kako Co. Japan in 99.1% purity and was dried over P_2O_5 under reduced pressure to a constant weight before use. Wang resin and Rink amide resin was purchased from Sigma Aldrich, and Tentagel S PHB resin from Advanced Chem Tech. Anhydrous solvents were obtained from a Braun SPS-800 system using MB-KOL-A and MB-KOL-M filter columns, and ultra-pure water from an Elgar Purelab® Classic UV system at 18.2 MΩ.

Freeze-drying: Solutions were freeze-dried with a Labconco Freezone 4.5 freeze-drier.

Chromatography: Thin layer chromatography (TLC) was carried out using aluminium backed 0.2 mm EMD Millipore silica gel 60 F254 plates and cyclodextrin compounds visualised by treatment with a naphthalene-1,3-diol solution (0.1% w/v) in ethanol:water:H_2SO_4 (200:157:43) and strong heating. Analytical HPLC was performed using a Hewlett Packard 1100 system and Chemstation Agilent software, with a YMC ODS-AQ 150x4.6 mml 3μm analytical column. Semi-Preparative and preparative HPLC was performed using a Waters 2996 photodiode array detector and Waters 600 controller and analysed with Waters Empower software. A Phenomenex Luna 250x10 mm 5μm semi-preparative column and a YMC ODS-AQ 200x20 mm 5μm preparative column were used. HPLC samples were filtered through a 0.45 μm nylon filter before analysis.

Ion Exchange: Cation exchange was performed using Toyopearl SP-650M resin or Waters Oasis® MCX 1cc cartridges, and anion exchange using Sep-Pak Plus QMA cartridges.

Nuclear Magnetic Resonance: ^{1}H NMR and 2D NMR spectra were recorded on a Varian Mercury 300 spectrometer, a Bruker Avance 400 spectrometer, a Varian Inova 500 spectrometer and a Bruker Avance 600 spectrometer. Residual solvent signal was used as an internal standard, and a TSPA-d_4 insert for ^{13}C NMR where D_2O was the solvent.

Mass Spectrometry: High resolution ESI mass spectrometry was obtained using a Waters LCT Premier XE oa-TOF mass spectrometer. LC-MS was performed using a Waters Aquity TQ detector and Waters 2695 separator with an Agilent Zorbax SB-C18 4.6x150 mm 3.5 μm column. Data was analysed using MassLynx software.

Melting Points: Melting points were measured on an Optimelt automated melting point system and analysed using SRS Optimelt V. 1.107 software.

Elemental Analysis: Elemental analyses were performed by the Australian National University microanalytical service at the Research School of Chemistry.

Isothermal Titration Calorimetry: ITC data was recorded on a Microcal VP-ITC calorimeter and analysed using Origin Version 7.0 software.

Circular Dichroism Spectrometry: Circular dichroism spectrometry was performed using a Chirascan circular dichroism spectrometer and analysed using Pro-data software. Samples were measured in a 10 mm Hellma QS cuvette in 5 mM phosphate buffer (pH 7.0). Spectra are the average of 5 scans using a 0.3 nm step and 1.5 s per point. T_m for samples were obtained in a stepped method from 5-90 °C with steps of 5 °C and a 30 s waiting period at each temperature.

UV-Vis Spectrometry and Photo-irradiation: Samples were irradiated using a Luzchem photoreactor with Luzchem 420 nm lamps, and a Spectroline 36-380 long wave UV 360 nm pencil lamp. UV data was obtained with a UV-2450 shimadzu spectrophotometer.

Fourier-transform Infrared Spectroscopy: FT-IR spectroscopy measurements were made on a Perkin Elmer Spotlight 400 FT-IR spectrophotometer equipped with a diamond crystal attenuated total reflectance (ATR) accessory. Solutions and gels were both prepared at 0.20 wt.% (2.14 mM) and pressed between the diamond crystal and substrate. All spectra were scanned 16 times over the range of 4000 - 650 cm^{-1}.

Rheology: Peptide solutions (0.20 wt.%, 2.14 mM) were made by dissolving in 50% acetonitrile/water with sonication. An aliquot (550 µL) of this solution was then cast onto an Anton Paar MCR 302 rheometer (parallel plate geometry) and left to gel over the course of 4 h. A solvent trap and Peltier hood was used to prevent any evaporation during gelation. Frequency sweeps were performed from 0.1-10 Hz, at a constant strain of 0.2% and three repeats performed on separate samples. Strain sweeps were performed from 0.1–100% at a constant frequency of 1 Hz.

AFM imaging: Peptide solutions (0.20 wt.%, 2.14 mM) were made by dissolving in the relevant solution with sonication. Gels were allowed to form, then samples for AFM were prepared by spread coating onto a freshly cleaved mica disc and leaving to dry overnight in ambient conditions to give the xerogel. Imaging was undertaken using a Bruker Multimode 8 in ScanAsyst mode under ambient conditions and with ScanAsyst Air tips (spring constant 0.4 N/m^2).

Manual Fmoc Solid Phase Peptide Synthesis: Wang resin was swollen overnight with DCM (~ 180 equivalents to resin loading) and DMF (~ 16.5 eq). Swelling solvents were then filtered from the resin and a solution of the Fmoc-protected amino acid (2.5 eq), HOBt (2.5 eq) and DIC (2.5 eq) in a minimum amount of DMF was added, followed by a solution of DMAP (0.1 eq) in DMF. The resin was then bubbled with N_2 for 3 h. The reaction mixture was filtered off and the resin washed with DMF (3x10 mL) and MeOH (3x10 mL) and dried under high vacuum. A small portion of resin (10 mg) was taken and the Fmoc protecting group cleaved by addition of 20% piperidine in DMF (1 mL) for 1 h. Completion of the first amino acid coupling to the resin was then found by Fmoc determination, by measuring UV absorbance at 278 nm. The resin was re-swollen with DMF (3 mL) for 1 h, then a solution of acetic anhydride (2 eq) and pyridine (2 eq) in a minimum amount of DMF added and bubbled with N_2 for 1 h. The reaction mixture was

filtered from the resin, washed with DMF (3x10 mL) and a solution of 20% piperidine in DMF (4.2 mL) added and bubbled with N_2 for 45 min. Subsequent amino acids were coupled by filtering off the reaction mixture, washing with DMF (3x10 mL) and adding a solution of Fmoc-protected amino acid (2 eq), HOBt (2 eq), HBTU (2 eq) and DIPEA (4 eq) in a minimum amount of DMF and bubbling with N_2 overnight. For some amino acids that did not couple with high efficiency, this reaction mixture was applied twice.

Automated Solid-Phase Peptide Synthesis: Synthesis was performed using Wang resin, preloaded with the first Fmoc-protected amino acid. Resin was swollen in DMF for 2 h before being loaded onto a CEM Liberty Automated Peptide Synthesiser. Amino acid solutions in DMF (0.2 M, 4 eq) were used, along with HBTU in DMF (0.45 M, 4 eq) as the activator, DIPEA in NMP (2 M, 3.6 eq) as the activator/base and HOBt (0.1 M, 4eq) in 20% piperidine in DMF (0.1 M, 4 eq) for deprotection. Couplings were performed in the CEM Discover Microwave Unit and sequences composed using PepDriver software.

Cleavage of Peptides from Wang and Tentagel Resin: The Fmoc protecting group was removed by filtering off the reaction mixture, washing with DMF (3x10 mL), adding a solution of 20% piperidine in DMF (4.2 mL) and bubbling with N_2 for 45 min. Peptides were cleaved from the resin by filtering off the reaction mixture, washing with DMF (3x10 mL) and MeOH (3x10 mL), then adding TIPS (1 eq) and H_2O (1 eq) followed by TFA (100 eq). The reaction mixture was left for 4 h, swirling every 30 min, then collected by filtering off from the resin.

9.2 Experimental for Chapter 2

6^A-*O*-(*p*-Toluenesulfonyl)-α-cyclodextrin 12

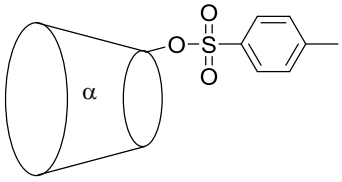

Natural α-cyclodextrin **11** (8.00 g, 8.22 mmol) was dissolved in dry pyridine (800 mL) and cooled to 5 °C. *p*-Toluenesulfonyl chloride (8.00 g, 42.1 mmol) was added in small portions, the ice bath was removed and the reaction mixture left to stir for ~4 h with a drying tube until TLC indicated the ratio of mono- and di-substituted products was equal. The reaction was quenched with the addition of water (50 mL) and the solution concentrated by rotary evaporation to 50 mL, then pipetted into ice-cold, vigorously stirring acetone (2.5 L). The resulting precipitate was recovered by filtration and dried to yield the crude product as a white solid. The crude product was dissolved in water (~3 L) and applied to a Diaion HP-20 column. The column was flushed with water until no more unreacted α-cyclodextrin was eluted, then a water-methanol gradient applied to elute the desired mono-substituted product (20-40% methanol). The combined fractions were reduced and lyophilised to yield the title compound **12** as a white solid (2.64 g, 29%).

TLC: (5:4:3 v/v/v *n*-butanol:ethanol:water) R_f = 0.61.

^{1}H NMR: (300 MHz, D_2O, δ): 7.82 (d, *J* = 7.5 Hz, 2H, Ar), 7.49 (d, *J* = 7.5 Hz, 2H, Ar), 5.01-4.89 (m, 6H, CD H1), 3.97-3.42 (m, 36H, CD H2-6), 2.43 (s, 3H, Me). (data consistent with lit.[57] values)

HRMS-ESI: (*m/z*) $[M + H]^+$ calcd for $C_{43}H_{67}O_{32}S$, 1127.3336; found 1127.3337, $[M + Na]^+$ calcd for $C_{43}H_{66}O_{32}NaS$, 1149.3156; found 1149.3156.

Melting point: 160 °C dec. (lit.[57] mp 159-162 °C dec.)

6^{A}-Azido-6^{A}-deoxy-α-cyclodextrin 34

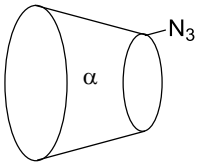

A stirring suspension of 6^{A}-*O*-(*p*-toluenesulfonyl)-α-cyclodextrin **12** (2.50 g, 2.22 mmol) in water (28 mL) was heated to 80 °C and sodium azide (1.59 g, 24.4 mmol) added. The reaction mixture was left to reflux for 8 h, until TLC indicated the consumption of the tosylate starting material. The solution was cooled to room temperature, then pipetted into ice-cold, stirring acetone (150 mL). The white precipitate was collected by filtration and dried under high vacuum to give the crude product as a white solid (1.51 g, 68%). The compound was used with no further purification.

TLC: (5:4:3 v/v/v *n*-butanol:ethanol:water) R_f = 0.41.

^{1}H NMR: (300 MHz, DMSO-d_6, δ): 5.58-3.26 (m, 59H, CD H). (data consistent with lit.[261] values)

HRMS-ESI: (*m/z*) [M + Na]$^{+}$ calcd for $C_{36}H_{59}N_3O_{29}Na$, 1020.3132; found 1020.3132.

Melting point: 220 °C dec. (lit.[261] mp 217 °C dec.)

6^{A}-Amino-6^{A}-deoxy-α-cyclodextrin 35

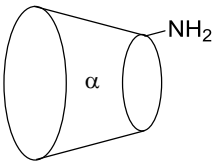

Crude 6^{A}-azido-6^{A}-deoxy-α-cyclodextrin **34** (1.51 g, 1.51 mmol), triphenylphosphine (0.75 g, 2.88 mmol) and aqueous ammonia (6 mL, 30% NH_3) were dissolved in DMF (25 mL) and the reaction mixture left to stir at room temperature for 5 h. The solution was then pipetted into ice-cold, stirring acetone (150 mL) and the precipitate recovered by filtration to give a white solid (0.94 g). The crude product was dissolved in water (~3.5

L) and applied to a SP-650M cationic column. The column was flushed with water until no more unreacted 6^A-azido-6^A-deoxy-α-cyclodextrin **34** starting material or triphenylphosphine eluted, then the product was obtained by elution with 0.5 M aqueous ammonia. Fractions containing the product were combined and reduced by rotary evaporation then lyophilised to yield the title compound **35** as a cream solid (0.87 g, 59%).

TLC: (5:4:3:2 v/v/v/v *i*-propanol:ethanol:water:acetic acid) R_f = 0.49.

^{1}H NMR: (300 MHz, D_2O, δ): 5.03-3.40 (m, 42H, CD H). (data consistent with lit.[261] values)

HRMS-ESI: (*m/z*) $[M + H]^+$ calcd for $C_{36}H_{62}NO_{29}$, 972.3408; found 972.3448.

Melting point: 205 °C dec. (lit.[261] mp 200 °C dec.)

(*E*)-*N*-(6^A-Deoxy-α-cyclodextrin 6^A-yl)-4-aminocarbonyl-4'-carboxyazobenzene 37

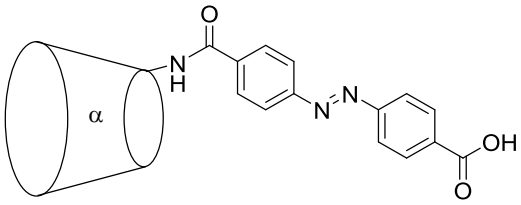

Azobenzene-4,4'-dicarboxylic acid **36** (210 mg, 0.78 mmol), BOP (140 mg, 0.32 mmol) and NEt_3 (0.4 mL, 2.7 mmol) were dissolved in anhydrous DMF (3 mL). A solution of 6^A-amino-6^A-deoxy-α-cyclodextrin **35** (200 mg, 0.21 mmol) and NEt_3 (20 μL, 0.14 mmol) in DMF (2.5 mL) was added dropwise to the reaction mixture and left to stir under N_2 for 24 h. The solution was pipetted into ice-cold, stirring acetone (120 mL) and the orange precipitate recovered by centrifugation. The crude product was dissolved in water (20 mL), acidified with HCl (0.5 M) to pH 2 and applied to a Diaion HP-20 column. The column was washed with water to remove unreacted starting material, then a water-methanol gradient (30-45%) applied to elute the desired product. Fractions containing the product were combined and lyophilised to yield the title compound **37** as an orange solid (110 mg, 44%).

TLC: (5:4:3 v/v/v *n*-butanol:ethanol:water) R_f = 0.41.

^{1}H NMR: (400 MHz, D_2O, δ): 8.07 (d, *J* = 8 Hz, 2H, azobenzene), 7.85 (d, *J* = 8 Hz, 2H, azobenzene), 7.33 (d, *J* = 8 Hz, 2H, azobenzene), 7.29 (d, *J* = 8 Hz, 2H, azobenzene), 4.76-4.59 (m, 6H, CD H1), 3.80-3.00 (m, 36H, CD H2-6). (data consistent with lit.[147] values)

HRMS-ESI: (*m/z*) $[M + Na]^+$ calcd for $C_{50}H_{69}N_3O_{32}Na$, 1246.3762; found 1246.3748.

Melting point: 225-228 °C dec. (lit.[147] mp 228-231 °C dec.)

(*E*)-*N*-(6^A-Deoxy-α-cyclodextrin-6^A-yl)-4-aminocarbonyl-4'-(3-aminopropylaminocarbonyl)azobenzene 39

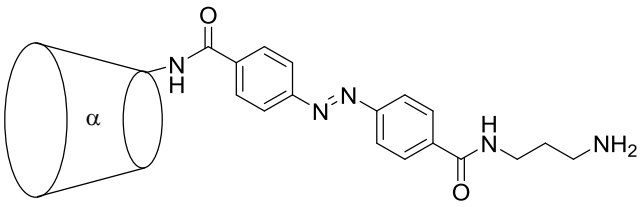

(*E*)-*N*-(6^A-Deoxy-α-cyclodextrin 6^A-yl)-4-aminocarbonyl-4'-carboxyazobenzene **37** (0.30 g, 0.25 mmol), *N*-Boc-1,3-propanediamine **38** (64 mg, 0.37 mmol), BOP (130 mg, 0.29 mmol) and NEt_3 (50 μL, 0.36 mmol) were dissolved in anhydrous DMF (5 mL) and the reaction mixture left to stir for 24 h. The solution was precipitated into ice-cold, stirring acetone (130 mL) and the precipitate recovered by centrifugation to give the intermediate 6^A-4-aminocarbonyl-4'-(1-aminopropyl-3'-*N*-Boc) azobenzene-6^A-deoxy-α-cyclodextrin as an orange solid. The crude intermediate was dissolved in 4M HCl (20 mL) and left to stir for 45 min, until TLC indicated the removal of the Boc protecting group. The solution was evaporated to dryness and the resulting solid taken up in water (0.5 L) before being applied to an SP-650M cationic column. The column was washed with water to remove any unreacted starting material, then the product eluted with 0.5 M aqueous ammonia. Fractions containing the product were reduced by rotary evaporation then lyophilised to yield the title compound **39** as an orange solid (260 mg, 81%).

TLC: (5:4:3:2 v/v/v/v *i*-propanol:ethanol:water:acetic acid) R_f = 0.13.

^{1}H NMR: (300 MHz, D_2O, δ): 8.30 (d, *J* = 9 Hz, 2H, azobenzene), 7.98 (d, *J* = 9 Hz, 2H, azobenzene), 7.48 (m, 4H, azobenzene), 4.92-4.83 (m, 6H, CD H1), 3.85-3.01 (m, 36H,

CD H2-6), 2.94-2.71 (m, 4H, -CONH-C*H*$_2$-CH$_2$ and -C*H*$_2$-NH$_2$), 1.84 (p, *J* = 9 Hz, 15 Hz, 2H, -C*H*$_2$-CH$_2$-NH$_2$). (data consistent with lit.[147] values)

HRMS-ESI: (*m/z*) [M + H]$^+$ calcd for $C_{53}H_{78}N_5O_{31}$, 1280.4681; found 1280.4679.

Melting Point: 218-220 °C dec. (lit.[147] mp 222-225 °C dec.)

8-*tert*-Butoxycarbonylamino-octanoic acid 41

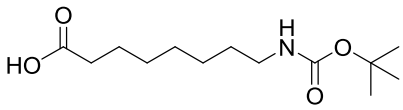

8-Aminooctanoic acid **40** (0.50 g, 3.1 mmol), NaOH (0.28 g, 6.9 mmol) and di-*tert*-butyl dicarbonate (0.82 g, 3.8 mmol) were dissolved in THF (16 mL) and water (16 mL) and the reaction mixture left to stir for 24 h. The solution was reduced by rotary evaporation to 5 mL then taken up in $CHCl_3$ (50 mL) before being washed with 1 M HCl (3x40 mL). The organic layer was dried over $MgSO_4$, filtered and dried by rotary evaporation to give the crude product as a white solid. The purified product was recrystallised from hexane to yield the title compound **41** as a white solid (0.67 g, 82%).

TLC: (1:1 v/v hexane:EtOAc) R_f = 0.58.

^{1}H NMR: (300 MHz, $CDCl_3$, δ): 4.59 (br s, 1H, N*H*), 3.08-3.00 (m, 2H, C*H*$_2$-NH), 2.30 (t, *J* = 7.5 Hz, 2H, HO$_2$C-C*H*$_2$), 1.62-1.57 (m, 2H, alkyl), 1.41 (s, 9H, Boc), 1.31-1.29 (m, 8H, alkyl).

^{13}C NMR: (75 MHz, $CDCl_3$, δ): 179.38 (C=O carboxylic acid), 156.17 (C=O carbamate), 79.23 (*C*-(CH$_3$)$_3$), 40.62 (*C*H$_2$-NH), 34.17, 30.00, 29.04, 28.98 (alkyl), 28.49 (*C*H$_3$), 26.65, 24.72 (alkyl).

HRMS-ESI: (*m/z*) [M + H]$^+$ calcd for $C_{13}H_{26}NO_4$, 260.1862; found 260.1862, [M + Na]$^+$ calcd for $C_{13}H_{25}NO_4Na$, 282.1681; found 282.1679, [M + K]$^+$ calcd for $C_{13}H_{25}NO_4K$, 298.1421; found 298.1421.

Elemental Analysis: Calcd for $C_{13}H_{25}NO_4$: C, 60.21; H, 9.72; N, 5.40%. Found: C, 60.41; H, 9.90; N, 5.40%.

Melting Point: 59 °C.

***N*-(6^A-Deoxy-α-cyclodextrin-6^A-yl)-8-aminooctanamide 42**

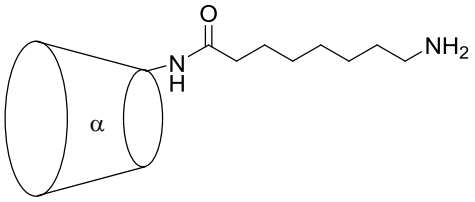

8-*tert*-Butoxycarbonylamino-octanoic acid **41** (0.12 g, 0.46 mmol), 6^A-amino-6^A-deoxy-α-cyclodextrin **35** (0.30 g, 0.31 mmol), BOP (0.16 g, 0.37 mmol) and NEt_3 (65 μL, 0.47 mmol) were dissolved in anhydrous DMF (3 mL) and the reaction mixture left to stir for 24 h. The solution was pipetted into ice-cold, stirring acetone (100 mL) and the precipitate recovered by centrifugation to give the Boc-protected intermediate as a white solid. The crude intermediate was dissolved in 4 M HCl (10 mL) and the reaction mixture left to stir for 2 h, until TLC indicated the removal of the Boc protecting group. The solution was evaporated to dryness and the resulting solid taken up in water (0.5 L) before being applied to an SP-650M cationic column. The column was washed with water to remove any unreacted starting material, then the product eluted with 0.5 M aqueous ammonia. Fractions containing the product were reduced by rotary evaporation then lyophilised to yield the title compound **42** as a cream solid (270 mg, 79%).

TLC: (5:4:3:2 v/v/v/v *i*-propanol:ethanol:water:acetic acid) R_f = 0.52.

^{1}H NMR: (300 MHz, D_2O, δ): 5.26-5.04 (m, 6H, CD H1), 3.77-3.05 (m, 36H, CD H2-6), 2.82-2.76 (m, 2H, NHCO-C*H*$_2$), 2.13-2.07 (m, 2H, C*H*$_2$-NH_2), 1.42-1.16 (m, 10H, alkyl).

^{13}C NMR: (75 MHz, D_2O, δ): 189.67 (C=O), 117.28 (CD C1), 96.31 (CD C4), 89.01 (CD C3), 87.28 (CD C5), 86.72 (CD C2), 74.49 (CD C6), 54.74, 54.69, 45.99, 45.87, 44.30, 43.22, 42.76 (alkyl).

HRMS-ESI: (*m/z*) $[M + H]^+$ calcd for $C_{44}H_{77}N_2O_{30}$, 1113.4561; found 1113.4571, $[M + Na]^+$ calcd for $C_{44}H_{76}N_2O_{30}Na$, 1135.4381; found 1135.4388.

HPLC-Analytical: t_R 11.7 min (gradient; MeCN (0.1% TFA): H_2O (0.1% TFA), 5:95 to 30:70 over 20 min, 30:70 up to 30 min, 0.5 mL min^{-1}).

Melting Point: 164-166 °C dec.

Attempted Synthesis of [(*E*)-*N*-(6^A-Deoxy-α-cyclodextrin-6^A-yl)-4-aminocarbonyl-4'-(3-(4,6-dimethoxy-1,3,5-triazin-2-ylamine)propylaminocarbonyl)azobenzene]-[*N*-(6^A-Deoxy-α-cyclodextrin-6^A-yl)-8-(4,6-dimethoxy-1,3,5-triazin-2-ylamine)aminooctanamide]-[*c*2]-daisy chain dimer 33

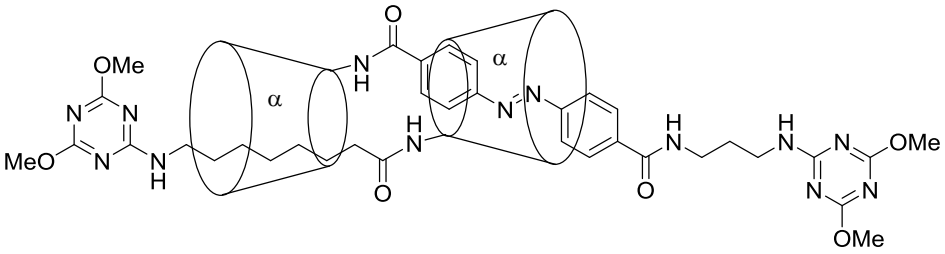

A solution of (*E*)-*N*-(6^A-deoxy-α-cyclodextrin-6^A-yl)-4-aminocarbonyl-4'-(3-aminopropylaminocarbonyl)azobenzene **39** (2 mg, 1.6 μmol) in water (400 μL) was brought to pH 9.5 with dilute NEt_3 and added dropwise to a solution of *N*-(6^A-deoxy-α-cyclodextrin-6^A-yl)-8-aminooctanamide **42** (8.7 mg, 7.8 μmol) in water (350 μL), also at pH 9.5. 2-Chloro-4,6-dimethoxy-1,3,5-triazine (1.7 mg, 9.4 μmol) was added and the reaction mixture left to stir for 24 h. More 2-chloro-4,6-dimethoxy-1,3,5-triazine (9.9 mg, 56.4 μmol) was then added and the reaction mixture left to stir for 24 h before analysis. Water (5 mL) was added and the solution washed with EtOAc (3x20 mL). The aqueous layer was reduced by rotary evaporation to 1 mL and applied to a sephadex G-20 column. The product was eluted with water and fractions containing the product were combined, reduced by rotary evaporation and lyophilised to yield an orange solid, identified as the trimeric species **49** (2 mg, 61%).

^{1}H NMR: (600 MHz, D_2O, δ): 8.48-8.45 (m, 4H, azobenzene), 8.15-8.13 (m, 4H, azobenzene), 7.69-7.55 (m, 8H, azobenzene), 5.07-5.02 (m, 18H, CD H1), 3.98-3.40 (m, 126H, CD H2-6 and O-C*H*$_3$), 3.04-2.92 (m, 6H, alkyl), 2.03-1.94 (m, 6H, alkyl), 1.56-1.26 (m, 14H, alkyl).

LRMS-ESI: (*m/z*) $[M + 3H]^{3+}$ calcd for $C_{165}H_{248}N_{21}O_{98}$, 1363.8; found 1364.5, $[M + 2H + Na]^{3+}$ calcd for $C_{165}H_{247}N_{21}O_{98}Na$, 1371.1, found 1373.5.

HPLC-Analytical: t_R 14.5 min (gradient; MeCN (0.1% TFA): H_2O (0.1% TFA), 5:95 to 30:70 over 10 min, 50:50 up to 11 min, 50:50 up to 30 min, 0.5 mL min^{-1}).

[(*E*)-*N*-(6^A-Deoxy-α-cyclodextrin-6^A-yl)-4-aminocarbonyl-4'-(3-(4,6-dimethoxy-1,3,5-triazin-2-ylamine)propylaminocarbonyl)azobenzene]$_2$-[*c*2]-daisy chain dimer 31

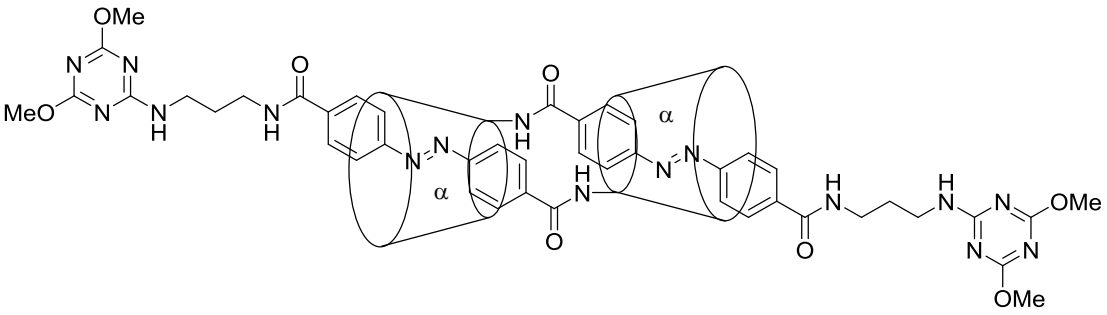

A solution of (*E*)-*N*-(6^A-deoxy-α-cyclodextrin-6^A-yl)-4-aminocarbonyl-4'-(3-aminopropylaminocarbonyl)azobenzene **39** (12 mg, 9.4 μmol) in water (750 μL) was allowed to equilibrate for 3 h. The solution was brought to pH 9.5 with dilute NEt_3 and 2-chloro-4,6-dimethoxy-1,3,5-triazine (12 mg, 68.3 μmol) added. The reaction mixture was left to stir for 24 h before analysis. The compound was not isolated, only identified in order to assign the target compound's and by-products' elution time in an HPLC method.

HRMS-ESI: (*m/z*) $[M + 2H]^{2+}$ calcd for $C_{116}H_{166}N_{16}O_{66}$, 1419.5080; found 1419.5084.
HPLC-Analytical: t_R 10.3 min (gradient; MeCN (0.1% TFA): H_2O (0.1% TFA), 5:95 to 30:70 over 20 min, 30:70 up to 30 min, 0.5 mL min^{-1}).

[(*E*)-*N*-(6^A-Deoxy-α-cyclodextrin-6^A-yl)-4-aminocarbonyl-4'-(3-(4,6-dimethoxy-1,3,5-triazin-2-ylamine)propylaminocarbonyl)azobenzene 45

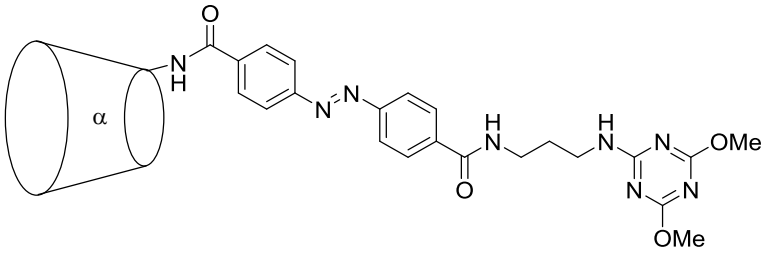

(*E*)-*N*-(6^A-deoxy-α-cyclodextrin-6^A-yl)-4-aminocarbonyl-4'-(3-aminopropylaminocarbonyl)azobenzene **39** (8 mg, 6.3 μmol) and 2-chloro-4,6-dimethoxy-1,3,5-triazine (1.3 mg, 7.5 μmol) were dissolved in anhydrous DMF (1 mL) and the solution brought to pH 9.5 with dilute NEt_3. The reaction mixture was left to stir for 2 h then evaporated to dryness and lyophilised to give an orange solid. The compound was used with no further purification and only characterised by mass spectroscopy as it was synthesised to verify the compound's elution time in an HPLC method.

HRMS-ESI: (*m/z*) $[M + Na]^+$ calcd for $C_{58}H_{82}N_8O_{33}Na$, 1441.4882, found 1441.4885.
HPLC-Analytical: t_R 14.5 min (gradient; MeCN (0.1% TFA): H_2O (0.1% TFA), 5:95 to 30:70 over 20 min, 30:70 up to 30 min, 0.5 mL min^{-1}).

9.3 Experimental for Chapter 3

Cbz-Ala-Ala-Ala-Ala-Ala-6^A-amino-6^A-deoxy-α-cyclodextrin 51

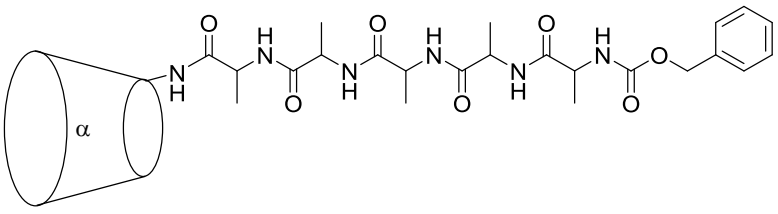

6^A-Amino-6^A-deoxy-α-cyclodextrin **35** (100 mg, 0.10 mmol), *N*-Cbz-penta-L-alanine (63 mg, 0.12 mmol), BOP (55 mg, 0.12 mmol) and NEt_3 (28 μL, 0.20 mmol) were dissolved in

anhydrous DMF (1.5 mL) and left to stir for 48 h. The reaction mixture was pipetted into ice-cold, stirring acetone (150 mL) and the white precipitate recovered by centrifugation. The solid was dissolved in water (~1 L) and applied to a cationic exchange cartridge, followed by an anionic exchange cartridge. The resulting solution was reduced by rotary evaporation then lyophilised to yield the product **51** as a white solid (75 mg, 50%).

TLC: (5:4:3:2 v/v/v/v *i*-propanol:ethanol:water:acetic acid) R_f = 0.92.

^{1}H NMR: (300 MHz, D_2O, δ): 7.47 (bs, 5H, Cbz), 5.04 (bs, 6H, CD H1), 5.12 (s, 2H, Ar-CH_2-O), 4.34-4.08 (m, 5H, Ala αH), 4.00-3.35 (m, 36H, CD H2-6), 1.50-1.18 (m, 15H, Ala βH).

HRMS-ESI: (*m/z*) $[M + Na]^+$ calcd for $C_{59}H_{92}N_6O_{36}Na$, 1483.5450; found 1483.5452.

Elemental Analysis: Calcd for $C_{59}H_{92}N_6O_{36}\cdot 6H_2O$: C, 45.15; H, 6.68; N, 5.35%. Found: C, 45.19; H, 6.79; N, 5.24%.

Melting Point: 225-232 °C dec.

H-Ala-Ala-Ala-Ala-Ala-6^A-amino-6^A-deoxy-α-cyclodextrin 52

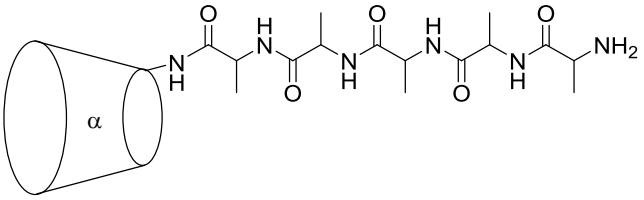

Cbz-Ala-Ala-Ala-Ala-Ala-6^A-amino-6^A-deoxy-α-cyclodextrin **51** (25 mg, 17.1 µmol) and Pd/C catalyst (10%, 10 mg) were suspended in MeOH (5 mL) and left to stir for 24 h under a H_2 balloon (~2 L). The reaction mixture was filtered and the resulting filtrate evaporated to dryness to yield the product as a white solid (14 mg, 61%).

TLC: (5:4:3:2 v/v/v/v *i*-propanol:ethanol:water:acetic acid) R_f = 0.31.

^{1}H NMR: (300 MHz, D_2O, δ): 5.07 (bs, 6H, CD H1), 4.33-4.27 (m, 5H, Ala αH), 4.02-3.38 (m, 36H, CD H2-6), 1.42-1.24 (m, 15H, Ala βH).

HRMS-ESI: (*m/z*) $[M + Na]^+$ calcd for $C_{51}H_{86}N_6O_{34}Na$, 1349.5083; found: 1349.5088.

Elemental Analysis: Calcd for $C_{51}H_{86}N_6O_{34}\cdot 12H_2O$: C, 39.69; H, 7.18; N, 5.44%. Found: C, 39.51; H, 6.89; N, 5.47%.

Melting Point: 224-236 °C dec.

(*E*)-(4-Azobenzoyl)-Ala-Ala-Ala-Ala-Ala-6^A-amino-6^A-deoxy-α-cyclodextrin 54

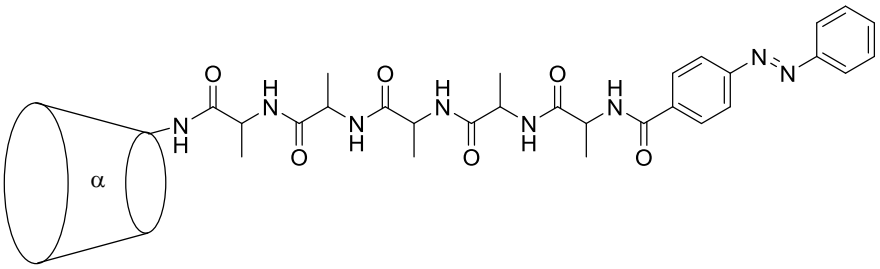

H-Ala-Ala-Ala-Ala-Ala-6^A-amino-6^A-deoxy-α-cyclodextrin **52** (30 mg, 22.6 µmol), 4-(phenylazo) benzoic acid **53** (6.5 mg, 27.1 µmol), BOP (12 mg, 27.1 µmol) and NEt_3 (7 µL, 49.7 µmol) were dissolved in anhydrous DMF (1 mL) and left to stir for 24 h. The reaction mixture was pipetted into ice-cold, stirring acetone (100 mL) and the orange precipitate recovered by centrifugation. The solid was dissolved in water (~20 mL) and applied to a cationic exchange cartridge, followed by an anionic exchange cartridge. The resulting solution was reduced by rotary evaporation then lyophilised to give an orange solid, which was further purified by semi-preparative HPLC to yield the product **54** as an orange solid (12 mg, 38%).

TLC: (5:4:3:2 v/v/v/v *i*-propanol:ethanol:water:acetic acid) R_f = 0.86.

^{1}H NMR: (400 MHz, D_2O, δ): 8.36 (bs, 2H, azobenzene), 8.12 (d, *J* = 8 Hz, 2H, azobenzene), 7.92 (bs, 2H, azobenzene), 7.81 (m, 3H, azobenzene), 5.06-4.90 (m, 6H, CD H1), 4.33-4.21 (m, 5H, Ala αH), 3.93-3.33 (m, 36H, CD H2-6), 1.57-1.28 ppm (m, 15H, Ala βH).

HRMS-ESI: (*m/z*) $[M + Na]^+$ calcd for $C_{64}H_{94}N_8O_{35}Na$, 1557.5719; found 1557.5732.

HPLC-Semi-preparative: t_R 28.05 min (gradient; MeCN (0.1% TFA): H_2O (0.1% TFA), 5:95 to 50:50 over 20 min, 50:50 until 30 min, 4 mL min^{-1}).

Elemental Analysis: Calcd for $C_{64}H_{94}N_8O_{35}\cdot 12H_2O$: C, 43.88; H, 6.79; N, 6.40%. Found C, 43.91; H, 6.61; N, 6.45%.

6^{A}-Amino-6^{A}-deoxy-β-cyclodextrin 56

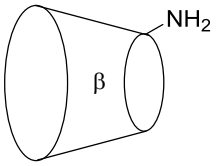

6^{A}-Azido-6^{A}-deoxy-β-cyclodextrin (synthesised previously in the group[167]) (2.64 g, 2.28 mmol), triphenylphosphine (1.11g, 4.23 mmol), and aqueous ammonia solution (10 mL, 30% NH_3) were dissolved in DMF (35 mL) and the reaction mixture left to stir for 24 h. The solution was pipetted into ice-cold, stirring acetone (250 mL) and the resulting precipitate recovered by filtration. The crude product was dissolved in water (200 mL) and applied to a cation exchange column. The column was washed with water until no further 6^{A}-azido-6^{A}-deoxy-β-cyclodextrin starting material eluted, then the product was eluted with 0.5 M aqueous ammonia. The resulting solution was reduced by rotary evaporation then lypholised to yield the title compound **56** as a white solid (0.84 g, 32.4%).

TLC: (5:4:3:2 v/v/v/v *i*-propanol:ethanol:water:acetic acid) R_f = 0.45.

^{1}H NMR: (300 MHz, D_2O, δ): 5.03-3.40 (m, 49H, CD H). (data consistent with lit.[262] values)

HRMS-ESI: (*m/z*) $[M + H]^+$ calcd for $C_{42}H_{70}NO_{34}Na$, 1155.3677; found 1155.3666.

Melting point: 200 °C dec. (lit.[263] melting point 203 °C)

Cbz-Ala-Ala-Ala-Ala-Ala-6^{A}-amino-6^{A}-deoxy-β-cyclodextrin 57

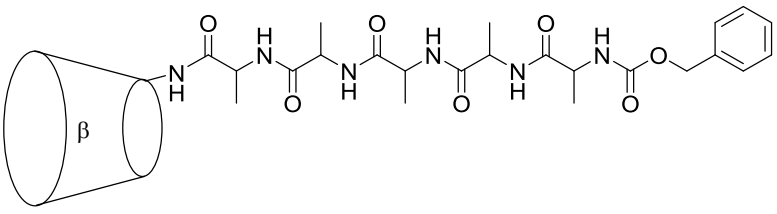

6^{A}-Amino-6^{A}-deoxy-β-cyclodextrin **56** (134 mg, 0.12 mmol), *N*-Cbz-penta-L-alanine (50 mg, 98.5 µmol), BOP (52 mg, 0.12 mmol) and NEt_3 (23 µL, 0.165 mmol) were dissolved

in anhydrous DMF (1.5 mL) and left to stir for 24 h. The reaction mixture was pipetted into ice-cold, stirring acetone (200 mL) and the white precipitate recovered by centrifugation. The solid was dissolved in water (500 mL) and applied to a cationic exchange cartridge, followed by an anionic exchange cartridge. The resulting solution was reduced by rotary evaporation then lyophilised to yield the product **57** as a white solid (100 mg, 63%).

TLC: (5:4:3 v/v/v *n*-butanol/ethanol/water) R_f = 0.76.

^{1}H NMR (300 MHz, D_2O, δ): 7.39-7.29 (m, 5H, Cbz), 5.01 (bs, 9H, CD H1 and Ar-CH_2-O), 4.28-4.03 (m, 5H, Ala αH), 3.89-3.34 (m, 42H, CD H2-6), 1.38-1.32 (m, 15H, Ala βH).

HRMS-ESI: (*m/z*) $[M + Na]^+$ calcd for $C_{65}H_{102}N_6O_{41}Na$, 1645.5979; found: 1645.5985.

Elemental Analysis: Calcd for $C_{65}H_{102}N_6O_{41}\cdot 8H_2O$: C, 44.17; H, 6.73; N, 4.75%. Found: C, 44.49; H, 6.73; N, 4.45%.

Melting Point: 240-249 °C dec.

H-Ala-Ala-Ala-Ala-Ala-6^A-amino-6^A-deoxy-β-cyclodextrin 58

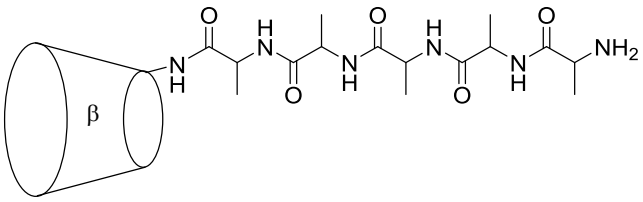

Cbz-Ala-Ala-Ala-Ala-Ala-6^A-amino-6^A-deoxy-β-cyclodextrin **57** (90 mg, 55.5 µmol) and Pd/C catalyst (10%, 10 mg) were suspended in MeOH (12 mL) and left to stir for 24 h under a H_2 balloon (~2 L). The reaction mixture was filtered and the resulting filtrate evaporated to dryness to yield the product as a white solid (52 mg, 63%).

TLC: (5:4:3:2 v/v/v/v *i*-propanol:ethanol:water:acetic acid) R_f = 0.26.

^{1}H NMR: (300 MHz, D_2O, δ): 5.04 (bs, 7H, CD H1), 4.29-4.25 (m, 3H, Ala αH), 3.95-3.35 (m, 42H, CD H2-6), 1.48-1.36 (m, 15H, Ala βH).

HRMS-ESI: (*m/z*) $[M + H]^+$ calcd for $C_{57}H_{97}N_6O_{39}$, 1489.5791; found 1489.5797.

Elemental Analysis: Calcd for $C_{57}H_{96}N_6O_{39}\cdot 2H_2O\cdot 2C_2HF_3O_2\cdot C_3H_6O$: C, 42.43; H, 6.01; N, 4.64%. Found C, 42.46; H, 6.27; N, 4.33%.

Melting Point: 229-238 °C dec.

Adamantane-1-carbonyl-Ala-Ala-Ala-Ala-Ala-6^A-amino-6^A-deoxy-β-cyclodextrin 60

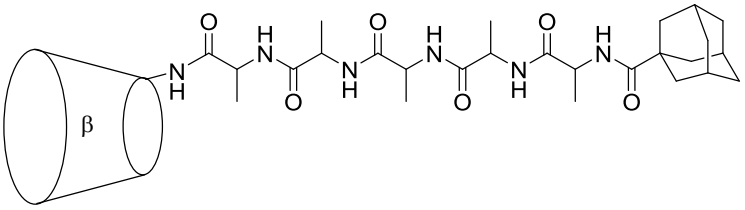

H-Ala-Ala-Ala-Ala-Ala-6^A-amino-6^A-deoxy-β-cyclodextrin **58** (100 mg, 67.0 µmol), 1-carboxyadamantane **59** (15 mg, 80.6 µmol), BOP (37 mg, 80.6 µmol) and NEt_3 (18 µL, 0.129 mmol) were dissolved in anhydrous DMF (1 mL) and left to stir for 24 h. The reaction mixture was pipetted into ice-cold, stirring acetone (150 mL) and the white precipitate recovered by centrifugation. The solid was dissolved in water (40 mL) and applied to a cationic exchange cartridge, followed by an anionic exchange cartridge. The resulting solution was reduced by rotary evaporation then lyophilised to yield the product **60** as a white solid (64 mg, 58%).

TLC: (5:4:3 v/v/v *n*-butanol:ethanol:water) R_f = 0.80.

^{1}H NMR: (400 MHz, D_2O, δ): 5.09 (s, 7H, CD H1), 4.35-4.28 (m, 5H, Ala αH), 3.93-3.28 (m, 42H, CD H2-6), 2.23 (bs, 3H, adamantane), 1.96-1.81 (m, 12H, adamantane), 1.43-1.38 ppm (m, 15H, Ala βH).

HRMS-ESI: (*m/z*) $[M + H]^+$ calcd for $C_{68}H_{111}N_6O_{40}$, 1651.6836; found 1651.6838.

HPLC-Analytical: t_R 12.9 min (gradient; MeCN (0.1% TFA): H_2O (0.1% TFA), 5:95 to 40:60 over 20 min, 0.5 mL min^{-1}).

Melting Point: 239-248 °C dec.

Penta-L-alanine 61

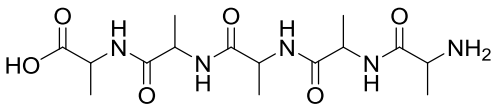

N-Cbz-penta-L-alanine **50** (50 mg, 98.5 μmol) and Pd/C catalyst (10%, 10 mg) were suspended in MeOH (25 mL) and left to stir for 24 h under a H_2 balloon (~2 L). The reaction mixture was filtered and the resulting filtrate evaporated to dryness to yield the product as a white solid (25 mg, 68%).

^{1}H NMR: (400 MHz, D_2O, δ): 4.38-4.20 (m, 5H, Ala αH), 1.41-1.33 (m, 15H, Ala βH).
HRMS-ESI: (*m/z*) $[M + H]^+$ calcd for $C_{15}H_{28}N_5O_6$, 374.2040; found 374.2034.
Melting Point: 201-207 °C dec.

Boc-Val-Val-Val-Val-Val-Val-6^A-amino-6^A-deoxy-α-cyclodextrin 63

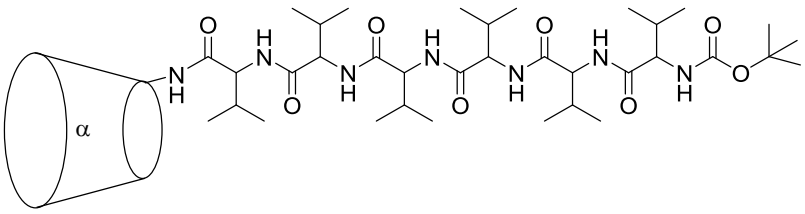

6^A-Amino-6^A-deoxy-α-cyclodextrin **35** (28 mg, 29.3 μmol), *N*-Boc-hexa-L-valine (25 mg, 35.1 μmol), BOP (16 mg, 35.1 μmol) and NEt_3 (8 μL, 57.4 μmol) were dissolved in anhydrous DMF (1 mL) and left to stir for 24 h. The reaction mixture was then pipetted into ice-cold, stirring acetone (100 mL) and the white precipitate recovered by centrifugation. The solid was dissolved in water (~2.5 L) and applied to a SP-650M cationic exchange column, followed by an anionic exchange cartridge. The resulting solution was reduced by rotary evaporation then lyophilised to yield the product as a white solid (25 mg, 51%).

TLC: (5:4:3:2 v/v/v/v *i*-propanol:ethanol:water:acetic acid) R_f = 0.92.

^{1}H NMR: (400 MHz, DMSO-d_6, δ): 5.57-5.42 (bs, 12H, CD OH2 and OH3), 4.81 (bs, 6H, CD H1), 4.53-4.46 (m, 5H, CD OH6), 4.29-4.18 (m, 6H, Val αH), 3.80-3.59 (m, 24H, CD H3, H5 and H6), 1.95-1.91 (m, 6H, Val βH), 1.38 (s, 9H, Boc), 0.86-0.81 (m, 36H, Val γH).

HRMS-ESI: (*m/z*) $[M + Na]^+$ calcd for $C_{71}H_{123}N_7O_{37}Na$, 1688.7856; found 1688.7856.

HPLC-Analytical: t_R 9.50 min (isocratic; MeCN (0.1% TFA): H_2O (0.1% TFA), 95:5, 0.5 mL min^{-1}).

Melting Point: 236-242 °C dec.

H-Val-Val-Val-Val-Val-Val-6^A-amino-6^A-deoxy-α-cyclodextrin 64

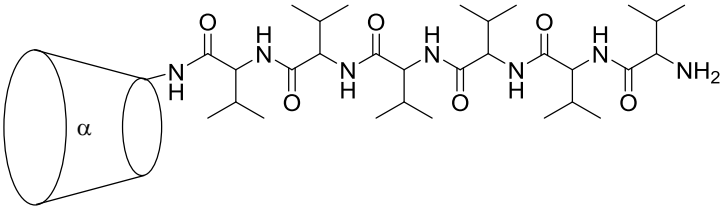

Boc-Val-Val-Val-Val-Val-Val-6^A-amino-6^A-deoxy-α-cyclodextrin **63** (106 mg, 63.8 μmol) was dissolved in 4 M HCl in water (80 mL) and left to stir for 3 h. The reaction mixture was then pipetted into ice-cold, stirring acetone (300 mL) and the resulting precipitate recovered by centrifugation, before being taken up in water and lyophilised to yield the crude product **64** as a white solid (32 mg, 35%). The compound was used with no further purification.

TLC: (5/4/3/2 v/v/v/v *i*-propanol:ethanol:water:acetic acid) R_f = 0.50.

^{1}H NMR: (300 MHz, DMSO-d_6, δ): 8.37-7.77 (m, 6H, NH), 5.58-5.47 (m, 12H, CD OH2 and OH3), 4.80 (br s, 6H, CD H1), 4.54-4.49 (m, 5H, CD OH6), 4.32-4.10 (m, 6H, Val αH), 3.79-3.57 (m, 24H, CD H6, H3 and H5), 2.03-1.91 (m, 6H, Val βH), 0.91-0.80 (m, 36H, Val γH).

HRMS-ESI: (*m/z*) $[M + H]^+$ calcd for $C_{66}H_{116}N_7O_{35}$, 1566.7512; found 1566.7512.

HPLC-Analytical: t_R 10.69 min (gradient; MeCN (0.1% TFA): H_2O (0.1% TFA), 5:95 to 95:5 over 30 min, 0.5 mL min^{-1}).

Melting Point: 191-195 °C dec.

Attempted Synthesis of (*E*)-(4-(4'-Carboxyl)-azobenzoyl-Val-Val-Val-Val-Val-Val-6^{A}-amino-6^{A}-deoxy-α-cyclodextrin 65

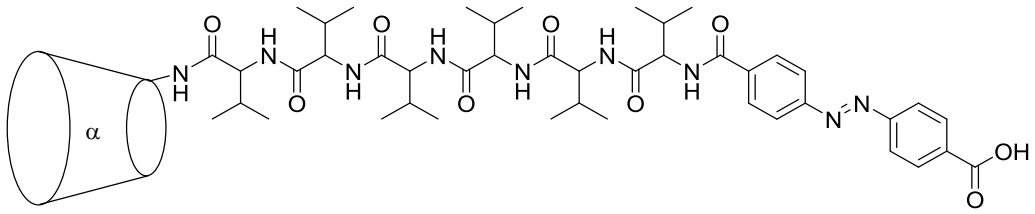

A solution of crude H-Val-Val-Val-Val-Val-Val-6^{A}-amino-6^{A}-deoxy-α-cyclodextrin **64** (50 mg, 31.9 µmol) and NEt_3 (10 µL, 71.7 µmol) in anhydrous DMF (1.5 mL) was added drop wise to a stirring solution of azobenzene-4,4'-dicarboxylic acid (33 mg, 122.1 µmol), BOP (22 mg, 49.5 µmol) and NEt_3 (100 µL, 717.0 µmol) in anhydrous DMF (1 mL). The reaction mixture was left to stir for 24 h then pipetted into ice-cold, stirring acetone (60 mL) and the orange precipitate recovered by centrifugation. Purification was attempted, however was unsuccessful as a consequence of solubility issues.

TLC: (5/4/3/2 v/v/v/v *i*-propanol:ethanol:water:acetic acid) R_f = 0.82.
HRMS-ESI: (*m/z*) $[M + Na]^+$ calcd for $C_{80}H_{124}N_9O_{38}Na$, 1841.7945; found 1841.7949.

Hexa-L-valine 66

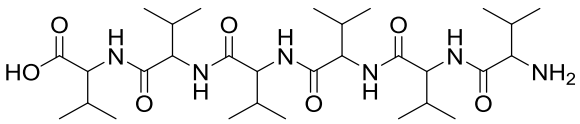

N-Boc-hexa-L-valine (20 mg, 0.028 mmol) was dissolved in 4 M HCl in water (1 mL) and left to stir for 4 h. The reaction mixture was then evaporated to dryness, taken up in water and lyophilised to yield the title product as a white solid (13 mg, 73%).

^{1}H NMR: (400 MHz, DMSO-d_6, δ): 8.85 (d, *J* = 8 Hz, 1H, NH), 8.12-8.05 (m, 4H, NH), 7.88 (d, 2H, *J* = 8 Hz, NH), 4.31-4.09 (m, 6H, Val αH), 2.07-1.86 (m, 6H, Val βH), 0.92-0.80 (m, 36H, Val γH).

HRMS-ESI: (*m/z*) $[M + H]^+$ calcd for $C_{30}H_{57}N_6O_7$, 613.4289; found 613.4288.

Melting Point: 195-206 °C dec.

9.4 Experimental for Chapter 4

***N*-Fmoc-tri-L-valine 67**

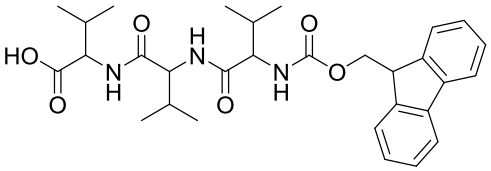

N-Fmoc-tri-L-valine **67** was prepared using standard manual Fmoc-coupling solid phase synthesis as described in general methods with the final deprotection step omitted, on a 0.25 mmol scale. The peptide was cleaved from the resin using the standard procedure described in general methods, and the resulting solution evaporated to dryness to give the crude product as a white solid (50 mg, 37%). The compound was used with no further purification.

^{1}H NMR: (400 MHz, DMSO-d_6, δ): 7.94 (d, J = 8 Hz, 1H, Fmoc), 7.89 (d, J = 8 Hz, 1H, Fmoc), 7.79-7.71 (m, 3H, Fmoc), 7.48 (d, J = 12 Hz, 1H, Fmoc), 7.41 (t, J = 8Hz, 1H, Fmoc), 7.32 (t, J = 8 Hz, 1H, Fmoc), 4.32-4.20 (m, 4H, Val αH and O-CH_2-Fmoc), 4.11 (dd, J = 7.5 Hz, 5.6 Hz, 1H, Fmoc), 3.92 (dd, J = 9 Hz, 7.5 Hz, 1H, Fmoc), 2.08-1.92 (m, 3H, Val βH), 1.04-0.83 (m, 18H, Val γH).

HRMS-ESI: (*m/z*) $[M + H]^+$ calcd for $C_{30}H_{40}N_3O_6$, 538.2917; found 538.2917, $[M + Na]^+$ calcd for $C_{30}H_{39}N_3O_6Na$, 560.2737; found 560.2739**.**

HPLC-Analytical: t_R 21.04 min (gradient; MeCN (0.1% TFA): H_2O (0.1% TFA), 5:95 to 95:5 over 30 min, 0.5 mL min^{-1}).

Melting point: 209-214 °C dec.

H-Val-Val-Val-6^{A}-amino-6^{A}-deoxy-α-cyclodextrin 68

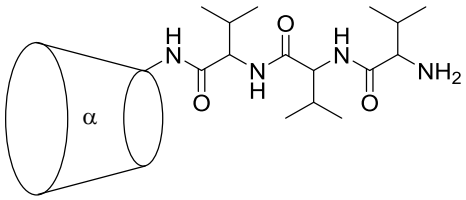

N-Fmoc-tri-L-valine **67** (40 mg, 74.4 μmol), 6^{A}-amino-6^{A}-deoxy-α-cyclodextrin **35** (87 mg, 89.3 μmol), BOP (39 mg, 89.3 μmol) and NEt_3 (20 μL, 143.4 μmol) were dissolved in anhydrous DMF (2 mL) and the reaction mixture left to stir overnight. The solution was pipetted into ice-cold, stirring acetone (100 mL) and the cream precipitate recovered by centrifugation. The crude product was dissolved in water (500 mL) and applied to a cation exchange cartridge. The resulting solution was lypholised to yield the title compound **68** as a white solid (12 mg, 13%).

TLC: (5:4:3:2 v/v/v/v *i*-propanol:ethanol:water:acetic acid) R_f = 0.60.

^{1}H NMR: (400 MHz, DMSO-d_6, δ): 5.58-5.45 (m, 12H, CD OH2 and OH3), 4.80 (br s, 6H, CD H1), 4.53-4.47 (m, 5H, CD OH6), 4.28-4.19 (m, 3H, Val αH), 3.77-3.57 (m, 24H, CD H3, H5 and H6), 2.01-1.91 (m, 3H, Val βH), 0.90-0.81 (m, 18H, Val γH).

HRMS-ESI: (*m/z*) $[M + H]^+$ calcd for $C_{51}H_{89}N_4O_{32}$, 1269.5460; found 1269.5453.

HPLC-Analytical: t_R 8.28 min (gradient; MeCN (0.1% TFA): H_2O (0.1% TFA), 5:95 to 95:5 over 30 min, 0.5 mL min^{-1}).

Melting point: 229-236 °C dec.

***N*-Fmoc-His(π-BOM)-Gly-OH 69**

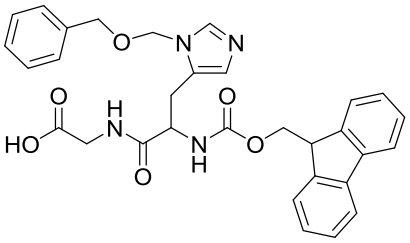

N-Fmoc-His(π-BOM)-Gly-OH **69** was prepared using standard manual Fmoc-coupling solid phase synthesis as described in general methods, on a 0.25 mmol scale. The peptide was cleaved from the resin using the standard procedure described in general methods, and the resulting solution evaporated to dryness to give a white solid (30 mg, 22%).

^{1}H NMR: (400 MHz, CD_3OD, δ): 8.92 (s, 1H, His εH), 7.78 (d, *J* = 10 Hz, 2H, Fmoc), 7.61 (t, *J* = 8 Hz, 2H, Fmoc), 7.37 (t, *J* = 10 Hz), 2H, Fmoc), 7.31-7.26 (m, 8H, Fmoc, BOM Ar and His δH), 5.71-5.62 (m, 2H, -N-C*H*$_2$-O-), 4.66-4.52 (m, 3H, -O-C*H*$_2$-BOM Ar and His αH), 4.45-4.33 (m, 2H, O-C*H*$_2$-Fmoc), 4.18-4.14 (m, 1H, Fmoc), 3.98-3.82 (m, 2H, Gly αH), 3.40-3.34 (m, 1H, His βH), 3.13-3.05 (m, 1H, His βH).

^{13}C NMR: (100 MHz, CD_3OD, δ): 171.25 (Gly carbonyl), 168.42 (His carbonyl), 156.75 (Fmoc carbamate), 143.78 (Fmoc), 141.19 (C-1 of BOM), 136.05, 135.76 (His γC and His εC), 130.88, 128.25, 127.97, 127.71, 127.41, 126.75, 124.61 (Fmoc and BOM), 119.55 (His δC), 118.96 (Fmoc), 76.14 (N-*C*H$_2$-O), 71.62 (O-*C*H$_2$-BOM), 66.48 (O-*C*H$_2$-Fmoc), 53.28 (His αC), 40.42 (Gly αC), 39.53 (OCH$_2$-*C*H-Fmoc), 25.66 (His βC).

HRMS-ESI: (*m/z*) $[M + H]^+$ calcd for $C_{31}H_{31}N_4O_6$, 555.2244; found 555.2246, $[M + Na]^+$ calcd for $C_{31}H_{30}N_4O_6Na$, 577.2063; found 577.2062.

HPLC-Analytical: t_R 25.3 min (gradient; MeCN (0.1% TFA): H_2O (0.1% TFA), 5:95 to 95:5 over 40 min, 0.5 mL min^{-1}).

Melting point: 56-59 °C.

(*E*)-(4-Azobenzoyl)-Val-Val-Val-OH 70

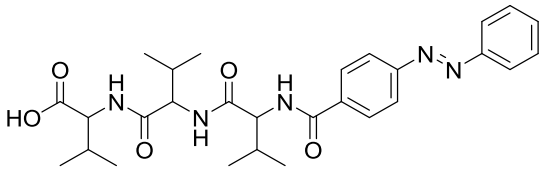

(*E*)-(4-Azobenzoyl)-Val-Val-Val-OH **70** was prepared using standard manual Fmoc-coupling solid phase synthesis as described in general methods, on a 0.20 mmol scale. 4-Carboxyazobenzene **53** was used in the final on-resin coupling step. The peptide was cleaved from the resin using the standard procedure described in general methods, and the resulting solution evaporated to dryness to give an orange solid. The crude product was dissolved in MeCN/H_2O (50:50) and subjected to reverse-phase semi-preparative HPLC. Fractions containing the product were combined and lypholised to yield the title compound **70** as an orange solid (22 mg, 21%).

^{1}H NMR: (400 MHz, $CDCl_3$, δ): 8.03-7.93 (m, 6H, azobenzene), 7.54-7.50 (m, 3H, azobenzene), 4.87-4.46 (m, 3H, Val αH), 2.44-2.18 (m, 3H, Val βH), 1.10-0.88 (m, 18H, Val γH)**.**

HRMS-ESI: (*m/z*) $[M + Na]^+$ calcd for $C_{28}H_{37}N_5O_5Na$, 546.2692; found 546.2684

HPLC-Semi-preparative: t_R 18.62 min (gradient; MeCN (0.1% TFA): H_2O (0.1% TFA), 50:50 isocratic over 30 min, 4 mL min^{-1}).

HPLC-Analytical: t_R 21.63 min (gradient; MeCN (0.1% TFA): H_2O (0.1% TFA), 5:95 to 95:5 over 30 min, 0.5 mL min^{-1}).

Melting point: 243-246 °C dec.

Adamantane-1-carbonyl-Val-Val-Val-OH 74

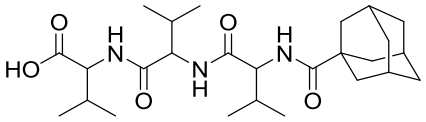

Adamantane-1-carbonyl-Val-Val-Val-OH **74** was prepared using standard manual Fmoc-coupling solid phase synthesis as described in general methods, on a 0.50 mmol scale. 1-Carboxyadamantane **59** was used in the final on-resin coupling step. The peptide was cleaved from the resin using the standard procedure described in general methods, and the resulting solution evaporated to dryness to give a white solid. The crude product was dissolved in MeCN/H_2O (60:40) and subjected to reverse-phase semi-preparative HPLC. Fractions containing the product were combined and lypholised to yield the title compound **74** as a white solid (25 mg, 11%).

^{1}H NMR: (400 MHz, DMSO-d_6, δ): 7.92 (d, J = 8 Hz, 1H, NH), 7.70 (d, J = 8 Hz, 1H, NH), 7.13 (d, J = 8 Hz, 1H, NH), 4.29-4.12 (m, 3H, Val αH), 2.09-2.00 (m, 3H, Val βH), 1.78 (br s, 12H, adamantane), 1.67 (br s, 3H, adamantane), 0.89-0.79 (m, 18H, Val γH).

HRMS: (m/z) $[M + H]^+$ calcd for $C_{26}H_{44}N_3O_5$, 478.3281; found 478.3283.

HPLC-Semi-preparative: t_R 22.95 min (gradient; MeCN (0.1% TFA): H_2O (0.1% TFA), 20:80 to 80:20 over 40 min, 4 mL min^{-1}).

HPLC-Analytical: t_R 20.06 min (gradient; MeCN (0.1% TFA): H_2O (0.1% TFA), 5:95 to 95:5 over 30 min, 0.5 mL min^{-1}).

Melting point: 107-110 °C dec.

(*E*)-(4-Azobenzoyl)-Val-Val-Val-His(π-BOM)-Gly-Val-Val-Val-OH 77

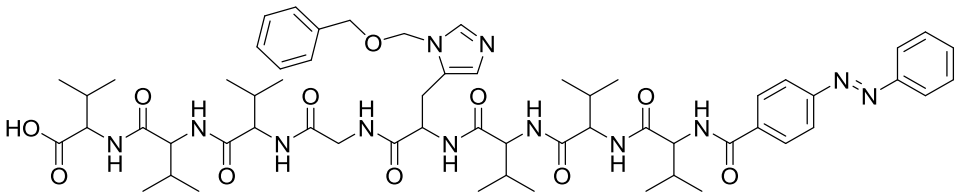

(*E*)-(4-Azobenzoyl)-Val-Val-Val-His(π-BOM)-Gly-Val-Val-Val-OH **77** was prepared using standard manual Fmoc-coupling solid phase peptide synthesis as described in general methods, on a 0.5 mmol scale. 4-Carboxyazobenzene **53** was used in the final on-resin coupling step. The peptide was cleaved from the resin using the standard procedure described in general methods, and the resulting solution evaporated to dryness to give the crude product as an orange solid (45 mg, 8%). The compound was used with no further purification.

^{1}H NMR: (400 MHz, DMSO-d_6, δ): 8.48 (d, *J* = 8 Hz, 1H, His εH), 8.08 (d, *J* = 8 Hz, 2H, azobenzene), 7.97-7.93 (m, 5H, azobenzene), 7.62 (d, *J* = 8 Hz, 2H, azobenzene), 7.37-7.27 (m, 6H, Ar, His δH), 4.81 (s, 2H, -N-CH_2-O-), 4.47 (t, *J* = 8 Hz, 1H, His αH), 4.30-4.13 (m, 8H, Val αH and Gly αH), 3.17 (s, 2H, Ar-CH_2-O-), 2.22-1.88 (m, 8H, His βH and Val βH), 0.93-0.76 (m, 36H, Val γH).

LRMS-ESI: (*m/z*) $[M + H]^+$ calcd for $C_{59}H_{83}N_{12}O_{11}$, 1135.63; found 1135.64, $[M + Na]^+$ calcd for $C_{59}H_{82}N_{12}O_{11}Na$, 1157.62; found 1157.62.

(*E*)-(4-Azobenzoyl)-Val-Val-Val-His(π-BOM)-Gly-Val-Val-Val-trivaline-6^{A}-amino-6^{A}-deoxy-α-cyclodextrin 71

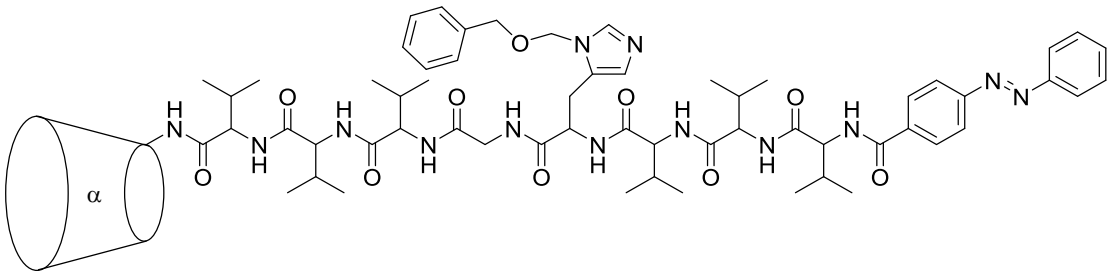

(*E*)-(4-Azobenzoyl)-Val-Val-Val-His(π-BOM)-Gly-Val-Val-Val-OH **77** (95 mg, 83.7 µmol), 6^{A}-amino-6^{A}-deoxy-α-cyclodextrin **35** (68 mg, 69.5 µmol), BOP (37 mg, 83.7 µmol) and NEt_3 (25 µL, 179.3 µmol) were dissolved in anhydrous DMF (5 mL) and the reaction mixture left to stir for 24 h. The solution was then pipetted into ice-cold, stirring acetone (80 mL) and the orange precipitate recovered by centrifugation. The crude product was dissolved in MeCN/H_2O (30:70) and subjected to reverse-phase preparative HPLC. Fractions containing the product were combined and lypholised to yield the title compound **71** as an orange solid (22 mg, 15%).

TLC: (5:4:3 v/v/v *n*-butanol:ethanol:water) R_f = 0.75.

^{1}H NMR: (400 MHz, DMSO-d_6, δ): 8.53 (d, *J* = 8 Hz, 1H, His εH), 8.08 (d, *J* = 8 Hz, 2H, azobenzene), 7.97-7.88 (m, 5H, azobenzene), 7.63 (d, *J* = 8 Hz, 2H, azobenzene), 7.36-7.28 (m, 6H, Ar, His δH), 5.70-5.44 (m, 12H, CD OH2, OH3), 4.98 (s, 2H, -N-CH_2-O-), 4.80 (s, 6H, CD H1), 4.53 (s, 5H, CD OH6), 4.36 (t, *J* = 8 Hz, 1H, His αH), 4.28-4.23 (m, 6H, Val αH), 4.13-4.10 (m, 2H, Gly αH), 3.80-3.58 (m, 24H, CD H6, H3 and H5), 3.17 (s, 2H, Ar-CH_2-O-), 2.18-2.09 (m, 2H, His βH), 2.00-1.87 (m, 6H, Val βH), 0.95-0.80 (m, 36H, Val γH).

HRMS-ESI: (*m/z*) $[M + H]^+$ calcd for $C_{95}H_{143}N_{13}O_{39}$, 2089.9606; found 2089.9619.

HPLC-Preparative: t_R 17.3 min (gradient; MeCN (0.1% TFA): H_2O (0.1% TFA), 40:60 to 60:40 over 40 min, 10 mL min^{-1}).

HPLC-Analytical: t_R 16.0 min (gradient; MeCN (0.1% TFA): H_2O (0.1% TFA), 40:60 to 60:40 over 40 min, 0.5 mL min^{-1}).

Melting point: 232-236 °C dec.

Attempted Synthesis of (*E*)-(4-Azobenzoyl)-Val-Val-Val-His-Gly-Val-Val-Val-trivaline-6^{A}-amino-6^{A}-deoxy-α-cyclodextrin 72

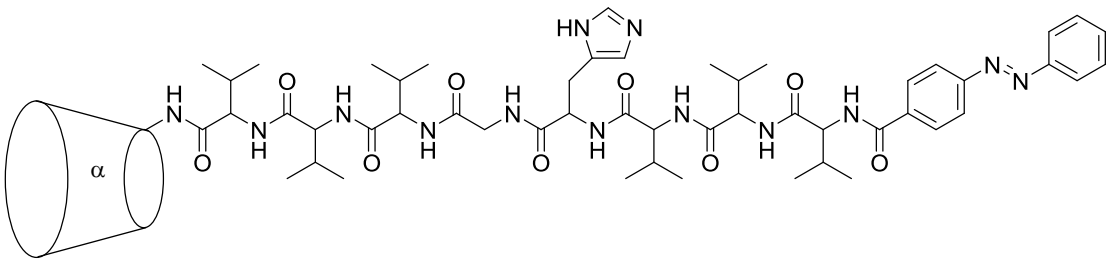

(*E*)-(4-Azobenzoyl)-Val-Val-Val-His(π-BOM)-Gly-Val-Val-Val-trivaline-6^{A}-amino-6^{A}-deoxy-α-cyclodextrin **71** (8 mg, 3.83 μmol) and Pd/C (10%, 5 mg) were suspended in MeOH (10 mL) and left to stir for 24 h under a H_2 balloon (~2 L). The reaction mixture was filtered and the resulting filtrate evaporated to dryness to give a cream-coloured solid. Although the product **72** could be detected by mass spectrometry, the ^{1}H NMR spectrum exhibited many small peaks in the 8.3-7.6 ppm region, indicating that the azobenzene moiety had also been reduced to give a large number of by-products.

HRMS-ESI: (*m/z*) $[M + Na]^+$ calcd for $C_{87}H_{133}N_{13}O_{38}Na$, 1990.8772; found 1990.8777.

Adamantane-1-carbonyl-Val-Val-Val-His(π-BOM)-Gly-Val-Val-Val-OH 78

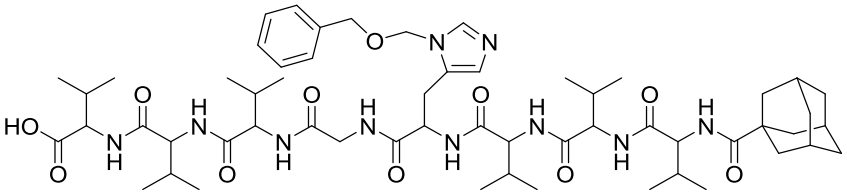

Adamantane-1-carbonyl-Val-Val-Val-His(π-BOM)-Gly-Val-Val-Val-OH **78** was prepared using standard automated Fmoc-coupling solid phase peptide synthesis as described in general methods, on a 0.1 mmol scale. Coupling was performed at 70 °C, apart from Fmoc-His(π-BOM) which was coupled at 50 °C. 1-Carboxyadamantane **59** was used in the final on-resin coupling step. The peptide was cleaved from the resin using the standard procedure described in general methods, and the resulting solution

evaporated to dryness to give a white solid. The crude product was dissolved in MeCN/H_2O (50:50) and subjected to reverse-phase semi-preparative HPLC. Fractions containing the product were combined and lypholised to yield the title compound **78** as a white solid (25 mg, 23%).

^{1}H NMR: (400 MHz, DMSO-d_6, δ): 8.41 (d, J = 8 Hz, 1H, His εH), 7.36-7.28 (m, 6H, Ar, His δH), 5.69 (s, 2H, -N-CH_2-O-), 4.65-4.59 (m, 1H, His αH), 4.55 (s, 2H, Ar-CH_2-O), 4.31-4.10 (m, 6H, Val αH), 3.76-3.74 (m, 2H Gly αH), 3.06-3.00 (m, 2H, His βH), 2.05-1.87 (m, 6H, Val βH), 1.77 (br s, 3H, adamantane), 1.66 (br s, 12H, adamantane).
HRMS-ESI: (m/z) $[M + H]^+$ calcd for $C_{57}H_{89}N_{10}O_{11}$, 1089.6712; found 1089.6722.
HPLC-Semi-preparative: t_R 25.4 min (gradient; MeCN (0.1% TFA): H_2O (0.1% TFA), 20:80 to 50:50 over 20 min, 50:50 to 80:20 up to 35 min, 4 mL min^{-1}).
HPLC-Analytical: t_R 24.8 min (gradient; MeCN (0.1% TFA): H_2O (0.1% TFA), 20:80 to 50:50 over 20 min, 50:50 to 80:20 up to 35 min, 0.5 mL min^{-1}).
Melting point: 208-216 °C dec.

Attempted Synthesis of Adamantane-1-carbonyl-Val-Val-Val-His(π-BOM)-Gly-Val-Val-Val-6^A-amino-6^A-deoxy-β-cyclodextrin 75

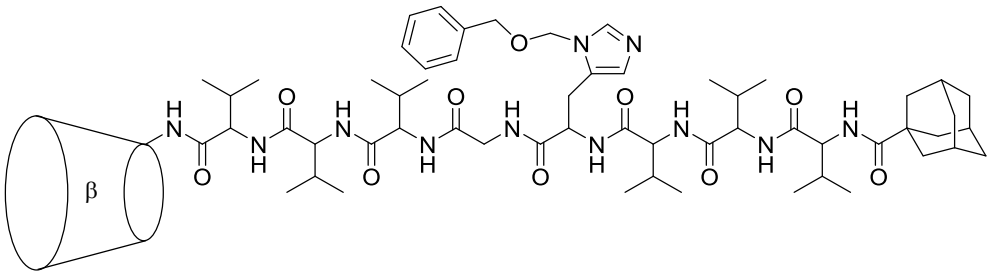

Adamantane-1-carbonyl-Val-Val-Val-His(π-BOM)-Gly-Val-Val-Val-OH **78** (25 mg, 22.9 µmol), 6^A-amino-6^A-deoxy-β-cyclodextrin **56** (31 mg, 27.5 µmol), BOP (12 mg, 27.5 µmol) and NEt_3 (500 µL, 3.59 mmol) were dissolved in anhydrous DMF (2 mL) and the reaction mixture left to stir for 5 days. TLC and analytical HPLC showed no evidence of any product formation.

2nd Attempted Synthesis of Adamantane-1-carbonyl-Val-Val-Val-His(π-BOM)-Gly-Val-Val-Val-6^A-amino-6^A-deoxy-β-cyclodextrin 75

H-Val-Val-Val-His(π-BOM)-Gly-Val-Val-Val-6^A-amino-6^A-deoxy-β-cyclodextrin **80** (20 mg, 9.9 µmol), 1-carboxyadamantane **59** (2.5 mg, 11.8 µmol), BOP (5 mg, 11.8 µmol) and NEt_3 (10 µL, 71.7 µmol) were dissolved in anhydrous DMF (5 mL) and the reaction mixture left to stir for 24 h. The solution was pipetted into ice-cold, stirring acetone (50 mL) and the resulting precipitate recovered by centrifugation, however TLC of the resulting solid indicated no product formation.

H-Val-Val-Val-His(π-BOM)-Gly-Val-Val-Val 79

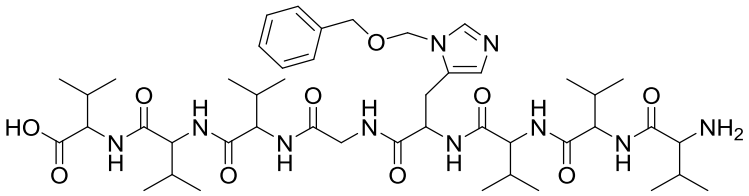

H-Val-Val-Val-His(π-BOM)-Gly-Val-Val-Val **79** was prepared using standard manual fmoc-coupling solid phase peptide synthesis as described in general methods, on a 0.5 mmol scale. The peptide was cleaved from the resin using the standard procedure described in general methods, and the resulting solution pipetted into ice-cold stirring ether (70 mL) to produce a precipitate which was recovered by centrifugation. The crude product was dissolved in MeCN/H_2O (80:20) and subjected to reverse-phase semi-preparative HPLC. Fractions containing the product were combined and lypholised to yield the title compound **79** as a white solid (41 mg, 9%).

^{1}H NMR: (400 MHz, D_2O, δ): 8.83 (s, 1H, His εH), 7.43-7.35 (m, 6H, Ar, His δH), 5.78 (s, 2H, N-C*H*$_2$-O), 4.69-4.61 (m, 3H, Ar-C*H*$_2$-O-, His αH), 4.33-4.12 (m, 6H, Val αH), 3.97-3.86 (m, 2H, Gly αH), 3.44-3.21 (m, 2H, His βH), 2.26-1.96 (m, 6H, Val βH), 1.04-0.82 (m, 36H, Val γH).

^{13}C NMR: (100 MHz, D_2O, δ): 188.14 (C=O carboxylic acid), 177.67, 176.02, 175.59, 175.29, 174.23, 173.08, 171.43 (C=O amide), 138.29, 138.12, 132.76, 131.37 (Ar),

131.49, 130.93, 121.20 (His), 78.77 (-O-*C*H_2-N-), 74.71 (Ar-*C*H_2-O), 62.19, 61.97, 61.77, 61.74, 60.99, 60.82 (Val αC), 54.40 (His αC), 44.96 (Gly αC), 33.09, 32.72, 32.61, 32.49, 32.47 (Val βC), 27.55 (His βC), 20.99, 20.90, 20.85, 20.78, 20.70, 20.55, 20.38, 20.15, 20.01, 19.53 (Val γC).

HRMS-ESI: (*m/z*) $[M + H]^+$ calcd for $C_{46}H_{75}N_{10}O_{10}$, 927.5668; found 927.5666, $[M + Na]^+$ calcd for $C_{46}H_{74}N_{10}O_{10}Na$, 949.5487; found 949.5479.

HPLC-Semi-preparative: t_R 16.8 min (gradient; MeCN (0.1% TFA): H_2O (0.1% TFA), 20:80 to 50:50 over 30 min, 4 mL min^{-1}).

HPLC-Analytical: t_R 15.6 min (gradient; MeCN (0.1% TFA): H_2O (0.1% TFA), 20:80 to 50:50 over 30 min, 0.5 mL min^{-1}).

Melting Point: 202- 209 °C dec.

H-Val-Val-Val-His(π-BOM)-Gly-Val-Val-Val-6^A-amino-6^A-deoxy-β-cyclodextrin 80

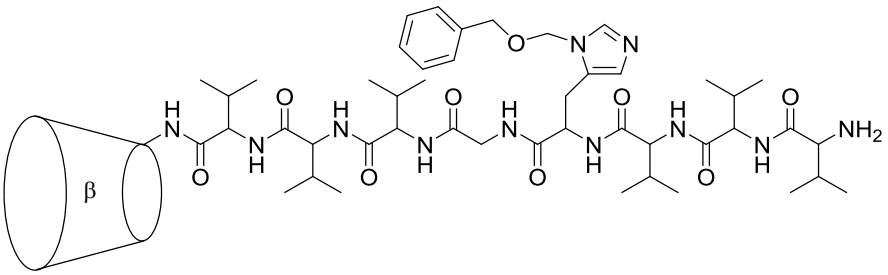

H-Val-Val-Val-His(π-BOM)-Gly-Val-Val-Val **79** (38 mg, 41.0 µmol), 6^A-amino-6^A-deoxy-β-cyclodextrin **56** (56 mg, 49.2 µmol), BOP (22 mg, 49.2 µmol) and NEt_3 (15 µL, 107.6 µmol) were dissolved in anhydrous DMF (4 mL) and the reaction mixture left to stir for 24 h. The solution was pipetted into ice-cold, stirring acetone (100 mL) and the resulting precipitate recovered by centrifugation. The crude product was dissolved in MeCN/ H_2O (50:50) and subjected to reverse-phase preparative HPLC. Fractions containing the product were combined and lypholised to yield the title compound **80** as a white solid (11 mg, 13%).

TLC: (5:4:3 v/v/v *n*-butanol:ethanol:water) R_f = 0.69.

^{1}H NMR: (400 MHz, D_2O, δ): 8.37 (br s, 1H, His εH), 7.38-7.32 (m, 5H, Ar), 7.14 (s, 1H, His δH), 6.77 (d, *J* = 12 Hz, 1H, O-C*H*$_2$-N), 6.70 (d, *J* = 12 Hz, 1H, O-C*H*$_2$-N), 4.99-4.92 (m, 7H, CD H1), 4.83-4.81 (m, 1H, His αH), 4.65-4.59 (m, 6H, Val αH), 4.18-4.15 (m, 2H, Gly αH), 3.92-3.45 (m, 42 H, CD H2-6), 3.27-2.36 (m, 2H, His βH), 2.05-1.89 (m, 6H, Val γH), 0.94-0.72 (m, 36H, Val γH).

HRMS-ESI: (*m/z*) $[M + H]^+$ calcd for $C_{88}H_{144}N_{11}O_{43}$, 2042.9419; found 2042.9434

HPLC-Preparative: t_R 8.28 min (gradient; MeCN (0.1% TFA): H_2O (0.1% TFA), 20:80 to 50:50 over 20 min, 10 mL min^{-1}).

HPLC-Analytical: t_R 8.20 min (gradient; MeCN (0.1% TFA): H_2O (0.1% TFA), 20:80 to 50:50 over 20 min, 0.5 mL min^{-1}).

Melting point: 216-220 °C dec.

_N_-Octanoyl-Val-Val-Val-His(π-BOM)-Gly-Val-Val-Val 81

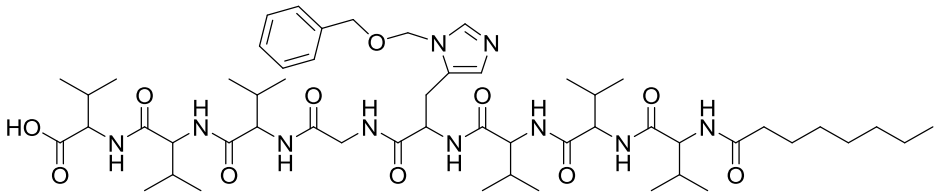

N-Octanoyl-Val-Val-Val-His(π-BOM)-Gly-Val-Val-Val **81** was synthesised using standard automated Fmoc-coupling solid phase peptide synthesis as described in general methods, on a 0.25 mmol scale. Coupling was performed at 70 °C, apart from Fmoc-His (π-BOM) which was coupled at 50 °C. *N*-Octanoic acid was used in the final on-resin coupling step and underwent double-coupling. The peptide was cleaved from the resin using the standard procedure described in general methods, and the resulting solution pipetted into ice-cold, stirring 10% MeCN in H_2O (100 mL) to produce a precipitate which was recovered by centrifugation. The crude product was dissolved in MeCN/H_2O (40:60) and subjected to reverse-phase semi-preparative HPLC. Fractions containing the product were combined and lypholised to yield the title compound **81** as a white solid (42 mg, 16%).

^{1}H NMR: (400 MHz, DMSO-d_6, δ): 8.35 (d, *J* = 8 Hz, 1H, His εH), 8.19-7.76 (m, 8H, NH), 7.38-7.28 (m, 6H, Ar, His δH), 5.70 (d, *J* = 12 Hz, 1H, O-C*H*$_2$-N), 5.64, (d, *J* = 12 Hz, O-C*H*$_2$-N), 4.64 (dd, *J* = 12, 8 Hz, 1H, His αH), 4.54 (s, 2H, Ar-C*H*$_2$-O), 4.30-4.08 (m, 6H, Val αH), 3.82-3.70 (m, 2H, Gly αH), 3.04-2.98 (m, 2H, His βH), 2.18-1.87 (m, 9H, Val βH and octyl), 1.50-1.43 (m, 3H, octyl), 1.22 (br s, 9H, octyl), 0.87-0.75 (m, 36H, Val γH).

^{13}C NMR: (100 MHz, DMSO-d_6, δ): 172.81, 172.74, 172.28, 171.20, 171.11, 170.93, 170.77, 169.85, 168.13 (carbonyl), 136.50 (BOM Ar), 136.09 (His εC), 130.30 (His γC), 128.39, 127.96, 127.73 (BOM Ar), 118.67 (His δC), 76.01 (-N-*C*H$_2$-O-), 70.70 (-O-*C*H$_2$-Ar), 57.82, 57.74, 57.72, 57.56, 57.36, 57.06 (Val αC), 51.12 (His αC), 41.99 (Gly αC), 35.15 (alkyl), 31.21, 30.80, 30.31, 30.27, 30.23, 29.77 (Val βC), 28.55, 28.45 (alkyl), 25.72 (His βC), 25.45, 22.05 (alkyl), 19.22, 19.13, 19.05, 18.40, 18.31, 18.20, 18.00, 17.89 (Val γC), 17.03, 13.95 (alkyl).

HRMS-ESI: (*m/z*) [M + H]$^+$ calcd for $C_{54}H_{89}N_{10}O_{11}$, 1053.6712; found 1053.6714, [M + Na]$^+$ calcd for $C_{54}H_{88}N_{10}O_{11}Na$, 1075.6532; found 1075.6532.

HPLC-Semi-preparative: t_R 7.30 mins (gradient; MeCN (0.1% TFA): H_2O (0.1% TFA), 50:50 to 90:10 over 30 mins, 4 mL min^{-1}).

HPLC-Analytical: t_R 28.07 min (gradient; MeCN (0.1% TFA): H_2O (0.1% TFA), 5:95 to 60:40 over 30 min, 0.5 mL min^{-1}).

Melting point: 238-242 °C dec.

_N_-Octanoyl-Val-Val-Val-His(π-BOM)-Gly-Val-Val-Val-6^{A}-amino-6^{A}-deoxy-α-cyclodextrin 82

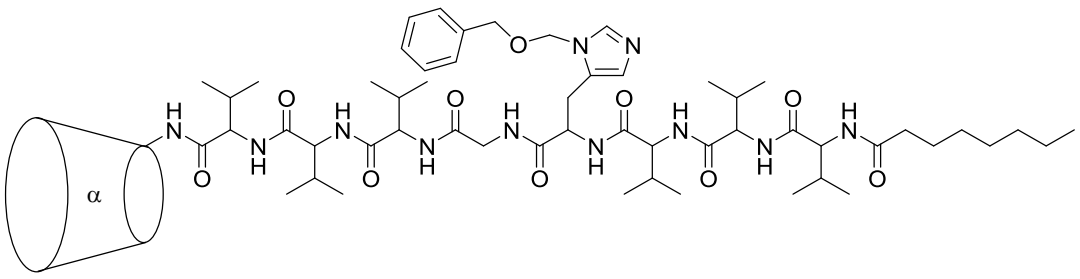

N-Octanoyl-Val-Val-Val-His(π-BOM)-Gly-Val-Val-Val **81** (50 mg, 47.5 µmol), 6^{A}-amino-6^{A}-deoxy-α-cyclodextrin **35** (55 mg, 57.0 µmol), BOP (25 mg, 57.0 µmol) and NEt_3 (250 µL,

1.8 mmol) were dissolved in anhydrous DMF (5 mL) and left to stir for 24 h. The solution was pipetted into ice-cold, stirring acetone (100 mL) and the precipitate recovered by centrifugation. The crude product was dissolved in MeCN/H_2O (50:50) and subjected to reverse-phase preparative HPLC. Fractions containing the product were combined and lypholised to yield the title compound **82** as a white solid (24 mg, 25%).

TLC: (5:4:3 v/v/v *n*-butanol:ethanol:water) R_f 0.39.

^{1}H NMR: (400 MHz, CD_3OD, δ): 9.33-9.25 (m, 2H, NH), 8.85 (br s, 1H, His εH), 8.56 (d, *J* = 12 Hz, 1H, NH), 8.41-8.34 (m, 2H, NH), 8.16-8.12 (m, 2H, NH), 7.97 (s, 1H, NH), 7.82 (d, *J* = 12 Hz, 1H, NH), 7.38-7.33 (m, 6H, Ar, His δH), 5.79 (d, *J* = 12 Hz, 1H, -O-C*H*$_2$-N-), 5.72 (d, *J* = 12 Hz, 1H, -O-C*H*$_2$-N-), 5.11 (br s, 6H, CD H1), 4.73-4.62 (m, 1H, His αH), 4.56-4.27 (m, 6H, Val αH), 4.20-4.07 (m, 2H, Gly αH), 4.02-3.45 (m, 36H, CD H2-6), 3.12-3.06 (m, 2H, His βH), 2.32-1.74 (m, 9H, Val βH), 1.47 (br s, 9H, octyl), 1.28 (br s, 3H, octyl), 1.06-0.70 (m, 36H, Val γH).

^{13}C NMR: (100 MHz, DMSO-d_6, δ): 172.26, 171.49, 171.24, 171.23, 170.94, 170.88, 170.85, 169.83, 167.97 (carbonyl), 136.46 (BOM Ar), 136.06 (His εC), 130.57 (His γC), 128.38, 127.95, 127.71 (BOM Ar), 118.45 (His δC), 101.98, 101.95, 101.94, 101.93, 101.92, 101.88 (CD C1), 82.12, 82.10, 82.00, 81.98, 81.92, 81.85 (CD C4), 75.98 (-N-*C*H_2-O-), 73.29, 73.27, 73.26, 73.24, 73.20, 73.16, 72.25, 72.17, 72.16, 72.12, 72.11, 72.09, 72.06, 72.04, 72.03, 72.00, 71.96, 71.91 (CD C2, C3 and C5), 70.66 (-O-*C*H_2-Ar), 60.31, 60.02, 60.00, 59.98, 59.96, 59.90 (CD C6), 46.32 (His αC), 40.29 (Gly αC), 35.33, 31.47 (alkyl), 31.21, 31.00, 30.88, 30.56, 30.41, 30.00 (Val βC), 28.63 (alkyl), 25.70 (His βC), 22.49, 22.21, 22.05 (alkyl), 19.20, 19.15, 19.07, 19.06, 18.65, 18.63, 18.46, 18.43, 18.21, 18.16, 18.00, 17.82 (Val γC), 14.04 (alkyl).

HRMS-ESI: (*m/z*) $[M + H]^+$ calcd for $C_{90}H_{148}N_{11}O_{39}$, 2006.9936; found 2006.9937.

HPLC Preparative: t_R 22.6 mins (gradient; MeCN (0.1% TFA): H_2O (0.1% TFA), 5:95 to 95:5 over 40 mins, 10 mL min^{-1}).

HPLC-Analytical: t_R 16.84 mins (gradient; MeCN (0.1% TFA): H_2O (0.1% TFA), 5:95 to 95:5 over 30 mins, 0.5 mL min^{-1}).

Melting point: 231-235 °C dec.

***N*-Octanoyl-Val-Val-Val-His-Gly-Val-Val-Val-6^A-amino-6^A-deoxy-α-cyclodextrin 83**

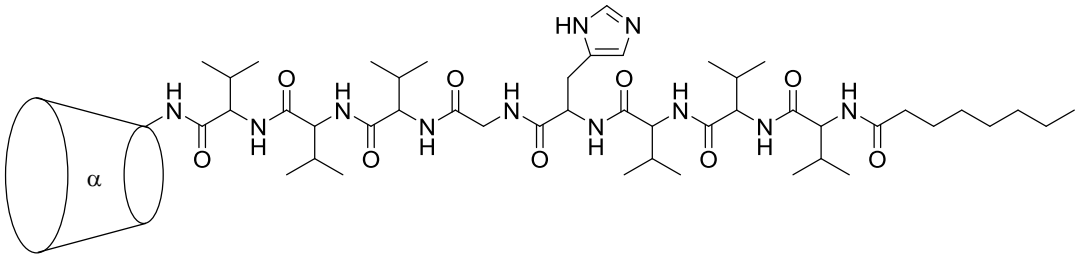

N-Octanoyl-Val-Val-Val-His(π-BOM)-Gly-Val-Val-Val-6^A-amino-6^A-deoxy-α-cyclodextrin **82** (20 mg, 10.0 μmol) and Pd/C catalyst (10%, 10 mg) were suspended in MeOH (20 mL) and left to stir for 24 h under a H_2 balloon (~2 L). The reaction mixture was filtered and the resulting filtrate evaporated to dryness to yield the title compound **83** as a white solid (12 mg, 63%). The product was used with no further purification.

^{1}H NMR: (600 MHz, D_2O, δ): 8.46 (s, 1H, His εH), 7.28 (s, 1H, His δH), 5.17-5.12 (m, 6H, CD H1), 4.55-4.52 (m, 1H, His αH), 4.45-4.38 (m, 6H, Val αH), 4.27-4.12 (m, 2H, Gly αH), 4.14-3.28 (m, 36H, CD H2-6), 3.11-3.07 (m, 2H, His βH), 2.26-1.73 (m, 8H, Val βH and octyl), 1.46 (br s, 10H, octyl), 1.25 (br s, 3H, octyl), 0.97-0.76 (m, 36H, Val γH).
HRMS-ESI: (*m/z*) $[M + H]^+$ calcd for $C_{82}H_{140}N_{11}O_{38}$, 1886.9361; found 1886.9316.
HPLC-Analytical: t_R 18.18 min (gradient; MeCN (0.1% TFA): H_2O (0.1% TFA), 5:95 to 95:5 over 45 min, 0.5 mL min^{-1}).
Melting point: 225-231 °C dec.

Crystal Structure with Zn: A crystal of the target molecule plus $ZnCl_2$ was grown using the technique of vapour diffusion from hanging drops from a solution containing 1M ammonium sulphate in a 0.1 M tris HCl buffer, pH = 7, that had been macro-seeded with crystals from a previous experiment. The resulting crystals were cryo-protected by soaking in a solution of the crystallisation buffer plus 35% ethylene glycol. A crystal with approximate dimensions 50 μm^3 was flashed cooled in a stream of nitrogen gas at 100 K and transferred in a dry shipper at liquid nitrogen temperature to the microfocus macromolecular beamline, MX2, at the Australian Synchrotron. The crystal was mounted and centred remotely using the SAM robot[264] under the control of BLU-ICE software[265]. The energy of the photons in the synchrotron beam was tuned to 9668 eV,

which is 9.4 EV above the Zn K-edge at 9658.6 eV. The imaginary scattering component of the anomalous scattering from the Zn atom, f", is 3.89 electrons at this energy.

X-ray images were collected from 180 contiguous one-degree rotations of the crystal. The synchrotron beam was attenuated by 99% and 0.5 second exposures were used to collect the diffraction images. Data reduction was undertaken using iMosflm[266] and the resulting statistics are listed in Table **9.1**.

The data were phased using the technique of single-wavelength anomalous diffraction (SAD) as implemented in phenix.autosol.[267] The program correctly phased the data and fitted four amino acid residues. In the resulting electron density maps there was clear data for both the Zn ion and the cyclodextrin moiety. These were manually fitted using an α-cyclodextrin template from the pdb file 2XFY[268] using COOT.[269] After further refinement using phenix.refine[270] the remaining atoms were fitted to the electron density, including ten solvent atoms (water). Further refinement yielded final R/R_{free} values of 0.204/0.2399.

	Overall	Inner Shell	Outer Shell
Low resolution limit	27.35	27.35	1.30
High resolution limit	1.27	5.53	1.27
Rmerege (within I+/I-)	0.053	0.034	0.466
Rmerge (all I+ and I-)	0.057	0.044	0.481
Rmeas (within I+/I-)	0.057	0.036	0.507
Rmeas (all I+ & I-)	0.059	0.047	0.502
Rpim (within I+/I-)	0.022	0.014	0.196
Rpim (all I+ & I-)	0.017	0.015	0.142
Rmerge in top intensity bin	0.035	-	-
Total number of observations	48131	600	3452
Total number unique	3870	60	285
Mean((I)/sd(I))	25.0	51.8	4.8
Mn(I) half-set correlation CC(1/2)	0.999	0.988	0.912
Completeness	99.9	96.7	100.0

Multiplicity	12.4	10.0	12.1
Anomalous completeness	100.0	100.0	100.0
Anomalous multiplicity	6.9	7.6	6.5
DelAnom correlation between half-sets	0.387	0.871	-0.076
Mid-Slope of Anom Normal Probability	1.045	-	-

Table 9.1 Data statistics from the crystal structure of *N*-octanoyl-Val-Val-Val-His-Gly-Val-Val-Val-6^{A}-amino-6^{A}-deoxy-α-cyclodextrin **83** with Zn^{2+}.

Estimates of resolution limits: overall

- from half-dataset correlation CC(1/2) > 0.50: limit = 1.27Å == maximum resolution
- from Mn(I/sd) > 2.00: limit = 1.27 Å == maximum resolution

Estimates of resolution limits in reciprocal lattice directions:

Along h k plane

- from half-dataset correlation CC(1/2) > 0.50: limit = 1.27 Å == maximum resolution
- from Mn(I/sd) > 2.00: limit = 1.27 Å == maximum resolution

Along l axis

- from half-dataset correlation CC(1/2) > 0.50: limit = 1.27 Å == maximum resolution
- from Mn(I/sd) > 2.00: limit = 1.27 Å == maximum resolution

Anisotropic deltaB (i.e. range of principal components), A^2: 0.94

Average unit cell: 32.06 32.06 52.44 90.00 90.00 90.00

Space group: I 4 2 2

Average mosaicity: 0.25

Minimum and maximum SD correction factors: Fulls 1.00 37.09 Partials 1.40 70.20

Anomalous flag switched ON in input, strong anomalous signal found

Full crystal data is listed in Appendix B.

Crystal Structure without Zn: Direct methods and charge flipping algorithms failed to solve the structure using *ab initio* methods.

The previously determined Zn-containing structure was used as a model to solve the structure using the technique of molecular replacement. To avoid model bias precluding a solution whereby two monomers form interlocking dimers in preference to the 'self-associating' monomer seen previously in the Zn containing structure, the Zn atom and residues His4 and Gly5 were deleted from the search model. These two residues are responsible for the forming the tight beta-turn that facilitates self-association. Using the program PHASER[271] as implemented in the CCP4 program suite[272] for the molecular replacement calculations yielded an unambiguous single solution with a refined translation function peak of 15.9 sigma. The resulting structure was refined using PHENIX[273] alternating with rounds of manual rebuilding using the program COOT.[269] The final R/R_{free} values after positional and anisotropic temperature factor refinement was 0.1904/0.2082.

The resulting model was virtually identical to the Zn containing model with the Zn atom replaced by water. The side chain imidazole group of His4 appears to be disordered in the absence of Zn binding and no electron density was observed for this side chain. Twelve ordered water molecules were also observed compared to ten in the Zn containing structure and some minor positional shifts of these solvent atoms was observed.

Full crystal data is listed in Appendix C.

H-Val-Val-Val-His-Gly-Val-Val-Val 84

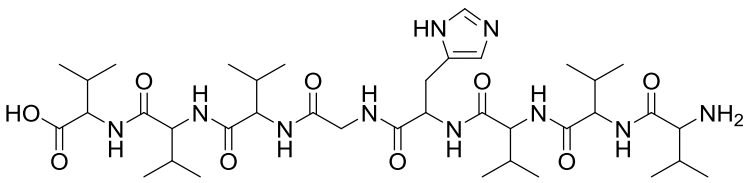

H-Val-Val-Val-His-Gly-Val-Val-Val **84** was synthesised using standard automated Fmoc-coupling solid phase peptide synthesis as described in general methods, on a 0.25 mmol scale. Coupling was performed at 70 °C, apart from Fmoc-His (Trt) which was coupled at

50 °C. The peptide was cleaved from the resin using the standard procedure described in general methods, and the resulting solution pipetted into ice-cold stirring ether (100 mL) to produce a precipitate which was recovered by centrifugation. The crude product was dissolved in MeCN/H_2O (20:80) and subjected to reverse-phase semi-preparative HPLC. Fractions containing the product were combined and lypholised to yield the title compound **84** as a white solid (38 mg, 19%).

^{1}H NMR: (400 MHz, D_2O, δ): 8.67 (s, 1H, His εH), 7.30 (s, 1H, His δH), 4.46 (t, *J* = 6 Hz, 1H, His αH), 4.37-4.05 (m, 6H, Val αH), 3.82 (d, *J* = 12 Hz, 1H, Gly αH), 3.71 (d, *J* = 4 Hz, 1H, Gly αH), 3.21 (m, 2H, His βH), 2.12-1.84 (m, 6H, Val βH), 0.94-0.79 (m, 36H, Val γH).
^{13}C NMR: (100 MHz, DMSO-d_6, δ): 172.74, 171.10, 170.90, 170.68, 170.65, 169.95, 168.60, 167.66 (carbonyl), 133.74 (His εC), 129.14 (His γC), 116.95 (His δC), 58.03, 57.86, 57.64, 57.53, 57.11, 57.01 (Val αC), 51.39 (His αC), 41.87 (Gly αC), 30.76, 30.42, 30.38, 30.21, 30.03, 29.71 (Val βC), 27.13 (His βC), 19.14, 19.11, 19.04, 19.01, 18.47, 18.32, 18.17, 18.12, 17.98, 17.92, 17.58 (Val γC).
HRMS-ESI: (*m/z*) $[M + H]^+$ calcd for $C_{38}H_{67}N_{10}O_9$, 807.5092; found 807.5092.
HPLC-Semi-preparative: t_R 16.4 min (gradient; MeCN (0.1% TFA): H_2O (0.1% TFA), 5:95 to 60:40 over 30 min, 0.5 mL min^{-1}).
HPLC-Analytical: t_R 14.97 min (gradient; MeCN (0.1% TFA): H_2O (0.1% TFA), 5:95 to 50:50 over 25 mins, 4 mL min^{-1}).
Melting Point: 228-230 °C dec.

Ac-Val-Val-Val-His-Gly-Val-Val-Val-Am 85

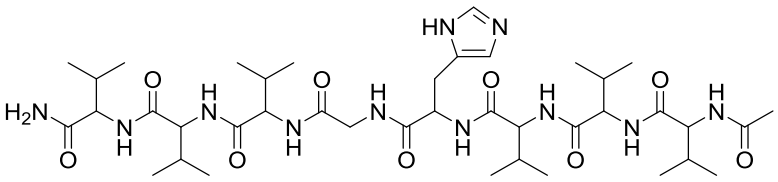

Ac-Val-Val-Val-His-Gly-Val-Val-Val-Am **85** was prepared using standard automated Fmoc-coupling solid phase peptide synthesis as described in general methods, on a 0.25 mmol scale. Rink amide resin was used in place of Wang resin in order to achieve *C*-

terminal amidation. Coupling was performed at 70 °C, apart from Fmoc-His(Trt) which was coupled at 50 °C. *N*-Terminal acetylation was achieved by loading the reacted resin onto a cintered column and washing with DMF. A solution of 10% acetic anhydride in pyridine (2 mL) was added and the reaction mixture left for 20 min. The resin was then washed with DMF (3x10 mL) and MeOH (3x10 mL). The peptide was cleaved from the resin using the standard procedure described in general methods, and the resulting solution evaporated to dryness to give a white solid. The crude product was dissolved in MeCN/H_2O (80:20) and subjected to reverse-phase semi-preparative HPLC. Fractions containing the product were combined and lypholised to yield the title compound **85** as a white solid (12 mg, 7%).

^{1}H NMR: (400 MHz, DMSO-d_6, δ): 8.49 (s, 1H, His εH), 7.21 (s, 1H, His δH), 4.44 (dd, *J* = 7.5 Hz, 12 Hz 1H, His αH), 4.32-4.26 (m, 6H, Val αH), 4.11-4.08 (m, 2H, Gly αH), 2.21-2.19 (m, 2H, His βH), 2.01-1.88 (m, 6H, Val βH), 0.94-0.82 (m, 36H, Val γH).
HRMS-ESI: (*m/z*) $[M + H]^+$ calcd for $C_{40}H_{70}N_{11}O_9$, 848.5358; found 848.5335.
HPLC-Semi-preparative: t_R 24.73 min (gradient; MeCN (0.1% TFA): H_2O (0.1% TFA), 50:50 to 95:5 over 25 min, 4 mL min^{-1}).
HPLC-Analytical: t_R 27.71 min (gradient; MeCN (0.1% TFA): H_2O (0.1% TFA), 5:95 to 95:5 over 30 min, 0.5 mL min^{-1}).
Melting point: 214-218 °C dec.

9.5 Experimental for Chapter 5

_N_-Fmoc-12-aminododecanoic acid 86

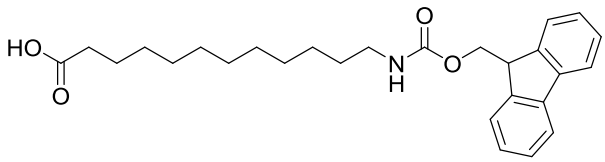

12-Aminododecanoic acid (0.5 g, 2.32 mmol) was suspended in water (30 mL) and heated under reflux to 85 °C. The pH of the solution was adjusted to 10 with a few drops of 10% aqueous Na_2CO_3 solution. A solution of 9-fluorenylmethyl *N*-succinimidyl carbonate (0.78 g, 2.32 mmol) in dioxane (15 mL) was then added dropwise to the

reaction mixture and left to reflux at 85 °C for 5 days. The solution was allowed to cool to room temperature, water (30 mL) added, and the product extracted with DCM (2x50 mL). The organic layer was dried over Na_2SO_4 and evaporated to dryness to give a yellow solid. The crude product was dissolved in chloroform and subjected to a silica gel column, eluted with 9:1 chloroform:ethanol. Fractions containing the product were combined and evaporated to dryness to yield the title compound **86** as a cream-coloured solid (0.34 g, 34%).

TLC: (9:1 v/v chloroform:ethanol) R_f = 0.67.

^{1}H NMR: (400 MHz, $CDCl_3$, δ): 7.76 (d, *J* = 8 Hz, 2H, Fmoc), 7.59 (d, *J* = 8 Hz, 2H, Fmoc), 7.40 (t, *J* = 8 Hz, 2H, Fmoc), 7.31 (t, *J* = 8 Hz, 2H, Fmoc), 4.40 (d, *J* = 8 Hz, Fmoc-C*H*$_2$-OCO-), 4.22 (m, 1H, Fmoc C*H*-), 3.21-3.14 (m, 2H, -C*H*$_2$-CO_2H), 2.34 (t, *J* = 8 Hz, 2H, -CONH-C*H*$_2$-), 1.66-1.59 (m, 2H, alkyl), 1.49-1.43 (m, 2H, alkyl), 1.28 (br s, 14H, alkyl). (data consistent with lit.[274] values)

HRMS-ESI: (*m/z*) $[M + H]^+$ calcd for $C_{27}H_{36}NO_4$, 438.2644; found 438.2645.

HPLC-Analytical: t_R 13.78 min (gradient; MeCN (0.1% TFA): H_2O (0.1% TFA), 5:95 to 95:5 over 30 min, 0.5 mL min^{-1}).

Melting point: 99-102 °C. (lit.[274] mp 102 °C)

Attempted Synthesis of *N*-(6^A-deoxy-α-cyclodextrin-6^A-yl)-12-((2,4,6-trinitrophenyl)amino)dodecaneamide 88

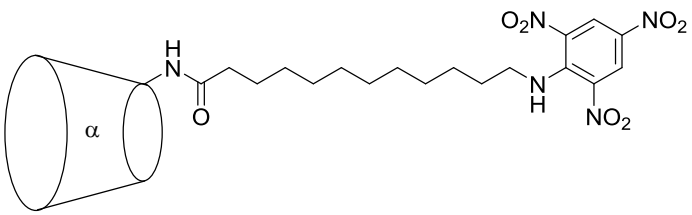

Tentagel resin (86 mg, 25.0 µmol) was swollen in DMF overnight. The resin was loaded onto a cintered column and a solution of DIC (10 µL, 62.5 µmol), DMAP (0.3 mg, 2.5 µmol), HOBt (8.5 mg, 62.5 µmol) and *N*-Fmoc-12-aminododecanoic acid **86** (27.5 mg, 62.5 µmol) in DMF (3 mL) added, and bubbled with N_2 for 4 h. The resin was washed with DMF (3x10 mL), then a solution of acetic anhydride (20 µL, 0.21 mmol) and pyridine

(20 µL, 0.25 mmol) in DMF (1 mL) added and bubbled with N_2 for 1 h. The resin was again washed with DMF (3x10 mL) and a deprotection solution of 20% piperidine in DMF (1.5 mL) added and bubbled with N_2 for 45 min. Resin was washed with DMF (3x10 mL), MeOH (3x10 mL) then water (3x10 mL). A solution of 6^A-azido-6^A-deoxy-α-cyclodextrin **34** (50 mg, 50.0 µmol) in 0.2 M carbonate buffer (2.5 mL, pH 10) was added and left to equilibrate overnight. TNBS (19 mg, 62.5 µmol) was added to the reaction mixture and bubbled with N_2 for 4 h. The resin was rinsed with water (3x10 mL), MeOH (3x10 mL) and DMF (3x10 mL) and a solution of triphenylphosphine (15 mg, 50 µmol) and aqueous ammonia (150 µL, 25%) in DMF (2 mL) added and bubbled with N_2 overnight. The resin was washed with DMF (3x10 mL) then a solution of HBTU (20 mg, 50 µmol), HOBt (7 mg, 50 µmol), DIPEA (20 µL, 0.1 mmol) and *N*-Fmoc-12-aminododecanoic acid **86** (22 mg, 50 µmol) in DMF (2 mL) added and bubbled with N_2 overnight. The resin was washed with DMF (3x10 mL) and a deprotection solution of 20% piperidine in DMF (2 mL) added and bubbled with N_2 for 45 min. The resin was washed with DMF (3x10 mL) and a solution of TNBS (19 mg, 62.5 µmol) in DMF (2 mL) added and bubbled with N_2 for 4 h. The resin was washed with MeOH (3x10 mL) and the daisy chain cleaved from the resin according to the standard procedure for peptide cleavage described in general methods. The resulting solution was evaporated to dryness to give a white solid, however analysis showed no product present. 12-((2,4,6-Trinitrophenyl)amino)dodecanoic acid **89** was identified from the cleaved reaction mixture.

H NMR: (400 MHz, DMSO-d_6, δ): 8.86 (s, 2H, Ar), 2.98 (t, *J* = 6 Hz, 2H, alkyl), 2.18 (t, *J* = 7 Hz, 2H, alkyl), 1.61 (t, *J* = 7 Hz, 2H, alkyl), 1.427 (t, *J* = 7 Hz, 2H, alkyl), 1.24 (m, 14H, alkyl).
LRMS-ESI: (*m/z*) $[M - H]^-$calcd for $C_{18}H_{25}N_4O_8$, 425.17; found 425.2.
HPLC-Preparative: t_R 14.3 min (gradient; MeCN (0.1% TFA): H_2O (0.1% TFA), 30:70 isocratic over 35 min, 10 mL min^{-1}).

6^A-(3-Carboxypropionamido)-6^A-deoxy-α-cyclodextrin 90

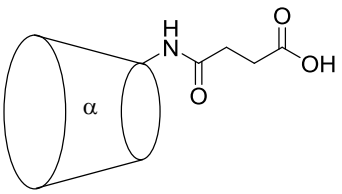

6^A-Amino-6^A-deoxy-α-cyclodextrin **35** (50 mg, 0.514 mmol) and succinic anhydride (51 mg, 0.514 mmol) were dissolved in DMF (25 mL) and the reaction mixture left to stir for 20 h. The solution was pipetted into ice-cold, stirring acetone (150 mL) and the precipitate recovered by centrifugation to give the title compound **90** as a white solid (516 mg, 94%). The crude product was used with no further purification.

TLC: (5:4:3 v/v/v *n*-butanol:ethanol:water) R_f = 0.36

^{1}H NMR: (400 MHz, D_2O, δ): 4.98 (br s, 6H, CD H1), 3.85-3.34 (m, 36H, CD H2-6), 2.48-2.40 (m, 4H, alkyl) (data consistent with lit.[275] values)

HRMS-ESI: (*m/z*) $[M + Na]^+$ calcd for $C_{40}H_{65}NO_{32}Na$, 1094.3387; found 1094.3387

Melting point: 182-191 °C dec.

12-((3,5-Dimethylphenyl)amino)-12-oxododecanoic acid 91

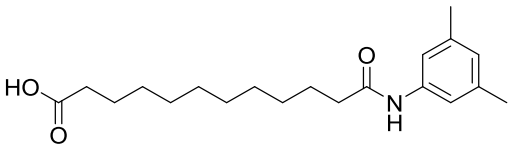

Dodecanedioic acid (0.50 g, 2.17 mmol), BOP (0.23 g, 0.521 mmol) and NEt_3 (300 µL, 2.1 mmol) were dissolved in anhydrous DCM (4 mL) and cooled to 0 °C. A solution of 3,5 dimethyl aniline (55 µL, 0.43 mmol) in anhydrous DCM (1 mL) was added dropwise to the reaction mixture, which was left to stir at room temperature for 24 h. The reaction mixture was evaporated to dryness, dissolved in EtOAc (30 mL) and washed with 1 M HCl (3x30 mL). The organic layer was dried over $MgSO_4$, filtered and evaporated to dryness to give a cream solid which was dried under high vacuum. The crude product

was then washed with acetone (80 mL) and dried under high vacuum to yield the title compound **91** as a white solid (33 mg, 23%).

TLC: (1:1 v/v EtOAc:hexane) R_f = 0.43.

^{1}H NMR: (400 MHz, DMSO-d_6, δ): 7.52 (s, 2H, Ar), 6.97 (s, 1H, Ar), 2.82 (s, 6H, Me), 1.89-1.78 (m, 4H, alkyl), 1.59-1.54 (m, 16H, alkyl).

HRMS-ESI: (*m/z*) $[M + H]^+$ calcd for $C_{20}H_{32}NO_3$, 334.2382; found 334.2383.

HPLC-Analytical: t_R 29.28 (gradient; MeCN (0.1% TFA): H_2O (0.1% TFA), 5:95 to 95:5 over 45 min, 0.5 mL min^{-1}).

Melting point: 124-126 °C.

Attempted Synthesis of [*N*-(6^A-deoxy-α-cyclodextrin-6^A-yl)-12-((3,5-dimethylphenyl)amino)dodecaneamide] [6^A-(3-Carboxypropionamido)-6^A-deoxy-α-cyclodextrin]-[*a*2]-daisy chain 93

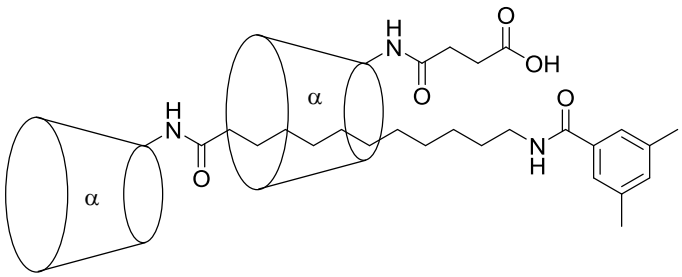

Tentagel resin (172 mg, 50.0 μmol) was swollen in DMF overnight. The resin was loaded onto a cintered column and a solution of DIC (20 μL, 125 μmol), DMAP (0.6 mg, 5 μmol), HOBt (17 mg, 125 μmol) and carboxypropionic acid-α-cyclodextrin **90** (134 mg, 125 μmol) in DMF (3 mL) added, and bubbled with N_2 for 6 h. The resin was washed with DMF (3x10 mL), ethanol (3x10 mL) and water (3x10 mL) then allowed to swell in water overnight. The resin was drained and a solution of 12-((3,5-dimethylphenyl)amino)-12-oxododecanoic acid **91** (25 mg, 75 μmol) and NEt_3 (20 μL, 150 μmol) in water (2 mL) added and left to equilibrate overnight. A solution of 6^A-amino-6^A-deoxy-α-cyclodextrin **35** (73 mg, 75 μmol), DMTMM (55 mg, 200 μmol) and NEt_3 (20 μL, 150 μmol) in water (0.5 mL) was then added and the reaction mixture bubbled with N_2 overnight. The resin

was washed with water (3x10 mL) and ethanol (3x10 mL) and the product cleaved from the resin according to the standard procedure for peptide cleavage described in general methods. The resulting solution was evaporated to dryness to give a white solid, however analysis showed no product present.

Attempted Synthesis of [*N*-(6^{A}-deoxy-α-cyclodextrin-6^{A}-yl)-12-((3,5-dimethylphenyl)amino)dodecaneamide] [6^{A}-(6-Carboxyhexionamido)-6^{A}-deoxy-α-cyclodextrin]-[*a*2]-daisy chain 95

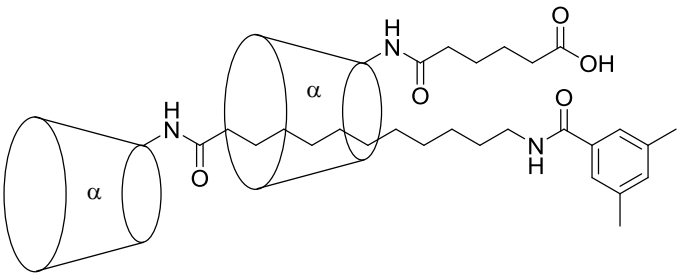

Tentagel resin (172 mg, 50.0 μmol) was swollen in DMF overnight. The resin was loaded onto a cintered column and a solution of DIC (20 μL, 125 μmol), DMAP (0.6 mg, 5 μmol), HOBt (17 mg, 125 μmol) and adipic acid (19 mg, 125 μmol) in DMF (3 mL) added, and bubbled with N_2 overnight. The resin was washed with DMF (3x10 mL), then a solution of HBTU (38 mg, 100 μmol), HOBt (14 mg, 100 μmol), DIPEA (35 μL, 200 μmol) and amino-α-cyclodextrin **35** (97 mg, 100 μmol) in DMF (3 mL) added and bubbled with N_2 overnight. The resin was washed with DMF (3x10 mL), ethanol (3x10 mL) and water (3x10 mL) then allowed to swell in water overnight. The resin was drained and a solution of 12-((3,5-dimethylphenyl)amino)-12-oxododecanoic acid **91** (25 mg, 75 μmol) and NEt_3 (30 μL, 0.21 mmol) in water (2 mL) added and left to equilibrate overnight. A solution of 6^{A}-amino-6^{A}-deoxy-α-cyclodextrin **35** (25 μL, 200 μmol), DMTMM (48 mg, 200 μmol) and NEt_3 (40 μL, 0.28 mmol) in water (0.5 mL) was then added and the reaction mixture bubbled with N_2 overnight. The resin was washed with water (3x10 mL) and ethanol (3x10 mL) and the product cleaved from the resin according to the standard procedure for peptide cleavage described in general methods. The resulting solution

was evaporated to dryness to give a white solid, however analysis showed no product present.

Attempted Synthesis of [(*E*)-4,4'-bis(3,5-dimethylphenylcarbonyl)azobenzene [di-(3,5 dimethylphenyl) amidoazobenzene] [6^A-(6-Carboxyhexionamido)-6^A-deoxy-α-cyclodextrin] rotaxane 98

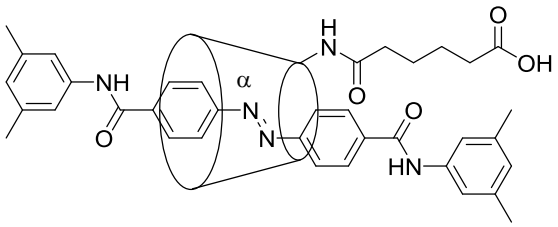

Tentagel resin (172 mg, 50.0 μmol) was swollen in DMF overnight. The resin was loaded onto a cintered column and a solution of DIC (20 μL, 125 μmol), DMAP (0.6 mg, 5 μmol), HOBt (17 mg, 125 μmol) and adipic acid (19 mg, 125 μmol) in DMF (3 mL) added, and bubbled with N_2 overnight. The resin was washed with DMF (3x10 mL), then a solution of HBTU (38 mg, 100 μmol), HOBt (14 mg, 100 μmol), DIPEA (35 μL, 200 μmol) and 6^A-amino-6^A-deoxy-α-cyclodextrin **35** (97 mg, 100 μmol) in DMF (3 mL) added and bubbled with N_2 overnight. The resin was washed with DMF (3x10 mL), ethanol (3x10 mL) and water (3x10 mL) then allowed to swell in water overnight. The resin was drained and a solution of azobenzene-4,4'-dicarboxylic acid **36** (27 mg, 100 μmol) in water (2 mL) added and left to equilibrate overnight. A solution of 3,5 dimethyl aniline **97** (25 μL, 200 μmol), DMTMM (48 mg, 200 μmol) and NEt_3 (40 μL, 0.28 mmol) in water (0.5 mL) was then added and the reaction mixture bubbled with N_2 overnight. The resin was washed with water (3x10 mL) and ethanol (3x10 mL) and the product cleaved from the resin according to the standard procedure for peptide cleavage described in general methods. The resulting solution was evaporated to dryness to give an orange solid, however analysis showed no product present.

2nd Attempted Synthesis of of [(*E*)-4,4'-bis(3,5-dimethylphenylcarbonyl)azobenzene [di-(3,5 dimethylphenyl) amidoazobenzene] [6^A-(6-Carboxyhexionamido)-6^A-deoxy-α-cyclodextrin] rotaxane 98

The synthesis for daisy chain **98** was repeated using Wang resin (42 mg, 50 μmol) in place of Tentagel resin. Upon analysis of the cleaved reaction mixture, no product was detected.

Attempted Synthesis of [(*E*)-4,4'-bis(2,4,6-trinitrophenylamino)azobenzene [di-(3,5 dimethylphenyl) amidoazobenzene] [6^A-(6-Carboxyhexionamido)-6^A-deoxy-α-cyclodextrin] rotaxane 100

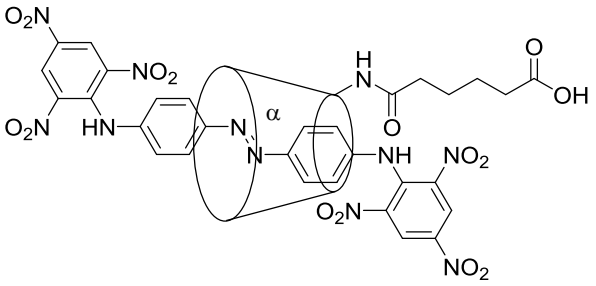

Tentagel resin (172 mg, 50.0 μmol) was swollen in DMF overnight. The resin was loaded onto a cintered column and a solution of DIC (20 μL, 125 μmol), DMAP (0.6 mg, 5 μmol), HOBt (17 mg, 125 μmol) and adipic acid (19 mg, 125 μmol) in DMF (3 mL) added, and bubbled with N_2 overnight. The resin was washed with DMF (3x10 mL), then a solution of HBTU (38 mg, 100 μmol), HOBt (14 mg, 100 μmol), DIPEA (35 μL, 200 μmol) and 6^A-amino-6^A-deoxy-α-cyclodextrin **35** (97 mg, 100 μmol) in DMF (3 mL) added and bubbled with N_2 overnight. The resin was washed with DMF (3x10 mL), ethanol (3x10 mL) and water (3x10 mL) then allowed to swell in water overnight. The resin was drained and a solution of azodianiline (22 mg, 100 μmol) in water (2 mL) added and left to equilibrate overnight. A solution of TNBS **87** (60 μL, 0.2 mmol) in water (0.5 mL) was then added and the reaction mixture bubbled with N_2 overnight. The resin was washed with water (3x10 mL) and ethanol (3x10 mL) and the product cleaved from the resin according to the standard procedure for peptide cleavage described in general methods. The

resulting solution was evaporated to dryness to give an orange solid, however analysis showed no product present.

Resin-bound 6^A-(6-carboxyhexionamido)-6^A-deoxy-α-cyclodextrin 101

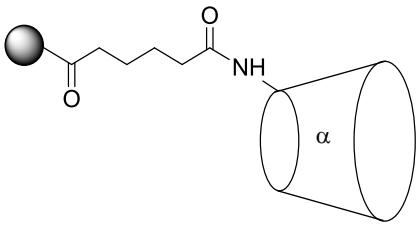

Tentagel resin (172 mg, 50.0 μmol) was swollen in DMF overnight. The resin was loaded onto a cintered column and a solution of DIC (20 μL, 125 μmol), DMAP (0.6 mg, 5 μmol), HOBt (17 mg, 125 μmol) and adipic acid (19 mg, 125 μmol) in DMF (3 mL) added, and bubbled with N_2 overnight. The resin was washed with DMF (3x10 mL), then a solution of HBTU (38 mg, 100 μmol), HOBt (14 mg, 100 μmol), DIPEA (35 μL, 200 μmol) and 6^A-amino-6^A-deoxy-α-cyclodextrin **35** (97 mg, 100 μmol) in DMF (3 mL) added and bubbled with N_2 overnight. The resin was rinsed with DMF (3x10 mL), ethanol (3x10 mL) and water (3x10 mL) and a small portion cleaved from the resin according to the standard procedure for peptide cleavage described in general methods and analysed by LC-MS to confirm that the desired product had coupled to the resin.

Resin-bound 4-carboxyazobenzene 102

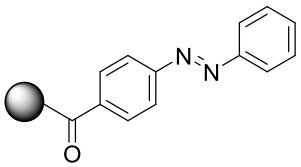

Tentagel resin (172 mg, 50.0 μmol) was swollen in DMF overnight. The resin was loaded onto a cintered column and a solution of DIC (20 μL, 125 μmol), DMAP (0.6 mg, 5 μmol), HOBt (17 mg, 125 μmol) and 4-phenylazobenzoic acid **53** (28 mg, 125 μmol) in DMF (3

mL) added, and bubbled with N_2 overnight. The resin was rinsed with DMF (3x10 mL), ethanol (3x10 mL) and water (3x10 mL) and a small portion cleaved from the resin according to the standard procedure for peptide cleavage described in general methods and analysed by LC-MS to confirm that the desired product had coupled to the resin.

9.6 Experimental for Chapter 6

(*E*)-(4((4-(6^A-Deoxy-α-cyclodextrin-6^A-ylcarbomyl)phenyl)diazenyl)benzoyl)-Val-Val-Val-OH 103

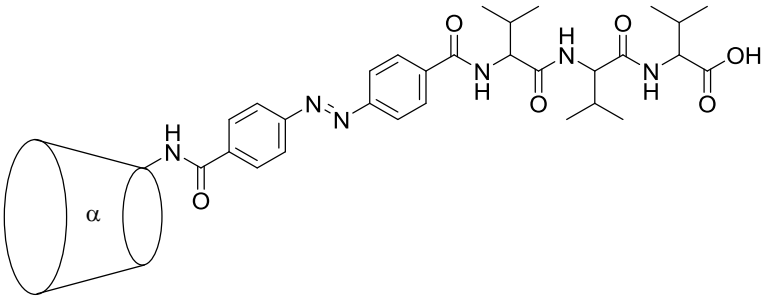

(*E*)-(4((4-(6^A-Deoxy-α-cyclodextrin-6^A-ylcarbomyl)phenyl)diazenyl)benzoyl)-Val-Val-Val-OH **103** was prepared using standard manual fmoc-coupling solid phase synthesis as described in general methods, on a 0.5 mmol scale. (*E*)-*N*-(6^A-Deoxy-α-cyclodextrin 6^A-yl)-4-aminocarbonyl-4'-carboxyazobenzene **37** was used in the final on-resin coupling step. The peptide was cleaved from the resin using the standard procedure described in general methods, and the resulting solution evaporated to dryness to give an orange solid. The crude product was dissolved in MeCN/H_2O (50:50) and subjected to reverse-phase semi-preparative HPLC. Fractions containing the product were combined and lypholised to yield the title compound **103** as an orange solid (91 mg, 12%).

^{1}H NMR: (400 MHz, D_2O, δ): 8.47 (d, *J* = 8 Hz, 2H, azobenzene), 8.33 (d, *J* = 8 Hz, 2H, azobenzene), 7.96-7.87 (m, 4H, azobenzene), 5.07-4.89 (m, 6H, CD H1), 4.19-3.80 (m, 36H, CD H2-6), 3.61-3.38 (m, 3H, Val αH), 2.14-1.92 (m, 3H, Val βH), 1.01-0.81 (m, 18H, Val γH).

HRMS-ESI: (*m/z*) $[M + Na]^+$ calcd for $C_{65}H_{96}N_6O_{35}Na$, 1543.5814; found 1543.5817.

HPLC-Semi-preparative: t_R 8.74 min (gradient; MeCN (0.1% TFA): H_2O (0.1% TFA), 5:95 to 95:5 over 30 min, 4 mL min^{-1}).

HPLC-Analytical: t_R 6.82 min (gradient; MeCN (0.1% TFA): H_2O (0.1% TFA), 5:95 to 95:5 over 30 min, 0.5 mL min^{-1}).

Melting point: 192-199 °C dec.

Tri-L-valine 104

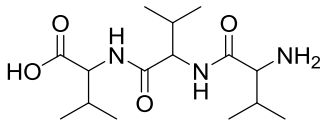

Tri-L-valine **104** was prepared using standard manual Fmoc-coupling solid phase synthesis as described in general methods, on a 0.5 mmol scale. The peptide was cleaved from the resin using the standard procedure described in general methods, and the resulting solution evaporated to dryness to give a white solid. The crude product was dissolved in MeCN:H_2O (50:50) and subjected to reverse-phase semi-preparative HPLC. Fractions containing the product were combined and lypholised to yield the title compound **104** as a white solid (70 mg, 43%).

^{1}H NMR: (400 MHz, D_2O, δ): 4.30-4.25 (m, 2H, Val αH), 3.91-3.89 (d, *J* = 7.5 Hz, 1H, Val αH), 2.26-2.05 (m, 3H, Val βH), 1.04-0.99 (m, 18H, Val γH).

^{13}C NMR: (100 MHz, D_2O, δ): 177.55, 175.75, 171.65 (carboynl), 62.13, 61.11, 60.83 (Val αC), 20.90, 20.78, 20.54, 20.13, 19.95, 19.46 (Val βC and Val γC).

HRMS-ESI: (*m/z*) $[M + H]^+$ calcd for $C_{15}H_{30}N_3O_4$, 316.2236; found 316.2237, $[M + Na]^+$ calcd for $C_{15}H_{29}N_3O_4Na$, 338.2056; found 338.2056.

HPLC-Semi-preparative: t_R 12.79 min (gradient; MeCN (0.1% TFA): H_2O (0.1% TFA), 5:95 to 95:5 over 30 min, 4 mL min^{-1}).

HPLC-Analytical: t_R 9.23 min (gradient; MeCN (0.1% TFA): H_2O (0.1% TFA), 5:95 to 95:5 over 30 min, 0.5 mL min^{-1}).

Melting point: 177-184 °C dec.

(*E*)-*N*-(6^{A}-Deoxy-β-cyclodextrin 6^{A}-yl)-4-aminocarbonyl-4'-carboxyazobenzene 105

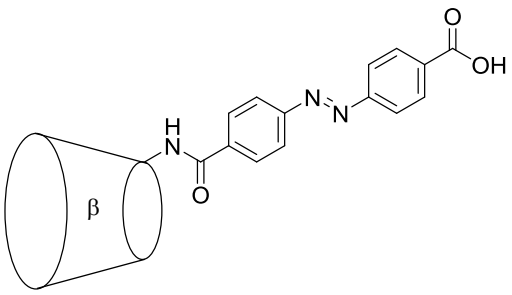

Azobenzene-4,4'-dicarboxylic acid **36** (90 mg, 0.335 mmol), BOP (60 mg, 0.137 mmol) and NEt_3 (500 µL, 3.6 mmol) were dissolved in anhydrous DMF (2 mL). A solution of 6^{A}-amino-6^{A}-deoxy-β-cyclodextrin **56** (100 mg, 88.1 µmol) and NEt_3 (100 µL, 0.70 mmol) in anhydrous DMF (3 mL) was added dropwise and the reaction mixture left to stir for 24 h. The solution was precipitated into ice-cold, stirring acetone (100 mL) and the orange precipitate recovered by centrifugation. The crude product was dissolved in water (100 mL) and acidified to pH 2 with 0.5 M HCl, before being applied to a HP-20 column. The product was eluted with 35-50% MeOH and fractions containing the product combined and lyophilised to yield the title compound **105** as an orange solid (20 mg, 17%).

TLC: (5:4:3 v/v/v *n*-butanol:ethanol:water) R_f = 0.42.

^{1}H NMR: (400 MHz, DMSO-d_6, δ): 8.10 (d, *J* = 8 Hz, 2H, azobenzene), 7.93 (d, *J* = 8 Hz, 2H, azobenzene), 7.90-7.80 (m, 4H, azobenzene), 5.92-5.80 (m, 14H, CD OH2 and OH3), 4.84 (br s, 7H, CD H1), 4.39 (br s, 7H, CD OH6), 3.68-3.63 (m, 28H, CD H3, H5 and H6).

HRMS-ESI: (*m/z*) $[M - 2H]^{2-}$ calcd for $C_{56}H_{77}N_3O_{37}$, 691.7118; found 691.7115.

HPLC-Analytical: t_R 5.09 min (gradient; MeCN (0.1% TFA): H_2O (0.1% TFA), 5:95 to 95:5 over 30 min, 0.5 mL min^{-1}).

Melting point: 185-191 °C dec.

Attempted Synthesis of (*E*)-(4((4-(6^{A}-Deoxy-β-cyclodextrin-6^{A}-ylcarbomyl)phenyl)diazenyl)benzoyl)-Val-Val-Val-OH 106

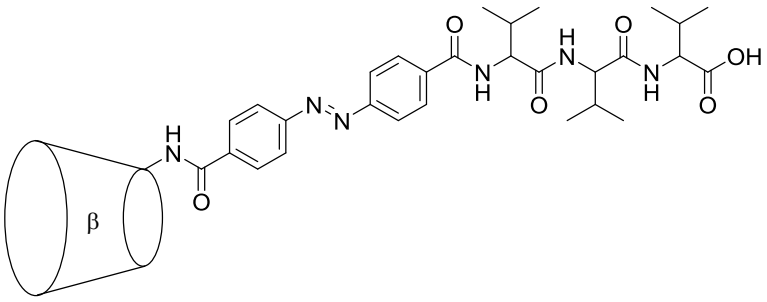

(*E*)-(4((4-(6^{A}-Deoxy-β-cyclodextrin-6^{A}-ylcarbomyl)phenyl)diazenyl)benzoyl)-Val-Val-Val-OH **106** was prepared using standard manual fmoc-coupling solid phase synthesis as described in general methods, on a 0.5 mmol scale. (*E*)-*N*-(6^{A}-Deoxy-β-cyclodextrin 6^{A}-yl)-4-aminocarbonyl-4'-carboxyazobenzene **105** was used in the final on-resin coupling step. The peptide was cleaved from the resin using the standard procedure described in general methods, however the product could not be detected.

Attempted Synthesis of [(*E*)-*N*-(6^{A}-Deoxy-α-cyclodextrin-6^{A}-yl)-4-aminocarbonyl-4'-(3-(Val-Val-Val)propylaminocarbonyl)azobenzene]$_2$-[*c*2]-daisy chain dimer of 107

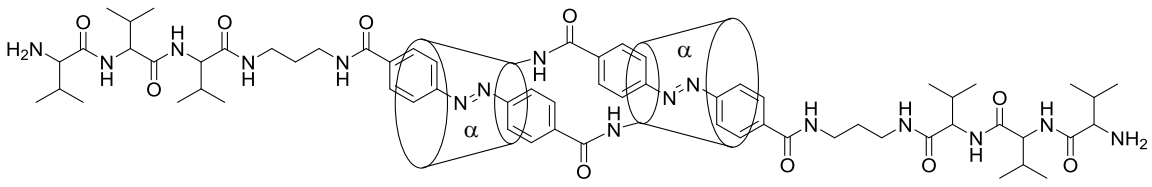

(*E*)-*N*-(6^{A}-Deoxy-α-cyclodextrin-6^{A}-yl)-4-aminocarbonyl-4'-(3-aminopropylaminocarbonyl)azobenzene **39** (25 mg, 39 μmol) and NEt_3 (10 μL, 0.07 mmol) were dissolved in water (5 mL) and allowed to equilibrate for 3 h. Tri-L-valine **104** (7.5 mg, 47 μmol) and DMTMM (6.5 mg, 47 μmol) were then added to the solution with some sonification to dissolve the peptide. The reaction mixture was left to stir overnight, then pipetted into ice-cold, stirring acetone (30 mL) and the precipitate recovered by

centrifugation. The crude product was dissolved in H_2O and subjected to reverse-phase analytical HPLC, however the desired product could not be detected.

Adamantane-1-carbonyl-Val-Val-Val-OH 111

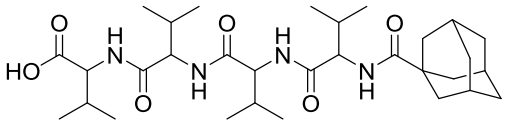

Adamantane-1-carbonyl-Val-Val-Val-OH **111** was prepared using standard automated Fmoc-coupling solid phase peptide synthesis as described in general methods, on a 0.25 mmol scale, with 1-carboxyadamantane **59** used in the final on-resin coupling step. The peptide was cleaved from the resin using the standard procedure described in general methods, and the resulting solution pipetted into ice-cold stirring ether (100 mL) to produce the crude product as a white precipitate (32 mg, 22%). The compound was used with no further purification.

^{1}H NMR: (400 MHz, DMSO-d_6, δ): 7.88 (d, J = 8 Hz, 1H, NH), 7.83 (d, J = 8 Hz, 1H, NH), 7.76 (d, J = 8 Hz, 1H, NH), 7.09 (d, J = 8 Hz, 1H, NH), 4.29-4.09 (m, 4H, Val αH), 2.08-1.91 (m, 4H, Val βH),1.78 (br s, 3H, adamantane), 1.66 (br s, 12H, adamantane), 0.88-0.78 (m, 18H, Val γH).

HRMS-ESI: (*m/z*) $[M + Na]^+$ calcd for $C_{31}H_{52}N_4O_6Na$, 599.3776; found 599.3785.

HPLC-Analytical: t_R 27.50 min (gradient; MeCN (0.1% TFA): H_2O (0.1% TFA), 5:95 to 95:5 over 45 min, 0.5 mL min^{-1}).

Melting Point: 196-200 °C dec.

9.7 Experimental for Chapter 7

Gelation: *N*-Octanoyl-Val-Val-Val-His-Gly-Val-Val-Val-OH **112** (1 mg) was weighed into a 1.5 mL RAM robotic sample vial and made up to the desired concentration with the relevant solvent. The sample was then sonicated to obtain a clear solution (~30 s) and left overnight. An inversion test was performed after ~12 h.

_N_-Octanoyl-Val-Val-Val-His-Gly-Val-Val-Val-OH 112

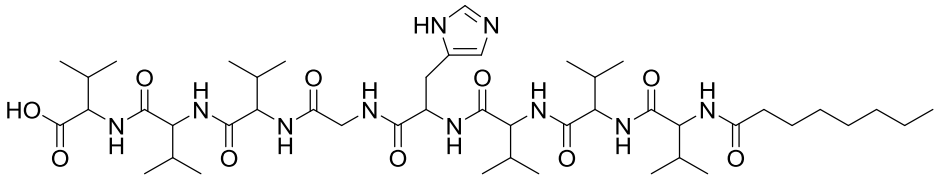

_N_-Octanoyl-Val-Val-Val-His-Gly-Val-Val-Val-OH **112** was prepared using standard automated Fmoc-coupling solid phase peptide synthesis as described in general methods, on a 0.25 mmol scale. Coupling was performed at 70 °C, apart from Fmoc-His(Trt) which was coupled at 50 °C. Octanoic acid was used in the final on-resin coupling step. The peptide was cleaved from the resin using the standard procedure described in general methods, and the resulting solution pipetted into ice-cold, stirring 10% acetonitrile/water (100 mL) to give a white precipitate which was recovered by centrifugation. The crude product was dissolved in MeCN/H_2O (50:50) and subjected to reverse-phase semi-preparative HPLC. Fractions containing the product were combined and lypholised to yield the title compound as a white solid (52 mg, 22%).

^{1}H NMR: (400 MHz, DMSO-d_6, δ): 8.70 (s, 1H, His εH), 8.23-7.79 (m, 8H, amide), 7.28 (s, 1H, His δH), 4.57-4.52 (br s, 1H, His αH), 4.31-4.09 (m, 6H, Val αH), 3.85-3.69 (m, 2H, Gly αH), 3.09-2.93 (m, 2H, His βH), 2.18-1.88 (m, 8H, Val βH, alkyl), 1.49-1.46 (m, 2H, alkyl), 1.23 (br s, 9H, alkyl), 0.88-0.79 (m, 38H, Val γH, alkyl).

^{13}C NMR: (100 MHz, DMSO-d_6, δ): 172.79, 172.21, 171.19, 171.07, 170.97, 170.93, 170.65, 169.94, 168.51 (carbonyl), 129.02 (His εC), 128.33 (His γC), 126.23 (His δC), 57.80, 57.70, 57.63, 57.59, 57.40, 57.02 (Val αC), 51.50 (His αC), 41.91 (Gly αC), 35.12 (alkyl), 31.18, 30.80, 30.27, 30.23, 30.21, 29.73 (Val βC), 28.52, 28.42 (alkyl), 25.41 (His βC), 22.02, 19.21, 19.11 (alkyl), 19.08, 19.06, 19.04, 18.40, 18.28, 18.19, 18.14, 18.00, 17.87, (Val γC) 13.93 (alkyl).

HRMS-ESI: (_m/z_) $[M+H]^+$ calcd for $C_{46}H_{81}N_{10}O_{10}$, 933.6137; found 933.6141, $[M+Na]^+$ calcd for $C_{46}H_{80}N_{10}O_{10}Na$, 955.5957; found 955.5961.

HPLC-Semi-preparative: t_R 5.80 min (gradient; MeCN (0.1% TFA): H_2O (0.1% TFA), 50:50 to 90:10 over 30 min, 4 mL min^{-1}).

HPLC-Analytical: t_R 35.87 min (gradient; MeCN (0.1% TFA): H_2O (0.1% TFA), 5:95 to 95:5 over 45 min, 0.5 mL min^{-1}).

Melting Point: 220-223 °C dec.

Chapter 10: References

1. J.-M. Lehn, *Supramolecular Chemistry*, Wiley-VCH, **1995**.
2. C. S. Mahon, D. A. Fulton, *Nat. Chem.* **2014**, *6*, 665-672.
3. A. Mulder, J. Huskens, D. N. Reinhoudt, *Org. Biomol. Chem.* **2004**, *2*, 3409-3424.
4. Z. He, W. Jiang, C. A. Schalley, *Chem. Soc. Rev.* **2015**, *44*, 779-789.
5. J. A. Sawitzke, L. C. Thomason, N. Costantino, M. Bubunenko, S. Datta, D. L. Court, *Recombineering: In Vivo Genetic Engineering in E-Coli, S-Enterica, and Beyond, Vol. 421*, Elsevier Academic Press Inc., San Diego, **2007**.
6. K. J. Edwards, D. G. Brown, N. Spink, J. V. Skelly, S. Neidle, *J. Mol. Biol.* **1992**, *226*.
7. R. H. Garrett, C. M. Grisham, S. Andreopoulos, W. G. Willmore, I. E. Gallouzi, *Biochemistry*, Nelson College Indigenous, **2012**.
8. T. A. Kunkel, *J. Biol. Chem.* **2004**, *279*, 16895-16898.
9. D. Philp, J. F. Stoddart, *Angew. Chem., Int. Edit.* **1996**, 1154-1196.
10. T. H. Newman, K. E. Williams, R. F. W. Pease, *J. Vac. Sci. Technol. B* **1987**, *5*, 88-91.
11. S. Hosoki, S. Hosaka, T. Hasegawa, *Appl. Surface Science* **1992**, *60-61*, 643-647.
12. J.-M. Lehn, *Angew. Chem., Int. Edit.* **2015**, 3276-3289.
13. M. Sakulsombat, Y. Zhang, O. Ramstrom, *Top. Curr. Chem.* **2012**, *322*, 55-86.
14. C. S. Mahon, A. W. Jackson, B. S. Murray, D. A. Fulton, *Polym. Chem.* **2013**, *4*, 368-377.
15. R. D. Vale, R. A. Milligan, *Science* **2000**, *288*, 88-95.
16. D. Carr, H. Craighead, *Cornell Chronicle*, Cornell University, **1997**.
17. www.rna.ucsc.edu/rnacenter/ribosome_images.html.
18. J. M. Baldwin, *J. Mol. Biol.* **1980**, *136*, 103-128.
19. K. E. Drexler, *Engines of Creation: The Coming Era of Nanotechnology*, Anchor Books, **1986**.
20. J. M. Tour, *Acc. Chem. Res.* **2000**, 791-804.
21. W. R. Browne, B. L. Feringa, *Nature Nanotechnology* **2006**, *1*, 25-35.
22. B. Lewandowski, G. De Bo, J. W. Ward, M. Papmeyer, S. Kuschel, M. J. Aldegunde, P. M. E. Gramlich, D. Heckmann, S. M. Goldup, D. M. D'Souza, A. E. Fernandes, D. A. Leigh, *Science* **2013**, *339*, 189-193.
23. R. P. Feynman, *American Physical Society*, Caltech, Pasadena, **1959**.
24. A. Caballero, F. Zapata, P. D. Beer, *Coord. Chem. Rev.* **2013**, *257*, 2434-2455.
25. J. F. Ayme, J. E. Beves, D. A. Leigh, R. T. McBurney, K. Rissanen, D. Schultz, *Nat. Chem.* **2012**, *4*, 15-20.
26. C. D. Meyer, C. S. Joiner, J. F. Stoddart, *Chem. Soc. Rev.* **2007**, *36*, 1705-1723.
27. C. J. Pedersen, *J. Am. Chem. Soc.* **1967**, *89*, 7017-7036.
28. P. J. Cragg, R. Vahora, Crown and Lariat Ethers, *Supramolecular Chemistry: From Molecules to Nanomaterials*, Eds. P. Gale, J. Steed, Wiley-VCH **2012**.
29. A. Bianchi, E. Garcia-Espana, Azacoronands and Azacyclophanes, *Supramolecular Chemistry: From Molecules to Nanomaterials*, Eds. P. Gale, J. Steed, Wiley-VCH **2012**.

30. L. F. Lindoy, K. M. Park, S. S. Lee, Cryptands and Spherands, *Supramolecular Chemistry: From Molecules to Nanomaterials*, Eds. P. Gale, J. Steed **2012**.
31. S. J. Cantrill, S. J. Rowan, J. F. Stoddart, *Org. Lett.* **1999**, *1*, 1363-1366.
32. W. Clegg, C. Gimenez-Saiz, D. A. Leigh, A. Murphy, A. M. Z. Slawin, S. J. Teat, *J. Am. Chem. Soc.* **1999**, *121*, 4124-4129.
33. H. Frisch, J. P. Unsleber, D. Ludeker, M. Peterlechner, G. Brunklaus, M. Waller, P. Besenius, *Angew. Chem., Int. Edit.* **2013**, *52*, 10097-10101.
34. M. J. Frampton, H. L. Anderson, *Angew. Chem., Int. Edit.* **2007**, *46*, 1028-1064.
35. S. Maniam, M. M. Cieslinski, S. F. Lincoln, H. Onagi, P. J. Steel, A. C. Willis, C. J. Easton, *Org. Lett.* **2008**, *10*, 1885-1888.
36. N. H. Evans, C. J. Serpell, P. D. Beer, *Chem. Commun.* **2011**, *47*, 8775-8777.
37. J. M. Spruell, A. Coskun, D. C. Friedman, R. S. Forgan, A. A. Sarjeant, A. Trabolsi, A. C. Fahrenbach, G. Barin, W. F. Paxton, S. K. Dey, M. A. Olson, D. Benitez, E. Tkatchouk, M. T. Colvin, R. Carmielli, S. T. Caldwell, G. M. Rosair, S. G. Hewage, F. Duclairoir, J. L. Seymour, A. M. Z. Slawin, W. A. G. III, M. R. Wasielewski, G. Cooke, J. F. Stoddart, *Nat. Chem.* **2010**, *2*, 870-879.
38. A. Harada, R. Kobayashi, Y. Takashima, A. Hashidzume, H. Yamaguchi, *Nat. Chem.* **2011**, *3*, 34-37.
39. A. Villiers, *Compt. Rend,* **1891**, *112*, 536.
40. K. Freudenberg, F. Cramer, *Zeitschrift Fur Naturforschung B* **1948**, *3*, 464.
41. M. L. Sinnott, *Carbohydrate Chemistry and Biochemistry*, The Royal Society of Chemistry, Cambridge, **2007**.
42. J. Szejtli, *Chem. Rev.* **1998**, *98*, 1743-1754.
43. M. J. Jozwiakowski, K. A. Conners, *Carbohydr. Res.* **1985**, *143*, 51.
44. J. Jacob, K. Gebler, D. Hoffmann, H. Sanbe, K. Koizumi, S. M. Smith, T. Takaha, W. Saenger, *Chem. Commun.* **1998**, *37*, 606-609.
45. W. Saenger, J. Jacob, K. Gessler, T. Steiner, D. Hoffmann, H. Sanbe, K. Koizumi, S. M. Smith, T. Takaha, *Chem. Rev.* **1998**, *98*, 1787-1802.
46. H. Taira, H. Nagase, T. Endo, H. Ueda, *J. Inclusion Phenom.* **2006**, *56*, 23-28.
47. Y. Terada, H. Sanbe, T. Takaha, S. Kitahata, K. Koizumi, S. Okada, *Appl. Environ. Microbiol.* **2001**, *67*, 1453-1460.
48. T. Fukami, A. Mugishima, T. Suzuki, S. Hidaka, T. Endo, H. Ueda, K. Tomono, *Chem. Pharm. Bull.* **2004**, *52*, 961-964.
49. H. Dodzuik, A. Ejchart, W. Anczewski, H. Ueda, E. Krinichnaya, G. Dolgonos, W. Kutner, *Chem. Commun.* **2003**, 986-987.
50. S. Machida, K. Hayashi, Patent No. 2001-261697, *Japan* **2001**.
51. F. Schardinger, *Zentralbl. Bakteriol. Parasitenk. Abt. 2* **1911**, *29*, 188.
52. K. Freudenberg, F. Cramer, H. Plieninger, Patent No. DE895769C, *Germany* **1953**.
53. B. Liu, *Clin. Lipidol.* **2012**, *7*, 289-301.
54. E. Bilensoy, *Cyclodextrins in Pharmaceutics, Cosmetics and Biomedicine: Current and Future Industrial Applications*, Wiley, **2011**.
55. T. Tamaki, T. Kokubu, *J. Incl. Phenom.* **1984**, *2*, 815-822.
56. K. Hamasaki, H. Ikeda, A. Nakamura, A. Ueno, F. Toda, I. Suzuki, T. Osa, *J. Am. Chem. Soc.* **1993**, *115*, 5035-5040.
57. L. D. Melton, K. N. Slessor, *Carbohydr. Res.* **1971**, *18*, 29-37.
58. H. Ikeda, Y. Nagano, Y. Q. Du, T. Ikeda, F. Toda, *Tetrahedron Lett.* **1990**, *31*, 5045-5048.
59. E. A. Lewis, L. D. Hansen, *J. Chem. Soc., Perkin Trans. 2* **1973**, 2081-2085.
60. H. Ogino, *J. Am. Chem. Soc.* **1981**, *103*, 1303-1304.

61. D. Armspach, P. R. Ashton, C. P. Moore, N. Spencer, J. F. Stoddart, T. J. Wear, D. J. Williams, *Angew. Chem., Int. Edit.* **1993**, *32*, 854-858.
62. B. L. Feringa, *J. Org. Chem.* **2007**, *72*, 6635-6652.
63. E. Kay, D. Leigh, F. Zerbetto, *Angew. Chem., Int. Edit.* **2007**, *46*, 72-191.
64. N. Koumura, R. W. J. Zijlstra, R. A. van Delden, N. Harada, B. L. Feringa, *Nature* **1999**, *401*, 152-155.
65. M. von Delius, E. M. Geertsema, D. A. Leigh, *Nat. Chem.* **2010**, *2*, 96-101.
66. H. Tian, Q. C. Wang, Cyclodextrin-Based Switches, *Molecular Switches*, Eds. B. L. Feringa, W. R. Browne, Wiley-VCH **2011** 9, 301-319.
67. S. Tsukagoshi, A. Miyawaki, Y. Takashima, H. Yamaguchi, A. Harada, *Org. Lett.* **2007**, *9*, 1053-1055.
68. Y. Zheng, A. Hashidzume, Y. Takashima, H. Yamaguchi, A. Harada, *Nat. Commun.* **2012**, *3*, 831.
69. R. J. Coulston, H. Onagi, S. F. Lincoln, C. J. Easton, *J. Am. Chem. Soc.* **2006**, *128*, 14750-14751.
70. Y. Liu, G. S. Chen, Y. Chen, F. Ding, T. Liu, Y. L. Zhao, *Bioconj. Chem.* **2004**, *15*, 300-306.
71. Y. L. Zhao, W. R. Dichtel, A. Trabolsi, S. Saha, I. Aprahamian, J. F. Stoddart, *J. Am. Chem. Soc.* **2008**, *130*, 11294-11296.
72. C. Garcia-Iriepa, M. Marazzi, L. M. Frutos, D. Sampedro, *RSC Advances* **2013**, 6241-6266.
73. R. E. Dawson, S. F. Lincoln, C. J. Easton, *Chem. Commun.* **2008**, 3980-3982.
74. J. M. Berg, J. L. Tymoczko, L. Stryer, *Biochemistry*, 6th Edition ed., W. H. Freeman and Company, New York, **2007**.
75. V. Hornak, S. Ahuja, M. Eilers, J. A. Goncalves, M. Sheves, P. J. Reeves, S. O. Smith, *J. Mol. Biol.* **2010**, *396*, 510-527.
76. B. H. Blehm, P. R. Selvin, *Chem. Rev.* **2014**, *114*, 3335-3352.
77. P. Karagiannis, Y. Ishii, T. Yanagida, *Chem. Rev.* **2014**, *114*, 3318-3334.
78. G. Oster, H. Wang, *Biochim. Biophys. Acta Bioenergetics* **2000**, *1458*, 482-510.
79. B. Lewandowski, G. De Bo, J. Ward, M. Papmeyer, S. Kuschel, M. Aldegunde, P. Gramlich, D. Heckmann, S. Goldup, D. D'Souza, A. Fernandes, D. Leigh, *Science* **2013**, *339*, 189-193.
80. R. Dawson, S. Lincoln, C. Easton, *Chem. Commun.* **2008**, 3980-3982.
81. M. Zelzer, R. V. Ulijn, *Chem. Soc. Rev.* **2010**, 3351-3357.
82. D. Mandal, A. N. Shirazi, K. Parang, *Org. Biomol. Chem.* **2014**, 3544-3561.
83. N. J. Greenfield, *Nat. Protoc.* **2006**, *1*, 2876-2890.
84. R. Chapman, M. Danial, M. L. Koh, K. A. Jolliffe, S. Perrier, *Chem. Soc. Rev.* **2012**, 6023-6041.
85. C. Q. Yan, D. J. Pochan, *Chem. Soc. Rev.* **2010**, *39*, 3528-3540.
86. C. A. E. Hauser, S. G. Zhang, *Chem. Soc. Rev.* **2010**, *39*, 2780-2790.
87. J. Rodriguez-Hernandez, S. Lecommandoux, *J. Am. Chem. Soc.* **2005**, *127*, 2026-2027.
88. D. P. Weimann, H. D. F. Winkler, J. A. Falenski, B. Koksch, C. A. Schalley, *Nat. Chem.* **2009**, *1*, 573-577.
89. H. Onagi, J. Rebek, *Chem. Commun.* **2005**, 4604-4606.
90. A. Moretto, I. Menegazzo, M. Crisma, E. J. Shotton, H. Nowell, S. Mammi, C. Toniolo, *Angew. Chem., Int. Edit.* **2009**, 8986-8989.
91. R. d. l. Rica, L. W. Chow, C. M. Horejs, M. Mazo, C. Chiappini, E. T. Pashuck, R. Bitton, M. M. Stevens, *Chem. Commun.* **2014**, 10648-10650.

92. N. Ashkenasy, W. S. Horne, M. R. Ghadiri, *Small* **2006**, *2*, 99-102.
93. D. Ivnitski, M. Amit, B. Rubinov, R. Cohen-Luria, N. Ashkenasy, G. Ashkenasy, *Chem. Commun.* **2014**, 6733-6736.
94. J. R. Dunetz, C. Sandstrom, E. R. Young, P. Baker, S. A. V. Name, T. Cathopolous, R. Fairman, J. C. d. Paula, K. S. Akerfeldt, *Org. Lett.* **2005**, *7*, 2559-2561.
95. J. Ryu, S. Y. Lim, C. B. Park, *Adv. Mater.* **2009**, 1577-1581.
96. K. J. Channon, G. L. Devlin, S. W. Magennis, C. E. Finlayson, A. K. Tickler, C. Silva, C. E. MacPhee, *J. Am. Chem. Soc.* **2008**, 5487-5491.
97. K. J. Channon, G. L. Devlin, C. E. MacPhee, *J. Am. Chem. Soc.* **2009**, 12520-12521.
98. L. Chen, S. Revel, K. Morris, D. J. Adams, *Chem. Commun.* **2010**, 4267-4269.
99. G. R. Dieckmann, A. B. Dalton, P. A. Johnson, J. Razal, J. Chen, G. M. Giordano, E. Munoz, I. H. Musselman, R. H. Baughman, R. K. Draper, *J. Am. Chem. Soc.* **2003**, 1770-1777.
100. J. Y. Shim, V. K. Gupta, *J. Colloid Interface Sci.* **2007**, 977-983.
101. D. A. Walker, V. K. Gupta, *Nanotechnology* **2008**.
102. A. Laromaine, L. Koh, M. Murugesan, R. V. Ulijn, M. M. Stevens, *J. Am. Chem. Soc.* **2007**, *14*, 4156-4157.
103. T. R. Soderling, J. T. Stull, *Chem. Rev.* **2001**, *101*, 2341-2351.
104. M. J. Pandya, E. Cerasoli, A. Joseph, R. G. Stoneman, E. Waite, D. N. Woolfson, *J. Am. Chem. Soc.* **2004**, 17016-17024.
105. W. Li, I.-s. Park, S.-K. Kang, M. Lee, *Chem. Commun.* **2012**, *48*, 8796-8798.
106. S. Zhang, M. A. Greenfield, A. Mata, L. C. Palmer, R. Bitton, J. R. Mantei, C. Aparicio, M. O. d. l. Cruz, S. I. Stupp, *Nat. Mater.* **2010**, 594-601.
107. W. Li, I. S. Park, S. K. Kang, M. Lee, *Chem. Commun.* **2012**, *48*, 8796-8798.
108. C. S. Chen, X. D. Xu, S. Y. Li, R. X. Zhuo, X. Z. Zhang, *Nanoscale* **2013**, 6270-6274.
109. M. Ueno, A. Murakami, K. Makino, T. Morii, *J. Am. Chem. Soc.* **1993**, *115*, 12575-12576.
110. U. Masaru, M. Akira, M. Keisuke, M. Takashi, *J. Am. Chem. Soc.* **1993**, *115*.
111. E. Oheix, A. F. A. Peacock, *Chem. Eur. J.* **2014**, 2829-2839.
112. J. Mosquera, M. I. Sanchez, M. E. Vazquez, J. L. Mascarenas, *Chem. Commun.* **2014**, 10975-10978.
113. D. T. Dang, H. D. Nguyen, M. Merkx, L. Brunsveld, *Angew. Chem., Int. Edit.* **2013**, 2915-2919.
114. S. Gordo, V. Martos, E. Santos, M. Menéndez, C. Bo, E. Giralt, J. de Mendoza, *Proc. Natl. Acad. Sci. U.S.A.* **2008**, *105*, 16426-16431.
115. J. J. Reczek, A. A. Kennedy, B. T. Halbert, A. R. Urbach, *J. Am. Chem. Soc.* **2009**, 2408-2415.
116. J. W. Lee, S. W. Heo, S. J. C. Lee, J. Y. Ko, H. Kim, H. I. Kim, *J. Am. Soc. Mass Spectrom.* **2013**, 21-29.
117. S. Sakamoto, K. Kudo, *J. Am. Chem. Soc.* **2008**, 9574-9582.
118. W. Szymanski, J. M. Beierle, H. A. V. Kistemaker, W. A. Velema, B. L. Feringa, *Chem. Rev.* **2013**, *113*, 6114-6178.
119. M. Blanco-Lomas, S. Samanta, P. Campos, G. Woolley, D. Sampedro, *J. Am. Chem. Soc.* **2012**, *134*, 6960-6963.
120. A. Ueno, T. Shimizu, H. Mihara, K. Hamasaki, K. Pitchumani, *J. Incl. Phenom. Macrocycl. Chem.* **2002**, *44*, 49-52.
121. S. Tashiro, M. Kobayashi, M. Fujita, *J. Am. Chem. Soc.* **2006**, *128*, 9280-9281.
122. C. Clavel, K. Fournel-Marotte, F. Coutrot, *Molecules* **2013**, 11553-11575.

123. A. J. Blake, N. R. Champness, P. Hubberstey, W.-S. Li, M. A. Withersby, M. Schroder, *Coord. Chem. Rev.* **1999**, *183*, 117-138.
124. J. H. K. K. Hirschberg, L. Brunsveld, A. Ramzi, J. A. J. M. Vekemans, R. P. Sijbesma, E. W. Meijer, *Nature* **2000**, *407*, 167.
125. B. D. Wall, A. E. Zacca, A. M. Sanders, W. L. Wilson, A. L. Ferguson, J. D. Tovar, *Langmuir* **2014**, *30*, 5946-5956.
126. S. Gonen, F. DiMaio, T. Gonen, D. Baker, *Science* **2015**, *348*, 1365-1368.
127. A. R. Hirst, B. Escuder, J. F. Miravet, D. K. Smith, *Angew. Chem., Int. Edit.* **2008**, *47*, 8002-8018.
128. H. Y. Lee, Ph.D. Thesis, The Australian National University **2014**.
129. K. Miyamae, M. Nakahata, Y. Takashima, A. Harada, *Angew. Chem., Int. Edit.* **2015**, *54*, 8984-8987.
130. A. Harada, J. Li, M. Kamachi, *Nature* **1992**, *356*, 325-327.
131. D. B. Amabilino, P. R. Ashton, A. S. Reder, N. Spencer, J. F. Stoddart, *Angew. Chem., Int. Edit.* **1994**, *33*, 1286-1290.
132. X. Wang, K. Han, J. Li, X. Jia, C. Li, *Polym. Chem.* **2013**, *4*, 3998-4003.
133. T. Kaneda, T. Yamada, T. Fujimoto, Y. Sakata, *Chemistry Letters* **2001**, 1264-1265.
134. Y. Liu, Z. Fan, H. Y. Zhang, Y. W. Yang, F. Ding, S. X. Liu, X. Wu, T. Wada, Y. Inoue, *J. Org. Chem.* **2003**, *68*, 8345-8352.
135. N. Tomimasu, A. Kanaya, Y. Takashima, H. Yamaguchi, A. Harada, *J. Am. Chem. Soc.* **2009**, *131*, 12339-12343.
136. M. Miyauchi, Y. Takashima, H. Yamaguchi, A. Harada, *J. Am. Chem. Soc.* **2005**, *127*, 2984-2989.
137. T. Hoshino, M. Miyauchi, Y. Kawaguchi, H. Yamaguchi, A. Harada, *J. Am. Chem. Soc.* **2000**, *122*, 9876-9877.
138. Y. Liu, Z. X. Yang, Y. Chen, *J. Org. Chem.* **2008**, *73*, 5298-5304.
139. G. Du, E. Moulin, N. Jouault, E. Buhler, N. Giuseppone, *Angew. Chem., Int. Edit.* **2012**, *51*, 12504-12508.
140. L. Gao, Z. Zhang, B. Zheng, F. Huang, *Polym. Chem.* **2014**, *5*, 5734-5739.
141. N. H. Evans, P. D. Beer, *Chem. Eur. J.* **2011**, *17*.
142. T. Fujimoto, A. Nakamura, Y. Inoue, Y. Sakata, T. Kaneda, *Tetrahedron Lett.* **2001**, *42*, 7987-7989.
143. S. H. Chiu, S. J. Rowan, S. J. Cantrill, J. F. Stoddart, A. J. P. White, *Chem. Commun.* **2002**, 2948-2949.
144. G. Dun, E. Moulin, N. Jouault, E. Buhler, N. Giuseppone, *Angew. Chem., Int. Edit.* **2012**, *51*, 12504-12508.
145. M. C. Jimenez, C. Dietrich-Buchecker, J. P. Sauvage, *Angew. Chem., Int. Edit.* **2000**, *39*, 3284-3287.
146. F. Coutrot, C. Romuald, E. Busseron, *Org. Lett.* **2008**, *10*, 3741-3744.
147. J. Zhang, Honour's Thesis, The Australian National University **2008**.
148. H. Ogino, *New Journal of Chemistry* **1993**, *17*, 683-688.
149. S. F. Lincoln, C. J. Easton, *Modified Cyclodextrins*, Blackwell, **1999**.
150. R. E. Dawson, S. Maniam, S. F. Lincoln, C. J. Easton, *Org. Biomol. Chem.* **2008**, *6*, 1814-1821.
151. Y. P. Wang, N. Ma, Z. Q. Wang, X. Zhang, *Angew. Chem., Int. Edit.* **2007**, *46*, 2823-2826.
152. M. V. Rekharsky, Y. Inoue, *Chem. Rev.* **1998**, *98*, 1875-1917.
153. N. Greenfield, *Nat. Protoc.* **2006**, *1*, 2527-2535.
154. S. Tsuda, Y. Aso, T. Kaneda, *Chem. Commun.* **2006**, 3072-3074.

155. H. Murakami, A. Kawabuchi, R. Matsumoto, T. Ido, N. Nakashima, *J. Am. Chem. Soc.* **2005**, *127*, 15891-15899.
156. T. P. Zhang, L. X. Mu, G. W. She, W. S. Shi, *Chem. Commun.* **2012**, *48*, 452-454.
157. D.-H. Qu, Q.-C. Wang, H. Tian, *Angew. Chem., Int. Edit.* **2005**, *44*, 5296-5299.
158. H. Tian, Q.-C. Wang, *Chem. Soc. Rev.* **2006**, *35*, 361-374.
159. J. Graf, P. H. Nguyen, G. Stock, H. Schwalbe, *J. Am. Chem. Soc.* **2007**, *129*, 1179-1189.
160. R. V. Pappu, G. D. Rose, *Protein Sci.* **2002**, *11*, 2437-2455.
161. G. Lanza, U. Chiacchio, S. Motta, S. Pellegrino, G. Broggini, *ChemPhysChem* **2011**, *12*, 2724-2727.
162. T. Asakura, M. Okonogi, K. Horiguchi, A. Aoki, H. Saito, D. P. Knight, M. P. Williamson, *Angew. Chem., Int. Edit.* **2012**, *51*.
163. M. Kodaka, *J. Am. Chem. Soc.* **1993**, *115*, 3702-3705.
164. A. A. Beharry, G. A. Woolley, *Chem. Soc. Rev.* **2011**, *40*, 4422-4437.
165. E. E. Tucker, S. D. Christian, *J. Am. Chem. Soc.* **1984**, *106*, 1942-1945.
166. J. Carrazana, A. Jover, F. Meijide, V. H. Soto, J. V. Tato, *J. Phys. Chem. B* **2005**, *109*, 9719-9726.
167. R. J. Coulston, Ph.D. Thesis, The Australian National University **2009**.
168. A. C. Gibbs, T. C. Bjorndahl, R. S. Hodges, D. S. Wishart, *J. Am. Chem. Soc.* **2002**, *124*, 1203-1213.
169. C. Toniolo, G. Bonora, M. Mutter, *J. Am. Chem. Soc.* **1979**, *101*, 450-454.
170. M. V. Rekharsky, M. P. Mayhew, R. N. Goldberg, P. D. Ross, Y. Yamashoji, Y. Inoue, *J. Phys. Chem. A* **1997**, *101*, 87-100.
171. M. S. Lin, L. Y. Chen, H. T. Tsai, S. S. S. Wang, Y. Chang, A. Higuchi, W. Y. Chen, *Langmuir* **2008**, *24*, 5802-5808.
172. J.-L. Foo, C. J. Jackson, P. D. Carr, H.-K. Kim, G. Schenk, L. R. Gahan, D. L. Ollis, *Biochem. J.* **2010**, *429*, 313-321.
173. N. Obradors, E. Cabiscol, J. Aguilar, J. Ros, *FEBS Journal* **1998**, *258*, 207-213.
174. F. Yu, V. M. Cangelosi, M. L. Zastrow, M. Tegoni, J. S. Plegaria, A. G. Tebo, C. S. Mocny, L. Ruckthong, H. Qayyum, V. L. Pecoraro, *Chem. Rev.* **2014**, *114*, 3495-3578.
175. T. R. Ward, *Acc. Chem. Res.* **2011**, *44*, 47-57.
176. F. Rosati, G. Roelfes, *ChemCatChem* **2010**, *2*, 916-927.
177. J.-N. Rebilly, B. Colasson, O. Bistri, D. Over, O. Reinaud, *Chem. Soc. Rev.* **2015**, *44*, 467-489.
178. Z. Dong, Q. Luo, J. Liu, *Chem. Soc. Rev.* **2012**, *41*, 7890-7908.
179. J. E. Padilla, C. Colovos, T. O. Yeates, *Proc. Natl. Acad. Sci. U.S.A.* **2001**, *98*, 2217-2221.
180. Y.-T. Lai, D. Cascio, T. O. Yeates, *Science* **2012**, *336*, 1129.
181. A. R. D. Voet, H. Noguchi, C. Addy, K. Y. J. Zhang, J. R. H. Tame, *Angew. Chem., Int. Edit.* **2015**, *54*, 9857-9860.
182. A. Medina-Morales, A. Perez, J. D. Brodin, F. A. Tezcan, *J. Am. Chem. Soc.* **2013**, *135*, 12013-12022.
183. B.-C. Lee, T. K. Chu, K. A. Dill, R. N. Zuckermann, *J. Am. Chem. Soc.* **2008**, *130*, 8847-8855.
184. J. P. Miller, M. S. Melicher, A. Schepartz, *J. Am. Chem. Soc.* **2014**, *136*, 14726-14729.
185. C. M. Rufo, Y. S. Moroz, O. V. Moroz, J. Stohr, T. A. Smith, X. Hu, W. F. DeGrado, I. V. Korendovych, *Nat. Chem.* **2014**, *6*, 303-309.

186. N. P. King, W. Sheffler, M. R. Sawaya, B. S. Vollmar, J. P. Sumida, I. Andre, T. Gonen, T. O. Yeates, D. Baker, *Science* **2012**, *336*, 1171-1174.
187. C. Kallay, K. Varnagy, G. Malandrinos, N. Hadjiliadis, D. Sanna, I. Sovago, *Inorg. Chim. Acta.* **2009**, *362*, 935-945.
188. V. K. Sarin, S. B. H. Kent, A. R. Mitchell, R. B. Merrifield, *J. Am. Chem. Soc.* **1984**, *106*, 7845-7850.
189. J. P. Tam, Y. A. Lu, *J. Am. Chem. Soc.* **1995**, *117*, 12058-12063.
190. L. Zhou, S. Li, Y. Su, X. Yi, A. Zheng, F. Deng, *J. Phys. Chem. B* **2013**, *117*, 8954-8965.
191. S. Barranco-Medina, S. Kakorin, J. J. Lazaro, K. J. Dietz, *Biochemistry* **2008**, *47*, 7196-7204.
192. M. Kabiri, I. Bushnak, M. T. McDermot, L. D. Unsworth, *Biomacromolecules* **2013**, *14*, 3943-3950.
193. R. I. Gelb, L. M. Schwartz, *J. Incl. Phenom. Mol. Recognit. Chem.* **1989**, *7*, 465-476.
194. P. Thordarson, *Chem. Soc. Rev.* **2011**, *40*, 1305-1323.
195. J. M. Stewart, J. D. Young, *Solid phase peptide synthesis*, Pierce Chemical Co., **1984**.
196. M. Amblard, J.-A. Fehrentz, J. Martinez, G. Subra, Fundamentals of Modern Peptide Synthesis, *Peptide Synthesis and Applications*, Ed. J. Howl, Humana Press **2005**.
197. www.rapp-polymere.com.
198. M. Amblard, J.-A. Fehrentz, J. Martinez, G. Subra, *Mol. Biotechnol.* **2006**, *33*, 239-254.
199. H. Onagi, C. J. Easton, S. F. Lincoln, *Org. Lett.* **2001**, *3*, 1041-1044.
200. H. Onagi, C. J. Blake, C. J. Easton, S. F. Lincoln, *Chem. Eur. J.* **2003**, *9*, 5978-5988.
201. A. Harada, J. Li, M. Kamachi, *Macromolecules* **1993**, *26*, 5698-5703.
202. C. Schmuck, M. Heil, *Org. Biomol. Chem.* **2003**, *1*, 633-636.
203. A. Aggeli, M. Bell, N. Boden, J. N. Keen, T. C. B. McLeish, I. Nyrkova, S. E. Radford, A. Semenov, *J. Mater. Chem.* **1997**, *7*, 1135-1145.
204. A. Aggeli, M. Bell, N. Boden, J. N. Keen, P. F. Knowles, T. C. B. McLeish, M. Pitkeathly, S. E. Radford, *Nature* **1997**, *386*, 259-262.
205. J. Dong, J. E. Shokes, R. A. Scott, D. G. Lynn, *J. Am. Chem. Soc.* **2006**, *128*, 3540-3542.
206. H. Kuhnle, H. G. Borner, *Angew. Chem., Int. Edit.* **2009**, *48*, 6431-6434.
207. S. Winkler, D. Wilson, D. L. Kaplan, *Biochemistry* **2000**, *39*, 12739-12746.
208. L. A. Haines, K. Rajagopal, B. Ozbas, D. A. Salick, D. J. Pochan, J. P. Schneider, *J. Am. Chem. Soc.* **2005**, *127*, 17025-17029.
209. S. Wang, Q. Shen, M. H. Nawaz, W. Zhang, *Polym. Chem.* **2013**, *4*, 2151-2157.
210. E. J. F. Klotz, T. D. W. Claridge, H. L. Anderson, *J. Am. Chem. Soc.* **2006**, *128*, 15374-15375.
211. J. H. Coates, C. J. Easton, S. J. v. Eyk, S. F. Lincoln, B. L. May, C. B. Whalland, M. L. Williams, *J. Chem. Soc., Perkin Trans. 1* **1990**, 2619-2620.
212. J. D. Hartgerink, E. Beniash, S. I. Stupp, *Proc. Natl. Acad. Sci. U.S.A.* **2002**, *99*, 5133-5138.
213. S. Bai, S. Debnath, N. Javid, P. W. J. M. Frederix, S. Fleming, C. Pappas, R. V. Ulijn, *Langmuir* **2014**, *30*, 7576-7584.
214. R. Afrasiabi, H.-B. Kraatz, *Chem. Eur. J.* **2013**, *19*, 15862-15871.
215. R. Gong, Y. Song, Z. Guo, M. Li, Y. Jiang, X. Wan, *Supramol. Chem.* **2013**, *25*, 269-275.

216. R. Jayakumar, M. Murugesan, C. Asokan, M. A. Scibioh, *Langmuir* **2000**, *16*, 1489-1496.
217. A. Mantion, A. G. Guex, A. Foelske, L. Mirolo, K. M. Fromm, M. Painsi, A. Taubert, *Soft Matter* **2008**, *4*, 606-617.
218. J. Makarevic, M. Jokic, L. Frkanec, V. Caplar, N. S. Vujicic, M. Zinic, *Beilstein J. Org. Chem.* **2010**, *6*, 945-959.
219. J. H. van Esch, B. L. Feringa, *Angew. Chem., Int. Edit.* **2000**, *39*, 2263-2266.
220. Y. Ohsedo, *Polymer. Adv. Tech.* **2016**, *27*, 704-711.
221. S. Bhattacharya, Y. Krishnan-Ghosh, *Chem. Commun.* **2001**, 185-186.
222. C.-C. Tsai, Y.-T. Cheng, L.-C. Shen, K.-C. Chang, I.-T. Ho, J.-H. Chu, W.-S. Chung, *Org. Lett.* **2013**, *15*, 5830-5833.
223. A. Vintiloiu, J.-C. Leroux, *J. Control. Release* **2008**, *125*, 179-192.
224. N. E. Hughes, A. J. Wright, M. A. Rogers, J. W. E. Rush, A. G. Marangoni, *Trends Food Sci. Technol.* **2009**, *20*, 470-480.
225. P. Kirilov, S. Rum, E. Gilbert, L. Roussel, D. Salmon, R. Abdayem, C. Serre, C. Villa, M. Haftek, F. Falson, F. Pirot, *Int. J. Cosmet. Sci.* **2014**, *36*, 336-346.
226. Z. Huo, S. Dai, C. Zhang, F. Kong, X. Fang, L. Guo, W. Liu, L. Hu, X. Pan, K. Wang, *J. Phys. Chem. B* **2008**, *112*, 12927-12933.
227. S. Srinivasan, P. A. Babu, S. Mahesh, A. Ajayaghosh, *J. Am. Chem. Soc.* **2009**, *131*, 15122-15123.
228. P. Koley, A. Pramanik, *Soft Matter* **2012**, *8*, 5364-5374.
229. K. Sugiyasu, N. Fujita, S. Shinkai, *Angew. Chem., Int. Edit.* **2004**, *43*, 1229-1233.
230. M. R. Caplan, E. M. Schwartzfab, S. Zhang, R. D. Kamm, D. A. Lauffenburger, *J. Biomater. Sci., Polm. Ed.* **2002**, *13*, 225-236.
231. E. T. Pashuck, H. Cui, S. I. Stupp, *J. Am. Chem. Soc.* **2010**, *132*, 6041-6046.
232. X. Luo, B. Liu, Y. Liang, *Chem. Commun.* **2001**, 1556-1557.
233. S. Fleming, R. V. Ulijn, *Chem. Soc. Rev.* **2014**, *43*, 8150-8177.
234. N. Greenfield, *Nat. Protoc.* **2006**, *1*, 2876-2890.
235. S. Y. Venyaminov, F. G. Prendergast, *Anal. Biochem.* **1997**, *248*, 234-245.
236. E. Goormaghtigh, J.-M. Ruysschaert, V. Raussens, *Biophys. J.* **2006**, *90*, 2946-2957.
237. Y. Yamaoki, H. Imamura, A. Fulara, S. Wojcik, L. Bozycki, M. Kato, T. A. Keiderling, W. Dzwolak, *J. Phys. Chem. B* **2012**, *116*, 5172-5178.
238. E. T. Pashuck, H. Cui, S. I. Stupp, *J. Am. Chem. Soc.* **2010**, *132*, 6041-6046.
239. J. D. Hartgerink, E. Beniash, S. I. Stupp, *Proc. Natl. Acad. Sci. U.S.A.* **2002**, *99*, 5133-5138.
240. J. H. Ortony, C. J. Newcomb, J. B. Matson, L. C. Palmer, P. E. Doan, B. M. Hoffman, S. I. Stupp, *Nat. Mater.* **2014**, *13*, 812-816.
241. T. Kar, S. K. Mandal, P. K. Das, *Chem. Eur. J.* **2011**, *17*, 14952-14961.
242. J. S. Fetrow, *FASEB J.* **1995**, *9*, 708-717.
243. M. Murphy, J. S. Fetrow, R. E. Burton, G. D. Brayer, *Protein Sci.* **1993**, *2*, 1429-1440.
244. Y. W. Bai, T. R. Sosnick, L. Mayne, S. W. Englander, *Science* **1995**, *269*, 192-197.
245. A. M. C. Marcelino, L. M. Gierasch, *Biopolymers* **2008**, *89*, 380-391.
246. K. C. Chou, *Anal. Biochem.* **2000**, *286*, 1-16.
247. B. L. Sibanda, J. M. Thornton, *Nature* **1985**, *316*, 170-174.
248. E. L. McCallister, E. Alm, D. Baker, *Nat. Struct. Bio.* **2000**, *7*, 669-673.
249. G. Bellot, S. Granier, W. Bourguet, R. Seyer, R. Rahmeh, B. Mouillac, R. Pascal, C. Mendre, H. Déméné, *J. Mol. Biol.* **2009**, *388*, 491-507.

250. J. C. Wei, J. Dobnikar, T. Curk, F. Song, *PLOS ONE* **2016**, *11*.
251. R. Chapanian, D. H. Kwan, I. Constantinescu, F. A. Shaikh, N. A. A. Rossi, S. G. Withers, J. N. Kizhakkedathu, *Nat. Commun.* **2014**, *5*.
252. A. C. Sohnel, W. Kohl, I. Gregor, J. Enderlein, B. Rieger, K. B. Busch, *Biochim. Biophys. Acta* **2016**, *1857*, 1290-1299.
253. S. Mittal, R. K. Chowhan, L. R. Singh, *Biochim. Biophys. Acta* **2015**, *1850*, 1822-1831.
254. N. C. Shirai, M. Kikuchi, *J. Chem. Phys.* **2016**, *144*, 055101.
255. B. C. McNulty, G. B. Young, G. J. Pielak, *J. Mol. Biol.* **2006**, *355*, 893-897.
256. C. F. Lee, S. Bird, M. Shaw, L. Jean, D. J. Vaux, *J. Biol. Chem.* **2012**, *287*, 38006-38019.
257. V. Rincón, R. Bocanegra, A. Rodríguez-Huete, G. Rivas, M. G. Mateu, *Biophys. J.* **2011**, *100*, 738-746.
258. S. Tímári, R. Cerea, K. Várnagy, *J. Inorg. Biochem.* **2011**, *105*, 1009-1017.
259. V. Joszai, I. Turi, C. Kallay, G. Pappalardo, G. D. Natale, E. Rizzarelli, I. Sovago, *J. Inorg. Biochem.* **2012**, *112*, 17-24.
260. S. S. Kidambi, D. K. Lee, A. Ramamoorthy, *Inorg. Chem.* **2003**, *42*, 3142-3151.
261. S. E. Brown, J. H. Coates, D. R. Coghlan, C. J. Easton, S. J. Vaneyk, W. Janowski, A. Lepore, S. F. Lincoln, Y. Luo, B. L. May, D. S. Schiesser, P. Wang, M. L. Williams, *Aus. J. Chem.* **1993**, *46*, 953-958.
262. K. Hamasaki, H. Ikeda, A. Nakamura, A. Ueno, F. Toda, I. Suzuki, T. Osa, *J. Am. Chem. Soc.* **1993**, *115*, 5035-5040.
263. V. Bonnet, R. Duval, V. Tran, C. Rabiller, *Eur. J. Org. Chem.* **2003**, *24*, 4810-4818.
264. S. M. Soltis, A. E. Cohen, A. Deacon, T. Eriksson, A. Gonzalez, S. McPhillips, H. Chui, P. Dunten, M. Hollenbeck, I. Mathews, M. Miller, P. Moorhead, R. P. Phizackerley, C. Smith, J. Song, H. van dem Bedem, P. Ellis, P. Kuhn, T. McPhillips, N. Sauter, K. Sharp, I. Tsyba, G. Wolf, *Acta Crystallogr. D* **2008**, *64*, 1210-1221.
265. T. McPhillips, S. McPhillips, H.-S. Chiu, A. E. Cohen, A. Deacon, P. J. Ellis, E. F. Garman, A. Gonzalez, N. Sauter, R. P. Phizackerley, S. M. Soltis, P. Kuhn, *J. Synchrotron Radiat.* **2002**, *9*, 401-406.
266. T. G. G. Battye, L. Kontogiannis, O. Johnson, H. R. Powell, A. G. W. Leslie, *Acta Crystallogr. D* **2011**, *67*, 271-281.
267. T. C. Terwilliger, P. D. Adams, R. J. Read, A. J. McCoy, N. W. Moriarty, R. W. Grosse-Kunstleve, P. V. Afonine, P. H. Zwart, L. W. Hung, *Acta Crystallogr. D* **2009**, *65*, 582-601.
268. M. Rejzek, C. E. Stevenson, A. M. Southard, D. Stanley, K. Denyer, A. M. Smith, M. J. Naldrett, D. M. Lawson, R. A. Field, *Mol. Biosyst.* **2011**, *7*, 718-730.
269. P. Emsley, K. Cowtan, *Acta Crystallogr. D* **2004**, *60*, 2126-2132.
270. P. V. Afonine, R. W. Grosse-Kunstleve, N. Echols, J. J. Headd, N. W. Moriarty, M. Mustyakimov, T. C. Terwilliger, A. Urzhumtsev, P. H. Zwart, P. D. Adams, *Acta Crystallogr. D* **2012**, *68*, 352-367.
271. A. J. McCoy, R. W. Grosse-Kunstleve, P. D. Adams, M. D. Winn, L. C. Storoni, R. J. Read, *J. Appl. Crystallogr.* **2007**, *40*, 658-674.
272. Collaborative Computational Project Number 4, *Acta Crystallogr. D* **1994**, *50*, 760-763.
273. P. D. Adams, R. W. Grosse-Kunstleve, L. W. Hung, T. R. Ioerger, A. J. McCoy, N. W. Moriarty, R. J. Read, J. C. Sacchettini, N. K. Sauter, T. C. Terwilliger, *Acta Crystallogr. D* **2002**, *58*, 1948-1954.

274. S. K. Sharma, A. K. Sharma, L. A. Samuelson, J. Kumar, A. C. Watterson, V. S. Parmar, *J. Macromol. Sci.* **2004**, *41*, 1459-1466.
275. H. Onagi, C. Blake, C. Easton, S. Lincoln, *Chem. Eur. J.* **2003**, *9*, 5978-5988.

Appendix A

Calculations used for determining % dimer at a particular concentration (c), using dimer dissociation constant (K_d):

$$K_d = \frac{[\text{Monomer}]^2}{[\text{Dimer}]}$$

$$c = [\text{Monomer}] + 2[\text{Dimer}]$$

$$[\text{Monomer}] = c - 2[\text{Dimer}]$$

$$K_d = \frac{(c - 2[\text{Dimer}])^2}{[\text{Dimer}]}$$

$$[\text{Dimer}]\,K_d = (c - 2[\text{Dimer}])^2$$

$$[\text{Dimer}]\,K_d = c^2 - 4c[\text{Dimer}] + 4[\text{Dimer}]^2$$

$$K_d = \frac{c^2}{[\text{Dimer}]} - 4c + 4[\text{Dimer}]$$

$$0 = \frac{c^2}{[\text{Dimer}]} - 4c + 4[\text{Dimer}] - K_d$$

$$0 = c^2 - 4c[\text{Dimer}] - K_d[\text{Dimer}] + 4[\text{Dimer}]^2$$

The value for c, the concentration at which % dimer is to be determined can then be inputted, and the value for [Dimer] obtained by solving the resulting quadratic equation.

$$\%\ \text{Dimer} = \frac{2[\text{Dimer}]}{c} \times 100\%$$

The calculated K_a can then be checked against the measured K_a.

$$K_a = \frac{[\text{Dimer}]}{[\text{Monomer}]^2}$$

Calculations used for determining the concentration (c) at which a particular % dimer will be present, using dimer dissociation constant (K_d):

$$\text{Fraction of dimer (d)} = \frac{\%\ \text{dimer}}{100}$$

$$[\text{Dimer}] = (d/2) \times c$$

$$0 = \frac{c^2}{(d/2 \times c)} - 4c + 4((d/2) \times c) - K_d$$

$$0 = c^2 - 4c((d/2) \times c) - K_d((d/2) \times c) + 4((d/2) \times c)^2$$

The value for d, the fraction of dimer that is present at the concentration to be calculated, can then be inputted and the value for c obtained by solving the resulting quadratic equation. The calculation can then be checked be re-entering the concentration into the equation for determining % dimer.

Appendix B

Coordinates from the crystal of peptide **83** with Zn^{2+}.

Atom no.	Atom	Residue	Residue no.	Coordinates			Occupancy	B-Factor
1	N	Val	1	15.115	8.054	8.982	1.00	11.46
2	Cα	Val	1	15.832	7.836	10.226	1.00	11.85
3	C	Val	1	14.935	8.221	11.411	1.00	11.68
4	O	Val	1	14.152	9.169	11.330	1.00	10.62
5	Cβ	Val	1	17.164	8.632	10.229	1.00	15.47
6	Cγ1	Val	1	16.912	10.138	10.320	1.00	11.95
7	Cγ2	Val	1	18.048	8.179	11.349	1.00	15.55
8	H3	Val	1	14.956	8.947	8.671	1.00	13.75
9	Hα	Val	1	16.046	6.893	10.306	1.00	14.22
10	Hβ	Val	1	17.632	8.460	9.397	1.00	18.56
11	Hγ11	Val	1	17.765	10.601	10.319	1.00	14.34
12	Hγ12	Val	1	16.384	10.416	9.555	1.00	14.34
13	Hγ13	Val	1	16.432	10.329	11.141	1.00	14.34
14	Hγ21	Val	1	18.871	8.692	11.328	1.00	18.66
15	Hγ22	Val	1	17.589	8.324	12.191	1.00	18.66
16	Hγ23	Val	1	18.242	7.236	11.236	100	18.66
17	O	Val	2	15.992	8.585	14.997	1.00	16.48
18	N	Val	2	15.032	7.473	12.503	1.00	13.28
19	Cα	Val	2	14.192	7.745	13.660	1.00	15.03
20	C	Val	2	14.860	8.759	14.577	1.00	15.66
21	Cβ	Val	2	13.827	6.452	14.430	1.00	18.54
22	Cγ1	Val	2	13.046	6.779	15.700	1.00	18.83
23	Cγ2	Val	2	13.011	5.526	13.539	1.00	17.62
24	H	Val	2	15.569	6.808	12.599	1.00	15.93
25	Hα	Val	2	13.362	8.139	13.348	1.00	18.04

26	Hβ	Val	2	14.642	5.990	14.685	1.00	22.25
27	Hγ11	Val	2	12.832	5.952	16.161	1.00	22.59
28	Hγ12	Val	2	13.591	7.344	16.270	1.00	22.59
29	Hγ13	Val	2	12.230	7.243	15.457	1.00	22.59
30	Hγ21	Val	2	12.792	4.722	14.036	1.00	21.14
31	Hγ22	Val	2	12.198	5.982	13.270	1.00	21.14
32	Hγ23	Val	2	13.537	5.298	12.756	1.00	21.14
33	O	Val	3	12.322	11.355	16.452	1.00	18.43
34	N	Val	3	14.135	9.830	14.858	1.00	15.66
35	Cα	Val	3	14.564	10.842	15.804	1.00	20.55
36	C	Val	3	13.436	10.964	16.805	1.00	21.44
37	Cβ	Val	3	14.821	12.196	15.122	1.00	20.16
38	Cγ1	Val	3	15.251	13.230	16.146	1.00	24.64
39	Cγ2	Val	3	15.871	12.046	14.025	1.00	20.14
40	H	Val	3	13.370	9.996	14.502	1.00	18.79
41	Hα	Val	3	15.370	10.555	16.262	1.00	24.66
42	Hβ	Val	3	13.998	12.504	14.711	1.00	24.20
43	Hγ11	Val	3	15.407	14.075	15.695	1.00	29.57
44	Hγ12	Val	3	14.548	13.332	16.806	1.00	29.57
45	Hγ13	Val	3	16.067	12.928	16.575	1.00	29.57
46	Hγ21	Val	3	16.018	12.910	13.609	1.00	24.17
47	Hγ22	Val	3	16.697	11.725	14.421	1.00	24.17
48	Hγ23	Val	3	15.550	11.411	13.366	1.00	24.17
49	O	His	4	11.783	8.421	18.403	1.00	23.31
50	N	His	4	13.732	10.620	18.052	1.00	24.68
51	Cα	His	4	12.718	10.530	19.083	1.00	21.17
52	C	His	4	11.575	9.616	18.620	1.00	17.64
53	Cβ	His	4	12.230	11.922	19.459	1.00	22.42
54	Cγ	His	4	13.304	12.788	20.043	1.00	33.11
55	Nδ1	His	4	14.029	12.421	21.157	1.00	36.55
56	Cδ2	His	4	13.779	14.000	19.668	1.00	36.33

57	Cε1	His	4	14.903	13.369	21.445	1.00	35.93
58	Nε2	His	4	14.773	14.339	20.556	1.00	36.16
59	H	His	4	14.526	10.432	18.326	1.00	29.61
60	Hα	His	4	13.112	10.131	19.875	1.00	25.41
61	Hβ2	His	4	11.891	12.361	18.664	1.00	26.90
62	Hβ3	His	4	11.522	11.839	20.118	1.00	26.90
63	Hδ1	His	4	13.927	11.689	21.596	1.00	43.86
64	Hδ2	His	4	13.488	14.508	18.945	1.00	43.60
65	Hε1	His	4	15.507	13.356	22.151	1.00	43.12
66	O	Gly	5	7.594	9.336	16.359	1.00	11.93
67	N	Gly	5	10.383	10.170	18.462	1.00	18.28
68	Cα	Gly	5	9.235	9.372	18.070	1.00	16.38
69	C	Gly	5	8.746	9.636	16.662	1.00	13.32
70	H	Gly	5	10.212	11.006	18.576	1.00	21.94
71	Hα2	Gly	5	9.464	8.432	18.138	1.00	19.66
72	Hα3	Gly	5	8.503	9.549	18.681	1.00	19.66
73	N	Val	6	9.605	10.200	15.809	1.00	12.53
74	Cα	Val	6	9.230	10.462	14.426	1.00	11.94
75	C	Val	6	10.265	9.900	13.453	1.00	13.42
76	O	Val	6	11.394	9.586	13.835	1.00	12.59
77	Cβ	Val	6	9.014	11.965	14.150	1.00	13.65
78	Cγ1	Val	6	7.903	12.506	15.035	1.00	16.08
79	Cγ2	Val	6	10.295	12.759	14.354	1.00	15.71
80	H	Val	6	10.406	10.439	16.010	1.00	15.04
81	Hα	Val	6	8.390	10.012	14.247	1.00	14.33
82	Hβ	Val	6	8.739	12.077	13.227	1.00	16.38
83	Hγ11	Val	6	7.782	13.450	14.848	1.00	19.29
84	Hγ12	Val	6	7.084	12.023	14.844	1.00	19.29
85	Hγ13	Val	6	8.152	12.382	15.964	1.00	19.29
86	Hγ21	Val	6	10.118	13.695	14.171	1.00	18.85
87	Hγ22	Val	6	10.591	12.651	15.271	1.00	18.85

88	Hγ23	Val	6	10.973	12.426	13.745	1.00	18.85
89	N	Val	7	9.852	9.755	12.203	1.00	10.46
90	Cα	Val	7	10.728	9.270	11.157	1.00	10.04
91	C	Val	7	10.991	10.440	10.238	1.00	8.82
92	O	Val	7	10.064	11.077	9.760	1.00	10.66
93	Cβ	Val	7	10.104	8.115	10.363	1.00	11.29
94	Cγ1	Val	7	11.131	7.504	9.405	1.00	12.30
95	Cγ2	Val	7	9.577	7.058	11.306	1.00	13.18
96	H	Val	7	9.055	9.934	11.933	1.00	12.56
97	Hα	Val	7	11.569	8.973	11.539	1.00	12.04
98	Hβ	Val	7	9.361	8.451	9.838	1.00	13.55
99	Hγ11	Val	7	10.713	6.778	8.916	1.00	14.76
100	Hγ12	Val	7	11.432	8.189	8.787	1.00	14.76
101	Hγ13	Val	7	11.882	7.169	9.919	1.00	14.76
102	Hγ21	Val	7	9.187	6.337	10.786	1.00	15.81
103	Hγ22	Val	7	10.310	6.719	11.843	1.00	15.81
104	Hγ23	Val	7	8.902	7.455	11.879	1.00	15.81
105	O	Val	8	14.148	10.605	7.818	1.00	9.30
106	N	Val	8	12.266	10.715	10.000	1.00	9.02
107	Cα	Val	8	12.684	11.869	9.217	1.00	8.58
108	C	Val	8	13.232	11.422	7.873	1.00	7.89
109	Cβ	Val	8	13.777	12.656	9.956	1.00	8.81
110	Cγ1	Val	8	14.185	13.883	9.181	1.00	10.14
111	Cγ2	Val	8	13.286	13.066	11.323	1.00	12.04
112	H	Val	8	12.921	10.238	10.287	1.00	10.82
113	Hα	Val	8	11.926	12.455	9.066	1.00	10.30
114	Hβ	Val	8	14.559	12.093	10.069	1.00	10.57
115	Hγ11	Val	8	14.874	14.354	9.675	1.00	12.17
116	Hγ12	Val	8	14.527	13.610	8.315	1.00	12.17
117	Hγ13	Val	8	13.410	14.455	9.066	1.00	12.17
118	Hγ21	Val	8	13.988	13.561	11.774	1.00	14.45

119	Hγ22	Val	8	12.500	13.624	11.221	1.00	14.45
120	Hγ23	Val	8	13.064	12.270	11.830	1.00	14.45
121	N	Gly	9	12.672	11.975	6.798	1.00	8.99
122	C1A	ACX		11.008	10.388	3.159	1.00	8.68
123	C2A	ACX		11.730	10.571	1.867	1.00	7.80
124	C3A	ACX		13.199	10.353	2.044	1.00	9.04
125	C4A	ACX		13.766	11.119	3.190	1.00	7.93
126	C5A	ACX		12.949	11.009	4.467	1.00	9.44
127	C6A	ACX		13.442	12.030	5.525	1.00	8.95
128	O1A	ACX		11.145	9.027	3.548	1.00	9.38
129	O2A	ACX		11.155	9.686	0.842	1.00	8.81
130	O3A	ACX		13.878	10.738	0.813	1.00	9.13
131	O5A	ACX		11.519	11.242	4.304	1.00	8.32
132	C1B	ACX		9.317	5.451	4.630	1.00	12.53
133	C2B	ACX		9.030	5.924	3.237	1.00	11.72
134	C3B	ACX		9.991	7.028	2.845	1.00	12.00
135	C4B	ACX		9.992	8.104	3.853	1.00	11.61
136	C5B	ACX		10.091	7.654	5.304	1.00	10.86
137	C6B	ACX		9.801	8.841	6.244	1.00	9.73
138	O1B	ACX		10.651	5.098	4.646	1.00	13.05
139	O2B	ACX		9.115	4.814	2.312	1.00	13.68
140	O3B	ACX		9.644	7.544	1.499	1.00	12.32
141	O5B	ACX		9.189	6.553	5.695	1.00	11.24
142	O6B	ACX		8.510	9.348	5.951	1.00	11.02
143	C1C	ACX		13.095	1.764	5.412	1.00	16.19
144	C2C	ACX		12.166	1.686	4.249	1.00	14.83
145	C3C	ACX		11.540	3.023	3.898	1.00	15.31
146	C4C	ACX		10.911	3.695	5.061	1.00	14.94
147	C5C	ACX		11.799	3.671	6.319	1.00	15.58
148	C6C	ACX		10.933	4.073	7.489	1.00	16.12
149	O1C	ACX		14.107	2.628	5.007	1.00	14.29

150	O2C	ACX		12.912	1.146	3.107	1.00	16.37
151	O3C	ACX		10.529	2.880	2.846	1.00	15.96
152	O5C	ACX		12.490	2.383	6.671	1.00	17.72
153	O6C	ACX		11.805	4.444	8.546	1.00	25.70
154	C1D	ACX		18.283	2.720	4.959	1.00	16.07
155	C2D	ACX		17.620	1.956	3.838	1.00	16.24
156	C3D	ACX		16.102	2.145	3.833	1.00	16.39
157	C4D	ACX		15.488	2.042	5.158	1.00	15.08
158	C5D	ACX		16.221	2.777	6.251	1.00	16.28
159	C6D	ACX		15.550	2.493	7.594	1.00	20.99
160	O1D	ACX		18.025	4.044	4.680	1.00	15.76
161	O2D	ACX		18.211	2.394	2.575	1.00	19.60
162	O3D	ACX		15.426	1.177	2.937	1.00	17.68
163	O5D	ACX		17.660	2.487	6.372	1.00	16.85
164	O6D	ACX		15.383	1.087	7.706	1.00	28.39
165	C1E	ACX		19.762	7.846	4.549	1.00	11.78
166	C2E	ACX		20.312	6.813	3.585	1.00	12.30
167	C3E	ACX		19.427	5.578	3.524	1.00	12.23
168	C4E	ACX		19.165	5.008	4.873	1.00	13.90
169	C5E	ACX		18.788	6.028	5.922	1.00	13.00
170	C6E	ACX		18.842	5.389	7.351	1.00	15.38
171	O1E	ACX		18.512	8.135	4.115	1.00	9.59
172	O2E	ACX		20.476	7.406	2.257	1.00	11.95
173	O3E	ACX		20.022	4.564	2.634	1.00	15.21
174	O5E	ACX		19.572	7.283	6.008	1.00	12.36
175	O6E	ACX		20.175	5.395	7.830	1.00	17.79
176	C1F	ACX		16.085	11.529	3.606	1.00	8.56
177	C2F	ACX		17.147	11.289	2.562	1.00	8.83
178	C3F	ACX		17.721	9.890	2.683	1.00	8.58
179	C4F	ACX		18.161	9.602	4.065	1.00	8.25
180	C5F	ACX		17.090	9.894	5.079	1.00	8.97

181	C6F	ACX		17.513	9.537	6.541	1.00	10.40
182	O1F	ACX		15.134	10.571	3.399	1.00	7.90
183	O2F	ACX		16.589	11.545	1.250	1.00	8.32
184	O3F	ACX		18.820	9.689	1.725	1.00	8.67
185	O5F	ACX		16.621	11.284	5.050	1.00	8.41
186	O6F	ACX		18.734	10.189	6.889	1.00	9.58
187	H1A	ACX		10.060	10.583	3.019	1.00	10.41
188	H2A	ACX		11.596	11.502	1.577	1.00	9.36
189	H3A	ACX		13.355	9.394	2.203	1.00	10.85
190	H4A	ACX		13.834	12.061	2.938	1.00	9.51
191	H5A	ACX		13.069	10.119	4.824	1.00	11.33
192	H6A1	ACX		13.319	12.939	5.183	1.00	10.74
193	H6A2	ACX		14.403	11.875	5.712	1.00	10.74
194	HO2A	ACX		11.443	9.945	0.020	1.00	10.57
195	HO3A	ACX		14.351	10.035	0.499	1.00	10.96
196	H1B	ACX		8.754	4.682	4.857	1.00	15.03
197	H2B	ACX		8.114	6.286	3.214	1.00	14.06
198	H3B	ACX		10.895	6.646	2.806	1.00	14.40
199	H4B	ACX		9.166	8.608	3.753	1.00	13.93
200	H5B	ACX		11.010	7.358	5.463	1.00	13.03
201	H6B1	ACX		9.833	8.538	7.176	1.00	11.68
202	H6B2	ACX		10.467	9.539	6.105	1.00	11.68
203	HO2B	ACX		8.328	4.720	1.883	1.00	16.42
204	HO3B	ACX		10.217	7.220	0.900	1.00	14.79
205	HO6B	ACX		8.335	10.031	6.482	1.00	13.22
206	H1C	ACX		13.464	0.880	5.612	1.00	19.43
207	H2C	ACX		11.446	1.060	4.474	1.00	17.79
208	H3C	ACX		12.248	3.607	3.562	1.00	18.38
209	H4C	ACX		10.054	3.252	5.263	1.00	17.93
210	H5C	ACX		12.489	4.355	6.207	1.00	18.69
211	H6C1	ACX		10.373	4.826	7.243	1.00	19.34

212	H6C2	ACX		10.378	3.323	7.765	1.00	19.34
213	HO2C	ACX		12.538	0.375	2.844	1.00	19.65
214	HO3C	ACX		10.092	2.113	2.957	1.00	19.16
215	HO6C	ACX		11.330	4.712	9.239	1.00	30.84
216	H1D	ACX		19.243	2.552	4.972	1.00	19.29
217	H2D	ACX		17.812	1.004	3.960	1.00	19.48
218	H3D	ACX		15.919	3.040	3.494	1.00	19.67
219	H4D	ACX		15.411	1.094	5.403	1.00	18.10
220	H5D	ACX		16.131	3.735	6.071	1.00	19.53
221	H6D1	ACX		16.118	2.820	8.326	1.00	25.18
222	H6D2	ACX		14.682	2.932	7.628	1.00	25.18
223	HO2D	ACX		18.474	1.701	2.123	1.00	23.52
224	HO3D	ACX		15.769	1.242	2.114	1.00	21.21
225	HO6D	ACX		14.955	0.897	8.466	1.00	34.06
226	H1E	ACX		20.317	8.643	4.557	1.00	14.14
227	H2E	ACX		21.195	6.537	3.909	1.00	14.76
228	H3E	ACX		18.568	5.846	3.143	1.00	14.68
229	H4E	ACX		19.944	4.524	5.167	1.00	16.68
230	H5E	ACX		17.861	6.282	5.752	1.00	15.60
231	H6E1	ACX		18.511	4.450	7.306	1.00	18.45
232	H6E2	ACX		18.271	5.908	7.964	1.00	18.45
233	HO2E	ACX		21.344	7.398	2.031	1.00	14.34
234	HO3E	ACX		20.881	4.624	2.666	1.00	18.26
235	HO6E	ACX		20.169	5.400	8.738	1.00	21.35
236	H1F	ACX		15.703	12.429	3.520	1.00	10.27
237	H2F	ACX		17.882	11.936	2.719	1.00	10.59
238	H3F	ACX		17.004	9.254	2.459	1.00	10.29
239	H4F	ACX		18.966	10.142	4.273	1.00	9.90
240	H5F	ACX		16.318	9.326	4.852	1.00	10.77
241	H6F1	ACX		16.809	9.822	7.160	1.00	12.49
242	H6F2	ACX		17.633	8.576	6.613	1.00	12.49

243	HO2F	ACX		17.046	12.173	0.858	1.00	9.99
244	HO3F	ACX		18.809	8.860	1.437	1.00	10.41
245	C1	OQQ		13.796	5.710	-0.359	1.00	21.74
246	C2	OQQ		14.453	5.405	0.978	1.00	23.76
247	C3	OQQ		13.890	6.276	2.065	1.00	16.22
248	C4	OQQ		14.755	6.251	3.320	1.00	13.62
249	C5	OQQ		14.007	6.851	4.490	1.00	12.35
250	C6	OQQ		14.724	6.665	5.809	1.00	12.96
251	C7	OQQ		13.906	7.214	6.964	1.00	12.98
252	C8	OQQ		14.644	7.174	8.271	1.00	12.64
253	O8	OQQ		14.765	5.842	8.644	1.00	14.77
254	H11	OQQ		12.709	5.590	-0.323	1.00	26.09
255	H12	OQQ		13.969	6.745	-0.654	1.00	26.09
256	H13	OQQ		14.183	5.089	-1.169	1.00	26.09
257	H21	OQQ		15.543	5.529	0.871	1.00	28.51
258	H22	OQQ		14.330	4.334	1.207	1.00	28.51
259	H31	OQQ		13.771	7.302	1.688	1.00	19.46
260	H32	OQQ		12.856	5.955	2.288	1.00	19.46
261	H41	OQQ		15.060	5.213	3.544	1.00	16.35
262	H42	OQQ		15.709	6.781	3.146	1.00	16.35
263	H51	OQQ		13.815	7.925	4.311	1.00	14.82
264	H52	OQQ		12.990	6.420	4.550	1.00	14.82
265	H61	OQQ		14.958	5.597	5.978	1.00	15.55
266	H62	OQQ		15.720	7.144	5.780	1.00	15.55
267	H71	OQQ		12.968	6.642	7.084	1.00	15.57
268	H72	OQQ		13.567	8.248	6.775	1.00	15.57
269	H81	OQQ		15.624	7.706	8.191	1.00	15.17
270	H82	OQQ		14.123	7.799	9.040	1.00	15.17
271	H83	OQQ		13.894	5.536	8.889	1.00	17.72
272	Zn	Zn		15.967	15.944	20.917	0.18	30.45

Appendix C

Coordinates from the crystal of peptide **83** in the absence of Zn^{2+}.

Atom no.	Atom	Residue	Residue no.	Coordinates			Occupancy	B-Factor
1	N	Val	1	1.008	7.997	61.661	1.00	6.75
2	Cα	Val	1	0.273	8.197	62.902	1.00	7.28
3	C	Val	1	1.138	7.780	64.096	1.00	7.49
4	O	Val	1	1.900	6.817	64.009	1.00	6.97
5	Cβ	Val	1	-1.066	7.419	62.872	1.00	8.81
6	Cγ1	Val	1	-0.829	5.912	62.912	1.00	9.13
7	Cγ2	Val	1	-1.959	7.859	64.006	1.00	11.40
8	H3	Val	1	1.010	7.135	61.238	1.00	8.10
9	Hα	Val	1	0.067	9.140	62.997	1.00	8.74
10	Hβ	Val	1	-1.524	7.622	62.041	1.00	10.57
11	Hγ11	Val	1	-1.685	5.457	62.891	1.00	10.96
12	Hγ12	Val	1	-0.299	5.655	62.140	1.00	10.96
13	Hγ13	Val	1	-0.355	5.689	63.728	1.00	10.96
14	Hγ21	Val	1	-2.789	7.359	63.966	1.00	13.68
15	Hγ22	Val	1	-1.509	7.687	64.847	1.00	13.68
16	Hγ23	Val	1	-2.139	8.808	63.915	1.00	13.68
17	O	Val	2	0.077	7.405	67.741	1.00	15.26
18	N	Val	2	1.033	8.511	65.201	1.00	11.16
19	Cα	Val	2	1.865	8.233	66.369	1.00	12.34
20	C	Val	2	1.204	7.213	67.288	1.00	13.67
21	Cβ	Val	2	2.189	9.513	67.169	1.00	15.37
22	Cγ1	Val	2	3.062	9.181	68.373	1.00	17.32
23	Cγ2	Val	2	2.887	10.529	66.282	1.00	17.11
24	H	Val	2	0.491	9.171	65.301	1.00	13.40

25	Hα	Val	2	2.705	7.854	66.066	1.00	14.80
26	Hβ	Val	2	1.363	9.907	67.491	1.00	18.45
27	Hγ11	Val	2	3.253	9.998	68.859	1.00	20.78
28	Hγ12	Val	2	2.587	8.558	68.945	1.00	20.78
29	Hγ13	Val	2	3.889	8.780	68.062	1.00	20.78
30	Hγ21	Val	2	3.080	11.323	66.804	1.00	20.53
31	Hγ22	Val	2	3.712	10.142	65.949	1.00	20.53
32	Hγ23	Val	2	2.303	10.754	65.541	1.00	20.53
33	O	Val	3	3.742	4.568	69.130	1.00	17.15
34	N	Val	3	1.923	6.124	67.542	1.00	13.97
35	Cα	Val	3	1.500	5.102	68.491	1.00	15.14
36	C	Val	3	2.625	4.927	69.500	1.00	17.78
37	Cβ	Val	3	1.229	3.753	67.795	1.00	16.06
38	Cγ1	Val	3	0.804	2.704	68.813	1.00	18.72
39	Cγ2	Val	3	0.169	3.908	66.714	1.00	15.04
40	H	Val	3	2.677	5.952	67.168	1.00	16.76
41	Hα	Val	3	0.698	5.388	68.955	1.00	18.16
42	Hβ	Val	3	2.046	3.446	67.372	1.00	19.27
43	Hγ11	Val	3	0.640	1.866	68.353	1.00	22.46
44	Hγ12	Val	3	1.514	2.590	69.464	1.00	22.46
45	Hγ13	Val	3	-0.006	3.003	69.255	1.00	22.46
46	Hγ21	Val	3	0.018	3.047	66.294	1.00	18.05
47	Hγ22	Val	3	-0.652	4.227	67.121	1.00	18.05
48	Hγ23	Val	3	0.481	4.548	66.055	1.00	18.05
49	O	His	4	4.201	7.384	71.401	1.00	25.16
50	N	His	4	2.324	5.181	70.771	1.00	20.39
51	Cα	His	4	3.342	5.184	71.812	1.00	20.97
52	C	His	4	4.444	6.177	71.440	1.00	21.56
53	H	His	4	1.532	5.355	71.056	1.00	24.47
54	Hα	His	4	2.943	5.474	72.648	1.00	25.16
55	Cβ	His	4	3.910	3.778	72.016	1.00	23.09

56	O	Gly	5	8.442	6.601	69.120	1.00	8.71
57	N	Gly	5	5.639	5.672	71.148	1.00	18.63
58	Cα	Gly	5	6.766	6.521	70.810	1.00	14.38
59	C	Gly	5	7.286	6.289	69.407	1.00	9.59
60	H	Gly	5	5.821	4.831	71.141	1.00	22.35
61	Hα2	Gly	5	6.502	7.451	70.887	1.00	17.26
62	Hα3	Gly	5	7.490	6.357	71.434	1.00	17.26
63	N	Val	6	6.443	5.747	68.532	1.00	8.79
64	Cα	Val	6	6.830	5.526	67.143	1.00	7.79
65	C	Val	6	5.788	6.101	66.192	1.00	8.30
66	O	Val	6	4.651	6.376	66.581	1.00	9.63
67	Cβ	Val	6	7.059	4.024	66.826	1.00	9.44
68	Cγ1	Val	6	8.167	3.455	67.699	1.00	11.05
69	Cγ2	Val	6	5.784	3.220	66.999	1.00	10.93
70	H	Val	6	5.642	5.498	68.718	1.00	10.55
71	Hα	Val	6	7.665	5.991	66.978	1.00	9.35
72	Hβ	Val	6	7.339	3.940	65.901	1.00	11.33
73	Hγ11	Val	6	8.290	2.518	67.481	1.00	13.26
74	Hγ12	Val	6	8.986	3.945	67.528	1.00	13.26
75	Hγ13	Val	6	7.914	3.548	68.630	1.00	13.26
76	Hγ21	Val	6	5.967	2.290	66.793	1.00	13.11
77	Hγ22	Val	6	5.482	3.302	67.918	1.00	13.11
78	Hγ23	Val	6	5.108	3.566	66.396	1.00	13.11
79	N	Val	7	6.203	6.290	64.945	1.00	6.74
80	Cα	Val	7	5.316	6.757	63.892	1.00	5.50
81	C	Val	7	5.057	5.578	62.961	1.00	5.54
82	O	Val	7	5.992	4.919	62.506	1.00	9.00
83	Cβ	Val	7	5.936	7.929	63.104	1.00	7.67
84	Cγ1	Val	7	4.911	8.542	62.161	1.00	7.87
85	Cγ2	Val	7	6.473	8.990	64.056	1.00	8.50
86	H	Val	7	7.010	6.153	64.682	1.00	8.09

87	Hα	Val	7	4.473	7.046	64.274	1.00	6.60
88	Hβ	Val	7	6.676	7.598	62.571	1.00	9.20
89	Hγ11	Val	7	5.325	9.275	61.679	1.00	9.45
90	Hγ12	Val	7	4.610	7.862	61.537	1.00	9.45
91	Hγ13	Val	7	4.160	8.869	62.681	1.00	9.45
92	Hγ21	Val	7	6.856	9.715	63.538	1.00	10.20
93	Hγ22	Val	7	5.743	9.323	64.601	1.00	10.20
94	Hγ23	Val	7	7.153	8.592	64.622	1.00	10.20
95	O	Val	8	1.894	5.429	60.500	1.00	5.65
96	N	Val	8	3.782	5.315	62.691	1.00	5.15
97	Cα	Val	8	3.365	4.158	61.904	1.00	4.80
98	C	Val	8	2.799	4.595	60.557	1.00	4.49
99	Cβ	Val	8	2.288	3.343	62.653	1.00	5.77
100	Cγ1	Val	8	1.879	2.118	61.854	1.00	8.21
101	Cγ2	Val	8	2.791	2.938	64.028	1.00	7.84
102	H	Val	8	3.126	5.802	62.960	1.00	6.18
103	Hα	Val	8	4.130	3.583	61.744	1.00	5.76
104	Hβ	Val	8	1.501	3.898	62.775	1.00	6.93
105	Hγ11	Val	8	1.203	1.629	62.350	1.00	9.86
106	Hγ12	Val	8	1.520	2.405	60.999	1.00	9.86
107	Hγ13	Val	8	2.658	1.558	61.715	1.00	9.86
108	Hγ21	Val	8	2.100	2.429	64.479	1.00	9.41
109	Hγ22	Val	8	3.589	2.395	63.924	1.00	9.41
110	Hγ23	Val	8	2.999	3.738	64.536	1.00	9.41
111	N	Gly	9	3.334	4.020	59.483	1.00	5.14
112	C1A	ACX		5.049	5.619	55.854	1.00	4.70
113	C2A	ACX		4.315	5.425	54.573	1.00	4.77
114	C3A	ACX		2.845	5.661	54.743	1.00	4.69
115	C4A	ACX		2.272	4.901	55.889	1.00	4.80
116	C5A	ACX		3.090	5.008	57.163	1.00	5.00
117	C6A	ACX		2.574	3.985	58.204	1.00	4.83

118	O1A	ACX		4.917	6.974	56.238	1.00	5.16
119	O2A	ACX		4.892	6.315	53.553	1.00	6.13
120	O3A	ACX		2.141	5.288	53.523	1.00	6.44
121	O5A	ACX		4.526	4.768	57.010	1.00	5.46
122	C1B	ACX		6.678	10.544	57.350	1.00	8.59
123	C2B	ACX		6.973	10.102	55.949	1.00	8.02
124	C3B	ACX		6.053	8.955	55.557	1.00	7.51
125	C4B	ACX		6.064	7.889	56.564	1.00	6.16
126	C5B	ACX		5.942	8.318	58.016	1.00	6.13
127	C6B	ACX		6.244	7.117	58.944	1.00	6.41
128	O1B	ACX		5.348	10.912	57.340	1.00	8.27
129	O2B	ACX		6.854	11.218	55.027	1.00	10.53
130	O3B	ACX		6.431	8.411	54.227	1.00	8.57
131	O5B	ACX		6.802	9.445	58.424	1.00	7.39
132	O6B	ACX		7.534	6.598	58.637	1.00	7.92
133	C1C	ACX		2.975	14.266	58.057	1.00	9.91
134	C2C	ACX		3.900	14.353	56.885	1.00	9.54
135	C3C	ACX		4.565	13.035	56.543	1.00	11.22
136	C4C	ACX		5.110	12.323	57.735	1.00	8.70
137	C5C	ACX		4.181	12.332	58.970	1.00	8.85
138	C6C	ACX		4.958	11.852	60.179	1.00	11.98
139	O1C	ACX		1.965	13.403	57.652	1.00	10.24
140	O2C	ACX		3.145	14.877	55.735	1.00	12.82
141	O3C	ACX		5.638	13.258	55.555	1.00	13.62
142	O5C	ACX		3.551	13.638	59.328	1.00	10.81
143	O6C	ACX		6.056	12.729	60.392	1.00	16.90
144	C1D	ACX		-2.222	13.252	57.642	1.00	12.34
145	C2D	ACX		-1.567	14.043	56.529	1.00	12.92
146	C3D	ACX		-0.052	13.864	56.513	1.00	12.41
147	C4D	ACX		0.575	13.976	57.837	1.00	11.12
148	C5D	ACX		-0.146	13.235	58.951	1.00	12.13

149	C6D	ACX		0.468	13.586	60.308	1.00	15.38
150	O1D	ACX		-1.961	11.946	57.330	1.00	10.49
151	O2D	ACX		-2.123	13.645	55.235	1.00	15.60
152	O3D	ACX		0.562	14.826	55.562	1.00	13.60
153	O5D	ACX		-1.605	13.451	59.067	1.00	13.72
154	O6D	ACX		0.376	14.986	60.495	1.00	19.10
155	C1E	ACX		-3.716	8.191	57.214	1.00	8.33
156	C2E	ACX		-4.275	9.201	56.237	1.00	8.71
157	C3E	ACX		-3.401	10.441	56.179	1.00	9.97
158	C4E	ACX		-3.139	11.025	57.520	1.00	10.98
159	C5E	ACX		-2.816	10.038	58.620	1.00	11.37
160	C6E	ACX		-3.030	10.745	60.004	1.00	19.98
161	O1E	ACX		-2.461	7.939	56.779	1.00	5.62
162	O2E	ACX		-4.405	8.584	54.909	1.00	9.54
163	O3E	ACX		-4.010	11.451	55.283	1.00	12.21
164	O5E	ACX		-3.551	8.747	58.678	1.00	10.12
165	O6E	ACX		-2.968	9.767	61.029	1.00	27.42
166	C1F	ACX		-0.052	4.505	56.317	1.00	5.75
167	C2F	ACX		-1.116	4.734	55.279	1.00	5.61
168	C3F	ACX		-1.697	6.136	55.381	1.00	4.71
169	C4F	ACX		-2.122	6.469	56.764	1.00	5.16
170	C5F	ACX		-1.049	6.171	57.778	1.00	5.79
171	C6F	ACX		-1.468	6.516	59.242	1.00	6.47
172	O1F	ACX		0.903	5.456	56.109	1.00	5.46
173	O2F	ACX		-0.536	4.467	53.972	1.00	5.19
174	O3F	ACX		-2.804	6.311	54.423	1.00	5.27
175	O5F	ACX		-0.592	4.770	57.755	1.00	5.95
176	O6F	ACX		-2.697	5.869	59.567	1.00	6.16
177	H1A	ACX		5.995	5.417	55.712	1.00	5.64
178	H2A	ACX		4.445	4.493	54.283	1.00	5.73
179	H3A	ACX		2.702	6.620	54.906	1.00	5.63

180	H4A	ACX		2.199	3.959	55.639	1.00	5.76
181	H5A	ACX		2.970	5.897	57.524	1.00	6.01
182	H6A1	ACX		2.665	3.079	57.843	1.00	5.80
183	H6A2	ACX		1.620	4.167	58.402	1.00	5.80
184	HO2A	ACX		4.635	6.036	52.727	1.00	7.36
185	HO3A	ACX		2.083	6.006	52.978	1.00	7.73
186	H1B	ACX		7.237	11.323	57.586	1.00	10.31
187	H2B	ACX		7.901	9.774	55.921	1.00	9.62
188	H3B	ACX		5.138	9.306	55.498	1.00	9.02
189	H4B	ACX		6.893	7.388	56.465	1.00	7.39
190	H5B	ACX		5.012	8.586	58.167	1.00	7.36
191	H6B1	ACX		6.225	7.413	59.879	1.00	7.69
192	H6B2	ACX		5.573	6.423	58.809	1.00	7.69
193	HO2B	ACX		7.587	11.256	54.504	1.00	12.64
194	HO3B	ACX		6.045	8.895	53.588	1.00	10.29
195	HO6B	ACX		7.699	5.896	59.147	1.00	9.50
196	H1C	ACX		2.601	15.149	58.258	1.00	11.89
197	H2C	ACX		4.606	14.998	57.106	1.00	11.45
198	H3C	ACX		3.891	12.457	56.132	1.00	13.47
199	H4C	ACX		5.971	12.734	57.984	1.00	10.43
200	H5C	ACX		3.461	11.692	58.803	1.00	10.62
201	H6C1	ACX		4.382	11.855	60.959	1.00	14.38
202	H6C2	ACX		5.287	10.950	60.018	1.00	14.38
203	HO2C	ACX		3.635	15.499	55.313	1.00	15.39
204	HO3C	ACX		6.243	13.816	55.895	1.00	16.34
205	HO6C	ACX		6.731	12.276	60.733	1.00	20.28
206	H1D	ACX		-3.183	13.414	57.658	1.00	14.80
207	H2D	ACX		-1.762	14.992	56.672	1.00	15.51
208	H3D	ACX		0.131	12.967	56.181	1.00	14.89
209	H4D	ACX		0.647	14.925	58.078	1.00	13.35
210	H5D	ACX		-0.005	12.277	58.802	1.00	14.56

211	H6D1	ACX		-0.024	13.124	61.023	1.00	18.45
212	H6D2	ACX		1.402	13.314	60.325	1.00	18.45
213	HO2D	ACX		-2.009	14.286	54.661	1.00	18.72
214	HO3D	ACX		0.636	14.444	54.757	1.00	16.31
215	HO6D	ACX		0.960	15.242	61.121	1.00	22.92
216	H1E	ACX		-4.249	7.379	57.212	1.00	10.00
217	H2E	ACX		-5.167	9.467	56.546	1.00	10.45
218	H3E	ACX		-2.541	10.180	55.796	1.00	11.96
219	H4E	ACX		-3.904	11.546	57.785	1.00	13.18
220	H5E	ACX		-1.865	9.824	58.545	1.00	13.65
221	H6E1	ACX		-3.922	11.188	60.019	1.00	23.97
222	H6E2	ACX		-2.324	11.418	60.146	1.00	23.97
223	HO2E	ACX		-5.163	8.865	54.522	1.00	11.44
224	HO3E	ACX		-4.726	11.763	55.647	1.00	14.65
225	HO6E	ACX		-2.131	9.751	61.381	1.00	32.90
226	H1F	ACX		0.327	3.602	56.242	1.00	6.90
227	H2F	ACX		-1.846	4.084	55.437	1.00	6.74
228	H3F	ACX		-0.985	6.767	55.132	1.00	5.65
229	H4F	ACX		-2.933	5.946	56.987	1.00	6.19
230	H5F	ACX		-0.273	6.734	57.553	1.00	6.95
231	H6F1	ACX		-0.769	6.214	59.859	1.00	7.76
232	H6F2	ACX		-1.578	7.477	59.326	1.00	7.76
233	HO2F	ACX		-0.856	3.720	53.661	1.00	6.22
234	HO3F	ACX		-3.011	7.162	54.367	1.00	6.32
235	C1	OQQ		2.179	10.562	52.359	1.00	23.72
236	C2	OQQ		1.502	10.712	53.703	1.00	20.02
237	C3	OQQ		2.047	9.751	54.731	1.00	14.73
238	C4	OQQ		1.278	9.814	56.031	1.00	12.07
239	C5	OQQ		2.022	9.128	57.151	1.00	9.49
240	C6	OQQ		1.334	9.295	58.486	1.00	8.33
241	C7	OQQ		2.159	8.762	59.632	1.00	8.19

242	C8	OQQ		1.441	8.950	60.947	1.00	8.76
243	O8	OQQ		1.509	10.306	61.319	1.00	11.22
244	H11	OQQ		3.135	10.732	52.456	1.00	28.47
245	H12	OQQ		2.041	9.656	52.025	1.00	28.47
246	H13	OQQ		1.797	11.203	51.729	1.00	28.47
247	H21	OQQ		0.544	10.554	53.601	1.00	24.03
248	H22	OQQ		1.630	11.624	54.027	1.00	24.03
249	H31	OQQ		1.998	8.842	54.377	1.00	17.67
250	H32	OQQ		2.981	9.974	54.905	1.00	17.67
251	H41	OQQ		1.142	10.750	56.271	1.00	14.49
252	H42	OQQ		0.408	9.386	55.911	1.00	14.49
253	H51	OQQ		2.097	8.176	56.948	1.00	11.39
254	H52	OQQ		2.919	9.510	57.211	1.00	11.39
255	H61	OQQ		1.165	10.245	58.636	1.00	9.99
256	H62	OQQ		0.480	8.823	58.463	1.00	9.99
257	H71	OQQ		2.998	9.260	59.660	1.00	9.83
258	H72	OQQ		2.352	7.815	59.496	1.00	9.83
259	H81	OQQ		0.508	8.680	60.854	1.00	10.52
260	H82	OQQ		1.871	8.406	61.633	1.00	10.52
261	H83	OQQ		2.150	10.415	61.924	1.00	13.46

Compound name	Lab book number	Thesis Number
Pentafoil knot	-	**1**
18-Crown-6	-	**2**
Hydrogen bond rotaxane	-	**3**
Cation nanotube peptide	-	**4**
Anion nanotube peptide	-	**5**
Molecular wire rotaxane	-	**6**
Ferrocene rotaxane	-	**7**
pi catenane	-	**8**
cyclodextrin gel	-	**9**
adamantane gel	-	**10**
alpha cyclodextrin	-	**11**
tosyl a cyclodextrin	1	**12**
tosyl a cyclodextrin secondary	-	**13**
cyclodextrin rotaxane	-	**14**
cyclodextrin catenane	-	**15**
cyclodextrin solvent switch	-	**16**
cyclodextrin competing guest switch	-	**17**
cyclodextrin redox switch	-	**18**
cyclodextrin light switch	-	**19**
bis pillar5arene bis guest polymer	-	**20**
azo naphthalene daisy chain	-	**21**
nitrophenyl daisy chain	-	**22**
secondary cinnamoyl daisy chain	-	**23**
secondary cinnamoyl boc daisy chain	-	**24**
primary cinnamino daisy chain	-	**25**
primary cinnamoyl daisy chain	-	**26**
azido daisy chain 1 4	-	**27**

azido daisy chain 1 5	-	**28**
crown ether metal polymer	-	**29**
pillar5arene metal polymer	-	**30**
azo propyl dicapped dimer	10	**31**
azo undecyl dicapped dimer	-	**32**
azo octyl dicapped dimer	11	**33**
azido a cyclodextrin	2	**34**
amino a cyclodextrin	3	**35**
dicarboxy azobenzene	-	**36**
carboxyazobenzene a cyclodextrin	4	**37**
boc propylamine	-	**38**
propylamine azo a cyclodextrin	9	**39**
amino octanoic acid	-	**40**
boc amino octanoic acid	5	**41**
octylamine a cyclodextrin	8	**42**
chloro dimethoxy triazine capping group	-	**43**
octyl dicapped dimer	-	**44**
azopropyl capped monomer	13	**45**
azo propyl monocapped dimer	-	**46**
octyl capped azo dimer		**47**
azo capped octyl dimer		**48**
trimer		**49**
cbz pentaalanine		**50**
cbz pentaalanine a cyclodextrin		**51**
pentaalanine a cyclodextrin		**52**
monocarboxy azobenzene	-	**53**
azo pentaalanine a cyclodextrin		**54**
azido b cd		**55**
amino b cd	43	**56**

cbz pentaalanine b cyclodextrin		**57**
pentaalanine b cyclodextrin		**58**
carboxyadamantane	-	**59**
ada pentaalanine b cyclodextrin		**60**
pentaalanine		**61**
boc hexavaline		**62**
boc hexavaline a cyclodextrin	18	**63**
hexavaline a cyclodextrin	12	**64**
carboxyazo aminohexavaline a cd	14	**65**
hexavaline		**66**
Fmoc trivaline	27	**67**
fmoc trivaline a cd	29	**68**
fmoc hisBOM gly	31	**69**
azo trivaline	30	**70**
azo vvvhBOMgvvv a cd	36	**71**
azo vvvhgvvv a cd	39	**72**
trivaline b cd		**73**
ada trivaline	44	**74**
ada vvvhBOMgvvv b cd	40	**75**
ada vvvhgvvv b cd		**76**
azo vvvhBOMgvvv	34	**77**
ada vvvhBOMgvvv	45	**78**
vvvhBOMgvvv	33	**79**
vvvhBOMgvvv b cd	38	**80**
octyl-vvvhBOMgvvv		**81**
octyl vvvhBOMgvvv a cd		**82**
octyl vvvhgvvv a cd		**83**
vvvhgvvv		**84**
Ac vvvhgvvv Am	56	**85**
Fmoc amino dodecanoic acid	52	**86**
TNBS	-	**87**

TNBS dodecaminoacid a cd	54	**88**
TNBS dodecaminoacid	-	**89**
carboxypropionamido a cd	50	**90**
dimethylphenyl dodecamino acid	57	**91**
dmp dodec amino a cd rotaxane	-	**92**
dmp dodec carboxyprop cd rotaxane	60	**93**
adipic acid	-	**94**
dmp dodec adipicacid cd rotaxane	61	**95**
adipic acid a cd	-	**96**
dimethyl aniline	-	**97**
dmp azo adipic acid a cd rotaxane	62	**98**
diamino azobenzene	-	**99**
TNBS azo adipicacid a cd rotaxane	67	**100**
resin adipicacid cd	64	**101**
resin azobenzene	63	**102**
trivaline azo a cd	42	**103**
trivaline	37	**104**
azo b cd		**105**
trivaline azo b cd		**106**
trivaline propyl azo a cd	66	**107**
hexavaline propyl azo a cd monomer	-	**108**
y cyclodextrin	-	**109**
bis b cd	-	**110**
ada tetravaline	65	**111**
vvvghvvv octyl		**112**
eeeaaavvv hexadecane		**113**